

Taxonomy and Dynamics of Small Solar System Body Populations

A Thesis submitted by
Timothy R. Holt

For the award of
Doctor of Philosophy (PhD)
21st of May 2021



School of Sciences
Faculty of Health, Engineering and Sciences
Centre for Astrophysics

Abstract

In the story of our Solar system, the captured, irregular satellites of the gas giants and the Jovian Trojan swarms provide key records of the dynamical history. When investigating small Solar system body populations such as these, we need to accommodate their complex and diverse dynamical and physical properties, and our incomplete empirical knowledge of individual objects. To discover more about our Solar system's small bodies using dynamical families and their histories, this thesis thus focuses on the use of astrocladistics, a novel taxonomic analysis adapted from the biological sciences, the 'Tree of Life'. The astrocladistical analyses in this thesis are then combined with n -body simulations of particular dynamical families, to gain insights as to their origins.

The first population examined in this Thesis comprises the irregular Satellites of the gas giants, providing a small-scale verification of the use of cladistics for Solar system research (Paper 1). Two dynamical studies on the Jovian Trojans then follow. The first of these (Paper 2) investigates the escape rate of the Jovian Trojans using large scale n -body simulations, with a focus on the collisional families in the population. The second Jovian Trojans study (Paper 3) reports the discovery of the first example of a Jovian Trojan dynamical pair. The final work (Paper 4) included in this thesis uses astrocladistics to examine the Jovian Trojan swarms, and identify a set of new priority targets. The priority target can also help place the targets of the *Lucy* mission spacecraft, set to visit in the late 2020s, into a wider context. In overall terms, this thesis establishes astrocladistics as a tool for analysis of small Solar system bodies, provides new insights into the history of different dynamical families, and forms a promising basis for the wider adoption of cladistics in comparative planetology.

The work that comprises this PhD was presented, as a whole, in a seminar on 13th of April, 2021. A recording is available.

Thesis certification

This Thesis is entirely the work of Timothy R. Holt except where otherwise acknowledged. The work is original and has not previously been submitted for any other award, except where acknowledged.

Principal Supervisor: Prof. Jonathan Horner (USQ)

Associate Supervisor: Prof. Bradley Carter (USQ)

Mentor: Dr. David Nesvorný (SwRI)

Student and supervisors signatures of endorsement are held at the University.

Acknowledgements

Many people helped in making this PhD project a success. Here I would like to acknowledge their tributes and assistance in this project.

The project would not have possible without the support of my supervisors at the University of Southern Queensland, Prof. Jonti Horner and Prof. Brad Carter. I can not express my gratitude for your support and and encouragement over the past few years.

Dr. David Nesvorný at the South-west Research Institute continues to be a mentor, an inspiration and invaluable source of knowledge. At the University of Southern Queensland, A/Prof Rachel King, has shared her knowledge of statistics. It was an honor to meet Dr. Didier Fraix-Burnet, the creator of Astrocladistics, at the Institut de Planétologie et d'Astrophysique de Grenoble (IPAG).

I am indebted to the hard work that Prof. David Vokrouhlický and Dr. Miroslav Brož, both from the Institute of Astronomy, Charles University in Prague Czech Republic put into the work on Paper 3, on the Jovian Trojan Pairs. Dr. Marcel Popescu, from Astronomical Institute of the Romanian Academy and Christopher C. E. Tylor, from the University of Southern Queensland, both assisted with Paper 4, the Astrocladistics of the Jovian Trojans. I need to thank Dr. Bryce Bolin, based at Caltech, and Dr. Marc Buie from the South-west Research Institute, for involving me in their studies.

Dr. Guido Grimm assisted with the cladistical methodology and terminology used in Paper 1, on the astrocladistics of the irregular satellites. Dr. Pablo Goloboff provided assistance with TNT, which is subsidized by the Willi Hennig Society, as well as additional comments on the cladistical methodology. I would like to thank Dr. Henry Throop for discussions regarding the gas giant ring systems. In Paper 2 and 3, the Trojan Dynamical papers, I thank Dr. Romina Di Sisto for their review and efforts in improving the papers.

As always, I need to acknowledge the support of my parents, who may not always understand the science, but knew that it was important to me. Finally, I can't thank my wife, partner and best friend, Dr. Rebecca Buchholz, enough for her faith in me. Together we finished this.

Funding for this PhD program was provided by the Australian Government Research Training Program Scholarship

The University of Southern Queensland and myself acknowledge the traditional custodians of the lands and waterways where the University is located. Further, we acknowledge the

cultural diversity of Aboriginal, Torres Strait Islander and First Nation peoples and pay respect to Elders past, present and future. The University of Southern Queensland, Toowoomba campus is located on lands of the Giabal and Jarowair peoples. The South-west Research Institute is situated on lands of the Arapaho and Cheyenne peoples.

Contents

Abstract	i
Table of Contents	v
List of Figures	viii
Chapter I Introduction	I
1.1 Hypothesis	7
1.2 Research Questions	7
1.3 Jovian and Saturnian Satellite systems	8
1.3.1 The Jovian System	9
1.3.2 The Saturnian System	10
1.3.3 Formation Theories	13
1.4 Jovian Trojans	15
1.4.1 Origins	15
1.4.2 Observations	18
1.4.2.1 History	18
1.4.2.2 Colours	20
1.4.2.3 Spacecraft observations	21
1.4.3 Physics	21
1.4.3.1 Lagrange points	21
1.4.3.2 Yarkovsky effect	23
1.4.4 Small Body Taxonomy	26
1.4.4.1 Spectral Classification	27
1.4.4.2 Multivariate Hierarchical Classification	28
1.4.4.3 Yarkovsky Drift	30
1.5 Orbital Dynamics	30
1.5.1 n -body simulations	31
1.5.2 Yarkovsky effect	33
1.5.3 Proper elements	35
1.5.4 Asteroid Pairs	37
1.6 Cladistics	40
1.6.1 History	41
1.6.2 Cladistical Methodology	41
1.6.2.1 Taxon-character Matrix	42

1.6.2.2	Tree Search	45
1.6.2.3	Tree statistics	46
1.6.3	Astrocladistics	47
1.6.3.1	Characteristics	48
1.6.4	Hierarchical Clustering Method	51
1.6.4.1	Limitations of the Hierarchical Clustering Method	51
1.7	Concluding remarks	52
Chapter 2	Paper 1 - Cladistical Analysis of the Jovian and Saturnian Satellite Systems	53
2.1	Abstract	53
2.1.1	New Satellites	54
2.2	Associated Presentations and Publications	56
2.2.1	Oct. 2017: DPS 49 - Oral presentation	56
Chapter 3	Paper 2 - Stability of the Jovian Trojans and their collisional families	77
3.1	Abstract	77
3.2	Associated Presentations and Publications	78
3.2.1	Oct. 2018: DPS 50 - Poster presentation	78
Chapter 4	Paper 3 - A pair of Jovian Trojans at the L ₄ Lagrange point	93
4.1	Abstract	93
4.1.1	Astrocladistical analysis of the Trojan Pair.	94
4.2	Associated Presentations and Publications	94
4.2.1	Aug. 2020: DDA 50 - Oral presentation	94
4.2.2	Jan. 2021: COSPAR - Oral presentation	95
Chapter 5	Paper 4 - Astrocladistics of the Jovian Trojan Swarms	117
5.1	Abstract	117
5.2	Associated Presentations and Publications	118
5.2.1	Aug. 2018: IAU XXX - Focus Meeting 1 - A Century of Asteroid Families - Oral presentation	118
5.2.2	Sept. 2019: EPSC-DPS joint meeting - Oral presentation	119
5.2.3	Oct. 2020: DPS 52 - Oral presentation	119
5.2.4	Jan. 2021: COSPAR - Oral presentation	120
Chapter 6	Additional works and Coauthor projects	160
6.1	Additional works	160
6.1.1	Simulations of a Synthetic Eurybates Collisional Family	160
6.1.2	Captured Small Solar System Bodies in the Ice Giant Region:	161
6.2	Coauthor	162
6.2.1	Horner et al. 2020 - Solar System Physics for Exoplanet Research	162
6.2.2	Bolin et al. 2020 - Characterization of Temporarily Captured Minimum 2020 CD ₃ by Keck Time-resolved Spectrophotometry	163
6.2.3	Horner et al. 2021 - Dynamical prospecting in the π Mensæ system	166

6.2.4	Bolin et al. 2021 - Initial Visible and Mid-IR Characterization of P/2019 LD ₂ (ATLAS), an Active Transitioning Centaur Among the Trojans, with Hubble, Spitzer, ZTF, Keck, APO and GROWTH Imaging and Spectroscopy	170
6.2.5	Buie et al. 2021 -Size and shape of (11351) Leucus from five stellar occultations	175
Chapter 7	Outcomes, Future works and conclusions	177
7.1	Outcomes	177
7.1.1	Additional Outcomes	179
7.2	Future works	181
7.2.1	Other small body populations	181
7.2.2	Future surveys	182
7.3	Concluding remarks	184
7.3.1	Dynamics of the Jovian Trojans	184
7.3.1.1	Jovian Trojan Escapes	184
7.3.1.2	Jovian Trojan Pair	185
7.3.2	Astrocladistics in Planetary science	187
References		190
Chapter A	Appendix	224
A.1	Calculations	224
A.1.1	Calculation of $\left(\frac{da}{dt}\right)_{JT}$	224
A.1.2	Mean obliquity of Yarkovsky	225

1.3	The distribution of bodies in the Solar system as seen face-on (xy left) and edge-on (xz right), showing the distribution of objects in Cartesian coordinates in the ecliptic coordinate system. The positions of the objects are those they occupied at epoch 2000-01-01 00:00:00 UT (from Horner et al., 2020). The data plotted were taken from the JPL HORIZONS database(https://ssd.jpl.nasa.gov/horizons.cgi). The objects in the inner Solar system are coloured as in Figure 1.2. Outer Solar system objects are also coloured according to their classification. Centaurs (brown) are shown between Jupiter and Neptune. The Neptune Trojans (orange-red) can be seen at 30 au, and the Plutinos (deep pink) at 39.5 au, just interior to the objects that make up the classical Edgeworth-Kuiper belt (orchid, between ~ 40 and 48 au). To higher eccentricities, the Scattered Disc objects (maroon) can be seen spreading outward in a curved population in the middle plot - objects whose perihelia fall between ~ 30 and 40 au that move on eccentric, chaotic orbits. Two cometary populations are shown, the Jupiter family comets (olive) and the Halley type comets (cyan).	4
1.4	A p[lot of the outer Solar system showing the individual populations in semi-major axis, eccentricity (top) and inclination (bottom) space (from Horner et al., 2020). The data plotted were taken from the JPL HORIZONS database (https://ssd.jpl.nasa.gov/horizons.cgi). The objects in the inner Solar system are coloured as in Figures 1.2 outer system as in Figure 1.3.	5
1.5	Distribution of asteroid types under the Bus-DeMeo spectral taxonomy. From Figure 3 in DeMeo and Carry (2014).	6
1.6	Polar (top row) and side (bottom row) views of the Jovian satellite system, as of 20th of November, 2020. The full system is shown on the left, only retrograde satellites in the center and the central system on the right. The colours represent terminology used in traditional classification: Amalthea inner regular family (magenta); Galilean family (blue); Themisto prograde Irregular (lime); Himalia prograde Irregular family (green); Carpo prograde Irregular (spring green); Ananke Irregular family (orange); Carme Irregular family (brown); Pasiphae Irregular group (red). Data retrieved from Sheppard database https://sites.google.com/carnegiescience.edu/sheppard/	11

1.7	Polar (top row) and side (bottom row) views of the Saturnian satellite system, as of 20th of November, 2020. The full system is shown on the left, only retrograde satellites in the center and the central system on the right. colours represent terminology used in traditional classification: Main ring group, with associated shepherd satellites (purple); Mid-sized icy satellites and Titan (dark blue); Trojan satellites (steel blue); Alkanoids and associated rings (deep sky blue); ‘Inuit’ prograde Irregular family (dark green); ‘Gallic’ prograde Irregular family (dark orange); ‘Norse’ retrograde Irregular family (dark red). Rings are shown in grey. Data retrieved from Sheppard database https://sites.google.com/carnegiescience.edu/sheppard/	13
1.8	Distribution of the Jovian Trojans after Horner et al. (2020). The upper panels show the positions of the Trojans relative to the planets on 01-01-2000 00:00 in XY (left) and XZ (right) planes of the ecliptic coordinate system. The lower panels show the Trojans in semi-major axis vs inclination space (left) and semi-major axis vs eccentricity space (right). All data from NASA HORIZONS (Giorgini et al., 1996), access on 13th October, 2020. Purple points are initially stable objects, from the AstDyS (Knežević and Milani, 2017) dataset. Grey points are transient objects.	16
1.9	Size-frequency distribution (left) and cumulative discoveries (right) of the Jovian Trojan asteroids. The solid line shows the distribution for the population as a whole, whilst the long-dash line shows the distribution among members of the leading L_4 swarm, and the dotted line shows the distribution for the trailing L_5 swarm. Data from NASA HORIZONS, as of 19th August 2019. Vertical grey, dashed line indicates observational completeness (Emery et al., 2015). The grey line shows the estimated complete size distribution (Nesvorný, 2018).	17
1.10	After DeMeo and Carry (2014), showing some major components of the dynamical history of small bodies in the Solar system based on models (Tsiganis et al., 2005a; Morbidelli et al., 2005; Walsh et al., 2011). These models may not represent the actual history of the Solar system, but are possible histories. They contain periods of radial mixing, mass removal and planet migration — ultimately arriving at the current distribution of planets and small-body populations.	19
1.11	A: Diagrammatic representation of libations in the Sun-Jupiter system. The reference frame is locked to the orbit of Jupiter, with arrows depicting the relative direction of travel. Lagrange points are indicated with a small circle. ‘Tadpole’ orbits at the L_4 and L_5 points are in blue. The ‘Horseshoe’ orbit is green. Adapted from (DePater and Lissauer, 2010). B: Gravitational potential of a three body system. After (Horner and Lykawka, 2011)	22

1.12	REBOUND simulation of the Jovian Trojan 624 Hektor as a mass-less particle showing semi-major axis (a), eccentricity (e) and inclination progression over 1×10^6 years. The location of 624 Hektor, in a rotating reference frame with Jupiter, is also shown (polar). Simulations were run with WHFAST integrator. The Sun, Jupiter, Saturn, Uranus and Neptune were included as particles with mass. The integration time-step was set to 0.3954 yr, or $1/30$ the orbital period of Jupiter (Barnes and Quinn, 2004).	24
1.13	Modern Bus-DeMeo spectral taxonomy of asteroids (DeMeo et al., 2009). Spectra are shown from approximately 0.45 μ m to 2.45 μ m. Each spectrum is indicative of a taxonomic class. Each complex approximates to broad compositional differences, S-complex (siliceous objects), C-complex (carbonaceous objects) and X-complex (metallic objects).	28
1.14	Yarkovsky drift shown for a synthetic family in the Main asteroid belt. Figure 3 in Deienno et al. (2020).	31
1.15	Eurybates and Ennomos families in proper semi-major axis (SMA) and absolute magnitude space (H mag.) space.	32
1.16	Simplistic examples of cladistical methodology. A: A taxon-character matrix, including an Outgroup (O) and three taxa (T_1, T_2, T_3), with character (C1-5) states, including an unknown (?); B: An example tree, showing each of the taxa and the three ancestral states (A_1, A_2, A_3); C: A tree with a different rearrangement to that shown in A. D: This tree is a isomorph of the one shown in A.	43
1.17	Flow diagram of the cladistical methodology. Each stage uses a different software package as indicated: Mesquite (Maddison and Maddison, 2017); TNT: Tree analysis using New Technology (TNT) 1.5 (Goloboff et al., 2008; Goloboff and Catalano, 2016).	44
1.18	Wavelengths of the filters surveys used in this study.	50

- 6.1 The orbital element distribution of the known near-Earth asteroids, in semi-major axis eccentricity space (top) after Horner et al. (2020). The four subgroups within the near-Earth asteroid population are shown in different shades of green. The Atira asteroids are shown in aquamarine, the Atens in chartreuse, Apollos in sea green and Amors in dark green. The impact of observational bias is clearly seen here, particularly in the upper panel. Objects are easier to detect when closer to Earth than farther away - and the smallest (but most numerous) objects can only be discovered during close approaches to our planet. For that reason, the greatest population in a-e space is bounded by lines of constant perihelion = 0.9833 au (curving outward to the right) and aphelion = 1.0167 au (moving inwards toward higher eccentricities), which we show in white in the top panel. The wedge bounded by these two lines contains those objects that can reach a heliocentric distance at a distance within the bounds set by Earth's perihelion and aphelion distances and can therefore experience very close encounters with our planet. 164
- 6.2 Top left panel: mean geocentric, co-rotating Cartesian y and x coordinates of 2020 CD₃ orbital clones ± 5 y centered on 2020 March 23 UTC encompassing its ~ 700 day capture completing ~ 5 revolutions around the Earth-Moon system. The red dotted line indicates the trajectory of 2020 CD₃ before 2020 March 23 UTC and the blue dotted line indicates the trajectory of 2020 CD₃ after 2020 March 23 UTC. A green circle with a radius of three times the Earth's Hill radii of ~ 0.03 au is overplotted. The direction towards the Sun in the co-rotating frame is indicated. Top right panel: same as the top left panel except for mean geocentric, co-rotating Cartesian x and z coordinates. Bottom left panel: the evolution of 2020 CD₃'s orbital clones' mean semi-major axes ± 5 y centered on 2020 March 23 UTC. The color code of the dotted lines is the same as in the top panels. Bottom right panel: the mean geocentric distance of 2020 CD₃ orbital clones ± 5 y centered on 2020 March 23 UTC. A horizontal green line indicates three times the Hill radii in distance. The color code of the dotted lines is the same as in the previous three panels. 167

6.3	Top left panel: mean geocentric Cartesian y and x coordinates of 2020 CD ₃ orbital clones integrated backwards 100 y from 2020 March 23 UTC (blue line) with the Earth's three Hill radii marked in green. Top right panel: same as the top left panel except for the mean geocentric Cartesian x and z coordinates of 2020 CD ₃ orbital clones integrated backwards 100 y from 2020 March 23 UTC. Bottom left panel: the evolution in 2020 CD ₃ 's orbital clones' mean semi-major axis integrated backwards 100 y from 2020 March 23 UTC with the Earth's orbit in black. Bottom right panel: the geocentric distance of 2020 CD ₃ orbital clones integrated backwards 100 y from 2020 March 23 UTC.	168
6.4	Top left panel: same as in Fig. 6.3 except for orbital clones of 2020 CD ₃ integrated forwards 100 y from 2020 March 23 UTC (red line) with the Earth's three Hill radii marked in green. Top right panel: same as the top left panel except for the mean geocentric Cartesian x and z coordinates of 2020 CD ₃ orbital clones integrated forwards 100 y from 2020 March 23 UTC. Bottom left panel: the evolution in 2020 CD ₃ 's orbital clones' mean semi-major axis integrated forwards 100 y from 2020 March 23 UTC with the Earth's orbit in black. Bottom right panel: the geocentric distance of 2020 CD ₃ orbital clones integrated forwards 100 y from 2020 March 23 UTC.	169
6.5	The distribution of test particles at the start (top) and end (bottom) of our simulations, in semi-major axis (<i>a</i>) vs eccentricity (<i>e</i>) space. We highlight the extent of the conservative and optimistic habitable zones for the system, following Kopparapu et al. (2013, 2014), in green - with the conservative habitable zone shown in dark green, and the optimistic zone marked in pale green. The influence of π Mensæ b is readily apparent – clearing the entirety of the optimistic habitable zone, and beyond (inwards to ~ 0.6 au), and exciting the eccentricities of particles inwards to within 0.2 au. Similarly, the influence π Mensæ c can be seen in the form of the 'wedge' of cleared space in the inner area of the system.	171
6.6	The distribution of test particles at the end of our simulations, in semi-major axis (<i>a</i>) vs eccentricity (<i>e</i>) space. The colour bar shows, in each plot, the normalised fractional change in the test particle's semi-major axis (top) and the distance that it has moved in eccentricity space (bottom). The regions shown in green mark the conservative (dark green) and optimistic (light green) habitable zones, following Kopparapu et al. (2013, 2014). It is immediately apparent that, through the great majority of the region studied, the surviving test particles exhibit excitation in orbital eccentricity without moving much in semi-major axis space. The exception to this comes in the form of those particles scattered by π Mensæ c along lines of constant periape and apoapse.	172

- 6.7 The distribution of the surviving test particles at the conclusion of our simulations, after 1 Myr of evolution, zoomed to the region where particles survived. The panels show the particle distribution in semi-major axis (a) vs. eccentricity (e) space, with the left panel showing a linear presentation of a , and the right plotting a logarithmically. The red lines denote paths of constant apoapse at 0.062 au and periapse at 0.074 au, and the locations of key mean-motion resonances with π Mensæ c are marked at the top. As in Figure 6.6, the colour scale shows the degree to which test particles are excited in semi-major axis (upper panels) and eccentricity (lower panels). The striped structure visible in the logarithmic plot is the result of the initial cloning process, showing the spacing of the innermost suite of test particles in a -space, which is preserved as those test particles are not strongly stirred in semi-major axis. The sculpting of the test particle disk exterior to ~ 0.2 au as a result of the influence of π Mensæ b is clearly visible. 173
- 6.8 The percentage of orbital P/2019 LD 2 clones that have escaped the Solar System (reached >1000 au from the Sun) per bin in duration of time. Each bin is $\sim 100,000$ years wide. Within the first million years of the simulation, 78.8% have escaped the Solar System. By 10 million years, $\sim 95\%$ have escaped the Solar System. 175

1

Introduction

Throughout antiquity, there were five known planets, Mercury, Venus, Mars, Jupiter and Saturn, named ‘The Wanderers’ for their apparent movement across the sky. With the discovery of Uranus, the first ice giant planet, in 1781 by Sir William Herschel, and four objects, 1 Ceres, 2 Pallas, 3 Juno and 4 Vesta in the early 19th Century (1801-1804) the apparent structure of the Solar system was starting to become more complex. This complexity increased in the mid 19th Century, including the discovery of Neptune, the other Solar system ice giant, in 1843-6. From 1845 to 1900, 448 asteroids, what are now termed ‘small Solar system bodies’ were discovered. This plethora of new discoveries increased steadily until the advent of computer-aided photometry in the later part of the 20th century, when the number of discoveries started to increase exponentially (see North, 2008, for review of these discoveries). As of 11th March, 2021, there are 1,043,047 small Solar system bodies in the Minor Planet Center catalogue¹.

The small Solar system bodies are the debris left over from the earliest period in its formation. The known objects range in size from meter sized Near Earth objects, through to several hundred km sized objects, such as 4 Vesta, 624 Hektor, 16 Psyche, and the dwarf planets Pluto, 1 Ceres, Eris, Makemake and Haumea. To date, over a million objects have been

¹<https://minorplanetcenter.net/>

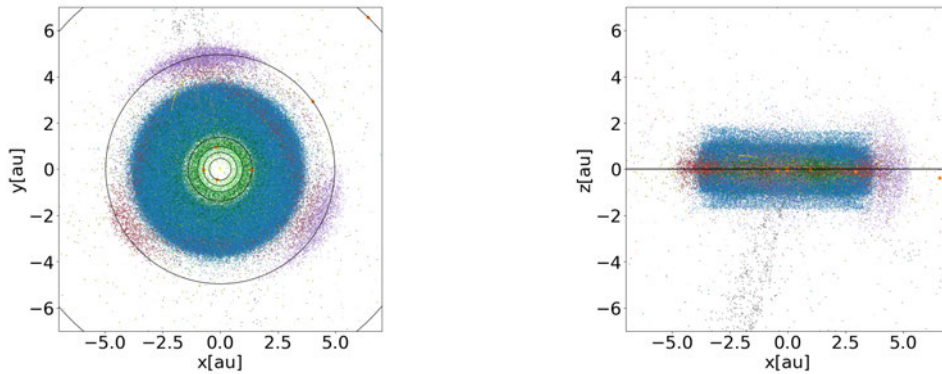


Figure 1.1: The distribution of objects in the inner six astronomical units (au) of the Solar system, shown in Cartesian coordinates in the ecliptic coordinate system. The left pane shows a top-down, xy view of the system, whilst the right pane shows a side-on xz view. The data plotted were taken from the JPL HORIZONS database <https://ssd.jpl.nasa.gov/horizons.cgi>, and the positions of the objects are shown at epoch 2000-01-01 00:00:00 UT. Inner Solar system showing the individual populations, including the Jovian Trojans in purple (after Horner et al., 2020). The various small body populations are colour coded as follows: the near-Earth asteroids (NEAs) in green (with the sub-populations as follows: Atiras in aquamarine, Atens in chartreuse, Apolos in sea green and Amors in dark green); Main belt asteroids in blue, the Hilda asteroids in red, the Jovian Trojans in purple, the Centaurs in brown, long-period comets in grey, Jupiter family comets in olive and Halley-type comets in cyan. The locations of the five innermost planets (Mercury, Venus, Earth, Mars and Jupiter) are marked in orange, with their orbits shown in white.

discovered, all clustered into various populations throughout the Solar system, see Figures 1.1 to 1.4. Two of these populations, the Jovian Trojans, and the Irregular satellites of the gas giants are of particular interest, as they are thought to have been captured to their current orbits during the chaotic, early days of the Solar system.

Taxonomy is the practice of grouping things into classes. In the context of small Solar system bodies, the current paradigm includes the dynamical populations (see Horner et al., 2020, for review), collisional families (see Nesvorný et al., 2015, for review) and a spectral classification system (the modern Bus-DeMeo system DeMeo et al., 2015), each explained further in section 1.4.4. There are some trends that can be seen using the spectral taxonomy across the Solar system, see Figure 1.5, though this complex area is the one of major interest and constantly under review (DeMeo and Carry, 2014; DeMeo et al., 2015).

The predominate method for analysis of taxonomy in the biological sciences is *Cladistics*, the ‘Tree of Life’. Recently works have expanded the use of this method out into astronomy, a new field termed ‘astrocladistics’. This PhD extends the use astrocladistics into the Planetary sciences for the first time, particularly the small Solar system body populations.

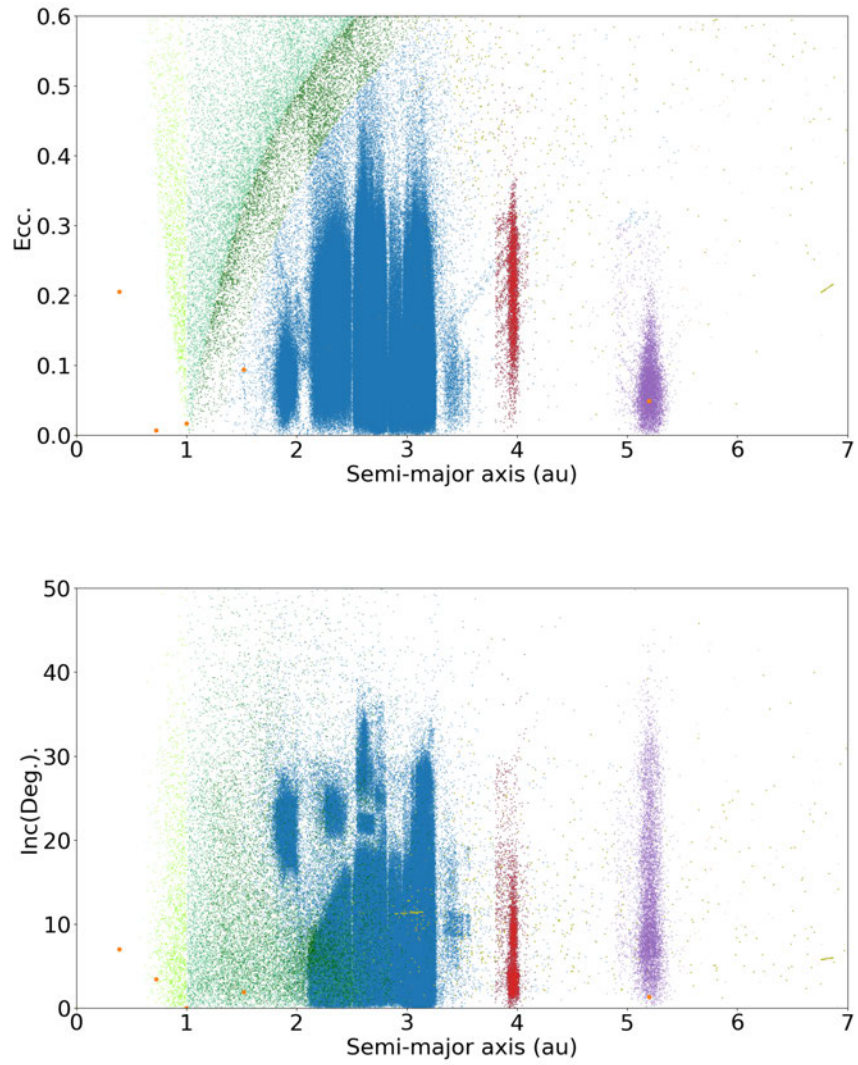


Figure 1.2: The observed distribution of the sma bodies in the inner So ar system, as a function of their semi-major axis, eccentricity, and inc ination. The various sma body popu ations are p otted in different co ours, using the same co our scheme as for Figure 1.1 The data p otted were taken from the JPL HORIZONS database <https://ssd.jpl.nasa.gov/horizons.cgi>.

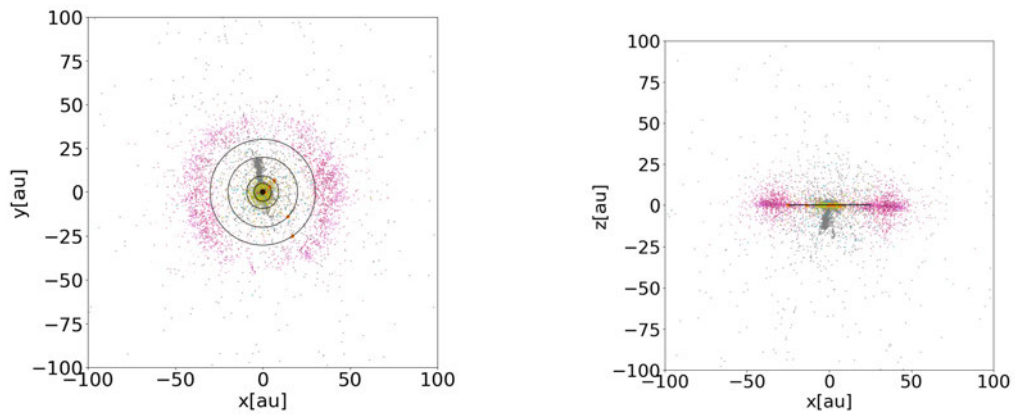


Figure 1.3: The distribution of bodies in the Solar system as seen face-on (xy left) and edge-on (xz right), showing the distribution of objects in Cartesian coordinates in the ecliptic coordinate system. The positions of the objects are those they occupied at epoch 2000-01-01 00 00 00 UT (from Horner et al., 2020). The data plotted were taken from the JPL HORIZONS database (<https://ssd.jpl.nasa.gov/horizons.cgi>). The objects in the inner Solar system are colored as in Figure 1.2. Outer Solar system objects are also colored according to their classification. Centaurs (brown) are shown between Jupiter and Neptune. The Neptune Trojans (orange-red) can be seen at 30 au, and the Plutinos (deep pink) at 39.5 au, just interior to the objects that make up the classical Edgeworth-Kuiper belt (orchid, between ~ 40 and 48 au). To higher eccentricities, the Scattered Disc objects (maroon) can be seen spreading outward in a curved population in the middle belt - objects whose perihelia fall between ~ 30 and 40 au that move on eccentric, chaotic orbits. Two cometary populations are shown, the Jupiter family comets (olive) and the Halley type comets (cyan).

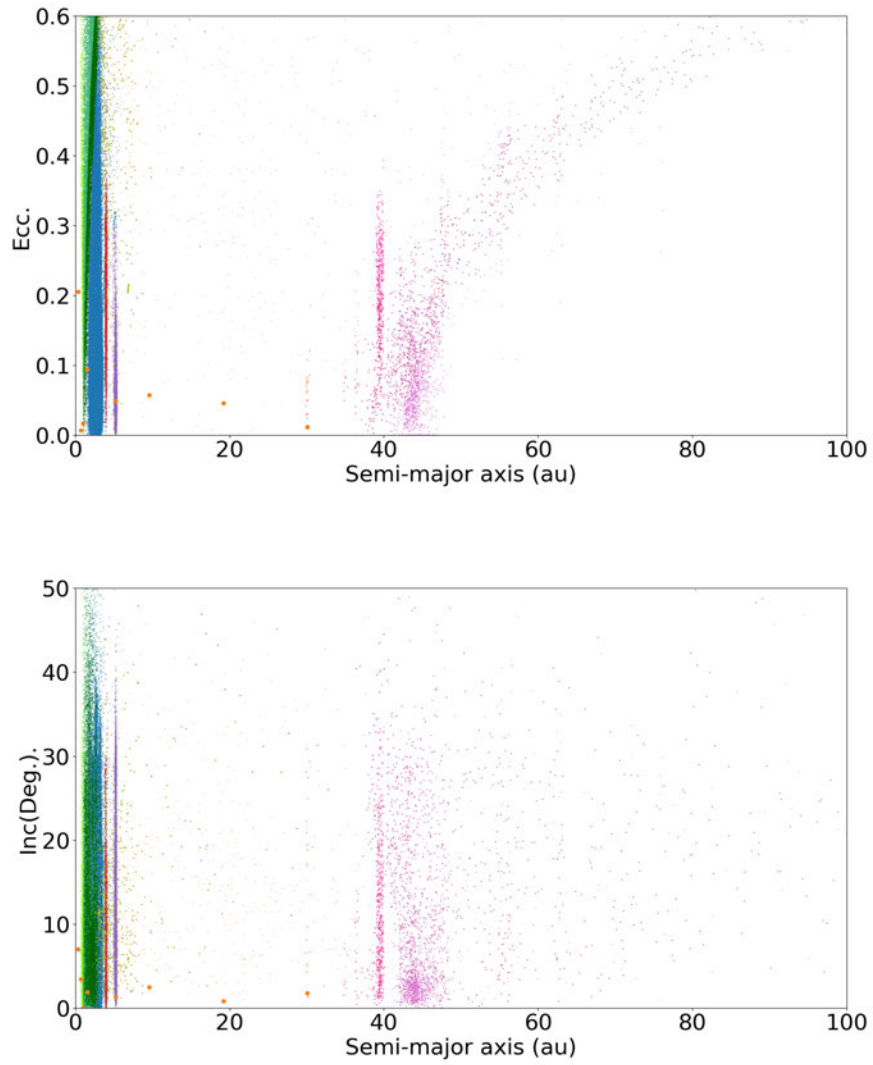


Figure 1.4: A plot of the outer Solar system showing the individual populations in semi-major axis, eccentricity (top) and inclination (bottom) space (from Horner et al., 2020). The data plotted were taken from the JPL HORIZONS database (<https://ssd.jpl.nasa.gov/horizons.cgi>). The objects in the inner Solar system are colored as in Figures 1.2 outer system as in Figure 1.3.

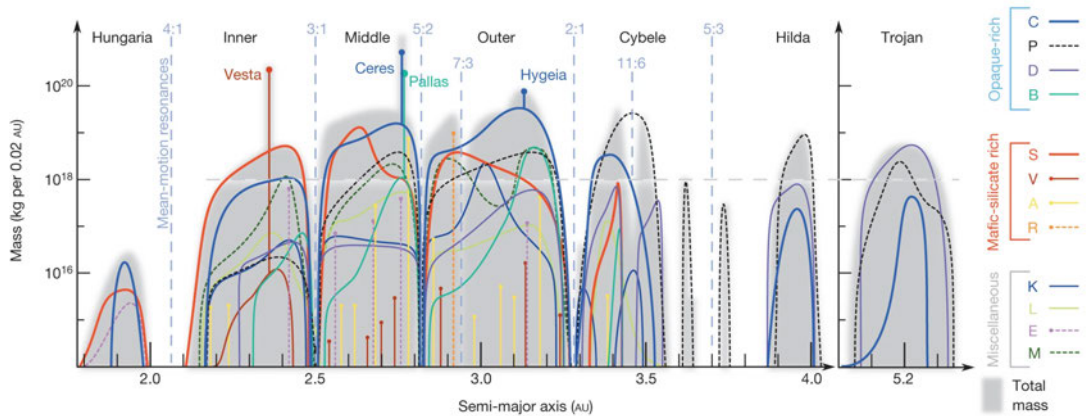


Figure 1.5: Distribution of asteroid types under the Bus-DeMeo spectra taxonomy. From Figure 3 in DeMeo and Carry (2014).

With a history of other taxonomic methods, these populations form a test case for the general expansion of astrocladistics as a tool for comparative planetology. The first population examined are the Irregular satellites of the gas giants, providing a small population to test cladistics. The primary focus of this PhD is the Jovian Trojan asteroids, a population several orders of magnitude larger than the satellites. The Jovian Trojans are two swarms of asteroids in Jupiter’s orbit, one leading and one trailing the gas giant. These objects provide a suitably sized population to extend the use of astrocladistics. The dynamical situation of the Jovian Trojans has also made traditional classifications systems problematic. In this PhD project, I use astrocladistics to investigate the classification of Jovian Trojans, and to place the resulting taxonomy into dynamical context. The combination of tool-sets provides insights into the history of these objects as well as providing an opportunity to incorporate astrocladistics into the narrative of the Solar system.

In this first chapter, I present an introduction to the project, including a hypothesis in section 1.1 and the scientific questions, with their objectives in section 1.2. The first paper of this PhD project looks at using astrocladistics to characterise Jovian and Saturnian Irregular satellite system. In section 1.3 I provide an overview of the satellite systems. Section 1.4 describes the small Solar system body population, the Jovian Trojans. The current state of relevant physics and dynamics of the Jovian Trojan swarms are also explored in section 1.4.3. I also look at how the current asteroid taxonomic systems relate to the Jovian Trojans, as well as their origins. Orbital dynamical methods form part of this work, and they are discussed in section 1.5. The application of astrocladistics to small Solar system bodies forms a major component of this work. In section 1.6 I explore some of the history of cladistics in the biological

sciences and its application in astronomy. The astrocladistical methodology is included in section 1.6.2. I finalise this section with some brief remarks in section 1.7.

1.1 HYPOTHESIS

Astrocladistics can be used to classify small Solar system objects into groups, including the Jovian Trojans and gas giant Irregular satellites, using incomplete datasets. The dynamical evolution of these populations can be simulated, giving insight into their long term stability and origins.

1.2 RESEARCH QUESTIONS

- *How can astrocladistics be used to give insights into the history of Solar system objects?*
Cladistics is used by biologists to create the ‘Tree of Life’. The technique was originally developed to incorporate incomplete fossils into the analysis. Traditional astronomy classification schemes require full, complete data for every object being investigated. This can become a major problem, as most objects in a given population are poorly characterised, and complete data is only available for a small fraction of them. As astrocladistics can be used for populations including incomplete data, it means more objects from a population can be included in a classification. In this PhD project, I use astrocladistics in an investigation of the satellite systems of the gas giants (Holt et al., 2016, 2018). Subsequent works in this project, by investigating the Jovian Trojans that have been observed in wide-field surveys, extends the use of the technique by an orders of magnitude. Previous investigations have indicated that there are several collisional families within the Jupiter Trojans (Emery et al., 2015), the results of collisions. One of the powers of cladistics is that it can analyse a multitude of different characteristics, particularly in incomplete datasets, allowing us to include dynamics as well as physical attributes in the analysis. The aim is to investigate the resulting classification that arises out of an astrocladistical analysis of the Jovian Trojans, and how it compares with existing methods.
- *What are the long term dynamics of the Jupiter Trojan families?*
Investigating the stability of the known collisional families in the Jovian Trojans (Nesvorný et al., 2015) can give us insights into the history of the population. Using a suite of simulations on Fawkes, the USQ High Performance Computer (HPC) cluster, we can simulate how these families evolve over time, giving us insights into their origins

and relationships. These results are expected to be of particular interest to the *Lucy* Mission (Levison et al., 2017), which is to visit the Jovian Trojans in 2025, as one of the targets, Eurybates is a collisional family member.

- *Are there any asteroid pairs in the Jovian Trojans, and what are the implications for the history of the population?*

Asteroid pairs, two objects with a common history, have been discovered in the Main belt and Hungaria populations (e.g. Pravec et al., 2019). The prevalence of these pairs informs us about dynamical history of the population. Despite searching in the sub 1000 km range (Pravec and Vokrouhlický, 2009), no pairs have been discovered in the Jovian Trojan swarms. Due to the unique dynamic environment of the Trojans, in collisional family searches, they require the use of a different proper semi-major axis parameter. In dynamical investigations of the Trojans, the delta to the semi-major axis of Jupiter, instead of just the orbital semi-major axis to the Sun, are used. The aim of this section is to use this alternative parameter to discover if there are any asteroidal pairs in the Jovian Trojan population.

1.3 JOVIAN AND SATURNIAN SATELLITE SYSTEMS

The two gas giants of the Solar system, Jupiter and Saturn, are host to a large number of satellites and rings. The satellites of both planets follow a similar progression pattern. The inner region of each system consists of small icy satellites, with an accompanying ring system (Thomas et al., 1998; Throop, 2004; Porco et al., 2005; Thomas et al., 2013). Farther out, there are larger icy/silicate satellites (Thomas, 2010; Deienno et al., 2014). Each of these satellites orbit the gas giant close to the equatorial plane, with minimal inclination, and prograde motion.

In the outer system, both planets have a series of Irregular satellites, small satellites with high eccentricities and inclinations (Nesvorný et al., 2003; Sheppard and Jewitt, 2003; Jewitt and Haghighipour, 2007), many of which have a retrograde orbit far from the host planet. It is thought that these satellites were captured from other populations of small Solar system bodies (Colombo and Franklin, 1971; Heppenheimer and Porco, 1977; Pollack et al., 1979; Sheppard and Jewitt, 2003; Nesvorný et al., 2004; Johnson and Lunine, 2005; Nesvorný et al., 2007, 2014). This is in contrast to the inner satellites, which are thought to have accreted in a circumplanetary disk (e.g. Canup and Ward, 2002; Canup, 2010). Such a formation mechanism is thought to resemble the accretion of planets in a protoplanetary disk around

a young star (Lissauer, 1987), a conclusion that is supported by the recent discovery of the TRAPPIST-1 planetary system (Gillon et al., 2016). That system features at least seven Earth-mass planets orbiting a very low mass star. While the host star, TRAPPIST-1, is considerably more massive than Jupiter it is similar in size, and its seven planets span orbital distances comparable to Jupiter's regular satellite system. Studying and understanding the gas giant systems in our own Solar system, can therefore provide context for future exploration of low-mass exoplanetary systems.

1.3.1 THE JOVIAN SYSTEM

Historically, Galilei (1610) discovered the first satellites in the Jovian system, the large Galileans, Io, Europa, Ganymede and Callisto. Our knowledge of these satellites has increased greatly in the past few decades, as a result of improved ground-based instrumentation (e.g. Vasundhara et al., 2017) and spacecraft flybys (e.g. Smith et al., 1979; Grundy et al., 2007; Greenberg, 2010).

Amalthea, one of the inner set of Jovian satellites, was discovered by Barnard (1892). A few years later, the first two small Irregular satellites, Himalia (Perrine, 1905) and Elara (Perrine and Aitken, 1905), were discovered in inclined, prograde orbits. The discovery of Pasiphae three years later by Melotte and Perrine (1908) is significant as this was only the second satellite in the Solar system to be found on a retrograde orbit, and the first such object found in the Jovian system. Several other Irregular satellites were discovered in the first half of the 20th century, Sinope (Nicholson, 1914), Lysithea (Nicholson, 1938), Carme (Nicholson, 1938) and Ananke (Nicholson, 1951). Leda, another small prograde Irregular, was discovered 20 years later by Kowal et al. (1975a). Themisto, the first Jovian satellite smaller than 10km to be discovered, was found that same year (Kowal et al., 1975b) and subsequently lost. Themisto was rediscovered by Sheppard et al. (2000) nearly 20 years later. The *Voyager* flybys of Jupiter discovered the remaining three inner satellites, Metis (Synnott, 1981), Adrastea (JEWITT et al., 1979) and Thebe (Synnott, 1980), along with a ring system (Smith et al., 1979). These three satellites, Amalthea and the ring system, would be imaged again by the *Galileo* (Ockert-Bell et al., 1999) and *Cassini* (Porco et al., 2005) spacecraft during their missions.

The Jovian Irregular satellites orbit the planet with semi-major axes an order of magnitude greater than the Galilean moons, and have large eccentricities and inclinations. In the early years of the 21st century, extensive surveys were carried out to search for the Jovian Irregular satellites (Scotti et al., 2000; Sheppard et al., 2001, 2002; Gladman et al., 2003a,b; Sheppard et al., 2003b; Sheppard and Marsden, 2003; Sheppard et al., 2003a; Sheppard and Jewitt, 2003;

Sheppard et al., 2004; Sheppard and Marsden, 2004; Beaugé and Nesvorný, 2007; Jacobson et al., 2011; Sheppard and Williams, 2012; Sheppard et al., 2018). These surveys increased the number of known Jovian satellites from 14 after *Voyager*, to the 79 known as of March, 2021. The inner five Irregular satellites, Leda, Himalia, Lystea, Elara and Dia, have prograde orbits and have previously been classified into the Himalia group (Nesvorný et al., 2003; Sheppard and Jewitt, 2003). Themisto and Carpo were proposed as single members of their own groups by Sheppard and Jewitt (2003). The remainder of the Irregular satellites have retrograde orbits. Based on similarities in semi-major axis, inclination and eccentricity, these satellites have been grouped into families by Sheppard and Jewitt (2003) and Nesvorný et al. (2003), the product of catastrophic collisions. These dynamical families are typified by their largest member, Himalia representing the inner prograde satellites, with the retrograde ones being broken down into the Ananke, Pasiphae and Carme families. Recently, several additional small Irregular satellites have been discovered (Jacobson et al., 2011; Sheppard and Williams, 2012; Sheppard et al., 2018) which are yet to be named or classified. With the discovery of new satellites (Scotti et al., 2000; Sheppard et al., 2001; Beaugé and Nesvorný, 2007; Jacobson et al., 2011; Sheppard and Williams, 2012; Sheppard et al., 2018) and additional information from the *Cassini* spacecraft (Porco et al., 2005; Denk and Mottola, 2019), a revisitation of the classification of the Jovian Irregular satellites (Nesvorný et al., 2003; Sheppard and Jewitt, 2003; Jewitt and Haghighipour, 2007) is warranted.

1.3.2 THE SATURNIAN SYSTEM

The Saturnian system is broadly similar to that of Jupiter, but exhibits greater complexity. One of the most striking features, visible to even the most modest telescope, is Saturn's ring system. First observed by Galileo in 1610, it was Huygens (1659) that observed that the objects surrounding Saturn were in fact rings. The rings themselves are composed of individual particles, from micrometer to meter size (Zebker et al., 1985). Embedded within several of the main rings are a series of small moonlets (Tiscareno et al., 2006) and several shepherd satellites (Showalter, 1991; Porco et al., 2007; Cuzzi et al., 2014). The co-orbitals Janus and Epimetheus (Yoder et al., 1983, 1989; Nicholson et al., 1992; Treffenstädt et al., 2015; El Moutamid et al., 2016), and their associated faint ring system (Winter et al., 2016) are unique to the Saturn system. Just beyond the Janus/Epimetheus orbit, there is a diffuse G-ring, the source of which is the satellite Aegaeon (Hedman et al., 2007).

Huygens (1659) also discovered Saturn's largest satellite, Titan. Earth-based observations highlighted the methane based atmosphere of Titan (Kuiper, 1944; Karkoschka, 1994), with

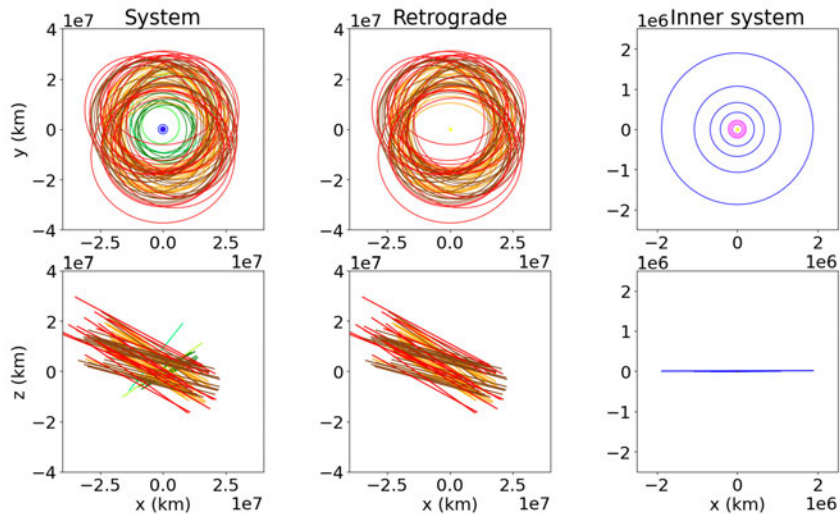


Figure 1.6: Polar (top row) and side (bottom row) views of the Jovian satellite system, as of 20th of November, 2020. The full system is shown on the left, on y retrograde satellites in the center and the central system on the right. The colors represent terminology used in traditional classification: Amalthea inner regular family (magenta); Galilean family (blue); Themisto prograde Irregular family (lime); Himalia prograde Irregular family (green); Carpo prograde Irregular family (spring green); Ananke Irregular family (orange); Carme Irregular family (brown); Pasiphae Irregular group (red). Data retrieved from Sheppard database <https://sites.google.com/carnegiescience.edu/sheppard/>.

further characterization by the *Cassini* spacecraft (Niemann et al., 2005) and Huygens lander (Lebreton et al., 2005). The bulk composition of Titan is analogous to that of the other icy satellites, with an icy shell, subsurface water ocean and silicate core (Hemingway et al., 2013). There are seven other mid-sized icy satellites, with semi-major axes on a similar order of magnitude to that of Titan. The five largest, Mimas, Enceladus, Tethys, Dione and Rhea are large enough to be in hydrostatic equilibrium, and are broadly spherical in shape. All of the mid-sized satellites are thought to be predominantly composed of water ice, with some contribution from silicate rock, and may contain subsurface liquid oceans (Matson et al., 2009; Filacchione et al., 2012). Those satellites closer to Saturn than Titan, Mimas, Enceladus, Tethys, Dione and Rhea, are embedded in the E-ring (Feibelman, 1967; Baum et al., 1981; Hillier et al., 2007; Hedman et al., 2012). The *Cassini* mission identified the source of this ring as the southern cryo-plumes of Enceladus (Spahn et al., 2006).

In addition to the larger icy satellites, there are four small Trojan satellites (Porco et al., 2005), situated at the leading and trailing Lagrange points, 60° ahead or behind the parent satellites in their orbit. Tethys has Telesto and Calypso as Trojan satellites, while Helene and Polydeuces are Trojan satellites of Dione. So far, these Trojan satellites are unique to the

Saturnian system.

Between the orbits of Mimas and Enceladus, there are the Alkyonides, Methone, Anthe and Pallene, recently discovered by the *Cassini* spacecraft (Porco et al., 2005). Each of the Alkyonides have their own faint ring arcs (Hedman et al., 2009) comprised of similar material to the satellite. Dynamical modelling by Sun et al. (2017) supports the theory of Hedman et al. (2009), that the parent satellite is the source of the rings.

In the outer Saturnian system there are a large number of smaller Irregular satellites, with 58 known as of March 2020. The first of these Irregular satellites to be discovered was Phoebe, which was the first planetary satellite to be discovered photographically (Pickering, 1899). Phoebe was also the second satellite, after Triton, a large satellite of Neptune (Lassell, 1849), to be discovered moving on a retrograde orbit (Pickering, 1905; Ross, 1905). Phoebe is the best studied gas giant Irregular satellite and the only one for which high quality in-situ spacecraft observations have been obtained (Clark et al., 2005). Recently, a large outer ring associated with Phoebe and the other Irregular satellites has been discovered (Verbiscer et al., 2009). It has been suggested that Phoebe may have originated in the Edgeworth-Kuiper Belt and captured into orbit around Saturn (Johnson and Lunine, 2005). The other Saturnian Irregular satellites were discovered in extensive surveys during the early 21st century (Gladman et al., 2001; Sheppard et al., 2003a; Jewitt et al., 2005; Sheppard et al., 2006, 2007). Due to the small size of the majority of these satellites, only their orbital information is available.

There are 11 prograde and 47 retrograde outer satellites as of March 2021, of which attempts have been made to place into collisional families based on dynamical (Gladman et al., 2001; Jewitt and Haghighipour, 2007; Turrini et al., 2008) and photometric (Grav et al., 2003; Grav and Bauer, 2007) information. In the traditional naming convention (Grav et al., 2003), the Inuit family, Ijiraq, Kiviuq, Paaliaq, Siarnaq and Tarqeq, are small prograde satellites, whose inclination is between 45° and 50° . The Gallic family, Albiorix, Bebhionn, Erriapus and Tarvos, is a similar, prograde group, but with inclinations between 35° and 40° . The retrograde satellites are all grouped into the Norse family, including Phoebe. There is a possibility that the Norse family could be further split into subfamilies, based on photometric studies (Grav et al., 2003; Grav and Bauer, 2007). The convention of using names from respective mythologies for the satellite clusters (Jewitt and Haghighipour, 2007), has become the default standard for the Irregular satellite families of Saturn. After these initial clusterings, a new set of 20 Irregular satellites were discovered, see section 2.1.1 for discussion on how these fit into the taxonomy

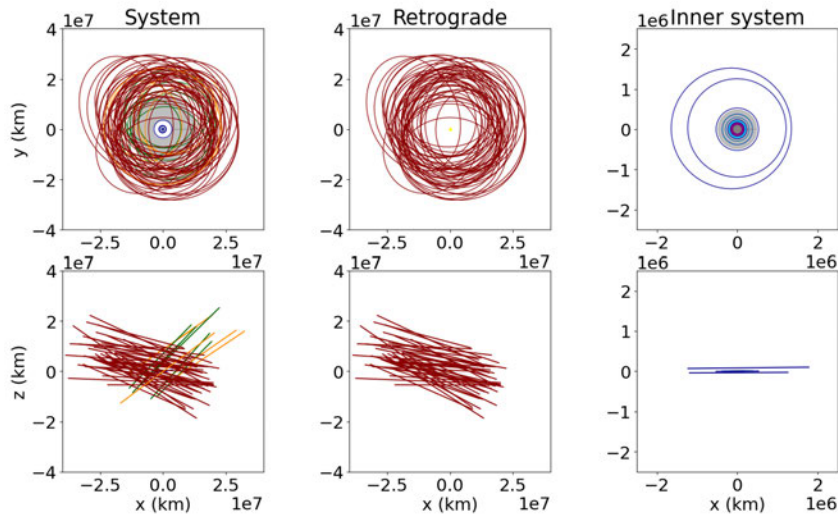


Figure 1.7: Polar (top row) and side (bottom row) views of the Saturnian satellite system, as of 20th of November, 2020. The full system is shown on the left, on y retrograde satellites in the center and the central system on the right. The colors represent terminology used in traditional classification: Main ring group, with associated shepherd satellites (purple); Mid-sized icy satellites and Titan (dark blue); Trojan satellites (steel blue); Amalthea and associated rings (deep sky blue); Inuit prograde Irregular family (dark green); 'Gallic' prograde Irregular family (dark orange); Norse retrograde Irregular family (dark red). Rings are shown in grey. Data retrieved from Sheppard database <https://sites.google.com/carnegiescience.edu/sheppard/>

1.3.3 FORMATION THEORIES

The purpose of taxonomy and classification, beyond simple grouping, is to investigate the origin of objects. The origin of the Irregular satellites is a topic of ongoing study (as reviewed in, Jewitt and Haghighipour, 2007; Nesvorný et al., 2014; Brozović and Jacobson, 2017). Here I present an overview for context. There are three main theories for the formation of the Jovian satellites: formation via disk accretion (Canup and Ward, 2002); capture via nebula drag (Pollack et al., 1979); or via dynamical capture (Nesvorný et al., 2003, 2007, 2014). In scenarios where satellites are captured, either by nebula drag or dynamical means, the idea is that those objects formed elsewhere in the Solar system, and were captured from unstable orbits crossing those of the giant planet host.

The disk accretion theory has generally been accepted as the mechanism for the formation of the inner prograde satellites of Jupiter (Canup and Ward, 2002). The satellites form from dust surrounding proto-Jupiter in a process analogous to the formation of planets around a star (Lissauer, 1987). This surrounding disk would have lain in the equatorial plane of Jupiter, with material being accreted to the planet itself through the disk. This would explain both

the prograde, coplanar orbits of the regular satellites and their near circular orbits.

The second theory requires satellites to be captured in the original Jovian nebula (Pollack et al., 1979; Čuk and Burns, 2004). Before it coalesced into a planet, Jupiter is proposed to have had a greater radius, and lower density than now. There was a ‘nebula’ surrounding this proto-Jupiter. As other pieces of Solar system debris crossed into the Hill sphere of this nebula, they would be slowed down by friction and be captured as a satellite. Related to this is the concept of a pull down mechanism (Heppenheimer and Porco, 1977). As a gas giant increases in mass from accretion (Pollack et al., 1996), the size of the Hill sphere increases. As a subsequent effect, small Solar system bodies can possibly be captured as Irregular satellites.

Dynamical capture can explain the retrograde orbits of the Jovian satellites (Nesvorný et al., 2003). The Hill sphere denotes the region where the gravitational pull from a planet dominates over the gravitational influence of other objects, and thus is the theoretical maximum distance that a stable satellite could exist. Although Agnor and Hamilton (2006) demonstrate that it would be possible to capture an Irregular satellite in a binary-planet gravitational encounter, a four body system, the theory (Nesvorný et al., 2003, 2007) states that it is impossible for a satellite to be captured in a three body system (Sun, planet and satellite), without some form of disruption, or non gravitational effect. The Nice model of the Solar system (Tsiganis et al., 2005a; Nesvorný et al., 2007, 2014) has a fourth body interaction placing the satellite into a stable orbit inside the Hill sphere of the gas giant. More recently the Nice model was updated to include a fifth giant planet (Nesvorný and Morbidelli, 2012). This updated theory has the new planet interacting with Jupiter and allowing for the capture of the satellites, before the fifth giant planet is ejected from the Solar system. Collisions between objects could also play a part in the dynamical capture of the Irregular satellites (Colombo and Franklin, 1971).

The formation of the Saturnian system, and indeed the other satellite systems of the gas giants, are thought to be similarly complex. The inner satellites are possibly formed from accretion within the ring system (Charnoz et al., 2010) or from the breakup of a large, lost satellite (Canup, 2010). Modelling of the Saturnian system by Salmon and Canup (2017) has shown that the mid-sized satellites could have formed from a large ice-dominated ring, with contamination of cometary material during the Late Heavy Bombardment, delivering the requisite silicate rock. Being the largest satellite in the Saturnian system, Titan is thought to have formed from accretion of proto-satellites (Asphaug and Reufer, 2013). The Saturnian Irregular satellites are predicted to be captured objects (Jewitt and Haghighipour, 2007), though their origins are still in dispute. Collisions are thought to have played a part in the capture of the Irregular satellites of Saturn (Turrini et al., 2009). The cratering data provided

by the *Cassini* spacecraft (Giese et al., 2006) supports this hypothesis.

1.4 JOVIAN TROJANS

The Jovian Trojans are two swarms of small Solar system bodies located at the Lagrange points of Jupiter, 60° ahead (L_4) and behind (L_5) in the gas giant's orbit, see Figure 1.2 and Figure 1.8. Each swarm is named after the characters of the epic Greek poems that detail the Trojan war, *The Iliad* and *The Odyssey* (Homer). The leading swarm in the L_4 position, are named after Greek figures in the poems (Nicholson, 1961). The trailing L_5 members are named for the Trojans. Due to no early adherence to this system there are two exceptions to this nomenclature. 624 Hektor, named for the Trojan prince, is in the L_4 Greek swarm. Also, 617 Patroclus, whose namesake is Greek, is in the L_5 Trojan swarm. To date, there have been a reported 9072 Jovian Trojans discovered². The majority of these asteroids are small, with most being less than 100km in diameter, see Figure 1.9 a. The only Jovian Trojan with a diameter larger than 150km, is the contact binary 624 Hektor at approximately 250km (Marchis et al., 2014), which also has a confirmed satellite (Marchis et al., 2014). More recently, a satellite has also been confirmed around 3548 Eurybates (Noll et al., 2020a).

1.4.1 ORIGINS

The origins of the Jovian Trojans are a complex issue, that inform us on the dynamical situation in the early Solar system. The interesting dynamics of the population, being relatively stable (e.g. Emery et al., 2015; Di Sisto et al., 2014; Nesvorný, 2018; Di Sisto et al., 2019; Holt et al., 2020a), and having high inclinations place unique constraints on theories of early Solar system history.

Historically, the relevance of the Trojans to early Solar system formation went unrecognised (Wyse, 1938) though this is mainly due to limitations in the number discovered. As more were discovered, the initial formation theory was that the Trojans formed in the same location as Jupiter (Nicholson, 1961; Rabe, 1968), with a potential link to the Jovian Irregular satellites (Hunter, 1967a,b). For the next few decades, several theories were proposed, namely that they were captured at the Lagrange points via the Yarkovsky effect or gas drag (Yoder, 1979; Peale, 1993; Kary and Lissauer, 1995), fragment injection from colliding planetesimals (Shoemaker et al., 1989) and the growth of a proto-Jupiter (Shoemaker et al., 1989). The issue is, that none of these scenarios reproduce the large inclinations of the Jovian Trojans, which

²Includes potentially transient objects, 5651 in L_4 , 3421 in L_5 . As of Dec. 8, 2020. Minor Planet Center <https://www.minorplanetcenter.net/iau/lists/JupiterTrojans.html>

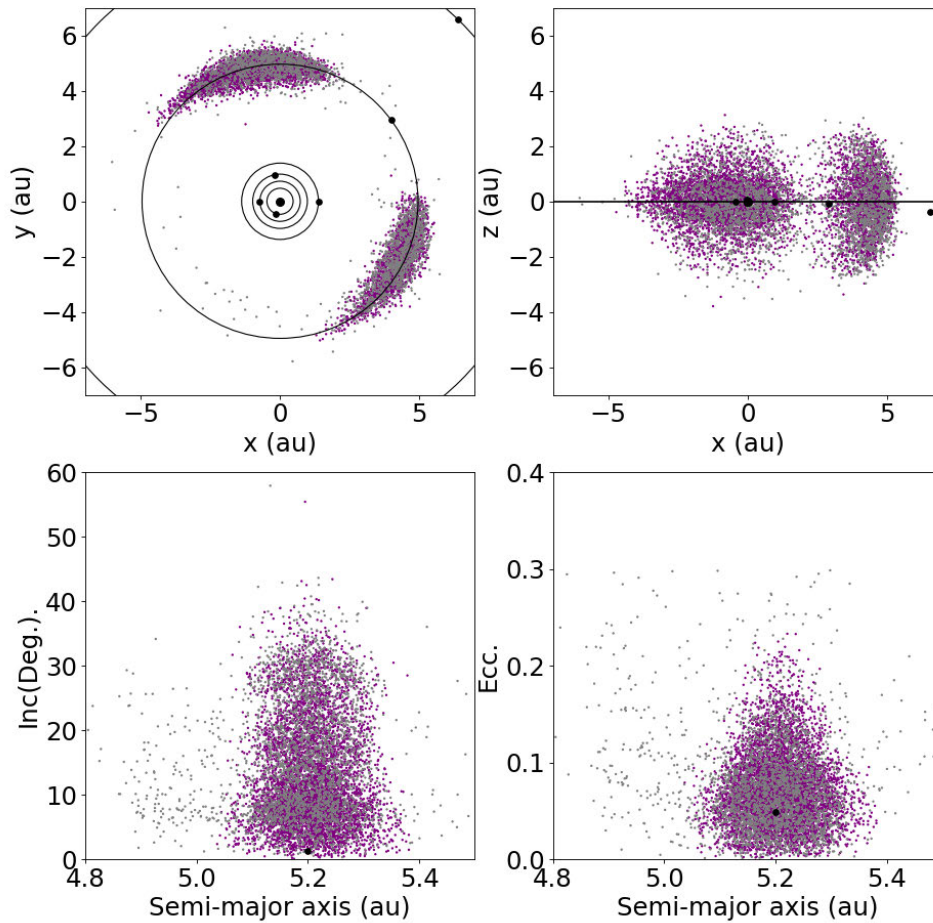


Figure 1.8: Distribution of the Jovian Trojans after Horner et al. (2020). The upper panels show the positions of the Trojans relative to the planets on 01-01-2000 00:00 in XY (left) and XZ (right) planes of the ecliptic coordinate system. The lower panels show the Trojans in semi-major axis vs inclination space (left) and semi-major axis vs eccentricity space (right). All data from NASA HORIZONS (Giorgini et al., 1996), accessed on 13th October, 2020. Purple points are initially stable objects, from the AstDyS (Knežević and Mianini, 2017) dataset. Grey points are transient objects.

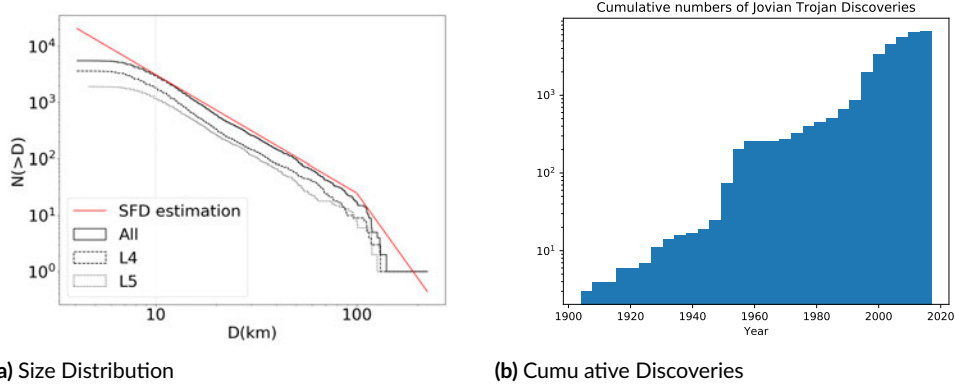


Figure 1.9: Size-frequency distribution (left) and cumulative discoveries (right) of the Jovian Trojan asteroids. The solid line shows the distribution for the population as a whole, whilst the long-dash line shows the distribution among members of the leading L_4 swarm, and the dotted line shows the distribution for the trailing L_5 swarm. Data from NASA HORIZONS, as of 19th August 2019. Vertical grey, dashed line indicates observational completeness (Emery et al., 2015). The grey line shows the estimated complete size distribution (Nesvorný, 2018).

even at the time was an observed feature of the population (Nicholson, 1961; Marzari et al., 2002). This feature of the population was one of the indications that the population did not form in their current orbits.

Given the dynamical situation of the Jovian Trojans, it is now well recognised that they did not form in their current orbits, but are thought to have been captured during a period of instability in the early Solar system (Morbideilli et al., 2005; Lykawka and Horner, 2010; Nesvorný et al., 2013). The specifics of the Trojan population, the high inclinations and spectral taxonomy (see section 1.4.4) linking to the outer Solar system, form constraints on this early Solar system history.

One leading theory to explain the capture of the Jovian Trojans is the proposed period of instability in the early Solar system (Nesvorný et al., 2013), the Nice model (Tsiganis et al., 2005a; Morbidelli, 2010; Levison et al., 2011; Nesvorný and Morbidelli, 2012). The Nice model invokes a period of instability triggered by the slow migration of Jupiter and Saturn, in response to their interactions with the debris left behind from planet formation. This second instability occurs after an early migration, the ‘Grand Tack’ (Walsh et al., 2011). Eventually, the later migration drove the two giant planets into an unstable architecture, leading to a period of chaotic evolution for objects throughout the Solar system. During that period of instability, any primordial Jovian Trojans would also have been destabilised, and ejected from the Solar system. As a result, some of the debris being flung around the system by the migrating giant planets would have experienced temporary capture to the Jovian Trojan swarms.

As Jupiter and Saturn migrated away from the location of the instability, the Jovian Trojan clouds would have become stable once again, freezing in place those temporarily captured Trojans, making their capture permanent.

More recently, it has been suggested that the required instability in the outer Solar system may have been triggered by the ejection of a fifth giant planet (Nesvorný and Morbidelli, 2012; Deienno et al., 2017) from the Solar system. This scenario has become known as the Jumping-Jupiter model, and has been invoked to explain a number of peculiarities in the distribution of Solar system small bodies, including the origin of the Jovian Trojans and the Irregular satellites (Nesvorný et al., 2007, 2014), as shown in Figure 1.10. This model is consistent with Wong and Brown (2016), who use the colour ratios of the objects in the populations to propose a hypothesis for a common origin between the Trojans and the Edgeworth-Kuiper belt objects (EKBOs). This model is also supported by compositional analysis across the small body populations (DeMeo and Carry, 2014).

An alternative to the scenarios painted above proposes instead that the Trojans were captured from the same region of the Solar system's protoplanetary disc as Jupiter, and were both captured and transported during the planet's proposed inward migration (Pirani et al., 2019a). A update to this *in-situ* transport model (Pirani et al., 2019b) explains the observed excitation in the orbital inclinations of the Jovian Trojans, which is a natural byproduct of the chaotic evolution proposed in the Nice and Jumping-Jupiter models (Nesvorný et al., 2013), by invoking mixing in the Jovian feeding region. Therefore, the observed inclinations are considered to be primordial in these simulations, and are preserved during transportation as Jupiter migrates. In contrast to the idea that the captured Trojans formed on inclined orbits, earlier studies of smooth, non-chaotic migration (e.g. Lykawka and Horner, 2010) showed that Jupiter could capture a significant population of Trojans. Lykawka and Horner (2010) also indicate a link between the Centaur population and the Jovian Trojans, though this is disputed by Jewitt (2018) due to differences in the colour distributions.

The common feature of all of the proposed models, however, is that the capture of the Jovian Trojans occurred during the Solar system's youth (Emery et al., 2015). These competing theories for the origins of the Trojans highlight the importance of the population in our understanding of the early Solar system.

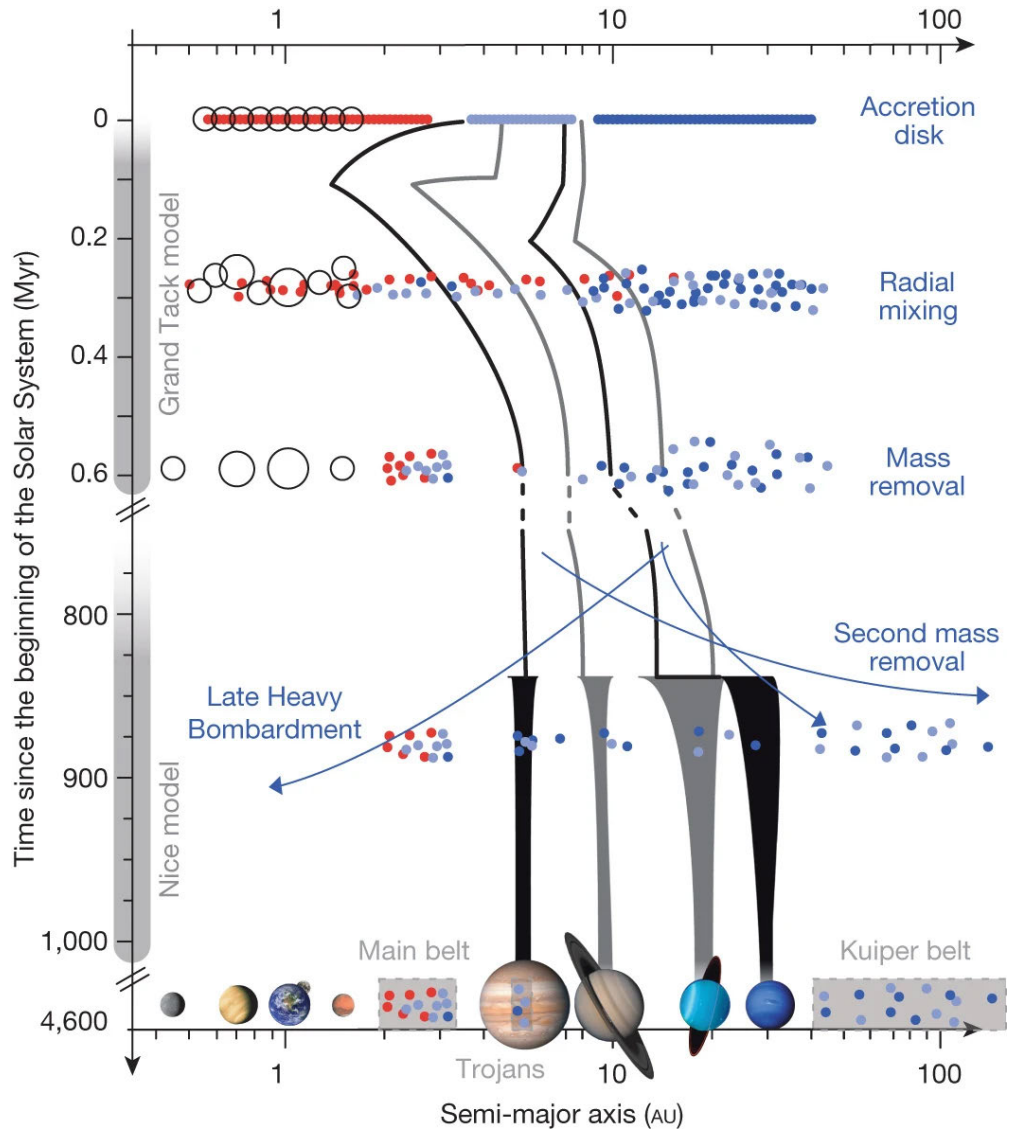


Figure 1.10: After DeMeo and Carry (2014), showing some major components of the dynamical history of small bodies in the Solar system based on models (Tsiganis et al., 2005a; Morbidelli et al., 2005; Walsh et al., 2011). These models may not represent the actual history of the Solar system, but are possible histories. They contain periods of radial mixing, mass removal and planet migration – ultimately arriving at the current distribution of planets and small-body populations.

1.4.2 OBSERVATIONS

1.4.2.1 HISTORY

The first accepted discovery of a Trojan asteroid was that of 588 Achilles by Wolf (1907) at the Heidelberg Observatory. Several more Trojan asteroids, 617 Patroclus (Heinrich, 1907), 624 Hektor (Strömgren, 1908; Kopff, 1909), 659 Nestor (Ebell, 1909; Kopff, 1909), and 884 Priamus (Wilkens, 1918) were also discovered at the start of the 20th century by the same group at the Heidelberg Observatory (Nicholson, 1961). Over the next several decades, several more Trojans, were discovered by Karl Reinmuth in Heidelberg (Slyusarev and Belskaya, 2014). With the advent of the photometry, the number of Trojan asteroid discoveries increased dramatically, see Figure 1.9.

1.4.2.2 COLOURS

There are several studies that have looked at the colours of the Jovian Trojans (Emery and Brown, 2003; Dotto et al., 2006). Initial observations were limited in number, totaling less than 100 objects in the infrared (Emery and Brown, 2003; Emery et al., 2006, 2011), visual (Fornasier et al., 2004; Dotto et al., 2006; Fornasier et al., 2007) and broadband UBVR_I (Karlsson et al., 2009).

Amongst these surveys, bimodality has been suggested amongst the Trojans, with red and less red groups being observed (Emery et al., 2011; Wong et al., 2014). Larger surveys conducted with *Wide-field Infrared Survey Explorer (WISE)* (Grav et al., 2012), Sloan Digital Sky Survey (SDSS) (Roig et al., 2008; Ryan et al., 2017) and Subaru (Wong and Brown, 2015) have confirmed this bimodality. Wong and Brown (2016) use location dependent volatile loss and subsequent capture to explain the different spectra seen. This hypothesis also explains the bimodality seen in the Edgeworth-Kuiper belt object (EKBO) population, and that suggests the two populations had a possible common origin. With only a small fraction of the Trojans observed in the surveys, confirmation of this hypothesis requires a larger sample-set, one that will be provided by the Vera Rubin Observatory, Legacy Survey of Space and Time (LSST), which is expected to see first light in 2023.

With the current generation of large ground-based facilities and space telescopes, recent years have seen a significant increase in the numbers of Trojans being observed and given preliminary classifications. Grav et al. (2012) observed 557 Trojans at infrared wavelengths, using two *WISE* filters. In doing so, they confirmed the prevalence of D-types in the Trojan population, with such asteroids dominating both the L₄ and L₅ swarms, independent of

the size of the Trojans studied (Grav et al., 2011). In the visual five-band SDSS catalogue (Carvano et al., 2010; Hasselmann et al., 2012), a total of 461 Trojans have been classified. Unlike previous surveys, the catalogue includes a measure of the confidence in the assigned taxonomy. Of the 461 objects in the SDSS dataset, only 106 have significantly high confidence value to be considered valid classifications. For more details on the taxonomy of the Trojans, see section 1.4.4.

1.4.2.3 SPACECRAFT OBSERVATIONS

To date, no spacecraft has conducted in-situ observations of the Jovian Trojans. A NASA discovery class mission, *Lucy*, is set to visit at least six Jovian Trojans between 2025 and 2033. One of the justifications for this mission is the diversity of asteroid classes found in the population (Levison et al., 2017). The first object, 3548 Eurybates (1973 SO) is the remnant of a large collisional family (Brož and Rozehnal, 2011; Nesvorný et al., 2015), and a well established C-type (Fornasier et al., 2007). The second target in the L₄ swarm, 15094 Polymele (1999 WB₂), is one of the smaller objects. It is thought to be a ‘P’-type, this has not been confirmed in any of the current generation of surveys. Though also a small target, 11351 Leucus (1997 TS₂₅), is a D-type (Fornasier et al., 2007), similar to the majority of the Trojans. The next object, 21900 Orus (1999 VQ₁₀), is also a preliminary D-type. The final two targets are in the L₅ swarm, the 617 Patroclus (1906 VY)/Menoetius binary (Marchis et al., 2006). Even in the early surveys, the binary was identified as a ‘P’-type (Tholen, 1989).

1.4.3 PHYSICS

In this section I introduce several of the physical concepts related to this PhD project. The dynamics of the Jovian Trojans are dominated by their motion around Lagrange points, explained in section 1.4.3.1. The Yarkovsky effect, a non-gravitational force, while minimal at the Jovian Trojans, is explained in section 1.5.2.

1.4.3.1 LAGRANGE POINTS

In classical Newtonian physics, the calculation of the forces (F) between two bodies (Kepler, 1609; Newton, 1687; DePater and Lissauer, 2010) is relatively straightforward and is represented in Equation 1.1, where G is the gravitational constant ($6.67408 \times 10^{-11} \text{ m}^3\text{kg}^{-1}\text{s}^{-2}$), M is the mass of the particles (in kilograms) and R is the relative distance between the centres

of the two masses, in meters.

$$F = G \frac{M_1 M_2}{R^2} \quad (1.1)$$

The motion of objects under their mutual gravitational pull can be perfectly calculated based on this simple relationship when there are only two objects in a system, but once you add a third object, the motion becomes non-integrable, and no simple analytical solution can be found, though it can be numerically calculated. This issue is known as the Three Body Problem.

A partial solution to the Three Body Problem was introduced by Euler and Lagrange (Euler, 1767; Lagrange, 1772), where the third particle has comparatively low mass, and is thus considered mass-less, as to not affect the orbits of the other two particles. Euler and Lagrange's solution revealed that, within the restricted three-body problem, there were five locations, in a co-rotating reference frame, at which the low-mass particle could be in equilibrium, collectively called Lagrange points. These points are graphically represented in Figure 1.11, with lines of equal gravitational potential shown in the right-hand diagram. As can be seen in Figure 1.11b, L_1 , L_2 and L_3 are saddle points, small areas of temporary stability, though minimal perturbations could destabilise a particle onto a potentially chaotic orbit. The other two Lagrange points, L_4 and L_5 , are the main focus of this study. In these locations, due to being areas of minimal slope in gravitational potential, an object can remain in a larger area of general stability for long time scales. In a co-rotating frame with the second massive object, these orbits appear as 'tadpole' orbits around the L_4 and L_5 Lagrange points. It is in these gravitational potential plateaus that we find the Jovian and Neptunian Trojan populations.

The Trojans are never exactly at the host Lagrange point, and librate in 'tadpole' orbits around it. As the Jovian Trojans orbit the Sun, their orbital rate, relative to Jupiter, changes. This is due to the interactions between the Jovian Trojan, Jupiter and the Sun. If a L_4 Trojan starts at a point just inside the orbit of Jupiter, due to the laws of angular momentum, it orbits the Sun faster. As it moves ahead of Jupiter, Jupiter's mass starts to slow its momentum. The drop will eventually cause it to increase to a semi-major axis outside that of Jupiter, with a lower relative velocity. This lower angular momentum causes the Trojan to approach the relative position of Jupiter. As it does so, the object is pulled into a lower orbit, for the cycle to start again. A graphical representation of this is shown in Figure 1.11A. Another way to consider this is that the Trojan orbits at an equal gravitational potential, as shown in Figure 1.11B. A trailing L_5 Trojan would act in a similar, but reversed manner. Collectively these are called tadpole orbits. It is this mechanism that causes the oscillating elements of 624 Hektor

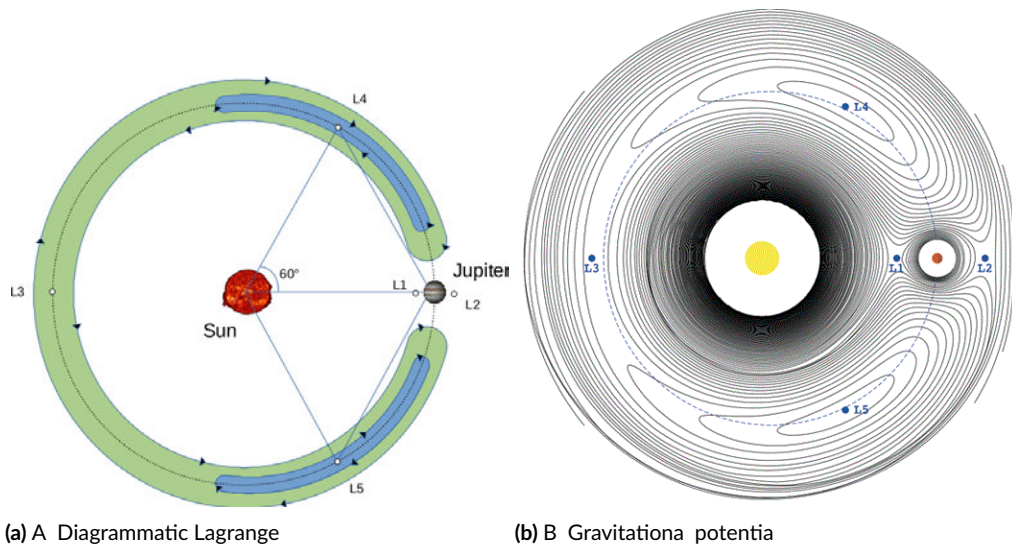
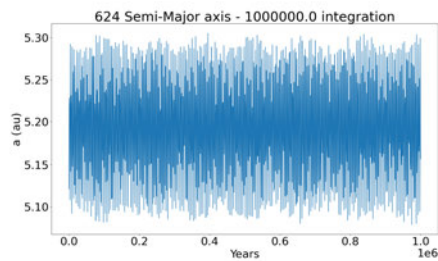


Figure 1.11: A Diagrammatic representation of libration in the Sun-Jupiter system. The reference frame is locked to the orbit of Jupiter, with arrows depicting the relative direction of travel. Lagrange points are indicated with a small circle. Tadpole orbits at the L_4 and L_5 points are in blue. The 'Horseshoe' orbit is green. Adapted from (DePater and Lissauer, 2010). B Gravitational potential of a three body system. After (Horner and Lykawka, 2011)

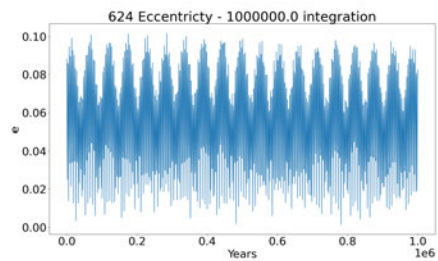
seen in Figure 1.12. A further semi-stable libration orbit, a horseshoe orbit, connects the L_4 and L_5 points through the L_3 . These horseshoe co-orbitals are much less stable than the L_4 and L_5 Trojans (e.g. Mikkola and Innanen, 1992; Zhou et al., 2019; Liberato and Winter, 2020). Though there is parameter space near Earth's orbit that could be stable for the life of the Solar system, these are ruled out due to the influence of the Yarkovsky effect (Zhou et al., 2019), see Section 1.4.3.2. As of July 2020, there have only 18 Earth co-orbitals discovered in horseshoe orbits (Christou and Asher, 2011; de la Fuente Marcos and de la Fuente Marcos, 2016; Kaplan and Cengiz, 2020), and none around other planets, excluding the unique co-orbital dynamics of Janus and Epimetheus (Yoder et al., 1983; Nicholson et al., 1992), two satellites of Saturn.

1.4.3.2 YARKOVSKY EFFECT

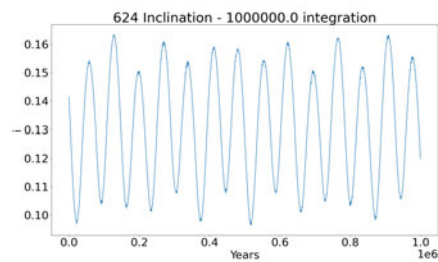
The diurnal Yarkovsky effect involves the absorption and re-emission of photons on an orbital body. Photons of light from the Sun hit an object and are absorbed, and are not immediately re-emitted. As the object is rotating, it will have rotated slightly before the photon's re-emission, and thus the infrared radiation of the photon happens at a different angle to the



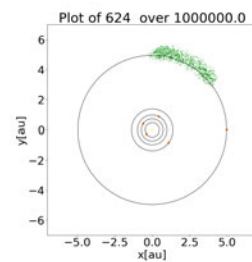
(a) Semi-major axis



(b) Eccentricity



(c) Inclination



(d) Position

Figure 1.12: REBOUND simulation of the Jovian Trojan 624 Hektor as a mass-less particle showing semi-major axis (a), eccentricity (e) and inclination progression over 1×10^6 years. The location of 624 Hektor, in a rotating reference frame with Jupiter, is also shown (position). Simulations were run with WHFAST integrator. The Sun, Jupiter, Saturn, Uranus and Neptune were included as particles with mass. The integration time-step was set to 0.3954 yr, or 1/30 the orbital period of Jupiter (Barnes and Quinn, 2004).

absorption. The result of this, on the scale of the whole object, is that the surface is heated by the insolation, causing the surface on the Sun-facing side to be warmer than the surface facing away from our star. As a result of the thermal inertia of the surface of the object, the hottest point on the asteroid will not be exactly at the sub-Solar point, but will instead be displaced somewhat by the object's rotation. The result of this process produces a small net force on the object. In a prograde rotator, the force has a additive affect in the orbital direction, creating a net increase in orbital rate (Bottke et al., 2006). The consequence of this small force is an increase in semi-major axis over time. For a retrograde rotator, the result is a decrease in orbital momentum, resulting in a decrease in semi-major axis. The magnitude of the force depends upon how close a body is to the Sun, the obliquity of the body's spin axis with respect to the orbital plane, and the body's thermophysical characteristics (Bottke et al., 2006). Mathematically, this is represented in Equation 1.2.

$$\left(\frac{da}{dt}\right)_{diurnal} = -\frac{8}{9} \frac{\alpha \Phi}{n} W(R'_\omega, \Theta_\omega) \cos \gamma \quad (1.2)$$

which includes correction for the obliquity of the spin axis ($\cos \gamma$), the albedo-factor ($\alpha = 1 - A$, where A is Bond Albedo) and the orbital mean motion (n). The radiative pressure coefficient (Φ , Equation 1.3) is dependent upon the radius of the object (R) and the Solar radiation flux (F), with corrections for the mass of the body (m) and the speed of light (c).

$$\Phi = \frac{\pi R^2 F}{(mc)} \quad (1.3)$$

The Stefan-Boltzmann constant ($\alpha = 1 - A$) comprises the bond albedo of the object (A). The thermal component of Equation 1.2, ($W(R'_\omega, \Theta_\omega)$) is dependent on the radius scaled for penetrative depth ($R'_\omega = R/l_v$) and the thermal parameter (Θ_ω). The thermal parameter (Θ_ω) is to account for the thermal properties of the body.

The area-to-mass ratio of the object has a major affect on the strength of the Yarkovsky effect. A large object has a small area-to-mass ratio, reducing the effect of such a small force. If an object is too small, the thermal gradient over the object lessens and the radiative difference becomes minimal. It is generally accepted that the size range where the diurnal Yarkovsky effect has the most influence is between a meter and approximately 10km (Bottke et al., 2006) for the Main belt asteroids. There are some known Jovian Trojans in this size range (Slyusarev and Belskaya, 2014), though the size-frequency distribution is incomplete below 10km, see Figure 1.9.

The diurnal Yarkovsky effect has been directly detected in the Near Earth Object popula-

tion (Chesley, 2003; Farnocchia et al., 2013). The effect has also been studied in the Main belt asteroid families (Bottke et al., 2001; Nesvorný and Bottke, 2004). One of the major science goals of the *OSIRIS-REx* mission to 101955 Bennu, a ~ 0.5 km diameter NEO is to measure the in-situ Yarkovsky effect (Lauretta et al., 2011). The spacecraft arrived at 101955 Bennu in August 2018, and observations (Hergenrother et al., 2019) confirm the predicted affect (Deo and Kushvah, 2017).

In addition to the diurnal Yarkovsky effect, a seasonal effect has been described (Bottke et al., 2006). Equation 1.4 shows how this relates to the change in semi-major axis. Unlike the diurnal Yarkovsky effect, the seasonal effect can only slow the object. This effect is much smaller, and may not play a part in the orbital evolution of the Jovian Trojans.

$$\left(\frac{da}{dt}\right)_{seasonal} = \frac{4}{9} \frac{\alpha\Phi}{n} W(R_n, \Theta_n) \sin^2 \gamma \quad (1.4)$$

The Yarkovsky-O’Keefe-Radzievskii-Paddack (YORP) effect (Rubincam, 2000) is related to the Yarkovsky effect, but affects the spin rate of the object. This in turn could affect the overall all Yarkovsky effect, if considered over long time periods (Bottke et al., 2006; Golubov and Scheeres, 2019). In a study of the YORP effect on Main belt families, Vokrouhlický et al. (2006) found on shorter time scales, < 50 Mya, the YORP spin rate alteration was not enough to affect the Yarkovsky effect on the members. This is possibly due to ‘YORP cycles’ (Vokrouhlický and Čapek, 2002; Bottke et al., 2006), where an object spins up, sheds mass, forms a binary and starts the cycle anew, which are thought occur on the scale of millions to hundreds of millions of years (Rubincam, 2000; Bottke et al., 2006).

The Yarkovsky, and the related YORP, effects have mainly been studied in the context of Main belt asteroids (Bottke et al., 2006). As the Yarkovsky effect is proportional to the distance from the Sun, it is thought to be a major factor in the stabilisation of the Martian Trojans (Ćuk et al., 2015). Objects in 2:1 resonance with Jupiter, near the Hecuba gap, one of the largest Kirkwood gaps (Roig et al., 2002) are thought to have instabilities caused by the Yarkovsky effect (Brož et al., 2005). In the Jovian Trojan swarms, Wang and Hou (2017) have modeled Jovian Trojans with and without a simplified version of the Yarkovsky system, mainly dealing with small bodies $< 100m$. They found that some of the smaller Jupiter Trojans experience the Yarkovsky effect, which may move them onto chaotic orbits and eventually eject them from the population. The study by Wang and Hou (2017) uses a simplistic model and theoretical Trojans. A more detailed study investigating the physical parameters of the Trojan (Hellmich et al., 2019), found that the Yarkovsky affect is not that relevant to escape analysis for Trojans over 1 km in size.

1.4.4 SMALL BODY TAXONOMY

There are several tools used in current asteroid taxonomy, and which have been used in the classification of the Jovian Trojans. The first broad taxonomy is a spectral classification, based on broad band colours. The other two methods, Multivariate Hierarchical Classification (MHC) and Yarkovsky drift, are related to the search for collisional families and determining their age.

1.4.4.1 SPECTRAL CLASSIFICATION

In spectral taxonomy, the current paradigm uses spectral slopes to classify the asteroids, regardless of location, into groups and types (Tholen, 1984; Bus, 2002; DeMeo et al., 2009). This form of classification started with broadband eight colour spectra of 978 asteroids, mainly from the Main belt (Tholen, 1984). In the initial classification scheme, there were 14 asteroidal types, including three larger groupings. The C-group (B, F, G and C types) are generally dark, carbonaceous asteroids. The S-types are primarily composed of Silicates. The X-group (mostly M-type with E and P differing in albedo) are metallic. Six smaller types (A, D, T, Q, R and V) form the remainder of the original ‘Tholin’ classification.

Bus (2002) used the Small Main-belt Spectroscopic Survey (SMASS) to extend and consolidate the taxonomy to 1447 asteroids with higher precession. The higher resolution also identified several additional types. An extension into the near-infrared by DeMeo et al. (2009) produced the modern spectral taxonomy. The three broad groups remain, C-complex (Carbonaceous objects, B-type, C-type, and Cg, Ch, Cgh, Cb transitional types), S-complex (Siliceous objects, A-type, Q-type, R-type, K-type, L-type, S-type, and Sa, Sq, Sr, Sv transitional types) and X-complex (Metallic objects, X-type and Xe, Xc, and Xk transitional types). In addition to these three broad groups, several additional types are included in the classification scheme, to account for particularly peculiar objects (T-type, D-type, O-type and V-type). Figure 1.13 shows the spectral features of each type in the modern Bus-DeMeo taxonomy. In the literature, there is often reference to M-type and P-type asteroids, a legacy from the (Tholen, 1984) taxonomy. These two classes have been merged into the X-complex of DeMeo et al. (2009). For this project, I follow the taxonomy of DeMeo et al. (2009), with notes on discrepancies where appropriate.

With regards to the Jovian Trojans, part of the difficulty lies in the limited number number of objects that are present in spectral catalogues. Taking data from each data-set (Tholen, 1989; Bendjoya et al., 2004; Fornasier et al., 2004, 2007; Lazzaro et al., 2004), including those Trojans classified in the SDSS catalogue with a confidence score of greater than 50 (Hassel-

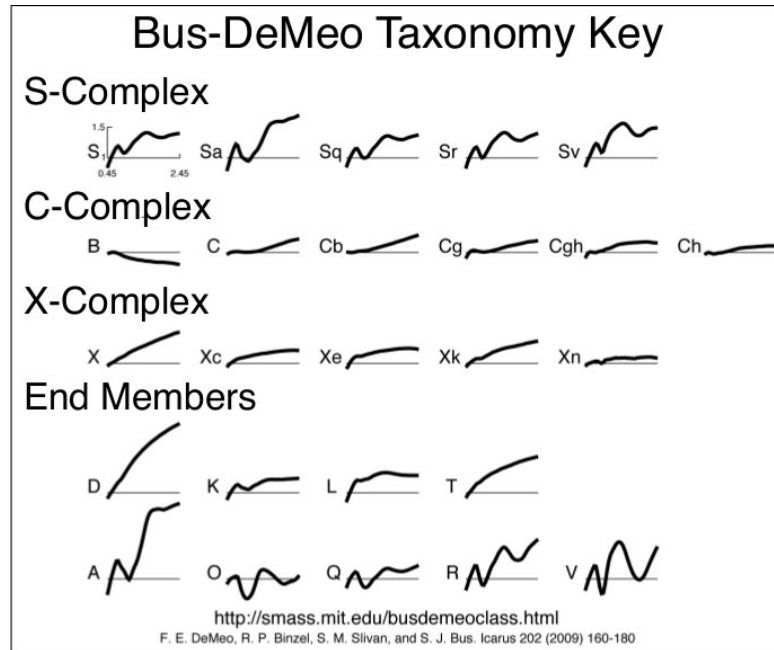


Figure 1.13: Modern Bus-DeMeo spectra taxonomy of asteroids (DeMeo et al., 2009). Spectra are shown from approximately 0.45 μm to 2.45 μm . Each spectrum is indicative of a taxonomic class. Each complex approximates to broad compositional differences, S-complex (siliceous objects), C-complex (carbonaceous objects) and X-complex (metallic objects).

mann et al., 2012), there is a canonical set of 214 Trojans that are classified under the Bus-DeMeo taxonomy. This represents less than 4 per cent of the population, and is biased towards larger objects. It is still valuable to use this spectral taxonomy, however, as it can inform on some general trends in the population. As other authors have noted (Grav et al., 2012; Haselmann et al., 2012; Emery et al., 2015; DeMeo and Carry, 2013), 72.2 per cent of the Jovian Trojans are classified as D-type, which is a much higher fraction than is seen in the Main belt (DeMeo et al., 2015; DeMeo and Carry, 2013; DeMeo et al., 2014) and in the Hilda (Wong and Brown, 2017) populations. This is consistent with the dynamical modelling, as the D-types are thought to have formed in the outer Solar system (Morbidelli et al., 2005; Levison et al., 2009) and those found in the Main belt are interlopers (DeMeo et al., 2014). The remainder of the Trojans classified to date in the canonical set are split between the C-types (10.8 per cent) and X-types (16.5 per cent). The diversity of asteroid spectral types in the Jovian Trojan swarm is indicative of diverse origins for the group and is part of the justification for the *Lucy* mission (Levison et al., 2017).

1.4.4.2 MULTIVARIATE HIERARCHICAL CLASSIFICATION

The Hierarchical Clustering Method (HCM, Zappala et al., 1990) has been applied to the proper elements (semi-major axis, eccentricity and inclination) of the Jovian Trojan swarm members (Milani, 1993; Beauge and Roig, 2001), resulting in the identification of several collisional families. This method of clustering uses Gauss equations to find clusters in n parameter space (Zappala et al., 1990), see section 1.6.4 for further details. Beauge and Roig (2001) use Fourier transformed proper elements, to account for librations present in the Jovian Trojan Dynamics. The rationale behind these calculations is that the dispersal velocities of the clusters would be similar to the escape velocities of the parent body. The unique dynamical situation of the Jovian Trojan asteroids makes the identification of dynamical families using the traditional HCM difficult. Despite the challenges involved in such analysis, such methods have suggested the presence of several dynamical families (Beauge and Roig, 2001) in the Jovian Trojans. Initial imaging surveys suggest that there is a spectral commonality to these dynamical families (Fornasier et al., 2007). More recent observational data has brought this into question (Roig et al., 2008), with a heterogeneity being seen in the spectra of the identified families. More modern dynamical analysis of the Jovian Trojans has identified a total of six families (Brož and Rozehnal, 2011; Emery et al., 2015; Vinogradova, 2015; Nesvorný et al., 2015; Rozehnal et al., 2016), see Table 1.1. Rozehnal et al. (2016) offer an expansion to the HCM developed by Zappala et al. (1990). This new ‘randombox’ method uses Monte Carlo simulations to gain statistics on the probability that the identified clusters are random in parameter space. While this new method adds a significance rating to the dynamical clustering seen in HCM, it still suffers from many of the same limitations, namely the requirement for complete datasets. Work has also been undertaken incorporating the known colours (Parker et al., 2008) and albedoes (Carruba et al., 2013) of the Main belt asteroids (Milani et al., 2014) into the classical method, though this reduces the dataset. From these methods, a canonical set of 317 family members, based on Nesvorný et al. (2015) can be generated.

1.4.4.3 YARKOVSKY DRIFT

In recent years, a number of studies have shown that drift of collisional fragments under the influence of the Yarkovsky effect can be used to improve the identification of ancestral dynamical families amongst the Main belt asteroids. These studies use Yarkovsky drift, the size dependent drift pattern due to the Yarkovsky effect, see section 1.4.3.2, to identify ancestral dynamic families in Main belt asteroids (Walsh et al., 2013; Bolin et al., 2017, 2018; Deienno et al., 2020). The Yarkovsky drift uses the size dependence of the Yarkovsky effect, to identify

Family Designation	$N_{members}$	Location	Method	Ref.
Eurybates	218	L ₄	MHC, RB	1, 2, 3
Hektor	12	L ₄	MHC, RB	2, 3
1996 RJ	7	L ₄	MHC, RB	2, 3
Arkesilaos	37	L ₄	RB	3
Ennomos	30	L ₅	RB	3
2001 UV ₂₀₉	6	L ₅	RB	3

Table 1.1: Dynamical families identified in the Jovian Trojan swarm using Multivariate Hierarchical Clustering (MHC) and Random Box (RB). Number of member objects ($N_{members}$) are taken from the canonical set in Nesvorný et al. (2015). References 1 Brož and Rozehna (2011), 2 Vinogradova (2015), 3 Rozehna et al. (2016)

these families in semi-major axis (a) vs size (diameter, d^{-1} , or absolute magnitude, H) space. A dynamical family created from a single event, would create a ‘V-shape’ due to Yarkovsky drift. The initial point of the V is dependent upon the amount of Yarkovsky drift that has occurred. The sides of the V-shape are dependent on the maximum Yarkovsky drift rate and the time since the disruption, as shown in Figure 1.14.

This technique, while useful in the Main belt, is less effective for the Jovian Trojans. This is due to the dependence of the Yarkovsky effect on the Solar flux, see equations 1.3 and 1.2. At the 5.2 au mean semi-major axis of the Jovian Trojans, the mean Yarkovsky effect is minimal, see Equation 1.9, particularly for Trojans over 1km in diameter (Wang and Hou, 2017; Hellmich et al., 2019). For these reasons, this technique has not been applied to the Jovian Trojan populations. In Figure 1.15, I have plotted the Eurybates and Ennomos families against the background population, in semi-major axis and absolute magnitude (H) space. These families were chosen as the largest in their respective swarms. What can be seen in Figure 1.15, is that, in this space, the families are indistinguishable from the background Trojans. Given that the age of the Eurybates family has been calculated to be approximately $1.045 \pm 0.364 \times 10^9$ years (Holt et al., 2020a), the shape would be similar to the 1 Gya panel in figure 3 of Deienno et al. (2020), reproduced in Figure 1.14.

1.5 ORBITAL DYNAMICS

Several of the papers that comprise this PhD thesis investigate the dynamics of the collisional families and the Trojan population as a whole. One current theory is that these objects were captured during a period of instability among the gas giants (Nesvorný et al., 2013), though this is still contentious, see section 1.4.1. There are several studies of the stability of the Jo-

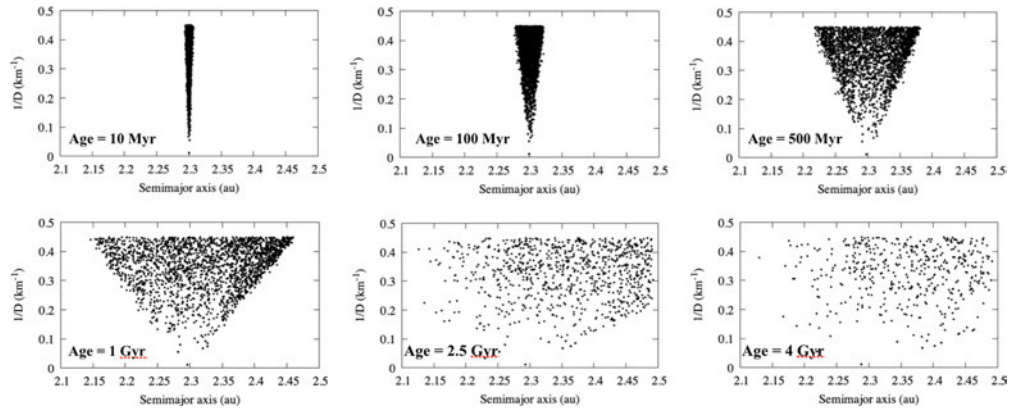


Figure 1.14: Yarkovsky drift shown for a synthetic family in the Main asteroid belt. Figure 3 in Deienno et al. (2020).

vian Trojans (Levison et al., 1997; Tsiganis et al., 2005b; Robutel et al., 2005; Lykawka and Horner, 2010; Horner et al., 2012; Di Sisto et al., 2014, 2019). These studies consider the asteroid swarm as a whole, regardless of family. They also only consider the numbered asteroids, with the largest study that of Di Sisto et al. (2014), numbering 2972 objects. In paper 2 (Holt et al., 2020a), I model the provisionally stable objects found in the AstDyS database, 5553 Jovian Trojans as of June, 2017 (Knežević and Milani, 2017), roughly double that of the previous largest investigation. Rozehnal et al. (2016) considered the Hektor family as a case for dynamical modelling of a Jovian Trojan Family. Their work showed that the dynamics of a specific family can be modeled. In this PhD, I focus on the families of the Jovian Trojans and the dynamical work considers individual objects, within the context of the collisional families. Recent modelling (Lykawka and Horner, 2010; Horner et al., 2012) has suggested that at least some of the Jovian Trojans are dynamically unstable on hundred-million year time scales.

1.5.1 *n*-BODY SIMULATIONS

REBOUND (Rein and Liu, 2012) is the main software used for the dynamical aspects of the project. REBOUND is an *n*-body simulator, encoded in C, with a Python interpreter, that is able to be parallelised for improved performance on the USQ Fawkes HPC cluster. Preliminary local testing, and post-process visualisation, were conducted locally on a Xeon based computer system.

REBOUND uses symplectic integrators to solve the *n*-body problem. Specifically, WHFAST is used in this project (Rein and Tamayo, 2015). The WHFAST symplectic integrator is based on Wisdom-Holman mapping system (Wisdom and Holman, 1991), similar to SWIFT (Levison and Duncan, 1994) and Symplectic Massive Body Algorithm (SyMBA Duncan et al., 1998).

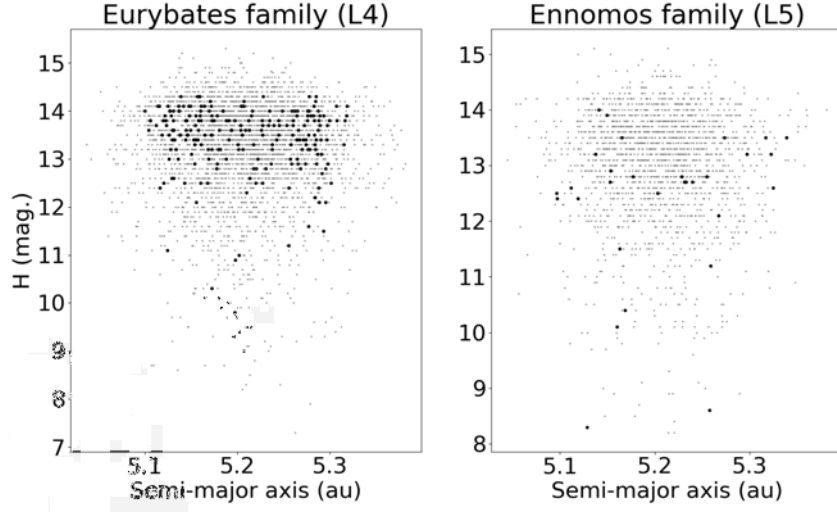


Figure 1.15: Eurybates and Ennomos families in proper semi-major axis (SMA) and absolute magnitude space (H mag.) space.

In these system, the Keplerian integrators (\mathcal{H}_{Kepler}) are separated out from other interactions ($\mathcal{H}_{Inter.}$), as expressed in Equation 1.5, with the Hamiltonian (\mathcal{H}) denoting the energy in the particle in the system. The system uses Jacobi coordinates. In this, r'_0 points to the center of the system, p'_0 is the total momentum and m'_0 is the total mass. The coordinator r'_i is relative to the center of mass of all particles interior to the i th particle (R_{i-1}). In the same way the Jacobi mass (m'_i) is the reduced mass of m_i and that internal to the particle. The Jacobi momentum (p'_i) is the product of these two factors ($p'_i = m_i r'_i$). A reminder that G is the gravitational constant ($6.67408 \times 10^{-11} \text{ m}^3 \text{ kg}^{-1} \text{ s}^{-2}$), and denotes the units used (m, kg, s), though these may be changed within REBOUND. Generally, I use the units astronomical units (au), Solar Mass (M_\odot) and years (yr) for the simulations.

$$\mathcal{H} = \mathcal{H}_0 + \mathcal{H}_{Kepler} + \mathcal{H}_{Inter.} \quad (1.5)$$

The components of the equation are each as follows:

$$\mathcal{H}_0 = \frac{p_0'^2}{2m'_0} \quad (1.6)$$

Equation 1.6 denotes the momentum of the central particle, in this case the Sun. Though not relevant to my investigation, Wisdom and Holman (1991) include it in order integrate

without any restriction to reference frame.

$$\mathcal{H}_{Kepler} = \sum_{i=1}^{N-1} \frac{p_i'^2}{2m_i'} - \sum_{i=1}^{N-1} \frac{Gm_i'M_i}{|r_i'|} \quad (1.7)$$

The Keplerian component of the Hamiltonian (\mathcal{H}_{Kepler}) is calculated using equation 1.7. This component of the integrator regulates the orbits of the particles around a central mass, in my simulations the Sun. This set of equations, is only based on the central mass and the particle, making this a two-body problem and easily calculated.

$$\mathcal{H}_{Inter.} = \sum_{i=1}^{N-1} \frac{Gm_i'M_i}{|r_i'|} - \sum_{i=0}^{N-1} \sum_{j=i+1}^{N-1} \frac{Gm_i'm_j}{|r_i - r_j|} \quad (1.8)$$

Equation 1.8 deals with the interactions between the particle and other masses in the system. The symplectic integration happens as an additive force applied to the original Keplerian component (\mathcal{H}_{Kepler}). Additional iterations of particles with mass add more complexity to the system. For this case, I use the major components of the Solar system (Sun, Jupiter, Saturn, Uranus and Neptune) as particles with their relative mass, as given by the REBOUND system (hard coded by Jon Giorgini; updated 10 May 2015). The Jovian Trojans are treated as massless particles, and replicated using the uncertainties in the HORIZONS database (Giorgini et al., 1996).

While the WHFAST integrator can handle dynamical interaction at a distance, it is less accurate for close encounters with the planets. In these instances a higher order integrator, one that accounts for more integration factors, is required. The issue with this is that it is more computationally expensive. Within the REBOUND package, such encounters are modelled using the IAS15 integrator (Rein and Spiegel, 2015), which is based on Gauss–Radau integration scheme (Everhart, 1985). The IAS15 integrator uses an adaptive timestep to effectively evaluate these close encounters. In order to use both types of integrators, hybrid systems have been developed. One of the other most commonly used hybrid integrators, is MERCURY (Chambers, 1999), which is written in Fortran. Within the REBOUND environment, the hybrid integrator is MECURIUS (Rein et al., 2019). This new integrator offers improvements in the switching algorithm, maintaining accuracy, with performance enhancements. Within this PhD program, MECURIUS was not released in time for Holt et al. (2018), where WHFAST was used. In two of the coauthor projects, Bolin et al. (2020) and Bolin et al. (2021), I use the new MECURIUS integrator, and will do so in future works.

1.5.2 YARKOVSKY EFFECT

The Yarkovsky effect is a non-gravitational force that acts on small Solar system bodies. The premise of the effect is that the thermal reemission of photons of light causes an asymmetric force on the object. The theoretical basis for the Yarkovsky effect is presented in section 1.4.3.2. Unfortunately, many of the parameters that are required for a full characterisation of the Yarkovsky effect are simply not known for the Jovian Trojans. An approximation of the $\frac{da}{dt}$ effect can be derived from better estimates conducted on the Main belt asteroids (Bottke et al., 2006). Using an approximate order of magnitude $\frac{da}{dt}$ of 10^{-5} auMya⁻¹ for a 10km Main belt object (Bottke et al., 2006), and values for the semi-major axis (5.2 au), density (0.8gcm⁻³, Marchis et al., 2006), and albedo (0.07, Grav et al., 2012), I derive an approximate dependence of $\frac{da}{dt}$ on the diameter (D km) and obliquity γ that is shown in Equation 1.9. See appendix A.1.1 for calculations.

$$\left(\frac{da}{dt}\right)_{JT} = 4.273 \times 10^{-11} \text{ auy}^{-1} \left(\frac{1\text{km}}{D}\right) \cos \gamma \quad (1.9)$$

With the diameter available for many of the Jovian Trojans (Giorgini et al., 1996), the issue then becomes the obliquity γ . Barucci et al. (2002) report on eight Jupiter Trojans with known obliquities, but do not give any details other than to say that they have a random distribution. Thus the obliquity may have to be investigated as part of this project, starting with a mean value (71.44°, see calculations in appendix A.1.2), and possibly continuing with randomly distributed values. From these equations, it can be seen that the Yarkovsky effect is minimal at the semi-major axis of the Jovian Trojans (5.2 au). Several studies (Wang and Hou, 2017; Hellmich et al., 2019) have modeled the Jovian Trojans, considering the Yarkovsky effect. They show that the effect is minimal, to the point of irrelevance, for any objects larger than approximately 1 km. To date (Nov. 2020), the smallest known Jovian Trojan is estimated at around 4 km. For the long term simulations, I therefore did not need to include the Yarkovsky effect.

Even though the Yarkosky effect has minimal affect on the Jovain population, it can still perturb individual objects. In the investigation into the Jovian Trojan pairs, particularly into the timing of the (258656) 2002 ES₇₆-2013 CC₄₁ pair, these small perturbations become important. As in Vokrouhlický and Nesvorný (2008), we can approximate thermal accelerations using a simple transverse component with the magnitude inversely proportional to the square of the heliocentric distance. The magnitude of this acceleration is adjusted

such that the resulting change in the semi-major axis (da/dt) matches predictions from the theoretical formulation of Yarkovsky effect (see also Farnocchia et al., 2013, where a classical formalism used in cometary dynamics was adopted). In order to estimate plausible da/dt values, I use a simple approach describing the diurnal Yarkovsky effect for a spherical body on a circular heliocentric orbit, presented in Vokrouhlický (1998). I use the following set of physical parameters: the surface thermal conductivity $K \simeq 0.01 - 0.03 \text{ W m}^{-1} \text{ K}^{-1}$, the surface thermal inertia $\Gamma \simeq 100 - 200 \text{ J m}^{-2} \text{ s}^{-1/2} \text{ K}^{-1}$ (for both see Delbó et al., 2015), the bulk density $\rho \simeq 1.5 \text{ g cm}^{-3}$ (e.g., Carry, 2012), rotation period $P \simeq 100 - 500 \text{ hr}$, and size $D \simeq 7 \text{ km}$. The maximum semi-major axis drift rate at zero obliquity is then $(da/dt)_{\text{max}} \simeq (0.15 \pm 0.07) \times 10^{-4} \text{ au Myr}^{-1}$.

1.5.3 PROPER ELEMENTS

The three main orbital characteristics of any dynamical object are the semi-major axis (a), eccentricity (e) and inclination (i). These three characteristics osculate in the Jovian Trojans (as shown in Figure 1.12), and thus need to be reduced to a single parameter. This reduction is the creation of the Proper elements. The method (Milani, 1993; Beauge and Roig, 2001) requires the use of oscillating elements, generated from short-term integrations, generally 1×10^7 years, though shorter simulations may be used for inner-Solar system objects, being passed through a Fourier transformation analysis (Šidlichovský and Nesvorný, 1996). The Fourier transformation collapses down the oscillations into usable, single value for each of the orbital parameters.

For the semi-major axis of the Jovian Trojans, the value is generally very close to that of Jupiter, approximately 5.2 au. In order to examine the nuances in this parameter space, the difference in the oscillating semi-major axis of the Trojan to that of Jupiter is used, the delta semi-major axis (da). The proper delta semi-major axis (da_p) can then be calculated for each individual Trojan, using the Fourier transformations (Šidlichovský and Nesvorný, 1996).

The eccentricity and inclination proper elements require some additional processing before the Fourier transformations are applied. The elements (eccentricity: ex , ey ; inclination: ix , iy) are broken into x and y components, to account for the longitude of the ascending node (Ω) and argument of periapsis (ω), see equations 1.10 to 1.13. These values can then be used as input into the aforementioned Fourier transformation process (Šidlichovský and Nesvorný, 1996).

$$ex = e \times \cos \omega \tag{1.10}$$

	Jupiter	Saturn	Uranus	Neptune
1×10^5 years				
Eccentricity Frequencies:	4.07	238.8	-0.08	1.38
Sine Inclination Frequencies:	-1.47	3.2	13.31	-0.27
1×10^6 years				
Eccentricity Frequencies:	4.17	28.25	11.62	0.9
Sine Inclination Frequencies:	0.03	-26.34	-0.28	-0.15
1×10^7 years				
Eccentricity Frequencies:	4.25	28.25	3.09	0.67
Sine Inclination Frequencies:	-26.34	-0.69	-2.99	-0.53

Table 1.2: Perturbation frequencies used in Fourier Transform analysis. Calculated for individual integration times using REBOUND WHFAST (Rein and Tamayo, 2015), with a timestep of 0.3954 years and 1024 outputs. Analyzed using the technique presented in Šidlichovský and Nesvorný (1996).

$$ey = e \times \sin \omega \quad (1.11)$$

$$ix = e \times \cos \Omega \quad (1.12)$$

$$iy = e \times \sin \Omega \quad (1.13)$$

The resulting output of the Fourier transformation, for eccentricity and inclination space, have perturbations from the four giant planets. The amplitude from these frequencies (Table 1.2) needs to be excluded to get the true proper element.

Several databases of asteroid proper elements already exist. The most commonly used is the AstDyS database (<https://newton.spacedys.com/astdys/index.php?pc=5>), maintained by the University of Pisa and SpaceDYS, both in Italy. For the generation of proper elements for the Trojans, AstDyS use the method described in Beauge and Roig (2001), to four significant figures. The latest AstDyS Jovian Trojan dataset (Knežević and Milani, 2017), contains proper elements for 5553 Jovian Trojans as of June 2017. In Holt et al. (2020a), I use this as a set of initially ‘stable’ Trojans. Brož and Rožehnal (2011), in their exploration of the families of Jovian Trojans, also generated a dataset (<https://sirrah.troja.mff.cuni.cz/~mira/mp/>) of 4143 Trojans, that correlates well with the AstDyS dataset of the time. For the investigation into the Jovian Trojan Pairs (Holt et al., 2020b), I used a similar method to generate a detailed proper element set of 7328 Jovian Trojans, as of April 2020. There are two major advantages of generating our own dataset. The first difference with this set, is that

it uses 16 decimal places, rather than the four used in AstDyS, allowing for a more accurate characterisation of the pairs. The second difference is a search in the 1775 Trojans discovered in the intervening two years, though no pairs were discovered in the additional sub-set.

1.5.4 ASTEROID PAIRS

The discovery of asteroid pairs, two objects sharing a very similar heliocentric orbit, recently brought yet another piece of evidence into the mosaic of small Solar system bodies' evolution on short timescales (e.g., Vokrouhlický and Nesvorný, 2008). Examples of these couples have been found in the Main belt and Hungaria populations (Vokrouhlický and Nesvorný, 2008; Pravec and Vokrouhlický, 2009; Rozek et al., 2011; Pravec et al., 2019). The similarity between the heliocentric orbits of the two members of an identified asteroid pair hints at a common and recent origin for the objects, that most likely involves their gentle separation from a parent object. Indeed, backward orbital propagation of heliocentric state vectors of the components in many pairs has allowed researchers to directly investigate the possibility of their past low-velocity and small-distance approach (see Vokrouhlický et al., 2017, for the most outstanding example discovered so far).

The well-documented cases of pairs among asteroids identified to date all feature separation ages of less than a million years. Vokrouhlický and Nesvorný (2008) speculated about three processes that could have led to the formation of those pairs: (i) collisional break-up of a single parent object, (ii) rotational fission of such an object driven by radiation torques, and (iii) instability and separation of the components of a binary system. Whilst each of these possibilities can explain the origin of asteroid pairs, with some being more likely than others for individual pair cases, evidence has been found that the majority of currently identified pairs were probably formed through the rotational fission of their parent object (e.g., Pravec et al., 2010, 2019). It is worth noting that Main belt binaries in the same size category (i.e., with primary diameters of one to a few kilometers), are also believed to be primarily formed through the rotational fission of their parent body (e.g., Pravec and Harris, 2007; Margot et al., 2015). This is an interesting population-scale result that informs us about a leading dynamical process for few-km size asteroids in the Main belt. It would certainly be desirable to extend this knowledge to other populations of small Solar system bodies.

Attempts to detect orbital pairs in other populations have, to date, either failed or were not strictly convincing. For instance, the orbital evolution of bodies in the near-Earth population is very fast and chaotic and, at the same time, the number of known objects is limited (see, e.g., Moskovitz et al., 2019, and references therein). Searches in populations beyond the

Main belt were not successful for a variety of reasons. Whilst dynamical chaos could also be relevant, a more important factor concerns the smallest size of bodies found at larger distance from the Sun. The smallest bodies found in Cybele zone, located between the 2:1 and 5:3 Jovian resonances, and amongst the Hildas or Jovian Trojans, are about an order of magnitude larger than the smallest known asteroids in the inner Main belt or the Hungarias (e.g. Emery et al., 2015). The proposed pair-formation processes have a characteristic timescale that rapidly increases as a function of parent body size. For that reason, it is no surprise that, to date, no recently formed (≤ 1 My) traditional pairs sharing the same heliocentric orbit have been detected beyond the Main belt. If any pairs do exist in these distant small-body populations, they should be revealed by their tight configuration in proper element space and long-term backward orbital propagation, if the stability in that particular zone of orbital phase space allows. With that guideline in mind, I focus here on the Jovian Trojan population. The leap to the Trojan population might appear to contradict the logical steps of gradually extending our knowledge of Main belt pairs by searches among the Cybele or Hilda populations first. However, I argue that the case of possible Jovian Trojan pairs is actually more interesting because of that population's entirely different origin.

The discovery of asteroid pairs was a direct by-product of a search for very young asteroid families (see Nesvorný, 2006; Nesvorný and Vokrouhlický, 2006). As a result, the primary ambition was to find pairs that formed recently, within the last Myr, amongst the Main belt and Hungaria populations. In fact, the necessity for proven pairs to be young is essentially related to the method that allows their identification.

Just like collisional families, asteroid pairs are identified as a result of the similarity of their heliocentric orbits. The search for classical collisional families has traditionally been performed using clustering techniques in proper orbital element space, examining the proper semi-major axis a_P , eccentricity e_P and the sine of proper inclination $\sin I_P$ (see, e.g., Nesvorný et al., 2015, for review). The use of the proper elements allows us, with some care, to search for both young and old families. This is because the proper elements are believed to be stable over much longer timescales than other types of orbital elements, such as osculating or mean, ideally on a timescale reaching hundreds of Myrs or Gyrs.

There are, however, limitations to this method. In the case of very old families, problems arise from instability of the proper orbital elements and the incompleteness of the dynamical model used to derive the proper elements. A different problem occurs for very young families. The issue has to do with the huge increase in the number of small-body objects discovered over the past decades. Despite the fact that the very young families and asteroid pairs must have very close values of the proper orbital elements, it is difficult to statistically discern them

from random fluctuations of background asteroids. Both occur at the same orbital distance in proper element space.

This fundamental obstacle arises due to the low dimensionality of proper element space, which consists of just three independent variables. In order to separate very young asteroid families and asteroid pairs from the random fluctuations of the background population, Nesvorný and Vokrouhlický (2006) and Vokrouhlický and Nesvorný (2008) realized that this problem can be overcome if the search is conducted in a higher-dimensional space. As a result, they used the five-dimensional space of the osculating orbital elements, neglecting just the mean longitude. The mean orbital elements are also suitable alternative parameters for such an analysis (e.g., Rozek et al., 2011). In order to effectively use the two extra dimensions, the searched structures must also be clustered in secular angles, the longitudes of ascending node and perihelion. This is perfectly justified for very young families and pairs that are expected to have separated at very low velocities.

Previous searches for these young structures in the space of osculating or mean orbital elements proved the usefulness of the method, provided the age of the pair was less than about one Myr. Asteroid pairs clearly exist that formed earlier than this limit, but the differential precession of their secular angles result in them becoming effectively randomized, which in turn, render the identification procedure described above ineffective. A key point here is that the population of Main belt asteroids is currently known to very small sizes, with objects detected with diameters of one kilometer, or even smaller. The proposed formation processes for very young families and pairs are expected to generate enough pairs within the last Myr that, even after accounting for discovery biases, we still have some of them in our catalogs.

Despite their importance as a source of information on the Solar system's past evolution, the fact that the Jovian Trojans are markedly farther from Earth than the Main Belt has made them significantly more challenging targets for study. As a result, our knowledge of the collisional history, binarity, and the presence/absence of pairs in the Trojan population remains far smaller than our knowledge of the Main belt (e.g. Margot et al., 2015). In fact, to date, no confirmed Trojan pairs have been discovered, and the true level of binarity in the population remains to be uncovered. The most famous confirmed binary in the Trojan population is (617) Patroclus, accompanied by a nearly equal size satellite Menoetius (both in the 100 km range; e.g., Marchis et al., 2006; Buie et al., 2015). The Patroclus-Menoetius system is fully evolved into a doubly synchronous spin-orbit configuration (see Davis and Scheeres, 2020, and references therein), and represents an example of the kind of binary systems which are expected to be common among the Trojans. A number of such binaries, comprising two components of almost equal size, have been found amongst the large trans-Neptunian ob-

jects (e.g. Noll et al., 2020b). This comparison is of particular interest, given that the Patroclus system was, in all likelihood, implanted to the Trojan region from the trans-Neptunian region source zone (e.g., Nesvorný et al., 2018). It seems likely that the Patroclus system represents the closest example of an Edgeworth-Kuiper belt binary system. Further information on the Patroclus system will become available in the coming decades, as the binary is a target for flyby in 2033 by the *Lucy* spacecraft (e.g., Levison et al., 2017). Similar smaller-scale systems may well exist among the Trojan population, but their abundance is uncertain. Observationally, such small-scale binaries remain beyond our detection, and theoretical models of their survival depend on a number of unknown parameters (e.g., Nesvorný et al., 2018; Noll et al., 2020b; Nesvorný and Vokrouhlický, 2019). The existence of Trojan binaries is interesting by itself, but in the context of this work, it is worth noting that, if such binaries exist, they likely serve as a feeding cradle for a population of Trojan pairs.

Following this logic, if the population of pairs among the Trojans can become known and well characterized, such that their dominant formation process is understood, that would in turn prove to be a source of new information about Trojan binaries. Milani (1993) in his pioneering work on Jovian Trojan orbital architecture noted a case of the L₄-swarm objects (1583) Antiochus and (3801) Thrasymedes. Their suspicious orbital proximity led the Milani (1993) to suggest that they may constitute a genetically related pair of bodies. A viable formation process would be through the instability and dissociation of a former binary. Unfortunately, the Antiochus–Thrasymedes interesting configuration has not since been revisited, nor further studied in a more detail.

1.6 CLADISTICS

The vast majority of work in cladistics, which is also known as phylogenetic systematics, has been undertaken in the biological sciences. The premise of the method is that characteristics are inherited through descent. From this, it may be inferred that organisms with similar characteristics are related to one another. The most well recognized use of the method is to create the ‘Tree of Life’ (e.g. Darwin, 1859; Hennig, 1965; Hug et al., 2016). Any reference to new living species (e.g. Van Dong et al., 1993; Ričan et al., 2011; Kvist et al., 2014) or interpretation of a fossil (e.g. Salisbury et al., 2006; Smith et al., 2017; Aria and Caron, 2017) uses cladistics to examine the relationships between organisms. Cladistics is therefore used as a method to investigate the common origins of life, and how different species are related to one another. The advantage of cladistics over other analytical techniques is the use of multiple characteristics, including those that are unknown in some objects. This allows for more detailed and

hierarchical relationships to be inferred, without truncating the dataset. While cladistics can account for unknown characteristics, the more that is known about an object, the more confidence that can be placed in the analysis. A reduction in missing data would also decrease the number of equally parsimonious trees produced during the analysis. A description of the method, and how it is to be applied in this project is discussed in section 1.6.2.

1.6.1 HISTORY

Historically, the investigation into relationships between different organisms reaches back to Darwin (1859). With early attempts at systematically applying cladistics in the early 20th century (Mitchell, 1901; Tillyard, 1926; Zimmermann and Schultz, 1931), the modern discipline started in the late 20th century. Hennig (1965) is regarded as the first to propose ‘phylogenetic systematics’, what would become modern cladistical analysis. The technique was quickly adopted by the biological community and used to analyse every form of life, from bacteria (e.g. Olsen et al., 1994) to Dinosauria (e.g. Bakker and Galton, 1974) and even our own ancestors (e.g. Chamberlain and Wood, 1987). During this era, and still with modern fossil cladistical analysis, physical characteristics are used in the cladistical analysis. With the advent of more powerful computing in the later years of the 20th century, the use of DNA led to the expansion into molecular cladistics (Suárez-Díaz and Anaya-Muñoz, 2008). As computing power improves, larger datasets can be examined, and our understanding of the ‘Tree of Life’ improves (Hug et al., 2016). For a detailed examination of the history of cladistics, I refer the interested reader to Hamilton (2014).

The methodology of this PhD project is to comprise two main areas of investigation, cladistics and dynamics. In section 1.6.2, I provide details on the Cladistical methodology and how it relates to other taxonomic tools. Section 1.6.3 describes the specifics of astrocladistics, how cladistics can be applied to an astronomical context. As part of the analysis of the results of astrocladistics, I also describe a previously derived method, the Hierarchical Clustering Method (HCM), and how it can be applied to the results of the astrocladistical analysis.

1.6.2 CLADISTICAL METHODOLOGY

The cladistical methodology, as pioneered by Hennig (1965), involves a sequence of steps to find the most parsimonious tree. This concept of parsimony, that the simplest explanation is the most likely to have occurred, is at the heart of the method. The method searches for

a dendritic tree with the least number of changes to explain the configuration. This tree is then a hypothesis for the relationships between the objects of interest.

The first stage of the methodology begins with the creation of a taxon-character matrix, including taxa, the object that you are interested in, and an outgroup, a related object, though outside your group of interest. In the Astrocladistical context, I have used two different objects as an outgroup. In paper 1 (Holt et al., 2018), I use the Sun as an outgroup. For astrocladistics of the Jovian Trojans (Holt et al., 2021), the dynamics make selection of the outgroup more difficult, as there is no true ancestral state from which ingroup characteristics are derived. As such a fictitious outgroup object is created, with a base 0 for each of the characteristics. The function of this outgroup is to root the trees. In the context of biological cladistics, a related clade, but one that is outside the group of interest, is selected as the outgroup (Farris, 1982). In doing this, the outgroup sets the base character state for each characteristic. For astrocladistics of the Trojans, the dynamics make selection of the outgroup more difficult, as there is no true ancestral state from which ingroup characteristics are derived. For the synthetic outgroup created for this study, the dynamical characteristics are set close to 0 in proper Δ semi-major axis (Δa_p), eccentricity (e_p) and sine inclination ($\sin i_p$). The calculated mean libration values would be at the closest approach to Jupiter (56.42° and 285.72° for the L_4 and L_5 swarms respectively), with low libration amplitudes (L_4 : 4.044° , L_5 : 2.73°). These values represent a very stable area of the parameter space. In terms of albedo (L_4 : 0.024, L_5 : 0.031) and colours, the object would be very dark, and have a featureless spectrum. Based on these parameters the outgroup served the purpose of rooting each consensus tree without being too close and considered part of the ingroups, or too far away so that the relationship to the populations of interest were lost.

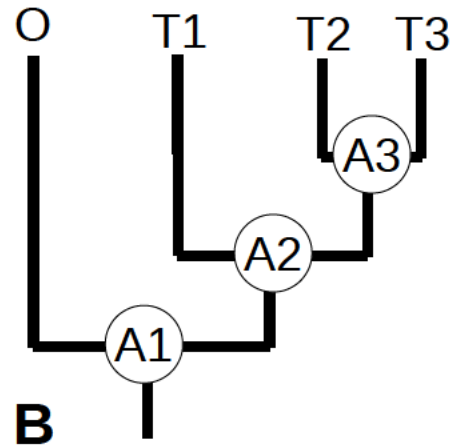
An example of a simple matrix is shown in Figure 1.16, with more details in section 1.6.2.1. This matrix is then used by `Tree analysis using New Technology (TNT) 1.5` (Goloboff et al., 2008; Goloboff and Catalano, 2016), to generate a number of equally parsimonious trees, that form the basis of the final consensus tree (Margush and McMorris, 1981), detailed in section 1.6.2.2. This process is shown in graphical form in Figure 1.17.

1.6.2.1 TAXON-CHARACTER MATRIX

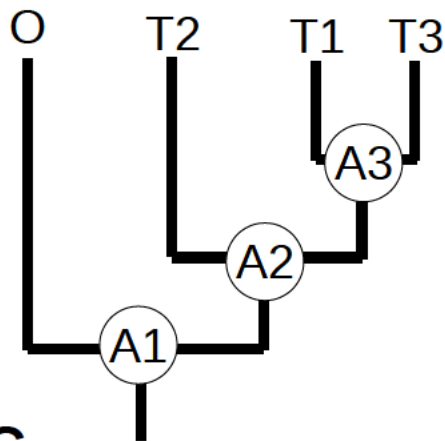
The cladistical methodology begins with the creation of a taxon-character matrix. Each matrix is a 2-d array, with the taxa, the objects of interest, in the rows, and each characteristic in the columns. The taxa used in this study are either the gas giant satellites or the Jovian Trojans (Holt et al., 2021). The orbital, physical and compositional properties, including the

	C1	C2	C3	C4	C5
Outgroup (O)	0	0	0	0	0
Taxon 1 (T1)	1	1	0	0	0
Taxon 2 (T2)	1	1	?	1	0
Taxon 3 (T3)	1	1	1	1	1

A



C



D

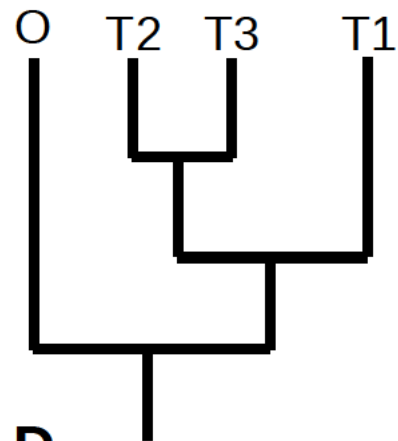


Figure 1.16: Simple examples of cladistic methodology. A A taxon-character matrix, including an Outgroup (O) and three taxa (T1, T2, T3), with character (C1-5) states, including an unknown (?); B An example tree, showing each of the taxa and the three ancestral states (A1, A2, A3); C A tree with a different rearrangement to that shown in A. D This tree is an isomorph of the one shown in A.

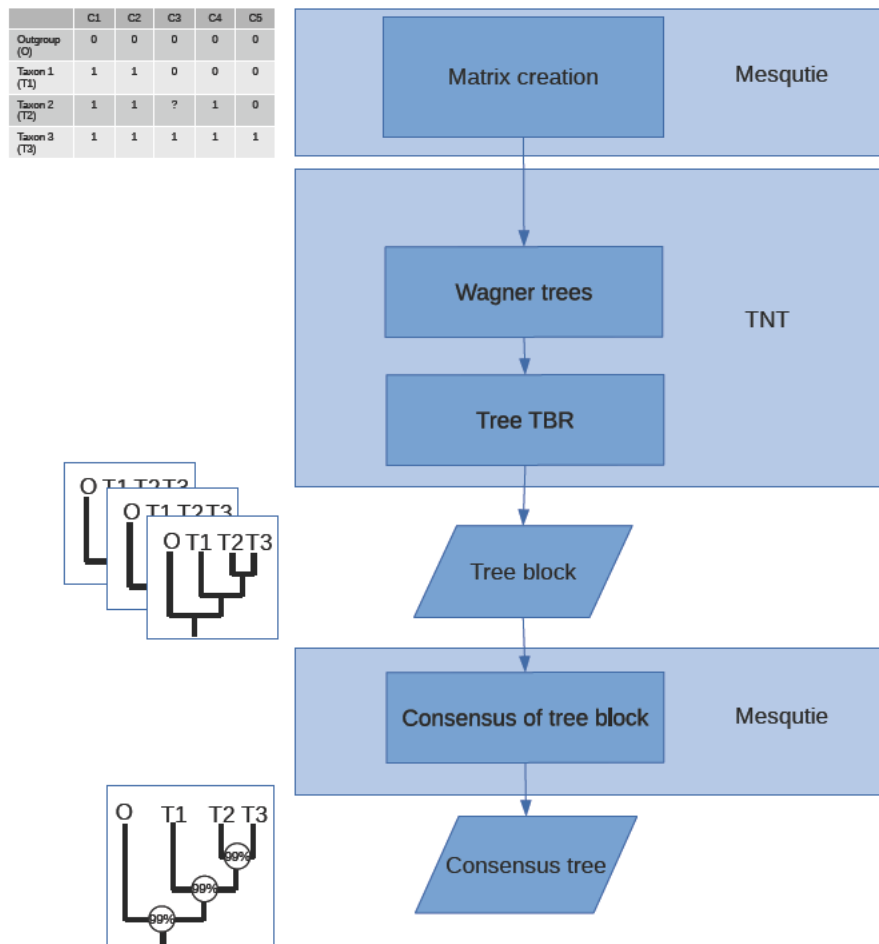


Figure 1.17: Flow diagram of the cladistics methodology. Each stage uses a different software package as indicated: Mesquite (Maddison and Maddison, 2017); TNT Tree analysis using New Technology (TNT) 1.5 (Gooboff et al., 2008; Gooboff and Catania, 2016).

wide-band survey colours, of the satellites or Jovian Trojan are used as characteristics, see section 1.6.3.1. For a given taxa, each corresponding characteristic is defined as a numerical state, usually a 0 or 1, though multiple, discrete states may be used. A 0 numerical state is used to indicate the original or ‘base’ state. An *outgroup*, or a taxa outside the area of interest, is used to dictate the 0 base state of a characteristic. An unknown character state can be accounted for, with a question mark (?). This taxon-character matrix is created using the `Mesquite` software package (Maddison and Maddison, 2017).

1.6.2.2 TREE SEARCH

A set of phylogenetic trees are subsequently created from the `Mesquite` taxon-character matrix, using `Tree analysis using New Technology (TNT) 1.5` (Goloboff et al., 2008; Goloboff and Catalano, 2016), via the `Zephyr Mesquite` package (Maddison and Maddison, 2015). The trees are created on the concept of maximum parsimony (Maddison et al., 1984), that the tree with the shortest lengths, the smallest number of changes, is most likely to show the true relationships (Camin and Sokal, 1965).

Some examples of basic trees are shown in Figure 1.16. I use these to explain some of the terminology of cladistics. The tree shown in B is the most parsimonious, with the least number of changes, five. Each node is shown as an Ancestral state (A_1 , A_2 and A_3).

A change between nodes, for example A_2 and T_1 in Figure 1.16B, can be mathematically expressed (after Camin and Sokal, 1965) as:

$$d(A_2, T_1) = \sum_i |X(A_2, i) - X(T_1, i)| \quad (1.14)$$

where $X(A_2, i)$ is the character state (i) matrix (X) for the node (A_2). The Tree length is then taken as the sum of the changes between nodes:

$$L(N, f) = \sum_{n \neq p} d(n, f(n)) \quad (1.15)$$

Between ancestral state 1 (A_1) and A_2 , there would be two changes, in characteristic 1 (C_1) and C_2 . Between A_2 and A_3 , there could be a further two changes (C_3 and C_4), but as the C_3 is unknown in Taxon 3, this is only a single change in C_4 . Between A_3 and T_3 there is a change in C_3 (from the assumption that there is no change in an unknown characteristic) and in C_5 . This gives a total of five changes, or a tree length of five. In tree C, there is another example, that is less parsimonious. A_1 to A_2 has three changes (C_1 , C_2 , C_4). There is one

change between A_2 and A_3 (C_3 to state 1), and then two reversals between A_3 and T_1 (C_3 and C_4 back to 0), and T_3 changes to state 1 in C_5 . This means that the tree has a length of seven, two greater than the one shown in Figure 1.16 B. An interesting feature of the trees is that each node is symmetric, so tree D in Figure 1.16 is an isomorph of tree B.

This system, while cumbersome to compute manually, is well suited to computational algorithms (Farris, 1970). For the works in this thesis, I use the modern TNT 1.5 (Goloboff, 1993, 1996). TNT uses a method of indirect tree length estimation (Goloboff, 1993, 1996), in its heuristic search for trees with the smallest length. TNT starts the drift algorithm (Goloboff, 1996) search by generating 100 Wagner trees (Farris, 1970), with 10 drifting trees per replicate. This drift algorithm randomly swaps terminal taxa to try to find the requested number of starting trees. These starting trees are then checked using a Tree bisection and reconnection (TBR) algorithm (Goloboff, 1996) to generate a block of equally parsimonious trees. The TBR algorithm takes the starting trees, and swaps branches to try find sets with smaller lengths. In this way, very large sets of trees can be tested.

Ideally, all equally parsimonious trees would be stored, but this is computationally prohibitive. For this analysis, 10000 equally parsimonious trees are requested from TNT, to create the tree block. Once a tree block has been generated and imported into Mesquite (Maddison and Maddison, 2017) for analysis, a 0.5 majority-rules consensus tree can be constructed using the a well established algorithm (Margush and McMorris, 1981). This tree is generated as a consensus of the block, with a tree branch being preserved if it is present in the majority of the trees. The resulting branching taxonomic tree is then a hypothesis for the relations between taxa.

1.6.2.3 TREE STATISTICS

I can assess how accurately a tree represents the true relationships between taxa. The number of steps it takes to create a tree is called the *tree length*. A smaller tree length indicates a more likely tree, as it is more parsimonious. Tree length estimation algorithms (Farris, 1970) continue to be improved, and are fully explored in a modern context by Goloboff (2015). Two other tree metrics, the consistency and retention indices, are a measure of *homoplasy*, or the independent loss or gain of a characteristic (Givnish and Sytsma, 1997). High amounts of homoplasy in a tree is indicative of random events, rather than the desired relationships between taxa (Brandley et al., 2009). Mathematically, homoplasy can be represented by the consistency index (CI) of a tree, (Equation (1.16), reproduced from Kluge and Farris, 1969) and is related to the minimum number of changes (M) and the number of changes on the

tree actually observed (S).

$$CI = M/S \quad (1.16)$$

A tree with no *homoplasy* would have a consistency index of 1. One of the criticisms of the consistency index is that it shows a negative correlation with the number of taxa and characteristics (Archie, 1989; Naylor and Kraus, 1995). In order to combat the issues with the consistency index, a new measure of homoplasy, the retention index, was created (Farris, 1989). The retention index (RI ; Farris, 1989) introduces the maximum number of changes (G) required into equation (1.17).

$$RI = \frac{G - M}{G - S} \quad (1.17)$$

As with the consistency index, a tree with a retention index of 1 indicates a perfectly reliable tree. Both of these metrics show how confidently the tree represents the most plausible relationships between taxa. Values closer to 1 of both the consistency and retention indices indicate that the tree represents the true relationships between taxa (Sanderson and Donoghue, 1989). For a detailed examination of the mathematics behind the algorithms and statistics used in cladistical analysis, I direct the interested reader to Gascuel (2005).

In my investigation of the Jupiter and Saturn satellite systems (Holt et al., 2016), I used the *Mesquite* (Maddison and Maddison, 2017) and TNT (Goloboff et al., 2008; Goloboff and Catalano, 2016) software packages, as described above. In order to investigate the parameter set, due to computation restrictions, a subset of the Jovian Trojans is required. Proper parameters are available through the JPL Small-body database (Giorgini et al., 1996) for all known Jovian Trojan asteroids. The subset is the intersect of albedo available from *WISE* (Grav et al., 2012), and the spin periods from Asteroid Lightcurve database (Warner et al., 2009). The subset is also to include colour indices from Sloan Digital Sky Survey Moving Object Catalogue (Szabo et al., 2007) and compositional information, where available. The subset includes all six Trojan targets of the *Lucy* spacecraft, as well as representatives from the known dynamical families (Brož and Rozehnal, 2011; Emery et al., 2015; Nesvorný et al., 2015; Vinogradova, 2015; Rozehnal et al., 2016).

1.6.3 ASTROCLADISTICS

In astronomy/astrophysics, astrocladistics has been used to look at the relationships between stars (Fraix-Burnet and Davoust, 2015; Jofré et al., 2017), gamma-ray bursts (Cardone and

Fraix-Burnet, 2013), globular clusters (Fraix-Burnet et al., 2009) and galaxies (Fraix-Burnet et al., 2006, 2010, 2012, 2015). These works, along with my own work on the Jovian and Saturnian satellites (Holt et al., 2016, 2018), form a body of work in the new field of ‘astrocladistics’ (Fraix-Burnet et al., 2015). There are good reasons to believe that cladistics can provide sensible groupings in a planetary science context. Objects that have similar formation mechanisms should have comparable characteristics. Daughter objects that are formed by breaking pieces off a larger object should also have similar characteristics. The advantage of this method over other multivariate analysis systems is the inclusion of a larger number of characteristics, enabling us to infer more detailed relationships. The work on the satellites of the gas giants (Holt et al., 2018) is the first to use the technique in a planetary science context. Extending the technique by investigating the Jovian Trojan asteroids, a population several orders of magnitude larger than each of the satellite systems, improves the validity of cladistics in a planetary science context (Holt et al., 2021).

1.6.3.1 CHARACTERISTICS

The characteristics used in astrocladistical analysis can be broken into three broad categories: orbital, physical and compositional parameters, as I initially used in the analysis of the satellite systems. I used the characteristics originally in (Holt et al., 2018) as a point for comparison. Additional characteristics are to be used to improve the dataset before expansion on to the full Jovian Trojans dataset (Holt et al., 2021). All numerical states are considered having equal weight. The discrete character sets are unordered. Any continuous characteristics are broken into bins, as cladistical analysis requires discrete characteristics. I developed a Python program to establish the binning of continuous characteristics. Each characteristic is binned independently of each other. The aforementioned Python program iterates the number of bins until a linear regression model between binned and unbinned sets achieves a coefficient of determination (R^2) score of > 0.99 . This is calculated using the stats package in SciPy (Jones et al., 2015). Each character set has a different number of bins, R^2 score, and delimiters. All characteristics are binned in a linear fashion, with the majority increasing in progression. The exception to the linear increase is the density character set, with a reversed profile. All of the continuous, binned characteristic sets are ordered, as used by Fraix-Burnet et al. (2006).

The first broad category includes the five orbital characteristics. Objects with similar orbital characteristics could be the result of a recent breakup, and form the basis of Multivariate Hierarchical Clustering (Zappala et al., 1990), see section 1.4.4.2. In the satellite systems, this is relatively straight forward, using the semi-major axis in km, eccentricity and inclinations of

the objects. Due to the unique dynamics of the Jovian Trojans, the instantaneous osculating orbital elements can not be used for taxonomic purposes (e.g., Beauge and Roig, 2001; Brož and Rozehnal, 2011). The *AstDyS* database (Knežević and Milani, 2017) provides a set of robust proper elements, in semi-major axis, eccentricity and inclination, for the Jovian Trojans. By moving from an instantaneous value for the object orbit to one that has been modified to take account of the periodic motion of the Trojans around the Lagrange points, these proper elements provide a much more accurate insight into a given object's provenance. Two objects with a common origin would be expected, in the absence of any major chaotic scattering events, to have similar proper elements, but might, at any given instant, be at a different part of their libration cycle, and hence have markedly different osculating elements. These proper elements can therefore, unlike the osculating elements, inform us about long term orbital relationships in the population. In addition to the proper elements obtained from *AstDyS*, I also include information on the libration of the Jovian Trojans around their host Lagrange point. To obtain these libration values, I performed 1×10^4 year integrations of the orbital evolution of the Trojans under the influence of the Sun and four giant planets, using the *REBOUND WHFAST* integrator (Rein and Liu, 2012). For these integrations, I used a timestep of 0.3954 years, and wrote out the instantaneous orbital elements of all objects simulated every 10 years. From these, I am able to calculate the amplitude of libration, as well as the mean angle in the Jovian reference frame.

The second category used to construct the matrix consists of two initial continuous physical characteristics, density and visual geometric albedo. Both of these characteristics would be passed down to daughter objects, during a breakup event. Similar physical properties would also be suggestive of analogous formation scenarios. I chose to not include mass, or any properties related to mass, as characters in the analysis. The inclusion of these characteristics could hide any relationships between a massive object and any daughter objects, as the result of collisions.

The third category, used specifically in the satellite study (Holt et al., 2018), describes the discrete compositional characteristics and details the presence or absence of 31 different chemical species. As with the physical characteristics, compositional characteristics can be passed down to daughter objects from a breakup event, or suggest similar formation scenarios. In order to account for any positional bias, the fundamental state, solid, liquid, gas or plasma was not considered. In the initial analysis, I make no distinction between surface, bulk and trace compositions. This is to account for the potential of daughter objects to have their bulk composition comprised of surface material from the parent. I compare the inclusion of this information as an additional investigation. The majority of chemical species have absence as

a base state (o), and presence as the derived (i). The exception are the first three molecules, elemental hydrogen (eH), hydrogen (H₂) and helium (He), all of which are found in the Sun. As the Sun is the designated outgroup, the base state (o) indicates the presence of these species. With the exception of elemental hydrogen, the remaining single element species are those found in compounds. The spectroscopy of an object often only reports on the presence of an ion, as opposed to a full chemical analysis. As more detailed analysis becomes available, characters may be added to the matrix. Several chemical species are used in this particular matrix which are either not present in any of the asteroids or unknown. These are included for future comparisons with other orbital bodies. The specific details of the compositions are shown in Holt et al. (2018).

The issue with using specific chemical presence as a characteristic is that this requires detailed spectral analysis, which is only currently available for two Jovian Trojans, 624 Hektor (1907 XM) (Marchis et al., 2014; Perna et al., 2018) and 911 Agamemnon (1919 FD) (Perna et al., 2018), although it is likely that this situation will change in the coming decade as a result of both the *Lucy* mission and observations with the *James Webb Space Telescope*. As a proxy for composition, broadband colours can be used in astrocladistics, as has been undertaken by Fraix-Burnet et al. (2010) in their studies of galaxies. Several of the Jovian Trojans have been imaged by large all-sky surveys, with data available from the Sloane Digital Sky Survey (SDSS) (Szabo et al., 2007), the *Wide-field Infrared Survey Explorer* (*WISE*) (Grav et al., 2012), *Gaia* DR2 (Spoto et al., 2018) and the Moving Objects from VISTA Survey (MOVIS) (Popescu et al., 2016). The wide range of wavelengths represented by these datasets are shown in Fig. 1.18. I use the ratio of colours in these surveys as characteristics in the analysis (Holt et al., 2021), in addition to the dynamical dataset described above. In total, combining the dynamical and observational data, this results in a maximum of 17 characteristics being included for each Trojan studied in this work.

1.6.4 HIERARCHICAL CLUSTERING METHOD

In the Astrocladistics works (Paper 1 and Paper 4 Holt et al., 2018, 2021), I use the inverse Gauss equations (as used by Zappala et al., 1990; Morbidelli et al., 1995; Zappala et al., 1996; Beauge and Roig, 2001; Nesvorný et al., 2002b, 2003, 2004; Ragozzine and Brown, 2007; Turini et al., 2008; Michel et al., 2011; Carruba and Nesvorný, 2016), equations 1.18, 1.19 and 1.20, substituted into Equation 1.21, to test the dispersal velocities of the clusters found through cladistics. This methodology forms the basis of the Hierarchical Clustering method (HCM) discussed in section 1.4.4. δa , δe and δi are the difference between the individual asteroids

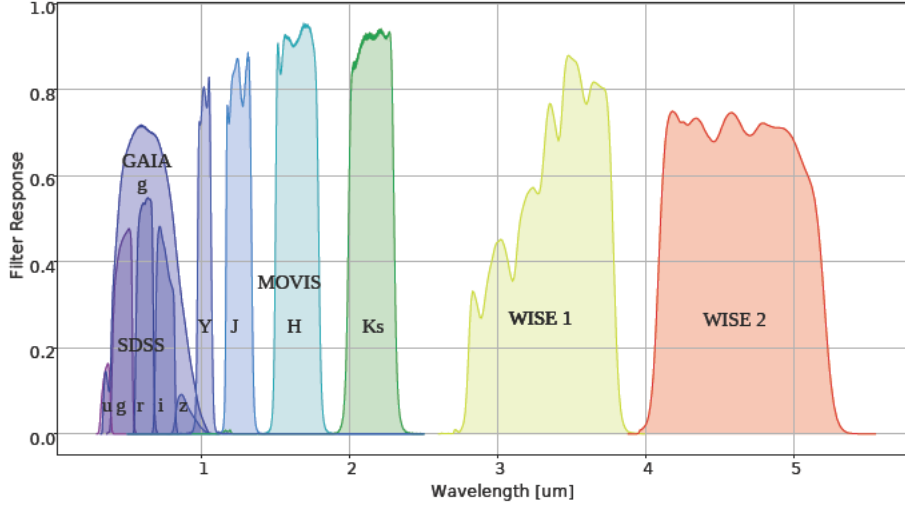


Figure 1.18: Wave lengths of the filters surveys used in this study.

and the reference object. a_r , e_r , i_r and orbital frequency (n_r) are parameters of the reference object. In this case, the reference object is taken as the largest member of the cluster. The true anomaly (f) and perihelion argument ($w + f$) at the time of disruption are unknown. Only in special cases, for example, for young asteroid families (e.g. Nesvorný et al., 2002a), the values of (f) and ($w + f$) can be inferred from observations. In this work I adopt $f = 90^\circ$ and $(f + w) = 45^\circ$ respectively as reasonable assumptions. Previous works by Nesvorný et al. (2003) and Turrini et al. (2008) using this method, do not indicate the true anomaly (f) and perihelion argument ($w + f$) used, nor the central reference point, making any comparison between them and this work relative rather than absolute. The final δV_d for the cluster is composed of the velocities in the direction of orbital motion (δV_T), the radial direction (δV_R) and perpendicular to the orbital plane (δV_W).

$$\delta V_T = \frac{n_r a_r (1 + e_r \cos f)}{\sqrt{1 - e_r^2}} \cdot \left[\frac{\delta a}{2a_r} - \frac{e_r \delta e}{1 - e_r^2} \right] \quad (1.18)$$

$$\delta V_R = \frac{n_r a_r}{(\sqrt{1 - e_r^2}) \sin f} \cdot \left[\frac{\delta e_r (1 + e_r \cos f)^2}{1 - e_r^2} - \frac{\delta a (e_r + e_r \cos^2 f + 2 \cos f)}{2a_r} \right] \quad (1.19)$$

$$\delta V_W = \frac{\delta i \cdot n_r a_r}{\sqrt{1 - e_r^2}} \cdot \frac{1 + e_r \cos f}{\cos(w + f)} \quad (1.20)$$

$$\delta V_d = \sqrt{\delta V_T^2 + \delta V_R^2 + \delta V_W^2} \quad (1.21)$$

1.6.4.1 LIMITATIONS OF THE HIERARCHICAL CLUSTERING METHOD

The disadvantage of this system is that it only identifies recent family breakups, with the vast majority of the asteroids considered ‘background’. Another issue with HCM is the issue of ‘chaining’ where families are identified, with interlopers included due to near proximity in phase space. This can be mitigated by the inclusion of colours (Parker et al., 2008), albedo (Carruba et al., 2013) and by incorporating taxonomy into the pipeline (Radović et al., 2017). Though these methods do improve some of the faults identified in HCM, they still suffer from the limitations inherent in the method. In order to use the HCM, a complete parameter space is required. This restricts the dataset in one of two ways, due to the limited information available for most small Solar system bodies. Either the parameters need to be restricted, usually down to just their proper elements, or the dataset is restricted down to those objects where a large amount of information is known. For example, Carruba et al. (2013) used a subset of only 11,609 Main belt asteroids, out of the approximately 60,000 available in the Sloan Digital Sky survey (SDSS) (Ivezić et al., 2002), 100,000 from the Wide-field Infrared Survey Explorer (WISE) (Masiero et al., 2011) and over 400,000 for which proper elements were available at the time. Cladistics is able to use all information available to examine relationships between objects, irrespective of the level of study. The Hierarchical Clustering Method remains useful in this project as a method of verifying and commenting on the age of the clusters identified by the Cladistical methodology. The rationale for this is that clusters with low dispersal velocities could indicate recent breakups, with larger velocities possibly indicating disruptions.

1.7 CONCLUDING REMARKS

In this chapter, I have provided an overview of the objects of interest, the Irregular satellites of the gas giant planets, and the Jovian Trojans. Both of these populations have similar origins, and are important in our understanding of early Solar system formation.

In order to investigate these populations further, I use two complimentary methodologies. Astrocladistics is a novel technique, based on cladistics, a biological method used to

create ‘the tree of life’. The method makes use of the limited datasets in the satellite systems of the gas giants (Paper 1 Holt et al., 2018) and the Jovian Trojans (Paper 4 Holt et al., 2021)) to investigate the relationships within the populations. I also use n -body simulations to look at the dynamical evolution of collisional families (Paper 2, Holt et al., 2020a) as well as looking for asteroid pairs in the population (Paper 3, Holt et al., 2020b). The four papers, and their peripheral presentations, form the core of this thesis, though there are several additional works outlined in chapter 6, including coauthor projects. Combined, these works improve our understanding of these small body populations, and bring astrocladistics into the context of Solar system research.

2

Paper 1 - Cladistical Analysis of the Jovian and Saturnian Satellite Systems

This is the first paper published in my PhD project, Holt et al. (2018). This work presents the first time that cladistics has been tried in a planetary science context. Currently (May, 2021), this paper has 9 citations on the ADS: <https://ui.adsabs.harvard.edu/abs/2018ApJ...859...97H/abstract>.

2.1 ABSTRACT

Jupiter and Saturn each have complex systems of satellites and rings. These satellites can be classified into dynamical groups, implying similar formation scenarios. Recently, a larger number of additional irregular satellites have been discovered around both gas giants that have yet to be classified. The aim of this paper is to examine the relationships between the satellites and rings of the gas giants, using an analytical technique called cladistics. Cladistics is traditionally used to examine relationships between living organisms, the “tree of life.” In this work, we perform the first cladistical study of objects in a planetary science context. Our method uses the orbital, physical, and compositional characteristics of satellites to clas-

sify the objects in the Jovian and Saturnian systems. We find that the major relationships between the satellites in the two systems, such as families, as presented in previous studies, are broadly preserved. In addition, based on our analysis of the Jovian system, we identify a new retrograde irregular family, the Iocaste family, and suggest that the Phoebe family of the Saturnian system can be further divided into two subfamilies. We also propose that the Saturnian irregular families be renamed, to be consistent with the convention used in Jovian families. Using cladistics, we are also able to assign the new unclassified irregular satellites into families. Taken together, the results of this study demonstrate the potential use of the cladistical technique in the investigation of relationships between orbital bodies.

2.1.1 NEW SATELLITES

After the publication of this paper, additional satellites around the giant planets have been discovered. In 2018, just after publication of Holt et al. (2018), an additional 13 objects were reported by Sheppard et al. (2018), presented in Table 2.1. In the Irregular satellites, nine of the objects are in taxonomic agreement between Holt et al. (2018) and Sheppard et al. (2018); four are in the Ananke subfamily (S/2016 J1, S/2017 J3, S/2017 J7, S/2017 J9), three in the Carme subfamily (S/2017 J2, S/2017 J5, S/2017 J8) and two (Pandia, S/2017 J4 and Ersa S/2018 J1) in the Himalia family. The two new members placed in the Pasiphae family (S/2017 J1 and S/2017 J6) by Sheppard et al. (2018) are most likely in the Iocvaste or Pasiphae subfamilies. Valetudo S/2016 J2 is also placed in the Himalia family, though Sheppard et al. (2018) placed the object in its own family.

Even more recently, 20 new satellites of Saturn have been discovered by the same team¹. Two of the objects (S/2004 S29 and S/2004 S31) are both clearly in the prograde ‘Inuit’ group, our Siarnaq family. S/2004 S24 poses an interesting problem. It is a prograde object that has a semi-major axis similar to that of the retrograde objects. In terms of inclination, the object matches the Gallic/Albiroix family, though the eccentricity and semi-major axis are smaller and larger respectively. Apart from the prograde motion, S/2004 S24 could belong in the Aegir subfamily, though it is more likely to be a dynamically altered prograde orbiter, than the remnant of a retrograde family, somehow altered to to a prograde orbit. The remaining 17 objects can be split into the Aegir (S/2004 S39, S/2004 S30, S/2004 S27, S/2004 S28, S/2004 S26, S/2004 S35, S/2004 S20) and Ymir (S/2004 S22, S/2004 S32, S/2004 S34, S/2004 S21, S/2004 S38, S/2004 S23, S/2004 S33, S/2004 S25, S/2004 S37, S/2004 S36) subfamilies of the Pheobe retrograde family.

¹<https://sites.google.com/carnegiescience.edu/sheppard/home/newsaturnmoons2019>

Name	$a(\text{km})$	i	e	tax_t	tax_{ac}
Jupiter					
Ersa S/2018 J1	11483000	30.61°	0.094	Himalia	Himalia family
Pandia S/2017 J4	11525000	28.15°	0.18	Himalia	Himalia family
Valetudo S/2016 J2	18980000	34°	0.222	Valetudo	Himalia family
S/2017 J7	20627000	143.4°	0.215	Ananke	Ananke subfamily
S/2016 J1	20650845	139.8°	0.141	Ananke	Ananke subfamily
S/2017 J3	20694000	147.9°	0.148	Ananke	Ananke subfamily
S/2017 J9	21487000	152.7°	0.229	Ananke	Ananke subfamily
S/2017 J6	22455000	155.2°	0.557	Pasiphae	Iocaste or Pasiphae family
S/2017 J5	23232000	164.3°	0.284	Carme	Carme subfamily
S/2017 J8	23232700	164.7°	0.312	Carme	Carme subfamily
S/2017 J2	23303000	166.4°	0.236	Carme	Carme subfamily
S/2017 J1	23547105	149.2°	0.397	Pasiphae	Iocaste or Pasiphae family
Saturn					
S/2004 S37	16003300	164°	0.506	Norse	Ymir subfamily
S/2004 S31	17402800	48.11°	0.242	Inuit	Siarnaq family
S/2004 S29	17470700	44.43°	0.472	Inuit	Siarnaq family
S/2004 S20	19211000	163.1°	0.204	Norse	Aegir subfamily
S/2004 S27	19776700	167.1°	0.12	Norse	Aegir subfamily
S/2004 S22	20379900	177.4°	0.257	Norse	Ymir subfamily
S/2004 S30	20424000	156.3°	0.113	Norse	Aegir subfamily
S/2004 S25	20544500	173.3°	0.457	Norse	Ymir subfamily
S/2004 S23	21427000	177.7°	0.399	Norse	Ymir subfamily
S/2004 S32	21564200	158.5°	0.262	Norse	Ymir subfamily
S/2004 S28	21791300	171°	0.133	Norse	Aegir subfamily
S/2004 S35	21953200	176.4°	0.182	Norse	Aegir subfamily
S/2004 S39	22790400	167.6°	0.081	Norse	Aegir subfamily
S/2004 S38	23006200	155°	0.381	Norse	Ymir subfamily
S/2004 S24	23231300	36.78°	0.049	Prograde	Unknown
S/2004 S36	23698700	147.6°	0.667	Norse	Ymir subfamily
S/2004 S33	23764800	161.5°	0.417	Norse	Ymir subfamily
S/2004 S21	23810400	154.6°	0.312	Norse	Ymir subfamily
S/2004 S34	24358900	165.7°	0.267	Norse	Ymir subfamily
S/2004 S26	26737800	171.3°	0.148	Norse	Aegir subfamily

Table 2.1: Newly discovered satellites of Jupiter and Saturn. Shown are $a(\text{km})$ Semi-major axis from planet in km; $i(\text{deg})$ inclination in degrees; e eccentricity; tax_t traditional taxonomy (Jewitt and Haghighipour, 2007; Sheppard et al., 2018); tax_{ac} astrodynamical taxonomy (Holt et al., 2018).

2.2 ASSOCIATED PRESENTATIONS AND PUBLICATIONS

There is a Github repository associated with this paper: <https://github.com/TimHoltastro/Holt-et-al-2018-Satellite-cladistics>

2.2.1 OCT. 2017: DPS 49 - ORAL PRESENTATION

Investigating the origins of the Irregular satellites using Cladistics

Holt, Timothy; Horner, Jonti; Tylor, Christopher; Nesvorny, David; Brown, Adrian; Carter, Brad

Abstract

The irregular satellites of Jupiter and Saturn are thought to be objects captured during a period of instability in the early solar system. However, the precise origins of these small bodies remain elusive. We use cladistics, a technique traditionally used by biologists, to help constrain the origins of these bodies. Our research contributes to a growing body of work that uses cladistics in astronomy, collectively called astrocladistics. We present one of the first instances of cladistics being used in a planetary science context. The analysis uses physical and compositional characteristics of three prograde Jovian irregular satellites (Themisto, Leda & Himalia), five retrograde Jovian irregular satellites (Ananke, Carme, Pasiphae, Sinope & Callirrhoe), along with Phoebe, a retrograde irregular satellite of Saturn, and several other regular Jovian and Saturnian satellites. Each of these members are representatives of their respective taxonomic groups. The irregular satellites are compared with other well-studied solar system bodies, including satellites, terrestrial planets, main belt asteroids, comets, and minor planets. We find that the Jovian irregular satellites cluster with asteroids and Ceres. The Saturnian satellites studied here are found to form an association with the comets, adding to the narrative of exchange between the outer solar system and Saturnian orbital space. Both of these results demonstrate the utility of cladistics as an analysis tool for the planetary sciences.

Publication: American Astronomical Society, DPS meeting 49, id.511.03

Pub Date: October 2017



Cladistical Analysis of the Jovian and Saturnian Satellite Systems

Timothy. R. Holt^{1,2} , Adrian. J. Brown³ , David Nesvorný⁴ , Jonathan Horner¹ , and Brad Carter¹ 
¹ University of Southern Queensland, Computational Engineering and Science Research Centre, Queensland, Australia; timothy.holt@usq.edu.au
² Swinburne University of Technology, Center for Astrophysics and Supercomputing, Victoria, Australia
³ Plancius Research LLC, Severna Park, MD, USA
⁴ Southwest Research Institute, Department of Space Studies, Boulder, CO, USA

Received 2017 June 4; revised 2018 April 9; accepted 2018 April 10; published 2018 May 29

Abstract

Jupiter and Saturn each have complex systems of satellites and rings. These satellites can be classified into dynamical groups, implying similar formation scenarios. Recently, a larger number of additional irregular satellites have been discovered around both gas giants that have yet to be classified. The aim of this paper is to examine the relationships between the satellites and rings of the gas giants, using an analytical technique called *cladistics*. Cladistics is traditionally used to examine relationships between living organisms, the “tree of life.” In this work, we perform the first cladistical study of objects in a planetary science context. Our method uses the orbital, physical, and compositional characteristics of satellites to classify the objects in the Jovian and Saturnian systems. We find that the major relationships between the satellites in the two systems, such as families, as presented in previous studies, are broadly preserved. In addition, based on our analysis of the Jovian system, we identify a new retrograde irregular family, the Iocaste family, and suggest that the Phoebe family of the Saturnian system can be further divided into two subfamilies. We also propose that the Saturnian irregular families be renamed, to be consistent with the convention used in Jovian families. Using cladistics, we are also able to assign the new unclassified irregular satellites into families. Taken together, the results of this study demonstrate the potential use of the cladistical technique in the investigation of relationships between orbital bodies.

Key words: methods: data analysis planets and satellites: composition planets and satellites: formation planets and satellites: general

Supporting material: machine readable tables

1. Introduction

The two gas giants of the Solar system, Jupiter and Saturn, are host to a large number of satellites and rings. The satellites of both planets follow a similar progression pattern. The inner region of each system consists of small icy satellites, with an accompanying ring system (Thomas et al. 1998, 2013; Throop et al. 2004; Porco et al. 2005). Further out, there are larger icy/silicate satellites (Thomas 2010; Deienno et al. 2014). In the outer system, both planets have a series of irregular satellites, small satellites with high eccentricities and inclinations (Nesvorný et al. 2003; Sheppard & Jewitt 2003; Jewitt & Haghighipour 2007). It is thought that these satellites were captured from other populations of small Solar system bodies (Colombo & Franklin 1971; Heppenheimer & Porco 1977; Pollack et al. 1979; Sheppard & Jewitt 2003; Nesvorný et al. 2004, 2007, 2014; Johnson & Lunine 2005). This is in contrast to the inner satellites, which are thought to have accreted in a circumplanetary disk (e.g., Canup & Ward 2002; Canup 2010). Such a formation mechanism is thought to resemble the accretion of planets in a protoplanetary disk around a young star (Lissauer 1987), a conclusion that is supported by the recent discovery of the TRAPPIST 1 planetary system (Gillon et al. 2016). That system features at least seven Earth mass planets orbiting a very low mass star. The star itself, TRAPPIST 1, is within two orders of magnitude more massive than Jupiter, and similar in size. The seven planets span an area comparable to that of Jupiter’s regular satellite system. Studying and understanding the gas giant systems in our own Solar system can therefore provide context for future exploration of low mass exoplanetary systems.

1.1. The Jovian System

Historically, Galilei (1610) discovered the first satellites in the Jovian system, the large Galileans, Io, Europa, Ganymede, and Callisto. Our knowledge of these satellites has increased greatly, as a result of both improved ground based instrumentation (e.g., Sparks et al. 2016; Vasundhara et al. 2017) and spacecraft visitations (e.g., Smith et al. 1979; Grundy et al. 2007; Greenberg 2010).

Amalthea, one of the inner set of Jovian satellites, was discovered by Barnard (1892). A few years later, the first two small irregular satellites, Himalia (Perrine 1905) and Elara (Perrine & Aitken 1905), were discovered in inclined, prograde orbits. The discovery of Pasiphae 3 years later by Melotte & Perrine (1908) is significant, as this was only the second satellite in the Solar system to be found on a retrograde orbit, and the first such object found in the Jovian system. Several other irregular satellites were discovered in the first half of the 20th century: Sinope (Nicholson 1914), Lysithea (Nicholson 1938), Carme (Nicholson 1938), and Ananke (Nicholson 1951). Leda, another small prograde irregular, was discovered 20 years later by Kowal et al. (1975b). Themisto, the first Jovian satellite smaller than 10 km to be discovered, was found that same year (Kowal et al. 1975a) and subsequently lost. Themisto was rediscovered by Sheppard et al. (2000) nearly 20 years later. The *Voyager* visitations of Jupiter discovered the remaining three inner satellites, Metis (Synnott 1981), Adrastea (Jewitt et al. 1979), and Thebe (Synnott 1980), along with a ring system (Smith et al. 1979). These three satellites, Amalthea, and the ring system would be imaged again by the

Galileo (Ockert Bell et al. 1999) and *Cassini* (Porco et al. 2005) spacecraft during their missions.

The irregular Jovian satellites orbit the planet with semimajor axes an order of magnitude greater than the Galilean moons, and have large eccentricities and inclinations. In the early years of the 21st century, extensive surveys were carried out to search for the Jovian irregular satellites (Scotti et al. 2000; Sheppard et al. 2001, 2002, 2003b, 2004; Gladman et al. 2003a, 2003b; Sheppard & Jewitt 2003; Sheppard & Marsden 2003a, 2003b, 2004; Beaugé & Nesvorný 2007; Jacobson et al. 2011; Sheppard & Williams 2012). These surveys increased the number of known Jovian satellites from 14 after *Voyager* to the 67 known today. The inner five irregular satellites, Leda, Himalia, Lystea, Elara and Dia, have prograde orbits and have previously been classified into the Himalia group (Nesvorný et al. 2003; Sheppard & Jewitt 2003). Themisto and Carpo were proposed as single members of their own groups by Sheppard & Jewitt (2003). The remainder of the irregular satellites have retrograde orbits. Based on similarities in semimajor axis, inclination, and eccentricity, these satellites have been grouped into families by Sheppard & Jewitt (2003) and Nesvorný et al. (2003). These dynamical families are typified by their largest member, Himalia, representing the inner prograde satellites, with the retrograde ones being broken down into the Ananke, Pasiphae, and Carme families. Recently, several additional small irregular satellites have been discovered (Jacobson et al. 2011; Sheppard & Williams 2012), which are yet to be named or classified. With the discovery of new satellites (Scotti et al. 2000; Sheppard et al. 2001; Beaugé & Nesvorný 2007; Jacobson et al. 2011; Sheppard & Williams 2012) and additional information from the *Cassini* spacecraft (Porco et al. 2005), a revisit of the classification of the Jovian irregular satellites (Nesvorný et al. 2003; Sheppard & Jewitt 2003; Jewitt & Haghighipour 2007) is warranted.

1.2. The Saturnian System

The Saturnian system is broadly similar to that of Jupiter, but exhibits greater complexity. One of the most striking features, visible to even the most modest telescope, is Saturn's ring system. First observed by Galileo in 1610, it was Huygens (1659) that observed that the objects surrounding Saturn were in fact rings. The rings themselves are composed of individual particles, from micrometer to meter size (Zebker et al. 1985). Embedded within several of the main rings are a series of small moonlets (Tiscareno et al. 2006) and several shepherd satellites (Showalter 1991; Porco et al. 2007; Cuzzi et al. 2014). The co-orbitals Janus and Epimetheus (Yoder et al. 1983, 1989; Nicholson et al. 1992; Treffenstädt et al. 2015; El Moutamid et al. 2016), and their associated faint ring system (Winter et al. 2016) are unique to the Saturn system. Just beyond the Janus/Epimetheus orbit, there is a diffuse G ring, the source of which is the satellite Aegaeon (Hedman et al. 2007b).

Huygens (1659) also discovered Saturn's largest satellite, Titan. Earth based observations highlighted the methane based atmosphere of Titan (Kuiper 1944; Karkoschka 1994), with further characterization by the *Cassini* spacecraft (Niemann et al. 2005) and Huygens lander (Lebreton et al. 2005). The bulk composition of Titan is analogous to that of the other icy satellites, with an icy shell, subsurface water ocean, and silicate core (Hemingway et al. 2013). There are seven other mid sized icy satellites, with semimajor axes on a similar order of magnitude to that of Titan. The five largest, Mimas, Enceladus,

Tethys, Dione, and Rhea, are large enough to be in hydrostatic equilibrium. All of the mid sized satellites are thought to be predominantly composed of water ice, with some contribution from silicate rock, and may contain subsurface liquid oceans (Matson et al. 2009; Filacchione et al. 2012). Those satellites closer to Saturn than Titan, Mimas, Enceladus, Tethys, Dione, and Rhea are embedded in the E ring (Feibelman 1967; Baum et al. 1981; Hillier et al. 2007; Hedman et al. 2012). The *Cassini* mission identified the source of this ring as the southern cryo plumes of Enceladus (Spahn et al. 2006).

In addition to the larger icy satellites, there are four small Trojan satellites (Porco et al. 2005), situated at the leading and trailing Lagrange points, 60° ahead or behind the parent satellites in their orbit. Tethys has Telesto and Calypso as Trojan satellites, while Helene and Polydeuces are Trojan satellites of Dione. So far, these Trojan satellites are unique to the Saturnian system. Between the orbits of Mimas and Enceladus, there are the Alkyonides, Methone, Anthe, and Pallene, recently discovered by the *Cassini* spacecraft (Porco et al. 2005). All of the Alkyonides have their own faint ring arcs (Hedman et al. 2009) composed of similar material to the satellite. Dynamical modeling by Sun et al. (2017) supports the theory of Hedman et al. (2009) that the parent satellite is the source of the rings.

In the outer Saturnian system there are a large number of smaller irregular satellites, with 38 known to date. The first of these irregular satellites to be discovered was Phoebe, which was the first planetary satellite to be discovered photographically (Pickering 1899). Phoebe was also the first satellite to be discovered moving on a retrograde orbit (Pickering 1905; Ross 1905). Phoebe is the best studied irregular satellite and the only one for which in situ observations have been obtained (Clark et al. 2005). Recently, a large outer ring associated with Phoebe and the other irregular satellites has been discovered (Verbiscer et al. 2009). It has been suggested that Phoebe may have originated in the Edgeworth Kuiper Belt and captured into orbit around Saturn (Johnson & Lunine 2005). The other Saturnian irregular satellites were discovered in extensive surveys during the early 21st century (Gladman et al. 2001; Sheppard et al. 2003a, 2006b, 2007; Jewitt et al. 2005). Due to the small size of the majority of these satellites, only their orbital information is available. There are 9 prograde and 29 retrograde outer satellites, of which attempts have been made to place into families based on dynamical (Gladman et al. 2001; Jewitt & Haghighipour 2007; Turrini et al. 2008) and photometric (Grav et al. 2003; Grav & Bauer 2007) information. In the traditional naming convention (Grav et al. 2003), the Inuit family, Ijiraq, Kiviuiq, Paaliaq, Siarnaq, and Tarqeq are small prograde satellites, whose inclination is between 45° and 50° . The Gallic family, Albiorix, Bebhionn, Erriapus, and Tarvos, is a similar, prograde group, but with inclinations between 35° and 40° . The retrograde satellites are all grouped into the Norse family, including Phoebe. There is a possibility that the Norse family could be further split into subfamilies, based on photometric studies (Grav et al. 2003; Grav & Bauer 2007). The convention of using names from respective mythologies for the satellite clusters (Jewitt & Haghighipour 2007) has become the default standard for the irregular satellite families of Saturn.

1.3. Formation Theories

The purpose of taxonomy and classification, beyond simple grouping, is to investigate the origin of objects. The origin of the irregular satellites is a major topic of ongoing study (Nesvorný & Morbidelli 2012; Nesvorný et al. 2014). Here we present an overview for context. There are three main theories in the formation of the Jovian satellites: formation via disk accretion (Canup & Ward 2002), via nebula drag (Pollack et al. 1979), or via dynamic capture (Nesvorný et al. 2003, 2007). The satellites that are captured, either by nebula drag or through dynamical means, are thought to be from Solar system debris, such as asteroids and comets.

The disk accretion theory has generally been accepted as the mechanism for the formation of the inner prograde satellites of Jupiter (Canup & Ward 2002). The satellites form from dust surrounding proto Jupiter in a process analogous to the formation of planets around a star (Lissauer 1987). This surrounding disk would have lain in the equatorial plane of Jupiter, with material being accreted to the planet itself through the disk. This would explain both the prograde, coplanar orbits of the regular satellites and their near circular orbits.

The second theory requires satellites to be captured in the original Jovian nebula (Pollack et al. 1979; Cuk & Burns 2004). Before it coalesced into a planet, Jupiter is proposed to have had a greater radius, and lower density than now. There was a “nebula” surrounding this proto Jupiter. As other pieces of Solar system debris crossed into the Hill sphere of this nebula, they would be slowed down by friction and be captured as a satellite. Related to this is the concept of a pull down mechanism (Heppenheimer & Porco 1977). As a gas giant increases in mass from accretion (Pollack et al. 1996), the Hill sphere increases. As a subsequent effect, small Solar system bodies can possibly be captured as irregular satellites.

Dynamical capture can explain the retrograde orbits of the Jovian satellites (Nesvorný et al. 2003). The Hill sphere of a planet dictates the limit of its gravitational influence over other bodies. The theory (Nesvorný et al. 2003, 2007) states that it is impossible for a satellite to be captured in a three body system (Sun, planet and satellite). The Nice model of the Solar system (Tsiganis et al. 2005; Nesvorný et al. 2007, 2014) has a fourth body interaction placing the satellite into a stable orbit inside the Hill sphere of the gas giant. Recently the Nice model was updated to include a fifth giant planet (Nesvorný & Morbidelli 2012). This updated theory has the new planet interacting with Jupiter and allowing for the capture of the satellites, before the fifth giant planet is ejected from the Solar system. Collisions between objects could also play a part in the dynamical capture of the irregular satellites (Colombo & Franklin 1971).

The formation of the Saturnian satellite system is thought to be similarly complex. The inner satellites are possibly formed from accretion within the ring system (Charnoz et al. 2010) or from the breakup of a large, lost satellite (Canup 2010). Modeling of the Saturnian system by Salmon & Canup (2017) has shown that the mid sized satellites could have formed from a large ice dominated ring, with contamination of cometary material during the Late Heavy Bombardment, delivering the requisite silicate rock. Being the largest satellite in the Saturnian system, Titan is thought to have formed from accretion of proto satellites (Asphaug & Reufer 2013). The Saturnian irregular satellites are predicted to be captured objects (Jewitt & Haghighipour 2007), though their origins are still in dispute. Collisions are thought to have played a part in

the capture of the irregular satellites of Saturn (Turrini et al. 2009). The cratering data provided by the *Cassini* spacecraft (Giese et al. 2006) supports this hypothesis.

1.4. This Project

With the discovery of several new irregular satellites (Scotti et al. 2000; Gladman et al. 2001, 2003a, 2003b; Sheppard et al. 2001, 2002, 2003a, 2003b, 2006b, 2007, 2004; Sheppard & Marsden 2003a, 2003b; Sheppard & Jewitt 2003; Sheppard & Marsden 2004; Jewitt et al. 2005; Jacobson et al. 2011; Sheppard & Williams 2012), along with the detailed examination of the Jovian and Saturnian system by the *Cassini* spacecraft (Brown et al. 2003; Porco et al. 2005, 2006; Cooper et al. 2006; Giese et al. 2006; Spahn et al. 2006; Filacchione et al. 2007, 2010, 2014, 2016, 2012; Nicholson et al. 2008; Matson et al. 2009; Buratti et al. 2010; Thomas 2010; Tosi et al. 2010; Clark et al. 2012; Spitale & Tiscareno 2012; Hirtzig et al. 2013; Brown 2014), there is an opportunity to revisit the classification of the satellite systems of the gas giants. We apply a technique called *cladistics* to characteristics of the Jovian and Saturnian satellites, in order to examine the relationships between objects in the systems. The purpose of this is twofold. First, due to their well established classification systems, the Jovian and Saturnian satellite systems offer an opportunity to test the cladistical technique in a planetary science context. This project is an extension of Holt et al. (2016), and together they form the first use of cladistics for planetary bodies. The second aim of the project is to classify recently discovered satellites, as well as providing context for future work.

In Section 2, we introduce the cladistical technique, and how it is used in this paper. The resulting taxonomic trees for the Jovian and Saturnian systems, along with their implications for the taxonomy of the satellites, are presented in Sections 3.1 and 3.2, respectively. Section 4 discusses the implications of cladistics in a planetary science context, along with some remarks on origins of the gas giant satellites and possible future work.

2. Methods

In this section, we present an overview of the cladistical method and how it is applied to the Jovian and Saturnian satellite systems. Following a general overview of cladistics, the section progresses into the specifics of this study, including characteristics used in the paper. The section concludes with an explanation on the specific matrices of the Jovian and Saturnian satellites and how they are applied to the cladistical method.

2.1. Cladistics

Cladistics is an analytical technique, originally developed to examine the relationships between living organisms (Hennig 1965). A *clade* is the term used for a cluster of objects, or *taxa*, that are related to each other at some level. In astronomy/astrophysics, the technique has been used to look at the relationships among stars (Fraix Burnet & Davoust 2015; Jofré et al. 2017), gamma ray bursts (Cardone & Fraix Burnet 2013), globular clusters (Fraix Burnet et al. 2009), and galaxies (Fraix Burnet et al. 2006, 2010, 2012, 2015). These works, along with this study, form a body of work in the new field of “Astrocladistics” (Fraix Burnet et al. 2015). There are good reasons to believe that cladistics can provide sensible groupings in a planetary science context. Objects that have similar formation mechanisms should have comparable characteristics.

Daughter objects that are formed by breaking pieces off a larger object should also have similar characteristics. The advantage of this method over other multivariate analysis systems is the inclusion of a larger number of characteristics, enabling us to infer more detailed relationships.

The vast majority of work in cladistics and phylogenetics has been undertaken in the biological and paleontological sciences. Biologists and paleontologists use cladistics as a method to investigate the common origins, or “tree of life” (Darwin 1859; Hennig 1965; Hug et al. 2016), and how different species are related to one another (e.g., Van Dong et al. 1993; Salisbury et al. 2006; Říčan et al. 2011; Aria & Caron 2017; Smith et al. 2017). Historically, the investigation into relationships between different organisms reaches back to Darwin (1859). Early attempts at using tree analysis techniques occurred in the early 20th century (Mitchell 1901; Tillyard 1926; Zimmermann & Schultz 1931). Hennig (1965) is regarded as one of the first to propose “phylogenetic systematics,” the technique that would become modern cladistical/phylogenetic analysis. The technique was quickly adopted by the biological community and used to analyze every form of life, from bacteria (e.g., Olsen et al. 1994) to Dinosauria (e.g., Bakker & Galton 1974) and our own ancestors (e.g., Chamberlain & Wood 1987). Recently the use of DNA led to the expansion of the technique to become molecular phylogenetics (Suárez Díaz & Anaya Muñoz 2008). As computing power improves, larger data sets can be examined, and our understanding of the tree of life improves (Hug et al. 2016). For a detailed examination of the history of cladistics and pyholgenetics, we refer the interested reader to Hamilton (2014).

The cladistical methodology begins with the creation of a taxon character matrix. Each matrix is a 2D array, with the taxa, the objects of interest, in the rows, and each characteristic in the columns. The taxa used in this study are the rings and satellites of the Jovian and Saturnian Systems. The orbital, physical and compositional properties of the rings and satellites are used as characteristics (see Section 2.2). For a given taxa, each corresponding characteristic is defined as a numerical state, usually a 0 or 1, though multiple, discrete states may be used. A 0 numerical state is used to indicate the original or “base” state. An *outgroup*, or a taxa outside the area of interest, is used to dictate the 0 base state of a characteristic. For this study, we use the Sun as an outgroup. An unknown character state can be accounted for with a question mark (?). This taxon character matrix is created using the Mesquite software package (Maddison & Maddison 2017).

A set of phylogenetic trees are subsequently created from the Mesquite taxon character matrix, with Tree analysis using New Technology (TNT) 1.5 (Goloboff et al. 2008; Goloboff & Catalano 2016), via the Zephyr Mesquite package (Maddison & Maddison 2015). The trees are created on the concept of maximum parsimony (Maddison et al. 1984) that the tree with the shortest lengths, the smallest number of changes, is most likely to show the true relationships. TNT uses a method of indirect tree length estimation (Goloboff 1994, 1996) in its heuristic search for trees with the smallest length. TNT starts the drift algorithm (Goloboff 1996) search by generating 100 Wagner trees (Farris 1970), with 10 drifting trees per replicate. These starting trees are then checked, using a tree bisection and reconnection algorithm (Goloboff 1996), to generate a block of equally parsimonious trees. Closely related taxa are grouped

together in the tree. Ideally, all equally parsimonious trees would be stored, but this is computationally prohibitive. For this analysis, 10,000 equally parsimonious trees are requested from TNT, to create the tree block. Once a tree block has been generated and imported into Mesquite (Maddison & Maddison 2017) for analysis, a 0.5 majority rules consensus tree can be constructed using a well established algorithm (Margush & McMorris 1981). This tree is generated as a consensus of the block, with a tree branch being preserved if it is present in the majority of the trees. The resulting branching taxonomic tree is then a hypothesis for the relations between taxa, the satellites, and rings of the gas giants.

We can assess how accurately a tree represents true relationships between taxa. The number of steps it takes to create a tree is call the *tree length*. A smaller tree length implies a more likely tree, as it is more parsimonious. Tree length estimation algorithms (Farris 1970) continue to be improved, and are fully explored in a modern context by Goloboff (2015). Two other tree metrics, the consistency and retention indices, are a measure of *homoplasy*, or the independent loss or gain of a characteristic (Givnish & Sytsma 1997). High amounts of homoplasy in a tree are suggestive of random events, rather than the desired relationships between taxa (Brandley et al. 2009). Mathematically, homoplasy can be represented by the consistency index (CI) of a tree (Equation (1)), Kluge & Farris (1969) and is related to the minimum number of changes (M) and the number of changes on the tree actually observed (S):

$$CI = M/S. \quad (1)$$

A tree with no *homoplasy* would have a consistency index of 1. One of the criticisms of the consistency index is that it shows a negative correlation with the number of taxa and characteristics (Archie 1989; Naylor & Kraus 1995). In order to combat the issues with the consistency index, a new measure of homoplasy, the retention index, was created (Farris 1989). The retention index (*RI*; Farris 1989) introduces the maximum number of changes (G) required into Equation (2):

$$RI = \frac{G - M}{G - S}. \quad (2)$$

As with the consistency index, a tree with a retention index of 1 indicates a perfectly reliable tree. Both of these metrics show how confidently the tree represents the most plausible relationships between taxa. Values closer to 1 of both the consistency and retention indices indicate that the tree represents the true relationships between taxa (Sanderson & Donoghue 1989). For a detailed examination of the mathematics behind the algorithms and statistics used in cladistical analysis, we direct the interested reader to Gascuel (2005).

A traditional form of multivariate hierarchical clustering is used in the detection of asteroid collisional families (Zappala et al. 1990, 1994). This method of clustering uses Gauss equations to find clusters in a parameter space, typically using semimajor axis, eccentricity, and inclination (Zappala et al. 1990). Work has also been undertaken incorporating the known colors (Parker et al. 2008) and albedo (Carruba et al. 2013) of the asteroids (Milani et al. 2014) into the classical method, though this reduces the data set significantly. The classical method of multivariate hierarchical clustering was used by (Nesvorný et al. 2003) to identify the Jovian irregular satellite families. Turrini et al. (2008) expanded the classical method into the Saturnian

irregular satellites, and utilized the Gauss equations, solved for velocities, in a similar way to Nesvorný et al. (2003) to verify the families found, using semimajor axis (a), eccentricity (e), and inclination (i) of the satellites. The rationale behind these calculations is that the dispersal velocities of the clusters would be similar to the escape velocities of the parent body. In this work we use the inverse Gauss equations, Equations (3)–(5), substituted into Equation (6), to test the dispersal velocities of the clusters found through cladistics. δa , δe , and δi are the respective differences between the individual satellites and the reference object. a_r , e_r , i_r , and orbital frequency (n_r) are parameters of the reference object. In this case, the reference object is taken as the largest member of the cluster. The true anomaly (f) and perihelion argument ($w + f$) at the time of disruption are unknown. Only in special cases (e.g., for young asteroid families; Nesvorný et al. 2002) can the values of (f) and ($w + f$) be inferred from observations. In this work we adopt $f = 90^\circ$ and $(f + w) = 45^\circ$, respectively, as reasonable assumptions. Previous works by Nesvorný et al. (2003) and Turrini et al. (2008) using this method do not specify the true anomaly (f) and perihelion argument ($w + f$) used, nor the central reference point, making any comparisons between them and this work relative rather than absolute. The final δV_d for the cluster is composed of the velocities in the direction of orbital motion (δV_T), the radial direction (δV_R), and perpendicular to the orbital plane (δV_W):

$$\delta V_T = \frac{n_r a_r (1 + e_r \cos f)}{\sqrt{1 - e_r^2}} \cdot \left[\frac{\delta a}{2a_r} - \frac{e_r \delta e}{1 - e_r^2} \right] \quad (3)$$

$$\delta V_R = \frac{n_r a_r}{(\sqrt{1 - e_r^2}) \sin f} \cdot \left[\frac{\delta e_r (1 + e_r \cos f)^2}{1 - e_r^2} - \frac{\delta a (e_r + e_r \cos^2 f + 2 \cos f)}{2a_r} \right] \quad (4)$$

$$\delta V_W = \frac{\delta i \cdot n_r a_r}{\sqrt{1 - e_r^2}} \cdot \frac{1 + e_r \cos f}{\cos(w + f)} \quad (5)$$

$$\delta V_d = \sqrt{\delta V_T^2 + \delta V_R^2 + \delta V_W^2}. \quad (6)$$

Cladistics offers a fundamental advantage over this primarily dynamics based clustering, via the incorporation of unknown values. Classical multivariate hierarchical clustering (Zappala et al. 1990) requires the use of a complete data set, and as such a choice is required. The parameters are either restricted to only known dynamical elements, or the data set is reduced to well studied objects. Cladistical analysis can incorporate objects with large amounts of unknown information, originally fossil organisms (Cobbett et al. 2007), without a reduction in the number of parameters.

2.2. Characteristics

We define 38 characteristics that can be broken into three broad categories: orbital, physical, and compositional parameters. All numerical states are considered to have equal weight. The discrete character sets are unordered. Any continuous characteristics are broken into bins, as cladistical analysis requires discrete characteristics. We developed a Python program to establish the binning of continuous characteristics. The pandas Cut module (McKinney 2010) is used to create the bins. Characteristics are binned independent of each other and for each of the Jovian and Saturnian systems.

The aforementioned Python program iterates the number of bins until a linear regression model between binned and unbinned sets achieves a coefficient of determination (r^2) score of >0.99 . This is calculated using the stats package in SciPy (Jones et al. 2001). Thus each character set will have a different number of bins, r^2 score, and delimiters. All characteristics are binned in a linear fashion, with the majority increasing in progression. The exception to the linear increase is the density character set, with a reversed profile. All of the continuous, binned characteristic sets are ordered, as used by Fraix Burnet et al. (2006). A full list of the characteristics used, the r^2 score for each of the binned characteristics, along with the delimiters are listed in Appendix A.

The first broad category includes the five orbital characteristics (Appendix A.1). This category is composed of two discrete characteristics: presence in orbit around the gas giant and prograde or retrograde orbit. The three remaining characteristics—semimajor axis (a), orbital inclination (i), and eccentricity (e)—are continuous and require binning using the aforementioned Python program.

The second category used to construct the matrix consists of two continuous physical characteristics, density, and visual geometric albedo (Appendix A.2). We chose to not include mass, or any properties related to mass, as characters in the analysis. The inclusion of these characteristics could hide any relationships between a massive object and any daughter objects, as the result of collisions.

The third category describes the discrete compositional characteristics and details the presence or absence of 31 different chemical species (Appendix A.3). In order to account for any positional bias, the fundamental state, solid, liquid, gas, or plasma was not considered. In this analysis, we make no distinction between surface, bulk, and trace compositions. This is to account for the potential of daughter objects to have their bulk composition comprising surface material from the parent. The majority of compounds have absence as a base state (0) and presence as the derived (1). The exceptions are the first three molecules—elemental hydrogen (eH), hydrogen (H_2), and helium (He)—all of which are found in the Sun. As the Sun is the designated outgroup, the base state (0) indicates the presence of these species. With the exception of elemental hydrogen, the remaining single element species are those found in compounds. The spectroscopy of an object often only reports on the presence of an ion, as opposed to a full chemical analysis. As more detailed analysis becomes available, characters may be added to the matrix. Several chemical species are used in this particular matrix that are either not present in any of the satellites or unknown. These are included for future comparisons with other orbital bodies.

2.3. Matrices

The Jovian taxon character matrix holds 68 taxa consisting of the Sun (outgroup), 4 inner satellites, the main ring, 4 Galilean satellites, and 59 irregular satellites. Appendix B (Table 3) contains the matrix, along with the references used in its construction.

The Saturnian matrix, presented in Appendix C (Table 4), is created with 76 taxa. These taxa are the Sun (outgroup), 6 main rings, 9 inner small satellites, 4 minor rings, 8 large icy satellites, 4 Trojan satellites, 3 Alkynoids and their associated rings, and the 38 irregular satellites. The references used in the construction of the Saturnian matrix are located in Appendix C. Both

matrices use the same characteristics, as discussed in Section 2.2, and are available in machine readable format.

3. Results

In this section we present the resulting taxonomic trees from the analysis of the Jovian and Saturnian satellites. The taxonomic trees are used to form the systematic classification of the Jovian (Table 1) and Saturnian (Table 2) satellite systems. Using inverse Gauss equations (Zappala et al. 1990), in a similar method to Nesvorný et al. (2003) and Turrini et al. (2008), we show in Tables 1 and 2 dispersal velocities (δV) for each of the taxonomic groups where a single origin object is hypothesized namely the irregular satellites. For these calculations we assume the largest representative of the cluster as the origin point. See Section 2.1 for further discussion.

3.1. Jovian Taxonomy

The results of the cladistical analysis of the individual Jovian satellites are shown in Figure 1. This 0.5 majority rules consensus tree has a tree length score of 128, with a consistency index of 0.46 and a retention index of 0.85. The low value of the consistency index is possibly due to the mixed use of ordered, multi state, continuous characteristics and bi modal compositional characteristics (Farris 1990). The high retention index suggests that the consensus tree is robust and demonstrates the most likely relationships between the satellites.

As can be seen in the Jovian taxonomic tree in Figure 1, the satellites cluster into clades resembling the taxonomy proposed by Nesvorný et al. (2003) and Sheppard & Jewitt (2003). The irregular satellites are a separate cluster to the prograde regular satellites.

We maintain the closest family to Jupiter, the Amalthea family, as a valid taxonomic cluster. The dispersal velocity is very large and may suggest that the Amalthea family did not form from a single object. This family, along with Jupiter’s main ring, is associated with the well known Galilean family.

In the analysis, we maintain the “irregular” satellite group. The Himalia family clusters with the retrograde satellites, separate to the other prograde satellites. The Himalia family has relatively low inclinations in comparison with the Jovian retrograde satellites, and their high eccentricity could be explained by disruptions (Christou 2005). The small satellites Themisto and Carpo cluster together with the other prograde satellites in the Himalia family. We propose that Themisto and Carpo be included in the Himalia family, as they are the sole members of the groups proposed by Sheppard & Jewitt (2003), and show similar orbital characteristics. The large mean dispersal velocity calculated for the Himalia family (see Table 1) was also noticed by Nesvorný et al. (2003) for the Prograde satellites. The large mean dispersal velocity is due to the dispersal velocities of Themisto and Carpo. Without including these members, the mean dispersal velocity for the classical Himalia family is $154.6 \pm 72.5 \text{ m s}^{-1}$, close to the escape velocity of Himalia (121.14 m s^{-1}). This dispersal velocity of the classical Himalia family was explained via gravitational scattering from Himalia by Christou (2005). Disruption and scattering could also be used to explain the large dispersal velocities of Themisto and Carpo, though further modeling is required.

The term “irregular” is maintained through the retrograde family for consistency with the literature (Nesvorný et al. 2003, 2004; Sheppard & Jewitt 2003; Beaugé & Nesvorný 2007;

Jewitt & Haghighipour 2007). The retrograde irregular satellites are a separate but related cluster to the Himalia, prograde irregulars. The broad classifications introduced by Sheppard & Jewitt (2003) and Nesvorný et al. (2003) are preserved, though the Ananke/Carme family is unresolved and may be split into subfamilies. Separating out the traditional families (Nesvorný et al. 2003; Sheppard & Jewitt 2003; see colors in Figure 1) gives smaller dispersal velocities. The traditional Ananke (escape velocity (eV) 23.10 m s^{-1}) family has a δV of $61.0 \pm 45.6 \text{ m s}^{-1}$, traditional Carme (eV 29.83 m s^{-1}) has $36.2 \pm 13.1 \text{ m s}^{-1}$, and a created Sinope (eV 27.62 m s^{-1}) family has $323.9 \pm 97.3 \text{ m s}^{-1}$. These are smaller than the δV of our unresolved Ananke/Carme Family ($457.2 \pm 445.7 \text{ m s}^{-1}$; see Table 1). Nesvorný et al. (2003) used similar small δV values to establish the Ananke and Carme dynamical families. The dynamical situation could be explained through a more recent capture and breakup event for Ananke, Carme, and Sinope that disrupted the ancestral irregular satellites. The identified Iocaste and Pasiphae families also have large dispersal velocities, suggestive of disruptions. Following the nomenclature of Sheppard & Jewitt (2003), each of the families and subfamilies are represented by the name of the largest contained satellite. Satellites within families are related by their retrograde orbit, high inclinations, and eccentricities. In addition to their linked orbital characteristics, the satellites of the retrograde irregular group all show a low albedo (Beaugé & Nesvorný 2007).

The Ananke subfamily is tightly constrained in its orbital characteristics, with a small dispersal velocity. While the characteristics listed in Table 1 would preclude them from being included in the Pasiphae family, their clustering around a common semimajor axis, inclination, and eccentricity suggest that they are a distinct young dynamical family. The members we include in the Ananke family for this analysis are all historical members of the family (Jewitt & Haghighipour 2007). Some of the satellites that have been historically included in the Ananke family (Jewitt & Haghighipour 2007) are moved to other families. We do not add any new satellites to this family.

The orbital characteristics of the Carme subfamily are tightly constrained. Satellites in this family orbit further from Jupiter, with higher orbital inclinations, but similar eccentricities to the Ananke family. As with the Ananke family, it is the highly constrained orbital characteristics and low mean dispersal velocity that justify the classification of this traditional family (Jewitt & Haghighipour 2007). According to the tree presented in Figure 1, there is a continuum between the Ananke and Carme families. However, differences in orbital characteristics, broken down in Table 1, distinguish both of these families from each other.

A new cluster, the Iocaste family, is defined as shown in Figure 1 and Table 1. The semimajor axis of this family spans most of the orbital space where irregular satellites have been discovered. The lower eccentricities and albedo are used to separate this family from the Pasiphae family. As with the Pasiphae family, the Iocaste family has a high mean dispersal velocity (510.2 ± 303.3 compared with a escape velocity of 3.16 m s^{-1}), suggestive of disruptions taking place at some point since the breakup of the original object (Christou 2005). Iocaste, being the largest member of this family, is proposed as the representative object. Also included are several members that have been previously included in other families (Jewitt & Haghighipour 2007), along with new unnamed satellites. For full details on included satellites and the descriptive properties of the family, see Table 1.

Table 1
Jovian Satellite Systematic Classification

Taxonomy	Members	Orbit	Semimajor Axis (km)	Inclination	Eccentricity	Density (kg m ⁻³)	Albedo	Composition	Velocity (δV) (m s ⁻¹)	References
Amalthea family	Thebe, Amalthea, Metis, and Adrastea	Prograde	$<3.0 \times 10^5$	$<0^\circ 02$	$<2^\circ$	<900	<0.1	Predominately water ice and silicates	3570.4 ± 491.8	1
Galilean family	Io, Ganymede, Europa, and Callisto	Prograde	4.0×10^5 – 2.0×10^6	$<0^\circ 5$	<0.01	>1800	>0.18	Water ice and silicates dominate; presence of SO ₂ ; other chemical species present.	...	2
Jovian irregular satellite group										
Himalia family	Leda, Elara, Lythea, Himalia, and Themisto	Prograde	7.5×10^6 – 1.8×10^6	25° – 55°	0.1–0.3	...	<0.1	Silicate-based	623.8 ± 750.3	3, 4
Ananke/Carme family	S/2003 J3, S/2003 J9, Ananke subfamily, Carme subfamily, and Sinope subfamily	Retrograde	1.88×10^7 – 2.5×10^7	143° – 166°	0.2–0.4	...	<0.07	...	457.2 ± 445.7	3, 4
Ananke subfamily	Euanthe, Thyone, Mneme, Harpalyke, Praxidike, Thelxinoe, and Ananke	Retrograde	2.0×10^7 – 2.15×10^7	145° – 152°	0.2–0.25	...	<0.07	...	61.0 ± 45.6	3, 4
Carme subfamily	Arche, Pasithee, Chaldene, Isonoe, Kale, Aitne, Erinome, Taygete, Carme, Kalyke, Eukelade, and Kallichore	Retrograde	2.2×10^7 – 2.4×10^7	164° – 166°	0.24–0.27	...	<0.07	...	36.1 ± 13.1	3, 4
Sinope subfamily	Eurydome, Autonoe, Sinope, and Callirrhoe	Retrograde	2.2×10^7 – 2.42×10^7	147° – 159°	0.27–0.35	...	<0.06	...	323.9 ± 97.3	
Iocaste family	Euporie, S/2003 J18, Hermippe, Helike, Iocaste, S/2003 J15, Herse, S/2003 J4, Aoede, S/2003 J5, and S/2003 J10	Retrograde	1.9×10^7 – 2.5×10^7	140° – 165°	0.1–0.45	...	<0.05	...	510.2 ± 303.3	
Pasiphae family	S/2003 J12, S/2011 J1, S/2010 J2, S/2003 J19, S/2010 J1, S/2011 J2, Sponde, Pasiphae, Megaclite, Hegemone, S/2003 J23, Cyllene, Kore, and S/2003 J2	Retrograde	1.9×10^7 – 2.9×10^7	145° – 164°	0.30–0.421	...	<0.1	...	412.3 ± 224.5	3, 4

References. (1) Barnard (1892), (2) Galilei (1610), (3) Nesvorný et al. (2003), (4) Sheppard & Jewitt (2003).

Table 2
Saturnian Satellite Systematic Classification

Taxonomy	Members	Orbit	Semimajor Axis (km)	Inclination	Eccentricity	Density (kg m ⁻³)	Albedo	Composition	Velocity (δV) (m s ⁻¹)	References
Saturnian inner system group, main ring and icy satellites	Atlas, Janus, Epimetheus, Prometheus, Janus/Epimetheus ring, G-ring, D-ring, Pan, Aegaeon, S/2009 S1, F-ring, B-ring, Cassini division, C-ring, Daphnis and A-ring. Possible members: Telesto, Calypso, Methone ring arc, Anthe ring arc, Pallene ring arc, Methone, Anthe, Pallene, Polydeuces Mimas, Tethys, Enceladus family, Hyperion, Titan, and Iapetus; see Section 3.2 for discussion.	Prograde	$<4.0 \times 10^6$	$<15^\circ$	<0.03	550–1900	0.1–1	Composition of water ice with silicates and presence of CO ₂ . Other chemical species may be present.	...	1, 2
Enceladus family	E-ring, Enceladus, Rhea, Dione, and Helene	Prograde	1.8×10^5 – 5.3×10^5	$<0.5^\circ$	0	1200–1700	>0.7	Complex composition, predominately water ice and silicates, with hydrocarbons and CO ₂ present	...	
∞ Saturnian irregular satellite group										
Albiorix family	Bebhionn, Erriapus, Albiorix, and Tarvos	Prograde	1.6×10^7 – 1.8×10^7	30° – 40°	0.4–0.6	...	<0.1	...	80.9 ± 1.6	3, 4, 5
Siamaq family	Tarqeq, Kiviuq, Ijiraq, Paaliaq, and Siamaq	Prograde	1.1×10^7 – 1.9×10^7	40° – 50°	0.1–0.4	...	<0.1	...	266.8 ± 60.0	3, 4, 5
Phoebe family	Phoebe ring, Phoebe, Fenrir, Loge, Aegir subfamily, and Ymir subfamily	Retrograde	1.1×10^7 – 2.51×10^7	$>145^\circ$	>0.1	...	<0.1	...	763.3 ± 259.0	3, 4, 5
Aegir subfamily	S/2007 S2, Mundilfari, Jarnsaxa, S/2006 S1, Bergelmir, Suttungr, Farbauti, S/2007 S3, Aegir, and Fornjot	Retrograde	1.6×10^7 – 2.51×10^7	$>150^\circ$	0.1–0.25	295.1 ± 125.0	5
Ymir subfamily	Skathi, Skoll, Greip, Hyrrokkin, S/2004 S13, S/2004 S17, Narvi, S/2004 S12, S/2004 S07, Hati, Bestla, Thrymr, S/2006 S3, Kari, Surtur, and Ymir	Retrograde	1.55×10^7 – 2.30×10^7	$>145^\circ$	0.25–0.6	...	<0.1	...	497.5 ± 247.7	5

References. (1) Huygens (1659), (2) Cassini (1673, 1686), (3) Nesvorný et al. (2003), (4) Sheppard & Jewitt (2003), (5) Turrini et al. (2008).

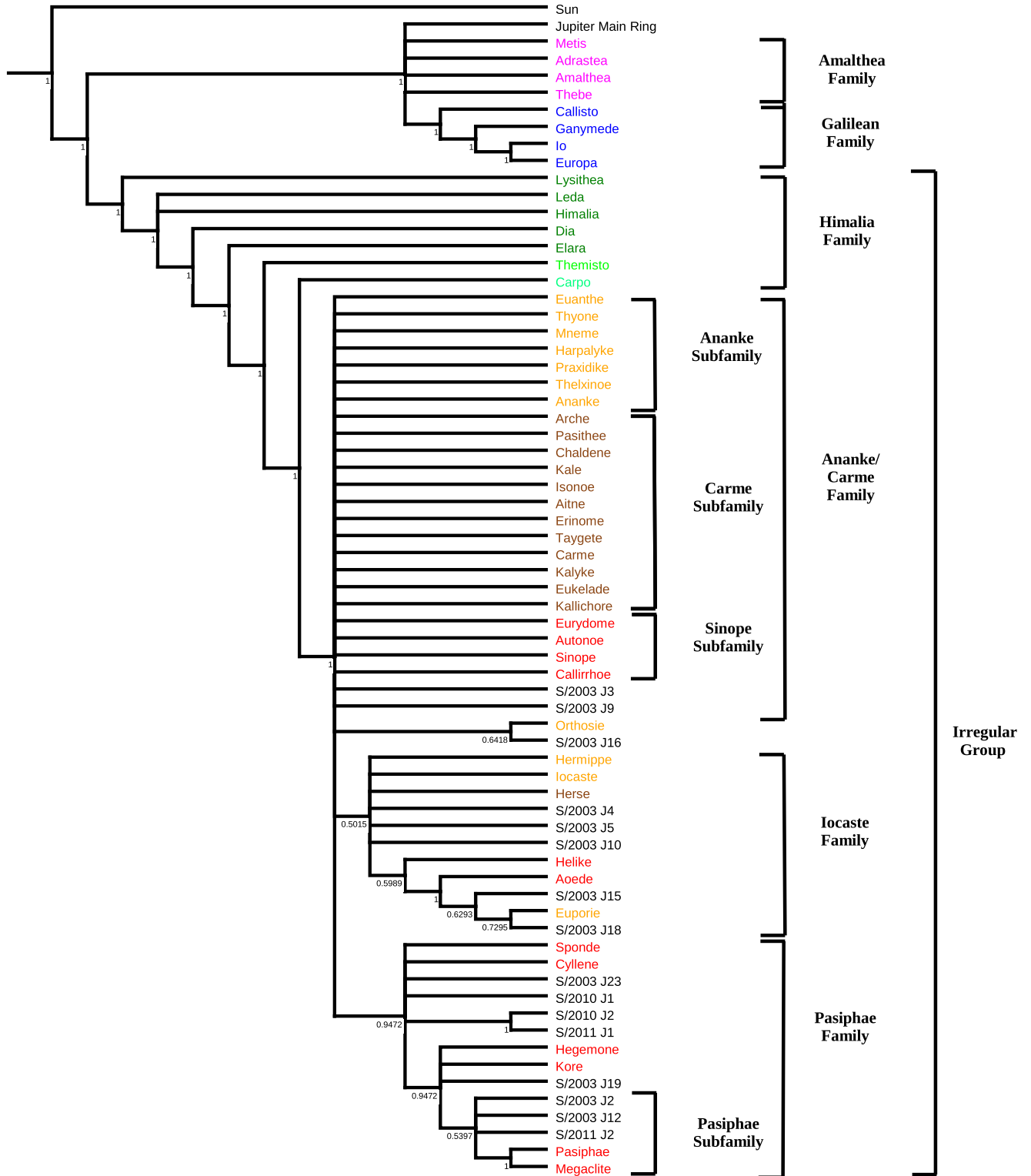


Figure 1. Majority consensus taxonomic tree of objects in the Jovian system. This tree has a tree length score of 128, with a consistency index of 0.46 and a retention index of 0.85. Numbers indicate the frequency of the node in the 10,000 most parsimonious tree block. Colors represent the terminology used in traditional classification: Amalthea inner regular family, Galilean family, Themisto prograde irregular, Himalia prograde irregular family, Carpo prograde irregular, Ananke irregular family, Carme irregular family, Pasiphae irregular group, and unnamed and unclassified. Proposed groups and families are shown on the right.

The Pasiphae family shows a broad range of orbital characteristics that, along with the large dispersal velocity (412.3 ± 224.5 compared with an escape velocity of 47.16 m s^{-1}), are suggestive of disruptions during the family's

lifetime (Christou 2005). The Pasiphae family has a broad range of semimajor axes and inclinations, with the Pasiphae family orbiting further from Jupiter and having larger eccentricities on average than the new Iocaste family (see

Table 1). A Pasiphae subfamily (see Figure 1), with a δV of $230.1 \pm 174.3 \text{ m s}^{-1}$, can be identified. This may imply a secondary, more recent breakup from Pasiphae. In addition, many of the unnamed satellites from recent observations (Gladman et al. 2003a, 2003b; Sheppard et al. 2003b, 2003a, 2004; Sheppard & Marsden 2003a, 2003b, 2004; Jacobson et al. 2011; Sheppard & Williams 2012) are associated with this family; see Table 1 and Figure 1 for a complete list.

3.2. Saturnian Taxonomy

Cladistical analysis of the Saturnian system yields the 0.5 majority rules consensus tree (Figure 2), constructed from the 10,000 parsimonious trees, with a tree length score of 186. The tree has a consistency index of 0.30 and a retention index of 0.81. The consistency index of the Saturnian tree is lower than that of the Jovian tree, though this could be due to the number of taxa used (Sanderson & Donoghue 1989). As with the Jovian tree, this low consistency index could be due to the mixed character states. This effect is to be explored further in a future paper. The high retention index indicates that the tree is suggestive of the true relationships (Farris 1989).

The tree shown in Figure 2 highlights the diversity of structures found in the orbit of Saturn. Satellites cluster into two main groupings around Saturn: the Inner group, comprised of rings and icy satellites, and the Irregular satellite group (see Table 2 for members and diagnostic properties of each clade). While the traditional classification nomenclature (Nesvorný et al. 2003; Sheppard & Jewitt 2003; Jewitt & Haghighipour 2007) is broadly conserved, several discrepancies require discussion. Table 2 shows our new taxonomy, along with included members of the families and their descriptive properties.

The Main ring and Icy satellite group form an unresolved, inner system group. This group includes the Saturnian ring system, the Alkynoids and their associated ring arcs, as well as the larger Icy satellites and their Trojans. We have confirmed the recently discovered S/2009 S1 (Spitale & Tiscareno 2012) is part of this group due to its orbital characteristics. Within this large group, there is the resolved Enceladus family.

Our results suggest the traditionally classified Alkyonides, Methone, Anthe, and Pallene, along with their associated rings, are not clustered with the the Enceladus family, as would be expected by their orbital location, between Mimas and Enceladus, within the E ring. Due to their bulk water ice composition, the Alkyonides associate with the Main ring objects (see Figure 2). The low density and mid range albedo of Pallene and Methone (Hedman et al. 2009) suggest that the association with the Main ring group is genuine. The dynamic resonances of both Methone and Anthe (Callegari & Yokoyama 2010) imply that these objects were captured, rather than forming in situ. As there is very little known about the composition of these objects, beyond their bulk water ice composition (Hedman et al. 2009), further study and dynamical modeling of the capture process is required to resolve their true origins.

Like the Alkynoids, the Trojan satellites of Tethys, Calypso, and Telesto also form an association with the main rings. The reason for this could be that Calypso and Telesto, like the Alkynoids, are also possible captured main ring objects. The capture dynamics could be similar to that of the Jovian Trojan asteroids (Morbidelli et al. 2005; Lykawka & Horner 2010; Nesvorný et al. 2013). Both the Tethys Trojans (Buratti et al. 2010) and main ring objects are chiefly composed of water ice,

implying a common origin. The bulk composition of Tethys is also prominently water ice (Buratti et al. 2010), with a very small fraction of silicates. Trojans may instead have formed from the same material as Tethys itself, either during accretion (Charnoz et al. 2011) or in the same orbit from a large debris disk (Canup 2010). As Tethys is also in the unresolved Main ring and Satellite group, we cannot differentiate between the two scenarios. Further compositional information about the Tethys Trojans could shed light on this issue. Polydeuces, a Trojan of Dione, also forms an association with the Main ring group in our analysis. This could be due to overemphasis on orbital and physical characteristics, since the bulk composition of Polydeuces is unknown (Thomas et al. 2013). Helene, the more well studied Trojan of Dione (Thomas et al. 2013), is well within the Enceladus Family. Helene and Dione are closely associated in our analysis, implying that Helene is a daughter object of Dione.

The outer icy satellites, Titan, Hyperion, and Iapetus, do not form a single cluster, and are therefore not considered a valid taxonomic group. They are associated with the Main ring and Icy satellite group. The Enceladus family is formed by the known association of the E ring, Enceladus, and Icy satellites (Verbiscer et al. 2007), which is mainly due to the detection of volatile chemicals, such as NH_3 , CH_4 , and other hydrocarbons. Plumes from Enceladus containing these chemicals (Porco et al. 2006), thought to be representative of the subcrust ocean (Porco et al. 2006), are the source of the E ring (Spahn et al. 2006). Titan itself also has an abundance of these volatiles (Hirtzig et al. 2013), implying a possible association between the Icy satellites of Saturn that remains unresolved in our analysis. Material from the outer satellites, particularly Pheobe and its associated ring (Tosi et al. 2010; Tamayo et al. 2011), is thought to play a role in the observed hemispherical dichotomy on Iapetus (Tosi et al. 2010). In Figure 2, Iapetus is unresolved in the Main ring and Icy satellite group.

The irregular satellites form a major cluster with each other separate from the inner Saturnian system, and are therefore collected under the Irregular satellite group. Along with their high inclinations, eccentricities, and semimajor axes, the Irregular satellite group is characterized by a dark albedo, comparative to the other objects in the Saturnian system. We follow the naming convention introduced with the Jovian satellites (Section 3.1), where each irregular satellite family is represented by the largest member (Jewitt & Haghighipour 2007). We therefore rename the classical Inuit group (Blunck 2010) as the Siarnaq family and the Gallic group (Blunck 2010) as the Albiorix family. Though this does change the formal name of the clusters, we encourage the discoverers of the unnamed satellites (Gladman et al. 2001; Sheppard et al. 2003a, 2006b, 2007; Jewitt et al. 2005) and any future discoveries that are placed in these groups, to follow IAU convention and use names from Inuit and Gallic mythology for satellites in the Siarnaq and Albiorix families, respectively. As in Turrini et al. (2008), the Albiorix family is distinct and has a low mean dispersal velocity (δV). The Siarnaq family has a higher δV , again suggestive of disruptions (Christou 2005). The mean δV of all prograde satellites is $364.8 \pm 114.9 \text{ m s}^{-1}$, only slightly higher than that of the Siarnaq family (Turrini et al. 2008). This could imply a disruption scenario, with a more recent capture of the Albiorix family parent body disrupting the older Siarnaq family. Our cladistical analysis supports this scenario, as the Siarnaq family shows a more branching structure than the Albiorix family. Further compositional information about these bodies, as well as dynamical modeling, could resolve this complex situation. In our

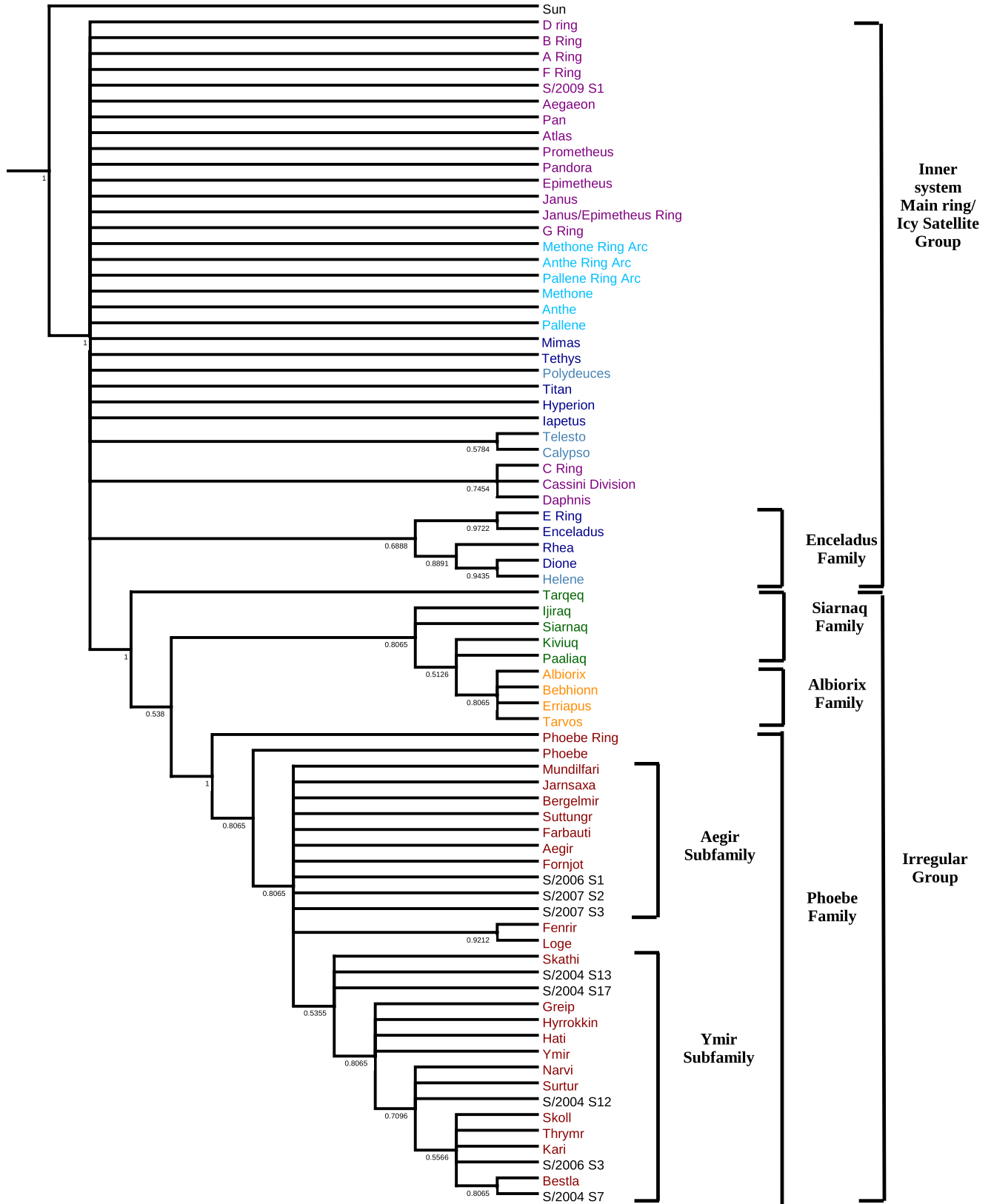


Figure 2. Majority Consensus taxonomic tree of objects in the Saturnian system. The tree has a consistency index of 0.30 and a retention index of 0.81. Numbers indicate frequency of the node in the 10,000 most parsimonious tree block. Colors represent terminology used in classical classification: the main ring group, with associated shepherd satellites; mid sized icy satellites and Titan; Trojan satellites; alkanoids and associated rings; “Inuit” prograde irregular family; “Gallic” prograde irregular family; “Norse” retrograde irregular family; and unnamed and unclassified. Proposed groups and families are shown to the right.

analysis, we separate out the retrograde irregular satellites, including Phoebe, from the prograde irregular satellites. In previous taxonomy, this group has been classified as the “Norse” group (Blunck 2010). In our revised nomenclature, this group should be termed the Phoebe family. We further separate out two clades, distinct from Phoebe and its associated ring. The first clade, the unresolved Aegir subfamily (previously identified as the S/2004 S10 group in Turrini et al. 2008), is characterized as having, on average, orbits further from Saturn, with low eccentricities and higher inclinations. The second clade is the Ymir subfamily and is categorized, on average, by being closer to Saturn, but with high eccentricities. This subfamily shows a branching structure and may be further split (Grav & Bauer 2007). This family was also identified by Turrini et al. (2008). We identify an association between Fenrir and Loge, with a low dispersal velocity ($\delta V = 114.4 \text{ m s}^{-1}$), suggestive of a recent breakup. The high dispersal velocity (δV) of the Phoebe family is due to the selection of Phoebe as a reference point. If Phoebe and the associated ring are removed from the family, and Ymir (with an escape velocity of 8.56 m s^{-1}) is selected as the reference object, the δV is halved from $763.3 \pm 259.0 \text{ m s}^{-1}$ to $439.9 \pm 215.1 \text{ m s}^{-1}$. The satellite with the lowest δV to Phoebe is S/2007 S2, with $\delta V = 248.0 \text{ m s}^{-1}$, still significantly larger than the escape velocity of Phoebe (100.8 m s^{-1}). Turrini et al. (2008) also found a dynamical separation between Phoebe and the other retrograde satellites. This is supportive of the narrative that Phoebe has a different origin than the other retrograde irregular satellites of Saturn (Turrini et al. 2008). The high δV among all the subfamilies shows that a complex dynamical situation is present in the Saturnian irregular satellites. Phoebe has been shown to clear its orbital parameter space (Turrini et al. 2008), which could have had a major disruptive effect on those remaining satellites (Turrini et al. 2008). The similarities between our analysis and that of Turrini et al. (2008) further validate cladistics as a method suitable for applications in Solar system astronomy. The addition of detailed compositional information from the other irregular satellites to an updated cladistical analysis could solve some of the minor discrepancies found between this analysis and that of Turrini et al. (2008).

We assign the currently unnamed irregular satellites to each of the subfamilies. S/2006 S1, S/2007 S2, and S/2007 S3 are part of the Aegir subfamily. We include S/2004 S13, S/2004 S17, S/2004 S12, S/2006 S3, and S/2007 S7 in the Ymir subfamily. See Table 2 for a full list of members in each subfamily. As with the Albiorix and Siarnaq families, we encourage discoverers of new satellites that fall within the Phoebe family to follow the Norse mythological naming convention as set by the IAU.

4. Discussion

In this study we have shown, using the Jovian and Saturnian satellite systems, that cladistics can be used in a planetary science context. We have ensured that the technique is objective by statistically creating bins for characteristics that are continuous in nature (see Section 2.2). By thus ensuring the objectivity of our analysis, we increase the confidence that cladistics is a valid technique that can be applied in the planetary sciences. Our results largely support the traditional classifications used in both the Jovian and Saturnian systems. However, the power of cladistics is shown in the ease of classifying new satellites, as well as identifying substructures within larger clusters. Cladistics also offers a method of analysis where limited information is available.

In our study we have examined well studied satellites, as well as those where only dynamical information is available. In traditional methods of analysis, either only dynamical information is considered, or the data set is truncated in favor of more well studied bodies. Cladistics offers a method that can incorporate as much information about an object as is available, while accounting for any unknown characteristics. As more detailed information becomes available, either of known or newly discovered satellites, cladistics offers a systematic method for inclusion or revision of the classification system.

The relationships that we noted between the satellites suggest common formation scenarios within the clusters. The prograde, inner families of Jupiter are the products of accretion from a circumplanetary disk (Canup & Ward 2002). The association of the Amalthea and Galilean families, along with the Main ring of Jupiter, in our analysis supports this hypothesis. Clustering of the Himalia family with other “irregular” satellites implies a capture scenario. The prograde nature of the Himalia family is possibly explained via a nebula drag capture mechanism (Ćuk & Burns 2004). Further modeling of the Himalia family is required to ascertain their true origins, particularly in light of the Jovian pebble formation hypothesis that may not include an extended nebula (Levison et al. 2015).

With the proposal that Sinope forms its own subfamily, each Jovian irregular satellite subfamily contains only a single large satellite. This strengthens the hypothesis that each of the families represents a capture event and subsequent breakup (Nesvorný et al. 2007) of an object external to the Jovian system. Two of the subfamilies, the Pasiphae and Sinope subfamilies, show a broad range of orbital characteristics and larger dispersal velocities. The other two, the Ananke and Carme subfamilies, show much more constrained characteristics and smaller dispersal velocities. This dichotomy between the two types of subfamilies, broad versus constrained, could imply at least two capture events, with the earlier Pasiphae and Sinope families being disrupted by later Ananke and Carme captures. The Iocaste family does not contain a large progenitor satellite, but has high dispersal velocities. This is suggestive of a possible ejection scenario. An alternative hypothesis is that the capture events happen simultaneously, but there were multiple disruption events. Both scenarios are supported by the dichotomy in dispersal velocities. Future analysis and simulations into the origins of the irregular satellites could help determine which theory is more probable.

As with the Jovian satellites, there are multiple origins for the origin of the Saturnian rings and satellites. The results from our analysis support a growing body of work showing the complexity of formation scenarios in the Saturnian system. The rings themselves possibly formed after the breakup of an inner icy satellite (Canup 2010).

The unresolved nature of the inner Saturnian system shows a complexity of formation scenarios. The main ring satellites, along with the Alkyonides and Tethys Trojans, possibly formed via accretion from the current ring system (Charnoz et al. 2010). The Alkyonides and Tethys Trojans are then secondarily captured in their current orbits. The major icy satellites, those in the E ring and outer satellites, probably formed in an accretion scenario, with delivery of the silicate from the outer system (Salmon & Canup 2017). Titan could be secondarily derived from multiple subsatellites that formed in the same disk (Asphaug & Reufer 2013). The volatiles are delivered from comets, with at least one, Phoebe, being captured in orbit. The size of Phoebe is not

traditionally associated with comet nuclei, but at least one comet, C/2002 VQ94, with a similar 100 km diameter has been observed (Korsun et al. 2014). The irregular satellite families and subfamilies form from collisional breakup events (Nesvorný et al. 2004) resulting from the captured comet nuclei. The large dispersal velocities of the subfamilies imply that this capture and disruption process is complex and requires detailed modeling.

We have shown that cladistics can be used in the classification of the Jovian and Saturnian satellite systems. Consequently, several related studies may be attempted in the future. Uranus and Neptune have similarly complex satellite systems as those of Jupiter and Saturn (Jewitt & Haghighipour 2007). These satellite systems could also be classified using cladistics, particularly the irregular satellites. Such a study is hampered by a lack of completeness in the irregular satellite data set (Sheppard et al. 2005, 2006a), but may become practical as observational technology improves and the hypothesized small irregular satellites are discovered. Cladistics could be used to further investigate the origins of the irregular satellites of Saturn and Jupiter. As the irregular satellites are thought to be captured bodies (e.g., Nesvorný et al. 2007), the question becomes from which small body population they originated. Comparisons between the well studied irregular satellites and other Solar system bodies could help constrain the origins of these satellites.

5. Conclusions

We have shown that the new application of cladistics on the Jovian and Saturnian satellite systems is valid for investigating the relationships between orbital bodies. In the Jovian system, the traditional classification categories (Nesvorný et al. 2003; Sheppard & Jewitt 2003; Jewitt & Haghighipour 2007) are preserved. We support the hypothesis put forward by Nesvorný et al. (2007) that each Jovian irregular satellite family can be represented by the largest member, and that each family comprises the remnants of a dynamical capture event and subsequent breakup. We can also assign recently discovered, as yet unnamed, satellites to each of their respective Jovian families. Cladistical analysis of the Saturnian system broadly preserves the traditional classifications (Nesvorný et al. 2003; Sheppard & Jewitt 2003; Jewitt & Haghighipour 2007; Turrini et al. 2008), strengthening the validity of the cladistical method. In the Phoebe family of retrograde, irregular satellites, we assign two subfamilies similar to those found by Turrini et al. (2008). We rename the classical

mythological designations for the Saturnian irregular satellites, to represent the largest member of the subfamily, in order to be consistent with the Jovian naming convention. Newly discovered, unnamed Saturnian satellites are easily assigned to various subfamilies. Through the application of the technique to the Jovian and Saturnian systems, we show that cladistics can be used as a valuable tool in a planetary science context, providing a systematic method for future classification.

This research was in part supported by the University of Southern Queensland's Strategic Research Initiative program. We wish to thank an anonymous reviewer for his/her comments, particularly on Multivariate Hierarchical Clustering. The AAS Statistics Reviewer provided valuable feedback on the methodology. Dr. Guido Grimm assisted with the cladistical methodology and terminology used in this paper. Dr. Pablo Goloboff provided assistance with TNT, which is subsidized by the Willi Hennig Society, as well as additional comments on the methodology. We would like to thank Dr. Henry Throop for discussions regarding the Ring systems.

Software: Mesquite 3.10 (Maddison & Maddison 2017), Python 3.5, Spyder 2.3.8 (Spyder Development Team 2015), Anaconda Python distribution package 2.40 (Continuum Analytics 2016), pandas Python package (McKinney 2010), SciPy Python package (Jones et al. 2001), TexMaker 4.1.1, Tree analysis using New Technology (TNT) 1.5 (Goloboff et al. 2008; Goloboff & Catalano 2016), Zephyr 1.1: Mesquite package (Maddison & Maddison 2015).

Appendix A List of Characteristics

Below you will find a list of characters used in the creation of the Jovian (Appendix B) and Saturnian (Appendix C) satellite matrices. See Section 2.2 for a full discussion.

A.1. Orbital Characteristics

1. In orbit around the gas giant (Orb): no (0); yes (1)
2. Revolution (Rev): Prograde revolution(0); Retrograde revolution (1)
3. Semimajor axis(a):
 - (i) Jovian: $r^2:0.990$ Bin delimiters 0 km (0); 3.67892625×10^6 km (1); 7.2348525×10^6 km (2); 1.079077875×10^7 km (3); 1.4346705×10^7 km (4);

- 1.790263125 $\times 10^7$ km (5); 2.14585575 $\times 10^7$ km (6);
2.501448375 $\times 10^7$ km (7)
- (ii) Saturnian: r^2 :0.991 Bin delimiters: 0 km (0);
3.644200 $\times 10^6$ km (1); 7.221500 $\times 10^6$ km (2);
1.0798800 $\times 10^7$ km (3); 1.4376100 $\times 10^7$ km (4);
1.7953400 $\times 10^7$ km (5); 2.1530700 $\times 10^7$ km (5)
4. Orbital inclination to the plane(i):
- (i) Jovian: r^2 :0.990 Bin delimiters: 0° (0); 16°55 (1);
33°1 (2); 49°65 (3); 66°2 (4); 82°75 (5); 99°3 (6);
115°85 (7); 132°4 (8); 148°95 (9)
- (ii) Saturnian: r^2 :0.993 Bin delimiters: 0° (0); 29°97 (1);
59°93 (2); 89°9 (3); 119°87 (4); 149°83 (5)
5. Orbital eccentricity(e):
- (i) Jovian: r^2 :0.99 Bin delimiters: 0(0); 0.036 (1); 0.072
(2); 0.108 (3); 0.144 (4); 0.18 (5); 0.216 (6); 0.252 (7);
0.288 (8); 0.324 (9); 0.36 (10); 0.396 (11)
- (ii) Saturnian: r^2 :0.993 Bin delimiters: 0 (0); 0.064 (1);
0.129 (2); 0.193 (3); 0.258 (4); 0.322 (5); 0.387 (6);
0.451 (7); 0.515 (8); 0.58 (9)

A.2. Physical Characteristics

1. Density:
- (i) Jovian: r^2 :0.996 Bin delimiters: 3084.5 kg m⁻³ (0);
2639 kg m⁻³ (1); 2193.5 kg m⁻³ (2); 1748 kg m⁻³ (3);
1302.5 kg m⁻³ (4); 854.3 kg m⁻³ (5)
- (ii) Saturnian: r^2 :99.2 Bin delimiters: 1880 kg m⁻³ (0);
1713.6 kg m⁻³ (1); 1547.3 kg m⁻³ (2); 1380.9 kg m⁻³
(3); 1214.5 kg m⁻³ (4); 1048.2 kg m⁻³ (5); 881.8 kg m⁻³
(6); 715.4 kg m⁻³ (7); 549.1 kg m⁻³ (8); 382.7 kg m⁻³
(9); 216.3 kg m⁻³ (10); 48.2 kg m⁻³ (11)
2. Visual geometric albedo:
- (i) Jovian: r^2 :0.991 Bin delimiters: 0 (0); 0.09 (1); 0.16
(2); 0.24 (3); 0.31 (4); 0.38 (5); 0.46 (6); 0.53 (7); 0.60
(8); 0.68 (9)
- (ii) Saturnian: r^2 :0.991 Bin delimiters: 0 (0); 0.13 (1);
0.26 (2); 0.38 (3); 0.51 (4); 0.63 (5); 0.75 (6); 0.87 (7)

A.3. Compositional Characteristics

1. Elemental Hydrogen (eH) Presence (0); Absence (1)
2. Hydrogen (H₂) Presence (0); Absence (1)
3. Helium (He) Presence (0); Absence (1)
4. Oxygen (O₂) Absence (0); Presence (1)
5. Ozone (O₃) Absence (0); Presence (1)
6. Sodium (Na) Absence (0); Presence (1)
7. Potassium (K) Absence (0); Presence (1)
8. Carbon dioxide (CO₂) Absence (0); Presence (1)
9. Nitrogen (N₂) Absence (0); Presence (1)
10. Sulphur dioxide (SO₂) Absence (0); Presence (1)
11. Argon (Ar) Absence (0); Presence (1)
12. Water (H₂O) Absence (0); Presence (1)
13. Carbon monoxide (CO) Absence (0); Presence (1)
14. Neon (Ne) Absence (0); Presence (1)
15. Nitrogen oxide (NO) Absence (0); Presence (1)
16. Methane (CH₄) Absence (0); Presence (1)
17. Sulphuric acid (H₂SO₄) Absence (0); Presence (1)
18. Iron (Fe) Absence (0); Presence (1)
19. Nickel (Ni) Absence (0); Presence (1)
20. Iron sulphide (FeS) Absence (0); Presence (1)
21. Iron oxide (FeO) Absence (0); Presence (1)
22. Silicone oxide (SiO) Absence (0); Presence (1)
23. Magnesium oxide (MgO) Absence (0); Presence (1)
24. Basalt (Bas) Absence (0); Presence (1)
25. Sulphur (S) Absence (0); Presence (1)
26. Silicates (Sil) Absence (0); Presence (1)
27. Carbonates (Carb) Absence (0); Presence (1)
28. Ammonia (NH₄) Absence (0); Presence (1)
29. Hydrocarbons (HyCarb) Absence (0); Presence (1)
30. Hydrogen peroxide (H₂O₂) Absence (0); Presence (1)
31. Tholins (Thol) Absence (0); Presence (1)

Appendix B Jovian Satellite Matrix

Here, Table 3 contains the Taxon character matrix used in the cladistical analysis of the Jovian satellite system.

Table 3
(Continued)

Identifier	Orb	Rev	a	i	e	D	Alb	eH	H ₂	He	O ₂	O ₃	Na	K	CO ₂	N ₂	SO ₂	Ar	H ₂ O	CO	Ne	NO	CH ₄	H ₂ SO ₄	Fe	Ni	FeS	FeO	SiO	MgO	Bas	S	Sil	Carb	NH ₃	HyCarb	H ₂ O ₂	Thol	Reference			
Megaclite	1	1	6	9	11	?	0	1	?	?	?	?	?	?	?	?	?	?	?	?	?	?	?	?	?	?	?	?	?	?	?	?	?	?	?	?	?	?	?	?	16, 17, 18	
Sinope	1	1	6	9	6	?	0	1	1	1	0	0	0	0	0	0	0	0	0	0	0	0	0	0	0	0	0	0	0	0	0	0	0	0	1	1	0	0	0	0	16, 17, 18, 19, 21	
Hegemone	1	1	6	9	9	?	?	1	?	?	?	?	?	?	?	?	?	?	?	?	?	?	?	?	?	?	?	?	?	?	?	?	?	?	?	?	?	?	?	?	16	
Aoede	1	1	6	9	1	?	?	1	?	?	?	?	?	?	?	?	?	?	?	?	?	?	?	?	?	?	?	?	?	?	?	?	?	?	?	?	?	?	?	?	16	
Callirrhoe	1	1	6	8	7	?	0	1	1	1	0	0	0	0	0	0	0	0	0	0	0	0	0	0	0	0	0	0	0	0	0	0	1	1	0	0	0	0	0	16, 17, 18, 19		
Cyllene	1	1	6	9	8	?	?	1	?	?	?	?	?	?	?	?	?	?	?	?	?	?	?	?	?	?	?	?	?	?	?	?	?	?	?	?	?	?	?	?	16	
Kore	1	1	6	8	9	?	?	1	?	?	?	?	?	?	?	?	?	?	?	?	?	?	?	?	?	?	?	?	?	?	?	?	?	?	?	?	?	?	?	?	?	16
S/2003 J2	1	1	7	9	10	?	?	1	?	?	?	?	?	?	?	?	?	?	?	?	?	?	?	?	?	?	?	?	?	?	?	?	?	?	?	?	?	?	?	?	16	
S/2003 J3	1	1	5	8	6	?	?	1	?	?	?	?	?	?	?	?	?	?	?	?	?	?	?	?	?	?	?	?	?	?	?	?	?	?	?	?	?	?	?	?	16	
S/2003 J4	1	1	6	8	5	?	?	1	?	?	?	?	?	?	?	?	?	?	?	?	?	?	?	?	?	?	?	?	?	?	?	?	?	?	?	?	?	?	?	?	16	
S/2003 J5	1	1	6	9	5	?	?	1	?	?	?	?	?	?	?	?	?	?	?	?	?	?	?	?	?	?	?	?	?	?	?	?	?	?	?	?	?	?	?	?	16	
S/2003 J9	1	1	6	9	7	?	?	1	?	?	?	?	?	?	?	?	?	?	?	?	?	?	?	?	?	?	?	?	?	?	?	?	?	?	?	?	?	?	?	?	16	
S/2003 J10	1	1	6	9	5	?	?	1	?	?	?	?	?	?	?	?	?	?	?	?	?	?	?	?	?	?	?	?	?	?	?	?	?	?	?	?	?	?	?	?	16	
S/2003 J12	1	1	5	8	10	?	?	1	?	?	?	?	?	?	?	?	?	?	?	?	?	?	?	?	?	?	?	?	?	?	?	?	?	?	?	?	?	?	?	?	16	
S/2003 J15	1	1	6	8	3	?	?	1	?	?	?	?	?	?	?	?	?	?	?	?	?	?	?	?	?	?	?	?	?	?	?	?	?	?	?	?	?	?	?	?	16	
S/2003 J16	1	1	5	8	7	?	?	1	?	?	?	?	?	?	?	?	?	?	?	?	?	?	?	?	?	?	?	?	?	?	?	?	?	?	?	?	?	?	?	?	16	
S/2003 J18	1	1	5	8	3	?	?	1	?	?	?	?	?	?	?	?	?	?	?	?	?	?	?	?	?	?	?	?	?	?	?	?	?	?	?	?	?	?	?	?	16	
S/2003 J19	1	1	6	9	9	?	?	1	?	?	?	?	?	?	?	?	?	?	?	?	?	?	?	?	?	?	?	?	?	?	?	?	?	?	?	?	?	?	?	?	16	
S/2003 J23	1	1	6	9	8	?	?	1	?	?	?	?	?	?	?	?	?	?	?	?	?	?	?	?	?	?	?	?	?	?	?	?	?	?	?	?	?	?	?	?	16	
S/2010 J1	1	1	6	9	8	?	?	1	?	?	?	?	?	?	?	?	?	?	?	?	?	?	?	?	?	?	?	?	?	?	?	?	?	?	?	?	?	?	?	?	16	
S/2010 J2	1	1	5	9	8	?	?	1	?	?	?	?	?	?	?	?	?	?	?	?	?	?	?	?	?	?	?	?	?	?	?	?	?	?	?	?	?	?	?	?	16	
S/2011 J1	1	1	5	9	8	?	?	1	?	?	?	?	?	?	?	?	?	?	?	?	?	?	?	?	?	?	?	?	?	?	?	?	?	?	?	?	?	?	?	?	16	
S/2011 J2	1	1	6	9	10	?	?	1	?	?	?	?	?	?	?	?	?	?	?	?	?	?	?	?	?	?	?	?	?	?	?	?	?	?	?	?	?	?	?	?	16	

Note. Character abbreviations: in orbit around the gas giant (Orb); revolution (Rev); semimajor axis (a); orbital inclination to the plane (i); orbital eccentricity (e); density (D); visual geometric albedo (Alb); elemental hydrogen (eH); hydrogen (H₂); helium (He); oxygen (O₂); ozone (O₃); sodium (Na); potassium (K); carbon dioxide (CO₂); nitrogen (N₂); sulphur dioxide (SO₂); argon (Ar); water (H₂O); carbon monoxide (CO); neon (Ne); nitrogen oxide (NO); methane (CH₄); sulphuric acid (H₂SO₄); iron (Fe); nickel (Ni); iron sulphide (FeS); iron oxide (FeO); silicone oxide (SiO); magnesium oxide (MgO); basalt (Bas); sulphur (S); silicates (Sil); carbonates (Carb); ammonia (NH₃); hydrocarbons (HyCarb); hydrogen peroxide (H₂O₂); and tholins (Thol). The compositional characters eH, H₂, and He have absence indicated by a 1. In the remainder of compositional characteristics, a 1 is indicative of presence of the chemical species.

References. (1) Lodders (2003), (2) Brooks et al. (2004), (3) Brown et al. (2003), (4) Burns et al. (1999), (5) Krüger et al. (2009), (6) Ockert-Bell et al. (1999), (7) Throop et al. (2004), (8) Wong et al. (2006), (9) Thomas et al. (1998), (10) Cooper et al. (2006), (11) Takato et al. (2004), (12) Dalton et al. (2010), (13) Dalton (2010), (14) Greenberg (2010), (15) Hussmann et al. (2006), (16) Beaugé & Nesvorný (2007), (17) Sheppard & Jewitt (2003), (18) Grav et al. (2003), (19) Grav et al. (2015), (20) Rettig et al. (2001), (21) Sykes et al. (2000), (22) Chamberlain & Brown (2004), (23) Emelyanov (2005).

(This table is available in machine-readable form.)

Table 4
(Continued)

Identifier	Orb.	Rev.	a	i	e	D	Alb	eH	H ₂	He	O ₂	O ₃	Na	K	CO ₂	N ₂	SO ₂	Ar	H ₂ O	CO	Ne	NO	CH ₄	H ₂ SO ₄	Fe	Ni	FeS	FeO	SiO	MgO	Bas	S	Sil	Carb	NH ₃	HyCarb	H ₂ O ₂	Thol	Reference		
Erriapus	1	0	4	1	7	?	0	1	?	?	?	?	?	?	?	?	?	?	?	?	?	?	?	?	?	?	?	?	?	?	?	?	?	?	?	?	?	?	?	24, 25, 27	
Tarvos	1	0	5	1	8	?	0	1	?	?	?	?	?	?	?	?	?	?	?	?	?	?	?	?	?	?	?	?	?	?	?	?	?	?	?	?	?	?	?	24, 25, 27	
Phoebe	1	1	3	5	2	2	0	1	1	1	0	0	0	0	1	0	0	0	1	0	0	0	0	0	0	1	0	0	0	0	0	0	1	0	1	1	0	1	16, 17, 18, 19, 24, 25, 26, 27		
Skathi	1	1	4	5	4	?	0	1	?	?	?	?	?	?	?	?	?	?	?	?	?	?	?	?	?	?	?	?	?	?	?	?	?	?	?	?	?	?	?	24, 25, 27	
Skoll	1	1	4	5	7	?	?	1	?	?	?	?	?	?	?	?	?	?	?	?	?	?	?	?	?	?	?	?	?	?	?	?	?	?	?	?	?	?	?	24	
Greip	1	1	5	5	5	?	?	1	?	?	?	?	?	?	?	?	?	?	?	?	?	?	?	?	?	?	?	?	?	?	?	?	?	?	?	?	?	?	?	24	
Hyrokkin	1	1	5	5	5	?	?	1	?	?	?	?	?	?	?	?	?	?	?	?	?	?	?	?	?	?	?	?	?	?	?	?	?	?	?	?	?	?	?	24	
Mundilfari	1	1	5	5	3	?	?	1	?	?	?	?	?	?	?	?	?	?	?	?	?	?	?	?	?	?	?	?	?	?	?	?	?	?	?	?	?	?	?	24, 25, 27	
Jarnsaxa	1	1	5	5	3	?	?	1	?	?	?	?	?	?	?	?	?	?	?	?	?	?	?	?	?	?	?	?	?	?	?	?	?	?	?	?	?	?	?	24	
Narvi	1	1	5	4	6	?	?	1	?	?	?	?	?	?	?	?	?	?	?	?	?	?	?	?	?	?	?	?	?	?	?	?	?	?	?	?	?	?	?	24	
Bergelmir	1	1	5	5	2	?	?	1	?	?	?	?	?	?	?	?	?	?	?	?	?	?	?	?	?	?	?	?	?	?	?	?	?	?	?	?	?	?	?	24	
Suttungr	1	1	5	5	1	?	0	1	?	?	?	?	?	?	?	?	?	?	?	?	?	?	?	?	?	?	?	?	?	?	?	?	?	?	?	?	?	?	?	24, 25, 27	
Hati	1	1	5	5	5	?	?	1	?	?	?	?	?	?	?	?	?	?	?	?	?	?	?	?	?	?	?	?	?	?	?	?	?	?	?	?	?	?	?	?	24
Bestla	1	1	5	4	8	?	?	1	?	?	?	?	?	?	?	?	?	?	?	?	?	?	?	?	?	?	?	?	?	?	?	?	?	?	?	?	?	?	?	?	24
Farbauti	1	1	5	5	3	?	?	1	?	?	?	?	?	?	?	?	?	?	?	?	?	?	?	?	?	?	?	?	?	?	?	?	?	?	?	?	?	?	?	?	24
Thrymr	1	1	5	5	7	?	0	1	?	?	?	?	?	?	?	?	?	?	?	?	?	?	?	?	?	?	?	?	?	?	?	?	?	?	?	?	?	?	?	24, 25, 27	
Aegir	1	1	5	5	3	?	?	1	?	?	?	?	?	?	?	?	?	?	?	?	?	?	?	?	?	?	?	?	?	?	?	?	?	?	?	?	?	?	?	?	24
Kari	1	1	6	5	7	?	?	1	?	?	?	?	?	?	?	?	?	?	?	?	?	?	?	?	?	?	?	?	?	?	?	?	?	?	?	?	?	?	?	?	24
Fenrir	1	1	6	5	2	?	?	1	?	?	?	?	?	?	?	?	?	?	?	?	?	?	?	?	?	?	?	?	?	?	?	?	?	?	?	?	?	?	?	?	24
Surtur	1	1	6	5	6	?	?	1	?	?	?	?	?	?	?	?	?	?	?	?	?	?	?	?	?	?	?	?	?	?	?	?	?	?	?	?	?	?	?	?	24
Ymir	1	1	6	5	5	?	0	1	?	?	?	?	?	?	?	?	?	?	?	?	?	?	?	?	?	?	?	?	?	?	?	?	?	?	?	?	?	?	?	24, 25, 27	
Loge	1	1	6	5	2	?	?	1	?	?	?	?	?	?	?	?	?	?	?	?	?	?	?	?	?	?	?	?	?	?	?	?	?	?	?	?	?	?	?	?	24
Forjot	1	1	6	5	3	?	?	1	?	?	?	?	?	?	?	?	?	?	?	?	?	?	?	?	?	?	?	?	?	?	?	?	?	?	?	?	?	?	?	?	24
S/2004 S07	1	1	5	5	8	?	?	1	?	?	?	?	?	?	?	?	?	?	?	?	?	?	?	?	?	?	?	?	?	?	?	?	?	?	?	?	?	?	?	?	24
S/2004 S12	1	1	5	5	6	?	?	1	?	?	?	?	?	?	?	?	?	?	?	?	?	?	?	?	?	?	?	?	?	?	?	?	?	?	?	?	?	?	?	?	24
S/2004 S13	1	1	5	5	4	?	?	1	?	?	?	?	?	?	?	?	?	?	?	?	?	?	?	?	?	?	?	?	?	?	?	?	?	?	?	?	?	?	?	?	24
S/2004 S17	1	1	5	5	4	?	?	1	?	?	?	?	?	?	?	?	?	?	?	?	?	?	?	?	?	?	?	?	?	?	?	?	?	?	?	?	?	?	?	?	24
S/2006 S1	1	1	5	5	2	?	?	1	?	?	?	?	?	?	?	?	?	?	?	?	?	?	?	?	?	?	?	?	?	?	?	?	?	?	?	?	?	?	?	?	24
S/2006 S3	1	1	5	5	7	?	?	1	?	?	?	?	?	?	?	?	?	?	?	?	?	?	?	?	?	?	?	?	?	?	?	?	?	?	?	?	?	?	?	?	24
S/2007 S2	1	1	4	5	3	?	?	1	?	?	?	?	?	?	?	?	?	?	?	?	?	?	?	?	?	?	?	?	?	?	?	?	?	?	?	?	?	?	?	?	24
S/2007 S3	1	1	5	5	2	?	?	1	?	?	?	?	?	?	?	?	?	?	?	?	?	?	?	?	?	?	?	?	?	?	?	?	?	?	?	?	?	?	?	?	24

Note. Character abbreviations: in orbit around the gas giant (Orb); revolution (Rev); semimajor axis (a); orbital inclination to the plane (i); orbital eccentricity (e); density (D); visual geometric albedo (Alb); elemental hydrogen (eH); hydrogen (H₂); helium (He); oxygen (O₂); ozone (O₃); sodium (Na); potassium (K); carbon dioxide (CO₂); nitrogen (N₂); sulphur dioxide (SO₂); argon (Ar); water (H₂O); carbon monoxide (CO); neon (Ne); nitrogen oxide (NO); methane (CH₄); sulphuric acid (H₂SO₄); iron (Fe); Nickel (Ni); iron sulphide (FeS); iron oxide (FeO); silicene oxide (SiO); magnesium oxide (MgO); basalt (Bas); sulphur (S); silicates (Sil); carbonates (Carb); ammonia (NH₃); hydrocarbons (HyCarb); hydrogen peroxide (H₂O₂); and tholins (Thol). The compositional characters eH, H₂, and He have absence indicated by a 1. In the remainder of compositional characteristics, a 1 is indicative of presence of the chemical species.

References. (1) Lodders (2003), (2) Hedman et al. (2007a), (3) Nicholson et al. (2008), (4) Filacchione et al. (2014), (5) Spitale and Tiscareno (2012), (6) Hedman et al. (2010), (7) Thomas et al. (2013), (8) Buratti et al. (2010), (9) Winter et al. (2016), (10) Hedman et al. (2007b), (11) Hedman et al. (2012), (12) Hillier et al. (2007), (13) Tamayo et al. (2014), (14) Verbiscer et al. (2009), (15) Hedman et al. (2009), (16) Filacchione et al. (2010), (17) Filacchione et al. (2012), (18) Hussmann et al. (2006), (19) Matson et al. (2009), (20) Spencer & Nimmo (2013), (21) Hirtzig et al. (2013), (22) Hemingway et al. (2013), (23) Niemann et al. (2005), (24) Beaugé and Nesvorný (2007), (25) Gladman et al. (2001), (26) Jewitt & Haghhighipour (2007), (27) Grav & Bauer (2007).

(This table is available in machine readable form.)

ORCID iDs

Timothy. R. Holt  <https://orcid.org/0000-0003-0437-3296>
 Adrian. J. Brown  <https://orcid.org/0000-0002-9352-6989>
 David Nesvorný  <https://orcid.org/0000-0002-4547-4301>
 Jonathan Horner  <https://orcid.org/0000-0002-1160-7970>
 Brad Carter  <https://orcid.org/0000-0003-0035-8769>

References

- Archie, J. W. 1989, *Systematic Zoology*, 38, 253
 Aria, C., & Caron, J. B. 2017, *Natur*, 545, 89
 Asphaug, E., & Reufer, A. 2013, *Icar*, 223, 544
 Bakker, R. T., & Galton, P. M. 1974, *Natur*, 248, 168
 Barnard, E. E. 1892, *AJ*, 12, 81
 Baum, W. A., Kreidl, T., Westphal, J. A., et al. 1981, *Icar*, 47, 84
 Beaugé, C., & Nesvorný, D. 2007, *AJ*, 133, 2537
 Blunck, J. 2010, in ASP Conf. Ser. 421, The Satellites of Saturn, ed. L. Verdes Montenegro, A. del Olmo, & J. Sulentic (Berlin: Springer), 53
 Brandley, M. C., Warren, D. L., Leaché, A. D., & McGuire, J. A. 2009, *Systematic Biol.*, 58, 184
 Brooks, S. M., Esposito, L. W., Showalter, M. R., & Throop, H. B. 2004, *Icar*, 170, 35
 Brown, A. J. 2014, *Icar*, 239, 85
 Brown, R. H., Baines, K. H., Bellucci, G., et al. 2003, *Icar*, 164, 461
 Buratti, B. J., Bauer, J. M., Hicks, M. D., et al. 2010, *Icar*, 206, 524
 Burns, J. A., Showalter, M. R., Hamilton, D. P., et al. 1999, *Sci*, 284, 1146
 Callegari, N., & Yokoyama, T. 2010, in IAU Symp. 263, Icy Bodies of the Solar System, ed. J. A. Fernandez et al. (Cambridge: Cambridge Univ. Press), 161
 Canup, R. M. 2010, *Natur*, 468, 943
 Canup, R. M., & Ward, W. R. 2002, *AJ*, 124, 3404
 Cardone, V. F., & Fraix Burnet, D. 2013, *MNRAS*, 434, 1930
 Carruba, V., Domingos, R. C., Nesvorný, D., et al. 2013, *MNRAS*, 433, 2075
 Cassini, G. D. 1673, *RSPT*, 8, 5178
 Cassini, G. D. 1686, *RSPT*, 16, 79
 Chamberlain, A., & Wood, B. A. 1987, *J. Hum. Evol.*, 16, 119
 Chamberlain, M. A., & Brown, R. H. 2004, *Icar*, 172, 163
 Charnoz, S., Crida, A., Castillo Rogez, J. C., et al. 2011, *Icar*, 216, 535
 Charnoz, S., Salmon, J., & Crida, A. 2010, *Natur*, 465, 752
 Christou, A. A. 2005, *Icar*, 174, 215
 Clark, R. N., Brown, R. H., Jaumann, R., et al. 2005, *Natur*, 435, 66
 Clark, R. N., Cruikshank, D. P., Jaumann, R., et al. 2012, *Icar*, 218, 831
 Cobbett, A., Wilkinson, M., Wills, M. A., & Sullivan, J. 2007, *Systematic Biol.*, 56, 753
 Colombo, G., & Franklin, F. A. 1971, *Icar*, 15, 186
 Continuum Analytics 2016, Anaconda Software Distribution, v. 2.4.0, <https://continuum.io>
 Cooper, N. J., Murray, C. D., Porco, C. C., & Spitale, J. N. 2006, *Icar*, 181, 223
 Čuk, M., & Burns, J. A. 2004, *Icar*, 167, 369
 Cuzzi, J. N., Whizin, A. D., Hogan, R. C., et al. 2014, *Icar*, 232, 157
 Dalton, J. B. 2010, *SSRv*, 153, 219
 Dalton, J. B., Cruikshank, D. P., Stephan, K., et al. 2010, *SSRv*, 153, 113
 Darwin, C. 1859, On the Origin of the Species by Natural Selection (London: Murray)
 Deienno, R., Nesvorný, D., Vokrouhlický, D., & Yokoyama, T. 2014, *AJ*, 148, 25
 El Moutamid, M., Nicholson, P. D., French, R. G., et al. 2016, *Icar*, 279, 125
 Emelyanov, N. V. 2005, *A&A*, 438, L33
 Farris, J. S. 1970, *Systematic Biol.*, 19, 83
 Farris, J. S. 1989, *Cladistics*, 5, 417
 Farris, J. S. 1990, *Cladistics*, 6, 91
 Feibelman, W. A. 1967, *Natur*, 214, 793
 Filacchione, G., Capaccioni, F., Ciarniello, M., et al. 2012, *Icar*, 220, 1064
 Filacchione, G., Capaccioni, F., Clark, R. N., et al. 2010, *Icar*, 206, 507
 Filacchione, G., Capaccioni, F., McCord, T. B., et al. 2007, *Icar*, 186, 259
 Filacchione, G., Ciarniello, M., Capaccioni, F., et al. 2014, *Icar*, 241, 45
 Filacchione, G., D'Aversa, E., Capaccioni, F., et al. 2016, *Icar*, 271, 292
 Fraix Burnet, D., Chattopadhyay, T., Chattopadhyay, A. K., Davoust, E., & Thuillard, M. 2012, *A&A*, 545, A80
 Fraix Burnet, D., Choler, P., & Douzery, E. J. P. 2006, *A&A*, 455, 845
 Fraix Burnet, D., & Davoust, E. 2015, *MNRAS*, 450, 3431
 Fraix Burnet, D., Davoust, E., & Charbonnel, C. 2009, *MNRAS*, 398, 1706
 Fraix Burnet, D., Dugué, M., Chattopadhyay, T., Chattopadhyay, A. K., & Davoust, E. 2010, *MNRAS*, 407, 2207
 Fraix Burnet, D., Thuillard, M., & Chattopadhyay, A. K. 2015, *FrASS*, 2, 3
 Galilei, G. 1610, Sidereus Nuncius (Venice: Tommaso Baglioni)
 Gascuel, O. 2005, Mathematics of Evolution and Phylogeny (Oxford: Oxford Univ. Press)
 Giese, B., Neukum, G., Roatsch, T., Denk, T., & Porco, C. C. 2006, *P&SS*, 54, 1156
 Gillon, M., Jehin, E., Lederer, S. M., et al. 2016, *Natur*, 533, 221
 Givnish, T., & Sytsma, K. 1997, *Mol. Phylogenetics Evol.*, 7, 320
 Gladman, B., Kavelaars, J. J., Holman, M., et al. 2001, *Natur*, 412, 163
 Gladman, B., Sheppard, S. S., & Marsden, B. G. 2003a, *IAUC*, 8125
 Gladman, B., Sheppard, S. S., & Marsden, B. G. 2003b, *IAUC*, 8138
 Goloboff, P. A. 1994, *Cladistics*, 9, 433
 Goloboff, P. A. 1996, *Cladistics*, 12, 199
 Goloboff, P. A. 2015, *Cladistics*, 31, 210
 Goloboff, P. A., & Catalano, S. A. 2016, *Cladistics*, 32, 221
 Goloboff, P. A., Farris, J. S., & Nixon, K. C. 2008, *Cladistics*, 24, 774
 Grav, T., & Bauer, J. 2007, *Icar*, 191, 267
 Grav, T., Bauer, J. M., Mainzer, A. K., et al. 2015, *ApJ*, 809, 3
 Grav, T., Holman, M. J., Gladman, B. J., & Aksnes, K. 2003, *Icar*, 166, 33
 Greenberg, R. 2010, *RPPH*, 73, 036801
 Grundy, W. M., Buratti, B. J., Cheng, A. F., et al. 2007, *Sci*, 318, 234
 Hamilton, A. 2014, The Evolution of Phylogenetic Systematics: Species and Systematics Vol. 5 (Berkeley, CA: Univ. California Press)
 Hedman, M. M., Burns, J. A., Hamilton, D. P., & Showalter, M. R. 2012, *Icar*, 217, 322
 Hedman, M. M., Burns, J. A., Showalter, M. R., et al. 2007a, *Icar*, 188, 89
 Hedman, M. M., Burns, J. A., Tiscareno, M. S., et al. 2007b, *Sci*, 317, 653
 Hedman, M. M., Cooper, N. J., Murray, C. D., et al. 2010, *Icar*, 207, 433
 Hedman, M. M., Murray, C. D., Cooper, N. J., et al. 2009, *Icar*, 199, 378
 Hemingway, D., Nimmo, F., Zebker, H., & Iess, L. 2013, *Natur*, 500, 550
 Hennig, W. 1965, *Annu. Rev. Entomology*, 10, 97
 Heppenheimer, T. A., & Porco, C. 1977, *Icar*, 30, 385
 Hillier, J. K., Green, S. F., McBride, N., et al. 2007, *MNRAS*, 377, 1588
 Hirtzig, M., Bézard, B., Lellouch, E., et al. 2013, *Icar*, 226, 470
 Holt, T. R., Brown, A. J., & Nesvorný, D. 2016, *LPSC*, 47, 2676
 Hug, L. A., Baker, B. J., Anantharaman, K., et al. 2016, *Nat. Microbiol.*, 1, 16048
 Hussmann, H., Sohl, F., & Spohn, T. 2006, *Icar*, 185, 258
 Huygens, C. 1659, Systema Saturnium (The Hague: Adriani Vlacq)
 Jacobson, R., Brozovic, M., Gladman, B., et al. 2011, *IAUC*, 9222
 Jewitt, D., & Haghhighipour, N. 2007, *ARA&A*, 45, 261
 Jewitt, D., Sheppard, S., Kleyna, J., & Marsden, B. G. 2005, *IAUC*, 8523
 Jewitt, D. C., Danielson, G. E., & Synnott, S. P. 1979, *Sci*, 206, 951
 Jofré, P., Das, P., Bertranpetit, J., & Foley, R. 2017, *MNRAS*, 467, 1140
 Johnson, T. V., & Lunine, J. I. 2005, *Natur*, 435, 69
 Jones, E., Oliphant, T., Peterson, P., et al. 2001, SciPy: Open source scientific tools for Python, <http://www.scipy.org/>
 Karkoschka, E. 1994, *Icar*, 111, 174
 Kluge, A. G., & Farris, J. S. 1969, *Systematic Zoology*, 18, 1
 Korsun, P. P., Rousselot, P., Kulyk, I. V., Afanasiev, V. L., & Ivanova, O. V. 2014, *Icar*, 232, 88
 Kowal, C., Roemer, E., Daniel, M. A., et al. 1975a, *IAUC*, 2855
 Kowal, C. T., Aksnes, K., Marsden, B. G., & Roemer, E. 1975b, *AJ*, 80, 460
 Krüger, H., Hamilton, D. P., Moissl, R., & Grün, E. 2009, *Icar*, 203, 198
 Kuiper, G. P. 1944, *ApJ*, 100, 378
 Lebreton, J. P., Witasse, O., Sollazzo, C., et al. 2005, *Natur*, 438, 758
 Levison, H. F., Kretke, K. A., & Duncan, M. J. 2015, *Natur*, 524, 322
 Lissauer, J. J. 1987, *Icar*, 69, 249
 Ladders, K. 2003, *ApJ*, 591, 1220
 Lykawka, P. S., & Horner, J. 2010, *MNRAS*, 405, 1375
 Maddison, W. P., Donoghue, M. J., & Maddison, D. R. 1984, *Systematic Biol.*, 33, 83
 Maddison, W. P., & Maddison, D. R. 2015, Zephyr: a Mesquite package for interacting with external phylogeny inference programs, v. 1.1, <https://mesquitezephyr.wikispaces.com>
 Maddison, W. P., & Maddison, D. R. 2017, Mesquite: a modular system for evolutionary analysis, v. 3.20, <http://mesquiteproject.org>
 Margush, T., & McMorris, F. R. 1981, *Bull. Math. Biol.*, 43, 239
 Matson, D. L., Castillo Rogez, J. C., Schubert, G., Sotin, C., & McKinnon, W. B. 2009, in The Thermal Evolution and Internal Structure of Saturn's Mid Sized Icy Satellites, ed. M. K. Dougherty, L. W. Esposito, & S. M. Krimigis (Amsterdam: Springer), 577
 McKinney, W. 2010, in Proc. 9th Python in Science Conf. 445, ed. S. van der Walt & J. Millman (Austin, TX: SciPy), 51
 Melotte, J., & Perrine, C. D. 1908, *PASP*, 20, 184
 Milani, A., Cellino, A., Knežević, Z., et al. 2014, *Icar*, 239, 46
 Mitchell, P. C. 1901, *Trans. Linnean Soc.*, 8, 173
 Morbidelli, A., Levison, H. F., Tsiganis, K., & Gomes, R. 2005, *Natur*, 435, 462

- Naylor, G., & Kraus, F. 1995, *Systematic Biol.*, 44, 559
- Nesvorný, D., Alvarellos, J. L. A., Dones, L., & Levison, H. F. 2003, *AJ*, 126, 398
- Nesvorný, D., Beaugé, C., & Dones, L. 2004, *AJ*, 127, 1768
- Nesvorný, D., Bottke, W. F., Jr., Dones, L., & Levison, H. F. 2002, *Natur*, 417, 720
- Nesvorný, D., & Morbidelli, A. 2012, *AJ*, 144, 117
- Nesvorný, D., Vokrouhlický, D., & Deienno, R. 2014, *ApJ*, 784, 22
- Nesvorný, D., Vokrouhlický, D., & Morbidelli, A. 2007, *AJ*, 133, 1962
- Nesvorný, D., Vokrouhlický, D., & Morbidelli, A. 2013, *ApJ*, 768, 45
- Nicholson, P. D., Hamilton, D. P., Matthews, K., & Yoder, C. F. 1992, *Icar*, 100, 464
- Nicholson, P. D., Hedman, M. M., Clark, R. N., et al. 2008, *Icar*, 193, 182
- Nicholson, S. B. 1914, *PASP*, 26, 197
- Nicholson, S. B. 1938, *PASP*, 50, 292
- Nicholson, S. B. 1951, *PASP*, 63, 297
- Niemann, H. B., Atreya, S. K., Bauer, S. J., et al. 2005, *Natur*, 438, 779
- Ockert Bell, M. E., Burns, J. A., Daubar, I. J., et al. 1999, *Icar*, 138, 188
- Olsen, G. J., Woese, C. R., & Overbeek, R. 1994, *J. Bacteriol.*, 176, 1
- Parker, A., Ivezić, Ž., Jurić, M., et al. 2008, *Icar*, 198, 138
- Perrine, C. D. 1905, *PASP*, 17, 62
- Perrine, C. D., & Aitken, R. G. 1905, *PASP*, 17, 62
- Pickering, E. C. 1899, *ApJ*, 9, 274
- Pickering, W. H. 1905, *AnHar*, 53, 85
- Pollack, J. B., Burns, J. A., & Tauber, M. E. 1979, *Icar*, 37, 587
- Pollack, J. B., Hubickij, O., Bodenheimer, P., et al. 1996, *Icar*, 124, 62
- Porco, C. C., Baker, E., Barbara, J., et al. 2005, *Sci*, 307, 1226
- Porco, C. C., Helfenstein, P., Thomas, P. C., et al. 2006, *Sci*, 311, 1393
- Porco, C. C., Thomas, P. C., Weiss, J. W., & Richardson, D. C. 2007, *Sci*, 318, 1602
- Rettig, T. W., Walsh, K., & Consolmagno, G. 2001, *Icar*, 154, 313
- Řičan, O., Pialek, L., Almirón, A., & Casciotta, J. 2011, *Zootaxa*, 2982, 1, <http://www.mapress.com/j/zt/article/view/11638>
- Ross, F. E. 1905, *AnHar*, 53, 101
- Salisbury, S. W., Molnar, R. E., Frey, E., & Willis, P. M. 2006, *RSPSB*, 273, 2439
- Salmon, J., & Canup, R. M. 2017, *ApJ*, 836, 109
- Sanderson, M. J., & Donoghue, M. J. 1989, *Evol.*, 43, 1781
- Scotti, J. V., Spahr, T. B., McMillan, R. S., et al. 2000, *IAUC*, 7460
- Sheppard, S. S., Gladman, B., & Marsden, B. G. 2003a, *IAUC*, 8116
- Sheppard, S. S., Gladman, B., & Marsden, B. G. 2004, *IAUC*, 8276
- Sheppard, S. S., Jewitt, D., & Kleyna, J. 2005, *AJ*, 129, 518
- Sheppard, S. S., Jewitt, D., & Kleyna, J. 2006a, *AJ*, 132, 171
- Sheppard, S. S., & Jewitt, D. C. 2003, *Natur*, 423, 261
- Sheppard, S. S., Jewitt, D. C., Fernandez, Y., et al. 2000, *IAUC*, 7525
- Sheppard, S. S., Jewitt, D. C., Fernandez, Y. R., et al. 2001, *IAUC*, 7555
- Sheppard, S. S., Jewitt, D. C., Kleyna, J., et al. 2003b, *IAUC*, 8087
- Sheppard, S. S., Jewitt, D. C., Kleyna, J., & Marsden, B. G. 2006b, *IAUC*, 8727
- Sheppard, S. S., Jewitt, D. C., Kleyna, J., & Marsden, B. G. 2007, *IAUC*, 8836
- Sheppard, S. S., Jewitt, D. C., Kleyna, J., Marsden, B. G., & Jacobson, R. 2002, *IAUC*, 7900
- Sheppard, S. S., & Marsden, B. G. 2003a, *IAUC*, 8088
- Sheppard, S. S., & Marsden, B. G. 2003b, *IAUC*, 8089
- Sheppard, S. S., & Marsden, B. G. 2004, *IAUC*, 8281
- Sheppard, S. S., & Williams, G. V. 2012, *IAUC*, 9252
- Showalter, M. R. 1991, *Natur*, 351, 709
- Smith, B. A., Soderblom, L. A., Johnson, T. V., et al. 1979, *Sci*, 204, 951
- Smith, S. Y., Stockey, R. A., Rothwell, G. W., & Little, S. A. 2017, *J. Systematic Paleontology*, 15, 69
- Spahn, F., Schmidt, J., Albers, N., et al. 2006, *Sci*, 311, 1416
- Sparks, W. B., Hand, K. P., McGrath, M. A., et al. 2016, *ApJ*, 829, 121
- Spencer, J. R., & Nimmo, F. 2013, *AREPS*, 41, 693
- Spitale, J. N., & Tiscareno, M. 2012, in AAS Meeting, 44, 414.04
- Spyder Development Team 2015, *Spyder: The Scientific Python Development Environment*, v. 2.3.8, <https://pythonhosted.org/spyder/>
- Suárez Díaz, E., & Anaya Muñoz, V. H. 2008, *Stud. Hist. Phil. Sci.*, 39, 451
- Sun, K. L., Seib, M., Hedman, M. M., & Spahn, F. 2017, *Icar*, 284, 206
- Sykes, M. V., Nelson, B., Cutri, R. M., et al. 2000, *Icar*, 143, 371
- Synnott, S. P. 1980, *Sci*, 210, 786
- Synnott, S. P. 1981, *Sci*, 212, 1392
- Takato, N., Bus, S. J., Terada, H., Pyo, T. S., & Kobayashi, N. 2004, *Sci*, 306, 2224
- Tamayo, D., Burns, J. A., Hamilton, D. P., & Hedman, M. M. 2011, *Icar*, 215, 260
- Tamayo, D., Hedman, M. M., & Burns, J. A. 2014, *Icar*, 233, 1
- Thomas, P. C. 2010, *Icar*, 208, 395
- Thomas, P. C., Burns, J. A., Hedman, M., et al. 2013, *Icar*, 226, 999
- Thomas, P. C., Burns, J. A., Rossier, L., et al. 1998, *Icar*, 135, 360
- Throop, H. B., Porco, C. C., West, R. A., et al. 2004, *Icar*, 172, 59
- Tillyard, R. J. 1926, *The Insects of Australia and New Zealand* (Sydney: Angus and Robertson)
- Tiscareno, M. S., Burns, J. A., Hedman, M. M., et al. 2006, *Natur*, 440, 648
- Tosi, F., Turrini, D., Coradini, A., & Filacchione, G. 2010, *MNRAS*, 403, 1113
- Treffenstädt, L. L., Mourão, D. C., & Winter, O. C. 2015, *A&A*, 583, A80
- Tsiganis, K., Gomes, R., Morbidelli, A., & Levison, H. F. 2005, *Natur*, 435, 459
- Turrini, D., Marzari, F., & Beust, H. 2008, *MNRAS*, 391, 1029
- Turrini, D., Marzari, F., & Tosi, F. 2009, *MNRAS*, 392, 455
- Van Dung, V., Giau, P. M., Chinh, N. N., et al. 1993, *Natur*, 363, 443
- Vasundhara, R., Selvakumar, G., & Anbazhagan, P. 2017, *MNRAS*, 468, 501
- Verbiscer, A., French, R., Showalter, M., & Helfenstein, P. 2007, *Sci*, 315, 815
- Verbiscer, A. J., Skrutskie, M. F., & Hamilton, D. P. 2009, *Natur*, 461, 1098
- Winter, O., Souza, A., Sfait, R., et al. 2016, in AAs Meeting, 48, 203.03
- Wong, M. H., de Pater, I., Showalter, M. R., et al. 2006, *Icar*, 185, 403
- Yoder, C. F., Colombo, G., Synnott, S. P., & Yoder, K. A. 1983, *Icar*, 53, 431
- Yoder, C. F., Synnott, S. P., & Salo, H. 1989, *AJ*, 98, 1875
- Zappala, V., Cellino, A., Farinella, P., & Knezevic, Z. 1990, *AJ*, 100, 2030
- Zappala, V., Cellino, A., Farinella, P., & Milani, A. 1994, *AJ*, 107, 772
- Zebker, H. A., Marouf, E. A., & Tyler, G. L. 1985, *Icar*, 64, 531
- Zimmermann, W., & Schultz, W. 1931, *Arbeitsweise der botanischen Phylogenetik und anderer Gruppierungswissenschaften* (Munich: Urban & Schwarzenberg)

3

Paper 2 - Stability of the Jovian Trojans and their collisional families

This paper was the result of dynamical simulations that I undertook on the Jovian Trojans (Holt et al., 2020a). The paper looks at the stability of the objects, as well as the population as a whole. In this paper, there is a focus on the collisional families previously identified in the swarms (Nesvorný et al., 2015). Even though this paper was only released in March 2020, it already (May 2021) has 4 citations on the ADS: <https://ui.adsabs.harvard.edu/abs/2020MNRAS.495.4085H/abstract>.

3.1 ABSTRACT

The Jovian Trojans are two swarms of objects located around the L_4 and L_5 Lagrange points. The population is thought to have been captured by Jupiter during the Solar system's youth. Within the swarms, six collisional families have been identified in previous work, with four in the L_4 swarm, and two in the L_5 . Our aim is to investigate the stability of the two Trojan swarms, with a particular focus on these collisional families. We find that the members of Trojan swarms escape the population at a linear rate, with the primordial L_4 (23.35% escape)

and L₅ (24.89% escape) population sizes likely 1.31 and 1.35 times larger than today. Given that the escape rates were approximately equal between the two Trojan swarms, our results do not explain the observed asymmetry between the two groups, suggesting that the numerical differences are primordial in nature, supporting previous studies. Upon leaving the Trojan population, the escaped objects move onto orbits that resemble those of the Centaur and short-period comet populations. Within the Trojan collisional families, the 1996 RJ and 2001 UV₂₀₉ families are found to be dynamically stable over the lifetime of the Solar system, whilst the Hektor, Arkesilos and Ennomos families exhibit various degrees of instability. The larger Eurybates family shows 18.81% of simulated members escaping the Trojan population. Unlike the L₄ swarm, the escape rate from the Eurybates family is found to increase as a function of time, allowing an age estimation of approximately $1.045 \pm 0.364 \times 10^9$ years.

3.2 ASSOCIATED PRESENTATIONS AND PUBLICATIONS

3.2.1 OCT. 2018: DPS 50 - POSTER PRESENTATION

Temporal stability of the Jovian Trojan Asteroids.

Holt, Timothy R.; Nesvorny, David; Horner, Jonti; Tylor, Christopher; Carter, Brad

Abstract

The Jovian Trojans are two swarms of asteroids, set at the Lagrange points of Jupiter. To date over 6800 have been discovered. The current paradigm is for these objects to be captured during an early Solar system instability, with most having stable orbits on the age of the Solar system. Though the majority of the objects are stable, long term modeling of the Jovian Trojans has indicated that at least some of these captures are temporary. Within each swarm several dynamical families have been identified. The aim of this work is to examine the temporal range of stabilities in the Jovian Trojan swarm, in the context of these dynamical families. Our simulations extend those of previous work by including all identified Jovian Trojans, roughly doubling the number of objects. Each of the Jovian Trojans that have been identified to date were simulated for the age of the Solar system, 4.5 Gigayear, using the REBOUND n-body integrator. We used a high resolution time step of 0.3954 yr, recording the test particle orbital elements every 100000 yr for each simulation. To account for uncertainties in the ephemeris, each asteroid was simulated with eight clones along the 1 sigma errors. Asteroids were monitored for when they escaped the Lagrange point stable regions, as well as Solar system ejection. We followed members of previously identified dynamical families to establish their temporal stabilities. The results are that several of the outlying Jovian Tro-

jans show stabilities on varying timescales. The short term stability of some of the Jovian Trojans is indicative of temporary captures. Prior to ejection, some of the ex-Jovian Trojans participate in other asteroid groups. This leads to a much more active participation between asteroid populations.

Publication: American Astronomical Society, DPS meeting 50, id.217.02

Pub Date: October 2018



Stability of Jovian Trojans and their collisional families

Timothy R. Holt^{1,2*}, David Nesvorný,² Jonathan Horner,¹ Rachel King,¹ Raphael Marschall,² Melissa Kamrowski,³ Brad Carter,¹ Leigh Brookshaw¹ and Christopher Tylor¹

¹Centre for Astrophysics, University of Southern Queensland, Toowoomba, Queensland 4350, Australia

²Department of Space Studies, Southwest Research Institute, Boulder, CO 80302, USA

³Physics, University of Minnesota, Morris, MN 56267, USA

Accepted 2020 May 7. Received 2020 May 5; in original form 2019 December 5

ABSTRACT

The Jovian Trojans are two swarms of objects located around the L₄ and L₅ Lagrange points. The population is thought to have been captured by Jupiter during the Solar system's youth. Within the swarms, six collisional families have been identified in previous work, with four in the L₄ swarm, and two in the L₅. Our aim is to investigate the stability of the two Trojan swarms, with a particular focus on these collisional families. We find that the members of Trojan swarms escape the population at a linear rate, with the primordial L₄ (23.35 per cent escape) and L₅ (24.89 per cent escape) population sizes likely 1.31 and 1.35 times larger than today. Given that the escape rates were approximately equal between the two Trojan swarms, our results do not explain the observed asymmetry between the two groups, suggesting that the numerical differences are primordial in nature, supporting previous studies. Upon leaving the Trojan population, the escaped objects move on to orbits that resemble those of the Centaur and short-period comet populations. Within the Trojan collisional families, the 1996 RJ and 2001 UV₂₀₉ families are found to be dynamically stable over the lifetime of the Solar system, whilst the Hektor, Arkesilos and Ennomos families exhibit various degrees of instability. The larger Eurybates family shows 18.81 per cent of simulated members escaping the Trojan population. Unlike the L₄ swarm, the escape rate from the Eurybates family is found to increase as a function of time, allowing an age estimation of approximately $1.045 \pm 0.364 \times 10^9$ yr.

Key words: methods: numerical – minor planets, asteroids: general.

1 INTRODUCTION

The Jovian Trojans are a population of small Solar system bodies comprising two swarms located around the leading (L₄) and trailing (L₅) Lagrange points of Jupiter. The larger and better known members of the Trojan swarms are named after the characters of the epic Greek poems that detail the Trojan war, The Iliad and The Odyssey (Homer 750 BC).

The Jovian Trojans were discovered in the early 20th Century, with the first (588 Achilles, Wolf 1907) being quickly followed by 617 Patroclus, 624 Hektor, and 659 Nestor (Heinrich 1907; Strömgren 1908; Ebell 1909; Kopff 1909). These objects were the first confirmation of a stable solution to the restricted three-body problem that had been proposed over a century earlier by Lagrange (1772).

At the time of writing, approximately 7200 objects have been discovered around the Lagrange points of Jupiter,¹ a number that is destined to rise still further in the coming years, as a result of the Rubin Observatory Legacy Survey of Space and Time (LSST), scheduled for first light in 2021 (Schwamb, Levison & Buie 2018b). Interestingly, the known Trojans are not evenly distributed between the two Trojan swarms. Instead, there is a marked asymmetry, with the leading L₄ swarm containing approximately 1.89 times the number of objects than the L₅ swarm. A number of studies have considered this asymmetry and have found it to be robust, a real feature of the population, rather than being the result of observational biases (Jewitt, Trujillo & Luu 2000; Nakamura & Yoshida 2008; Yoshida & Nakamura 2008; Vinogradova & Chernetenko 2015).

Although more than 7200 objects have been found in the region surrounding the Jovian Lagrange points, many of those objects may

* E-mail: timothy.holt@usq.edu.au

¹Taken from the JPL HORIZONS Solar System Dynamics Database <https://ssd.jpl.nasa.gov/> (Giorgini et al. 1996), on 2019 November 13.

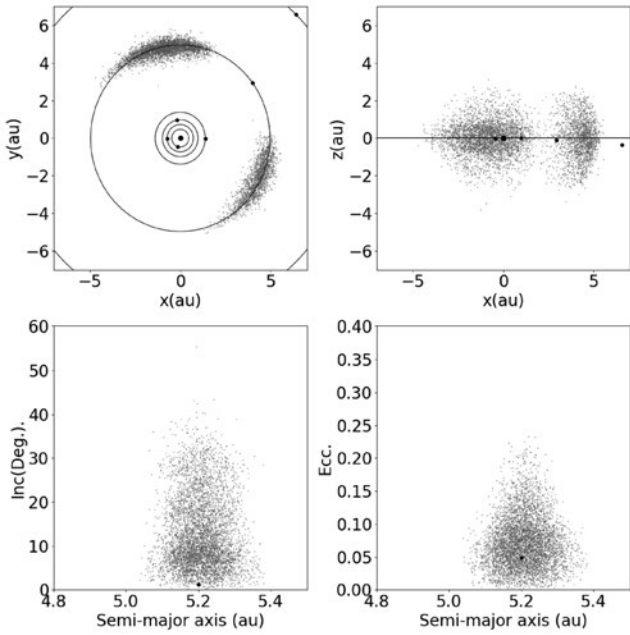


Figure 1. Distribution of 5553 Jovian Trojans for which proper elements have been generated (Knežević & Milani 2017). The top figures indicate the positions of the Trojans relative to the planets on 01-01-2000 00:00 in a face-on (xy ; left) and edge-on (xz ; right) orientation, in the ecliptic reference system. Bottom figures show the Trojans in osculating inclination (Inc.), eccentricity (Ecc), and semimajor axis space. Larger black dots indicate planets, with Jupiter being shown in the bottom diagrams. Data from NASA HORIZONS, as of 2019 August 19.

be temporarily captured objects, rather than permanent members of the Trojan population. Whilst the ‘true’ Trojans move on stable orbits that keep them librating around the L_4 and L_5 Lagrange points on billion year time-scales (e.g. Emery et al. 2015), temporarily captured objects would be expected to escape from the Trojan swarms on time-scales of thousands or tens of thousands of years. To confirm that a given object is truly a member of the Trojan population requires confirmation that the object’s proper orbital elements (Milani & Knežević 1992) are stable, and that the object is truly trapped in 1:1 resonance with Jupiter. Simulations spanning more than 1×10^6 yr and transformation using Fourier transform analysis (Šidlichovský & Nesvorný 1996; Beaugé 2001; Brož & Rozehnal 2011) are used to devolve the osculations of potential Trojans to determine whether or not their orbits are truly resonant. The data base of those objects for which such analysis has been carried out can therefore be considered a set of contemporary stable Jovian Trojans, and includes 5553 numbered and multioppositional objects (Knežević & Milani 2017). Fig. 1 shows the current known configuration of the Jovian Trojan population.

In order to assess the observational completeness of the Trojan population, an examination of their size distribution is needed. The observed population of Jovian Trojans ranges in diameter from the largest, 624 Hektor, at ~ 250 km (Marchis et al. 2014), down to objects several kilometres across (Emery et al. 2015). The size-frequency distribution for these objects is generally considered to be observationally complete to approximately 10 km in size (Grav et al. 2011; Emery et al. 2015), as shown in Fig. 2. The power law that best describes this size distribution is similar to that of the collisionally evolved Asteroid belt (Bottke et al. 2005). From this, it has been inferred that the Jovian Trojan population could contain as many as

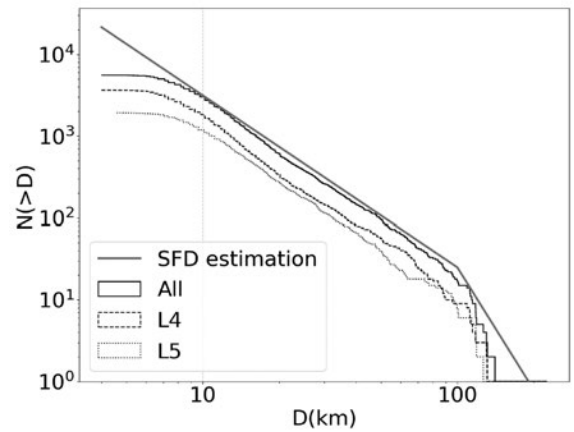


Figure 2. Cumulative size-frequency distribution of the Jovian Trojans. The solid line shows the distribution for the population as a whole, whilst the long-dash line shows the distribution among members of the leading L_4 swarm, and the dotted line shows the distribution for the trailing L_5 swarm. Data from NASA HORIZONS, as of 2019 August 19. Vertical grey, dashed line indicates observational completeness (Emery et al. 2015). The grey line shows the estimated complete size distribution (Nesvorný 2018).

a million objects greater than 1 km in diameter (Jewitt et al. 2000; Yoshida & Nakamura 2008; Yoshida & Terai 2017), though there are also indications that these may be optimistic estimates that grossly overestimate the true situation (e.g. Nakamura & Yoshida 2008).

1.1 The dynamics and origins of the Jovian Trojans

Due to their stability, it is thought that the Jovian Trojans date back to the early Solar system (e.g. Emery et al. 2015; Nesvorný 2018). Attempts to ascertain the origins of the Jovian Trojans need to explain their unique dynamical situation. As can be seen in Fig. 1, the population is dynamically ‘warm’, occupying two broad tori around the Lagrange points, with high orbital inclinations and eccentricities. An *in situ* formation would be expected to produce a ‘cold’ disc, with low orbital eccentricities and inclinations, reflective of the primordial protoplanetary disc. The mismatch between the observed population and the distribution that would be expected from *in situ* formation has led to the conclusion that the Jovian Trojans most likely did not form in their current orbits, but were in fact captured early in the Solar system’s history (e.g. Morbidelli et al. 2005; Lykawka & Horner 2010; Nesvorný, Vokrouhlický & Morbidelli 2013; Pirani et al. 2019a).

One explanation for the observed orbital distribution of the Jovian Trojans comes in the form of the ‘Nice’ Model. This model invokes a period of chaotic disruption in the outer Solar system to explain the origin of the Late Heavy Bombardment (Tsiganis et al. 2005a; Morbidelli 2010; Levison et al. 2011; Nesvorný & Morbidelli 2012; Deienno et al. 2017; Nesvorný 2018), during which the Trojans were trapped in their current orbits from a population of dynamically unstable objects that were being scattered through the outer Solar system (Morbidelli et al. 2005; Lykawka & Horner 2010; Nesvorný et al. 2013). A recent attempt to explain the observed asymmetry, which is not explained by the ‘Nice’ model, proposes an alternative, that the Trojans were captured from the same region of the disc as Jupiter, and were transported during the planet’s proposed inward migration (Pirani et al. 2019a). In an update to this *in situ* transport model, Pirani, Johansen & Mustill (2019b) explains the inclinations by invoking mixing in the Jovian feeding

region. These two competing theories for the origins of the Trojans highlight the importance of the population in our understanding of the early Solar system.

Previous long-term simulations of the Jovian Trojans (Levison, Shoemaker & Shoemaker 1997; Tsiganis, Varvoglis & Dvorak 2005b; Di Sisto, Ramos & Beaugé 2014; Di Sisto, Ramos & Gallardo 2019) have indicated that at least some of the members of both the L₄ and L₅ swarms are actually temporary captures, and will escape from the Trojan swarms on time-scales of $\sim 1 \times 10^6$ yr. The estimated fraction of Trojans that will escape the population on these time-scales varies somewhat between these studies, with Levison et al. (1997) proposing an escape rate of ~ 12 per cent and Tsiganis et al. (2005b) estimating 17 per cent. More recent works, by Di Sisto et al. (2014, 2019), suggest a still higher escape rate, at 23 per cent for the L₄ and 28 per cent for the L₅ swarm. To some extent, the disparity among these results can be explained by the growth in the known Trojan population that occurred between one study and the next. Levison et al. (1997) considered a sample of only 178 numbered objects. In contrast, Tsiganis et al. (2005b) studied 246 numbered objects. The 2972 numbered Trojans that were simulated by Di Sisto et al. (2014, 2019) make it the largest previous study.

To further complicate the picture, detailed modelling of (1173) Anchises (Horner, Müller & Lykawka 2012) has shown that at least some of the unstable Jovian Trojans could still be primordial in nature. Indeed, that work, along with other studies in stability (Levison et al. 1997; Nesvorný et al. 2002c; Tsiganis et al. 2005b; Di Sisto et al. 2014, 2019), suggests that the original population of Jovian Trojans was larger than that observed today, and that it likely included objects with a range of stabilities. (1173) Anchises is stable on time-scales of hundreds of millions of years, and so might well be a representative of a once larger population of such objects, which have slowly escaped from the Trojan population since their formation. Following a similar argument, Lykawka & Horner (2010) propose a link between the Centaur population and the Jovian Trojans that escape, though this is disputed by Jewitt (2018) due to differences in the colour distributions of the two populations. Wong & Brown (2016) also use the observed colours of members of the Jovian Trojan population to propose a hypothesis for a common origin between the Trojans and the Edgeworth–Kuiper Belt objects. Such an origin is a good fit with the results of dynamical models that invoke an instability in the outer Solar system as the origin of the Jovian Trojans, in which the Jovian Trojans are captured from a similar source region to the Edgeworth–Kuiper Belt objects (Morbiddelli et al. 2005; Nesvorný et al. 2013).

1.2 Collisional families amongst the Jovian Trojans

Elsewhere in the Solar system, other evolved populations contain dynamical families, the results of the collisional disruption of large parent bodies. Such collisional families have been identified in the asteroid main belt (see Hirayama 1918; Gradie et al. 1979; Zappala et al. 1984; Knežević & Milani 2003; Carruba et al. 2013; Milani et al. 2014; Nesvorný, Brož & Carruba 2015; Milani et al. 2017), the Hilda (Brož & Vokrouhlický 2008) and Hungaria (Warner et al. 2009; Milani et al. 2010) populations, the irregular satellites of the giant planets (Grav et al. 2003; Nesvorný et al. 2003; Sheppard & Jewitt 2003; Nesvorný, Beaugé & Dones 2004; Grav & Bauer 2007; Jewitt & Haghhighipour 2007; Turrini, Marzari & Beust 2008; Turrini, Marzari & Tosi 2009; Bottke et al. 2010; Holt et al. 2018) and the Haumea family in the Edgeworth–Kuiper belt (Brown et al. 2007; Levison et al. 2008; de la Fuente Marcos & de la Fuente Marcos 2018). The traditional methodology for identifying these

Table 1. Identified collisional families in the Jovian Trojan swarms, after Nesvorný et al. (2015).

Family	FIN	n	D_{LM} (km)	Tax.
L ₄				
Hektor	1	12	225	D
Eurybates	2	218	63.88	C/P
1996 RJ	3	7	68.03	–
Arkesilaos	4	37	20.37	–
L ₅				
Ennomos	5	30	91.43	–
2001 UV ₂₀₉	6	13	16.25	–

Note. FIN: family identification number, used throughout this manuscript; n : number of family members; D_{LM} : diameter of the largest member; Tax.: identified taxonomic type (Bus 2002; Grav et al. 2012).

families in small body populations was developed by Zappala et al. (1990, 1994) and is known as the Hierarchical Clustering Method (HCM) and utilizes distances in semimajor axis, eccentricity, and inclination parameter space to identify family members.

Historically, studies that attempted to identify such collisional families amongst the Jovian Trojans were limited by the number of objects that had been discovered at that time (Milani 1993). Additionally, as the Jovian Trojans librate around the Lagrange points, the calculation of proper elements used in family identification is problematic (Emery et al. 2015). For that reason, Beaugé (2001) used transformed proper elements to account for the librations present in the Jovian Trojan dynamics. As the number of known Jovian Trojans increased, additional dynamical clusters have been identified (e.g. Roig, Ribeiro & Gil-Hutton 2008; De Luise et al. 2010; Brož & Rozehnal 2011; Nesvorný et al. 2015; Vinogradova 2015; Rozehnal et al. 2016). Rozehnal et al. (2016) offer an expansion to the HCM developed by Zappala et al. (1990). This new ‘randombox’ method uses Monte Carlo simulations to determine the probability that the identified clusters are random in parameter space. Canonically, six collisional families, four in the L₄ swarm and two in the L₅, are now considered valid in the Jovian Trojan population (Nesvorný et al. 2015). Independent HCM analysis undertaken by Vinogradova (2015) has confirmed the four L₄ families, though they dispute the validity of the L₅ families. See Table 1 for details on the families we consider in this work.

Early imaging surveys suggest that there is a spectral commonality within the dynamical families (Fornasier et al. 2007) in the Jovian Trojans. More recent observational data have brought this into question (Roig et al. 2008), with a heterogeneity being seen in some unconfirmed families from the Sloan Digital Sky Survey (SDSS) colours. The confirmed Eurybytes and Hektor families, however, show a distinctive colour separation from the rest of the population (Roig et al. 2008; Brož & Rozehnal 2011; Rozehnal et al. 2016). Vinogradova (2015) also make comments on the taxonomy of the L₄ families, based on SDSS taxonomy (Carvano et al. 2010). In these studies, the Eurybates family is found to consist mainly of C-types, and the Hektor family mostly D-types, under the Bus–Demeo taxonomy (Bus 2002; DeMeo et al. 2009).

Unlike collisional families in the asteroid belt, the determination of ages for the Trojan families remains elusive. Currently, there are two general methods used to determine family ages (Nesvorný et al. 2015). The first involves reverse integration n -body simulations of the identified family. A relatively young family, such as the Karin family (Nesvorný et al. 2002a), would show convergence in both longitude of ascending node and argument of pericentre as those simulations approach the time of the family’s birth. However, such

simulations are not able to provide firm constraints on the ages of older families, as a result of the chaotic diffusion experienced by the members of those families over time. Once such diffusion has had sufficient time to act, reverse integration of family members will fail to show such convergence. A variation on this uses synthetic families to estimate the collisional family age (Milani & Farinella 1994; Nesvorný et al. 2002b). Some synthetic simulations by Brož & Rožehnal (2011) and Rožehnal et al. (2016) have calculated the age of the Hektor, Eurybates, and Ennomos families in the Trojan population, though these have relatively large, Gigayear ranges. In order to circumvent some of these issues, a second method of family age estimation was developed. This method relies on the modelling of asteroidal Yarkovsky drift (Vokrouhlický et al. 2006; Spoto, Milani & Knežević 2015; Bolin et al. 2017). The technique takes advantage of the fact that any collisional family will contain a large number of different sized objects, which would be expected to experience Yarkovsky drift (Bottke et al. 2006) at different rates. As a result, when the members of a collisional family are plotted in size, or its proxy absolute magnitude, versus orbital semimajor axis, they will form a characteristic ‘V shape’ (Vokrouhlický et al. 2006; Spoto et al. 2015; Paolicchi et al. 2019). The slope of the ‘V’ can then be used to estimate the age of the family. Using this method, a 4×10^9 yr old meta-family has been identified in the asteroid belt (Delbó et al. 2017). This method has been attempted with the Eurybates family (Milani et al. 2017), though due to the negligible Yarkovsky effect experienced by the Jovian Trojans, the age is unreasonably estimated at 1.4×10^{10} yr. This indicates that the method is inappropriate for age estimation of collisional families in the Jovian Trojan swarms.

1.3 This work

In this work, we utilize n -body simulations of the known Jovian Trojan population to consider the stability of previously identified collisional families (Nesvorný et al. 2015). This work considers 5553 numbered and multioppositional objects, a sample nearly double that of the previous largest study (Di Sisto et al. 2014, 2019), who considered 2972 numbered objects. By simulating the whole known population, we can include all identified collisional family members in the study. We divide this work into the following sections. Section 2 describes the methodology of the n -body simulations used as the basis for this work. We discuss the L_4 and L_5 swarms in Section 3. In Section 3.1, we use our simulations to study the rate at which objects escape from the Trojans, and discuss the implications of our results for the original size of the population, including the L_4/L_5 asymmetry and formation scenarios. We consider the stability of the collisional families in Section 4, with a particular focus on the large Eurybates family in Section 4.1.1. Concluding remarks are presented in Section 5.

2 METHODS

We selected the Jovian Trojan population for our simulations based on several criteria. An initial data set was obtained from the JPL Small-Body Database (Giorgini et al. 1996) by searching for and selecting all objects with orbital semimajor axes between 4.6 and 5.5 au and an orbital eccentricity less than 0.3. This process yielded an initial selection of 7202 objects, obtained on 2018 April 17. The ephemeris were retrieved from the NASA HORIZONS data base (Giorgini et al. 1996) for all objects using an initial time point of A.D. 2000-Jan-01 00:00:00.0000. We then filtered our sample to discard temporarily captured objects by limited selection to those

objects present in the AstDys proper element data base (Knežević & Milani 2017). Since objects in this list require the completion of simulations spanning 1×10^6 yr to generate the proper elements of their orbits (Knežević & Milani 2017), this set can be considered initially stable objects. Once our sample was filtered in this way, we were left with a total of 5553 nominally ‘stable’ Trojans for this study, including 4780 numbered and 773 multioppositional objects.

In order to investigate the long-term dynamical evolution of the Jovian Trojan population, we carried out a suite of n -body integrations using the WFAST symplectic integrator within the *REBOUND* n -body dynamics package (Rein & Liu 2012; Rein & Tamayo 2015). Eight clones of each reference Trojan were created, distributed across the $\pm 1\sigma$ positional uncertainties from the HORIZONS data base (Giorgini et al. 1996). These eight 1σ clones were generated at the vertices of a cuboid in x - y - z space, with the reference particle in the centre. Therefore, in this work, we followed the evolution of a total of 49 977 collisionless, massless test particles in our simulations, nine particles for each of the 5553 Trojans. Our integrations modelled the evolution of our test particle swarms under the gravitational influence of the Sun and the four giant planets (Jupiter, Saturn, Uranus, and Neptune). Each individual simulation thus consisted of the Sun, four giant planets, the initial HORIZONS reference particle and the eight 1σ clones, with ephemeris in Solar system barycentric coordinates. All simulations were conducted on the University of Southern Queensland’s High Performance Computing Cluster, Fawkes. We ran each simulation forward for 4.5×10^9 yr, with an integration time-step of 0.3954 yr, 1/30th of the orbital period of Jupiter (Barnes & Quinn 2004). The orbital elements of every test particle were recorded every 1×10^5 yr.

The Yarkovsky effect is a non-gravitational force that can act on small bodies (Bottke et al. 2006). The effect involves the asymmetric thermal radiation of photons from an object, which imparts a thrust on the object in question. This thrust will gradually change the semimajor axis of a body, with the scale and direction of the induced drift dependent on the thermal properties, axis of rotation and size of the object (Brož et al. 2005; Bottke et al. 2006). In the case of the Jovian Trojans, simulations of hypothetical objects have indicated that at small sizes (< 1 km), the Yarkovsky effect could impact the stability of the objects (Wang & Hou 2017; Hellmich et al. 2019). As we are simulating known Jovian Trojans, the majority of the objects are greater than several kilometres in size (Emery et al. 2015), and have unknown or highly uncertain thermal properties (Slyusarev & Belskaya 2014; Sharkey et al. 2019). For these reasons, we have not included the Yarkovsky effect in our simulations.

3 ESCAPES FROM THE L_4 AND L_5 SWARMS

In each of our simulations, we track the position of a particle and record the time it escapes the Jovian Trojan population. A data base of the escape times of each particles is presented in the online supplementary material. We define these escapes as occurring once the test particle obtains an osculating semimajor axis of less than 4.6 au or greater than 5.5 au. In Table 2, we present the results of our simulations, showing the fraction of the total population that escaped from the Trojan population during our simulations. As part of our calculations, we include the volume of the object, as a proxy for mass. The density is only known for a single C-type Trojan, (617) Patroclus (Marchis et al. 2006). With the diversity of taxonomic types seen in even a small number of classified Trojans (Carvano et al. 2010; Grav et al. 2012; DeMeo & Carry 2013), using mass instead of volume could further propagate errors. The volumes were calculated from diameters in the HORIZONS data

Table 2. Escape percentages of Jovian Trojan swarm members.

	n	n_{test}	f_{EscR} (per cent)	$f_{V\text{EscR}}$ (per cent)	f_{EscP} (per cent)	$f_{V\text{EscP}}$ (per cent)	f_{Esc9C} (per cent)	$f_{V\text{Esc9C}}$ (per cent)	$>10\text{km}f_{\text{EscP}}$ (per cent)	$>10\text{km}f_{V\text{EscP}}$ (per cent)
L ₄	3634	32 706	22.23	22.97	23.19	23.35	5.01	7.36	23.28	23.37
L ₅	1919	17 271	24.80	32.22	24.89	24.89	5.04	6.07	24.27	24.88
Total	5553	49 977	23.12	26.58	23.77	23.95	5.02	6.56	23.67	23.96

Note. n : Number of real Trojan members considered in the simulations; n_{test} : number of test particles simulated (eight clones, plus initial reference particle); f_{EscR} : numerical percentage of reference particles that escape; $f_{V\text{EscR}}$: volumetric percentage of reference particles that escape; f_{EscP} : numerical percentage Trojan particle pool, Reference and eight 1σ clones, that escape; $f_{V\text{EscP}}$: volumetric percentage Trojan particle pool, Reference and eight 1σ clones, that escape; f_{Esc9C} : numerical percentage Trojans where all nine particles escape; $f_{V\text{Esc9C}}$: volumetric percentage of Trojans where all nine particles escape; $>10\text{km}f_{\text{EscP}}$: numerical percentage of Trojan particle pool greater than 10 km that escape; $>10\text{km}f_{V\text{EscP}}$: volumetric percentage of Trojan particle pool greater than 10 km that escape.

base to a assumed sphere. Where diameters were unavailable, due to no recorded albedo, we made an estimate based on the H magnitude and mean geometric albedo (from NASA HORIZONS) of each Jovian Trojan swarm, following the methodology of Harris (1997). We use separate geometric albedos for the L₄ (0.076) and L₅ (0.071) swarms, as they are significantly different (Romanishin & Tegler 2018), though close to the mean geometric albedo (0.07) identified by Grav et al. (2011, 2012). There may be a size dependence on the albedos in the Trojan population (Fernández, Jewitt & Ziffer 2009; Grav et al. 2011, 2012), though only a relatively small number of objects have been studied in this way. In choosing to use consistent albedos, there may be some discrepancies between this work and future studies, as more robust albedos, diameters, and shape models are presented. We note that the observed L₄/L₅ asymmetry is lower when volume is considered (L₄ 1.56 larger) than simply considering the number of known objects (L₄ 1.89 larger).

The escape percentages of our reference particles are larger than the 12 per cent seen by Levison et al. (1997). In order to investigate this discrepancy, we consider the instability of the subset of the 178 Jovian Trojans known at the time of Levison et al. (1997). Using our simulations, we find a reference particle escape rate of 15 per cent, consistent with Levison et al. (1997) and similar to the 17 per cent found by Tsiganis et al. (2005b). Di Sisto et al. (2014, 2019) considered the 2972 numbered Trojans known at that time and found escape rates of 23 per cent and 28.3 per cent for the L₄ and L₅ swarms, respectively. The Di Sisto et al. (2014, 2019) results are closer to our escape rates for the reference particles, and the L₄ particle pool escapees. The escape percentages in the L₅ clone pool are lower in our simulations, closer to that of the L₄ swarm and the population as a whole.

The similar ratios in escape percentages between the two swarms confirm the findings of others (Nesvorný & Dones 2002; Tsiganis et al. 2005b; Nesvorný et al. 2013; Di Sisto et al. 2014, 2019), who argued that the observed Jovian Trojan swarm asymmetry cannot be the result of differences in the escape rate between the two Trojan swarms. The difference is therefore more likely due to differences in the number of objects that were initially captured to the swarms.

At first glance, the escape volume differences between the two swarms, shown in Table 2, could account for the asymmetry, particularly in terms of the reference particles ($f_{V\text{EscR}}$ in Table 2). This can be explained by the escape of several large (<100 km diameter) reference objects. In the L₄ swarm, the reference particles of (1437) Diomedes and (659) Nestor escape the Trojan population. The reference particles of (3451) Mentor, (1867) Deiphobus, and (884) Priamus in the L₅ swarm also escape. (3451) Mentor and (659) Nestor are classified as X-type (Tholen 1984; Bus 2002). Once the 1σ clones are taken into account, $f_{V\text{EscP}}$ in Table 2, this escape asymmetry in the volume is negated, resulting in near identical

escape rates for the L₄ and L₅ swarms. This volumetric escape fraction ($f_{V\text{EscP}}$ in Table 2) is very similar to the numerical escape fraction (f_{EscP} in Table 2) for the population and in each of the swarms. In order to further investigate the volumetric escapes, we can limit our selection to just objects for which the population can be considered to be observationally complete, those larger than 10 km (Emery et al. 2015). This reduces the numerical size of the population to 3003. When we repeat the analysis, the percentage of particles that escape only changes by fractions of a per cent in the population, as well as each swarm, see $>10\text{km}f_{\text{EscP}}$ and $>10\text{km}f_{V\text{EscP}}$ in Table 2. This additional analysis supports the hypothesis that the observed asymmetry between the swarms is due to implantation, rather than any volumetric differences.

We generate a conservative subset of the escape population, one where all nine particles of a given object escape. In this subset, f_{Esc9C} and $f_{V\text{Esc9C}}$ in Table 2 escape percentages are much lower. These escapes represent the minimal set of escapes and show that the majority of the escaping population are statistically borderline. Those objects where all nine particles escape are deep into the parameter space identified as unstable by Levison et al. (1997) and Nesvorný et al. (2002c). With regards to the large Trojans, all particles of (1437) Diomedes escape the L₄ swarm by the end of our simulations.

The timing of the reference particle escapes are shown in Fig. 3. With larger changes in semimajor axis (Δa_p) and eccentricity (e_p), there is an increase in the instability. Proper inclination ($\sin - i_p$) appears to have little effect on the general instability of the particles. This general trend is consistent with other studies (Nesvorný & Dones 2002; Tsiganis et al. 2005b; Di Sisto et al. 2014, 2019). With the inclusion of the timing of escape, we show that there is a gradient to the instability trends, particularly in the Δa_p to e_p relationship. This is in a similar unstable parameter space to that identified in Nesvorný & Dones (2002).

3.1 Escape analysis

During our 4.5×10^9 yr simulations, we track the timing of any particles that escape the Jovian Trojan population. As the orbital elements of our test particles are recorded at intervals of 1×10^5 yr, the escape times are only accurate to that resolution. For this analysis, we pool our results for all test particles considered in this work, including the reference object and each of the eight 1σ clones, as independent objects. This gives statistical robustness to the analysis. A histogram of the escape percentages for the population as a whole, and each of the L₄ and L₅ swarms is presented in Fig. 4.

We create linear regression equations to the escape percentages as a function of time, independently for the combined population, and for the L₄/L₅ swarms. These equations along with their associated

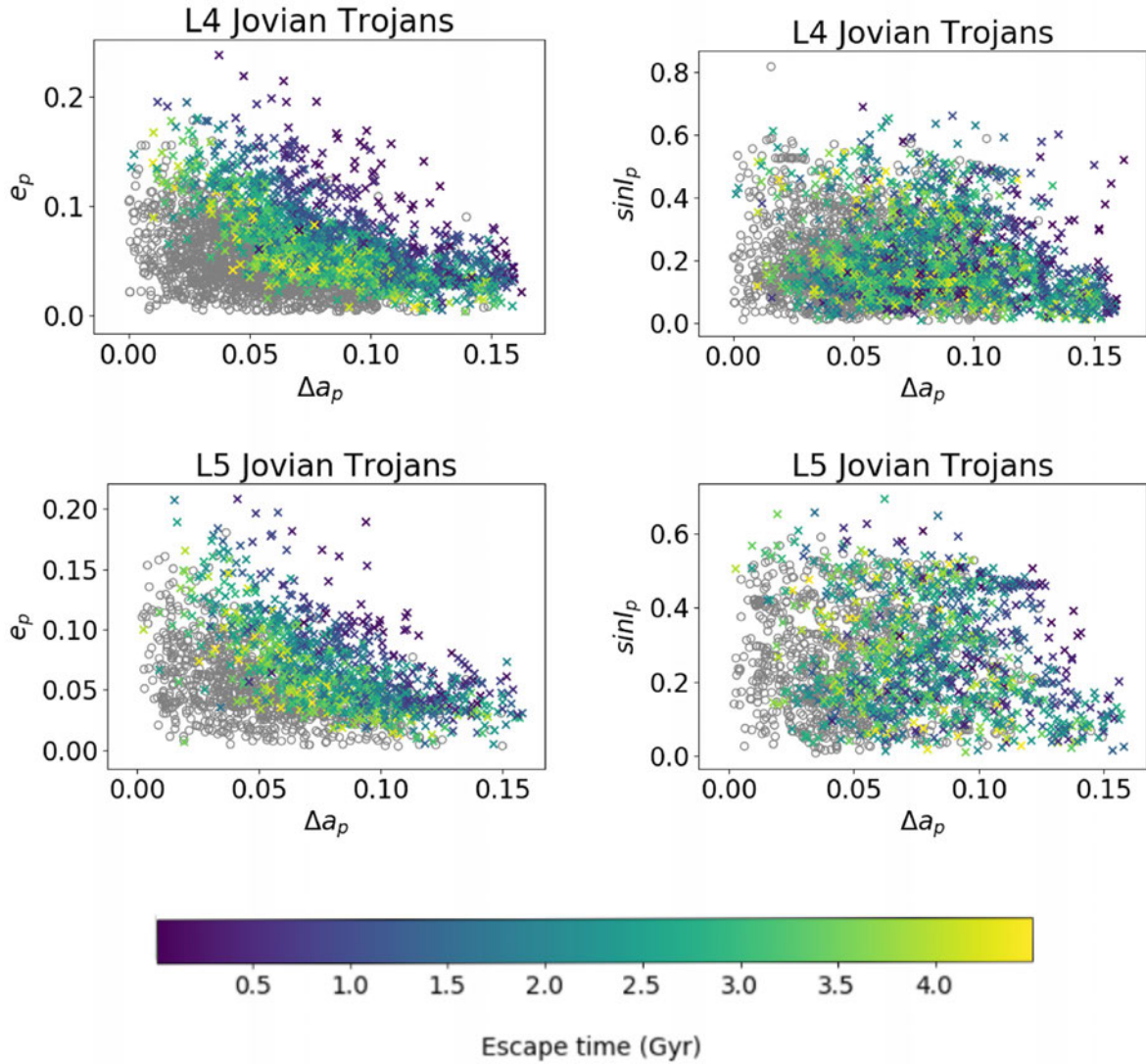


Figure 3. Escape analysis of Jovian Trojans in the L₄ and L₅ swarms simulated over 4.5 Gyr. Proper elements, semimajor axis (Δa_p), eccentricity (e_p), and sine inclination ($\sin i_p$), are taken from the AstDys data base (Knežević & Milani 2017). o indicates objects that are stable over the simulated time frame. X shows objects that have at least one particle escaping the population, with their mean respective escape times indicated by colour.

coefficients of determination (R^2) and 1σ errors are presented in Fig. 4. These linear fits are shown in equations (1) for the population, equation (2) for the L₄ swarm, and equation (3) for the L₅. In these equations, the escape percentages (y) are per 1×10^7 yr (x) of the contemporary size of the population (equation 1) and each individual swarms (equations 2–3). These equations are similar, once the bins are taken into account, to those found by Di Sisto et al. (2019), validating our results:

$$y_{pop} = -9.328 \times 10^{-14}x + 0.0007384, \quad (1)$$

$$y_{L4} = -8.581 \times 10^{-14}x + 0.0007085, \quad (2)$$

$$y_{L5} = -1.078 \times 10^{-14}x + 0.000796. \quad (3)$$

Using linear equations (1)–(3), we can calculate the predicted original size of the Jovian population and L₄/L₅ swarms, see Fig. 5, under the assumption that the historical decay of the Trojan population proceeded in the same manner as we see in our simulations. Though the known Jovian Trojan size-frequency distribution, Fig. 2,

is only complete to a fraction of the theoretical size, we can still make predictions of the number of objects, placing constraints on their formation and capture. The original population, based on the integration of equation (1), is approximately 1.332 ± 0.004 times the current population. There is an observed difference in the past size of the L₄ and L₅ swarms. Due to the difference in their escape rates, the past L₄ swarm is predicted to be 1.319 ± 0.005 times larger than the contemporary swarm, while the L₅ is 1.358 ± 0.008 times larger. The predicted implantation sizes, based on modern numbers and the escape rates, are 4792 ± 19 for the L₄ and 2606 ± 15 for the L₅. This past ratio reduces the current 1.89 numerical asymmetry to 1.84 ± 0.003 . This small difference in past/contemporary size ratio does not account for the modern observed numerical asymmetry, as previously noted (Nesvorný & Dones 2002; Tsiganis et al. 2005b; Di Sisto et al. 2014, 2019).

The *in situ* transport model (Pirani et al. 2019a,b) predicts that the initial mass the Jovian Trojan population was three to four times the magnitude of the observed population. Our escape analysis estimates a primordial population size only 1.332 ± 0.004 times

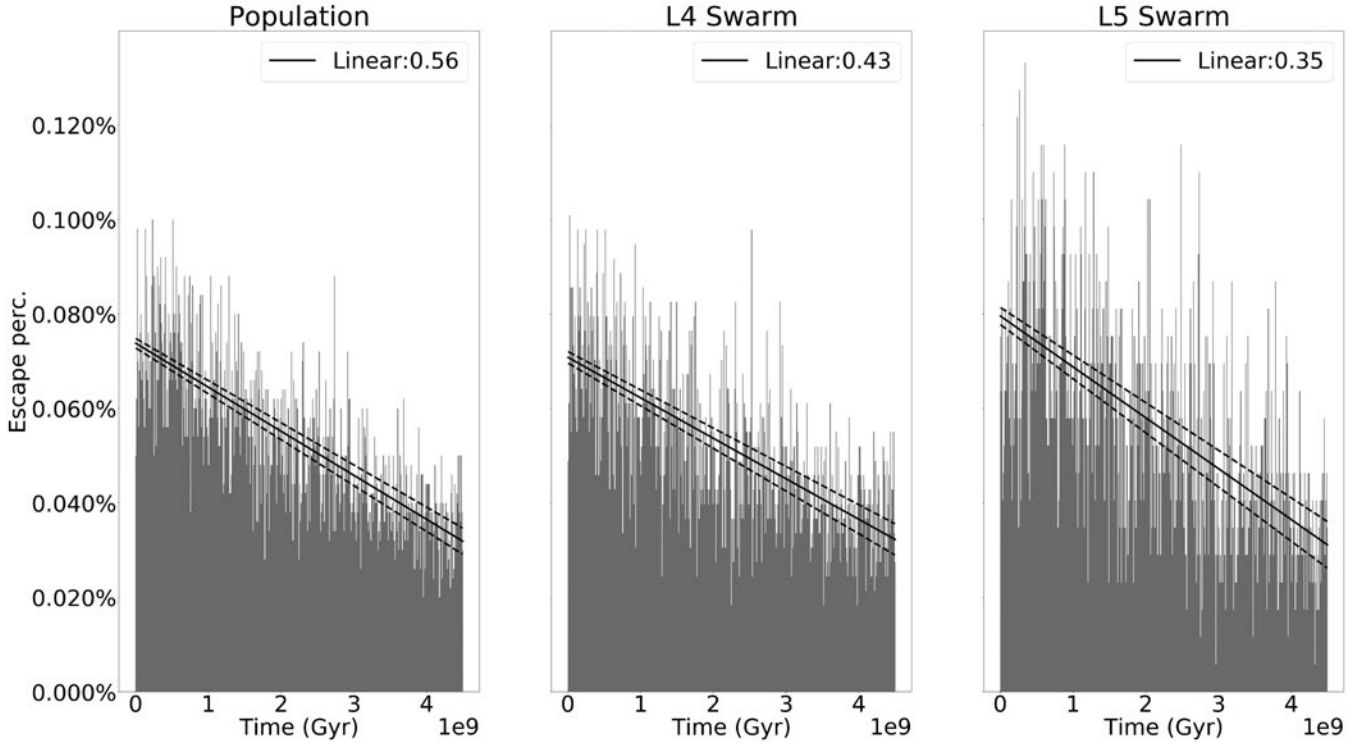


Figure 4. Histograms of escape percentages of the contemporary number, per 1×10^7 yr, of a pool of Jovian Trojan particles, in the combined population, L₄ and L₅ swarms. Lines are linear best fit along with associated R^2 values. Dotted lines are 1σ errors.

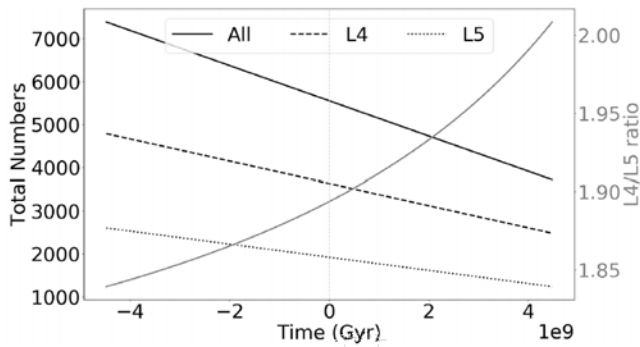


Figure 5. Number of objects, calculated from the contemporary total population (solid line), L₄ (dashed line) and L₅ (dotted line) Jovian Trojan swarms, as a function of time, with 0 time being the present. Right axis shows changing ratio (grey line) between L₄ and L₅ swarms. Plotted from equations discussed in Section 3.1.

larger than today. This is still several orders of magnitude smaller than the most conservative predictions of Pirani et al. (2019a). However, it should be noted that our estimates for the initial population are based on the assumption that the current linear decay has remained consistent since the origin of the Trojan population. In the population's youth, it is possible that the decay rate could have been markedly higher, had objects been efficiently captured to the less stable regions of the Trojan population. Pirani et al. (2019b) do report on interactions with Saturn affecting Trojans larger inclinations, though this is still insufficient to explain the current escape rate.

The majority of escape particles are eventually ejected from the Solar system, by achieving a heliocentric distance of 1000 au, in the same 1×10^5 time-step. This is longer than the expected lifetime

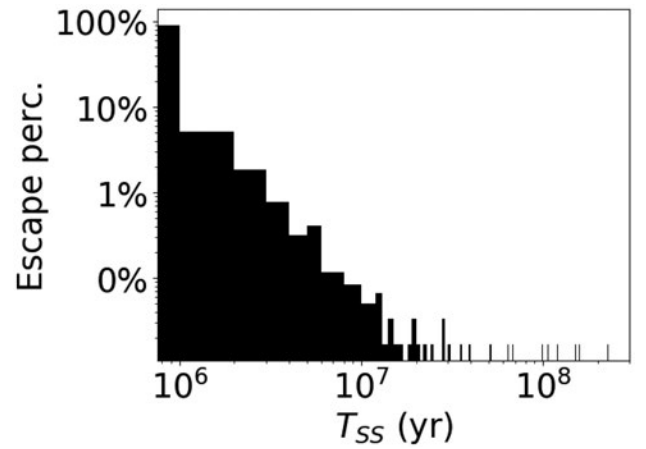


Figure 6. Histogram (1×10^6 yr bins) of time spent in the Solar system prior to ejection (T_{SS}) of objects that escape the Jovian Trojan population. Escape percentages are based of nine particles generated for each of 5553 Jovian Trojans.

of most Centaurs (Horner, Evans & Bailey 2004a), particularly those starting on orbits close to that of Jupiter. A fraction of the population escapees, approximately 41.41 per cent, stay within the Solar system for a longer period of time, prior to being ejected. This fraction is similar between the L₄ and L₅ populations, 41.37 per cent and 41.45 per cent, respectively. This similarity between swarms is not unexpected, since the chaotic evolution of test particles once they leave the Trojan population would be expected to quickly erase any ‘memory’ of their original orbit. Fig. 6 shows the length of time that these particles spend in the Solar system, with over 88.58 per cent escaping in the first 1×10^6 yr, and an additional

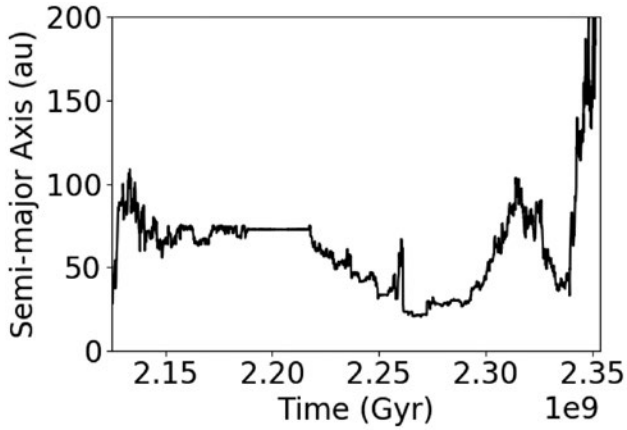


Figure 7. The behaviour of the longest lived escapee, clone 2 of (312627) 2009 TS₂₆ in semimajor axis over time. Start time is the point when the particle escapes the L₄ Jovian swarm. End time is when the particle escapes the Solar system.

6.15 per cent escaping in the next 1.0×10^6 yr. By 1.0×10^7 yr, 99.25 per cent of the particles have been ejected. These short lifetimes are consistent with the expected lifetimes of Centaurs (Horner et al. 2004a). Horner et al. (2012) show that at least one escaped Jovian Trojan, (1173) Anchises, can participate in the Centaur population before being ejected. Despite this high number of short-lived objects, 13 particles survive longer than 3.2×10^7 yr, the expected lifetime of the longest Centaur (Horner et al. 2004a). These long-lived particles are not unexpected, as Horner et al. (2004a) and Horner, Evans & Bailey (2004b) also reported on several long-lived particles. Each of our clone particles have a different reference object. The longest lived particle is clone 2 of (312627) 2009 TS₂₆, which lives for 2.286×10^8 yr, shown in Fig. 7, and represents a typical chaotic pattern for escaped Trojans.

Less than 10 per cent, 547 objects, of the Jovian Trojan population have been classified under the Bus-Demeo system (Tholen 1984; Bus 2002; Bendjoya et al. 2004; Fornasier et al. 2004, 2007; DeMeo et al. 2009; Carvano et al. 2010; Grav et al. 2012; DeMeo & Carry 2013). The majority, 65.08 per cent, are considered D-types, with several other minor classes X-type (15.17 per cent), C-type (12.79 per cent), and other classes below 5 per cent (P-type, L-type, S-type, V-type, and F-type). The rate at which the three major classes, D-type, X-type, and C-type objects escape, 23.00 per cent, 27.66 per cent, and 24.13 per cent, respectively, is roughly constant with the overall population. Many of the smaller taxonomic classes come from Carvano et al. (2010), Hasselmann, Carvano & Lazzaro (2012), and have low classification confidence levels. If we reduce the taxonomic data set to only those in Carvano et al. (2010) and Hasselmann et al. (2012) with a confidence classification of greater than 50, it reduces the classified Trojans down to 2 per cent of the population, and only D-type (79.24 per cent), X-type (14.15 per cent), and C-type (6.6 per cent) objects. This restriction does not change the escape rates significantly for the D-types at 23.41 per cent. The X-types and C-types do increase to 32.59 per cent and 31.75 per cent, respectively, though these classes suffer from the variances of small number statistics. This classification analysis is something that may merit further study once data becomes available from the Rubin Observatory LSST (Schwamb et al. 2018a,b), and our escape analysis can then be placed in a wider taxonomic context.

4 COLLISIONAL FAMILIES

In order to further investigate the escapes of collisional family members, we have increased the number of clones simulated to 125 for each of the canonical family members in Nesvorný et al. (2015). This increases the statistical significance of the escape analysis. For comparison purposes, the wider, non-canonical family data sets found by Brož & Rozehnal (2011) and Rozehnal et al. (2016) use the original eight clones, as in Section 3, and only those objects found in the AstDys data base (Knežević & Milani 2017).

The specific numbers of canonical collisional family members that are simulated in this work are shown in Table 3, after Nesvorný et al. (2015). Of particular interest is the Eurybates family. This is the largest known family in the Jovian Trojan population and is discussed separately in Section 4.1.1. When all of the particles are considered independently, f_{EscP} and f_{VEscP} in Table 3, the percentage that escape is similar to the escape rate of the reference particles (f_{EscR} and f_{VEscR} in Table 3). This is comparable to the trends seen in the overall swarms (see Section 3).

In general terms, the members of known collisional families within our integrations show lower escape percentages than the total of the swarms. This is due to the fact that the majority of the known collisional families are located in the more stable regions of the delta semimajor axis, eccentricity, and $\sin i$ parameter space, as discussed in Sections 4.1 and 4.2.

There are also potentially a significant number of undetected family members (Yoshida & Nakamura 2008; Vinogradova & Chernetenko 2015) in the Jovian Trojan population. The numerical escape percentages may increase as a larger number of objects are discovered by new surveys, such as the Rubin Observatory LSST (Schwamb et al. 2018a), which is expected to commence science operations in 2023. As these new objects are discovered, their allocation to collisional families and long-term stabilities will need to be investigated.

4.1 L₄ collisional Families

In the L₄ swarm, shown in Fig. 8, a total four families have been identified. The largest L₄ cluster, the Eurybates family is discussed in Section 4.1.1.

4.1.1 Eurybates family

The Eurybates family is the largest and most consistently identified (Brož & Rozehnal 2011; Nesvorný et al. 2015; Vinogradova 2015) collisional cluster in the Trojan population. The largest fragment of the family, (5348) Eurybates, is also the target of future visitation by the *Lucy* spacecraft in 2027 (Levison et al. 2017). In our simulations, we consider the canonical 218 identified members of the family (Nesvorný et al. 2015). From the 310 members identified by Brož & Rozehnal (2011), 293 are in the AstDys data base. In the canonical members, there is a 19.59 per cent escape percentage for the particle pool. If we consider the larger set identified by Brož & Rozehnal (2011), this escape percentage only decreases slightly to 19.07 per cent.

As was seen in the L₄ swarm (Fig. 3), there is a gradient to the escape from the Eurybates family (Fig. 9) with larger changes in semimajor axis (Δa_p) and eccentricity (e_p), causing particles to escape the swarm sooner. Contrary to the overall decreasing escape rates seen in the L₄ swarm, we found the escape rate of the Eurybates family to be increasing with time, as can be seen in Fig. 10. A possible explanation for this is the ongoing diffusion of

Table 3. Escaping collisional family members; n : number of objects in each canonical collisional family (Nesvorný et al. 2015); the n_{EscR} : number of reference particles that escape; f_{EscR} : numerical percentage of reference particles that escape; f_{VEscR} : volumetric percentage of reference particles that escape; f_{EscP} : numerical percentage Trojan particle pool, Reference and 125 1σ clones, that escape; f_{VEscP} : volumetric percentage Trojan particle pool, Reference and 125 1σ clones, that escape.

	n	n_{EscR}	f_{EscR} (per cent)	f_{VEscR} (per cent)	f_{EscP} (per cent)	f_{VEscP} (per cent)
L4 Families						
Eurybates (1)	218	43	19.72	7.43	19.59	8.05
Hektor (2)	12	2	16.66	0.06	11.99	28.53
1996 RJ (3)	7	0	0.00	0.00	0.00	0.00
Arkesilaos (4)	37	1	2.70	1.13	3.09	3.47
L5 Families						
Ennomos (5)	30	15	50.00	66.39	34.29	17.47
2001 UV ₂₀₉ (6)	13	0	0.00	0.00	0.00	0.00
Total	317	61	19.24	12.45	17.67	24.75%

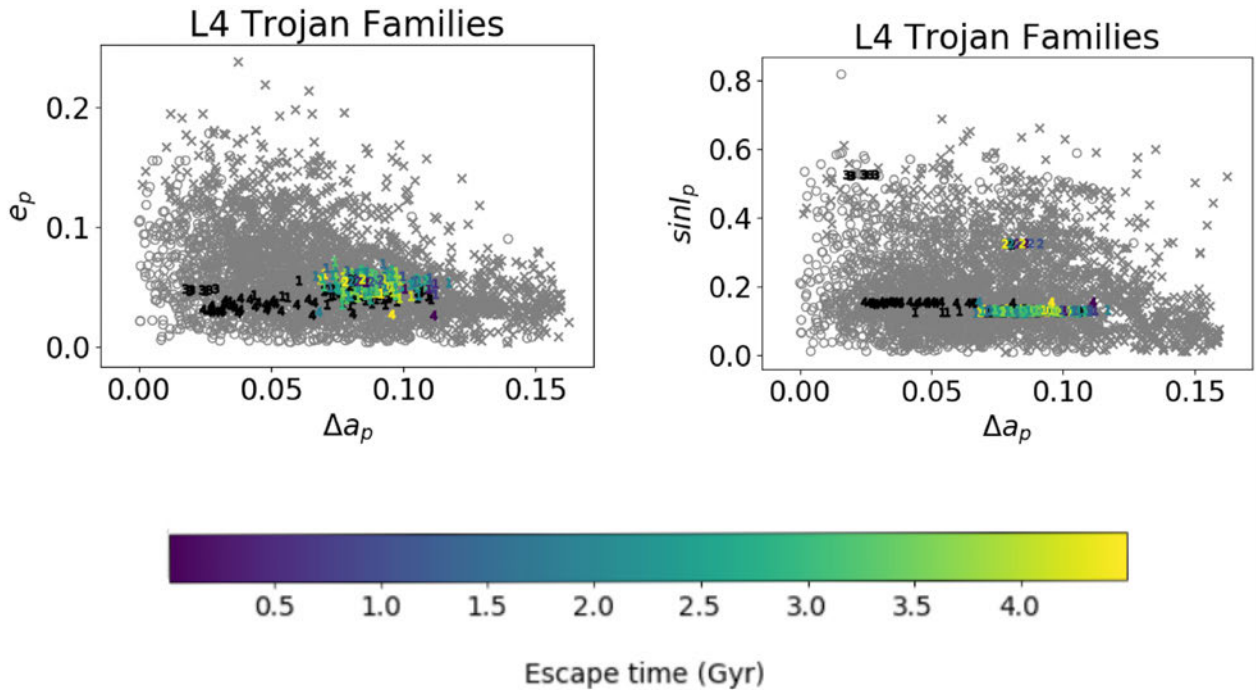


Figure 8. Escape analysis of collisional family members located in the L₄ Jovian Trojan swarm simulated for 4.5×10^9 yr. Shown are the instabilities of the reference object. Proper elements, semimajor axis (Δa_p), eccentricity (e_p), and sine inclination ($\sin i_p$), are taken from the AstDys data base (Knežević & Milani 2017). o indicates objects that are stable over the simulated time frame. x are unstable background objects. Family membership: Eurybates (1), Hektor (2), 1996 RJ (3), Arkesilaos (4). Black numbers are stable, with colours showing mean particle escape time.

family members into less stable parameter space, as they disperse chaotically from the initial location of the breakup event. Such dispersion can be seen in main belt families (Milani & Knežević 1992; Bottke et al. 2005; Brož & Morbidelli 2013; Aljbaae et al. 2019), with members gradually diffusing into Jovian resonances and being ejected from the main belt. Future simulations of a synthetic Eurybates family would be required to confirm this, and are beyond the scope of this paper.

As with the L₄ swarm escape analysis, a standard linear regression offers the most reliable fit for the data. We did attempt to create a second-order polynomial, along with using cumulative linear and polynomial regression to improve the fit in this case, though as Fig. 10 demonstrates, this did not improve the coefficient of

determination. The coefficient of determination for the linear fit ($R^2 = 0.42$) is similar to the L₄ swarm, due to number of particles being considered being an order of magnitude smaller. We attempted to take account for this by using an order of magnitude larger bins to increase the number of ejections per bin to a reasonable number. The y-intercept of this linear equation, which represents the time at which the escape rate from the Eurybates family equals zero, might be considered to be an indication of the age of the family. If such a conclusion is reasonable, our data would place the family formation event some $1.045 \pm 0.364 \times 10^9$ yr ago. This age is presented as a minimum age, though preliminary simulations of a synthetic Eurybates family (Holt et al. 2019) indicate that the observed dynamical situation could be achieved within 1×10^5 yr.

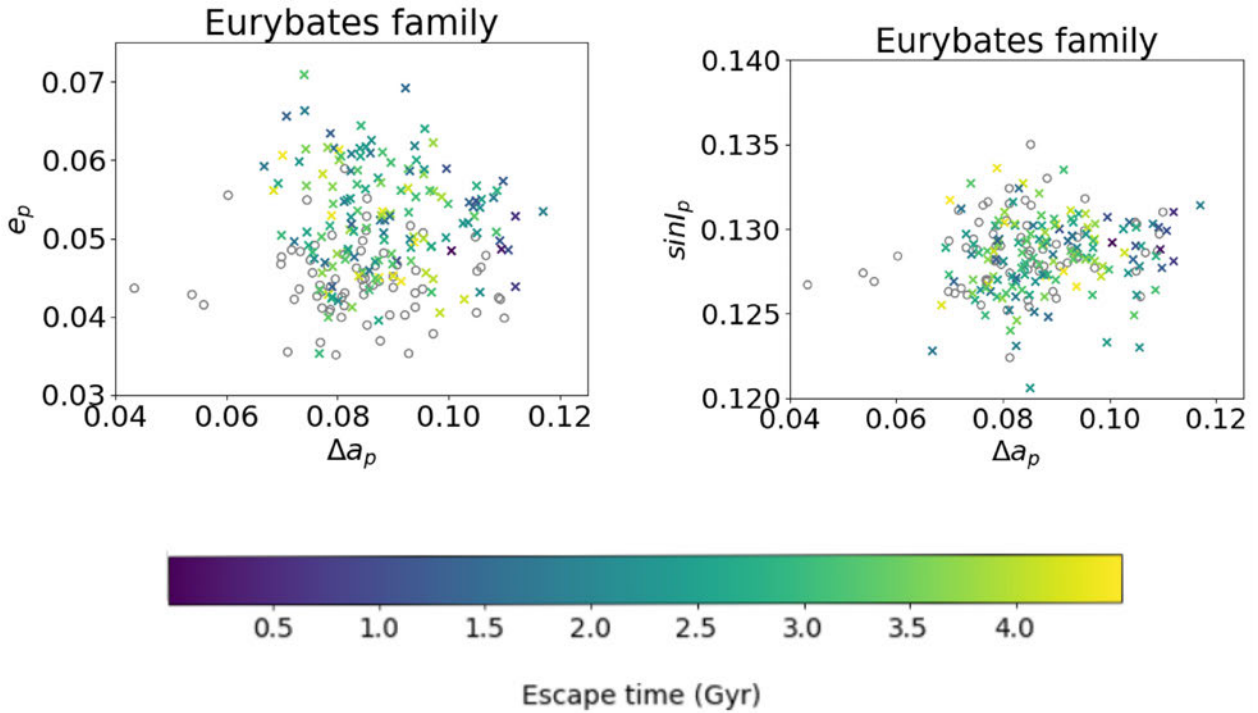


Figure 9. Escape analysis of the canonical Eurybates collisional family members identified in Nesvorný et al. (2015), simulated for 4.5×10^9 yr. Shown are the mean escape time of 126 particles for the object (coloured x). Proper elements, semimajor axis (Δa_p), eccentricity (e_p), and sine inclination ($\sin I_p$) are taken from the AstDys data base (Knežević & Milani 2017). o indicates objects that are stable over the simulated time frame.

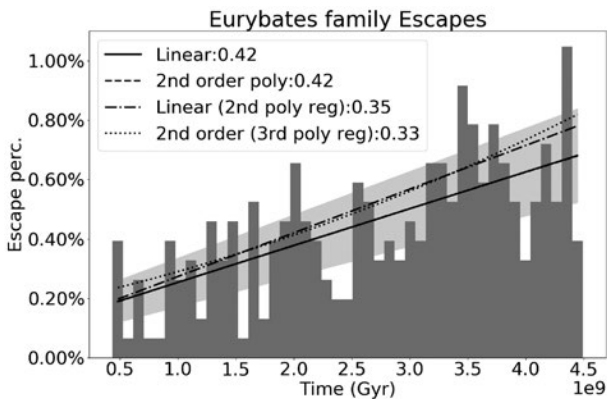


Figure 10. Histogram (1×10^8 yr bins) of escapes from the Eurybates collisional family. Lines indicate best-fitting analysis scaled to the histogram bins, with R^2 scores for linear fit (solid, with light grey shading indicating 1σ error) and second degree polynomial (dashed) lines. Fits are also shown from the results of linear regression analysis on second (dot-dashed) and third-order polynomial (dotted) generated from a cumulative histogram.

As previously stated, the two other methods of collisional family age estimation, high precision reverse integration (Nesvorný et al. 2002a) and Yarkovsky ‘V’ (Milani et al. 2017) are inappropriate for the Trojan families. Using a small number of synthetic members, Brož & Rozehnal (2011) also calculated a wide time range, 1–4Gyr, for the family creation event. Our age is therefore one of the first estimations that give a reasonable order of magnitude age and constrained range for the Eurybates family. As larger numbers of family members are identified, a re-investigation should improve the statistical reliability of this analysis.

4.1.2 Hektor family

Rozehnal et al. (2016) identified 90 objects in this family, using the Random box method. We use the canonical 12 objects from Nesvorný et al. (2015), and note where there could possibly be a different escape rate. The family is characterized by a moderate Δa_p and e_p , with a comparatively high $\sin I_p$. The parent body, (624) Hektor has been classified under the Bus-Demeo spectral taxonomy (DeMeo et al. 2009) as a D-type asteroid (Emery, Cruikshank & Van Cleve 2006; Emery, Burr & Cruikshank 2011; Rozehnal et al. 2016). It is also a contact binary, with a confirmed satellite (Marchis et al. 2014). The canonical Hektor family has a low escape rate, with only two reference particles from the family eventually escaping the swarm. One of these is the reference particle of (624) Hektor itself, which also has a 28.8 per cent particle escape rate. These particles account for the large volume of escapes, nearly double that of the numerical escape fraction. Unfortunately, the small number of identified members of the Hektor family, 12 known objects, means that a statistical analysis of these results would prove problematic. Using the larger number of clones, we can assign a numerical escape percentage of 12 per cent. If the wider numbers, 77 objects from Rozehnal et al. (2016) are used, then 18.18 per cent of particles escape.

4.1.3 1996 RJ family

The compact 1996 RJ family has a small Δa_p and e_p . This places it firmly within the predicted stability region from Nesvorný & Dones (2002). The high inclinations of the family members do not seem to have an effect on their stability. Our results show that this family is completely stable, with no escapes. Those members from Rozehnal et al. (2016) are also stable, except for the single particle, clone 6 of

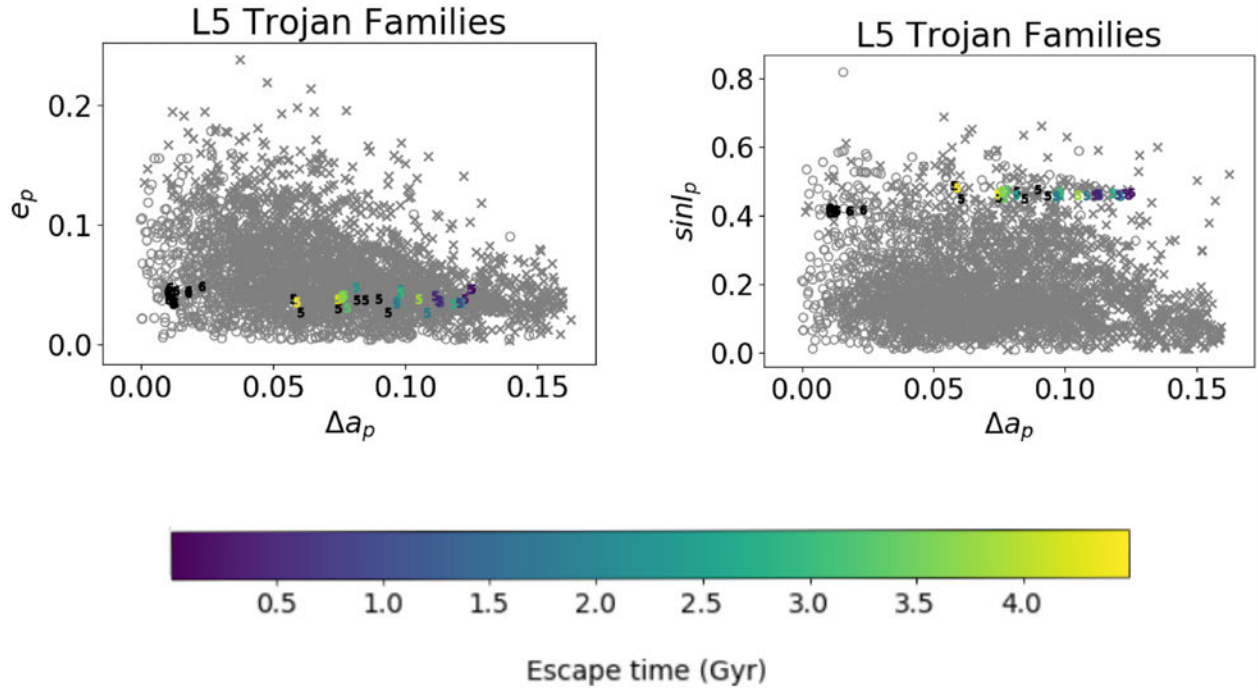


Figure 11. Escape analysis of collisional family members located in the L₅ Jovian Trojan Swarm simulated for 4.5e9 yr. Proper elements, delta semimajor axis (Δa_p), eccentricity (e_p), and sine inclination ($\sin I_p$), are taken from the AstDys data base (Knežević & Milani 2017). o indicates objects that are stable over the simulated time frame. x are unstable background objects. Numbers indicate collisional family membership: Ennomos (5), 2001 UV₂₀₉ (6). Black numbers are stable, with colours showing mean escape time of 126 particles for the object.

(195104) 2002 CN₁₃₀. This particular object has a higher Δa_p than the rest of the family, and is a probable outlier.

4.1.4 Arkesilaos family

This is a medium-sized family, with 37 canonical members. It is confirmed by Vinogradova (2015), though they use (2148) Epeios as the main object and have a larger number of members (130). Rozehnal et al. (2016) chose (20961) Arkesilaos as the primary objects due to consistency at the centre of the family parameter space, even at low cut-off velocities. The family has a wide distribution of Δa_p values and a compact range of e_p and $\sin I_p$ values. Predictably, the family is stable with three small outliers that escape. (356237) 2009 SA₃₂₈ is the most unstable, with 72 per cent of the particles escaping. This is due to its high Δa_p , placing it in the unstable parameter space. (394808) 2008 RV₁₂₄ and (20961) Arkesilaos also have some particles escape, but only 28.9 per cent and 14.4 per cent, respectively. The escape fraction of the family only changes slightly to 2.24 per cent, considering the additional members identified by Rozehnal et al. (2016). The small escape percentages of this family preclude any additional statistical analysis.

4.2 L5 Collisional families

Within the L₅ swarm, there are only two identified collisional families (Nesvorný et al. 2015), the Ennomos and 2001 UV₂₀₉ families. Contrary to Rozehnal et al. (2016) and the canonical Nesvorný et al. (2015), Vinogradova (2015) do not consider either of the families valid, though they note that there is some clustering around the largest members. We show the escape times of the L₅ families in Fig. 11.

4.2.1 Ennomos family

The most unstable cluster in the L₅ swarm is the Ennomos family. This is a medium-sized cluster, with 30 identified objects in Nesvorný et al. (2015). There are a larger number of objects, 104, of which 85 are in the AstDys data base, identified by Rozehnal et al. (2016). The family members have relatively high Δa_p and $\sin I_p$, with low e , placing them on the edge of the stable parameter space. Consequently, a large fraction of Ennomos family members, 50 per cent of reference particles, escape the swarm. When considering just the reference particles, 66.66 per cent of the volume escape during our simulations. This is due to the reference particle and a low number of clones (14.28 per cent) of (1867) Deiphobus, a 59 km object, escaping the L₅ swarm. In the more statistically robust particle pool, the escape percentage by volume drops to 17.47 per cent. This family is characterized by its high inclination and delta semimajor axis, so a high amount of instability is not unexpected. In this family, there are three members, (48373) Gorgythion, (381987) 2010 HZ₂₁ and (287454) 2002 YX₇ where all particles escape. This is unsurprising, as (48373) Gorgythion has the largest proper Δa_p and e_p of the family. In addition to these three, six objects have over 50 per cent of their particles escape. Including the larger number of members from Rozehnal et al. (2016), decreases the escape rate to 23.14 per cent, closer to the overall L₅ rate.

As in Section 4.1.1, we attempted regression analysis to ascertain the age of this family. Brož & Rozehnal (2011) estimate the age of the family to be approximately 1–2 Gya. Similar to the L₅ swarm and unlike the Eurybates family, the slope of the linear regression analysis is negative, though fairly flat (-1.62×10^{-12}). The R^2 score is only 0.13, so until additional family members are identified, these are only preliminary indications.

4.2.2 2001 UV₂₀₉

This small family, with thirteen canonical members, is located well within the stable Δa_p - e parameter space. It is then not unexpected that the 2001 UV₂₀₉ family members are stable in our simulations. Considering the expanded 36 objects identified by Rozehnal et al. (2016), this jumps to 13.89 per cent. These unstable members are not considered valid by Nesvorný et al. (2015), and with higher Δa_p are probable background objects, rather than members of the family.

5 CONCLUSIONS

The Jovian Trojans are a fascinating collection of objects, remnants of the early stages of the Solar system's formation. In this work, we present the results of detailed n -body simulations of the known Jovian Trojan population, using nearly double the number of objects of the previous largest study (Di Sisto et al. 2014, 2019). We simulate the orbital evolution of a population of 49 977 massless test particles, nine particles for each of the 5553 known Jovian Trojans, for a period of 4.5×10^9 yr into the future, under the gravitational influence of the Sun and the four giant planets. Our simulations reveal that the populations of both the L₄ and L₅ swarms are predominately stable; however, a significant number of objects from both swarms can escape over the lifetime of the Solar system. In the case of the leading L₄ swarm, we find that 23.35 per cent of objects escape, by volume. Similarly, only 24.89 per cent escape the trailing L₅ swarm. Overall, 23.95 per cent by volume of all test particles simulated in this work escape the Jovian population. As discussed by other authors (Nesvorný & Dones 2002; Tsiganis et al. 2005b; Nesvorný et al. 2013; Di Sisto et al. 2014, 2019), we find that the escape rates cannot explain the current observed asymmetry between the two swarms. This supports the conclusion that the observed asymmetry between the L₄ and L₅ swarms are the result of their initial capture implantation (Nesvorný et al. 2013; Pirani et al. 2019a).

The escape rates of objects from the two Trojan swarms are in accordance with the idea that the Jovian Trojans act as a source of material to the other small Solar system body populations, as noted in Levison et al. (1997), Di Sisto et al. (2014), Di Sisto et al. (2019), particularly with regards to the Centaurs (Horner et al. 2004a, 2012). The majority of escaped Trojans, 58.63 per cent, are ejected from the population and the Solar system within a single 1×10^5 yr time-step. For those that remain in the Solar system, 99.25 per cent are ejected by 1×10^7 yr, after joining the Centaur population.

In the Jovian Trojan swarms, a total of six collisional families have been identified to date (Nesvorný et al. 2015), with four in the L₄ swarm and two located around L₅. We find that three of the families are highly dynamically stable, with no particles escaping the Trojan population through the course of our integrations (the 1996 RJ, Arkesilaos and 2001 UV₂₀₉ families). Two other collisional groups, the L4 Hektor and L5 Ennomos families did have members that escape. These unstable families all have a small number of known members, which limits our ability to study their stability further in this work. The largest known Trojan family, the Eurybates L4 family, has a smaller escape rate than the overall population. Contrary to the escape trends in the population, however, the escape rate of the Eurybates family is found to increase with time in our simulations. This might point to the diffusion of its members into unstable parameter space as they evolve away from the location of the family's creation. From this escape rate, we can obtain an estimate of the age of the Eurybates family on the order of $1.045 \pm 0.364 \times 10^9$ yr.

In the future, as more members of the Jovian Trojans and their taxonomic groupings are identified, it will be interesting to see whether these dynamical methods can be used to help constrain the ages of the smaller clusters. If this is possible, such results would shed light on the variability of the collision rates within the Jovian Trojan swarms. The results we present in this paper, and these potential future works, highlight the impotence of the Jovian Trojan swarms, their taxonomic groups and collisional families, to understanding the history of the Solar system.

ACKNOWLEDGEMENTS

This research was in part supported by the University of Southern Queensland's Strategic Research Initiative programme. TRH was supported by the Australian Government Research Training Program Scholarship. This work makes use of the Anaconda Python software environment (Continuum Analytics 2016). We thank Hal Levison for discussions on the paper and for providing previously unpublished data. We also thank Douglas Hamilton and Romina Di Sisto (as a reviewer) for providing comments and insights on this paper. This research has made use of NASA Astrophysics Data System Bibliographic Services.

REFERENCES

- Aljbaae S., Souchay J., Prado A. F. B. A., Chanut T. G. G., 2019, *A&A*, 622, A39
- Barnes R., Quinn T. R., 2004, *AJ*, 611, 494
- Beaugé C., 2001, *Icarus*, 153, 391
- Bendjoya P., Cellino A., Di Martino M., Saba L., 2004, *Icarus*, 168, 374
- Bolin B. T., Delbó M., Morbidelli A., Walsh K. J., 2017, *Icarus*, 282, 290
- Botke W. F., Durda D. D., Nesvorný D., Jedicke R., Morbidelli A., Vokrouhlický D., Levison H. F., 2005, *Icarus*, 179, 63
- Botke W. F., Vokrouhlický D., Rubincam D., Nesvorný D., 2006, *Ann. Rev. Earth Planet. Sci.*, 34, 157
- Botke W. F., Nesvorný D., Vokrouhlický D., Morbidelli A., 2010, *AJ*, 139, 994
- Brown M. E., Barkume K. M., Ragozzine D., Schaller E. L., 2007, *Nature*, 446, 294
- Brož M., Morbidelli A., 2013, *Icarus*, 223, 844
- Brož M., Rozehnal J., 2011, *MNRAS*, 414, 565
- Brož M., Vokrouhlický D., 2008, *MNRAS*, 390, 715
- Brož M., Vokrouhlický D., Roig F., Nesvorný D., Botke W. F., Morbidelli A., 2005, *MNRAS*, 359, 1437
- Bus S. J., 2002, *Icarus*, 158, 146
- Carruba V., Domingos R. C., Nesvorný D., Roig F., Huaman M. E., Souami D., 2013, *MNRAS*, 433, 2075
- Carvano J. M., Hasselmann P. H., Lazzaro D., Mothé-Diniz T., 2010, *A&A*, 510, A43
- Continuum Analytics, 2016, Anaconda Software Distribution. Version 2.4.0. Available at: <https://continuum.io>
- de la Fuente Marcos C., de la Fuente Marcos R., 2018, *MNRAS*, 474, 838
- De Luise F., Dotto E., Fornasier S., Barucci M. M. A., Pinilla-Alonso N., Perna D., Marzari F., 2010, *Icarus*, 209, 586
- Deienno R., Morbidelli A., Gomes R. S., Nesvorný D., 2017, *AJ*, 153, 153
- Delbó M., Walsh K., Bolin B., Avdellidou C., Morbidelli A., 2017, *Science*, 357, 1026
- DeMeo F. E., Carry B., 2013, *Icarus*, 226, 723
- DeMeo F. E., Binzel R. P., Slivan S. M., Bus S. J., 2009, *Icarus*, 202, 160
- Di Sisto R. P., Ramos X. S., Beaugé C., 2014, *Icarus*, 243, 287
- Di Sisto R. P., Ramos X. S., Gallardo T., 2019, *Icarus*, 319, 828
- Ebell M., 1909, *Astron. Nachr.*, 180, 213
- Emery J. P., Cruikshank D. P., Van Cleve J., 2006, *Icarus*, 182, 496
- Emery J. P., Burr D. M., Cruikshank D. P., 2011, *AJ*, 141, 25

- Emery J. P., Marzari F., Morbidelli A., French L. M., Grav T., 2015, in Michel P., DeMeo F., Bottke W., eds, *Asteroids IV*. Univ. Arizona Press, Tucson, AZ, p. 203
- Fernández Y. R., Jewitt D., Ziffer J. E., 2009, *AJ*, 138, 240
- Fornasier S., Dotto E., Marzari F., Barucci M., Boehnhardt H., Hainaut O., Debergh C., 2004, *Icarus*, 172, 221
- Fornasier S., Dotto E., Hainaut O., Marzari F., Boehnhardt H., Deluise F., Barucci M., 2007, *Icarus*, 190, 622
- Giorgini J. D. et al., 1996, American Astronomical Society, DPS meeting #28, id.25.04
- Gradie J. C., Chapman C. R., Williams J. G., Gradie J. C., Chapman C. R., Williams J. G., 1979, in Gehrels T., ed., *Asteroids*. Univ. Arizona Press, Tucson, AZ, p. 359
- Grav T., Bauer J. M., 2007, *Icarus*, 191, 267
- Grav T., Holman M. J., Gladman B. J., Aksnes K., 2003, *Icarus*, 166, 33
- Grav T. et al., 2011, *Astrophys. J.*, 742, 40
- Grav T., Mainzer A. K., Bauer J. M., Masiero J. R., Nugent C. R., 2012, *Astrophys. J.*, 759, 49
- Harris A. W., 1997, *Icarus*, 126, 450
- Hasselmann P. H., Carvano J. M., Lazzaro D., 2012, NASA Planetary Data System. Available at: <https://pds.nasa.gov/ds-view/pds/viewDataset.jsp?dsid=EAR-A-I0035-5-SDSSTAX-V1.1>
- Heinrich V., 1907, *Astron. Nachr.*, 176, 193
- Hellmich S., Mottola S., Hahn G., Kühr E., de Niem D., 2019, *A&A*, 630, A148
- Hirayama K., 1918, *AJ*, 31, 185
- Holt T. R., Brown A. J., Nesvorný D., Horner J., Carter B., 2018, *ApJ*, 859, 97
- Holt T., Nesvorný D., Horner J., King R., Carter B., Brookshaw L., 2019, AAS Division on Dynamical Astronomy Meeting #50, id. 100.01
- Homer, 750 BC, *The Iliad & The Odyssey*, 2013 edn. Barnes & Noble, New York, NY
- Horner J., Evans N. W., Bailey M. E., 2004a, *MNRAS*, 354, 798
- Horner J., Evans N. W., Bailey M. E., 2004b, *MNRAS*, 355, 321
- Horner J., Müller T. G., Lykawka P. S., 2012, *MNRAS*, 423, 2587
- Jewitt D. C., 2018, *AJ*, 155, 56
- Jewitt D. C., Haghhighipour N., 2007, *ARA&A*, 45, 261
- Jewitt D. C., Trujillo C. A., Luu J. X., 2000, *AJ*, 120, 1140
- Knežević Z., Milani A., 2003, *A&A*, 403, 1165
- Knežević Z., Milani A., 2017, *AstDys: Synthetic Proper Elements 5553 Numbered and Multiopposition Trojans*. Available at: https://newton.spacedys.com/~astdys2/propsynth/tro_syn
- Kopff A., 1909, *Astron. Nachr.*, 182, 25
- Lagrange J.-L., 1772, *Prix de l'académie Royale des Sciences de Paris*, 9, 292
- Levison H. F., Shoemaker E. M., Shoemaker C. S., 1997, *Nature*, 385, 42
- Levison H. F., Morbidelli A., Vokrouhlický D., Bottke W. F., 2008, *AJ*, 136, 1079
- Levison H. F., Morbidelli A., Tsiganis K., Nesvorný D., Gomes R., 2011, *AJ*, 142, 152
- Levison H. F., Olkin C. B., Noll K., Marchi S., Lucy Team, 2017, 48th Lunar and Planetary Science Conference, held 20–24 March 2017, at The Woodlands, Texas, ID: 2025
- Lykawka P. S., Horner J., 2010, *MNRAS*, 405, 1375
- Marchis F. et al., 2006, *Nature*, 439, 565
- Marchis F. et al., 2014, *Astrophys. J.*, 783, L37
- Milani A., 1993, *Celest. Mech. Dyn. Astron.*, 57, 59
- Milani A., Farinella P., 1994, *Nature*, 370, 40
- Milani A., Knežević Z., 1992, *Icarus*, 98, 211
- Milani A., Knežević Z., Novaković B., Cellino A., 2010, *Icarus*, 207, 769
- Milani A., Cellino A., Knežević Z., Novaković B., Spoto F., Paolicchi P., 2014, *Icarus*, 239, 46
- Milani A., Knežević Z., Spoto F., Cellino A., Novaković B., Tsirvoulis G., 2017, *Icarus*, 288, 240
- Morbidelli A., 2010, *Comptes Rendus Physique*, 11, 651
- Morbidelli A., Levison H. F., Tsiganis K., Gomes R., 2005, *Nature*, 435, 462
- Nakamura T., Yoshida F., 2008, *PASJ*, 60, 293
- Nesvorný D., 2018, *ARA&A*, 56, 137
- Nesvorný D., Dones L., 2002, *Icarus*, 160, 271
- Nesvorný D., Morbidelli A., 2012, *AJ*, 144, 117
- Nesvorný D., Bottke W. F., Dones L., Levison H. F., 2002a, *Nature*, 417, 720
- Nesvorný D., Morbidelli A., Vokrouhlický D., Bottke W. F., Brož M., 2002b, *Icarus*, 157, 155
- Nesvorný D., Thomas F., Ferraz-Mello S., Morbidelli A., 2002c, *Celest. Mech. Dyn. Astron.*, 82, 323
- Nesvorný D., Alvarro J. L. A., Dones L., Levison H. F., 2003, *AJ*, 126, 398
- Nesvorný D., Beaug C., Dones L., 2004, *AJ*, 127, 1768
- Nesvorný D., Vokrouhlický D., Morbidelli A., 2013, *ApJ*, 768, 45
- Nesvorný D., Brož M., Carruba V., 2015, in Michel P., DeMeo F. E., Bottke W. F., eds, *Asteroids IV*. Univ. Arizona Press, Tucson, AZ, p. 297
- Paolicchi P., Spoto F., Knežević Z., Milani A., 2019, *MNRAS*, 484, 1815
- Pirani S., Johansen A., Bitsch B., Mustill A. J., Turrini D., 2019a, *A&A*, 623, A169
- Pirani S., Johansen A., Mustill A. J., 2019b, *A&A*, 631, A89
- Rein H., Liu S.-F., 2012, *A&A*, 537, A128
- Rein H., Tamayo D., 2015, *MNRAS*, 452, 376
- Roig F., Ribeiro A. O., Gil-Hutton R., 2008, *A&A*, 483, 911
- Romanishin W., Tegler S. C., 2018, *AJ*, 156, 19
- Rozehnal J., Brož M., Nesvorný D., Durda D. D., Walsh K. J., Richardson D. C., Asphaug E., 2016, *MNRAS*, 462, 2319
- Schwamb M. E. et al., 2018a, preprint ([arXiv:1802.01783](https://arxiv.org/abs/1802.01783))
- Schwamb M. E., Levison H. F., Buie M. W., 2018b, *Res. Notes AAS*, 2, 159
- Sharkey B. N. L., Reddy V., Sanchez J. A., Izawa M. R. M., Emery J. P., 2019, *AJ*, 158, 204
- Sheppard S. S., Jewitt D. C., 2003, *Nature*, 423, 261
- Šidlichovský M., Nesvorný D., 1996, *Celest. Mech. Dyn. Astron.*, 65, 137
- Slyusarev I. G., Belskaya I. N., 2014, *SoSyR*, 48, 139
- Spoto F., Milani A., Knežević Z., 2015, *Icarus*, 257, 275
- Strömgren E., 1908, *Astron. Nachr.*, 177, 123
- Tholen D. J., 1984, PhD thesis, Univ. Arizona, Tucson
- Tsiganis K., Gomes R., Morbidelli A., Levison H. F., 2005a, *Nature*, 435, 459
- Tsiganis K., Varvoglis H., Dvorak R., 2005b, *Celest. Mech. Dyn. Astron.*, 92, 71
- Turrini D., Marzari F., Beust H., 2008, *MNRAS*, 391, 1029
- Turrini D., Marzari F., Tosi F., 2009, *MNRAS*, 392, 455
- Vinogradova T. A., 2015, *MNRAS*, 454, 2436
- Vinogradova T. A., Chernetenko Y. A., 2015, *Solar Syst. Res.*, 49, 391
- Vokrouhlický D., Brož M., Bottke W. F., Nesvorný D., Morbidelli A., 2006, *Icarus*, 182, 118
- Wang X., Hou X., 2017, *MNRAS*, 471, 243
- Warner B. D., Harris A. W., Vokrouhlický D., Nesvorný D., Bottke W. F., 2009, *Icarus*, 204, 172
- Wolf M., 1907, *Astron. Nachr.*, 174, 47
- Wong I., Brown M. E., 2016, *AJ*, 152, 90
- Yoshida F., Nakamura T., 2008, *Publ. Astron. Soc. Japan*, 60, 297
- Yoshida F., Terai T., 2017, *AJ*, 154, 71
- Zappala V., Farinella P., Knežević Z., Paolicchi P., 1984, *Icarus*, 59, 261
- Zappala V., Cellino A., Farinella P., Knežević Z., 1990, *AJ*, 100, 2030
- Zappala V., Cellino A., Farinella P., Milani A., 1994, *AJ*, 107, 772

SUPPORTING INFORMATION

Supplementary data are available at [MNRAS](https://www.mnras.org/) online.

Holtetal2020_JovTrojanEscapes.csv

Please note: Oxford University Press is not responsible for the content or functionality of any supporting materials supplied by the authors. Any queries (other than missing material) should be directed to the corresponding author for the article.

This paper has been typeset from a $\text{\TeX}/\text{\LaTeX}$ file prepared by the author.

4

Paper 3 - A pair of Jovian Trojans at the L₄ Lagrange point

This third paper came out of discussions with Prof. David Vokrouhlický, who was visiting SwRI in at the beginning of 2020 (Holt et al., 2020b). The original idea would be that any pairs identified in the Trojans could help verify the astrocladistical method of paper 4. Once I found that none had been discovered, we tried using the existing pair discovery methodology (Vokrouhlický and Nesvorný, 2008), using the proper elements of the Trojans. From this, we discovered the first pair, (258656) 2002 ES₇₆ and 2013 CC₄₁, in the Jovian Trojans.

4.1 ABSTRACT

Asteroid pairs, two objects that are not gravitationally bound to one another, but share a common origin, have been discovered in the Main belt and Hungaria populations. Such pairs are of major interest, as the study of their evolution under a variety of dynamical influences can indicate the time since the pair was created. To date, no asteroid pairs have been found in the Jovian Trojans, despite the presence of several binaries and collisional families in the population. The search for pairs in the Jovian Trojan population is of particular interest,

given the importance of the Trojans as tracers of planetary migration during the Solar system's youth. Here we report a discovery of the first pair, (258656) 2002 ES₇₆ and 2013 CC₄₁, in the Jovian Trojans. The two objects are approximately the same size and are located very close to the L₄ Lagrange point. Using numerical integrations, we find that the pair is at least 360 Myr old, though its age could be as high as several Gyrs. The existence of the (258656) 2002 ES₇₆–2013 CC₄₁ pair implies there could be many such pairs scattered through the Trojan population. Our preferred formation mechanism for the newly discovered pair is through the dissociation of an ancient binary system, triggered by a sub-catastrophic impact, but we can not rule out rotation fission of a single object driven by YORP torques. A by-product of our work is an up-to-date catalog of Jovian Trojan proper elements, which we have made available for further studies.

4.1.1 ASTROCLADISTICAL ANALYSIS OF THE TROJAN PAIR.

Due to their small size, the physical characteristics of (258656) 2002 ES₇₆ and 2013 CC₄₁ have not, to date, been determined. They are also not present in any of the wide-field surveys used in Holt et al. (2021), *WISE*, SDSS, *Gaia* DR₂ and MOVIS. It is, however, possible to estimate the properties of these objects based on the dynamics of the pair - though obviously, such estimates should be taken with caution until supported by observations. From the AstDys dataset (Knežević and Milani, 2017), the proper elements (da:0.0006; e:0.057, sinI:0.0659) are similar to the proper element dynamical range of the Epios clan Holt et al. (2021). Within this clan are 5283 Pyrrhus (1989 BW), a oddity with a negative spectral slope (Bendjoya et al., 2004), and 12921 (1998 WZ₅), an X-type (Fornasier et al., 2007). This would indicate that the Trojan pair are most likely not typical D-type Trojans, but some other form of object. Observations of the objects themselves would be problematic (H-mag 14.1), though, through their association with 5283 Pyrrhus (1989 BW) (H-mag 9.76), some potential inferences could be made about their origin.

4.2 ASSOCIATED PRESENTATIONS AND PUBLICATIONS

4.2.1 AUG. 2020: DDA 50 - ORAL PRESENTATION

A pair of Jovian Trojans

Holt, T. R.; Vokrouhlicky, D.; Nesvorny, D.; Broz, M.; Horner, J.

Abstract

Asteroid pairs have been discovered in the main belt and Hungaria small body populations.

These objects are of major interest, as they inform us about dynamic processes related to their lifetime. To date, no asteroid pairs have been found in the Jovian Trojans, despite the presence of several binaries and collisional families in the population. At the same time, this population is particularly important in our understanding of the beginning of the Solar system, having been formed in the trans-Neptunian zone and only later captured around the Jupiter Lagrange points. Here we report the discovery of the first pair, 258656 and 2013 CC41, in the Jovian Trojan population. A couple of approximately equal size bodies, diameters ≈ 7.7 km and ≈ 6.7 km, is located very close to the L₄ Lagrange point. Not only this location helps to increase the statistical significance of the pair, but it also facilitates attempts in determining past orbital convergence of their orbits. Using numerical integrations, including Yarkovsky clones, we find the pair is at least approximately 380 Myr old, but its age may also be several Gyrs. The existence of the 258656-2013 CC41 implies there should be many more of them in the Trojan population. Our preferred formation mechanism is a split of a formerly binary system, but rotation fission driven by YORP torques may not be excluded too.

Publication: AAS Division on Dynamical Astronomy meeting 51, id. 203.06. Bulletin of the American Astronomical Society, Vol. 52, No. 4, id. 2020n4i203p06

Pub Date: August 2020

4.2.2 JAN. 2021: COSPAR - ORAL PRESENTATION

Identification of an Asteroid pair in the Jovian Trojan population

Holt, T. R.; Vokrouhlicky, D.; Nesvorný, D.; Brož, M.; Horner, J.

Abstract

Asteroid pairs have been discovered in the Main Belt, Hungarian, Hilda and Cybele small body populations. These objects are of major interest, as they inform the collisional history of the Solar system. They are thought to have formed one of three ways, catastrophic disruption, YORP fission or binary disruption. To date, no asteroid pairs have been found in the Jovian Trojans, despite the presence of several binaries and collisional families in the population. This population is particularly important in our understanding of the beginning of the Solar system, having been captured around the Lagrange points. The *Lucy* spacecraft, launching in 2021 is due to visit several of these objects. In this work, we report on the discovery of the first asteroid pair, 258656 and 2013 CC41 in the Jovian Trojan population. This approximately equal mass pair, diameters of 7.7km and 6.7km respectively, is located very close to the Jovian L₄ Lagrange point. The pair was discovered using a modified version of the existing distance parameter space search. In order to confirm the pair, we use n-body

code to reverse integrate the two bodies for the age of the Solar system, with high-resolution outputs. As each of these bodies are relatively small, we also create a set of Yarkovsky clones for each. Using the convergence of the longitude of the ascending node and argument of periapsis, we can confirm the pair as a binary disruption, and comment on the timing of the event. With the assumption that the current dynamical orbits of the two objects were created by binary separation, we can put constraints on the collisional history of the Jovian Trojan populations.

Publication: 43rd COSPAR Scientific Assembly, id. B1.1-0042-21

Pub Date: January 2021



A pair of Jovian Trojans at the L4 Lagrange point

Timothy R. Holt^{1,2*}, David Vokrouhlický³, David Nesvorný², Miroslav Brož³ and Jonathan Horner¹¹Centre for Astrophysics, University of Southern Queensland, Toowoomba, Queensland 4350, Australia²Southwest Research Institute, Department of Space Studies, 1050 Walnut St., Ste 300, Boulder, CO-80302, USA³Institute of Astronomy, Charles University, V Holešovičkách 2, Prague 8 CZ-180 00, Czech Republic

Accepted 2020 September 24. Received 2020 September 14; in original form 2020 August 3

ABSTRACT

Asteroid pairs, two objects that are not gravitationally bound to one another, but share a common origin, have been discovered in the Main belt and Hungaria populations. Such pairs are of major interest, as the study of their evolution under a variety of dynamical influences can indicate the time since the pair was created. To date, no asteroid pairs have been found in the Jovian Trojans, despite the presence of several binaries and collisional families in the population. The search for pairs in the Jovian Trojan population is of particular interest, given the importance of the Trojans as tracers of planetary migration during the Solar system's youth. Here we report a discovery of the first pair, (258656) 2002 ES₇₆ and 2013 CC₄₁, in the Jovian Trojans. The two objects are approximately the same size and are located very close to the L4 Lagrange point. Using numerical integrations, we find that the pair is at least 360 Myr old, though its age could be as high as several Gyrs. The existence of the (258656) 2002 ES₇₆–2013 CC₄₁ pair implies there could be many such pairs scattered through the Trojan population. Our preferred formation mechanism for the newly discovered pair is through the dissociation of an ancient binary system, triggered by a sub-catastrophic impact, but we can not rule out rotation fission of a single object driven by YORP torques. A by-product of our work is an up-to-date catalogue of Jovian Trojan proper elements, which we have made available for further studies.

Key words: minor planets, asteroids: general – methods: numerical.

1 INTRODUCTION

The discovery of asteroid pairs, two objects sharing a very similar heliocentric orbit, recently brought yet another piece of evidence into the mosaic of small Solar system bodies' evolution on short time-scales (e.g. Vokrouhlický & Nesvorný 2008). Examples of these couples have been found in the Main belt and Hungaria populations (Vokrouhlický & Nesvorný 2008; Pravec & Vokrouhlický 2009; Rožek, Breiter & Jopek 2011; Pravec et al. 2019). The similarity between the heliocentric orbits of the two members of an identified asteroid pair hints at a common and recent origin for the objects, that most likely involves their gentle separation from a parent object. Indeed, backward orbital propagation of heliocentric state vectors of the components in many pairs has allowed researchers to directly investigate the possibility of their past low-velocity and small-distance approach (see Vokrouhlický et al. 2017, for the most outstanding example discovered so far).

The well-documented cases of pairs among asteroids identified to date all feature separation ages of less than a million years. Vokrouhlický & Nesvorný (2008) speculated about three processes that could have led to the formation of those pairs: (i) collisional break-up of a single parent object, (ii) rotational fission of such an object driven by radiation torques, and (iii) instability and separation of the components of a binary system. Whilst each of these possibilities can explain the origin of asteroid pairs, with some

being more likely than others for individual pair cases, evidence has been found that the majority of currently identified pairs were probably formed through the rotational fission of their parent object (e.g. Pravec et al. 2010, 2019). It is worth noting that Main belt binaries in the same size category (i.e. with primary diameters of one to a few kilometers), are also believed to be primarily formed through the rotational fission of their parent body (e.g. Pravec & Harris 2007; Margot et al. 2015a). This is an interesting population-scale result that informs us about a leading dynamical process for few-km size asteroids in the Main belt. It would certainly be desirable to extend this knowledge to other populations of small Solar system bodies.

Attempts to detect orbital pairs in other populations have, to date, either failed or were not strictly convincing. For instance, the orbital evolution of bodies in the near-Earth population is very fast and chaotic and, at the same time, the number of known objects is limited (see e.g. Moskovitz et al. 2019, and references therein). Searches in populations beyond the Main belt were not successful for different reasons. Whilst dynamical chaos could also be relevant, a more important factor concerns the smallest size of bodies found at larger distance from the Sun. The smallest bodies found in Cybele zone, and amongst the Hildas or Jovian Trojans, are about an order of magnitude larger than the smallest known asteroids in the inner Main belt or the Hungarias (e.g. Emery et al. 2015). The proposed pair-formation processes have a characteristic time-scale that rapidly increases as a function of parent body size. For that reason, it is no surprise that, to date, no recently formed (≤ 1 Myr) traditional pairs sharing the same heliocentric orbit have been detected beyond the Main belt. If any pairs do exist in these distant small-body

* E-mail: timothy.holt@usq.edu.au

populations, they should be revealed by their tight configuration in proper element space and long-term backward orbital propagation, if the stability in that particular zone of orbital phase space allows. With that guideline in mind, we focus here on the Jovian Trojan population. The leap to the Trojan population might appear to contradict the logical steps of gradually extending our knowledge of Main belt pairs by searches among the Cybele or Hilda populations first. However, we argue that the case of possible Jovian Trojan pairs is actually more interesting because of that population’s entirely different origin.

The Jovian Trojan population consists of two swarms of objects, librating on tadpole trajectories about the Jovian L4 and L5 Lagrange points. Indeed, 588 Achilles Wolf (1907) was the first discovered object to serve as an example of a solution to the restricted three-body problem (Lagrange 1772). Whilst originally considered to be just an extension of the main belt, and particularly the Hilda and Thule populations, towards the orbit of Jupiter, the Jovian Trojans were soon realized to be a totally distinct group of objects, with a unique history (see Emery et al. 2015, for a review). Most importantly, the majority of the Jovian Trojans are thought to have formed in a vast trans-Neptunian disc of planetesimals, at a heliocentric distance beyond $\simeq 20$ au, and became captured on to their current orbits during the planetesimal-driven instability of giant planets (see Nesvorný 2018, for review). The physical properties of the Trojans, such as their material strength or bulk density, are therefore most likely different from most of the asteroidal populations, resembling rather those of comets and Centaurs with which they share the birth-zone. Though relatively stable, the Jovian Trojans can escape their stable region (e.g. Di Sisto, Ramos & Beaugé 2014; Holt et al. 2020, and references therein), and contribute to other populations, most notably the Centaurs (see Di Sisto, Ramos & Gallardo 2019, and references therein). An example of this, (1173) Anchises, exhibits significant dynamical instability on time-scales of hundreds of millions of years, with the result that it will likely one day escape the Jovian Trojan population and become a Centaur before being ejected from the Solar system, disintegrating, or colliding with one of the planets (Horner, Müller & Lykawka 2012).

Despite their importance as a source of information on the Solar system’s past evolution, fact that the Jovian Trojans are markedly farther from Earth than the Main Belt has made them significantly more challenging targets for study. As a result, our knowledge of the collisional history, binarity, and the presence/absence of pairs in the Trojan population remains far smaller than our knowledge of the main Asteroid belt (e.g. Margot et al. 2015b). In fact, to date, no confirmed Trojan pairs have been discovered, and the true level of binarity in the population remains to be uncovered. The most famous confirmed binary in the Trojan population is (617) Patroclus, accompanied by a nearly equal size satellite Menoetius (both in the 100 km range; e.g. Marchis et al. 2006; Buie et al. 2015). The Patroclus–Menoetius system is fully evolved into a doubly synchronous spin–orbit configuration (see Davis & Scheeres 2020, and references therein), and represents an example of the kind of binary systems which are expected to be common among Trojans. A number of such binaries, comprising two components of almost equal size, have been found amongst the large trans-Neptunian objects (e.g. Noll et al. 2020). This comparison is of particular interest, given that the Patroclus system was, in all likelihood, implanted to the Trojan region from the trans-Neptunian region source zone (e.g. Nesvorný et al. 2018). It seems likely that the Patroclus system represents the closest example of an Edgeworth–Kuiper belt binary system. Further information on the Patroclus system will become available in the coming decades, as the binary is a target for flyby in 2033 by the *Lucy* spacecraft (e.g. Levison et al. 2017). Similar smaller scale systems

may well exist among the Trojan population, but their abundance is uncertain. Observationally, such small-scale binaries remain beyond our detection, and theoretical models of their survival depend on a number of unknown parameters (e.g. Nesvorný et al. 2018, 2020; Nesvorný & Vokrouhlický 2019). The existence of Trojan binaries is interesting by itself, but in the context of our work, it is worth noting that, if such binaries exist, they likely serve as a feeding cradle for a population of Trojan pairs.

Following this logic, then if the population of pairs among the Trojans can become known and well characterized, such that their dominant formation process is understood, that would in turn prove to be a source of new information about Trojan binaries. Milani (1993) in his pioneering work on Jovian Trojan orbital architecture noted a case of L4-swarm objects (1583) Antiochus and (3801) Thrasymedes. Their suspicious orbital proximity led the author to suggest that they may constitute a genetically related couple of bodies. A viable formation process would be through the instability and dissociation of a former binary (Milani and Farinella, personal communication). Unfortunately, the Antiochus–Thrasymedes interesting configuration has not since been revisited, nor further studied in a more detail.

This background information motivates us to conduct a search for Jovian Trojan pairs. Unfortunately, even now the problem is not simple, and we consider our work to be an initial attempt, rather than providing a definitive solution. In Section 2, we explain our strategy, and describe the difficulties in Trojan pair identification. This strategy led us to preliminarily identify the Jovian Trojans (258656) 2002 ES₇₆ and 2013 CC₄₁ as a potential pair. To test this hypothesis, we attempted to prove that these two bodies could be genetically related using backward orbital integration, as described in Section 3. In Section 4, we discuss potential formation processes for the pair, before presenting our concluding remarks and a call for observations in Section 5. Appendix A describes our methods for the construction of Jovian Trojan proper elements. An up-to-date catalogue of those elements, which we have made publicly available online, is actually a fruitful by-product of our work that may prove useful for future studies. We discuss some additional candidate pairs in Appendix B.

2 SELECTION OF CANDIDATE PAIRS

The discovery of asteroid pairs was a direct by-product of a search for very young asteroid families (see Nesvorný & Vokrouhlický 2006; Nesvorný, Vokrouhlický & Bottke 2006; Vokrouhlický & Nesvorný 2008). As a result, the primary ambition was to find pairs that formed recently, within the last Myr, amongst the Main belt and Hungaria populations. In fact, the necessity for proven pairs to be young is essentially related to the method that allows their identification.

Just like collisional families, asteroid pairs are identified as a result of the similarity of their heliocentric orbits. The search for classical collisional families has traditionally been performed using clustering techniques in proper orbital element space, examining the proper semimajor axis a_p , eccentricity e_p , and the sine of proper inclination $\sin I_p$ (see e.g. Benjoya & Zappalà 2002; Nesvorný, Brož & Carruba 2015, for reviews). The use of the proper elements allows us, with some care, to search for both young and old families. This is because the proper elements are believed to be stable over much longer time-scales than other types of orbital elements, such as osculating or mean, ideally on a time-scale reaching hundreds of Myrs or Gyrs.

There are, however, limitations to this method. In the case of very old families, problems arise from instability of the proper orbital elements and the incompleteness of the dynamical model used to

derive the proper elements. A different problem occurs for very young families. The issue has to do with the huge increase in the number of small-body objects discovered over the past decades. Despite the fact that the very young families and asteroid pairs must have very close values of the proper orbital elements, it is difficult to statistically discern them from random fluctuations of background asteroids. Both occur at the same orbital distance in proper element space.

This fundamental obstacle arises due to the low dimensionality of proper element space, which consists of just three independent variables. In order to separate very young asteroid families and asteroid pairs from the random fluctuations of the background population, Nesvorný, Vokrouhlický & Bottke (2006) and Vokrouhlický & Nesvorný (2008) realized that this problem can be overcome if the search is conducted in a higher dimensional space. As a result, they used the 5D space of the osculating orbital elements, neglecting just the mean longitude. The mean orbital elements are also suitable alternative parameters for such an analysis (e.g. Rožek, Breiter & Jopek 2011). In order to effectively use the two extra dimensions, the searched structures must also be clustered in secular angles, the longitudes of ascending node and perihelion. This is perfectly justified for very young families and pairs that are expected to have separated at very low velocities.

Previous searches for these young structures in the space of osculating or mean orbital elements proved the usefulness of the method, provided the age of the pair was less than about 1 Myr. Asteroid pairs will clearly exist that formed earlier than this limit, but a differential precession of their secular angles will result in them becoming effectively randomized, which will, in turn, render the identification procedure described above ineffective. A key point here is that the population of Main belt asteroids is currently known to very small sizes, with objects detected with diameters of 1 km, or even smaller. The proposed formation processes for very young families and pairs are expected to generate enough pairs within the last Myr that, even after accounting for discovery biases, we still have some of them in our catalogues.

The situation is, however, different in the case of the Jovian Trojan swarms. First, the characteristic size of the smallest Trojans is $\simeq 5$ km, with few objects being discovered that are smaller than this limit. Secondly, the formation processes of putative Trojan pairs, such as a rotational fission or collisions, are significantly less efficient than in the main belt. As a result, no identifiable pairs among Trojans are expected to have been formed in the last 10–30 Myr, over which time, one would expect secular angles of any such pairs to diverge from each other. We conducted a traditional search for pairs in the 5D space of osculating orbital elements (as in Vokrouhlický & Nesvorný 2008), but did not find any candidates. If pairs do exist amongst the known Trojans, their ages must be larger. In that case, however, their secular angles would be randomized, as is the case for old pairs in the main belt. Our candidate selection method then returns back to the analysis of the Trojan proper elements, with further considerations based on additional criteria.

2.1 A new catalogue of proper orbital elements

The AstDyS website, founded at the University of Pisa, and currently run by SpaceDys company (see <https://newton.spacedys.com/astdys/>), is a world renowned storehouse of proper orbital elements for Solar system minor bodies. It also contains data on the Jovian Trojans, namely synthetic proper elements based on mathematical methods presented in the pioneering work of Milani (1993). We also note the work of Beaugé & Roig (2001), which discusses an

alternative approach to the calculation of Trojan proper elements, but these authors neither make their results readily available online, nor update them on a regular basis. For that reason, one possibility for this study would be to use the AstDyS data. However, those data have at least two drawbacks for our application. First, their last update occurred in 2017 June. As a result, they provide information for a total of 5553 numbered and multi-opposition Jovian Trojans. Given the efficiency of all-sky surveys, this number has increased significantly in the years since that update, with more than 7000 Jovian Trojans now known for which observations span multiple oppositions. Secondly, the proper elements provided at AstDyS are given to a precision of just four decimal places, which is not sufficient for our work. The AstDyS data base would, as a result, allow the determination of the orbital distance in the proper element space – equation (1) – with only $\simeq 2$ to 5 m s^{-1} accuracy, which is insufficient to characterize the low velocity tail. For both of these reasons, in this work, we decided to determine our own synthetic proper elements. Details of the approach are given in Appendix A. Here, we only mention that our proper element definition and mathematical methods follow the work of Milani (1993), with substantial differences only for those orbits with very small libration amplitudes. Previous applications using this technique may be found in Brož & Rozehnal (2011) and Rozehnal et al. (2016).

Fig. 1 shows our results, namely proper elements computed for 7328 Jovian Trojans (numbered and multi-opposition objects as of 2020 April) projected on to the $(da_p, \sin I_p)$ and (da_p, e_p) planes for the L4 swarm (‘Greeks’ leading Jupiter on its orbit; left-hand panels) and the L5 swarm (‘Trojans’ trailing behind Jupiter; right-hand panels). The L4 swarm is more numerous, partly as a result of four major collisional families that have been recognized in recent years (e.g. Rozehnal et al. 2016), and contains 4607 objects. The smaller L5 swarm contains only 2721 known objects, including the 2001 UV₂₀₉ and Ennomos collisional families. To proceed with an investigation of the orbital similarity between members of the Trojan population, the basis of the pair and family recognition process, one must introduce a metric function in the space of the proper orbital elements. Several choices have been discussed by Milani (1993). We opt for the d_3 metric, also favoured by the author of that work, though we slightly adjust that metric, such that the orbital distance is given in velocity units. Given two orbits in the Trojan L4 or L5 proper element space, obviously without mixing the two swarms, we define their distance δV_p as a quadratic form using the differences δa_p , δe_p , and $\delta \sin I_p$ as

$$\delta V_p = V_J \sqrt{\frac{1}{4} \left(\frac{\delta da_p}{a_J} \right)^2 + 2(\delta e_p)^2 + 2(\delta \sin I_p)^2}, \quad (1)$$

where $V_J \simeq 13\,053 \text{ m s}^{-1}$ and $a_J \simeq 5.207 \text{ au}$ are mean orbital velocity and semimajor axis of Jupiter. Milani (1993) argued that this particular choice of the coefficients – (0.25, 2, 2) – helps to equally weight contributions from all three dimensions.

2.2 Metrics-based analysis

Given the metric shown in equation (1), we computed distances of all possible pairs in the L4 and L5 Trojans swarms, and organized them in the form of a cumulative distribution $N(< \delta V_p)$ (see also Vokrouhlický & Nesvorný 2008, for context). The results of this process are shown in Fig. 2. Whilst the largest δV_p values of approximately V_J are set by the maximum extension of the stable phase space of tadpole orbits associated with Jupiter (Fig. 1), the smallest δV_p values of the order of $\sim 1\text{--}2 \text{ m s}^{-1}$ are determined by a

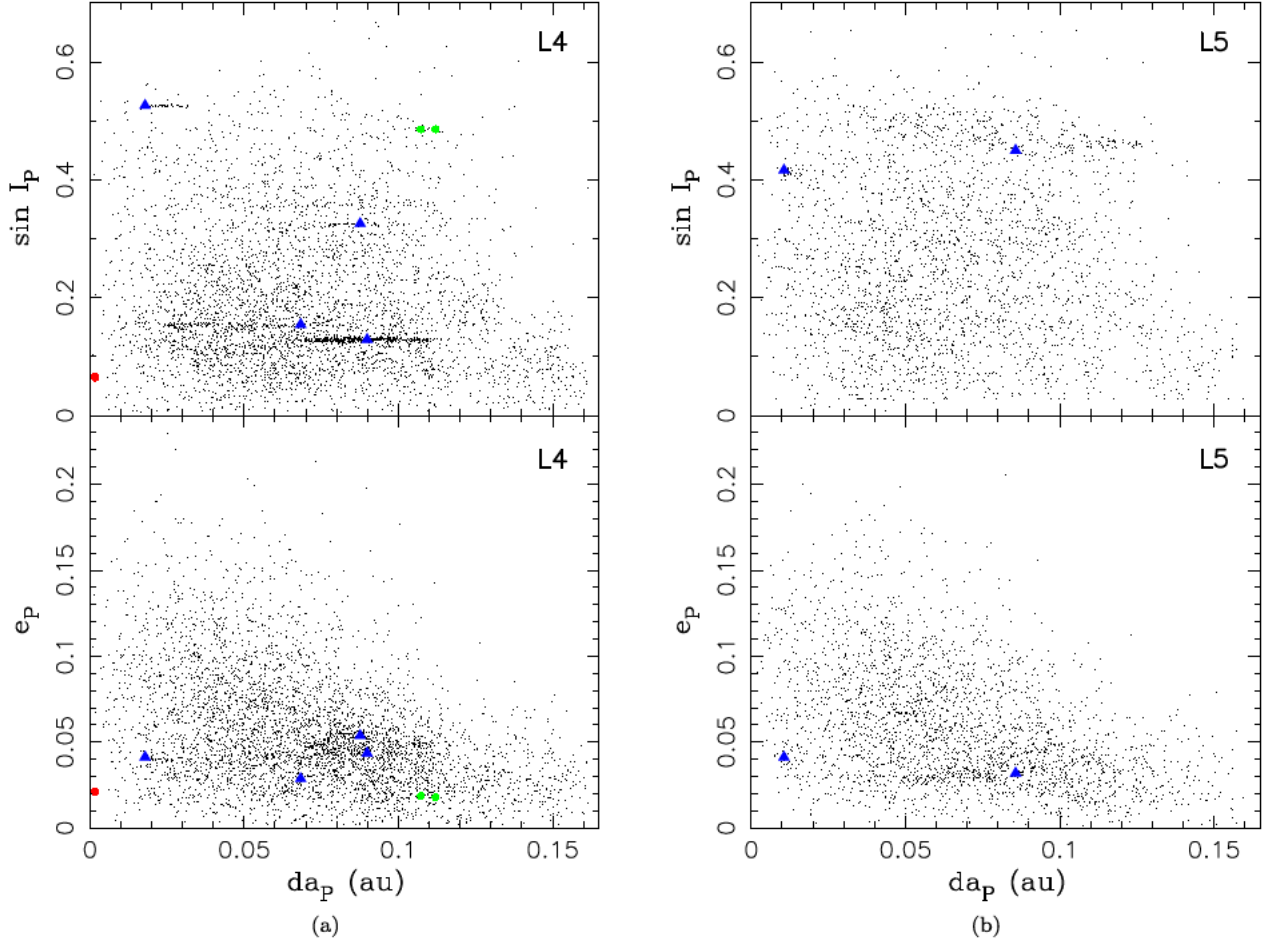


Figure 1. Proper orbital elements of Jovian Trojans: semimajor axis da_P versus sine of inclination $\sin I_P$ (top panels), and semimajor axis da_P versus eccentricity e_P (bottom panels). The left panels show the orbits of 4607 objects at the L4 libration zone, whilst the right panels show the orbits of 2721 objects at the L5 libration zone. These data were computed using the method described in Appendix A and display numbered and multi-opposition orbits as of April 2020. Blue triangles indicate the largest objects of the previously identified Trojan families (e.g. Rozehnal et al. 2016): (a) Eurybates, Hektor, Arkesilaos and 1996 RJ in the L4 zone, and (b) Ennomos and 2001 UV₂₀₉ in the L5 zone. The two green circles denote position of Jovian Trojans (1583) and (3801) that were previously identified as constituting a suspiciously close pair (see Milani 1993). The two overlapping red circles denote the location of our proposed pair candidate of (258656) 2002 ES₇₆ and 2013 CC₄₁.

combination of several factors. The number of known Jovian Trojans filling the stable orbital space is the first factor, compared with the typical smallest values $\delta V_P \simeq 100 \text{ m s}^{-1}$ found by Milani (1993), who studied just 80 and 94 Trojans in the L4 and L5 swarms, respectively. Additionally, small velocity differences occur when bodies become organized in structures like families. Last, the inevitable uncertainty of the proper elements contributes to the noise in δV_P . We determine the uncertainties of δV_P by a propagation of the proper element uncertainties described in Appendix A. This effect is obviously not uniform, but organized in a complicated structure of a chaotic web, generally increasing towards the border of the stable tadpole zone (see e.g. Robutel & Gabern 2006). Interestingly, the characteristic noise level from such deterministic chaos is of the order of a few meters per second, about the same as minimum distances between the orbits, as can be seen in Fig. 2, where we show uncertainty intervals of δV_P for the low-velocity tail.

It is also worth noting that for reasonably small values of δV_P (hundred m s^{-1} or so), one would expect $N(< \delta V_P) \propto (\delta V_P)^3$ provided that: (i) Trojans fill the available stable phase space at random, and (ii) the weighting coefficients in the metric function (1) truly express isotropy, the exponent 3 is then a measure of the proper element

space dimension. For large δV_P values the cumulative distributions $N(< \delta V_P)$ become shallower because of the finite extent of the stable orbital region. We also note that $N(< \delta V_P)$ holds global information about the whole L4 and L5 populations, while local structures, such as families and clusters, are almost not seen in this distribution.

We find it interesting that $N(< \delta V_P)$ are broadly similar for the L4 and L5 swarms, but they also differ in some important characteristics, in particular, the smallest and the largest δV_P values. This is due to the directly comparable populations of the two swarms and basically identical volumes of their stable phase space. However, the $\delta V_P < 100 \text{ m s}^{-1}$ parts of the distributions have a different behaviour when approximated with a power-law $N(< \delta V_P) \propto (\delta V_P)^\alpha$: (i) the L4 swarm has the canonical value $\alpha \simeq 3$, while (ii) the L5 swarm is shallower, with approximately $\alpha \simeq 7/3$. We hypothesize that this difference is caused by a presence of the prominent Trojan families in the L4 population. Family members efficiently contribute to the low- δV_P part of the distribution. Given their small extent, it is also conceivable that the mutual orbital distribution in families is approximately isotropic. The L5 population is less influenced by Trojan families, and, as a result, $N(< \delta V_P)$ may reflect the parameters of the background Trojan population. This is affected both by the resonances that sculpt the

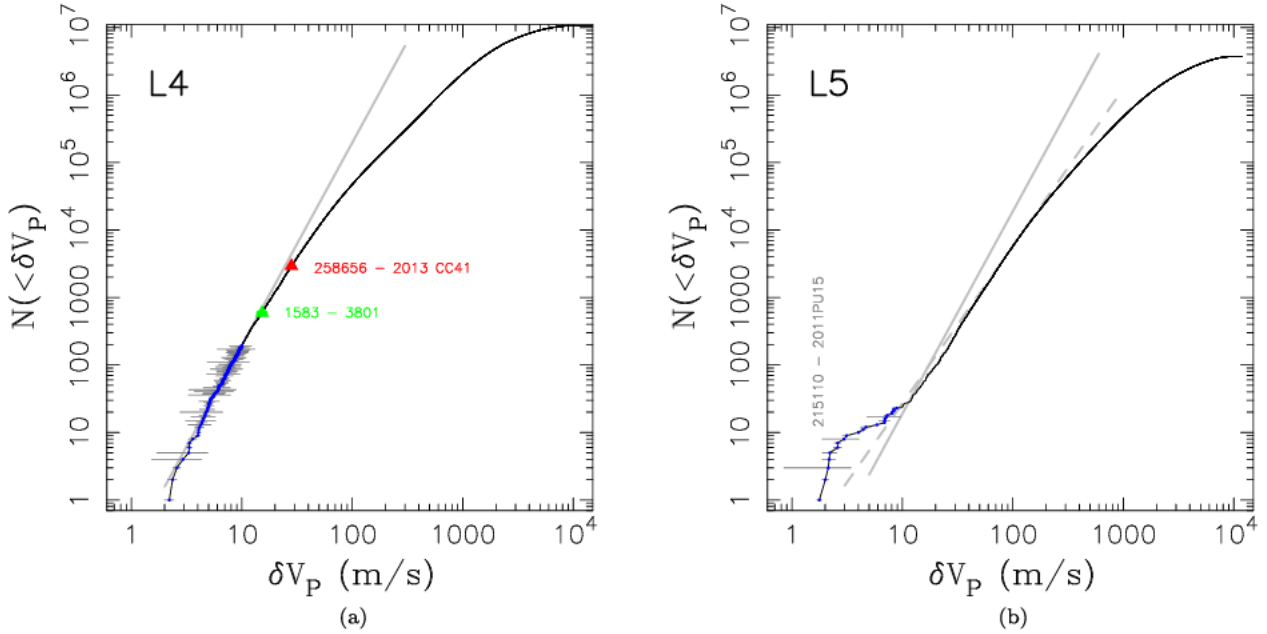


Figure 2. Cumulative distribution $N(< \delta V_P)$ of Trojans with velocity distance δV_P in the proper elements space using the metric described in equation (1): the left-hand panel presents the results for the 4607 objects of the L4 Trojan swarm, with the right-hand panel showing the 2721 members of the L5 Trojan swarm. The light grey solid lines indicate the $N(< \delta V_P) \propto (\delta V_P)^3$ relationship, for reference; curiously, the L5 distribution is better matched with $N(< \delta V_P) \propto (\delta V_P)^{7/3}$, shown with a dashed grey line. The blue symbols denote the population with the smallest δV_P values, namely $\delta V_P \leq 10 \text{ m s}^{-1}$ for both the L4 and L5 Trojans. For sake of interest, we also show uncertainties in the determination of δV_P for these low-velocity couples with grey horizontal intervals. Position of three couples of interest is highlighted by labels. These are the (1583)-(3801) couple with $\delta V_P = (15.2 \pm 1.0) \text{ m s}^{-1}$ and (258656) 2002 ES₇₆-2013 CC₄₁ couple $\delta V_P = (28.2 \pm 0.9) \text{ m s}^{-1}$ among L4 Trojans, and (215110) 1997 NO₅-2011 PU₁₅ couple with $\delta V_P = (1.8 \pm 0.1) \text{ m s}^{-1}$ among L5 Trojans.

stable orbital zone in a complicated way and, perhaps, the initial filling of the Trojan region by planetesimals. Finally, the weighting coefficients of the metric function (1), that express how differences in semimajor axis, eccentricity, and inclination contribute to the whole, may also slightly affect the result (though our experiments with small changes in those values did not yield significant differences). If combined altogether, the α value may be slightly shallower than 3, such as $7/3$ we found for the L5 population

We paid some attention to the smallest-distance couple (215110) 1997 NO₅-2011 PU₁₅, and could not conclusively prove that it represents a real pair of related objects (Appendix B). A closer analysis of the second to sixth closest couples in the L5 population indicates the possibility of a very compact cluster about Trojan (381148) 2007 GZ₁, but its status needs to be confirmed with more data in the future. In any case, because our interest here focuses on Trojans in the low-velocity tail of the $N(< \delta V_P)$ distribution, seeking putative pairs, we also show in Fig. 3 location of couples that have $\delta V_P < 10 \text{ m s}^{-1}$ in both Trojan swarms. These would be the most logical candidates for further inspection.

Seeking details that could explain the difference in the population exponents α in further detail, we analysed distributions of the proper elements. The most significant difference concerns proper inclination I_p . Fig. 4 shows L4 and L5 Trojan distributions of I_p for all bodies. The dashed lines are simple approximations with a function $I_p \exp(-I_p/C)$, where the adjustable constant C characterizes width of the distribution (the prominent families, such as Eurybates at $\approx 8^\circ$ among L4 or Ennomos at $\approx 30^\circ$ among L5, were excluded from the fit). We found $C \approx 6.0^\circ$ for L4 and $C \approx 8.7^\circ$ for L5, implying the inclination distribution at L5 is slightly broader. This confirms results in Di Sisto, Ramos & Beaugé (2014). It is not clear, whether this is due to the details of the capture process, or whether

the escapees from the prominent Eurybates and Arkesilaos families in the L4 swarm contribute to the difference, and how it may affect the exponent α of the $N(< \delta V_P)$ distribution discussed above. A full analysis of these interesting findings is beyond the aims of our work. Regarding the smallest δV_P values, neither of the two distribution functions $N(< \delta V_P)$ show a change in behaviour. In the context of our work, this implies no hint of a statistically significant population of very close orbits, a tracer of a possible Trojan pair population. In fact, given the low dimensionality of the proper element space, this was not unexpected, given that the asteroid pairs in the Main belt would not manifest themselves using a similar analysis. The slight deviation of $N(< \delta V_P)$ below $\approx 7 \text{ m s}^{-1}$ velocity to a shallower trend for the L5 swarm is interesting, but likely not statistically robust enough to allow firm conclusions to be drawn at the current time.

A full frontal approach to this data would be to analyse the results from backward orbital integrations for these little more than 200 putative couples using the methods described in Section 3. However, this would require a significant computational effort, and thus we chose to adopt further criteria for candidate selection. For instance, data in the L4 swarm show that the lowest δV_P couples are strongly concentrated in the recognized families. The locally increased density of Trojans in these regions obviously imply small distances δV_P , but this also means such couples are most likely not the objects that we seek. The correlation with Trojan families is somewhat weaker in the L5 swarm, though several of the small-distance couples are found in both the Ennomos and 2001 UV₂₀₉ families. Other constitute compact clusters scattered in the background population, like that around (381148) 2007 GZ₁, as mentioned above.

Sifting the $\delta V_P < 10 \text{ m s}^{-1}$ couples unrelated to families would still leave us with too many candidates to pursue with backward n -body

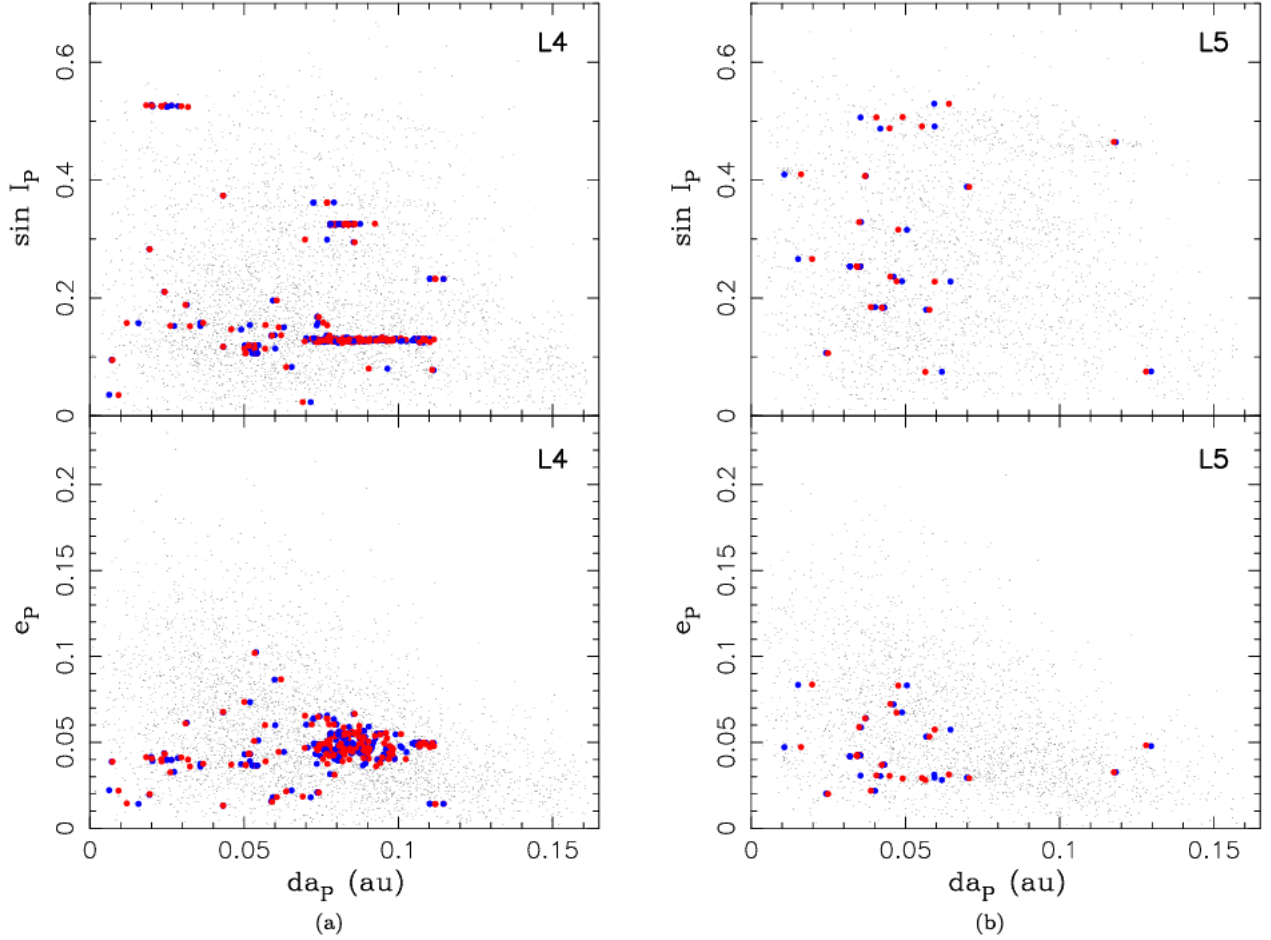


Figure 3. Proper orbital elements of Jovian Trojans as in Fig. 1. The red symbols in both L4 and L5 swarms show couples of Trojans with $\delta V_P < 10 \text{ m s}^{-1}$, namely the lowest velocity tail in the distributions shown in Fig. 2: the primary component of each couple is shown using a filled red circle, whilst the secondary is shown using a blue circle. In the L4 case their relation to the recognized families is apparent. In the L5 case their distribution is more scattered, though some are also associated with the 2001 UV₂₀₉ and Ennomos families.

simulations. Having experimented with several cases, we adopted the strategy of focusing on those low- δV_P couples characterized by (i) the least populated background, and (ii) located in the most dynamically stable zones of the orbital phase space. The former condition increases the likelihood that the candidate couple is a real pair, and not just a fluke, whilst the latter condition would allow us to investigate the past orbital configuration of the putative pair across as lengthy a time-scale as possible. This is particularly important for pairs in the Jovian Trojan population, since no recently formed pairs are to be expected, as described above. Moreover, the expected large ages of possible Trojan pairs do not allow us to seek their past orbital convergence in full 6D Cartesian space of positions and velocities. Even the most stable Trojan orbits have an estimated Lyapunov time-scale of about 10–20 Myr. In this situation, our convergence scheme should rely on the behaviour of secular angles, the longitudes of node and perihelion, and the related eccentricity and inclination (Section 3). It is then advantageous to suppress the role of the last two elements, the semimajor axis, and the mean longitude, by letting them vary as little as possible. This favours locations very near the tadpole libration centre of either the L4 or L5 swarms, where also the previous two conditions, low background population and maximum orbital stability, are satisfied.

2.3 A prospective candidate Trojan pair

With all these criteria in mind, we found a candidate couple of L4 objects, (258656) 2002 ES₇₆ and 2013 CC₄₁. The proximity of these two objects to the libration centre is reflected by the small values of all proper elements (see Fig. 1), namely $da_p \simeq (1.6180 \pm 0.0001) \times 10^{-3} \text{ au}$, $e_p \simeq (2.12713 \pm 0.00001) \times 10^{-2}$, and $\sin I_p \simeq (6.578 \pm 0.003) \times 10^{-2}$ for (258656) 2002 ES₇₆, and $da_p \simeq (1.6890 \pm 0.0001) \times 10^{-3} \text{ au}$, $e_p \simeq (2.10588 \pm 0.00001) \times 10^{-2}$ and $\sin I_p \simeq (6.427 \pm 0.004) \times 10^{-2}$ for 2013 CC₄₁. The close proximity to L4 also indicates that the pair have been in stable orbits for the life of the Solar system (e.g. Holt et al. 2020). For reference, we also mention their libration amplitude, in the angular measure, which is only about 0.33° , resp. 0.34° . There are only four other L4 objects in our sample that have smaller libration amplitudes, and none among the known L5 objects, though these have generally larger proper eccentricity and/or inclination values. The similarity of the two orbits is immediately apparent and quantitatively expressed with $\delta da_p \simeq 7.1 \times 10^{-5} \text{ au}$ and $\delta e_p \simeq 2.12 \times 10^{-4}$, both with negligible uncertainty, while $\delta \sin I_p \simeq 1.51 \times 10^{-3}$ with a small uncertainty of 4.8×10^{-5} . This uncertainty amounts to about 0.085° difference in the proper inclination. All these values result in the velocity difference $\delta V_P \simeq 28.2 \pm 0.9 \text{ m s}^{-1}$, using our adopted metric (1),

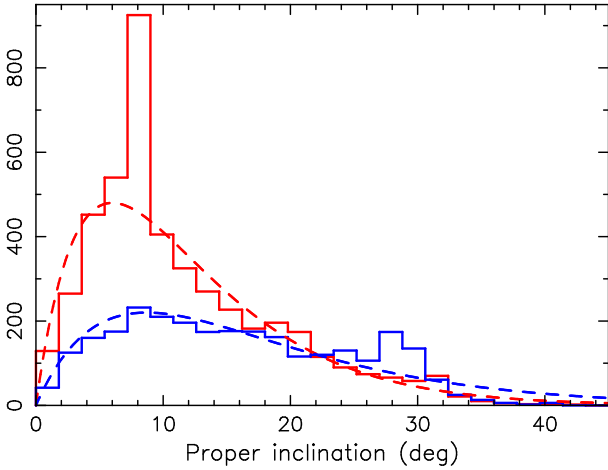


Figure 4. Number of Jovian Trojans with proper inclination I_P (in degrees), showing the L4 (red) and L5 (blue) swarms. The dashed lines represent an approximation $I_{P\text{exp}}(-I_P/C)$ for the background population (significant peaks due to Trojan families eliminated), where we found $C \simeq 6.0^\circ$ for L4 and $C \simeq 8.7^\circ$ for L5.

dominated by the inclination contribution the contribution from the difference in proper eccentricities is about 10 per cent of the total, and the difference in proper semimajor axes is negligible). With that said, this couple would qualify among the closest in the population if it were not for the slight inclination offset of the two orbits.

Not much physical information is available about these two objects. Various data bases providing orbital solutions (such as AstDyS, JPL, or MPC) yield an absolute magnitude for (258656) 2002 ES₇₆ in the range 14.0 to 14.2, and values in the range 14.3 to 14.4 for 2013 CC₄₁. Given the mean albedo, $p_V \simeq 0.075$, for small Trojans (a value with an admittedly large scatter; e.g. Grav et al. 2011, 2012), we estimate their sizes to be $D \simeq 7.0\text{--}7.7$ km for (258656) 2002 ES₇₆ and $D \simeq 6.4\text{--}6.7$ km for 2013 CC₄₁. Unless the assumption of similar albedoes is significantly in error, it is clear that the two bodies are similar in size, though not exactly the same. No other physical parameters, such as the rotation period, thermal inertia, and/or spectral colours, are known at the present time. Further observational follow-up on these objects is therefore highly recommended.

2.4 Assessment of the statistical significance of the selected pair

The small libration amplitude zone of the proper element space contains a relatively small number of bodies, as can be seen in the left-hand panel (a) in Fig. 5. Here, we used the range $da_P \leq 0.014$ au, expressing the proximity to the libration centre, but left $e_P \leq 0.15$ and $\sin I_P \leq 0.6$, generally capturing the width of the stable Trojan phase space (Levison, Shoemaker & Shoemaker 1997; Nesvorný et al. 2002a; Tsiganis, Varvoglis & Dvorak 2005; Di Sisto et al. 2014; Holt et al. 2020). We could have also more strongly restricted the proper eccentricity and inclination values, but if this is done too aggressively, it would result in the sample of observed Trojans available for our analysis becoming too small. With our limits, we find $k = 91$ Trojans in the L4 space, including our candidate pair (258656) 2002 ES₇₆ and 2013 CC₄₁.

The proper element differences in the (258656) 2002 ES₇₆ and 2013 CC₄₁ couple are $\delta a_P = 7.11 \times 10^{-5}$ au, $\delta e_P = 0.000212$, $\delta \sin I_P = 0.00151$, much smaller than the scale of the chosen zone, assuming that all dimensions are taken equally. In the first approximation,

taking all dimensions equally, and thus neglecting the weighting coefficients from equation (1) which are all of the order of unity, the $(\delta a_P, \delta e_P, \delta \sin I_P)$ differences in this couple define a small box of which represents only a $\simeq 1.81 \times 10^{-8}$ fraction of the analysed target zone. For statistical calculations, it is useful to imagine ‘numbered’ boxes of the $(\delta a_P, \delta e_P, \delta \sin I_P)$ volume in the whole zone. Their total number of such boxes would then be $n \simeq 5.53 \times 10^7$.

The simplest estimate of the statistical significance of the (258656) 2002 ES₇₆–2013 CC₄₁ pair is based on the assumption that bodies were distributed in the analysed zone randomly/uniformly. We choose k numbers from n possibilities (i.e. one for each body from a set of ‘numbered’ boxes). Ordered, repeated selections are given as variations $V(n, k) = n^k$, while ordered, non-repeated as $V(n, k) = n!/(n-k)!$. The likelihood that among the trials the box-numbers do not repeat is simply the ratio $V(n, k)/V(n, k)$, and we are interested just in the complementary probability:

$$p = 1 - \frac{V(n, k)}{V(n, k)} \simeq 7.4 \times 10^{-5}. \quad (2)$$

We verified this result by directly running a Monte Carlo simulation of the selection process. Thus, we find the probability that the selected couple is only a random orbital coincidence to be very low. Shrinking the width of the e_P and $\sin I_P$ to half the previously mentioned values did not change our result significantly.

As can be seen in the left-hand panel (a) of Fig. 5, the assumption of a uniform distribution of background Trojans in the target zone is fair, but not exactly satisfied. This is the result of the decreasing number of Trojans towards the libration centre (i.e. at very small values da_P). We therefore repeated our analysis in a different system of coordinates. Keeping e_P and $\sin I_P$, we now changed da_P with $S = 4\pi(da_P)^2$. The background reasoning is that the libration point, $da_P = 0$, represents a centre about which the tadpole orbits move in 3D. In a Cartesian view centred at L4 the radial coordinate is to be replaced with the surface area $S = 4\pi(da_P)^2$. Re-mapping and re-binning our analysis in the $(S, e_P, \sin I_P)$ coordinate system, we obtained the situation shown in the right-hand panel (b) of Fig. 5. Whilst still keeping the same number $k = 91$ of Trojans in the analysed zone, their distribution is now more uniform. Given the new box-definition by the (258656) 2002 ES₇₆ and 2013 CC₄₁ couple, we now find the number of thus defined small boxes to be increased to $n \simeq 2.34 \times 10^9$. This is the result of the candidate couple’s close proximity to the libration centre. As a result, the likelihood (equation 2) of the couple being just a fluke in a uniform distribution of objects now becomes smaller, namely $p \simeq 1.75 \times 10^{-5}$.

The probability p , defined and computed for the (258656) 2002 ES₇₆–2013 CC₄₁ couple above, is appreciably small. It is both interesting and important to compare this result with the similarly defined quantity for other Trojan couples, especially amongst those that have a small δV_P distance in the metrics (1). This will tell us whether the probability p for (258656) 2002 ES₇₆–2013 CC₄₁ is sufficiently small in absolute measure for the couple to be considered a true pair, whilst at the same time enabling our algorithm to better connect our p definition with the velocity metrics used above. Here we analyse the L4-swarm population, but the same approach could equally be applied to the L5 case.

The potentially complicated part of the procedure is that, for each selected couple, we have to (i) adapt the box size $(\delta a_P, \delta e_P, \delta \sin I_P)$, and (ii) the zone size $(\Delta a_P, \Delta e_P, \Delta \sin I_P)$, as well as the position to which the box size refers. The choice of the latter obviously varies because the local number density of bodies differs from place to place. In order to prevent excessively small boxes in one of the dimensions (as an example, due to an almost zero difference $\delta e_P = 0$),

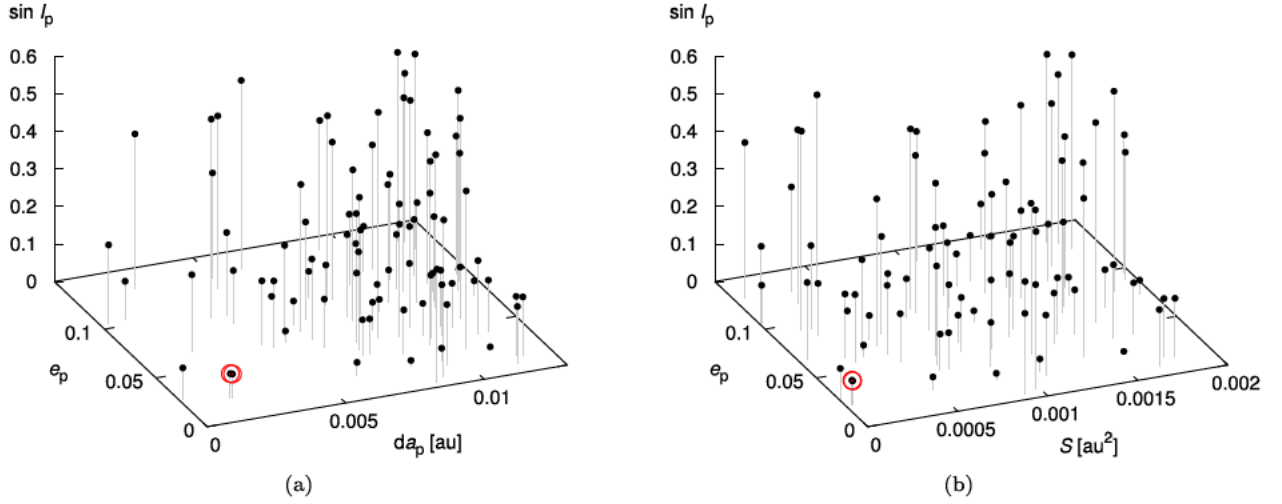


Figure 5. Left-hand panel (a): The small-libration portion of the L4 stable orbital zone in the 3D proper element coordinates (da_p , e_p , $\sin I_p$). The proximity to the libration was arbitrarily set by $da_p \leq 0.014$ au, whilst the extent of e_p and $\sin I_p$ is limited by orbital stability. We find 91 objects (black symbols) in this zone for our data set of Trojans. The candidate pair (258656) 2002 ES₇₆ and 2013 CC₄₁ is highlighted with a red circle. The vertical intervals help to appreciate 3D nature of the display. Right-hand panel (b): The same as on the left-hand panel, but the da_p was replaced with a surface area $S = 4\pi(da_p)^2$. In this case, the small-amplitude Trojans are distributed more uniformly.

we use the metric δV_p as a measure of the ‘diagonal’ of the box and we define its respective volume as $(\delta V_p)^3/\sqrt{3}$. Observing the typical spatial variation of the number density of Trojans, we use a fixed value for $\Delta a_p = 0.02$ au, rejecting pairs with $\delta a_p > 0.3\Delta a_p$. In order to prevent a low number of bodies k in the zone, both Δe_p and $\Delta \sin I_p$ are then sequentially increased until $k \geq 50$. Once we set the zone, we again define its volume as $(\Delta V_p)^3/\sqrt{3}$, with ΔV_p the velocity distance of the corners connected with a diagonal. The number of boxes n , as well as the probability p , is then computed as before (equation 2). Obviously, the whole algorithm cannot be done manually, but an automated computer script was written to run the method.

The statistical results of our analysis are shown in Fig. 6. The pairs seem to be well organized in the (p , δV_p) plane, expressing an overall correlation between the two quantities. As might be expected, the general trend is $p(\delta V_p) \propto (\delta V_p)^3$, namely volume of the box. Nevertheless, the p versus δV_p values do not follow a single curve, due to the local number density being different for each of the couples. Those couples located within known families generally have relatively high p values. This is to be expected, since the surrounding zones are densely populated by Trojans, which causes the dimensions of the zone to be small. To illustrate this effect, we coloured data for pairs in the largest families in the Fig. 6, identifying those in the (i) Eurybates family (blue), (ii) the core of the Hektor family (light blue), and (iii) the (9799) 1996 RJ family (cyan), after Nesvorný, Brož & Carruba (2015). The Eurybates family, the largest and most populous in the Trojan population, has systematically the largest p values. This is because even a small zone quickly contains our threshold number of $k = 50$ Trojans. We note that $p \simeq 1$, or even formally larger, just indicates that a couple of Trojans in this zone is fully expected at their distance δV_p . An exception to this rule is the (9799) 1996 RJ family, where we find the smallest p values, which are clearly correlated with δV_p . This is because (9799) 1996 RJ is a very compact family located in isolation in a high-inclination portion of the Trojan phase space (see also Fig. 1). For each of the couples selected in this family, the reference zone needs to be large to contain the minimum required number of objects.

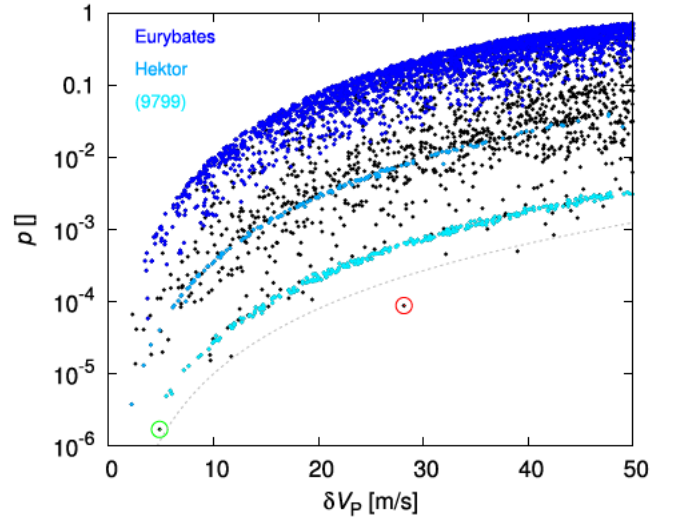


Figure 6. The probability p that a pair is random fluke, computed using the method described in the text, versus its distance δV_p , computed for all low-velocity pairs in the L4 zone using equations (2) and (1). The pair (258656) 2002 ES₇₆ and 2013 CC₄₁ is highlighted with a red circle. The pair (219902) 2002 EG₁₃₄ and (432271) 2009 SH₇₆, discussed briefly in Appendix B, is highlighted with a green circle. The coloured symbols denote pairs in the identified L4 families: (i) Eurybates (blue), (ii) the core of the Hektor family (light blue), and (iii) (9799) 1996 RJ (cyan). The dashed line, $p = 10^{-5} (\delta V_p / (10 \text{ m s}^{-1}))^3$, is used to emphasize that the candidate pair (258656) 2002 ES₇₆ and 2013 CC₄₁ is an outlier in this population.

Whilst the collisional families could clearly contain dynamical pairs, their recognition is confused by the locally high background of family members. We therefore exclude objects located in families from our work. What remains is then a diffuse background population of Trojans. For every fixed δV_p value, there are some background couples for which p extends to small values. The true Trojan dynamical pairs, namely those objects genetically related to a common parent, form the basis for our search among this population of a low- p tail for sufficiently small δV_p values. There are possibly a number of such

cases, but amongst them, the one which is the most outlying from the $p(\delta V_p) \propto (\delta V_p)^3$ reference level shown by the dashed curve in Fig. 6 is the case of (258656) 2002 ES₇₆–2013 CC₄₁ (highlighted with red circle). Its p value is an order of magnitude lower when compared to couples with similar δV_p values. This justifies the validity of the (258656) 2002 ES₇₆–2013 CC₄₁ couple as a true asteroid pair, based on our statistical analysis alone. There are also some family-unrelated couples with p values comparable or smaller, and these are briefly discussed in Appendix B.

In the next Section 3, we conduct a search for past orbital convergence of the selected (258656) 2002 ES₇₆ and 2013 CC₄₁ couple. If successful, this process adds an important piece of evidence justifying the couple as a real pair of genetically related objects. We explain our methods in detail. These methods are also briefly applied to several other candidate couples, with less success (Appendix B).

3 NUMERICAL SIMULATIONS

The dynamics of the Jovian Trojans have been extensively studied using both analytical and numerical means (e.g. Milani 1993; Beaugé & Roig 2001; Robutel & Gabern 2006; Di Sisto et al. 2014; Holt et al. 2020, and references therein). Here, we confine ourselves to briefly recalling only the information necessary for understanding and interpreting our numerical simulations of the (258656) 2002 ES₇₆ – 2013 CC₄₁ pair.

As previously noted, the objects in this pair are not typical, but are instead exceptional representatives of Trojan population. This is because they reside extremely close to the L₄ libration centre. As a result, the evolution of their semimajor axis a and the resonant argument $\lambda - \lambda_J$ be characterized by many small-amplitude and high-frequency terms. Those are, however, of the least importance for our analysis. More relevant is the behaviour of the eccentricity e , the inclination I , the longitude of ascending node Ω , and the longitude of perihelion ϖ . Due to the small values of the eccentricity and inclination, it is also useful to think about complex non-singular elements $z = e \exp(i\varpi)$ and $\zeta = \sin I \exp(i\Omega)$. In linear perturbation theory, a fairly satisfactory zero approximation, both z and ζ are represented by a finite number of Fourier terms, namely the proper term and a few forced planetary terms. A simpler description concerns ζ , whose Fourier representation is dominated by the proper term with $I_p \simeq 3.7^\circ$, followed only by small contributions from the s_6 term, with $I_6 \simeq 0.36^\circ$, and a number of significantly smaller contributions. As a result, the osculating inclination I is well represented by a constant I_p and a periodic term with amplitude I_6 . Correspondingly, the osculating longitude of the ascending node, Ω , steadily circulates with a period given by the proper s frequency, and experiences only very small perturbation from the s_6 term. The evolution of z is more complicated because it is represented by three terms of comparable amplitude. The largest amplitude contribution, $\simeq 0.044$, is provided by the term with frequency g_5 , followed by proper g and g_6 terms with comparable amplitudes of $\simeq 0.021$ and $\simeq 0.015$. Whilst still very simple in the Cartesian representation of z , the polar variables in this plane (i.e. the eccentricity and especially longitude of perihelion) exhibit a non-linear evolution, characteristic of many low-eccentricity asteroid orbits.

3.1 Short-term simulations

Equipped with this knowledge, we can now turn to investigating the common origin of (258656) 2002 ES₇₆ and 2013 CC₄₁. In studies of asteroid pairs, researchers seek to demonstrate a convergence of heliocentric orbits of the proposed pair at some moment in the

past (e.g. Vokrouhlický & Nesvorný 2008). This is considered to be the origin of the two objects from a common parent body, and the corresponding time in the past representative of the age of the pair. As typically achievable ages of the asteroid pairs in the Main belt are less than 1 Myr, with many less than 100 kyr, a convergence is often sought in Cartesian space. This approach means to demonstrate that the two orbits meet at the same point in space and have a very small relative velocity.

The same condition can be expressed in heliocentric orbital elements by making them basically equal at the formation moment of the pair. For this work, we find it markedly more useful to work with the orbital elements of our candidate pair, as they can teach us more readily about the evolution of the orbits of the two objects. Therefore, in Fig. 7, we show the results of our initial numerical experiment. We provide the differences between the osculating heliocentric elements of the nominal orbits of (258656) 2002 ES₇₆ and 2013 CC₄₁ over a short time interval of the past 10 Myr. We use the `swift_rmvs4` integrator (Levison & Duncan 1994) which allows us to efficiently include gravitational perturbations from all eight planets. The integration time-step used was 3 d, and the state vectors of all propagated bodies, planets, and the two Trojans, were output every 50 yr. We use a reference system defined by the invariable plane of the planetary system. The initial conditions of (258656) 2002 ES₇₆ and 2013 CC₄₁ at MJD58800 epoch were obtained from the `AstDyS` website.

The differences in the orbital elements shown in Fig. 7 oscillate with the dominant frequencies identified by the analysis of z and ζ themselves. For instance, the principal periodicity seen in δI and $\delta \Omega$ corresponds to the frequency $s_6 - s$, whilst the principal periodicity seen in δe and $\delta \varpi$ corresponds to frequencies g and $g_5 - g_6$. Differences δa and $\delta \lambda$ are characterized by higher frequencies, such as the planetary orbital frequencies, the libration frequency, and then followed by a ‘forest’ of lower frequencies starting with g .

We also note a markedly different behaviour of $\delta \varpi$ and $\delta \Omega$, which can be understood from the above mentioned description of the z and ζ non-singular elements of the two objects. Observing the general behaviour of the amplitude in the $(\delta a, \delta e, \delta \varpi, \delta \lambda)$ terms, we note a curious fact that those amplitudes become very small simultaneously for semimajor axis, eccentricity, longitude of perihelion and longitude in orbit $\simeq 7.11$ Myr ago (upper four panels in Fig. 7). However, any hope for a clear orbital convergence at that epoch is removed by looking at behaviour of the inclination and longitude of ascending node differences (bottom two panels in Fig. 7). We note that δI keeps steadily oscillating about a mean value of $\simeq -0.08^\circ$, namely a difference in the proper inclinations of (258656) 2002 ES₇₆ and 2013 CC₄₁, without the amplitude of those oscillations showing any tendency to shrink. At the same time, the nodal difference stays large, and only slowly decreases from $\simeq -56^\circ$ to $\simeq -45^\circ$. This rate of decrease in $\delta \Omega$ fits perfectly the difference in proper frequencies s of the two objects as to be expected. Hence some $\simeq 7.11$ Myr ago, the two orbits had basically identical (a, e, ϖ, λ) values, but the nodes were still offset by about 50° . This is inconsistent with any believable low-velocity separation of the two objects from a common parent body at their origin. Whilst inconclusive about the origin of the (258656) 2002 ES₇₆ and 2013 CC₄₁ couple, this 10 Myr integration provides useful hints for further analyses.

3.2 Long-term simulations

Extrapolating the trend seen in Fig. 7, we can estimate that the nodes of (258656) 2002 ES₇₆ and 2013 CC₄₁ became coincident some

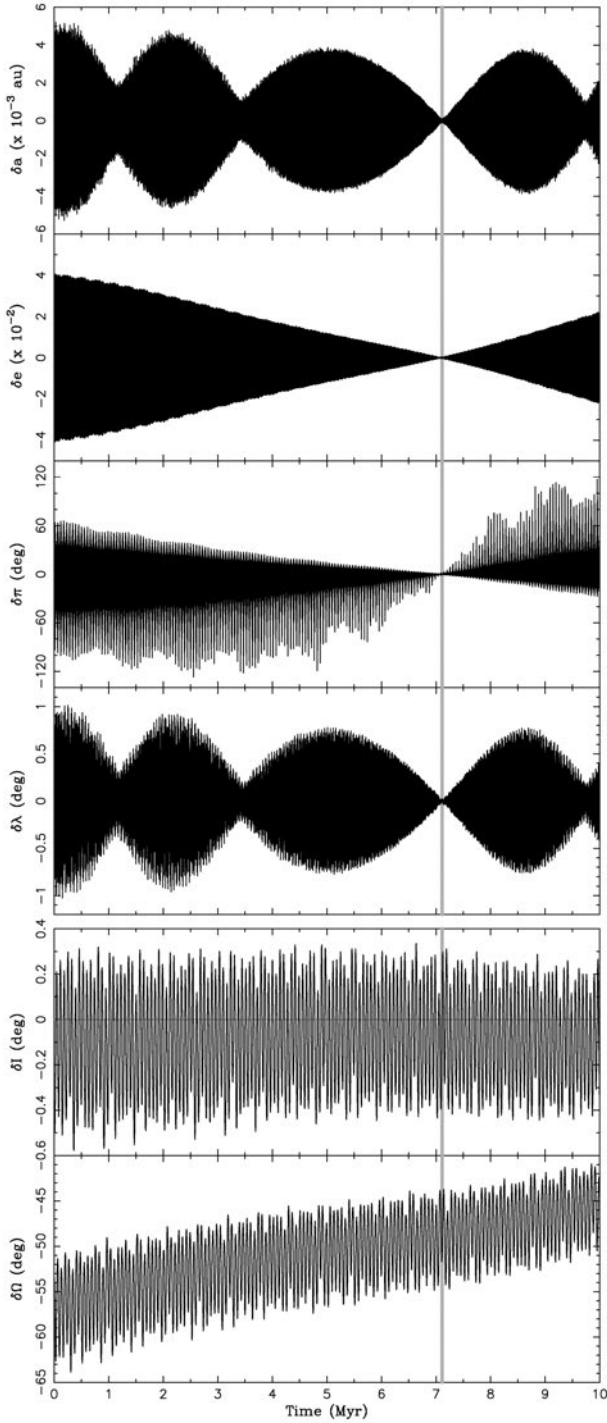


Figure 7. Differences between the osculating orbital elements of (258656) 2002 ES₇₆ and 2013 CC₄₁ from a 10 Myr backward integration of their nominal orbits. Gravitational perturbations from all planets were included and an invariable-plane reference system used. The differences of semimajor axis δa , eccentricity δe , longitude of pericentre $\delta \varpi$, and longitude in orbit $\delta \lambda$ (top four panels) indicate a simultaneous collapse to near zero values at ≈ 7.11 Ma (grey vertical line). In contrast, the differences of inclination δl and longitude of ascending node $\delta \Omega$ (the bottom two panels) do not converge at that epoch: the nodal longitudes of the two objects are still $\approx 50^\circ$ away from each other, and the inclination difference shows steady oscillation about the mean value of $\approx -0.08^\circ$, namely a difference in their proper inclinations. The steady trend in $\delta \Omega$ has a slope $\approx 0.004 \text{ arcsec yr}^{-1}$, very close to the difference in proper frequencies s of (258656) 2002 ES₇₆ and 2013 CC₄₁.

50 Myr ago. Obviously, this is only the first such configuration in the historical evolution of the two objects. Assuming orbital stability, we also predict that the configuration will repeat with a ≈ 320 Myr periodicity. To probe the long-term changes in the orbital architecture of the (258656) 2002 ES₇₆–2013 CC₄₁ couple, we extended our previous simulation to 1200 Myr in the past. We note in passing that the necessity to seek this pair’s age over such a long time-span forces us to abandon any hopes of finding a convergence in Cartesian coordinates. This is because of the small but non-negligible chaoticity of the integrated orbits, and principally results from an uncertainty in the thermal accelerations that the objects would experience (as discussed below). Both of these factors would require a large number of clones of (258656) 2002 ES₇₆ and 2013 CC₄₁ to investigate their past histories, and thus are computationally prohibitive to pursue. We therefore choose to downsize the dimensionality of the space where a convergence is quantified, and focus on the behaviour of secular evolution in just the non-singular elements z and ζ . Fig. 8 shows the differences between the osculating $\delta \Omega$ and $\delta \varpi$ of the two objects, and pays special attention to the time interval near $\delta \Omega \approx 0$ configurations.

As expected, the first such configuration occurred about 50 Myr ago. However, a closer look at the relevant panel of Fig. 8 indicates that suitable orbital convergence conditions did not occur at that time. Unlike ≈ 7.11 Mya, the orbital planes converge, but the perihelion longitudes are at the maximum of their oscillations. An even closer look at the epochs near nodal convergence shows that when $\delta \varpi$ crosses zero, δe is large, and vice versa. Once again, we therefore find that the conditions of a low-velocity separation of the two orbits cannot be met at that epoch.

Inspecting further epochs of nodal crossing, as shown in Fig. 8, we conclude that $\delta \Omega \approx 0$ in fact never exactly coincides with $\delta \varpi \approx 0$, a convergence pre-requisite. Here, however, we must revisit some of the assumptions made in our simulation. In particular, recall that (i) we used only nominal realizations of the orbits of both (258656) 2002 ES₇₆ and 2013 CC₄₁, and (ii) we included only gravitational perturbations from planets in our dynamical model. Both of these approximations are insufficient for a full analysis of our problem (see a similar discussion of the attempts to determine the origin of young asteroid clusters/families and pairs in Nesvorný & Vokrouhlický 2006, or Vokrouhlický & Nesvorný 2008).

First, the nominal orbital solution represents the best-fit of the available astrometric data. The inevitable uncertainties of the latter implies the uncertainty of the orbital fit itself. Well-behaved orbital solutions are represented by fixed confidence-level regions in the 6D orbital space, using an ellipsoidal geometry, mathematically expressed by elements organized in the covariance matrix. Each orbit starting in a high confidence-level zone (≥ 80 – 90 per cent, say) is statistically equivalent to the best-fitting solution. Whilst initially very compact, these different solutions typically diverge with time. We thus need to consider in our simulation not only the best-fitting orbits, but also a sample of those starting from the high-confidence zone. We call these ‘geometrical clones’.

The second issue that needs to be considered is the validity of the dynamical model used. The long-term dynamics of small objects are known to be subject to perturbations due to the thermal acceleration known as the Yarkovsky effect (e.g. Bottke et al. 2006; Vokrouhlický et al. 2015). Nominally, within the Trojan population, objects are only minimally affected by the Yarkovsky effect (Wang & Hou 2017; Hellmich et al. 2019), which has the greatest influence at smaller sizes. However, the two components in the (258656) 2002 ES₇₆–

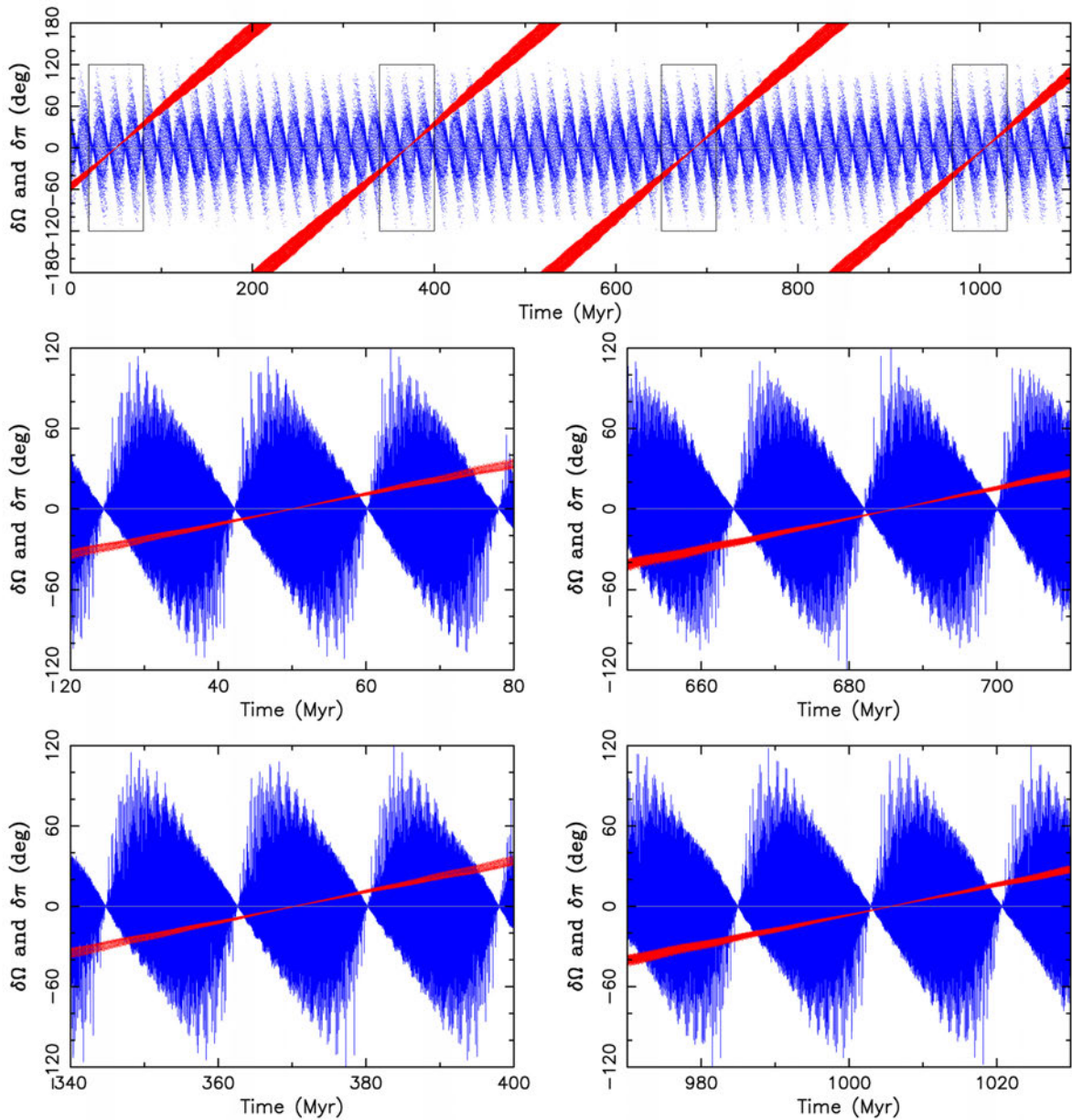


Figure 8. The long-term behaviour of the difference in osculating nodal and perihelion longitudes $\delta\Omega$ (red) and $\delta\varpi$ (blue) for the nominal orbits of (258656) 2002 ES₇₆ and 1013 CC₄₁. The top panel shows the results from a backward integration in time to 1200 Myr. The four panels below show a zoom around the configurations where $\delta\Omega$ becomes small, also indicated by the black rectangles in the top panel. As inferred from data in Fig. 7, the first such situation occurs $\simeq 50$ Myr in the past, and repeats with a period of $\simeq 320$ Myr. The configuration of the nominal orbit becomes closest to true convergence at $\simeq 680$ Myr and $\simeq 1010$ Myr in the past (right middle and bottom panels).

2013 CC₄₁ couple are well within this size range, and so it is warranted to see what dynamical effects might be produced by Yarkovsky accelerations. Since none of the parameters needed for evaluation of the thermal accelerations, such as the rotation state, the surface thermal inertia, and the bulk density, are known for either (258656) 2002 ES₇₆ or 2013 CC₄₁, we need to consider a suite of potential orbit histories, each generated by numerical integration of test particles experiencing a range of physically plausible thermal accelerations. These will be called the Yarkovsky clones. We also note that the effect of thermal accelerations was included in *swift_rmvs4* using the same method as described in Vokrouhlický & Nesvorný (2008).

3.3 Clone sets

We conducted two sets of numerical simulations, one considering only the geometrical clones (Section 3.3.1), and the other considering only the Yarkovsky clones (Section 3.3.2) of (258656) 2002 ES₇₆ and 2013 CC₄₁. In each simulation set, we include the nominal orbit of the objects, complemented by a set of 20 clones. We ran a backward integration of all orbits for 1.5 Gyr with an integration time-step of 3 d. Every 500 yr, we evaluated the differences between the osculating orbital elements of the 21 realizations of (258656) 2002 ES₇₆ with each of those of 2013 CC₄₁, and searched for the possibility of a convergent configuration. To quantify the latter, we

used two conditions. First, as in Nesvorný & Vokrouhlický (2006), we evaluated the target function

$$\delta V = na\sqrt{(\sin I \delta\Omega)^2 + 0.5(e \delta\varpi)^2}, \quad (3)$$

where (n, a, e, I) are the arithmetically mean values of the mean motion, semimajor axis, eccentricity, and inclination of the two considered clones, and $\delta\Omega$ and $\delta\varpi$ are the differences between the osculating longitude of the ascending node and perihelion for the two clones, respectively. This way, δV has the dimension of velocity, and is constructed to provide, in a statistically mean sense, the necessary velocity perturbation required for a transfer between the secular angles of the two orbits. However, the analysis of the results presented in Fig. 8 has shown that even a configuration with potential $\delta\Omega \simeq 0$ and $\delta\varpi \simeq 0$, and therefore $\delta V \simeq 0$, is not enough to guarantee a satisfactory orbital convergence, provided that δe and δI are simultaneously large. For that reason, we admit as a potentially convergent configuration a case where the orbits of the two clones satisfy

- (i) $\delta V \leq V_{\text{lim}}$, where V_{lim} is some small value, we use typically $1\text{--}3 \text{ m s}^{-1}$, and
- (ii) $\delta e \leq e_{\text{lim}}$ and $\delta I \leq I_{\text{lim}}$, where again we use suitably small values of $e_{\text{lim}} \simeq 5 \times 10^{-4}$ and $I_{\text{lim}} \simeq 0.1^\circ$ namely differences in the corresponding proper elements of (258656) 2002 ES₇₆ and 2013 CC₄₁.

We output information about these potentially converging configurations for further analysis. In the next two sections, we comment on the results of our numerical experiments that use geometrical (Section 3.3.1) and Yarkovsky clones (Section 3.3.2) separately.

3.3.1 Geometric clones

Information about the orbit determination, needed for a construction of the geometrical clones, was taken from the `AstDyS` data base. The orbits of both (258656) 2002 ES₇₆ and 2013 CC₄₁ are rather well constrained, reflecting numerous astrometric observations. Even the poorer of the two, 2013 CC₄₁, was observed over seven oppositions, leading to a fractional accuracy of $\simeq 10^{-7}$ in the semimajor axis, a , and the Cartesian components of the non-singular elements, z and ζ . Only the mean longitude, λ , has a slightly worse accuracy, namely $\simeq 2 \times 10^{-5}$ deg. These are the characteristic differences between the six orbital osculating elements $\mathbf{E} = (a, z, \zeta, \lambda)$ of the clones in $\simeq 68$ per cent confidence zone and the best-fitting solution \mathbf{E}_* . The solution is given at the initial epoch MJD58800. Complete information about the parameters of the 6D confidence zone ellipsoid in the space of elements \mathbf{E} is given by the covariance and normal matrices, also provided at the `AstDyS` website. Denoting Σ the normal matrix, we may construct the initial orbital elements \mathbf{E} of the geometric clones using

$$\mathbf{E} = \mathbf{T}^T \xi + \mathbf{E}_*, \quad (4)$$

where ξ is a 6D vector whose components are random deviates of normal distribution (with variance equal to unity), and the matrix \mathbf{T} satisfies $\mathbf{T}^T \mathbf{T} = \Sigma$ (e.g. Milani & Gronchi 2010); \mathbf{T} is obtained using the Cholesky decomposition method. As mentioned above, we constructed 20 geometric clones of both (258656) 2002 ES₇₆ and 2013 CC₄₁ at the initial epoch of our simulation.

The bottom panel of Fig. 9 shows the maximum nodal difference between the clones of (258656) 2002 ES₇₆ and its nominal orbit. Tiny differences between the orbital parameters imply that the s frequency of the clone orbits is not exactly the same as that of the

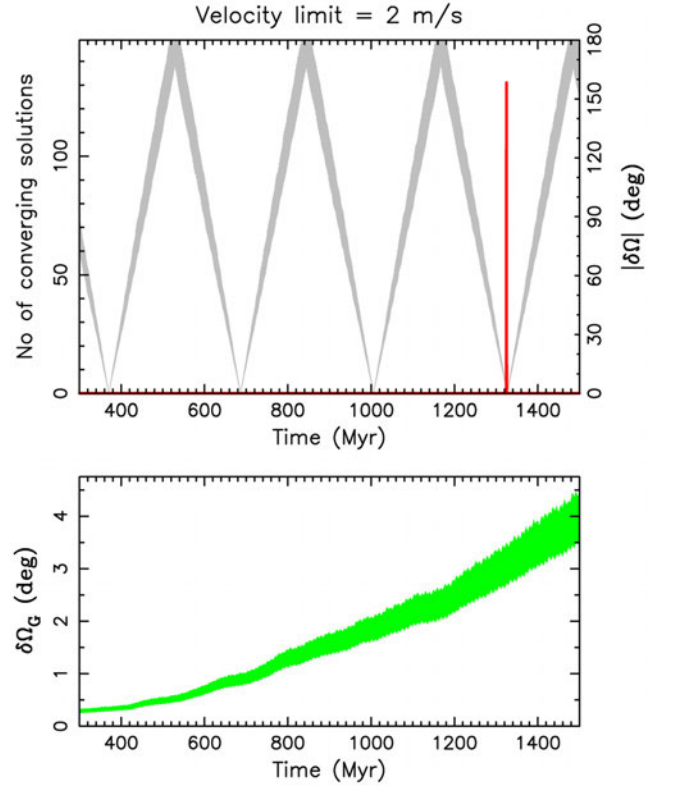


Figure 9. The statistical distribution of convergent solutions for geometric clones of (258656) 2002 ES₇₆ and 2013 CC₄₁ from simulations of the nominal orbits of the two objects, plus 20 clones each, using the velocity cutoff $\delta V \leq 2 \text{ m s}^{-1}$, and eccentricity and inclination limits discussed in the text. Abscissa is time to the past starting from 300 Mya (there are no earlier solutions). The left ordinate in the upper two panels gives the number of recorded solutions in 50 kyr bins (red histogram). The grey line gives $|\delta\Omega|$ of the nominal orbits of (258656) 2002 ES₇₆'s and 2013 CC₄₁ (see the right ordinate and the red line on Fig. 8), aiming to aid interpretation of the results. The green line in the bottom panel shows the maximum difference in the longitude of the ascending node between the clones of (258656) 2002 ES₇₆ and the longitude of ascending node of its nominal orbit; up to about 200 Myr this trend is nearly linear, but becomes more complicated beyond this epoch due to very weak orbital chaos.

nominal orbit. However, the stability of this orbital zone ensures that the configuration of the clone orbits does not evolve, and thus initially the nodal divergence is basically linear in time. Only beyond about 0.5 Gyr does the divergence become stronger than linear. This is an expression of a very weak instability that manifests itself in the behaviour of the secular angle solely Gyr time-scales. The formal Lyapunov time-scale of the orbits of both (258656) 2002 ES₇₆ and 2013 CC₄₁ is only $\simeq 20$ Myr (see the `AstDyS` data base). This implies that a divergence in λ is dominant, whilst the divergence in the secular angles is slower, as shown in Fig. 9. At 1 Gyr, the nodal longitudes of clones of (258656) 2002 ES₇₆ are thus spread over a $\simeq 2^\circ$ range. A similar, and potentially slightly larger, effect is seen among the clones of 2013 CC₄₁, principally due to their larger differences at the initial epoch. This divergence may overcome the difficulties we experienced in attempting to find an epoch at which the nominal orbits achieve a converging configuration. For instance, in the bottom right-hand panel of Fig. 8, we note that the nodal difference of the nominal orbits misses the epoch at which the difference of pericentres basically shrinks to zero by about 3° at $\simeq 1$ Gyr. This may be compensated for if the orbits of suitable clones are used, instead of the nominal orbits.

Obviously, a satisfactorily large nodal spread of the clone orbits must be attained.

The top panel of Fig. 9 shows the statistical distribution of the converging geometric clones of the two Trojans, organized in 50 kyr wide bins. Obviously, the rather small number of clones in our test run does not allow us to probe the convergence properties in great detail. For that reason, and with the rather tight limit $\delta V \leq 2 \text{ m s}^{-1}$ chosen, the possible solutions cluster only near the $\approx 1325 \text{ Myr}$ epoch, though we note that, if a looser criterion $\delta V \leq 4 \text{ m s}^{-1}$ was chosen, more solutions would also exist at $\approx 1003 \text{ Myr}$. Taken naively at a face value, we would conclude a possible origin of the (258656) 2002 ES₇₆–2013 CC₄₁ couple at this time in the past, if the couple are not older than 1.5 Gyr, beyond which we did not continue our simulation. However, as is often in the case of a pair configuration which is not very young, the so far neglected thermal accelerations in the dynamical model can prove to be a source of considerable uncertainty. This is analysed in Section 3.3.2.

3.3.2 Yarkovsky clones

Our Yarkovsky clones all have the same initial conditions as the nominal orbit, but they differ in the magnitude of thermal accelerations used for their orbital propagation. As in Vokrouhlický & Nesvorný (2008), we approximate thermal accelerations using a simple transverse component with the magnitude inversely proportional to the square of the heliocentric distance. The magnitude of this acceleration is adjusted such that the resulting change in the semimajor axis da/dt matches predictions from the theoretical formulation of Yarkovsky effect (see also Farnocchia et al. 2013, where a classical formalism used in cometary dynamics was adopted). In order to estimate plausible da/dt values, we use a simple approach describing the diurnal Yarkovsky effect for a spherical body on a circular heliocentric orbit, presented in Vokrouhlický (1998). We use the following set of physical parameters: the surface thermal conductivity $K \approx 0.01\text{--}0.03 \text{ W m}^{-1} \text{ K}^{-1}$, the surface thermal inertia $\Gamma \approx 100\text{--}200$ [SI units] (for both see Delbó et al. 2015), the bulk density $\rho \approx 1.5 \text{ g cm}^{-3}$ (e.g. Carry 2012), rotation period $P \approx 100\text{--}500 \text{ h}$, and size $D \approx 7 \text{ km}$. The maximum semimajor axis drift rate at zero obliquity is then $(da/dt)_{\text{max}} \approx (0.15 \pm 0.07) \times 10^{-4} \text{ au Myr}^{-1}$. Our choice of a slow rotation period is tied to the working assumption that (258656) 2002 ES₇₆ and 2013 CC₄₁ are indeed a real Trojan pair. We argue in Section 4.1 that the most plausible formation mechanism for such a pair is the destabilization of a Trojan binary. If this is indeed the case, then before their separation, the two components were most likely spin–orbit synchronized to periods of $\geq 100 \text{ h}$ (e.g. Nesvorný et al. 2020). If, however, the formation mechanism of the pair was different, such as the YORP-driven fission of a parent object (see Section 4.2), the rotation periods P of (258656) 2002 ES₇₆ and 2013 CC₄₁ could well be as short as a few hours. In that case, $(da/dt)_{\text{max}}$ would be smaller by a factor of 3 to 5. Indeed, as a confirmation of our reasoning, we note that scaling the value of the detected Yarkovsky signal $19 \times 10^{-4} \text{ au Myr}^{-1}$ for the 500 m size near-Earth asteroid 101955 Benu with $P \approx 4.3 \text{ h}$ (e.g. Chesley et al. 2014), we would have $(da/dt)_{\text{max}} \approx 0.06 \times 10^{-4} \text{ au Myr}^{-1}$. In our simulation, we consider only the case of long rotation periods, and fix $(da/dt)_{\text{max}} \approx 0.15 \times 10^{-4} \text{ au Myr}^{-1}$. For each of the two Trojans, (258656) 2002 ES₇₆ and 2013 CC₄₁, we consider the nominal orbit with $da/dt = 0$, and 20 Yarkovsky clones. In both cases, 10 clones have positive da/dt and 10 clones have negative da/dt . Additionally, because in the case of the diurnal variant of the Yarkovsky effect $da/dt \propto \cos \gamma$, where γ is the spin axis obliquity, the positive/negative

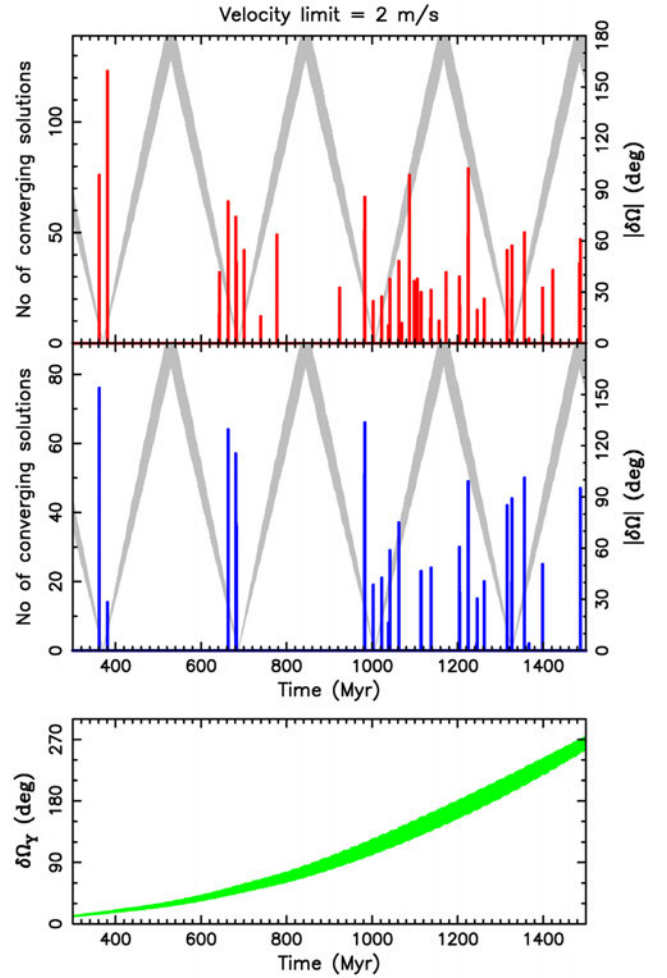


Figure 10. The statistical distribution of convergent solutions for the Yarkovsky clones (nominal orbits plus 20 clones each) of (258656) 2002 ES₇₆ and 2013 CC₄₁, using the velocity cutoff $\delta V \leq 2 \text{ m s}^{-1}$, and eccentricity and inclination limits discussed in the text. Abscissa is time to the past starting from 300 Mya (there are no earlier solutions). The left ordinate in the upper two panels gives the number of recorded solutions in 50 kyr bins. The top panel (red histogram) gives the number of solutions for all possible combinations of clones. The middle panel (blue histogram) for the case when only clones with the same sign of da/dt were compared. The grey line gives $|\delta\Omega|$ of the (258656) 2002 ES₇₆'s and 2013 CC₄₁'s nominal orbits (see the right ordinate and the red line on Fig. 8), aiming to aid interpretation of the results. The green line in the bottom panel shows the difference in the longitude of ascending node between the Yarkovsky clone with maximum positive drift rate $(da/dt)_{\text{max}}$ and the nominal orbit of (258656) 2002 ES₇₆.

close da/dt values uniformly sample the interval 0 to $(da/dt)_{\text{max}}$, resp. $-(da/dt)_{\text{max}}$ to 0.

Fig. 10 shows the results from our Yarkovsky clone simulations. In contrast to the simulations where only the geometrical clones were used (Fig. 9), there are many more convergent solutions, starting from 360 Mya. The reason is illustrated in the bottom panel of Fig. 10, which shows the divergence of the osculating longitude of the ascending node between the nominal orbit (no Yarkovsky effect) and the clone with the maximum positive drift-rate $(da/dt)_{\text{max}}$ of (258656) 2002 ES₇₆. Clones with smaller da/dt values have nodal differences smaller than the signal seen in Fig. 10, proportionally to their $\cos \gamma$ value.

The nodal differences between various clones are now much larger, reaching the maximum possible value of 360° after at $\simeq 1.1$ Gya. The nodal difference to the nominal orbit of the clone with the maximum negative drift-rate value is about the same but negative. This is because $\delta\Omega$ now propagates nearly quadratically in time as opposed to the quasi-linear trend for the geometrical clones. Such a quadratic trend in node propagation is characteristic of Yarkovsky studies of asteroids (e.g. Vokrouhlický & Nesvorný 2008). In that case, the phenomenon was easily associated with the principal dynamical perturbation produced by the Yarkovsky effect, namely the secular drift in semimajor axis. As a result, the semimajor axis dependence of the s frequency produces, after a straightforward integration, a quadratic-in-time drift of the node. In our case of Jovian Trojans, the effects are slightly subtler. This is because, in spite of a permanent transverse perturbing acceleration in orbits of the clones, their semimajor axis does not show any constant drift in time due to the resonant locking inherent to their presence in the Trojan population. However, other elements – eccentricity and inclination – do display such a secular drift, as previously found in Wang & Hou (2017) and Hellmich et al. (2019). As the s frequency is also dependent on these values, it still displays a linear change as a function of time, explaining the quadratic effect in node seen in the Fig. 10.

Returning to the pattern in the distribution of converging solutions seen in Fig. 10, we note their clustering near epochs when $\delta\Omega$ of the (258656) 2002 ES₇₆ and 2013 CC₄₁ nominal orbits has been found to reach zero (the grey line in the top panels). This is to be expected, since the nodal difference exhibits the most stable evolution in time. Therefore, when nominal orbits of the two Trojans have large $\delta\Omega$ values, the clones will also follow the same pattern. This conclusion will, however, weaken further into the past because of the clone nodal divergence discussed above. As a result, beyond ~ 1 Gyr into the past, the solution distribution spreads more in time. This is because specific clone combinations may now satisfy more easily our convergence conditions. Additionally, convergent solutions cluster in peaks separated by about 19 Myr, rather than exhibiting a continuous distribution about the $\delta\Omega \simeq 0$ nodal conditions. This is due to the $\delta\varpi \simeq 0$ perihelion condition also facilitating the convergence criteria we adopted.

The middle panel in Fig. 10 shows the statistical distribution of the number of converging solutions for a subsample of cases in which clones of (258656) 2002 ES₇₆ and 2013 CC₄₁ both have the same sign of the associated da/dt drift. Translated using the diurnal Yarkovsky theory, this also implies that the two clones have the same sense of rotation: either both prograde, or both retrograde. The proposed formation mechanisms for this pair, namely a binary split or rotation fission, would both predict this property. There are obviously fewer solutions found, but the general pattern of their distribution is about the same as in the general case when all clones are taken into account.

Fig. 11 shows the conditions at convergence for two pairs of the Yarkovsky clones of (258656) 2002 ES₇₆ and 2013 CC₄₁: the left-hand panels at the most recent possible cluster of solutions in the past (namely at $\simeq 381.07$ Mya), whilst the right-hand panel shows the cluster at an epoch which is more distant in the past by two cycles of the differential motion of their orbital nodes (namely at $\simeq 1062.33$ Mya). In general, the quality of the convergence is similar, including those solutions beyond 1 Gya. In both cases, the formal convergence of the secular angles is better than 0.004° .

When inserted into equation (3), the equivalent velocity difference is negligibly small $\delta V \leq 0.04 \text{ m s}^{-1}$. At the convergence epoch, the osculating eccentricity values are also satisfactorily close to each other, namely $\delta e \simeq 7.5 \times 10^{-5}$. Using the Gauss equations (e.g.

Nesvorný & Vokrouhlický 2006), we estimate that this tiny eccentricity difference corresponds to an orbital velocity change smaller than 1 m s^{-1} in a statistical sense. This change is actually smaller than the difference in proper eccentricity values of (258656) 2002 ES₇₆ and 2013 CC₄₁. The inclination convergence turns out to be the most troublesome element of the simulation: the persisting differences of $\simeq 0.085^\circ$ statistically correspond to a velocity change of $\simeq 25 \text{ m s}^{-1}$. Such a difference in the osculating values of inclinations corresponds to the difference of their proper values. In contrast, the acceptable true separation velocity of the objects should be a fraction of the escape velocity from the effective parent body. With its size of $\simeq 9 \text{ km}$, the ideal condition of the separation in this pair would require a velocity difference of $\leq 4 \text{ m s}^{-1}$. The inclination difference at converging solutions is therefore nearly an order of magnitude larger.

One possibility to explain this mismatch may be related to our approximation of the Yarkovsky effect. By representing it using the transverse acceleration only, the inclination is not perturbed. In fact, a complete model of the thermal accelerations may admit an out-of-plane component, provided that the obliquities of the components of the pair are not extreme (e.g. Vokrouhlický 1998). However, to fully use such a model, we would need to sample a multiparametric space of possible spin orientations and physical parameters for Yarkovsky clones, an effort which is postponed to further studies.

An alternative dynamical mechanism, that has not been included in our simulations, consists of perturbations from the largest Trojans in the L₄ swarm. As an example, we consider the influence 624 Hektor, whose mass is estimated to be $\simeq 10^{17} \text{ kg}$ (e.g. Carry 2012), about 10^{-4} of the mass of dwarf-planet 1 Ceres. Nesvorný et al. (2002b) found that, statistically, the mean perturbation of the orbital inclination produced by Ceres in the inner and middle parts of the Main belt is $\simeq 1.5^\circ$ in 4 Gyr. Assuming the effect scales with the square root of the perturber mass, we estimate that the approximate effect of Hektor on small L₄ Trojans would be $\simeq 0.015^\circ$ over 4 Gyr, in a statistical sense. Therefore, at least a part of the inclination mismatch reported above could well be due to the ongoing scattering influence of the most massive Trojans.

4 FORMATION OF THE TROJAN PAIR

We now briefly discuss possible formation processes for the (258656) 2002 ES₇₆–2013 CC₄₁ pair. In principle, these mechanisms coincide with the suggestions outlined in Section 6 of Vokrouhlický & Nesvorný (2008). Building on that work, we will skip for now the possibility that these two Trojans are the two largest objects in a compact, collisionally born family. Given their comparable size, the collision required to form such a family must have been supercatastrophic, with many kilometre size fragments created and dominating the mass. Without information about them, it is hard to say anything more about the putative collision conditions, including the probability of such a collision actually having occurred.

4.1 Collisional dissociation of a synchronous binary

The first possible origin for the (258656) 2002 ES₇₆–2013 CC₄₁ pair consists of a model, in which the two objects were formerly components in a binary system which underwent some kind of instability. We assume that the instability was not of a dynamical origin. Indeed, even if formed by gravitational collapse, the initial angular momentum of the binary would exceed that of a critically rotating single body of an equivalent mass by a factor of $\simeq (3-10)$ (Nesvorný et al. 2019). This is not sufficient to drive tidal evolution, whilst conserving angular momentum, to the stability

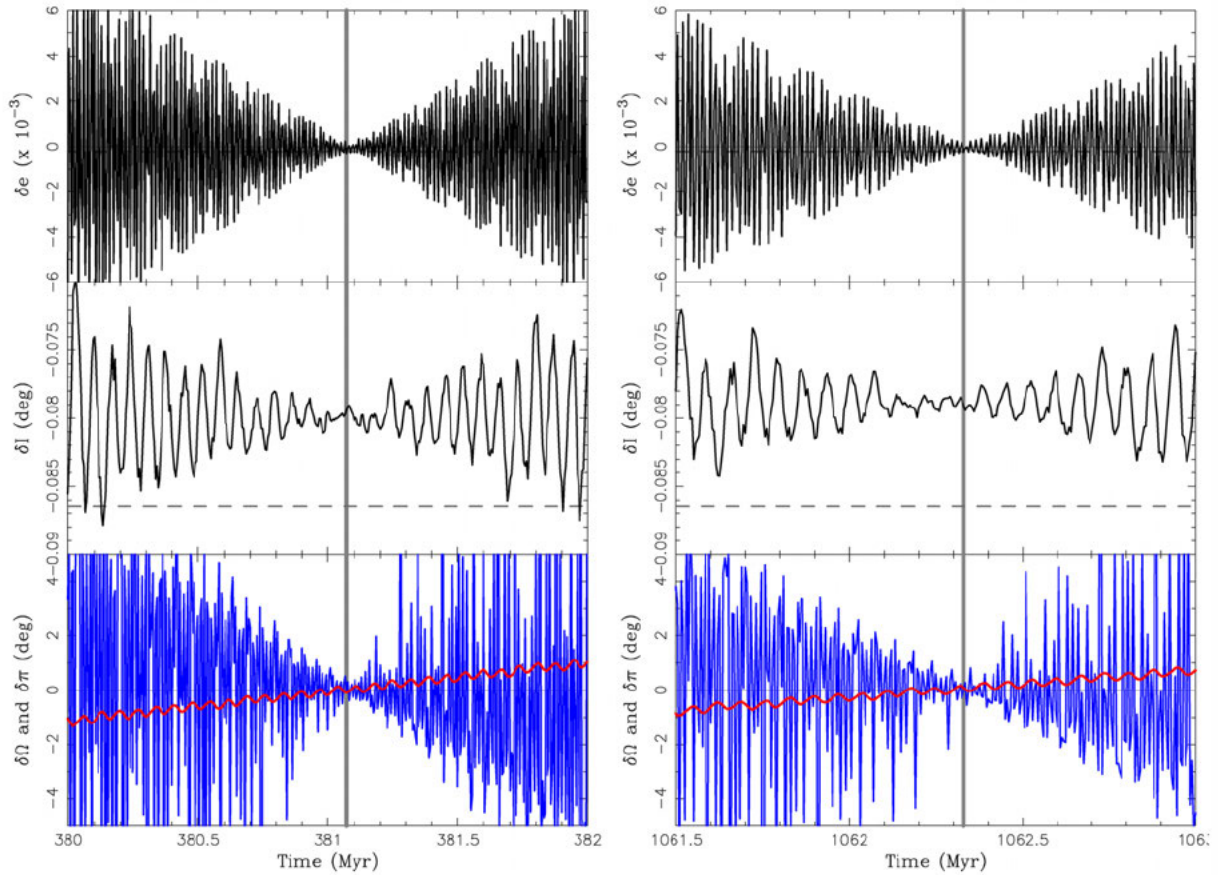


Figure 11. Two examples of converging solutions between Yarkovsky clones of (258656) 2002 ES₇₆ and 2013 CC₄₁: left-hand panels at ≈ 381.07 Mya, right-hand panels at ≈ 1062.33 Mya (grey vertical lines show the nominal convergence epochs). Each of the panels shows the differences between the osculating orbital elements of the clones: eccentricity (top), inclination (middle), and longitude of node (red) and perihelion (blue; bottom). The secular angles Ω and ϖ converge to better than 0.004° , corresponding to a negligible value of the target function $\delta V \leq 0.04 \text{ m s}^{-1}$ (see equation 3). Differences in e and I are relatively larger, namely $\delta e \approx 7.5 \times 10^{-5}$ and $\delta I \approx 0.079^\circ$ (left), resp. $\delta I \approx 0.078^\circ$ (right). The dashed horizontal lines show the differences between the respective proper elements of (258656) 2002 ES₇₆ and 2013 CC₄₁. Note the ordinate of the middle panel (inclination) which is offset from zero.

limit at about half of the Hill sphere, even in the Trojan zone. The limiting configuration would require angular momentum at least twice as large. Additionally, time constraints may prevent evolution to such large separations within ≤ 4.5 Gyr. Therefore, the nature of the parent binary instability must be different. We assume instead that this instability was triggered by a gentle-enough impact on one of the components. We leave aside other possibilities, such as binary instability produced during a close three-body encounter with a massive Trojan (Agnor & Hamilton 2006; Nesvorný & Vokrouhlický 2019), for future investigations, once the mechanisms are better understood in the Jovian Trojan population.

Let us start the likelihood analysis of the formation of the (258656) 2002 ES₇₆–2013 CC₄₁ pair via the subcritical impact dissociation of a previously existing synchronous binary with a very simple, order-of-magnitude estimate. Assume that the needed imparted velocity by the impact on to a ≈ 7 km size component in the binary is about 1 m s^{-1} . Then, using the simple formulation in Nesvorný et al. (2011), a projectile of ≈ 0.53 km size is required. The characteristic impact velocity assumed was $V_{\text{imp}} \approx 4.6 \text{ km s}^{-1}$ (Davis et al. 2002). The Trojan population contains very approximately $N \approx 400\,000$ such objects (e.g. Emery et al. 2015; Wong & Brown 2015; and Fig. 12).

Using the mean impact probability $p_i \approx 7 \times 10^{-18} \text{ km}^{-2} \text{ yr}^{-1}$ (e.g. Davis et al. 2002), we can therefore estimate the order-of-magnitude likelihood that such an event would occur within a timeframe of T

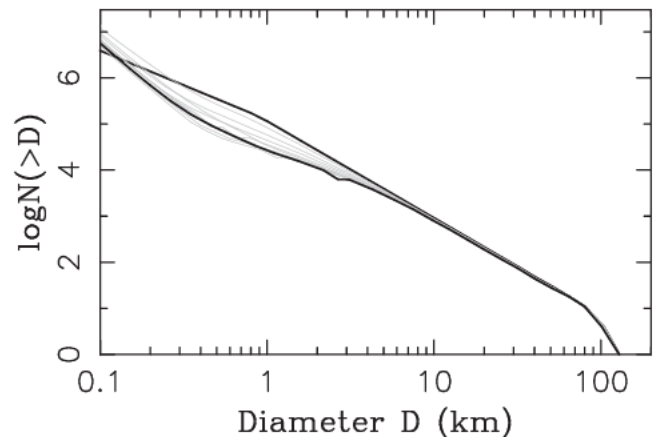


Figure 12. The effects of collisional grinding on the cumulative size distribution of Jovian Trojans. The upper bold line is the initial distribution. The lower bold line is the size distribution at $T = 4.5$ Gyr. The grey lines show the changing size distribution in 500 Myr intervals. The dip in the final distribution near $D = 0.5$ km is produced by the strength-to-gravity transition of the disruption law.

$\simeq 4.5$ Gyr, namely $p_i R^2 NT \simeq 0.15$ (here $R = 3.5$ km is the radius of the target body). This suggests that every such binary implanted to the Trojan population has a non-negligible (15 per cent) chance to be split via this process. Assuming that, initially, at least hundreds of binaries were captured intact to the Trojan population, a non-negligible number of Trojan pairs might have been created over the age of the Solar system. Obviously, in many cases, our ability to identify the pair produced in this manner is low, due to unsuitable locations in the Trojan orbital phase space. Nonetheless, this result suggest that sufficiently many such pairs could be produced that future study might well reveal several more.

We now substantiate this order-of-magnitude estimate using a more involved numerical simulation. As outlined above, the mutual orbit of a binary can be affected by small impacts on to its components. The binary may become unbound if the velocity change imparted by an impact exceeds binary’s orbital speed $\sim 0.2\text{--}2$ m s $^{-1}$ for bodies with $D \simeq 7$ km (Petit & Mousis 2004).

We investigate this process with the previously developed collisional code (Morbidelli et al. 2009; Nesvorný et al. 2011). The code, known as `Boulder`, employs a statistical method to track the collisional fragmentation of planetesimal populations. A full description of the `Boulder` code, tests, and various applications can be found in Morbidelli et al. (2009), Levison et al. (2009), and Bottke et al. (2010). The binary module in `Boulder` accounts for small, non-disruptive impacts on binary components, and computes the binary orbit change depending on the linear momentum of impactors (see Nesvorný et al. 2011; Nesvorný & Vokrouhlický 2019).

We account for impacts over the life of the Solar system, 4.5 Gyr. The captured population of Jovian Trojans is assumed to be similar to the present population, for objects with large diameters. There are $\simeq 25$ Trojans with $D > 100$ km. The population is assumed to follow a power-law profile below 100 km, with a cumulative index equal to -2.1 (Fig. 12). The intrinsic impact probability and impact velocity is the same as used for the order-of-magnitude estimate above. We adopt a standard disruption law for solid ice from Benz & Asphaug (1999). Fragments are generated according to the method described in Morbidelli et al. (2009). These rules are implemented in the `Boulder` code, which is then used to determine the collisional survival of Trojan binaries (e.g. Nesvorný et al. 2018).

Fig. 12 shows the evolution of the size distribution for the Jovian Trojans. The size distribution for $D > 10$ km remains unchanged over 4.5 Gyr, but below $D \simeq 5$ km the slope becomes shallower. This is consistent with Jovian Trojan observations that detect a shallower slope for $D \simeq 3$ km (e.g. Wong & Brown 2015). If this interpretation is correct, the slope should become steeper below approximately 500 m, for bodies that are too faint to be detected from the ground using the current generation of observatories. The dip in the size distribution is produced by the transition from strength-to-gravity dominated branches of the disruption law (e.g. Nesvorný et al. 2018).

We find that the survival chances of Trojan binaries are generally good, but drop significantly when the binary separation approaches $0.5 R_H$ (R_H being the Hill sphere of gravitational influence, see Fig. 13). This is expected because binaries with semimajor axis $a_B > 0.5 R_H$ are dynamically unstable (e.g. Porter & Grundy 2012). For a characteristic separation of $a_B/(R_1 + R_2) \simeq 10\text{--}100$, where a_B is the binary semimajor axis and R_1 and R_2 are the binary component radii, consistent with the pair (258656) 2002 ES $_{76}$ –2013 CC $_{41}$ ($R_1 + R_2 = 7.2$ km), which is quite common among equal-size binaries in the Edgeworth-Kuiper belt (e.g. Noll et al. 2020), the survival probability is 7–40 per cent. There is plenty of room in this parameter space for Trojan pair formation by this mechanism. Assuming that the

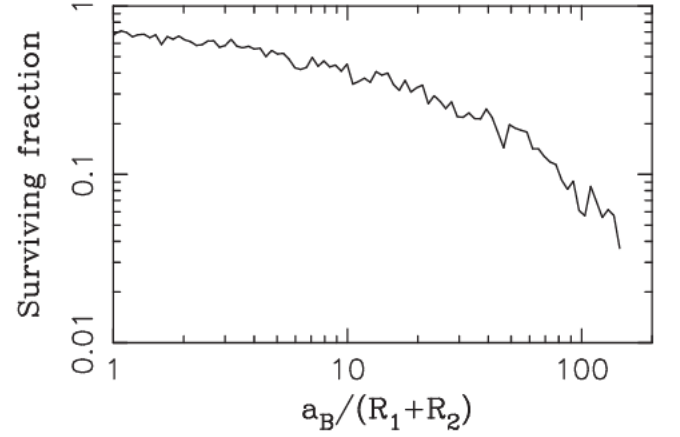


Figure 13. The survival probability of binaries with (258656) 2002 ES $_{76}$ –2013 CC $_{41}$ components as a function of separation, here normalized to the sum of physical radii, $R_1 + R_2$. The survival probability decreases with separation because wide binaries have smaller orbital speeds and are easier to dissolve by a small impact. For reference, the Hill radius R_H of a binary with (258656) 2002 ES $_{76}$ –2013 CC $_{41}$ components, corresponding to mass $\sim 5 \times 10^{17}$ g (for 1 g cm $^{-3}$ density), is $R_H \simeq 3,400$ km, or nearly $a_B/(R_1 + R_2) = 500$.

pair (258656) 2002 ES $_{76}$ –2013 CC $_{41}$ is an impact-dissolved binary, we find that there should be 0.08–0.7 surviving binaries for each pair such as (258656) 2002 ES $_{76}$ –2013 CC $_{41}$. Given that the vast majority of Trojan pairs remain undetected (see the difficulties briefly outlined in Appendix B), the obvious implication is that there should also be several equal-size binaries among Jovian Trojans in this size range.

4.2 Rotational fission of a parent object

An alternative formation mechanism that could explain the observed properties of the (258656) 2002 ES $_{76}$ –2013 CC $_{41}$ pair is that they might be the result of the rotational fission of their common parent object (this is indeed the favourite mechanism for asteroid pair formation in the main belt; e.g. Pravec et al. 2010). The most probable driving process for such a fission event is the Yarkovsky–O’Keefe–Radzievski–Paddack (YORP) effect, a radiative torque resulting from the combination of reflected and thermally emitted radiation by the surface (being thus a complementary phenomenon to the Yarkovsky effect; e.g. Bottke et al. 2006; Vokrouhlický et al. 2015). The YORP effect is able to constantly accelerate an asteroid’s rotation up to speeds that meet the requisite conditions to cause the object to fission. The rotation frequency change $\dot{\omega}$ satisfies general scaling properties, such that $\dot{\omega} \propto 1/[\rho (aD)^2]$, where ρ is the bulk density, a the orbital semimajor axis, and D the size. However, the problematic part of the YORP effect, unlike the Yarkovsky effect, is its large sensitivity to details of the surface roughness. For that reason it is troublesome to determine the exact value of the strength of the YORP effect for a given object, and we must satisfy ourselves with an order-of-magnitude estimate in our case.

If we were to determine the doubling time-scale $\tau_{\text{YORP}} = \omega/\dot{\omega}$ (sometimes also the YORP cycle time-scale; e.g. Rubincam 2000), it would be reasonable to use the YORP detection of the small near-Earth asteroid (101955) Bennu as a template, as we did above for the Yarkovsky effect in Section 3.3.2. (101955) Bennu has $\tau_{\text{YORP}} \simeq 1.5$ Myr (e.g. Hergenrother et al. 2019). Adopting plainly the scaling $\tau_{\text{YORP}} \propto \rho (aD)^2/P$ (with P being the rotation period), we obtain $\tau_{\text{YORP}} \simeq 11$ Gyr for a $D \simeq 9$ km Trojan, the estimated size of a putative

parent object of the (258656) 2002 ES₇₆–2013 CC₄₁ pair. Note that τ_{YORP} provides an estimate of a time-scale for doubling ω , as an example changing rotation period from 5 to 2.5 h, an approximate fission limit for a large internal strength Trojan model. Another $\tau_{\text{YORP}}/2 \simeq 5.5$ Gyr time would be needed if the initial rotation period of the parent object was 10 h. This shorter time-scale would also be an appropriate estimate to reach the fission limit at a longer period of $\simeq 5$ h when the internal strength and bulk densities are low (e.g. French et al. 2015; Szabó et al. 2017).

If, however, we were to consider the results from numerical simulations of the YORP effect for a large statistical sample of Gaussian-sphere shapes Čapek & Vokrouhlický (2004), which obtained $\tau_{\text{YORP}} \simeq 15$ Myr for a typical main belt S-type asteroid of a 2 km size, we would have $\tau_{\text{YORP}} \simeq 1.5$ Gyr for changing the parent object period from 5 to 2.5 h. Whilst these results are known to typically overestimate the strength of the YORP effect by a factor of 3–5, when compared to detections of the YORP effect for small near-Earth asteroids, we none the less get a time-scale shorter by a factor 2 to 3 than for the Benu case. The takeaway message is that the estimate of the YORP doubling time-scale prior the fission of the putative parent object of the (258656) 2002 ES₇₆ and 2013 CC₄₁ pair is very uncertain, with values ranging possibly from 2 Gyr to some 12 Gyr.

Taken at a face value, the smaller values in this interval are plausible as an explanation for the origin of the pair when compared to the lifetime of the Solar system. It may not be surprising to find that some $D \simeq 9$ km Jupiter Trojan objects undergo a rotational fission during their lifetime. However, a more detailed inspection of the (258656) 2002 ES₇₆ and 2013 CC₄₁ parameters speaks against this possibility. First, we note that the known rotation periods of Jovian Trojans rarely have values smaller than 8–10 h (e.g. French et al. 2015; Ryan, Sharkey & Woodward 2017; Szabó et al. 2017), which suggests in turn that more than one τ_{YORP} time-scale would be needed to reach fission from a typical initial rotation state (though, admittedly, these known data concern larger objects). More importantly, though, we note that the absolute magnitude difference of (258656) 2002 ES₇₆ and 2013 CC₄₁ is $\simeq (0.2-0.3)$, depending on the data base used. This implies that the two objects are nearly of the same size. Pravec et al. (2010) argued that the typical conditions of fission mechanics require at least 1 magnitude difference between the two components in pair. This is because some degree of size disparity is needed to make the two components separate on to distinct heliocentric orbits. Whilst exceptions have been found to this guideline (see e.g. Pravec et al. 2019), the majority of the known asteroid pairs, more than 90 per cent, satisfy this condition of having a large enough magnitude disparity. The components in the (258656) 2002 ES₇₆–2013 CC₄₁ pair violate this rule and would require special conditions for their separation to feasibly be the result of rotational fission.

5 CONCLUSIONS

In this work, we identified the first potential dynamical pair in the Jovian Trojan population. In particular, we analysed the distribution of Trojans in their proper orbital element space. Using information about the local density of objects, we also assessed the statistical significance of the proximity of potential couples. This procedure lead us to select a pair of bodies, (258656) 2002 ES₇₆ and 2013 CC₄₁, in the L4 swarm as a potential candidate pair. Interestingly, this suggested pair is located very close to the L4 Lagrange point, with low proper elements, semimajor axis (da_p), eccentricity e_p , and sine of inclination ($\sin I_p$) values. Finally, as part of our effort,

we developed an up-to-date, highly accurate set of proper elements for the all Jovian Trojans, which we have made publicly available (Appendix A).

In order to further investigate the selected pair, we ran a series of n -body simulations, which were used to look for past convergences in the osculating nodal ($\delta\varpi$) and perihelion longitude ($\delta\Omega$) value for the two objects, whilst ensuring that, at the time of such convergences the differences in the osculating eccentricity and inclination were also sufficiently small. Our simulations included both geometric clones, created from the uncertainties in the orbital elements of the bodies, and Yarkovsky clones, based on the estimated thermal accelerations that the two objects could experience, for a variety of realistic rotation rates. As a result, we obtained a statistical set of convergences, finding a larger pool of possibilities once the Yarkovsky clones were included. Our results reveal that the pair is at least $\simeq 360$ Myr old, but are compatible with the age being significantly older, potentially in the Gyr time-scale. By finding such possible convergences, we increase the confidence that the (258656) 2002 ES₇₆–2013 CC₄₁ couple is a legitimate pair.

We then considered the mechanisms by which the (258656) 2002 ES₇₆–2013 CC₄₁ pair could have formed (compared with Vokrouhlický & Nesvorný 2008). The pair is not associated with any known collisional family, and as such we do not favour the possibility of the pair having been formed as a result of a catastrophic impact on a putative parent body. The pair might have been formed through the rotational fission of their parent Trojan, since, for certain initial conditions, the time-scale for such an object to be spun-up by the YORP effect to the point that it undergoes fission could be somewhat shorter than the age of the Solar system. However, this pair consists of two nearly equal-sized components, whilst the vast majority of observed pairs formed by rotational fission have a size ratio of at least 1.5 (see Pravec et al. 2010, 2019). For that reason, we consider that the pair most likely formed as a result of the dissociation of an equal-size binary. We can confirm that such a scenario is indeed feasible using an estimation of the binary survival rate in the size range of the (258656) 2002 ES₇₆–2013 CC₄₁ pair, $D \simeq 7$ km, over 4.5 Gyr, after implantation to the Trojan population early in Solar system’s history. Statistically, this indicates that there should be many such pairs within the Trojan population in this 5–10 km size range. As the Rubin Observatory’s Legacy Survey of Space and Time (LSST) comes online, it is expected to discover many Jovian Trojans in this size range (e.g. Schwamb et al. 2018). As new Trojans are discovered, our results suggest that further pairs should be revealed.

The (258656) 2002 ES₇₆–2013 CC₄₁ pair provides an interesting clue to the past history of the Jovian Trojans, and the Solar system as a whole. So far, we know little beyond their dynamical properties and size estimations. In particular, light-curve analysis could assist in constraining the formation mechanism, as this would provide an estimate of the rotational periods of the two objects. Due to their small size, and dark albedo, the objects have relatively low apparent magnitudes, at best $\simeq 20.5$ magnitude in visible band. In order to further characterize these objects, observations using large Earth-based facilities, such as the SUBARU (Kashikawa et al. 2002) or Keck (Oke et al. 1995) telescopes, will be required. These objects would also benefit from future observations using the *James Web* (JWST; Rivkin et al. 2016) and *Nancy Grace Roman Space Telescopes* (RST, formerly known as *WFIRST*; Holler et al. 2018). Time on these telescopes is competitive, but we recommend proposals for observations of (258656) 2002 ES₇₆ and 2013 CC₄₁ be selected to further extend our understanding of this interesting pair of Trojans.

ACKNOWLEDGEMENTS

TRH was supported by the Australian Government Research Training Program Scholarship. The work of DV and MB was partially supported by the Czech Science Foundation (grant 18-06083S). This research has made use of NASA Astrophysics Data System Bibliographic Services. We thank Dr. Romina Di Sisto for their valuable review of this manuscript.

We dedicate this paper to the memory of Andrea Milani and Paolo Farinella, who were the first to propose the idea of a genetically connected pair of objects in the Jovian Trojan population (Milani 1993).

DATA AVAILABILITY

The data base of Jovian Trojan proper elements is accessible at https://sirrah.troja.mff.cuni.cz/~mira/mp/trojans_hildas/, and is available for community use. See Appendix A for details.

REFERENCES

- Agnor C. B., Hamilton D. P., 2006, *Nature*, 441, 192
- Beaugé C., Roig F., 2001, *Icarus*, 153, 391
- Benjoya P., Zappalà V., 2002, in Bottke W. F., Cellino A., Paolicchi P., Binzel R. P., eds, Asteroids III. University of Arizona Press, Tucson, p. 613
- Benz W., Asphaug E., 1999, *Icarus*, 142, 5
- Bottke W. F., Vokrouhlický D., Rubincam D. P., Nesvorný D., 2006, *Annu. Rev. Earth Planet. Sci.*, 34, 157
- Bottke W. F., Nesvorný D., Vokrouhlický D., Morbidelli A., 2010, *AJ*, 139, 994
- Brož M., Rožehnal J., 2011, *MNRAS*, 414, 565
- Buie M. W. et al., 2015, *AJ*, 149, 113
- Carry B., 2012, *Planet. Space Sci.*, 73, 98
- Chesley S. R. et al., 2014, *Icarus*, 235, 5
- Davis A. B., Scheeres D. J., 2020, *Icarus*, 341, 113439
- Davis D. R., Durda D. D., Marzari F., Campo Bagatin A., Gil-Hutton R., 2002, in Bottke W. F., Cellino A., Paolicchi P., Binzel R. P., eds, Asteroids III. University of Arizona Press, Tucson, p. 545
- Delbó M., Mueller M., Emery J. P., Rozitis B., Capria M. T., 2015, in Michel P., DeMeo F. E., Bottke W. F., eds, Asteroids IV. University of Arizona Press, Tucson, p. 107
- Di Sisto R. P., Ramos X. S., Beaugé C., 2014, *Icarus*, 243, 287
- Di Sisto R. P., Ramos X. S., Gallardo T., 2019, *Icarus*, 319, 828
- Emery J. P., Marzari F., Morbidelli A., French L. M., Grav T., 2015, in Michel P., DeMeo F. E., Bottke W. F., eds, Asteroids IV. University of Arizona Press, Tucson, p. 203
- Farnocchia D., Chesley S. R., Vokrouhlický D., Milani A., Spoto F., Bottke W. F., 2013, *Icarus*, 224, 1
- French L. M., Stephens R. D., Coley D., Wasserman L. H., Sieben J., 2015, *Icarus*, 254, 1
- Grav T. et al., 2011, *ApJ*, 742, 40
- Grav T., Mainzer A. K., Bauer J. M., Masiero J. R., Nugent C. R., 2012, *ApJ*, 759, 49
- Hellmich S., Mottola S., Hahn G., Kürt E., de Niem D., 2019, *A&A*, 630, A148
- Hergenrother C. W. et al., 2019, *Nat. Commun.*, 10, 1291
- Holler B. J., Milam S. N., Bauer J. M., Alcock C., Bannister M. T., Bjoraker G. L., 2018, *J. Astron. Telesc. Instrum. Syst.*, 4, 1
- Holt T. R. et al., 2020, *MNRAS*, 495, 4085
- Horner J., Müller T. G., Lykawka P. S., 2012, *MNRAS*, 423, 2587
- Kashikawa N. et al., 2002, *PASJ*, 54, 819
- Lagrange J.-L., 1772, Essai sur le Problème des Trois Corps, Prix de l'Académie Royale des Sciences de Paris printed in 1868, Œuvres de Lagrange, Tome VI. Gauthier-Villars, Paris, France, p. 229
- Laskar J., Robutel P., 2001, *Celest. Mech. Dyn. Astron.*, 80, 39
- Levison H. F., Duncan M. J., 1994, *Icarus*, 108, 18
- Levison H. F., Shoemaker E. M., Shoemaker C. S., 1997, *Nature*, 385, 42
- Levison H. F., Bottke W. F., Gounelle M., Morbidelli A., Nesvorný D., Tsiganis K., 2009, *Nature*, 460, 364
- Levison H. F., Olkin C. B., Noll K., Marchi S., Lucy Team, 2017, in Lunar Planet. Sci. Conf, p. 2025, <http://adsabs.harvard.edu/abs/2017LPI....48.2025L>
- Marchis F. et al., 2006, *Nature*, 439, 565
- Margot J.-L., Pravec P., Taylor P., Carry B., Jacobson S., 2015a, in Michel P., DeMeo F. E., Bottke W. F., eds, Asteroids IV. University of Arizona Press, Tucson, p. 355
- Margot J.-L., Pravec P., Taylor P., Carry B., Jacobson S., 2015b, in Michel P., DeMeo F. E., Bottke W. F., eds, Asteroids IV. University of Arizona Press, Tucson, p. 355
- Milani A., 1993, *Celest. Mech. Dyn. Astron.*, 57, 59
- Milani A., Gronchi G. F., 2010, Theory of Orbital Determination. Cambridge University Press, Cambridge
- Morbidelli A., Bottke W. F., Nesvorný D., Levison H. F., 2009, *Icarus*, 204, 558
- Moskovitz N. A. et al., 2019, *Icarus*, 333, 165
- Nesvorný D., 2018, *Annu. Rev. Astron. Astrophys.*, 56, 137
- Nesvorný D., Vokrouhlický D., 2006, *AJ*, 132, 1950
- Nesvorný D., Vokrouhlický D., 2019, *Icarus*, 331, 49
- Nesvorný D., Thomas F., Ferraz-Mello S., Morbidelli A., 2002a, *Celest. Mech. Dyn. Astron.*, 82, 323
- Nesvorný D., Morbidelli A., Vokrouhlický D., Bottke W. F., Brož M., 2002b, *Icarus*, 157, 155
- Nesvorný D., Vokrouhlický D., Bottke W. F., 2006, *Science*, 312, 1490
- Nesvorný D., Vokrouhlický D., Bottke W. F., Noll K., Levison H. F., 2011, *AJ*, 141, 159
- Nesvorný D., Brož M., Carruba V., 2015, in Michel P., DeMeo F. E., Bottke W. F., eds, Asteroids IV. University of Arizona Press, Tucson, p. 297
- Nesvorný D., Vokrouhlický D., Bottke W. F., Levison H. F., 2018, *Nat. Astron.*, 2, 878
- Nesvorný D., Li R., Youdin A. N., Simon J. B., Grundy W. M., 2019, *Nat. Astron.*, 3, 808
- Nesvorný D., Vokrouhlický D., Bottke W. F., Levison H. F., Grundy W. M., 2020, *ApJ*, 893, L16
- Noll K., Grundy W. M., Nesvorný D., Thirouin A., 2020, in Priainik D., Barucci M. A., Young L., eds, The Trans-Neptunian Solar System. University of Arizona Press, Tucson, p. 201
- Oke J. B. et al., 1995, *Publ. Astron. Soc. Pacific*, 107, 375
- Petit J. M., Mousis O., 2004, *Icarus*, 168, 409
- Porter S. B., Grundy W. M., 2012, *Icarus*, 220, 947
- Pravec P. et al., 2010, *Nature*, 466, 1085
- Pravec P. et al., 2019, *Icarus*, 333, 429
- Pravec P., Harris A. W., 2007, *Icarus*, 190, 250
- Pravec P., Vokrouhlický D., 2009, *Icarus*, 204, 580
- Quinn T. R., Tremaine S., Duncan M., 1991, *AJ*, 101, 2287
- Rivkin A. S., Marchis F., Stansberry J. A., Takir D., Thomas C., 2016, *Publ. Astron. Soc. Pacific*, 128, 018003
- Robutel P., Gabern F., 2006, *MNRAS*, 372, 1463
- Rožehnal J., Brož M., Nesvorný D., Durda D. D., Walsh K., Richardson D. C., Asphaug E., 2016, *MNRAS*, 462, 2319
- Rožek A., Breiter S., Jopek T. J., 2011, *MNRAS*, 412, 987
- Rubincam D. P., 2000, *Icarus*, 148, 2
- Ryan E. L., Sharkey B. N. L., Woodward C. E., 2017, *AJ*, 153, 116
- Schwamb M. E. et al., 2018, preprint ([arXiv:1802.01783](https://arxiv.org/abs/1802.01783))
- Szabó G. M. et al., 2017, *A&A*, 599, A44
- Tsiganis K., Varvoglis H., Dvorak R., 2005, *Celest. Mech. Dyn. Astron.*, 92, 71
- Vokrouhlický D. et al., 2017, *AJ*, 153, 270
- Vokrouhlický D., 1998, *A&A*, 335, 1093
- Vokrouhlický D., Nesvorný D., 2008, *AJ*, 136, 280
- Vokrouhlický D., Bottke W. F., Chesley S. R., Scheeres D. J., Statler T. S., 2015, in Michel P., DeMeo F. E., Bottke W. F., eds, Asteroids IV. University of Arizona Press, Tucson, p. 509
- Wang X., Hou X., 2017, *MNRAS*, 471, 243
- Wolf M., 1907, *Astron. Nachr.*, 174, 47

Wong I., Brown M. E., 2015, *AJ*, 150, 174

Čapek D., Vokrouhlický D., 2004, *Icarus*, 172, 526

Šidlichovský M., Nesvorný D., 1996, *Celest. Mech. Dyn. Astron.*, 65, 137

APPENDIX A: DETERMINATION OF THE JOVIAN TROJAN PROPER ELEMENTS

Here we briefly review our approach to compute synthetic proper elements for the currently known Jovian Trojan population. The method is based on Milani (1993), see also Brož & Rozehnal (2011), though we needed several modifications of the digital filters in order to stabilize determination of the proper elements for Trojans having very small libration amplitude. Our dynamical model included four giant planets, with barycentric corrections to compensate for the indirect perturbations for terrestrial planets. This arrangement suitably speeds up computations when dealing with the whole population of many thousands of Trojans. Nevertheless, we also checked validity of our results using a dynamical model including also the terrestrial planets in a full-fledged manner for a sub-sample of Trojans (notably the low- δV_p that is of interest here). No significant differences were observed. The initial planetary state vectors were taken from the JPL ephemerides and those of the Trojans from the *AstOrb* catalogue as of 2020 April 28, from which their population was also identified.

We used well-tested numerical package *swift* (e.g. Levison & Duncan 1994), specifically the MVS2 symplectic integrator (e.g. Laskar & Robutel 2001), that we adapted for our application in several ways. The most important was an implementation of digital filters, helping us to eliminate short-period and forced terms from osculating orbital elements, necessary for identification of the proper terms. Due to the absence of the direct perturbations from the terrestrial planets, we can allow a fixed integration time-step of 0.25 yr. The input sampling into the filtering routines was 1 yr. We used a sequence of the convolution (Kaiser-window) filters A A B (e.g. Quinn, Tremaine & Duncan 1991) with decimation factors 10 10 3, which were applied to the non-singular elements $z = k + ih = e \exp(i\varpi)$ and $\zeta = q + ip = \sin I \exp(i\Omega)$. The intermediate time window for this filtering procedure and output time-step was 300 yr. At this stage, the short-period terms with periods comparable to planetary orbital periods or the libration period were efficiently suppressed from the resulting mean values \bar{z} and $\bar{\zeta}$ of eccentricity and inclination variables. We then accumulated batches of 2048 values of \bar{z} and $\bar{\zeta}$, and applied Fourier transformation (in particular the FMFT method from Šidlichovský & Nesvorný 1996), on the output. After rejecting signal associated with forced planetary frequencies (such as g_5 , g_6 , or s_6 to recall the principal ones), we were left with the proper values e_p for the eccentricity and I_p for the inclination as the amplitude of the remaining dominant terms. Our simulation spanned the total of 30 Myr, and we computed proper elements in the $\simeq 600$ kyr window described above many times over intervals with 100 kyr shift in their origin. This way we had a series of many tens of proper element realizations, allowing to access their stability and compute their mean and variance. We also observed that the series of individual e_p and I_p still contained long-period signal (periods > 1 Myr), which in future studies may call for extension of integration windows. At this moment, we however, satisfied ourselves with our set-up. We also used the above outlined procedure for the semimajor axis a , but instead of applying FMFT on its mean values we simply computed its mean value \bar{a} over a 1 Myr interval. This helps us to determine semimajor axis value of the libration centre for a given Trojan orbit.

In order to obtain a reliable information about a stable libration amplitude we need to apply a different method that has been

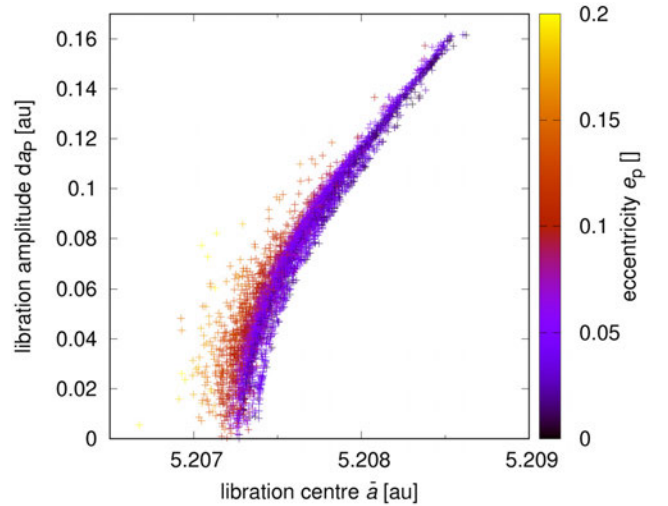


Figure A1. Libration amplitude da_p versus libration centre \bar{a} for Trojans in the L4 region. Colour corresponds to the proper eccentricity e_p . The dependence of $\bar{a}(da_p, e_p)$ is systematic, indicating a functional dependence.

implemented in our code in parallel to computation of e_p and I_p . This is because the corresponding libration frequency is fast, $f \simeq 2.434 \text{ deg yr}^{-1}$ and $360^\circ/f \simeq 148 \text{ yr}$, and must not be under-sampled. A delicate issue consists of the fact that, at the same time, one has to suppress terms with period even shorter than the libration period, namely those which are related to orbital periods of giant planets (principally Jupiter $\simeq 11.86 \text{ yr}$). We thus applied convolution filters B B, with decimation factors 3 3, to the osculating values of the semimajor axis a and the longitude difference $\lambda - \lambda'$ (the orbital elements labelled with prime correspond to Jupiter), a resonant argument of the Trojan tadpole motion. These intermediate (mean) values of a and $\lambda - \lambda'$ are computed with a 9 yr cadence. In the next step, the intermediate $a - a'$ were fitted by a straight line and the constant term a_0 was subtracted. In the same way, the intermediate angle $\phi = \lambda - \lambda' - \chi$, where $\chi = \pm 60^\circ$ depending on the L4 and L5 libration points, was fitted by a straight line and the constant term ϕ_0 was subtracted. Effectively, after subtractions of the mean values was done, the tadpole motion around the Lagrange point centres in these rescaled, zero-averages $a - a'$ versus ϕ coordinates is centred at the origin. Consequently, the polar angle ψ defined as (see e.g. Milani 1993, a and a' in au)

$$\psi = \arctan\left(\frac{a - a'}{0.2783 \phi}\right) \quad (\text{A1})$$

can be unfolded by 360° , fitted by a straight line, with the slope defining the libration frequency f . The libration amplitudes da_p (in au) and D (in deg) are computed by the Fourier transform as amplitudes of spectral terms with frequency f . This second step uses a 1 kyr cadence. Finally, we apply another averaging of da_p and D values, defined on a simple running window with the output time-step of 1 Myr. Both da_p and D may be considered as the third proper orbital element alongside of e_p and I_p .

We note that the value of libration centre \bar{a} is not universal for all Trojans. Instead, its value functionally depends on the proper elements (da_p, e_p, I_p) or (D, e_p, I_p), see Fig. A1. Some authors (e.g. Brož & Rozehnal 2011; Rozehnal et al. 2016) thus define an alternative set of proper elements ($a_p = \bar{a} + da_p, e_p, I_p$).

We determined the above-introduced parameters, including different variants of orbital proper values and their uncertainty, for 7328

Jovian Trojans, population as of 2020 April. These data can be found on https://sirrah.troja.mff.cuni.cz/~mira/mp/trojans_hildas/.

APPENDIX B: ARE THERE MORE LOW- δV_P COUPLES?

As also suggested by data in Fig. 6, the brief answer to the topic of this Appendix is probably positive, but a full analysis of this issue is left to the future work. Here we only restrict ourselves to illustrate difficulties one would quickly face in attempting to prove the past orbital convergence on a Gyr time-scales for most of the candidates.

Let us consider another low- δV_P candidate couple characterized by small values of proper orbital elements (da_P , e_P , $\sin I_P$), which helps to minimize the unrelated background Trojan population (Section 2). Staying near the L4 libration point, we find 219902 (2002 EG₁₃₄) and 432271 (2009 SH₇₆) at $\delta V_P \simeq 4.9 \text{ m s}^{-1}$ distance. This couple has also appreciably small probability $p \simeq 1.5 \times 10^{-6}$ to be a random fluke and it has been highlighted by a green circle in Fig. 6. The proper elements read $da_P \simeq (7.0372 \pm 0.0004) \times 10^{-3} \text{ au}$, $e_P \simeq (3.87534 \pm 0.00004) \times 10^{-2}$ and $\sin I_P \simeq (9.496 \pm 0.003) \times 10^{-2}$ for (219902) 2002 EG₁₃₄, and $da_P \simeq (7.2950 \pm 0.0006) \times 10^{-3} \text{ au}$, $e_P \simeq (3.87652 \pm 0.00004) \times 10^{-2}$ and $\sin I_P \simeq (9.469 \pm 0.002) \times 10^{-2}$ for (432271) 2009 SH₇₆ (for reference, we again mention their quite small libration amplitudes 1.44° , resp. 1.48°). This is a configuration reminiscent of the (258656) 2002 ES₇₆–2013 CC₄₁ case, though each of the three proper elements is slightly larger now. The relative velocity δV_P is again entirely dominated by the proper inclination difference, this time somewhat smaller than in the (258656) 2002 ES₇₆–2013 CC₄₁ case (only $\simeq 0.015^\circ$). Assuming geometric albedo value 0.075, we obtain sizes of $\simeq 12.8 \text{ km}$ and $\simeq (7.3\text{--}8.1) \text{ km}$ for (219902) 2002 EG₁₃₄ and (432271) 2009 SH₇₆, considering absolute magnitude values from the major three small-body ephemerides sites as above. While little larger, it still places this couple into the same category of very small Trojans as (258656) 2002 ES₇₆–2013 CC₄₁.

We repeated the convergence experiment using geometrical clones from Section 3.3.1. In particular we considered nominal (best-fitting) orbits of (219902) 2002 EG₁₃₄ and (432271) 2009 SH₇₆, and for each of them we constructed 20 geometrical clone variants of the initial data at MJD58800 epoch. We again used information from the AstDyS website and noted that both initial orbits of components in this possible couple have smaller uncertainties in all orbital elements than the orbits of (258656) 2002 ES₇₆ and 2013 CC₄₁. This is because their longer observation arcs and more data available for the orbit determination. We propagated these 42 (21+21) test bodies backwards in time to 1.5 Gyr before present. Perturbations from all planets were included and every 500 yr configuration of the nominal orbits and accompanied clones for the two bodies compared. A criterion for convergence included $\delta V \leq 2 \text{ m s}^{-1}$ from equation (3), and small eccentricity and inclination differences. In particular, we required $\delta e \leq 10^{-4}$ and $\delta I \leq 0.029^\circ$. These values are only slightly larger than the difference in the corresponding proper values and each represent a few metres per second contribution in (1).

Results are shown in Fig. B1 which has the same structure as the Fig. 9, previously given for the (258656) 2002 ES₇₆ and 2013 CC₄₁ couple. The main take-away message is in the bottom panel, which shows maximum nodal difference between clones of (219902) 2002 EG₁₃₄ and its nominal orbit as a function of time to the past. The slope of the initially linear trend (lasting approximately 50 Myr) is simply given by maximum δs proper frequency among clones from the initial data difference. The non-linearity, which develops at later

epochs, is due to orbital long-term chaoticity. While for the (258656)

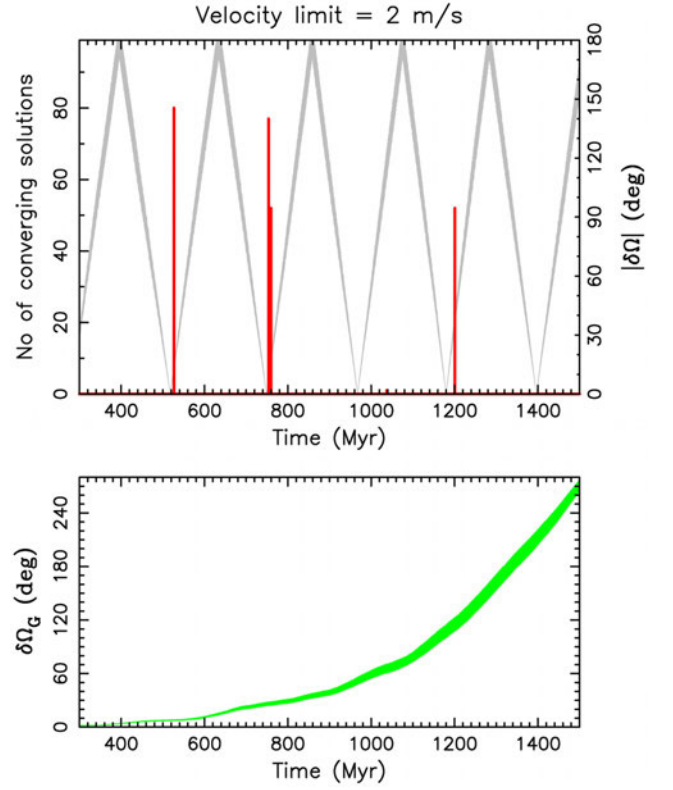


Figure B1. The same as Fig. 9 but for the (219902) 2002 EG₁₃₄–(432271) 2009 SH₇₆ couple of Trojans: past orbital histories of nominal orbits and 20 geometrical clones each compared every 500 yr and convergent solutions within $\delta V \leq 2 \text{ m s}^{-1}$ limit combined in 50 kyr bins. Top panel gives the number of solutions for all possible combinations of clones (red histogram). The grey line gives $|\delta\Omega|$ of the nominal orbit of (219902) 2002 EG₁₃₄ and (432271) 2009 SH₇₆ (see also the right ordinate). The green line at the bottom panel shows the maximum difference in longitude of ascending node between the clones of (219902) 2002 EG₁₃₄ and the longitude of ascending node of its nominal orbit, compared with the same information for (258656) 2002 ES₇₆ given in Fig. 9.

2002 ES₇₆ and 2013 CC₄₁ couple the chaotic effects were very minimum, the nodal difference between (258656) 2002 ES₇₆ clones and the nominal orbit increased to only $\simeq 4^\circ$ in 1.5 Gyr. At the end of our run the nodal difference expanded to $\simeq 260^\circ$. Given the very limited number of clones we had, this works again identification of convergent solutions. Note that beyond $\simeq 970 \text{ Myr}$, where we would expect more convergent cases, we could satisfy the convergence criteria of only few metres per second described above only rarely. CPU-demanding effort with many more clones would be needed to achieve the desired convergence limits.

We repeated the same experiment for several other candidate couples from the small- δV_P sample, including the case of (215110) 1997 NO₅–2011 PU₁₅ (see Fig. 2), but observed even faster onset of the clone diffusion in the Trojan orbital phase space. This was due to their large e_P and/or $\sin I_P$ values, as well as larger libration amplitudes. Their systematic analysis is beyond the scope of this paper.

This paper has been typeset from a \LaTeX file prepared by the author.

5

Paper 4 - Astrocladistics of the Jovian Trojan Swarms

This is the culmination of the PhD project. This paper was published April 2021 (Holt et al., 2021). In this paper I expand on the astrocladistical method to include wide-field surveys. This paper will form the basis of the astrocladistical methodology in the planetary science context.

5.1 ABSTRACT

The Jovian Trojans are two swarms of small objects that share Jupiter's orbit, clustered around the leading and trailing Lagrange points, L_4 and L_5 . In this work, we investigate the Jovian Trojan population using the technique of astrocladistics, an adaptation of the 'tree of life' approach used in biology. We combine colour data from *WISE*, *SDSS*, *Gaia* DR2 and *MOVIS* surveys with knowledge of the physical and orbital characteristics of the Trojans, to generate a classification tree composed of clans with distinctive characteristics. We identify 48 clans, indicating groups of objects that possibly share a common origin. Amongst these are several that contain members of the known collisional families, though our work identifies subtleties

in that classification that bear future investigation. Our clans are often broken into subclans, and most can be grouped into 10 superclans, reflecting the hierarchical nature of the population. Outcomes from this project include the identification of several high priority objects for additional observations and as well as providing context for the objects to be visited by the forthcoming *Lucy* mission. Our results demonstrate the ability of astrocladistics to classify multiple large and heterogeneous composite survey datasets into groupings useful for studies of the origins and evolution of our Solar system.

5.2 ASSOCIATED PRESENTATIONS AND PUBLICATIONS

There is a GitHub associated with this paper: <https://github.com/TimHoltastro/holt-etal-2021-Jovian-Trojan-astrocladistics>. The University of Southern Queensland also created a press release associated with the paper: [University of Southern Queensland researcher swaps dinosaur bones for fossils of the Solar system]

5.2.1 AUG. 2018: IAU XXX - FOCUS MEETING 1 - A CENTURY OF ASTEROID FAMILIES - ORAL PRESENTATION

Cladistics as a tool in Asteroid Taxonomy: The Jovian Trojan Asteroids.

Holt, Timothy. R., Horner, Jonathan., Nesvorny, David., Carter, Brad., Tylor, Christopher. and Brookshaw, Leigh

Abstract

Cladistics is traditionally used in the biological sciences to examine the relationships between organisms, commonly referred to as the ‘tree of life’. Recent works in galactic taxonomy, stellar phylogenetics and satellite classification have expanded the technique into astronomy, collectively called astrocladistics. The advantage of this method over other analytical techniques is the inclusion of objects with limited information. A full data-set can then be used without truncation. Our aim is to present how cladistics may be used to study asteroid taxonomy. We start by using the Jovian Trojan asteroids as an example population. The Jovian Trojan asteroids are two swarms of captured asteroids, located at the L₄ and L₅ Lagrange points of Jupiter. The Jovian Trojans provide a test case, as several have well known characteristics, while the majority have limited information available, with the complete population of computationally manageable size. The cladistical method involves the use of algorithms to link possibly related objects in a parsimonious fashion. The results are presented as a dendritic tree, where related objects are closer to one another. Using the cladistical method, we classify the Jovian Trojan swarms, using the inherent characteristics of the asteroids. The resulting

taxonomic system can then be compared with existing classifications and identified dynamical families. We present preliminary results from this study, with an indication of how the cladistical technique could be expanded to larger data-sets, and used in the of future asteroid taxonomy.

Publication: International Astronomy Union General Assembly XXX, Focus Meeting 1 - A Century of Asteroid Families. Vienna, Austria.

Pub Date: September 2018

5.2.2 SEPT. 2019: EPSC-DPS JOINT MEETING - ORAL PRESENTATION

The use of Multiple large-scale Surveys in Astrocladistics: The Jovian Trojans

Holt, Timothy; Horner, Jonathan; Nesvorny, David; King, Rachael; Carter, Brad; Tylor, Christopher

Abstract

Cladistics is traditionally used to study the relationships between living things. We expand the use of the technique in the planetary sciences, specifically the Jovian Trojans, adding to the field of astrocladistics. By incorporating data from three surveys, WISE, SDSS and GAIA, we can improve our understanding of these objects. This work establishes a framework for the technique that could be used in the next generation of surveys, including LSST.

Publication: EPSC-DPS Joint Meeting 2019, held 15-20 September 2019 in Geneva, Switzerland, id. EPSC-DPS2019-289

Pub Date: September 2019

5.2.3 OCT. 2020: DPS 52 - ORAL PRESENTATION

Holt, T. R.; Horner, J.; Nesvorny, D.; King, R.; Carter, B. D.; Tylor, C. C.

Abstract

A recently developed technique, ‘astrocladistics’, has been used to analyze a variety of astronomical objects, from galaxies to the satellite systems of the giant planets. The method was originally developed in a biological context, the ‘Tree of Life’, and adapted for use in astronomy. In this work, we use the novel astrocladistical method to examine the relationships between objects in the Jovian Trojan population - two swarms of small Solar system bodies that librate around the L₄ and L₅ Lagrange points of Jupiter. These objects are of particular interest for researchers as it is thought they were captured to their current location early in the Solar system’s history. Given the importance of such studies, six Trojans are due to be visited by the *Lucy* spacecraft, launching in 2021. For each Trojan in our astrocladistical analysis, a

set of binned characteristics are used, including dynamical properties, albedo, density, along with color ratios from SDSS, WISE, Gaia DR2, and the MOVIS surveys. Not all Trojans are present in each survey, and these differences in available data are accounted for in the algorithm. This highlights one of the advantages of astrocladistics, namely its ability to work with incomplete datasets and return meaningful results. We limit the selection for this study to those Jovian Trojans that have color measurements from at least one survey, including each of the *Lucy* targets. The results are dendritic trees, which allow us to visualize the relationships between the Jovian Trojans. One of the outcomes of this project is the ability to identify additional, high priority targets for observation. By clustering the population into clans, several mid-sized objects are identified that could provide valuable additional information from follow-up observations. An additional outcome from the analysis is that we are able to make preliminary characterization of objects, even where information is limited. We demonstrate this with some remarks on a recently identified Trojan pair, the first such relationship to be identified in the population. These outcomes highlight two of the potential ways that astrocladistics can be used in a planetary science context. Publication: AAS Division of Planetary Science meeting 52, id. 401.06D. Bulletin of the American Astronomical Society, Vol. 52, No. 6 e-id 2020n6i4o1p06D
Pub Date: October 2020

5.2.4 JAN. 2021: COSPAR - ORAL PRESENTATION

Using astrocladistics in Small Body research: The Jovian Trojans

Holt, T. R.; Horner, J.; Nesvorný, D.; King, R.; Carter, B. D

Abstract

Astrocladistics is a recently developed technique that has been used to analyse a variety of astronomical objects, from Galaxies to the satellite systems of the Giant Planets. The method borrows from biology, the ‘Tree of Life’, to examine the relationships between various astronomical objects. In this work, we apply the novel astrocladistical method to the Jovian Trojan population. The Jovian Trojans are two swarms of small Solar system bodies that are located at the Lagrange points of Jupiter. These objects represent a test case for astrocladistics, as they include several collisional families, as well as a history dating back to the early Solar system. The population is also due to be visited by the *Lucy* spacecraft, launching in 2021. The astrocladistical method begins with the creation of a 2d matrix. For each object, in this case, the Jovian Trojans, a set of binned characteristics are used. We used the proper orbital and libration dynamical characteristics, albedo, density, and color ratios where available. The colour

ratios are sourced from multiple datasets, including the SDSS, WISE, GIA DR2, and MOVIS surveys. Not all Trojans are present in each survey and these are accounted for in the algorithm, highlighting one of the advantages of astrocladistics, its use in incomplete datasets. We do limit the selection for this study to those Jovian Trojans that have colours in at least one survey, creating two matrices, one for each of the L₄ and L₅ swarms. The result are dendritic trees, visualising the relationships between the Jovian Trojans. Here we present the results of astrocladistical analysis performed on the two Jovian Trojan swarms. Each swarm can be split into many clans, and several superclans. Some of these clans correlate with previously identified collisional families, and the limited number of taxonomic classes identified in the swarms. In analysing the Jovian Trojan swarms, we highlight the advantages of astrocladistics, further validating its applicability to the Planetary sciences. The example of the Jovian Trojans provides a basis for the use of astrocladistics in future analysis of larger populations of small Solar system bodies.

Publication: 43rd COSPAR Scientific Assembly, id. B1.1-0041-21

Pub Date: January 2021



Astrocladistics of the Jovian Trojan Swarms

Timothy R. Holt^{1,2*}, Jonathan Horner,¹ David Nesvorný,² Rachel King,¹ Marcel Popescu^{1,3},
Brad D. Carter¹ and Christopher C. E. Tylor¹

¹Centre for Astrophysics, University of Southern Queensland, Toowoomba, QLD, 4350, Australia

²Department of Space Studies, Southwest Research Institute, Boulder, 80302 CO, USA

³Astronomical Institute of the Romanian Academy, Bucharest, 052034, Romania

Accepted 2021 March 17. Received 2021 March 16; in original form 2020 November 9

ABSTRACT

The Jovian Trojans are two swarms of small objects that share Jupiter’s orbit, clustered around the leading and trailing Lagrange points, L_4 and L_5 . In this work, we investigate the Jovian Trojan population using the technique of astrocladistics, an adaptation of the ‘tree of life’ approach used in biology. We combine colour data from *WISE*, *SDSS*, *Gaia* DR2, and *MOVIS* surveys with knowledge of the physical and orbital characteristics of the Trojans, to generate a classification tree composed of clans with distinctive characteristics. We identify 48 clans, indicating groups of objects that possibly share a common origin. Amongst these are several that contain members of the known collisional families, though our work identifies subtleties in that classification that bear future investigation. Our clans are often broken into subclans, and most can be grouped into 10 superclans, reflecting the hierarchical nature of the population. Outcomes from this project include the identification of several high priority objects for additional observations and as well as providing context for the objects to be visited by the forthcoming *Lucy* mission. Our results demonstrate the ability of astrocladistics to classify multiple large and heterogeneous composite survey data sets into groupings useful for studies of the origins and evolution of our Solar system.

Key words: methods: data analysis – astronomical data bases: miscellaneous – surveys – minor planets, asteroids: general.

1 INTRODUCTION

At the Jovian Lagrange points, 60° ahead (L_4) and behind (L_5) the giant planet in its orbit, there are two swarms of small Solar system objects, collectively termed the Jovian Trojans. Members of the leading swarm, which librate around Jupiter’s L_4 Lagrange point, are named after the Greek heroes in the *Iliad* (Nicholson 1961), with members of the trailing swarm being named for the Trojan heroes. The first Jovian Trojans, 588 Achilles (1906 TG), 617 Patroclus (1906 VY), 624 Hektor (1907 XM), and 659 Nestor (1908 CS) were discovered in the early 20th century (Heinrich 1907; Wolf 1907; Strömngren 1908; Ebell 1909). In the decades that followed, the number of known Trojans grew slowly, as a result of ongoing work at the Heidelberg observatory (e.g. Nicholson 1961; Slyusarev & Belskaya 2014). With the advent of CCD imaging, in the later part of the 20th century, the rate at which Trojans were discovered increased markedly, such that, by the end of the century, a total of 257 had been confirmed (Jewitt, Trujillo & Luu 2000).

Over the last twenty years, the rate at which Jovian Trojans have been discovered has increased still further, as a result of new instrumentation and automated surveys coming online to scour the skies. As a result, more than 8700 Jovian Trojans have been discovered to date.¹ We show the current distribution of objects

around the Jovian Lagrange points in Fig. 1. Whilst objects can still be temporarily captured to orbits within the Trojan clouds, without the destabilization of the clouds caused by planetary migration, such captures are very short-lived (e.g. 2019 LD₂; Steckloff et al. 2020; Bolin et al. 2021; Hsieh et al. 2021). At any time, it is likely that there are a number of such ‘temporary Trojans’, whose residence in the swarms can be measured in years, decades, or centuries at most (e.g. Horner & Wyn Evans 2006).

It is now well established that the Jovian Trojans did not form in their current orbits (see Emery et al. 2015, for review). Instead, they are thought to have been captured as a byproduct of the migration of Jupiter. Such capture would require some mechanism by which the Trojans could become trapped in such dynamically stable orbits.

One leading theory to explain the capture of the Jovian Trojans is the proposed period of instability in the early Solar system (Nesvorný, Vokrouhlický & Morbidelli 2013) that has come to be known as the ‘Nice’ model (Tsiganis et al. 2005b; Morbidelli 2010; Levison et al. 2011; Nesvorný & Morbidelli 2012; Nesvorný 2018). The Nice model invokes a period of instability triggered by the slow migration of Jupiter and Saturn, in response to their interactions with the debris left behind from planet formation. Eventually, that migration drove the two planets into an unstable architecture, leading to a period of chaotic evolution for objects throughout the Solar system. During that period of instability, the Jovian Trojan clouds would also have been destabilized. As a result, some of the debris being flung around the system by the migrating giant planets would have experienced temporary capture to the Jovian Trojan clouds. As

* E-mail: timothy.holt@usq.edu.au

¹Taken from the NASA-JPL HORIZONS Solar system Dynamics Data base <https://ssd.jpl.nasa.gov/> (Giorgini et al. 1996) taken 2020 October 13

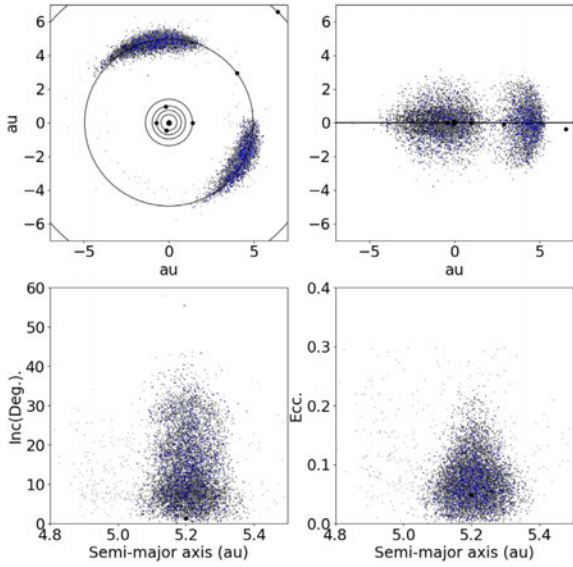


Figure 1. Distribution of the Jovian Trojans after Horner et al. (2020). The upper panels show the positions of the Trojans relative to the planets on 2000 January 1, 00:00 in XY (left-hand panel) and XZ (right-hand panel) planes. The lower panels show the Trojans in semimajor axis versus inclination space (left-hand panel) and semimajor axis versus eccentricity space (right-hand panel). All data from NASA HORIZONS (Giorgini et al. 1996), access on 2020 October 13. The black points are initially stable objects, from the *ASTDyS* (Knežević & Milani 2017) data set. The grey points are potentially transient objects. The blue points identify those objects used in this work.

Jupiter and Saturn migrated away from the location of the instability, the Jovian Trojan clouds would have become stable once again, freezing in place those temporarily captured Trojans, making their capture permanent (Roig & Nesvorný 2015). More recently, it has been suggested that the required instability in the outer Solar system may have been triggered by the ejection of a fifth giant planet (Nesvorný & Morbidelli 2012; Deienno et al. 2017) from the Solar system. This scenario has become known as the Jumping-Jupiter model, and has been invoked to explain a number of peculiarities in the distribution of Solar system small bodies, including the origin of the Jovian Trojans.

A recent alternative to the scenarios painted above proposes instead that the Trojans were captured from the same region of the Solar system’s protoplanetary disc as Jupiter, and were both captured and transported during the planet’s proposed inward migration (Pirani et al. 2019a). A recent update to this *in-situ* transport model (Pirani, Johansen & Mustill 2019b) explains the observed excitation in the orbital inclinations of the Jovian Trojans, which is a natural byproduct of the chaotic evolution proposed in the Nice and Jumping-Jupiter models, by invoking mixing in the Jovian feeding region. Therefore, the observed inclinations are considered to be primordial in these simulations, and are preserved during transportation as Jupiter migrates. In contrast to the idea that the captured Trojans formed on inclined orbits, earlier studies of smooth, non-chaotic migration (e.g. Lykawka & Horner 2010) showed that Jupiter could capture a significant population of Trojans. The common feature of all of the proposed capture models, however, is that the capture of the Jovian Trojans occurred during the Solar system’s youth (Emery et al. 2015). These two competing theories for the origins of the Trojans highlight the importance of the population in our understanding of the early Solar system.

1.1 Taxonomy and wide field surveys

The methods by which the Solar system’s small bodies are classified can be broken down into two broad categories. First, the objects are grouped based on their orbital parameters, in combination with any evidence of cometary activity, into broad dynamical clusters (Near-Earth Asteroid; Main Belt Asteroid; Centaur etc. see Horner et al. 2020, for review). Those objects can then be further classified based on their visual and infrared spectra. This classification is useful as the resulting taxonomy can indicate that certain objects share a common origin.

Building on an original taxonomy by Tholen (1984, 1989), the modern iteration of this observationally motivated categorization is based on the works of Bus (2002) and DeMeo et al. (2009, 2015), and is collectively termed the Bus–DeMeo taxonomy (see DeMeo et al. 2015, for summary). In this taxonomy, spectra are used to place objects into categories known as ‘types’. Each type reflects a major compositional category, for example, the C-types are the most numerous and correspond to Carbonaceous chondrite meteorites. Since the Bus–DeMeo taxonomy requires spectral information in order to classify asteroids, its use is naturally limited to those objects bright enough for such data to have been obtained – either through wide-field surveys, or targeted observations. As a result, to date less than 1 per cent of the Trojan population have been officially classified under this scheme. In the initial Tholen (1984, 1989) data set, 22 Trojans were classified, with a further 12 in the small Solar system Object Spectral Survey (*S³OS³*) (Lazzaro et al. 2004). In these initial surveys, D-types (85.29 per cent) were found to dominate the population. This is consistent with the dynamical modelling, as the D-types are thought to have formed in the outer Solar system (Morbidelli et al. 2005; Levison et al. 2009) and those found in the Main belt are interlopers (DeMeo et al. 2014).

Two large members of the Trojan population, 617 Patroclus (1906 VY) and 588 Achilles (1906 TG), were initially classified as P-type objects, though in recent years, that category (P-type) has been degenerated into the X-types (Bus 2002; DeMeo et al. 2009). For this work, we substitute any members of the ‘P-type’ from their original works into the X-types, including the hybrid ‘DP-type’ (now DX-type) and ‘PD-type’ (now XD-type). Amongst the small number of Trojans classified in those initial studies, the population was found to include another X-type, 3451 Mentor (1984 HA₁), and an Xc-type, 659 Nestor (1908 CS), as well as two C-types, namely 4060 Deipylus (1987 YT₁) and 1208 Troilus (1931 YA).

Following these initial spectral surveys, Bendjoya et al. (2004) investigated 34 Trojans spectrally between 0.5 and 0.9 μm , finding again that the majority were D-type (70.6 per cent), with several X-types (11.7 per cent) and C-types (5.8 per cent). There were two objects, 7641 (1986 TT₆) and 5283 Pyrrhus (1989 BW), that showed a negative slope and were not classified, although 7641 (1986 TT₆) was later classified as D-type by Hasselmann, Carvano & Lazzaro (2012), based on new observations. In a larger set of visual spectral surveys, Fornasier et al. (2004, 2007) examined a further 80 Jovian Trojans, and added their classifications. Though these classifications comprise a total of just 2.14 per cent of the Trojan population, they can still provide indications of the compositional distribution of the population as a whole.

In recent years, a number of studies have begun to gather data on the colour and physical properties of the Trojans. Wide-band surveys can give indications of taxonomic classification, circumventing the need for full spectra to be obtained of object. Several studies have investigated the colours of the Jovian Trojans (e.g. Emery & Brown 2003; Dotto et al. 2006). Once again, the initial observations were

limited in number, yielding data for less than 100 objects in the Jovian swarm in the infrared (Emery & Brown 2003; Emery, Cruikshank & Van Cleve 2006; Emery, Burr & Cruikshank 2011), visual (Fornasier et al. 2004; Dotto et al. 2006; Fornasier et al. 2007), and broad-band *UBVRI* (Karlsson, Lagerkvist & Davidsson 2009). As in the prior studies, these initial surveys found that the majority of objects studied were best classified as D-types.

With the current generation of large ground-based facilities and space telescopes, recent years have seen a significant increase in the numbers of Trojans being observed and given preliminary classifications. Grav et al. (2012) observed 557 Trojans at infrared wavelengths, using two *Wide-field Infrared Survey Explorer (WISE)* filters. In doing so, they confirmed the prevalence of D-types in the Trojan population, with such objects dominating both the L_4 and L_5 swarms, independent of the size of the Trojans studied (Grav et al. 2011). Grav et al. (2011, 2012) noted that the population in the *WISE* data set was quite heterogeneous, with a mean albedo of 0.07 ± 0.03 . In the visual five-band Sloan Digital Sky Survey (SDSS) catalogue (Carvano et al. 2010; Hasselmann et al. 2012), a total of 461 Trojans have been classified. Unlike previous surveys, the catalogue includes a measure of the confidence in the assigned taxonomy. Of the 461 objects in the SDSS data set, only 106 have significantly high confidence value, greater than 50, to be considered valid classifications. In using this data set to make inferences about asteroid taxonomy as across the Solar system, DeMeo & Carry (2013, 2014) noted that again, the Jovian Trojans are heterogeneous in comparison to other populations.

In summary, taking data from each of these data sets (Tholen 1989; Bendjoya et al. 2004; Fornasier et al. 2004, 2007; Lazzaro et al. 2004), including those Trojans classified in the SDSS catalogue with a confidence score of greater than 50 (Hasselmann et al. 2012), there is a canonical set of 214 Trojans that are classified under the Bus–DeMeo taxonomy.² As other authors have noted (Grav et al. 2012; Hasselmann et al. 2012; DeMeo & Carry 2013; Emery et al. 2015), 72.2 per cent are classified as D-type, which is a much higher fraction than is seen in the Main Belt (DeMeo & Carry 2013; DeMeo et al. 2014; DeMeo et al. 2015) and in the Hilda (Wong & Brown 2017) populations. The remainder of the Trojans classified to date in the canonical set are split between the C-types (10.8 per cent) and X-types (16.5 per cent).

The current generation of surveys are laying the groundwork for our future exploration of the Trojan population. A NASA discovery class mission, *Lucy*, is set to visit six Jovian Trojans between 2025 and 2033. One of the justifications for this mission is the diversity of taxonomic classes found in the population (Levison et al. 2017), with the mission visiting two C-types, two D-types and two X-types. The mission will also visit 3548 Eurybates (1973 SO), a C-type and the parent body of a collisional family. In combination with the *Lucy* mission, in the coming decades, several relevant observational surveys coming online including the Vera Rubin Observatory, with the Legacy Survey of Space and Time (Rubin Obs. LSST; LSST Science Collaboration 2009), the *James Web Space telescope (JWST)*; Rivkin et al. 2016), *Twinkle* (Savini et al. 2018), and *Nancy Grace Roman Space Telescope (RST)*, formally *WFIRST*; Milam et al. 2016). We explore these in further depth, with a specific focus on how they relate to the Jovian Trojans and our work, in Section 6.

²The taxonomy is included in the online data sets, available from the Github repository for this study <https://github.com/TimHoltastro/holt-et-al-2021-Jovian-Trojan-astrocladistics.git>

1.2 Clustering methods

Contemporary studies of the Jovian Trojans have attempted to identify groups of objects within the population that share common dynamical properties. The most effective of these models to date has been the Hierarchical Clustering Method (HCM; Zappala et al. 1990). Several collisional families have already been identified in the Trojan population using this method, despite the number of known Trojans being some two orders of magnitude smaller than the known population of the main belt (e.g. Milani 1993; Beauge & Roig 2001; Nesvorný, Brož & Carruba 2015). Another family identification method uses the size-dependent drift pattern due to the Yarkovsky effect (Bottke et al. 2006) to identify ancestral dynamic families in main-belt Asteroids (Walsh et al. 2013; Bolin et al. 2017, 2018; Deienno, Walsh & Delbo 2020). The technique, while useful in the Main belt, has reduced usefulness in the Trojans. This is due to the dependence of the Yarkovsky effect on the Solar flux. At the 5.2 au mean semimajor axis of the Jovian Trojans, the mean Yarkovsky effect is minimal, particularly for Trojans over 1 km in diameter (Wang & Hou 2017; Hellmich et al. 2019).

The HCM is a technique that uses Gauss' equations to find groups in proper element (semimajor axis, eccentricity, and inclination) parameter space (Zappala et al. 1990). The rationale behind these calculations is that the dispersal velocities of the clusters created by the collisional disruption of an object would be similar to the escape velocities of the parent body. The unique dynamical situation of the Jovian Trojans makes the identification of dynamical families using the traditional HCM difficult. Despite this, several collisional families are thought to be present amongst the Trojan population (e.g. Nesvorný et al. 2015). More modern dynamical analysis of the Jovian Trojans has identified a total of six canonical families (Brož & Rozehnal 2011; Emery et al. 2015; Nesvorný et al. 2015; Vinogradova 2015; Rozehnal et al. 2016). The individual members and numbers in each work are inconsistent, and for this work we follow the canonical six families found in Nesvorný et al. (2015), with their associated members. There are two other modern sets that could be considered, Rozehnal et al. (2016) or Vinogradova & Chernetenko (2015). Vinogradova & Chernetenko (2015) found families in the L_4 swarm using HCM with independently derived proper elements, though questioned the existence of any families in the L_5 swarm. Rozehnal et al. (2016) is incorporated into the canonical set Nesvorný et al. (2015), with several exceptions in the population. In our discussion, we note where these differ from the canonical set (Nesvorný et al. 2015). Initial imaging surveys suggested that there is some spectral conformity within these dynamical families in the Jovian Trojans (Fornasier et al. 2007). More recent observational data has brought this into question (Roig, Ribeiro & Gil-Hutton 2008), with a heterogeneity being seen in the colours of the identified family members.

The disadvantage of the HCM system is that it only identifies recent family breakups, with the vast majority of objects considered 'background'. Another issue with HCM is the issue of 'chaining', where families are identified with interlopers included due to near proximity in phase space. In an attempt to overcome some of these issues Rozehnal et al. (2016) offer an expansion to the HCM developed by Zappala et al. (1990). This new 'randombox' method uses Monte Carlo simulations to gain statistics on the probability that the identified clusters are random in parameter space. Carruba & Michtchenko (2007) also tried using elements in the proper frequency domain instead of orbital element space to overcome some of the issues of the HCM. The inclusion of 'background objects' can be further mitigated by the inclusion of colours (Parker et al.

2008), albedo (Carruba et al. 2013), and taxonomy into the family identification pipeline (Milani et al. 2014; Radović et al. 2017), though these methodologies have focused on the Main-belt families.

Though these methods do improve some of the faults identified in HCM, they still suffer from the issues inherent to the method. In order to use the HCM, a complete parameter space is required. This restricts the data set in one of two ways, due to the limited information available for most small Solar system bodies. For the majority of family identification work, (for review, see Nesvorný et al. 2015), only the dynamical elements are used. In order to expand the technique to include photometric information, albedo and colours, the number of objects needs to be restricted. For example, Carruba et al. (2013) used a subset of only 11 609 main belt asteroids, out of the approximately 60 000 available in the Sloan Digital Sky survey (SDSS) (Ivezić et al. 2002), 100 000 from *WISE* (Masiero et al. 2011), and over 400 000 for which proper elements were available at the time. In the main-belt, Milani et al. (2014) similarly attempted to combine together the AstDys data base consisting of $\sim 340\,000$ asteroids, the *WISE* (Masiero et al. 2011) data base consisting of $\sim 95\,000$ asteroids and the SDSS data base (Ivezić et al. 2002) consisting of $\sim 60\,000$ asteroids into family classifications.

In order to overcome some of the issues inherent in the HCM, as well as incorporating disparate colour surveys, in this work, we apply a technique called ‘cladistics’ to the Jovian Trojan swarms. Cladistics is traditionally used to examine the relationships between biological organisms, and has played an important role in the study of our own history as a species. The namesake of the *Lucy* mission, a near complete *Australopithecus afarensis*, was used in some of the first hominid cladistical investigations (Johanson & White 1979; Chamberlain & Wood 1987), and continues to be an important resource for studies into human origins today (Parins-Fukuchi et al. 2019).

The premise of the cladistical method is that characteristics are inherited through descent. It is then inferred that organisms with similar characteristics are related to one another. As cladistics was originally developed to incorporate incomplete fossil records (Hennig 1965), not all characteristics need to be known in order for a cladistical analysis to be carried out. This allows for the use of a larger number of characteristics and organisms, without needing to truncate the data set due to missing values. Whilst cladistics can account for these unknown characteristics, the more that is known about an object/organism, the more confidence that can be placed in the analysis. Minimizing missing data in the analysis would also decrease the number of equality parsimonious trees, trees that minimize the number of changes, produced during the analysis. The result of a biological cladistical analysis is a hierarchical dendritic tree, the ‘Tree of Life’ (e.g. Darwin 1859; Hennig 1965; Hug et al. 2016), in which those organisms that are most closely related to one another are joined by the shortest branch lengths. The advantage of cladistics over other analytical techniques is that it allows the use of multiple characteristics from disjointed data sets, including those that are unknown in some objects.

The application of cladistics in an astronomical context is analogous to the biological framework, in that it facilitates the identification of groups of objects that likely share a common origin. For example, the members of collisional families are expected to cluster together, due to similarities in their orbital and physical elements. The previously identified collisional families can thus be used to comment on the cladistical methodology. The technique has already been used in a growing body of work called ‘astrocladistics’ (Fraix-Burnet, Choler & Douzery 2006). Astrocladistics has been used to study a wide range of astronomical objects, including galaxies (e.g.

Fraix-Burnet et al. 2006), gamma-ray bursts (e.g. Cardone & Fraix-Burnet 2013), and stellar phylogeny (Jofré et al. 2017). Within the planetary sciences, Holt et al. (2018) used the technique to investigate the satellite systems of Jupiter and Saturn.

1.3 This work

This is the first time that astrocladistics has been applied to large Solar system survey data sets. The extension of the technique presented in Holt et al. (2018) to these large data sets could greatly improve our understanding of the relationships between Solar system objects. By increasing the number of Solar system objects that can be studied using astrocladistics, this project will help us to establish the method as a valid analytical tool for the planetary science community. To do this, we combine proper orbital elements (Knežević & Milani 2017), *WISE* albedos (Grav et al. 2012), SDSS colours (Hasselmann et al. 2012), *G*-band colour from the *Gaia* DR2 (Spoto et al. 2018) data sets, and the Moving Objects from VISTA Survey (MOVIS) near-infrared colours (Popescu et al. 2018), into a single cladistical analysis. As a result, this paper will provide a methodological basis for future astrocladistical studies in the planetary sciences.

In Section 2, we present an overview of the methodology of our work, and describe how astrocladistics is applied in the context of the Jovian Trojan population. Section 3 shows the results of the Jovian Trojan L₄ and L₅ swarm taxonomic analysis, including the dendritic trees and a discussion of the previously identified collisional families. As part of our analysis, we identify multiple objects of interest, presented in Section 4. The implications for the targets of the *Lucy* mission are discussed in Section 5. In Section 6, we discuss the implications of our work in the context of the next generation of wide-field surveys that are coming online in the next decade. Finally, we draw our conclusions in Section 7.

2 DATA SETS AND METHODS

Here we present an overview of the cladistical methodology used in a planetary science context. For a more detailed overview of the techniques involved, we direct the interested reader to Holt et al. (2018).

2.1 Matrix and characteristics

Each analysis begins with the creation of a 2D matrix that contains all known information about the objects of interest – in this case, the Jovian Trojans. Individual objects are allocated a row in that matrix. The columns of the matrix contain information on a different characteristic of the objects studied – including their physical properties and orbital elements.

The great advantages of using the cladistical methodology is that it can take a wide and disparate set of characteristics for a group of objects, and can cope with incomplete data sets. To illustrate the breadth of characteristics that can be incorporated into a cladistical study, in this work we bring together the proper elements of the Jovian Trojans, retrieved from AstDys (Knežević & Milani 2017), geometric albedos from NASA HORIZONS (Giorgini et al. 1996), simulated libration properties, the *WISE* albedos (Grav et al. 2011), SDSS (Carvano et al. 2010) colours, *Gaia* DR2 *G*-band colour (Spoto et al. 2018), and MOVIS colours (Popescu et al. 2016, 2018; Morate et al. 2018).

Due to the unique dynamics of the Jovian Trojans, the instantaneous osculating orbital elements cannot be used for taxonomic proposes (e.g. Beauge & Roig 2001; Brož & Rozehnal 2011). The

AstDyS data base (Knežević & Milani 2017) provides a set of robust proper elements, in semimajor axis, eccentricity, and inclination, for the Jovian Trojans. Those proper elements are generated from the results of 1×10^6 yr simulations, from which the osculating elements of the target objects are output at regular intervals. The resulting data base of osculating elements are then processed using Fourier Transform analysis. This technique removes oscillations due to planetary perturbations, with the final result being three proper elements (Δa_p : proper delta in semimajor axis to the Jovian mean (5.2 au), e_p : proper eccentricity; $\sin i_p$: sine of the proper inclination). By moving from an instantaneous value for the objects orbit to one that has been modified to take account of the periodic motion of the Trojans around the Lagrange points, these proper elements provide a much more accurate insight into a given object's provenance. Two objects with a common origin would be expected, in the absence of any major chaotic scattering events, to have similar proper elements, but might, at any given instant, be at a different part of their libration cycle, and hence have markedly different osculating elements. These proper elements can therefore, unlike the osculating elements, inform us about long-term orbital relationships in the population.

The Jovian Trojans are unique in that they are trapped in 1:1 mean motion resonance with Jupiter, which means that their proper semimajor axes lie very close to that of Jupiter, approximately 5.2 au. The proper semimajor axis for the Trojans is therefore expressed, in this work, as a distance from the 5.2 au baseline (δa_p). An additional benefit to using these elements is that, due to the requirement that the object's exhibit 1×10^6 yr of stable osculations around their host Lagrange point in simulations of their dynamical evolution, the AstDyS data base represents a data set of Jovian Trojans that are at least relatively dynamically stable, and should exclude any objects that have otherwise been misclassified, such as objects temporarily captured from the Jupiter family comet and Centaur populations (e.g. Horner & Wyn Evans 2006). It should be noted that stability for 1×10^6 yr does not equate to, or even imply, stability on time-scales comparable to the age of the Solar system (Levison, Shoemaker & Shoemaker 1997; Tsiganis, Varvoglis & Dvorak 2005a; Horner, Müller & Lykawka 2012; Di Sisto, Ramos & Beaugé 2014; Di Sisto, Ramos & Gallardo 2019; Holt et al. 2020a). We use this stability level to exclude objects temporarily captured near the Jovian Lagrange points, such as P/2019 LD₂ (Steckloff et al. 2020; Bolin et al. 2021; Hsieh et al. 2021).

In addition to the proper elements obtained from AstDyS, we also include information on the libration of the Jovian Trojans around their host Lagrange point. To obtain these libration values, we performed 1×10^4 yr integrations of the orbital evolution of the Trojans under the influence of the Sun and four giant planets, using the REBOUND WHFAST integrator (Rein & Liu 2012). For these integrations, we used a time-step of 0.3954 yr, and wrote out the instantaneous orbital elements of all objects simulated every 10 yr. From these, we were able to calculate the amplitude of libration, as well as the mean angle in the Jovian reference frame.

Similar physical properties, such as albedos and colours, would also be suggestive of analogous formation scenarios. We chose to not include mass, or any properties related to mass, as characteristics in the analysis. Their inclusion could hide any relationships between a massive object and any daughter objects, the result of collisions resulting in families. We do include visual geometric albedo (Giorgini et al. 1996), as this represents analogous physical properties.

In Holt et al. (2018), the presence or absence of various chemical species were used as characteristics in the cladistical analysis. This information requires detailed spectral analysis, which is only currently available for two Trojans, 624 Hektor (1907 XM) (Marchis

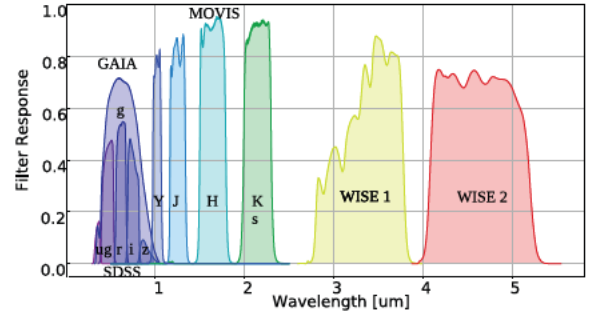


Figure 2. Wavelengths of the filters surveys used in this study.

et al. 2014; Perna et al. 2018) and 911 Agamemnon (1919 FD) (Perna et al. 2018), although it is likely that this situation will change in the coming decade as a result of both the *Lucy* mission and observations with the *James Webb Space Telescope*. As a proxy for composition, broad-band colours can be used in astrocladistics, as has been undertaken by Fraix-Burnet et al. (2010) in their studies of galaxies.

Several of the Jovian Trojans have been imaged by large all-sky surveys, with data available from the Sloan Digital Sky Survey (SDSS) (Szabo et al. 2007), the *Wide-field Infrared Survey Explorer* (WISE) (Grav et al. 2012), *Gaia* DR2 (Spoto et al. 2018), and MOVIS (Popescu et al. 2016). The wide range of wavelengths represented by these data sets are shown in Fig. 2. We include these colours as characteristics in our analysis, in addition to the dynamical data set described above. In total, combining the dynamical and observational data, this results in a maximum of 17 characteristics being included for each Trojan studied in this work. Each of these characteristics, along with their coefficient of determination (R^2) and ranges, are presented in appendix A.

Once all characteristics are collated for our objects of interest, they are binned to give each object a unique integer value for each characteristic. This was carried out using a Python program developed for Holt et al. (2018).³ The binning of the data has multiple benefits. The primary reason for binning is the requirement of the cladistical methodology to have whole numbers for analysis, representing character states. This has the added benefit of normalizing each of the independent data sets. By normalizing the data sets, the binning program also reduces the heterogeneity seen in the colours of the population (Grav et al. 2011, 2012; DeMeo & Carry 2013; DeMeo et al. 2014), mitigating some of the effects of the ‘information content’ (Milani et al. 2014) from each catalogue. The maximum number of bins for each characteristic, is set at 15, though if a co-efficient of determination (R^2) of greater than 0.99 is reached, a smaller number is used, shown in appendix A. Those characteristics with a smaller number are then weighted, to standardize their contribution to the analysis. All binned characteristics have R^2 values larger than 0.95. The binned matrices are then imported into Mesquite (Maddison & Maddison 2017), a program used for management of cladistical matrices and trees, for further analysis.

The dynamical characteristics and albedo are ordered as in Holt et al. (2018) and Fraix-Burnet et al. (2006), with the colours unordered. The reasoning behind the ordering of dynamical characteristics is related to the stability of the Jovian Trojans. In dynamical

³Available from <https://github.com/TimHoltastro/holt-et-al-2021-Jovian-Trojan-astrocladistics.git>.

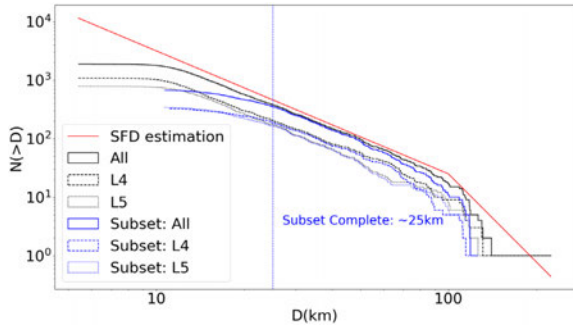


Figure 3. Size–Frequency distribution (SFD) of the Jovian Trojan population (black solid), L₄ (black dashed), and L₅ (black dot) swarms. We show the SFD of objects used in this work in blue, showing a completeness to 25 km. An estimated complete SFD distribution of the Jovian Trojans (red) is also shown (Nesvorný 2018).

space, the Jovian Trojans are relatively stable (e.g. Nesvorný 2002; Robutel & Gabern 2006; Emery et al. 2015; Holt et al. 2020a), and therefore any changes in dynamical properties represent large differences. In contrast to this, the colour ratios represent estimations in compositional structure of the objects. These broad-band colours can be affected by single changes in mineralogy (e.g. DeMeo et al. 2015; Reddy et al. 2015), and are thus unordered.

Simulations have suggested that some of the Jovian Trojans are unstable on relatively short time-scales (e.g. Levison et al. 1997; Tsiganis et al. 2005a; Di Sisto et al. 2014, 2019; Holt et al. 2020a). In order to account for this, we use only those objects that are present in the *ASTDYS* data base (Knežević & Milani 2017). As the creation of proper elements requires a degree of stability (e.g. Knežević & Milani 2003), these objects are stable in the swarms for at least 1×10^6 yr. In this initial phase, we also only select those Trojans that have available observational data from at least one of the four surveys, *WISE*, *SDSS*, *Gaia*, or *MOVIS*. The result of this is the generation of two distinct matrices, one for each of the two Jovian Swarms. The L₄ data set is smaller with 398 objects, whilst the L₅ matrix contains 407 objects. Though these subsets are markedly smaller than the total known populations of the two swarms, they offer a significant advantage over a possible HCM set. For comparison, in the L₄ swarm there are only five objects, 4060 Deipylus (1987 YT₁), 3793 Leonteus (1985 TE₃), 5027 Androgeos (1988 BX₁), 5284 Orsilocus (1989 CK₂) and 4063 Euforbo (1989 CG₂), and one, 7352 (1994 CO), in the L₅ that are present in all four surveys. Even if only the largest photometric data set (*SDSS*; Szabo et al. 2007) is considered, our subsets are nearly double those of a restricted HCM-type study (L₄:176 objects, L₅:232 objects).

The objects in our subsets are shown in the context of the swarms in Fig. 1. In selecting only those objects with observational data available from one or other of the named surveys, we acknowledge that we are introducing a size bias, since larger objects are more likely to have been surveyed. We show the size–frequency distribution of our chosen objects in Fig. 3. This shows that our subset is complete to approximately 25 km diameter.

In addition to the Jovian Trojans, a fictitious outgroup object is created, with a base 0 for each of the characteristics. The function of this outgroup is to root the trees. In the context of biological cladistics, a related clade, but one that is outside the group of interest, is selected as the outgroup (Farris 1982). In doing this, the outgroup sets the base character state for each characteristic. For astrocladistics of the Trojans, the dynamics make selection

of the outgroup more difficult, as there is no true ancestral state from which ingroup characteristics are derived. For the synthetic outgroup created for this study, the dynamical characteristics are set close to 0 in proper Δ semimajor axis (Δa_p), eccentricity (e_p), and sine inclination ($\sin i_p$). The calculated mean libration values would be at the closest approach to Jupiter (56.42° and 285.72° for the L₄ and L₅ swarms, respectively), with low libration amplitudes (L₄: 4.044° , L₅: 2.73°). These values represent a very stable area of the parameter space. In terms of albedo (L₄: 0.024, L₅: 0.031) and colours, the object would be very dark, and have a featureless spectrum. Based on these parameters the outgroup served the purpose of rooting each consensus tree without being too close and considered part of the ingroups, or too far away so that the relationship to the populations of interest were lost.

Each matrix is available in the online supplemental material⁴ in binned and unbinned form.

2.2 Trees

Each *Mesquite* taxon-character matrix is then used to create a set of phylogenetic trees using *Tree analysis using New Technology (TNT)* v1.5 (Goloboff, Farris & Nixon 2008; Goloboff & Catalano 2016), via the *Zephyr Mesquite* package (Maddison & Maddison 2015). This tree search is based on the concept of maximum parsimony (Maddison, Donoghue & Maddison 1984). Each tree generated in the block has a length and in this case, is a characteristic of the tree itself, and not of the individual branches. This tree length is calculated on the bases of characteristics changing states, for example a change from a 0 to a 1 would constitute a 1 step value. In ordered characteristics, a change from 0 to 2 would be two steps, whereas in the unordered, would only be one step. A tree with more changes in character state would have a longer tree length. The TNT algorithm (Goloboff et al. 2008; Goloboff & Catalano 2016) rearranges the configuration of the trees, attempting to find the set of trees with the lowest tree length, creating a block of the most equally parsimonious trees, those with the same minimum tree length. We use a drift algorithm (Goloboff 1996) search by generating 100 Wagner trees (Farris 1970), with 10 drifting trees per replicate. These starting trees are then checked using a *Tree bisection and reconnection (TBR)* algorithm (Goloboff 1996) to generate a block of 10 000 equally parsimonious dendritic trees. The Nexus files for both matrices, both with and without the tree blocks, are available on the GITHUB repository.⁵ A 0.5 majority-rules consensus tree can be constructed (Margush & McMorris 1981) once the tree block is imported back into *Mesquite* (Maddison & Maddison 2017). This tree is then a hypothesis for the relationships between the Jovian Trojans in the individual swarms.

As part of the consensus tree, each node (see Figs 4, 5 and 6) shows the fraction of trees in the block that contain that node (F_{node}). This fraction is indicated in the relevant sections, Section 3.1 for the L₄ swarm and Section 3.2 for the L₅ swarm, for each subclan, clan, and superclan. The higher the prevalence of the node, with 1.0000 indicating that the node is in all 10 000 trees, gives higher confidence in the grouping.

⁴<https://github.com/TimHoltastro/holt-et-al-2021-Jovian-Trojan-astrocladistics.git>

⁵Available from <https://github.com/TimHoltastro/holt-et-al-2021-Jovian-Trojan-astrocladistics.git>

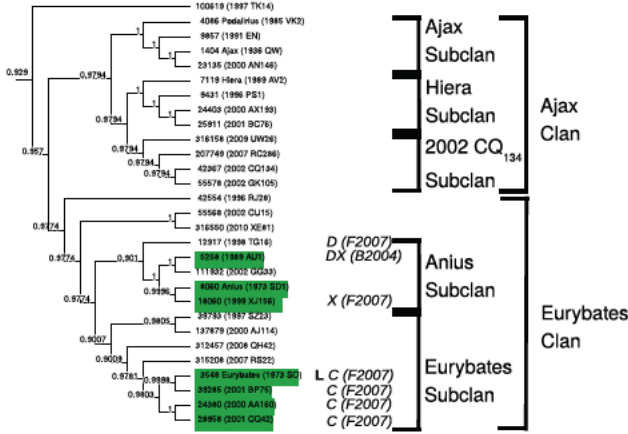


Figure 4. Consensus trees of Greater Ajax superclan, including Ajax and Eurybates clans. An example of trees shown in Appendix B. Letters associate objects with Bus–Demeo taxonomy (Bus 2002; DeMeo et al. 2009), classified by associated reference T1989: Tholen (1989); B2004: Bendjoya et al. (2004); F2007: Fornasier et al. (2007); H2012, with associated confidence rating: Hasselmann et al. (2012). L indicates objects to be visited by the *Lucy* spacecraft (Levison et al. 2017). The green highlights are members of the Eurybates collisional family.

2.3 Dispersal velocities, diameter calculations, and escape analysis

The taxonomic clusters produced by the cladistical methodology can be verified using the established inverse Gauss equations (e.g. Zappala et al. 1996; Turrini, Marzari & Beust 2008; Holt et al. 2018), in much the same way that asteroid collisional families are identified and confirmed (e.g. Nesvorný et al. 2015). Holt et al. (2018) provide a demonstration of the use of those equations in conjunction with their cladistical analysis of the Jovian and Saturnian satellite systems. In that work, the inverse Gauss equations are used to comment on the relative timing of creation and validity of the clusters in the irregular satellites identified by astrocladistics. The rationale for this is that clusters with low dispersal velocities would most likely indicate families produced by recent breakups, with larger velocities possibly indicating either more energetic disruptions of the family’s parent body, or an older family that has had longer to disperse.

We extend the methodology used in Holt et al. (2018) to investigate the mean dispersal velocity in the dynamical parameter space of the clusters we identify in the Jovian Trojan population.⁶ In the traditional methodology, the largest object is used as a point of reference for the parameters used in the calculations (specifically a_r , e_r , i_r , and n_r in equations 5–6 in Holt et al. 2018). In this work, we calculate two different dispersal velocities for each Jovian Trojan. As in the original work, we determine the dispersal velocity of each object in a given cluster to the largest object in that cluster (ΔV_{ref}). In addition, we calculate the dispersal velocity from a fictitious centroid at the mean of the cluster proper element space (Δa_{prop} , e_p , $\sin i_p$ and period n : $\Delta V_{m_{\text{cent}}}$). The inverse Gauss equations also require knowledge of the values of ω and $\omega + f$ at the initial point of disruption (e.g. Zappala et al. 1996; Nesvorný, Beaug & Dones 2004; Nesvorný et al. 2015). For ease of comparison, we have used ω as 90° and $\omega + f$ as 45° .

⁶Python 3 program is available from the GITHUB repository: <https://github.com/TimHoltastro/holt-etal-2021-Jovian-Trojan-astrocladistics.git>

Data sets for each of the clusters are available from the Github repository.⁷

Only 1857 of the 5553 (33.44 per cent) canonical Trojan have measured albedos, and therefore reliable diameters in the NASA HORIZONS data base. In order to investigate the size distribution of each swarm, we created an estimate of the diameter and volume of each of the 5553 Jovian Trojans in the AstDyS data base (Knežević & Milani 2017). The unknown diameters (D) were calculated from the absolute magnitude (H) of the object in the NASA HORIZONS data base, combined with an estimate of the mean geometric albedo values for the population ($P_v = 0.075$) using equation (1) (Fowler & JR Chillemi 1992).

$$D(\text{km}) = \frac{1329}{\sqrt{P_v}} 10^{-0.2H}. \quad (1)$$

It should be noted that it is highly likely that most Jovian Trojans, particularly the smaller members of the population, are markedly aspherical. Indeed, shapes inferred from occultation observations suggest that several of the targets for the *Lucy* mission are likely irregular in shape (Buie et al. 2015; Mottola et al. 2020). Given the known shapes in this size regime, from the Main belt and Near Earth populations (e.g. Durech et al. 2015), it is expected that other Jovian Trojans are also irregular in shape. From this our calculated diameter values should only be taken as estimations, and are available in the Github associated with this study.

As part of our analyses, we track the dynamical evolution of the chosen objects, using data presented in Holt et al. (2020a) which presented escape fractions of the Trojan swarms and collisional families on a time-scale of 4.5×10^9 yr. The best-fitting orbital solution for each Jovian Trojan studied in that work was integrated forwards in time under the gravitational influence of the Sun and four giant planets for 4.5×10^9 yr. In addition, eight ‘clones’ of each object were studied, with initial orbital parameters perturbed from the best-fitting solution along the Cartesian uncertainties presented in the HORIZONS data base. We use this information to comment on the stability of the individual members, and each cluster as a whole.

2.4 Full population analysis

In addition to the subset analysis, we also conducted an analysis of the full L_4 swarm (3620 objects) and full L_5 swarm (1920 objects), using same techniques presented in Section 2. Since many of the objects in each swarm remain poorly characterized, with many lacking for any information other than an apparent magnitude and orbital solution, there is insufficient information in the matrices for us to place great weight in the results of this additional analysis. We only include this as a computational note for future work, as presented in Table 1.

3 RESULTS AND DISCUSSION

Here, we present the taxonomic trees resulting from our cladistical analysis of the Jovian Trojan swarms. Each swarm is presented and discussed separately, and we compare our results to the previously identified collisional families (Nesvorný et al. 2015). In order to avoid confusion with a specific cluster identified in our cladistics analysis, we use the term ‘clan’ to identify the groups of objects that share a similar heritage. We borrow two conventions from the biological Linnean taxonomy (Linnaeus 1758), namely the inclusion

⁷<https://github.com/TimHoltastro/holt-etal-2021-Jovian-Trojan-astrocladistics.git>

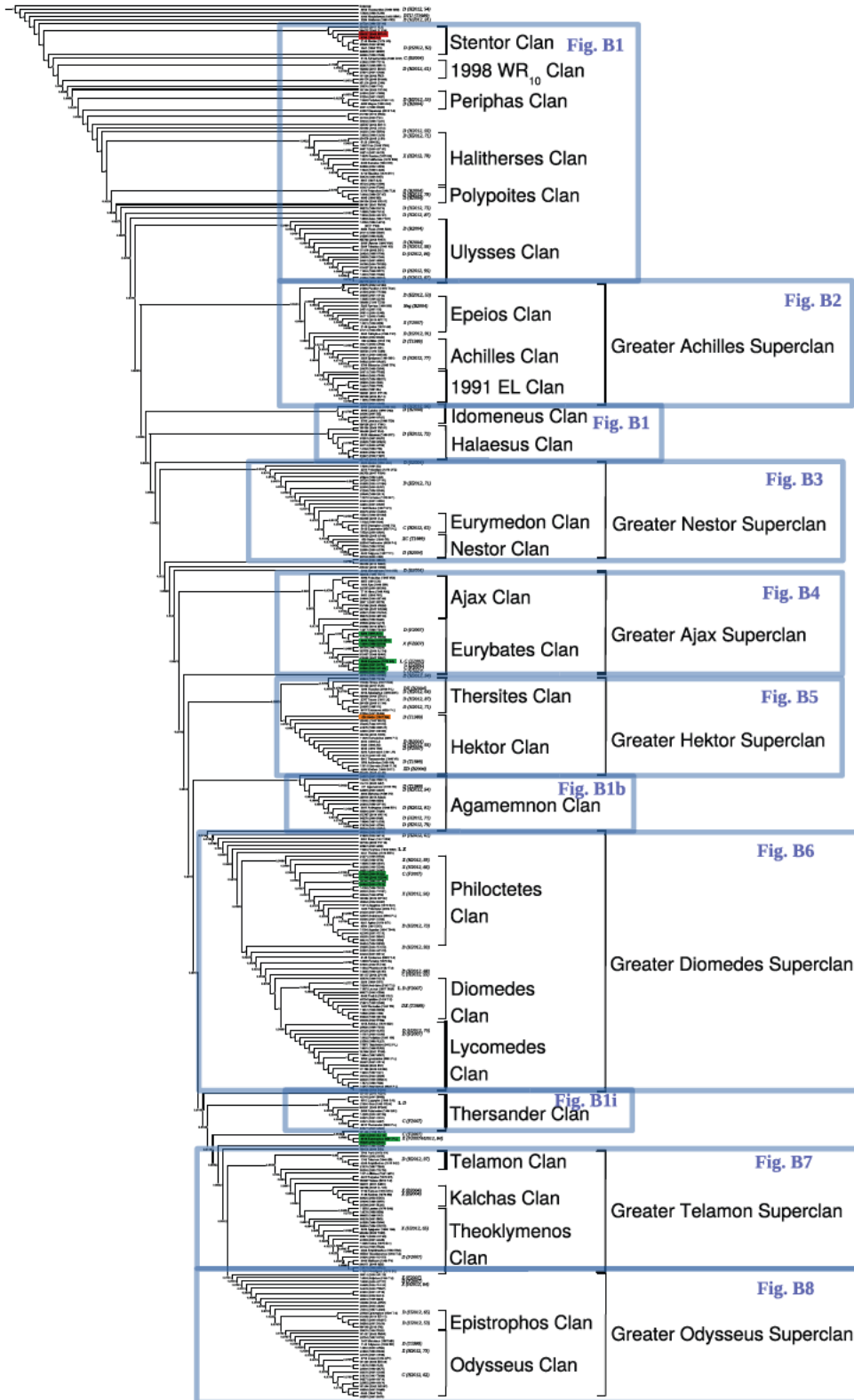


Figure 5. Consensus tree of cladistical analysis of 398 L₄ Jovian Trojans. Numbers indicate the proportion of the 10 000 generated trees where a given branch is present. Colours are indicative of previously identified collisional families: Green: Eurybates; Orange: Hektor; Red; 1996 RJ; after Nesvorný et al. (2015). Letters associate objects with Bus–DeMeo taxonomy (Bus 2002; DeMeo et al. 2009), from different sources, T1989: Tholen (1989); B2004: Bendjoya et al. (2004); L2004: Lazzaro et al. (2004); F2007: Fornasier et al. (2007); H2012, with associated confidence rating: Hasselmann et al. (2012). *Lucy* Targets are indicated by an L. A high resolution, expanded form of this figure is available in online supplemental material. The blue rectangles correspond to detailed figures in Appendix B.

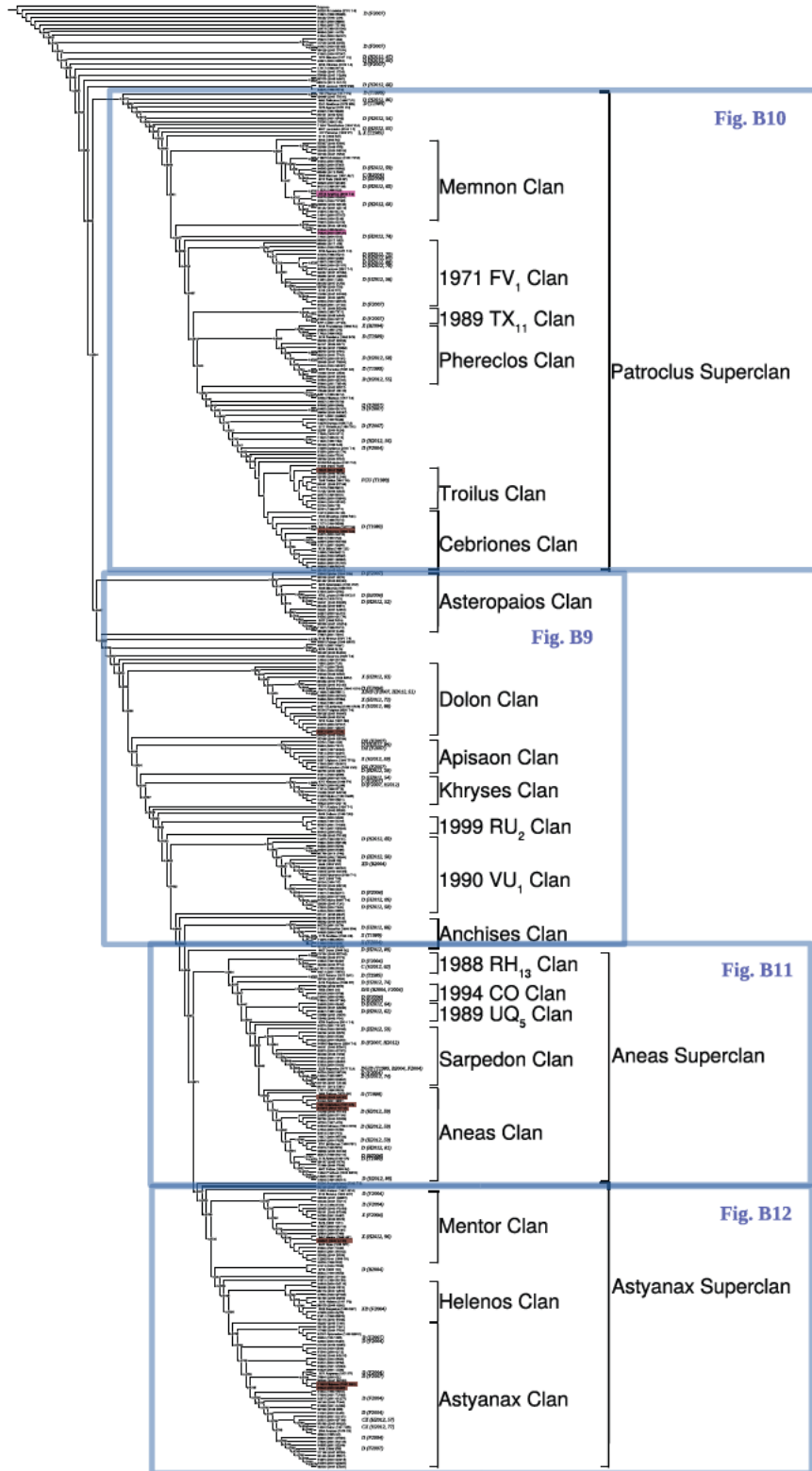


Figure 6. Consensus tree of cladistical analysis of 407 L₅ Jovian Trojans. Numbers indicate fraction of 10000 trees where branch is present. Colours are indicative of previously identified collisional families: Brown: Ennomos; Purple: 2001 UV₂₀₉ after Nesvorný et al. (2015). Letters associate objects with Bus–Demeo taxonomy (Bus 2002; DeMeo et al. 2009) from different sources, T1989: Tholen (1989); B2004: Bendjoya et al. (2004); F2004: (Fornasier et al. 2004); F2007: Fornasier et al. (2007); H2012, with associated confidence rating: Hasselmann et al. (2012). *Lucy* Targets are indicated by an L. A high resolution, expanded form of this figure is available in online supplemental material. The blue rectangles correspond to detailed figures in Appendix B.

Table 1. Comparison of times taken to generate each 10 000 tree blocks, as described in Section 2.2. (subset) are the matrices used in this work, where as (Pop) are the full known population at their respective Lagrange points. No.: Number of objects in the matrix; Hrs_{cpu}: number of CPU hours taken to generate tree block on a single core of Intel Xeon W-2133 CPU at 3.60GHz; L_{tree} : Tree length; I_c : consensus index (Brooks, O’Grady & Wiley 1986) of the 0.5 consensus tree; I_r : retention index (Naylor & Kraus 1995) of the 0.5 consensus tree.

	No.	Hrs _{cpu}	L_{tree}	I_c	I_r
L_4 (subset)	398	10.72	1635.37	0.123	0.751
L_5 (subset)	407	10.69	1984.79	0.113	0.712
L_4 (Pop)	3620	420.15	3926	0.041	0.899
L_5 (Pop)	1920	372.2	2794	0.054	0.883

of a type object and the use of prefixes. Each clan is named after the member that was first discovered. This object is designated the ‘type object’. Due to observational bias, in most cases, the type object is the largest member of the clan. The largest member of the group is used as a reference point for the dispersal velocities explained in Section 2.3, and termed the ‘reference object’. It is important to note that the type object and the reference object in a clan can be the same object, though this is not always the case. In order to assist with any hierarchical grouping, we use the super and sub-prefixes, to denote higher and lower groups. To further improve the clarity of the hierarchical clusters, the superclan’s have ‘Greater’ affixed to the representative name. We choose five members as the minimum number for a clan or subclan. This terminology forms a basis for future expansion of the small Solar system body taxonomic framework.

The Greater Ajax superclan, shown in Fig. 4, highlights the hierarchical nature of this new terminology. The superclan is split into two clans, the Ajax and Eurybates clans. The type object of both the Greater Ajax superclan and the Ajax clan is 1404 Ajax (1936 QW), whereas 3548 Eurybates (1973 SO) is the type object of the Eurybates clan. Within both clans, there are two subclans. In the Eurybates clan, there is the Anius subclan with type object 8060 Anius (1973 SD₁), and the Eurybates subclans, along with three other objects, namely 42554 (1996 RJ₂₈), 55568 (2002 CU₁₅), 316550 (2010 XE₈₁), not associated with either subclan. In this example set, the Trojan 3548 Eurybates (1973 SO) is therefore the type object of both the Eurybates subclan and Eurybates clan, and is also a member of the Greater Ajax superclan. In this example, 3548 Eurybates (1973 SO) is also the reference object used in dispersal velocity calculations for the Eurybates clan and subclan.

3.1 L_4 swarm

In the L_4 Trojan swarm, we analyse a total of 398 objects using the astrocladistical methodology. A total of 10 000 equally parsimonious trees were generated, a process that took 10 h, 43 min using a single core of Intel Xeon W-2133 CPU at 3.60 GHz. The resulting consensus tree is presented in Fig. 5. The tree has a consistency index of 0.123 (Brooks et al. 1986) and a retention index of 0.751 (Naylor & Kraus 1995). The consensus tree has a length of 1635.37.⁸

⁸The tree length, retention index, and consistency index are measures of how accuracy a tree represents the true relationships. A smaller tree length implies a more parsimonious, and thus likely tree (Goloboff 2015). The two other indices are measures of homoplasy, the independent loss or gain of a characteristic (Brandley et al. 2009). In both indices, a value of 1 indicates no homoplasy, and thus no random events. The consistency index is the ratio of

The superclans, clans, and subclans identified in the L_4 swarm are listed in Table 2. In the L_4 swarm, we identify a total of ten unaffiliated clans and eight superclans containing an additional seventeen clans. Each of these trees are shown in detail in Appendix B.

In the L_4 swarm, there are four canonical collisional families (Nesvorný et al. 2015). Here three are represented in the subset, the 1996 RJ, Hektor and Eurybates families. All members of the Eurybates, 1996 RJ, and Hektor families in the canonical set used in this study are also in Rozehnal et al. (2016) and Vinogradova (2015). There are no representatives of the canonical Arkesilaos family, though Vinogradova (2015) associated this family with their Epeios non-canonical family, of which the largest member, 2148 Epeios (1976 UW) is the type object of the Epeios clan. The only member of the Hektor family, 624 Hektor (1907 XM), is the type object of the Hektor clan, in the Greater Hektor superclan. The Eurybates collisional family provides some place for comment. Seven of the thirteen identified members are clustered the Ajax clan, around 3548 Eurybates (1973 SO), the type object. There are two other clusters of Eurybates family members, three objects in the Philoctetes Clan, and another three that are unassociated with any clan. The fact that these are clustered, but separated in the consensus tree, may indicate that they are victims of ‘chaining’ in HCM, and thus not truly members of the collisional family.

3.1.1 Unaffiliated L_4 clans

Our results reveal ten clans in the L_4 swarm that are unaffiliated with any identified superclan, presented in Fig. B1. None of the unaffiliated clans can be further split into subclans. Six of the unaffiliated clans, namely the Stentor, 1998WR₁₀, Periphias, Halitherses, Polypoites, and Ulysses clans, are located at the base of the L_4 tree. Each of the ten unaffiliated clans in the L_4 swarm contain at least one D-type object. The Agamemnon and Ulysses clans containing five and six D-type members, respectively. The Halitherses clan contains one X-type, 13475 Orestes (1973 SX), along with a single D-type, 13362 (1998 UQ₁₆), indicating that there may be some heterogeneity to these clans.

The dynamical stability of all members of the identified unaffiliated clan members was assessed by Holt et al. (2020a). Comparing our list of those clans with the dynamical data from that work, we find that most of the clans exhibit significant dynamic stability, at a level that exceeds the mean stability of the L_4 Trojan population as a whole (with the simulations described in Holt et al. 2020a yielding a mean escape fraction of 0.24 for the L_4 cloud over the age of the Solar system). The exception is the Periphias clan, which displays a higher escape fraction (0.44) over the course of those simulations.

In the following sections, we discuss three of these unaffiliated clans, the Stentor, Idonmeneus, and Thersander clans, highlighting several interesting cases. The other seven clans, as shown in Fig. B1, may contain objects of interest, though we leave further detail discussion for future research.

Stentor clan: The first clan identified in our consensus tree of the L_4 Trojans (Fig. 5) is the Stentor clan, shown in more detail in Fig. B1(h), after the type object 2146 Stentor (1976

the minimum number of changes in a tree, to the actual number (Givnish & Sytsma 1997). The retention index is similar, but incorporates the maximum number of changes into the index (Farris 1989). We direct the interested reader to Gascuel (2005) for a more detailed analysis of the mathematics behind these indices.

Table 2. Clans, superclans, and subclans identified in the L₄ Trojan swarm. Name: Clan Name; N : Number of objects; D_{ref} : Reference object diameter; V_{esc} : Escape velocity of reference object; F_{esc} : fraction of objects that escape the L₄ Lagrange point, from Holt et al. (2018); ΔV_{mref} : mean dispersal velocity calculated from inverse Gauss equations, see Section 2.3, to the reference object, with 1σ standard deviation; ΔV_{mcen} : as ΔV_{mref} , with calculations to the fictitious cluster centre; F_{node} : faction of trees in the block that contain the node.

Name	N	D_{ref} (km)	V_{esc} (m s ⁻¹)	F_{esc}	ΔV_{mref} (m s ⁻¹)	ΔV_{mcen} (m s ⁻¹)	F_{node}
L4-Stentor	8	71.84	24.02	0.07	11.38 ± 7.85	10.25 ± 6.51	1.0000
L4-1998 WR ₁₀	5	34.95	11.69	0.02	26.02 ± 8.11	10.61 ± 5.33	0.7628
L4-Periphias	5	80.17	26.81	0.44	13.02 ± 6.11	10.61 ± 4.56	0.9216
L4-Halitherses	15	37.7	12.61	0.01	21.53 ± 12.28	15.63 ± 9.9	0.9422
L4-Polypoites	5	68.73	22.98	0	30.67 ± 9.95	15.49 ± 8.5	0.9799
L4-Ulysses	17	76.15	25.46	0.08	24.15 ± 12.43	14.25 ± 8.25	0.9694
L4-Idomeneus	6	112.05	37.47	0	9.81 ± 3.51	8.37 ± 3.7	1.0000
L4-Halaesus	10	50.77	16.98	0.06	12.3 ± 9.36	10.56 ± 6.34	1.0000
L4-Agamemnon	16	131.04	43.82	0.12	28.34 ± 12.5	21.41 ± 11.01	1.0000
L4-Thersander	10	65.92	22.04	0.14	21.82 ± 10.93	17.5 ± 12.43	0.9795
L4-Greater Achilles	35	130.1	43.51	0.06	16.91 ± 11.24	14.4 ± 8.6	0.9501
L4-Epeios	10	48.36	16.17	0	19.55 ± 7.42	8.57 ± 4.42	0.9987
L4-Achilles	9	130.1	43.51	0.15	9.9 ± 5.96	8.65 ± 6.54	0.9707
L4-1991EL	10	68.98	23.07	0.06	17.37 ± 13.76	12.69 ± 8.48	0.9799
L4-Greater Nestor	27	112.32	37.56	0.63	34.04 ± 20.11	29.81 ± 12.31	0.9507
L4-Eurymedon	6	45.68	15.28	0.3	20.96 ± 15.31	13.48 ± 6.9	0.9013
L4-Nestor	7	112.32	37.56	0.4	20.71 ± 13.1	14.84 ± 5.4	0.9709
L4-Greater Ajax	29	85.5	28.59	0.38	40.33 ± 26.27	32.91 ± 16.75	0.9290
L4-Ajax	12	85.5	28.59	0.6	18.06 ± 14.39	16.82 ± 10.65	0.9794
<i>L4-Ajax Sub</i>	4	85.5	28.59	0.64	11.29 ± 0.93	7.34 ± 2.62	1.0000
<i>L4-Hiera Sub</i>	4	59.15	19.78	0.36	8.31 ± 1.19	4.35 ± 0.85	1.0000
<i>L4-2002 CQ₁₃₄ Sub</i>	4	32.16	10.75	0.81	36.08 ± 17.87	20.26 ± 11.97	0.9794
L4-Eurybates	16	63.88	21.36	0.23	32.58 ± 28.94	24.59 ± 14.67	0.9774
<i>L4-Anius Sub</i>	5	53.28	17.82	0.27	12.61 ± 10.34	10.42 ± 4.62	0.9010
<i>L4-Eurybates Sub</i>	8	63.88	21.36	0.24	25.23 ± 20.27	19.43 ± 2.22	0.9007
L4-Greater Hektor	28	225	75.24	0.54	31.47 ± 19.35	28.99 ± 21.63	0.9593
L4-Thersites	11	89.43	29.91	0.83	34.57 ± 33.85	27.49 ± 23.04	0.9792
L4-Hektor	17	225	75.24	0.35	31.43 ± 16.53	27.93 ± 16.05	1.0000
L4-Greater Diomedes	75	117.79	39.39	0.43	108.79 ± 36.64	41.85 ± 23.23	0.9782
L4-Philoctetes	26	33.96	11.36	0.38	25.19 ± 7.9	19.07 ± 11.21	0.9998
<i>L4-Andraimon Sub</i>	10	33.96	11.36	0.77	27.48 ± 6.64	23.91 ± 7.2	0.9796
L4-Diomedes	12	117.79	39.39	0.76	56.9 ± 28.09	40.6 ± 19.19	0.9427
L4-Lycomedes	20	31.74	10.61	0.45	33.18 ± 16.71	29.44 ± 16.14	0.9809
<i>L4-Amphiaraios Sub</i>	8	26.83	8.97	0.57	13.3 ± 4.33	10.18 ± 1.9	1.0000
L4-Greater Telamon	35	111.66	37.34	0.05	27.16 ± 15.83	21.68 ± 11.82	0.8646
L4-Telamon	5	64.9	21.7	0.27	26.96 ± 18.11	20.7 ± 6.98	0.9600
L4-Kalchas	6	46.46	15.54	0	16.88 ± 10.79	12.47 ± 4.59	1.0000
L4-Theoklymenos	19	111.66	37.34	0.03	25.71 ± 17.83	20.08 ± 12.5	0.8390
<i>L4-Makhaon Sub</i>	5	111.66	37.34	0.09	13.39 ± 6.05	8.22 ± 1.17	0.9691
L4-Greater Odysseus	36	114.62	38.33	0.11	24.17 ± 12.28	18.41 ± 9.07	0.9701
L4-Epistrophos	5	24	8.02	0	8.32 ± 3.94	6.99 ± 2.47	1.0000
L4-Odysseus	20	114.62	38.33	0	17.6 ± 11.75	12.54 ± 8.43	0.9797

UQ), and consists of a total of eight objects. The clan includes the two identified members of the 1996 RJ collisional family, 226027 (2002 EK₁₂₇ and 9799 (1996 RJ), (Nesvorný et al. 2015), and it seems likely that the other members of the clan represent previously undetected members of the collisional family. The type object of this clan, 2146 Stentor (1976 UQ), is chosen over 9799 (1996 RJ), due to it being discovered nearly 20 yr earlier. In this clan, although 2146 Stentor (1976 UQ) (50.76 km) is the type object, 7641 (1986 TT₆) is used as the reference frame for our calculations of the clan member's dispersion in ΔV_{ref} , as the available observational data suggest that it has the largest diameter in the clan (71.84 km).

Unfortunately, no members of this clan have been classified under the Bus–Demeo system. Almost all members of this clan were found to be dynamically stable in the simulations carried out by Holt et al. (2020a), with the one exception being the clones of the type object, 2146 Stentor (1976 UQ). More than half of the clones of that object (56 per cent) escaped from the Jovian Trojan population over the 4.5×10^9 yr of those simulations. The stability of the remainder of the clan is likely the result of most of the members having low δa_{prop} (<0.036 au), mean libration angles ($<3.5^\circ$ from the Lagrange point) and range ($<14^\circ$).

The clan has relatively compact *Gaia* G magnitude values (17.56 to 18.11 mag), though there are only two similar sized members,

Table 3. Clans, **superclans**, and **subclans** identified in the L₅ Trojan swarm. *Name*: Family Name; *N*: Number of members; *D*_{ref}: Reference object diameter; *V*_{esc}: Escape velocity of reference object; *F*_{esc}: fraction of objects that escape the L₅ Lagrange point, from Holt et al. (2018); ΔV_{ref} : dispersal velocity relative to the reference object (calculated using the inverse Gauss equations; see section 2.3), with 1σ standard deviation; ΔV_{cent} : as ΔV_{ref} , with calculations to the fictitious cluster centre; *F*_{node}: fraction of trees in the block that contain the node.

Name	No.	<i>D</i> _{refobj} (km)	<i>V</i> _{esc} (m s ⁻¹)	<i>F</i> _{esc}	ΔV_{ref} (m s ⁻¹)	ΔV_{cent} (m s ⁻¹)	<i>F</i> _{node}
L5-Asteropaios	17	57.65	19.28	0.06	25.94 ± 11.96	15.48 ± 6.14	0.9304
<i>L5-Lykaon Sub</i>	5	50.87	17.01	0.07	10.22 ± 2.14	7.06 ± 1.84	0.9588
<i>L5-1988 RS₁₀ Sub</i>	7	32.14	10.75	0.02	9.97 ± 6.12	8.31 ± 5.99	0.8942
L5-Dolon	20	42.52	14.22	0.31	46.28 ± 27.85	34.71 ± 19.81	0.9999
<i>L5-Erichthonios Sub</i>	5	27.53	9.21	0.04	13.36 ± 10.86	9.95 ± 6.73	0.9999
<i>L5-Dolon Sub</i>	11	42.52	14.22	0.35	25.77 ± 13.42	23.52 ± 14.58	1.0000
L5-Apisaon	9	40.67	13.6	0.67	26.29 ± 7.75	20.31 ± 7.29	0.9794
L5-Khryses	8	53.2	17.79	0.53	14.41 ± 5.08	8.02 ± 3.15	0.9784
L5-1999 RU ₁₂	5	24.01	8.03	0.84	29.24 ± 11.18	17.87 ± 4.84	1.0000
L5-1990 VU ₁	21	63.19	21.13	0.52	28.35 ± 28.23	24.87 ± 18.96	0.9391
<i>L5-1990 VU₁ Sub</i>	7	59.3	19.83	0.73	61.38 ± 30.9	31.94 ± 9.74	0.9788
<i>L5-Idaios Sub</i>	8	44.55	14.9	0.38	13.72 ± 5.31	8.93 ± 3.59	0.9395
L5-Anchises	8	99.55	33.29	0.88	32.88 ± 10.82	22.51 ± 13.02	0.9612
L5-Greater Patroclus	133	140.36	46.94	0.1	31.57 ± 20.49	31.62 ± 15.09	0.8377
L5-Memnon	23	118.79	39.72	0.11	15.31 ± 7.57	15.05 ± 6.59	0.9534
<i>L5-Memnon Sub</i>	9	118.79	39.72	0.15	16.02 ± 7.97	12.24 ± 7.9	0.9332
<i>L5-Amphios Sub</i>	9	38.36	12.83	0.14	14.06 ± 8.13	13.04 ± 7.89	0.9727
L5-1971 FV ₁	18	75.66	25.3	0.07	12.76 ± 7.58	9.43 ± 5.5	0.9065
<i>L5-Lampos Sub</i>	6	35.39	11.83	0.22	21.47 ± 4.71	11.11 ± 1.99	1.0000
<i>L5-1971 FV₁ Sub</i>	8	75.66	25.3	0	6.35 ± 0.93	5.28 ± 2.55	0.9801
L5-1989 TX ₁₁	5	28.26	9.45	0	10.8 ± 1.35	4.33 ± 2.38	0.9248
L5-Phereclos	17	94.62	31.64	0.01	9.97 ± 5.41	8.14 ± 3.84	0.8886
<i>L5-Pandarus Sub</i>	5	82.03	27.43	0.04	18.61 ± 0.94	7.48 ± 3.44	0.9996
<i>L5-Phereclos Sub</i>	12	94.62	31.64	0	10.61 ± 5.66	7.29 ± 3.49	0.889
L5-Troilus	13	100.48	33.6	0.09	18.95 ± 7.41	12.88 ± 5.81	1.0000
<i>L5-Troilus Sub</i>	5	100.48	33.6	0	15.95 ± 5.0	8.2 ± 4.36	1.0000
<i>L5-1988 RV₁₁ Sub</i>	5	39.75	13.29	0.2	22.58 ± 6.65	10.33 ± 4.42	1.0000
L5-Cebriones	17	95.98	32.09	0.23	24.9 ± 10.97	19.04 ± 7.42	1.0000
<i>L5-Bitias Sub</i>	7	47.99	16.05	0.35	23.47 ± 9.83	13.74 ± 4.09	0.9798
L5-Greater Aeneas	64	118.22	39.53	0.2	65.85 ± 34.23	38.7 ± 20.27	0.8884
L5-1988 RH ₁₃	6	53.1	17.76	0.65	36.74 ± 22.51	23.44 ± 15.43	0.9350
L5-1994 CO	5	47.73	15.96	0.13	28.95 ± 5.47	21.4 ± 11.93	0.9997
L5-1989 UQ ₅	5	25.91	8.66	0	25.34 ± 4.92	9.72 ± 7.17	1.0000
L5-Sarpedon	17	77.48	25.91	0.04	23.15 ± 13.77	18.98 ± 6.16	0.9596
<i>L5-Hippokoon Sub</i>	5	18.43	6.16	0	12.03 ± 4.65	9.9 ± 5.74	1.0000
<i>L5-Sarpedon Sub</i>	11	77.48	25.91	0.04	16.65 ± 13.65	15.97 ± 9.07	0.9596
L5-Aeneas	26	118.22	39.53	0.2	34.55 ± 18.97	22.42 ± 13.03	0.9544
<i>L5-Helicaon Sub</i>	5	32.54	10.88	0.27	8.95 ± 3.27	7.18 ± 3.51	1.0000
<i>L5-Iphidamas Sub</i>	5	49.53	16.56	0.33	15.8 ± 6.57	13.08 ± 5.2	0.9795
<i>L5-Aeneas Sub</i>	8	118.02	39.47	0.07	30.7 ± 20.66	23.17 ± 13.27	0.9744
L5-Greater Astyanax	80	126.29	42.23	0.45	92.28 ± 43.46	50.89 ± 28.51	0.9647
L5-Mentor	20	126.29	42.23	0.41	48.51 ± 24.27	32.58 ± 18.62	0.9732
<i>L5-1988 RR₁₀ Sub</i>	5	29.08	9.72	0	19.21 ± 3.39	9.84 ± 4.86	1.0000
<i>L5-Mentor Sub</i>	10	126.29	42.23	0.58	36.72 ± 8.02	24.68 ± 11.69	0.9732
L5-Helenos	11	34.05	11.39	0.12	40.81 ± 19.19	21.03 ± 11.21	1.0000
L5-Astyanax	41	53.98	18.05	0.55	141.79 ± 42.59	42.8 ± 28.01	0.9735
<i>L5-Ophelestes Sub</i>	5	32.39	10.83	0.18	20.79 ± 12.53	13.7 ± 6.25	1.0000
<i>L5-Astyanax Sub</i>	6	53.98	18.05	0.54	99.92 ± 57.95	55.04 ± 28.89	0.9796
<i>L5-Acamas Sub</i>	6	43.86	14.67	0.74	102.44 ± 11.67	31.58 ± 31.34	1.0000
<i>L5-1989 UX₅ Sub</i>	9	32.19	10.76	0.56	15.28 ± 8.38	12.97 ± 7.93	0.9735

2146 Stentor (1976 UQ) and 9799 (1996 RJ), in the data set. Three additional objects, 7641 (1986 TT₆), 83983 (2002 GE₃₀) and 88225 (2001 BN₂₇), have a corresponding SDSS ($g - r$) colour (0.57 to 0.7), indicating that perhaps there is a diagnostic feature for the clan in the visible range.

Idomeneus clan: The small Idomeneus clan (six members), Fig. B1 (c) contains two D-types, 2759 Idomeneus (1980 GC) and 4063 Euforbo (1989 CG₂), along with a small ΔV_m ($9.81 \pm 3.51 \text{ ms}^{-1}$), and large reference object, 3793 Leonteus (1985 TE₃). This clan also includes 4063 Euforbo (1989 CG₂), a 95.62 km

object. The clan is entirely stable, with no clones of any member escaping. The members have a relatively low range of reference angle values, fairly close to the 60° Lagrange point (60.44° to 61.77°), though with a comparatively low libration range (19.43° to 29.64°). The clan has a small spread of SDSS colours, particularly in the $(u - g)$ colour (1.23–1.51). In the MOVIS survey there are narrow $(Y - J)$ (0.29 to 0.38) and $(J - K_s)$ colour ratios (0.49–0.72). The narrow ranges indicate that the colours, along with the dynamics are diagnostic for this clan.

Thersander clan: The Thersander clan, named after 9817 Thersander (6540 P–L) contains 10 objects, and is highlighted in Fig. B1 (i). This unaffiliated clan, includes 21900 Orus (1999 VQ₁₀), a provisionally allocated D-type that is the target of the *Lucy* mission. In the clan, there is also 24341 (2000 AJ₈₇), an identified C-type (Fornasier et al. 2007). Close to this clan, there are several members of the Eurybates family, 24341 (2000 AJ₈₇), a C-type, 9818 Eurymachos (6591 P–L), a P/X-type (Fornasier et al. 2007; Hasselmann et al. 2012) and 65225 (2002 EK₄₄). This could have implications for classification of 21900 Orus (1999 VQ₁₀), see Section 5 for discussion. The compact SDSS colours are due to only a single object, 53477 (2000 AA₅₄), found in the survey. In terms of escapes, a low number of clones escape the swarm, mainly from 14268 (2000 AK₁₅₆) and 24531 (2001 CE₂₁).

3.1.2 Greater Achilles superclan

The Greater Achilles superclan contains 35 objects, grouped into three distinct groups, the Epeios (discussed below), 1991 EI and Achilles clans, as shown in Fig. B2. The type object, 588 Achilles (1906 TG), has been classified as a DU-type (Tholen 1989). The majority of the objects in the superclan are classified as D-type, with just two exceptions, both of which are members of the Epeios clan: 12921 (1998 WZ₅), a X-type, and 5283 Pyrrhus (1989 BW), which is unclassified, but has an unusual negative spectral slope in Bendjoya et al. (2004).

If the more traditional δV_{ref} of the superclan is considered, the Eios ($19.55 \pm 7.42 \text{ m s}^{-1}$) and 1991EI ($17.37 \pm 13.7 \text{ m s}^{-1}$) clans have larger dispersal velocities than the Greater Achilles superclan ($16.91 \pm 11.2 \text{ m s}^{-1}$), whilst the Epeios ($8.57 \pm 4.42 \text{ m s}^{-1}$) and Achilles ($8.65 \pm 6.54 \text{ m s}^{-1}$) clans have smaller ΔV cent than the superclan ($4.4 \pm 8.6 \text{ m s}^{-1}$).

The Greater Achilles superclan is relatively stable ($0.057 F_{\text{esc}}$). Only 160534 (1996 TA₅₈), a member of the Achilles clan, has a high escape fraction (0.78). This is not surprising, as the superclan has a low range of δa_{prop} (0.0 to 0.05 au), and is close to the 60° Lagrange point (59.1° to 63.1°).

Epeios clan: The Epeios clan, named for 2148 Epeios (1976 UW), contains 10 members. The type object was also in the non-canonical Epeios collisional family (Vinogradova 2015). This non-canonical family was associated with the canonical Arkesilaos family (Nesvorný et al. 2015), of which we have no members represented. This could indicate with further characterization in future surveys, members of the Arkesilaos family could form part of this clan. This is supported by the fact that both the Epeios clan and Epeios collisional family (Vinogradova 2015) contain X-type objects.

In this clan, 5283 Pyrrhus (1989 BW) was unclassified, though it has an interesting negative slope in Bendjoya et al. (2004). Also, within this clan is 12921 (1998 WZ₅), an identified X-type (Fornasier et al. 2007). The Epeios clan is entirely stable, with no unstable members. There are a narrow range of SDSS colours, though there are only two members, 37710 (1996 RD₁₂) and 168364 (1996 TZ₁₉),

in the survey. Dynamically, this clan is close to the Lagrange point (59.1° to 61.77°), with small libration amplitudes (4.04° to 14.33°) and eccentricities (0.01 to 0.1).

This clan may contain a dynamical pair of objects, 258656 (2002 ES₇₆) and 2013 CC₄₁ (Holt et al. 2020b), the first such objects identified in the Trojan population. Unfortunately neither of these objects are included in this analysis, due to their lack of presence in wide-field surveys. The Epeios clan does not include any D-types, but has a X-type, 12921 (1998 WZ₅) (Fornasier et al. 2007), and an object with a potential negative slope, 5283 Pyrrhus (1989 BW) (Bendjoya et al. 2004). These associations are an indication that the 258656-2013 C₄₁ pair may have different properties to the majority of the Jovian Trojans.

3.1.3 Greater Nestor superclan

The Great Nestor superclan consists of 37 objects shown in Fig. 4 and includes two distinct clans, Eurymedon and Nestor, as well as several additional members that are not associated with any individual clan. We discuss the Nestor clan in detail below. Whilst most of the Trojans are D-types (72.2 per cent), the Greater Nestor superclan contains two large members of other taxonomic types, 659 Nestor (1908 CS), a XC-type (Tholen 1989) and 5012 Eurymedon (9507 P–L), a C-type (Hasselmann et al. 2012), each is the type object of their respective clan. Based on the simulations described in Holt et al. (2020a), the Greater Nestor superclan has the largest escape fraction of any superclan in the L₄ swarm, with fully 63 per cent of all test particles generated based on clan members escaping from the Trojan population on a time-scale of 4×10^9 yr. The more stable members are located in the two clans, but though those clans still exhibit escape fractions higher than the base L₄ escape fraction (at 0.3 and 0.4, respectively). The superclan, as a whole, has an average δa range (0.03 to 0.11 au), with relatively high eccentricities (0.07 to 0.17).

Nestor clan: This clan contains seven objects, two of which have been taxonomically identified, the XC-type 659 Nestor (1908 CS), and D-type 4060 Deipylos (1987 YT₁) (Bendjoya et al. 2004). Holt et al. (2020a) noted a slightly larger escape rate amongst the X-types in the Trojans, and this is reflected in this clan. The Nestor Clan has a relatively high escape fraction (0.4), versus that of the L₄ swarm (0.23) as a whole. The members of the clan all display centres of libration that are slightly ahead of the 60° point (60.44° to 64.43°), though the range of amplitudes is relatively small (14.33° to 24.54°). With the diversity of taxonomic types within the clan, it is not surprising that the members also display a wide range of SDSS colours, $(b - v)$: 0.65–0.99, $(u - g)$: 1.62–2.29, $(g - r)$: 0.43–0.77, $(r - i)$: 0.18–0.27. The narrow range of MOVIS values are due to only a single representative of the clan, 4060 Deipylos (1987 YT₁), $(Y - J)$: 0.241, $(J - K_s)$: 0.547, $(H - K_s)$: 0.137, in the survey.

3.1.4 Greater Ajax superclan

The 29 objects in this superclan, and the associated Ajax and Eurybates clans, are shown in Fig. 4. We use this superclan, and the following detailed discussion of both clans, as examples for the rest of the consensus trees, found in Appendix B. This superclan includes the many members of the Eurybates collisional family. The cluster is not named the ‘Eurybates superclan’, as 1404 Ajax (1936 QW) was discovered in 1936 (Wyse 1938), nearly 40 yr before 3548 Eurybates (1973 SO). This superclan is one of the most complex in the L₄ swarm, with multiple subclans in each clan. Apart from one unassociated object, 100619 (1997 TK₁₄), all objects are in one of the

clans. In terms of escapes, the Greater Ajax superclan has a higher escape fraction (0.38) than the L₄ swarm as a whole. The group is dynamically diverse, though they have a compact δa_{prop} range (0.07° to 0.11°). Relatively compact SDSS values, $(b - v)$: 0.65–0.93, $(u - g)$: 1.25–1.72, $(g - r)$: 0.43–0.7, $(r - i)$: 0.15–0.29, may be an actual feature of this superclan, as eight of the 29 superclan objects are represented in the SDSS survey, though the $(i - z)$ colour has quite a wide range (−0.03–0.26).

Ajax clan: In this clan there are three subclans (Ajax, Hiera, and 2002 CQ₁₃₄), each consisting of four objects in a branching format. The Hiera and 2002 CQ₁₃₄ subclans form a sister group to the Ajax subclan. Unfortunately, there are no taxonomically identified members of this clan. With the close association to the Eurybates family, this makes the three largest members of the clan, 1404 Ajax (1936 QW), 4086 Podalirius (1985 VK₂), and 7119 Hiera (1989 AV₂), all of which have an absolute H-magnitude greater than 9, of particular interest for future telescope observations (see Section 4). Most of the escapes in the Greater Ajax superclan come from this clan. The 2002 CQ₁₃₄ subclan has a large escape fraction (0.81), with all members having an escape fraction over 0.65.

The clan is located well ahead of the 60° point, with mean libration angle between 63.1° and 65.76°. The clan does have a relatively narrow range of dynamical values (Δa_{prop} : 0.09 au–0.11 au, e_{prop} : 0.03–0.08, $\text{sin} i_{\text{prop}}$: 0.28–0.49), that could be diagnostic. In addition, some of the SDSS values may also be diagnostic, $(b - v)$: 0.86–0.93, $(u - g)$: 1.44–1.63, $(g - r)$: 0.63–0.7, $(r - i)$: 0.15–0.24, with three members of the clan represented, 4086 Podalirius (1985 VK₂), 24403 (2000 AX₁₉₃), and 42367 (2002 CQ₁₃₄). Two additional members, 207749 (2007 RC₂₈₆) and 316158 (2009 UW₂₆), are represented in the MOVIS data set with similar values, $(Y - J)$: 0.469–0.494, $(J - K_s)$: 0.608–0.712. The range of *Gaia* values from six different sized members is broader (17.29–18.93 mag), highlighting the need for further investigations into members of this clan.

Eurybates clan: There are two subclans (Anius and Eurybates) in this clan. The Anius subclan has five members, with two duos and a single object, in a 1:2:2 format. The Eurybates subclan (eight members), as expected for the group containing many members of the Eurybates collisional family (Brož & Rozehnal 2011; Nesvorný et al. 2015), has a comparatively complex structure (three duos and two singles in 2:1:1:2:2 format). The type object of Eurybates clan, 3548 Eurybates (1973 SO) is a target for the *Lucy* mission. There are three other Eurybates family members, 39285 (2001 BP₇₅), 24380 (2000 AA₁₆₀), 28958 (2001 CQ₄₂), all C-types (Fornasier et al. 2007), in close association under the Eurybates subclan. The other four members of the Eurybates subclan, 39793 (1997 SZ₂₃), 137879 (2000 AJ₁₁₄), 312457 (2008 QH₄₂), 315208 (2007 RS₂₂), and possibly two in the Anius subclan, 12917 (1998 TG₁₆) and 111932 (2002 GG₃₃), are likely previously unidentified members of the collisional family. The age of this collisional family has been identified as approximately $1.045 \pm 0.364 \times 10^9$ yr (Holt et al. 2020a). With that long an age, the possibility for interlopers is quite high, as the true members of the collisional family disperse. 18060 (1999 XJ₁₅₆) is a X-type in Fornasier et al. (2007), and the corresponding SDSS colours, $(b - v)$: 0.70, $(u - g)$: 1.69, $(g - r)$: 0.48, $(r - i)$: 0.21, $(i - z)$: 0.06, are different to other members. The Eurybates clan, which includes members of the Eurybates collisional family, has a lower escape fraction (0.23) than the superclan as a whole (0.38). The clan escape fraction (0.23) is similar to the escape fraction of the Eurybates collisional family (0.1881) found by Holt et al. (2020a). If we disregard the X-type (18060 (1999 XJ₁₅₆), $(g - r)$: 0.48), the SDSS $(g - r)$ colour is contained within a single bin, $(g - r)$: 0.633–0.7.

3.1.5 Greater Hektor superclan

This superclan contains the only member of the Hektor collisional family (Rozehnal et al. 2016), 624 Hektor (1907 XM), considered in our analysis. The superclan also contains many other objects identified as D-type (Roig et al. 2008; Rozehnal et al. 2016). The exception, 5285 Krethon (1989 EO₁₁), is a XD-type (Bendjoya et al. 2004) in the Thersites clan, which with further examination could be reidentified as a true D-type. In the superclan, the ΔV_{ref} and ΔV_{cent} are similar (31.47 ± 19.35 and 28.99 ± 21.63 ms^{−1}), as well as in both clans (Thersites clan: 34.57 ± 33.85 and 27.49 ± 23.04 ms^{−1}, Hektor clan: 31.43 ± 16.53 and 27.93 ± 16.05 ms^{−1}), with each of mean velocities being smaller than the V_{esc} of 624 Hektor (1907 XM) (75.24 ms^{−1}).

Dynamically, the superclan is ahead of the Lagrange point (63.1° to 68.4°), with a fairly high libration range (34.75° to 60.27°) and δa_{prop} (0.09 to 0.12 au). Some of the compact range of SDSS values, $(b - v)$: 0.72–0.86, $(u - g)$: 1.16–1.63, $(g - r)$: 0.5–0.63, $(i - z)$: 0.09–0.2, could be diagnostic, but a wider range of other colours, $(r - i)$: 0.18–0.29, MOVIS, $(Y - J)$: 0.02–0.46, $(J - K_s)$: 0.37–1.18, and *Gaia* (15.11–18.38 mag) are indicative of heterogeneity in the superclan.

Thersites clan: As with the superclan, almost all members of this clan are identified as D-types (1868 Thersites (2008 P-L), 4946 Askalaphus (1988 BW₁), 2797 Teucer (1981 LK), 20995 (1985 VY); Bendjoya et al. 2004; Hasselmann et al. 2012). Most of the unstable members of the Hektor superclan are in the Thersites clan, with six members of the clan having all nine clones escape, 2797 Teucer (1981 LK), 4946 Askalaphus (1988 BW₁), 8317 Eurysaces (4523 P-L), 20995 (1985 VY), 37298 (2001 BU₈₀), and 266869 (2009 UZ₁₅₁). This clan has higher eccentricity (0.03 to 0.11) and libration range (39.85°–60.27°) compared with the Hektor clan. As with the superclan, the SDSS colours are compact, $(b - v)$: 0.79–0.86, $(u - g)$: 1.35–1.53, $(g - r)$: 0.57–0.63, $(r - i)$: 0.23–0.29, $(i - z)$: 0.09–0.2, and with four members in the survey, 2797 Teucer (1981 LK), 4946 Askalaphus (1988 BW₁), 20995 (1985 VY) and 38606 (1999 YC₁₃), could be diagnostic. There are three members represented in MOVIS, 173086 Nireus (2007 RS₈), 200023 (2007 OU₆), 264155 (2009 VJ₁₀₉), and 266869 (2009 UZ₁₅₁), though 264155 (2009 VJ₁₀₉), has quite different colours, $(Y - J)$: 0.294, $(J - K_s)$: 1.004, compared to the other three, $(Y - J)$: 0.398–0.492, $(J - K_s)$: 0.309–0.909.

Hektor clan: The type object of this clan, 624 Hektor (1907 XM), is the largest object in the Jovian Trojan population (225 km; Marchis et al. 2014). It is also the largest member of the Hektor collisional family (Rozehnal et al. 2016). Unfortunately, 624 Hektor (1907 XM) is the only member of the collisional family studied in this analysis, therefore any conclusions about potential family memberships are speculative at best. Most of the instability in this clan is confined to two members, 24275 (1999 XW₁₆₇) and 42230 (2001 DE₁₀₈), both of which have only a single clone remaining at the end of the Holt et al. (2020a) simulations. The clan has a reasonably high Δa_{prop} values (0.09–0.12 au). As with the Hektor superclan, most of the SDSS colours, $(b - v)$: 0.72–0.86, $(u - g)$: 1.16–1.63, $(g - r)$: 0.5–0.63, $(i - z)$: 0.09–0.2, are compact, with a range of $(r - i)$ (0.18–0.29), MOVIS, $(Y - J)$: 0.02–0.46, $(J - K_s)$: 0.49–1.18, and *Gaia* (15.11–18.38 mag) values. The type object, 624 Hektor (1907 XM), shows a level of heterogeneity in the spectra (Perna et al. 2018), agreeing with the compact values for the clan. Interestingly, 1583 Antiochus (1950 SA) and 3801 Thrasymedes (1985 VS), were identified as potential asteroid pair (Milani 1993), though this was not confirmed by Holt et al. (2020b). In our analysis these two objects are next to one another in the dendritic tree (Fig. B5), lending strength to our analysis.

3.1.6 Greater Diomedes superclan

This is the largest superclan in the L₄ swarm, with 71 members. It also has the largest ΔV_{ref} of any superclan ($108.79 \pm 36.64 \text{ ms}^{-1}$). The ΔV_{cent} is more reasonable ($41.85 \pm 23.23 \text{ ms}^{-1}$), closer to the V_{esc} of 1437 Diomedes (1937 PB) (39.3 ms^{-1}), the type object of the superclan. The superclan includes two *Lucy* targets, 11351 Leucus (1997 TS₂₅) and 15094 Polymele (1999 WB₂). They are both provisionally classified differently, with 15094 Polymele (1999 WB₂) being a X-type (Buie et al. 2018; Souza-Feliciano et al. 2020) and 11351 Leucus (1997 TS₂₅) a D-type (Buie et al. 2018). They are in two separate clusters, with 5094 Polymele (1999 WB₂) not in any clan, and 11351 Leucus (1997 TS₂₅) in the Diomedes clan with another DX-type, 1437 Diomedes (1937 PB). The dynamical stability of the different clans within the superclan is markedly variable, with some significantly less stable than others (e.g. Diomedes clan which has an escape fraction of 0.76, compared to the Philoctetes clan, with an escape fraction of 0.38). The escape rates within each clan, however, are relatively consistent – so all objects within an unstable clan are similarly unstable, whilst those in the stable clans are all relatively stable, and each of these clans has a larger escape fraction than that of the overall L₄ swarm (0.2335).

Philoctetes clan: This clan with 26 members, displays a high diversity of taxonomic types, three X-types (19725 (1999 WT₄), 24233 (1999 XD₉₄) and 23963 (1998 WY₈); Hasselmann et al. 2012), a C-type (24420 (2000 BU₂₂); Fornasier et al. 2007), and a D-type (9590 (1991 DK₁); Hasselmann et al. 2012) in the Andraimon subclan. This clan also contains three members of the Eurybates family (24420 (2000 BU₂₂), 111805 (2002 CZ₂₅₆) and 24426 (2000 CR₁₂); Nesvorný et al. 2015), and a fourth non-canonical member (63291 (2001 DU₈₇); Rozehnal et al. 2016). A large fraction of this clan is represented in the SDSS data base (0.6923), with relatively compact colours, ($b - v$): 0.58–0.93, ($u - g$): 1.16–1.63, ($g - r$): 0.37–0.7, ($i - z$): –0.03–0.2, though there is a wide ($r - i$) range (0.1–0.24). There is only a single representative of the clan in the *Gaia* survey (19725 (1999 WT₄), 18.67 mag), so the value range here is only indicative. As the largest object in the clan, 1869 Philoctetes is relatively small (33.96 km), the V_{esc} (11.36 ms^{-1}) is lower than the ΔV_{ref} ($25.1 \pm 7.9 \text{ ms}^{-1}$).

Diomedes clan: This mid-sized (12 members) clan contains 11351 Leucus (1997 TS₂₅), a D-type (Fornasier et al. 2007) *Lucy* target. The type object of the clan, 1437 Diomedes (1937 PB) is also classified as a DX-type (Tholen 1989). The ΔV_{cent} for the clan is relatively high ($56.9 \pm 28.09 \text{ ms}^{-1}$), though close to the V_{esc} of the large type object (39.3 ms^{-1}). With relatively high Δa_{prop} values (0.11 to 0.16 au) and mean centre of libration values (67.09° to 73.74° ; Amplitude: 50.06° to 75.59°), it is unsurprising that this clan has a high escape rate (0.76). In the SDSS data set, there are only three members represented, 5209 (1989 CW₁), 43706 Iphiklos (1416 T-2), and 83977 (2002 CE₈₉), and with only two in the MOVIS data base, 11397 (1998 XX₉₃) and 65228 (2002 EH₅₈), it is difficult to make any conclusions regarding colour distribution. The wide range of *WISE* (W1: 0.08–0.26, W2: 0.06–0.28) albedos indicate that there is a variety of compositions in this clan.

3.1.7 Greater Telamon superclan

The Greater Telamon superclan which has 35 members, including three separated clans, Telmon, Kalchas, and Theoklymenos. The Telmon and Kalchas clans are relatively small, with 5 and 6 members, respectively. The Theoklymenos clan is larger, at 19 members, and contains a X-type (5023 Agapenor (1985 TG₃); Hasselmann et al.

2012), and two D-types (24390 (2000 AD₁₇₇ and 3063 Makhaon (1983 PV); Lazzaro et al. 2004; Fornasier et al. 2007). We discuss the Kalachas clan in more detail below.

This is one of the most stable superclans (F_{esc} : 0.05) in the Trojan population. Most of the escape values in the superclan originate with the type object, 1749 Telamon (1949 SB), where all nine particles escape (Holt et al. 2020a). Within this only superclan 3063 Makhaon (1983 PV) has a higher escape fraction (0.33) higher than the L₄ swarm (0.23).

Other superclan members have all nine clones stay in the L₄ Trojan region. With moderate Δa values (0.04–0.09 au) and a location near the Lagrange point (59.61° to 64.43°), this stability is not surprising. In general, the clan has low *WISE* albedos (W1: 0.102–0.239, W2: 0.102–0.251). The exception is 24225 (1999 XV80) (W1:0.378, W2:0.378), which extends the ranges of the superclan as well as the Theoklymenos clan. The SDSS values are relatively diverse, ($b - v$): 0.65–0.93, ($u - g$): 1.35–1.72, ($g - r$): 0.43–0.7, ($i - z$): –0.03–0.26), particularly the ($r - i$) colour (0.16–0.34).

Kalachas clan: The Kalachas clan contains two X-type objects, 4138 Kalchas (1973 SM) and 7152 Euneus (1973 SH₁) (Bendjoya et al. 2004), both of similar size (46.46 and 45.52 km, respectively). The smaller of the two, 7152 Euneus (1973 SH₁) has a low ΔV_{ref} (5.4 ms^{-1}) to 138 Kalchas (1973 SM), which is the reference object for the clan. Even though they were not identified in Holt et al. (2020b), their ΔV_{ref} , similar properties and sizes, indicate that these two large objects could be an ancient disrupted binary pair (Vokrouhlický & Nesvorný 2008; Pravec et al. 2019).

All members of this clan are stable over the life of the Solar system (Holt et al. 2020a). The clan has very low proper eccentricities (0.0161–0.0532) and $\sin i$ (0.0102–0.119) values, and with mid-range δa_{prop} values, places the clan within the stable parameter space (Nesvorný 2002; Di Sisto et al. 2014; Hellmich et al. 2019; Holt et al. 2020a). The ΔV_{ref} of the clan is relatively small ($16.88 \pm 10.7 \text{ ms}^{-1}$), and close to the V_{esc} of 4138 Kalchas (1973 SM) (15.5 ms^{-1}). With a relatively high fraction of objects (50 per cent) represented in the SDSS catalogue, the ($b - v$), ($u - g$), ($g - r$), and ($i - z$) colours are possibly diagnostic, ($b - v$): 0.72–0.86, ($u - g$): 1.44–1.72, ($g - r$): 0.5–0.7, ($i - z$): 0.09–0.15. The range of ($r - i$) SDSS colours (0.16–0.23) are mainly due to 89924 (2002 ED₅₁), ($r - i$): 0.225 being a possible outlier.

3.1.8 Greater Odysseus superclan

The Odysseus superclan (36 members) contains two clans, Epistrophs (5 members) and Odysseus (20 members), neither of which is discussed here in detail. There is a diversity of taxonomic types in this superclan. The type object, 1143 Odysseus (1930 BH) is classified as a D-type (Tholen 1989), though there are two other objects with taxonomic classifications, namely 24882 (1996 RK₃₀) which is an X-type, and 21372 (1997 TM₂₈) classified as a C-type (Hasselmann et al. 2012). The Epistrophos clan contains two D-types (39293 (2001 DQ₁₀) and 23382 Epistrophos (4536 T-2); Hasselmann et al. 2012). There is a X-type (13463 Antiphos (5159 T-2); Fornasier et al. 2007), another D-type (15535 (2000 AT₁₇₇); Fornasier et al. 2007), and a X-type (24485 (2000 YL₁₀₂); Hasselmann et al. 2012), that are not associated with any clan.

The range of albedos and colours reflect the diversity in the superclan. Much of this can, however, be explained by several outliers, for example, 9713 Oeax (1973 SP₁) in the Odysseus clan has high *WISE* (W1:0.336, W2:0.336) and geometric (0.168) albedos compared with the rest of the objects. A particularly interesting object

is 128383 (2004 JW₅₂), in terms of its colours. The SDSS colours for 128383 (2004 JW₅₂) are high for $(b - v)$ (1.55) and $(g - r)$ (1.3), but low for $(i - z)$, (-0.55), the opposite of the rest of the superclan, $(b - v)$: 0.649–0.857, $(g - r)$: 0.433–0.7, $(i - z)$: -0.0167 – -0.25 . This one outlier accounts for much of the SDSS variation.

The superclan (ΔV_{cent} : $18.41 \pm 9.07 \text{ ms}^{-1}$) and clans (Odysseus: ΔV_{cent} : $12.54 \pm 8.43 \text{ ms}^{-1}$) are fairly compact, particularly the Epistrophos clan (ΔV_{cent} : $6.99 \pm 2.47 \text{ ms}^{-1}$). This superclan is also quite stable (F_{esc} : 0.11), with the majority of the instability coming from the unaffiliated superclan members, such as 22404 (1995 ME₄), where all the clones escape. The Epistrophos and Odysseus clan members are all completely stable, due to both sets being close to the Lagrange point (60.44° to 61.77° and 59.1° to 61.77° , respectively).

3.2 L₅ swarm

In our analysis of the L₅ swarm, we present a consensus tree of 407 objects in Fig. 6. A total of 10 000 equally parsimonious trees took approximately 10 h 26 min to find using a single core of Intel Xeon W-2133 CPU at 3.60 GHz. The consensus tree has a length of 1984.79, with a consensus index of 0.113 (Brooks et al. 1986) and retention index of 0.712 (Naylor & Kraus 1995). The superclans, clans, and subclans identified in the L₅ swarm are listed in Table 3. In the L₅ swarm, there are seven clans unaffiliated with any superclan with six subclans within them. There is a small number of large superclans (three), compared with the L₄ swarm, and each superclan contains a larger number of clans and subclans. In total there are 14 clans containing a total of 14 subclans. Overall, the L₅ swarm contains more hierarchical structure than the L₄ swarm, shown in Fig. 6.

In the L₅ swarm, there are two canonical collisional families, 2001 UV₂₀₉ and the larger Ennomos family (Nesvorný et al. 2015). Vinogradova (2015) questioned the existence of any collisional families in the L₅ swarm, though they did note some clustering around 247341 2001 UV₂₀₉, 11487 (1988 RG₁₀), and 4709 Ennomos (1988 TU₂). Rožehnal et al. (2016) has a similar data set to the canonical one, with a few extra objects. The non-canonical 2001 UV₂₀₉ and several Ennomos family members are in the Cebriones and Troilus clans of the Greater Patroclus superclan, along with the two canonical Ennomos family members. The Ennomos family is more problematic. In our subset, there are nine members, spread throughout the L₅ swarm. There is a small cluster of three members in the Aeneas clan, though the largest member of the collisional family, 4709 Ennomos (1988 TU₂), is located in the Cebriones clan, Greater Pratoclus superclan, with two other non-canonical members. The hierarchical structure seen in the L₅ swarm through astrocladistics could indicate that the dynamical history of the swarm is more complex than can be reliably identified by HCM, and as indicated by the lack of confident clusters in Vinogradova (2015).

3.2.1 Unaffiliated L₅ clans

There are seven clans that are unaffiliated with any superclan in the L₅ swarm. In this section, we discuss the Dolan (20 members), 1990 VU₁ (21 members) and Anchises (8 members) clans. The values for the other four clans, Asteropaios (17 members), Apisaon (9 members), Khryses (8 members), and 1990 VU₁ are available in the Github repository.⁹ In the superclan, the Asteropaios, Dolan and 1990 VU₁ each have two subclans, shown in Fig. B9, unlike the L₄

clans. All unaffiliated clans in the L₅ swarm are located between the Patroclus and Aeneas superclans in the tree. Except for the 1999 RU₂ clan, which does not contain any taxonomically identified objects, each clan contains at least one D-type object. Most of the unaffiliated clans have escape fractions higher than that of the L₅ swarm (0.2489; Holt et al. 2020a). The exception is the stable Asteropaios clan (F_{esc} : 0.06). The 1992 RU₂ (F_{esc} : 0.84) and Anchises clans (F_{esc} : 0.88) are particularly unstable.

Dolon clan: This clan contains 55419 (2001 TF₁₉), which is a member of the Ennomos collisional family (Nesvorný et al. 2015). In this clan there are three X-type objects (11554 Asios (1993 BZ₁₂), 32482 (2000 ST₃₅₄), and 29314 Eurydamas (1994 CR₁₈); Hasselmann et al. 2012), along with two D-types (9430 Erichthonios (1996 HU₁₀) and 11488 (1988 RM₁₁); Fornasier et al. 2004; Hasselmann et al. 2012), both located in the Erichthonios subclan. This diversity in types is reflected in the geometric (0.03–0.14) and WISE (W1: 0.07–0.29, W2: 0.08–0.3) albedo ranges of the clan. The clan is close (295.12° to 297.46°) to the L₅ Lagrange point (300°) resulting in an overall escape fraction (F_{esc} : 0.31) similar to the overall L₅ swarm (0.2489; Holt et al. 2020a), though the Erichthonios subclan is much more stable (F_{esc} : 0.04). The overall ΔV_{ref} and ΔV_{cent} of the clan are relatively high (46.28 ± 27.85 and $34.71 \pm 19.81 \text{ ms}^{-1}$, respectively), in comparison to the small reference object (V_{esc} : 14.22 ms^{-1}). The SDSS ($u - g$) (1.51–1.62), $(g - r)$ (0.48–0.64), and $(i - z)$ (0.01–0.18) as well as the MOVIS ($J - K_s$) (0.53–0.9) colours are compact and fairly diagnostic for the clan.

1990 VU₁ clan: There are two identified subclans (1990 VU₁ and Idaios subclans) in this clan. The type object, 1990 VU₁ has been identified as a XD-type (Bendjoya et al. 2004), with five other D-types (16070 (1999 RB₁₀₁), 58008 (2002 TW₂₄₀), 15977 (1998 MA₁₁), 30705 Idaios (3365 T-3) and 47969 (2000 TG₆₄); Fornasier et al. 2004; Hasselmann et al. 2012) present in the clan. In terms of stability, this clan has an escape fraction (0.52), nearly double that of the L₅ swarm as a whole (0.2489; Holt et al. 2020a). There is a wide variety of escape fraction of members in this clan, with all nine particles of the type object 1990 VU₁ escaping, but two other members, 30705 Idaios (3365 T-3) and 301760 (2010 JP₄₂), being completely stable. This range of stability is not unexpected, as the clan has a wide variance in ΔV_{cent} ($24.87 \pm 18.96 \text{ ms}^{-1}$), e_{prop} (0.04–0.14) and $\sin i_{\text{prop}}$ (0.01–0.43). The *Gaia* G magnitude is constrained (17.67–18.19 mag), with only four similar sized objects represented, more analysis is needed. The $(i - z)$ SDSS colour (0.05–0.317) has a narrow range in this clan.

Anchises clan: This clan is unstable (F_{esc} : 0.88), including all clones of the type object 1173 Anchises (1930 UB). This particular object was studied by Horner et al. (2012), who found that it will most likely escape the Trojan population and evolve to become either a Centaur or Jupiter family comet on hundred-million year time-scales. The clan is located a few degrees from the 300° Lagrange point (291.6° to 296.29°) with a decent range (32.05° to 51.55°) and δa_{prop} (0.08 to 0.12). The type object 1173 Anchises (1930 UB), along with 11089 (1994 CS₈) are X-types (Tholen 1989; Fornasier et al. 2004). There is also a D-type, (11552 Boucolion (1993 BD₄); Hasselmann et al. 2012) in this clan. In the *Gaia* G band, 1173 Anchises (1930 UB) shows a different value (16.75 mag) to the other two smaller, measured objects, 11089 (1994 CS₈) and 11552 Boucolion (1993 BD₄) (18.47 and 18.32 mag, respectively). Unfortunately, 1173 Anchises (1930 UB) was not observed in either of SDSS or MOVIS surveys. This is of note, as the SDSS ($b - v$) (0.69–0.93), $(g - r)$ (0.48–0.7), $(r - i)$ (0.2–0.27), as well as the

⁹<https://github.com/TimHoltastro/holt-et-al-2021-Jovian-Trojan-astrocladistics.git>

MOVIS ($Y - J$) (0.23–0.32) and ($J - K_s$) (0.44–0.53) colours are plausibly diagnostic of the clan.

3.2.2 Greater patroclus superclan

This large (133 members) superclan contains six clans, as shown in Fig. B10. Of these, we discuss the Memnon (23 members), Troilus (13 members), and Cebriones (17 members) clans in the following sections. The details of the other clans, 1971 FV₁ (18 members), 1989 TX₁₁ (5 members), and Phereclos (17 members), are available on the Github repository.¹⁰ There is a diversity of taxonomic types represented in this superclan, though as with other superclans, the members are predominantly D-types. Overall, the superclan is more stable (F_{esc} : 0.1) than the L₅ swarm as a whole. Each of the clans has a lower escape rate than the L₅ swarm, with several having no escapees, see Table 3, for details. The clan is clustered close to the 300° Lagrange point (296.29°–303.31°), with relatively low δa_{prop} (0.0–0.11 au).

The largest member of the Ennomos collisional family (4709 Ennomos (1988 TU₂); Nesvorný et al. 2015), is within this superclan, though it is not used as the type object. The actual type object, 617 Patroclus (1906 VY) was discovered over 80 yr earlier and thus is considered the type for the superclan, though it is not associated with any clan in this analysis. The binary 617 Patroclus (1906 VY) (Merline et al. 2001) is currently the only *Lucy* target in the L₅ swarm. The ΔV_{ref} to 617 Patroclus (1906 VY) ($31.57 \pm 20.49 \text{ ms}^{-1}$) is smaller than the V_{esc} (46.94 ms^{-1}) and similar to the ΔV_{cent} ($31.62 \pm 15.09 \text{ ms}^{-1}$).

Memnon clan: The Memnon clan has several D-types (30505 (2000 RW₈₂), 3317 Paris (1984 KF), 80119 (1999 RY₁₃₈), and 105808 (2000 SZ₁₃₅); Bendjoya et al. 2004; Hasselmann et al. 2012), though the type object, 2895 Memnon (1981 AE₁) is a C-type (Bendjoya et al. 2004). As with the superclan, this clan is stable (F_{esc} : 0.11) and close to the L₅ Lagrange point (296.29°–303.31°).

A representative of the 2001 UV₂₀₉ collisional family (37519 Amphios (3040 T-3); Nesvorný et al. 2015), is within this clan, and is the type object of the Amphios subclan, which has a small ΔV_{ref} ($14.06 \pm 8.13 \text{ ms}^{-1}$) and ΔV_{cent} ($13.04 \pm 7.89 \text{ ms}^{-1}$), close to the V_{esc} (12.83 ms^{-1}). The objects in this subclan may represent unidentified members of the 2001 UV₂₀₉ collisional family, or at least closely associated objects.

The clan has mid-range ($b - v$) (0.74–0.93), ($u - g$) (1.18–1.73), and ($g - r$) (0.52–0.7) SDSS colours, with high ($i - z$) values (0.12–0.34). The two MOVIS objects 295336 (2008 HY₈), ($Y - J$): 0.559373, ($J - K_s$): 0.973755, ($H - K_s$): 0.407764, and 369886 (2012 RM₆), ($Y - J$): 0.318022, ($J - K_s$): 0.585282, show quite different colours. Further characterization of the large objects in the clan, 2895 Memnon (1981 AE₁), 3317 Paris (1984 KF), and 37519 Amphios (3040 T-3), would be required to resolve this dichotomy in the colours.

Troilus clan: Within the clan there are two small subclans, the Troilus and 1988 RY₁₁ subclans. The Troilus subclan, which includes the type object, 1208 Troilus (1931 YA), of the clan, is entirely stable. The members of the 1988 RY₁₁ subclan have a higher escape fraction (F_{esc} : 0.2), though even this is lower than the overall L₅ escape fraction (0.2489).

The type object, 1208 Troilus (1931 YA), is an interesting case. It is the type object of the Troilus clan, which also contains a single

member of the Ennomos collisional family (76867 (2000 YM₅); Nesvorný et al. 2015). It is classified as FCU-type (Tholen 1989), designating it as an unusual object. It is the only ‘F-type’ in the Trojan swarm. This type was degenerated under the modern Bus–Demeo system (Bus 2002) into the B-types, closely associated with the other C-types in the Trojans. As the type object is relatively large, the ΔV_{ref} ($18.95 \pm 7.41 \text{ ms}^{-1}$) and ΔV_{cent} ($12.88 \pm 5.81 \text{ ms}^{-1}$) of the clan is lower than the V_{esc} (33.6 ms^{-1}). The clan is clustered centrally around the L₅ Lagrange point (298.63° to 302.14°), which likely indicates that it dates back to the time the Jovian Trojans were captured. The SDSS ($b - v$) (0.72–0.91), ($g - r$) (0.5–0.7), and ($i - z$) (0.07–0.23) colours are relatively constrained. An initial tight MOVIS bin is due to only a single object (299491 (2006 BY₁₉₈); Popescu et al. 2018).

Cebriones clan: 4709 Ennomos (1988 TU₂), the largest member of the Ennomos collisional family, is in the Cebriones clan (Nesvorný et al. 2015). Again, 4709 Ennomos (1988 TU₂) is not used as the type object, as the chosen type object, 2363 Cebriones (1977 TJ₃) was discovered earlier. A non-canonical family member, 32496 (2000 WX₁₈₂) (32496 (2000 WX₁₈₂); Rozehnal et al. 2016), is also in the clan. This is complicated by two members of the non-canonical 2001 UV₂₀₉ family (17171 (1999 NB₃₈) and 24470 (2000 SJ₃₁₀); Rozehnal et al. 2016) that are also present in the clan.

2363 Cebriones (1977 TJ₃) is a D-type object (Tholen 1989), and the only classified member of the clan. This clan has the highest escape rate in the Greater Patroclus superclan (F_{esc} : 0.23), and even this is lower than that of the overall L₅ swarm (0.2489; Holt et al. 2020a). In terms of colours, there are an insufficient number of multispectral observations to ascertain any trends, with only two members represented in the SDSS data, 17415 (1988 RO₁₀) and 129135 (2005 AD₂₁), and two different objects in MOVIS, 51969 (2001 QZ₂₉₂) and 53419 (1999 PJ₄).

3.2.3 Greater Aeneas superclan

This superclan (64 members) contains five clans, 1988 RH₁₃ (6 members), 1994 CO (5 members), 1989 UQ₅ (5 members), Sarpedon (17 members), and Aeneas (26 members) clans, with subclans in the Aeneas clan (Hippokoon and Sarpedon subclans) and Aeneas clans (Helicaon, Iphidamas and Aeneas subclans). The only clan discussed in detail here is the Aeneas clan. Almost all taxonomically identified members of this superclan are D-types (Tholen 1989; Bendjoya et al. 2004; Fornasier et al. 2004; Hasselmann et al. 2012). The only exception is 17419 (1988 RH₁₃), the type object of the 1988 RH₁₃ Clan, a C-type, though with a comparatively low confidence score (62; Hasselmann et al. 2012). Overall the superclan has a relatively low escape rate (F_{esc} : 0.2), when compared with the L₅ swarm (0.2489; Holt et al. 2020a). Within the Greater Aeneas superclan, the majority of unstable members are in the 1988 RH₁₃ Clan, which has an escape rate of 0.65. Other clans have a similar or lower escape rate than the superclan. Though 1172 Aeneas (1930 UA) is a large object (118.02 km), the reference object for the dispersal velocities in the superclan is 1867 Deiphobus (1971 EA) (118.22 km). The ΔV_{ref} ($65.85 \pm 34.23 \text{ ms}^{-1}$) is high. The ΔV_{cent} ($38.7 \pm 20.27 \text{ ms}^{-1}$), though still quite high, is closer to the V_{esc} (39.53 ms^{-1}).

Aeneas clan: The Aeneas clan contains several D-type objects, including the type object 1172 Aeneas (1930 UA) (Tholen 1989). The three members of the Ennomos collisional family present in the clan (36624 (2000 QA₁₅₇), 1867 Deiphobus (1971 EA), and 247967 (2003 YD₁₄₉); Nesvorný et al. 2015) form a cluster with 34746 2001 QE₉₁, however this does not fulfill the minimum requirements for

¹⁰<https://github.com/TimHoltastro/holt-et-al-2021-Jovian-Trojan-astrocladistics.git>

a subclan (five objects). There are three other subclans Helicaon, Iphidamas, and Aneas subclans, each containing at least one D-type. As in the Greater Aneas superclan, 1172 Aneas (1930 UA) is the dynamical reference object for ΔV_{ref} calculations. The overall escape fraction of the clan ($F_{\text{esc}}:0.2$) is similar to the Greater Aneas superclan ($F_{\text{esc}}:0.2$), though the Helicaon ($0.27 F_{\text{esc}}$) and Iphidamas ($0.33 F_{\text{esc}}$) subclans have a slightly higher rates. In the SDSS colours, ($b - v$) (0.649–0.857), ($g - r$) (0.5–0.633), and ($i - z$) (–0.0167–0.25) are relatively constrained. The ($u - g$) (1.294–1.847) and ($r - i$) (0.0682–0.267) values would also be relatively compact, except for the outlier 129147 (2005 CY70), which has comparatively high values, ($u - g$): 2.28, ($r - i$): 0.37.

3.2.4 Greater Astyanax superclan

This is the terminal superclan in the L_5 tree. It contains 809 members, of which 41 are in the Astyanax clan, discussed in detail below. The Mentor clan (20 members) is also discussed. The remaining Helenos clan contains 11 members, and the values are presented in the Github repository.¹¹

This superclan has a diversity of taxonomic types. The majority of the superclan is D-types, but the type object of the Mentor clan, 3451 Mentor (1984 HA₁) is a well recognized X-type (Bus 2002; Hasselmann et al. 2012). There are also two CX-types in the Astyanax clan (24454 (2000 QF₁₉₈) and 16560 Daitor (1991 VZ₅); Hasselmann et al. 2012). The Helenos clan contains one taxonomic identified member, 4829 Sergestus (1988 RM1), an XD-type (Fornasier et al. 2004). This diversity of taxonomic types is reflected in the wide range of all colour values (W1: 0.07–0.4, W2: 0.03–0.4, G-mag: 15.86–18.7 mag, ($b - v$): 0.65–0.91, ($u - g$): 1.18–1.95, ($g - r$): 0.44–0.68, ($r - i$): 0.07–0.4, ($i - z$): –0.26–0.29, ($Y - J$): 0.05–0.46, ($J - K_s$): 0.07–1.18, ($H - K_s$): 0.04–0.81). The superclan has a large ΔV_{ref} ($92.28 \pm 43.46 \text{ ms}^{-1}$) compared to the V_{esc} of the largest member, 3451 Mentor (42.2 m s^{-1}), though the ΔV_{cent} ($50.89 \pm 28.51 \text{ m s}^{-1}$) is more reasonable. The escape fraction of the supergroup (0.42) is higher than the L_5 swarm. The superclan has a large range of high δa_{prop} values (0.07–0.15 au), though the smaller values are limited to the 1988RR₁₀ subclan (δa_{prop} : 0.07–0.11) within the Mentor clan.

Mentor clan: 3451 Mentor (1984 HA₁), the type object of the Mentor clan, is a large (126.29 km) X-type (Bus 2002; Hasselmann et al. 2012). There is also a X-type (34785 (2001 RG₈₇); Fornasier et al. 2004), and two D-types (5130 Ilioneus (1989 SC₇) and 17416 (1988 RR₁₀); Fornasier et al. 2004). The ΔV_{ref} ($48.51 \pm 24.27 \text{ ms}^{-1}$) is close to the F_{esc} of 3451 Mentor (1984 HA₁) (42.23 ms^{-1}), and the ΔV_{cent} ($32.58 \pm 18.62 \text{ ms}^{-1}$). Even amongst the Trojans, which are some of the darkest objects in the Solar system (Grav et al. 2012), the Mentor clan has a range of low geometric (0.0367–0.107) and *WISE* (W1: 0.0557–0.171, W2: 0.0276–0.177; Grav et al. 2011, 2012) albedos. Unfortunately, there are only two representatives in the SDSS data set: 3451 Mentor (1984 HA₁) and 133862 (2004 BR₃₈), and only a single representative in the *MOVIS* data base, 289501 (2005 EJ₁₃₃), and therefore any comments on colours are preliminary.

Astyanax Clan: This is one of the largest clans in our analysis and at 41 members is larger than some superclans. Consequently, it does have a large ΔV_{ref} ($141.79 \pm 42.59 \text{ ms}^{-1}$) and ΔV_{cent} ($42.8 \pm 28.01 \text{ ms}^{-1}$) relative to the V_{esc} (18.05 ms^{-1}) of the small type object (1871 Astyanax (1971 FF), 53.98 km). Two of the subclans,

Table 4. Physical and observational parameters for the priority targets identified in this work, taken from the Asteroid Light-curve Data base (<http://www.minorplanet.info/lightcurvedatabase.html>, retrieved 2020 October 22; Warner, Harris & Pravec 2009). Here, P denotes the rotation period of the asteroid, and A_{min} and A_{max} are the minimum and maximum amplitudes of the asteroid’s light curve. H is the absolute magnitude of the asteroid, and p_V the geometric albedo.

Ast.no.	P (h)	A_{min} (mag)	A_{max} (mag)	H (mag)	p_V
659	15.98	0.22	0.31	8.71	0.040 ± 0.004
1173	11.60	0.16	0.73	8.91	0.035 ± 0.002
1208	56.17	–	0.20	9.00	0.037 ± 0.002
1404	29.38	–	0.30	9.41	0.050 ± 0.003
1437	24.49	0.34	0.70	8.21	0.028 ± 0.001
2456	7.24	0.05	0.27	9.37	0.026 ± 0.002
2895	7.52	0.08	0.48	10.14	–
4086	10.43	0.08	0.16	9.29	0.056 ± 0.004
4138	29.20	0.10	0.40	10.12	0.057 ± 0.007
4709	12.28	0.31	0.47	8.77	0.078 ± 0.005
5283	7.32	–	0.11	9.76	0.072 ± 0.007
7119	400.00	–	0.10	9.85	0.036 ± 0.005
7152	9.73	–	0.09	10.34	–
37519	50.93	–	0.30	11.10	–

Ophelestes (ΔV_{ref} : $20.79 \pm 12.5 \text{ ms}^{-1}$, ΔV_{cent} : $3.7 \pm 6.25 \text{ ms}^{-1}$) and 1989 UX (ΔV_{ref} : 15.28 ± 8.38 , ΔV_{cent} : $12.97 \pm 7.93 \text{ ms}^{-1}$), have low dispersal velocities, though these are higher than the V_{esc} of the respective type objects (52767 Ophelestes (1998 MW₄₁): 10.83 ms^{-1} and 9030 (1989 UX₅): 10.76 ms^{-1} , respectively). Within this clan, there are two members of the Enominos collisional family in this clan (17492 Hippasos (1991 XG₁) and 98362 (2000 SA₃₆₃); Nesvorný et al. 2015) clustered close together in the Astyanax subclan. The small *Gaia* range (17.836–18.381 mag) is due to only two objects being represented, 16560 Daitor (1991 VZ₅) and 17492 Hippasos (1991 XG₁). The majority of the objects (60.09 per cent) are in the SDSS colour set. The ($b - v$) (0.649–0.926) and ($g - r$) (1.183–1.958) values are low and constrained, where as the ($u - g$) (0.5–0.633) and ($i - z$)(–0.15–0.317) are on the high end and broad.

4 IDENTIFIED PRIORITY TARGETS

One of the outcomes of this work is to identify priority targets for future observations. Here, we collate these objects and describe the rationale for their selection. A summary of these objects is presented in Table 4.

1404 Ajax (1936 QW), 4086 Podalirius (1985 VK₂) and 7119 Hiera (1989 AV₂): These three objects are located in the Ajax clan. All three are fairly large, with H magnitudes brighter than 9. They are of interest due to a lack of taxonomically identified objects in the Ajax clan. This clan is close to the Eurybates clan, which contains multiple members of the Eurybates collisional family, along with 3548 Eurybates (1973 SO), a *Lucy* target.

2456 Palamedes (1966 BA₁): The largest object (H magnitude of 9.3) for the Thersites clan, which contains 21900 Orus (1999 VQ₁₀), a *Lucy* target. Only a single member of the clan, 53477 (2000 AA₅₄), has SDSS colour values. Further classification and observations of 2456 Palamedes (1966 BA₁) would help to provide context for the smaller *Lucy* target, 21900 Orus (1999 VQ₁₀), and the clan as a whole.

5283 Pyrrhus (1989 BW): This object is the largest in the Epeios clan. In Bendjoya et al. (2004), it is reported as having a negative spectral slope. Unfortunately, it not represented in either of the multiband

¹¹<https://github.com/TimHoltastro/holt-et-al-2021-Jovian-Trojan-astrocladistics.git>

surveys. This clan is of interest, as the only taxonomically identified object, 12921 (1998 WZ₅), a X-type amongst the prominently D-types of the Greater Achilles superclan. The 258656 (2002 ES₇₆)–(2013 CC₄₁) pair identified by Holt et al. (2020b) is also potentially in the Epeios clan, close to 5283 Pyrrhus (1989 BW).

659 Nestor (1908 CS): An XC-type amongst the mostly D-types of the L₄ Trojan swarm. It is also one of the largest members of the population (with a H magnitude of 8.99), and is the type member of the Greater Nestor superclan, which has a variety of taxonomic types. Additional observations of this object would help to understand the diversity of objects in the Trojan population.

1437 Diomedes (1937 PB): This is the type object of the Diomedes clan, which includes 11351 Leucus (1997 TS₂₅), a small *Lucy* target. Further observations of this object could provide more details on 11351 Leucus (1997 TS₂₅) (H mag: 10.7), and being a brighter object (with an absolute magnitude of 8.3), is able to be observed more easily. Like 2456 Palamedes (1966 BA₁), 1437 Diomedes (1937 PB) offers an opportunity to provide some context, prior to visitation of a related object by *Lucy*.

4138 Kalchas (1973 SM) and 7152 Euneus (1973 SH₁): These objects are identified X-types in a very stable clan, with absolute magnitudes of 10.1 and 10.2, respectively. Another large X-type in the population, 617 Patroclus (1906 VY), is part of a binary, and a *Lucy* target. Though not in the same clan, further investigations on 4138 Kalchas (1973 SM) and 7152 Euneus (1973 SH₁) could provide some details on other X-types in a stable configuration.

1173 Anchises (1930 UB): The subject of dynamical and thermophysical studies by Horner et al. (2012) and the type object of the unaffiliated L₅ Anchises clan. This object is one of the darkest objects (0.05 albedo) in the Trojan population, though it is quite large, over 100 km, and has an H -magnitude of 8.89. We echo the call of Horner et al. (2012) for further investigation into this object, particularly in broad-band colours, as the object is not represented in SDSS or MOVIS data bases.

2895 Memnon (1981 AE₁) and 37519 Amphios (3040 T-3): Both of these objects are located in the stable L₅ Memnon clan, part of the Greater Patroclus superclan. One of only two members of the 2001 UV₂₀₉ collisional family included in this analysis, is 37519 Amphios (3040 T-3) (Nesvorný et al. 2015), also in the Memnon clan. The objects are the type of their respective subclans. The Memnon clan is also the closest clan to 617 Patroclus (1906 VY), a *Lucy* target not affiliated with any clan. Both of these objects could provide additional information about the context of 617 Patroclus (1906 VY), though 2895 Memnon (1981 AE₁) is the cladistically closer object. 37519 Amphios (3040 T-3) is an interesting object in its own right, due to its affiliation with the 2001 UV₂₀₉ collisional family, and may be the largest remnant of the collision that created that family.

1208 Troilus (1931 YA): A relatively large object (H mag 8.99), 1208 Troilus (1931 YA) is the only F/B-type object identified in the Trojan swarm (Tholen 1989; Bus 2002). Though this taxonomic type is associated with the C-types, there are none identified in the Troilus clan. This could indicate that the object is unique in the Trojan population. Further detailed observations could help us to place this object in a wider small Solar system body context, and possibly identify previously unknown associations between the Jovian Trojans and other populations.

4709 Ennomos (1988 TU₂): The largest member of the Ennomos collisional family (Brož & Rozehnal 2011). The object is a member of the Cebriones clan, which has limited colour information. Further characterization of this object would help us to understand the diversity of collisional family members in the Jovian Trojans.

128383 (2004 JW₅₂): This relatively small object (H mag 13.1) was removed at the binning stage from the analysis, due to its anomalous colour. If the object was included, the SDSS colours would consist of two bins, this object and everything else. The object has high ($b - v$) and ($g - r$) colours (1.55 and 1.3, respectively) in comparison to the rest of the Jovian Trojan population (0.10–1.275 and 0.300–1.045), as well as low ($i - z$) values (−0.55, compared with −0.37–0.45). These anomalous values could be explained if the object was an interloper in the Trojan population, but this is contradicted by the stability. The object has an approximately 0.55 fractional escape rate, though only after spending an average of 3.7×10^9 in the L₄ Trojan swarm (Holt et al. 2020a). Further characterization and investigations into this object could help us to resolve this discrepancy and discover the history of the object.

5 Lucy CONTEXT

At the time of writing, five of the Jovian Trojans have been selected as targets to be visited by the *Lucy* spacecraft in the late 2020's to early 2030's (Levison et al. 2017). Each of these objects are included in our astrocladistical analysis, which allows us to provide additional information on the context of those targets, in advance of the mission.

3548 Eurybates (1973 SO) is the largest fragment of the Eurybates collisional family (Brož & Rozehnal 2011), and a member of the Greater Ajax superclan, as described in Section 3.1.4. Six other members of the preciously identified Eurybates collisional family, are also located within the clan. The majority of the objects that are thought to be closely associated with 3548 Eurybates (1973 SO) can be found in the Eurybates subclan, and are all classified as C-types (Fornasier et al. 2007). The C-types are relatively rare in the Trojan population, comprising only approximately 12.79 per cent by number, compared with over 60, by mass in the Main Belt (DeMeo & Carry 2013). Other members of the Eurybates clan include two D-types, 12917 (1998 TG₁₆) (Fornasier et al. 2007) and 5258 (1989 AU₁) (Bendjoya et al. 2004), and a X-type, 18060 (1999 XJ₁₅₆) (Fornasier et al. 2007), with all three in the Anius subclan, a sister subclan to the Eurybates subclan. This complexity of closely associate subclans, may indicate that 3548 Eurybates (1973 SO) may be different to other C-types.

15094 Polymele (1999 WB₂) is a member of the Greater Diomedes superclan, as described in Section 3.1.6, along with 11351 Leucus (1997 TS₂₅). It is not associated with any clan, though it is worth noting that if falls relatively close to the Philoctetes clan, which contains several X-types, a C-type, a D-type, and three members of the Eurybates collisional family. The diversity in this superclan, and the associated Philoctetes clan, means that it is hard to anticipate the physical nature of 15094 Polymele. It may have a shared heritage with any of the other members of the clan, and observations by *Lucy* may well shed new light on its true nature and affiliation.

11351 Leucus (1997 TS₂₅), like 15094 Polymele (1999 WB₂), is a member of the Greater Diomedes superclan. Specifically, 11351 Leucus (1997 TS₂₅) is located well within the Diomedes clan, and the type object 1437 Diomedes (1937 PB) (Tholen 1989) is a well recognized DX-type. This suggests that 11351 Leucus (1997 TS₂₅) is representative of the majority of D-type Jovian Trojans (Fornasier et al. 2007). This close association could imply that 11351 Leucus (1997 TS₂₅) has a common origin and physical composition to that larger object, and as such, that *Lucy*'s visit will provide valuable data on an object that could be representative of the majority of the Trojan population that is associated with the D-types.

21900 Orus (1999 VQ₁₀), located in the unaffiliated Thersander Clan, is another provisional D-type. The only other classified object

in the clan, 24341 (2000 AJ₈₇), is a C-type (Fornasier et al. 2007). In addition, there are several other closely associated C-types. This could suggest that 21900 Orus (1999 VQ₁₀) has a different composition to 11351 Leucus (1997 TS₂₅), despite both being designated D-types. This further highlights the diversity of taxonomic types in the Trojan swarms, and could be confirmed with analysis of the *Lucy* data, as it becomes available. Indications of the differences between 21900 Orus (1999 VQ₁₀) and 121351 Leucus (1997 TS₂₅) could be investigated using observations of 2456 Palamedes (1966 BA₁), the largest object in the Thersander clan, of which 21900 Orus (1999 VQ₁₀) is a member.

The 617 Patroclus (1906 VY)/Menoetius binary system is, so far the only *Lucy* target in the L₅ swarm. Being a large object, it is very well studied (Merline et al. 2001; Marchis et al. 2006), and has a well-established taxonomy as a X-type (Tholen 1989), though we note that in the original classification, as well as the *Lucy* documentation (Levison et al. 2017), it is a ‘P-type’. In our analysis, 617 Patroclus (1906 VY) is the type object for the Greater Patroclus superclan. The binary is not, itself, associated with any of the clans, although it is close to the Memnon clan. Part of the issue is that in our analysis 617 Patroclus (1906 VY) is not represented in the SDSS catalogue. The inclusion of these data could potentially bring the object into the Memnon clan. Being close to the Memnon clan may associate it with other large members, 2895 Memnon (1981 AE₁) and 37519 Amphios (3040 T-3), though neither of these have any colour values, beyond the size-dependent *Gaia* G magnitudes. The relatively large 37519 Amphios (3040 T-3) is interesting due to its inclusion in the 2001 UV₂₀₉ collisional family. While inclusion of 617 Patroclus (1906 VY) in the family would be unreasonable, as the family creation event would have disrupted the binary (Nesvorný & Vokrouhlický 2019), this may indicate a link between the family and the binary. Further analysis of several of these objects, as discussed in Section 4, could help further classify these objects, and place 617 Patroclus (1906 VY) in context prior to *Lucy*’s arrival, in 2033.

6 FUTURE SURVEYS

In this work, we use astrocladistics to investigate the Jovian Trojan population, drawing upon observational data obtained by the latest generation of wide-field surveys. In the coming decade, several new surveys will come online, providing a wealth of new data that could be incorporated in future studies. Here, we comment on the potential for the use of the astrocladistical methodology in the analysis of that data, and discuss how those surveys will improve our understanding of the Jovian Trojan population.

***Gaia* DR3:** In this work we use single *G*-band (330 to 1050 nm) data taken from *Gaia* DR2 (Spoto et al. 2018). Whilst this single band data can provide some information about the objects, The *Gaia* *G*-band magnitudes are clearly linked to size, to first approximation, but also to some extent albedo and distance. Albedos within the Jovian Trojans are low, and relatively consistent (Romanishin & Tegler 2018). Distance is also normalized somewhat, due to the librations of the population around the Lagrange points. In the *Gaia* DR2 data set, there are two additional two bands, *G*_{BP}-band (330–680 nm) and *G*_{RP}-band (630–1050 nm) (Evans et al. 2018) for stellar objects, but data in these bands is not available for Solar system objects. These data are expected to be included in the full *Gaia* DR3 release, which is currently scheduled for release in early 2022, and once available, could be incorporated into future astrocladistical surveys in a similar way to the SDSS and *MOVIS* colours.

The Vera Rubin Observatory, with the Legacy Survey of Space and Time (Rubin Obs. LSST), is expected to receive first light in

2023. During the first few years that Vera Rubin is active, estimates suggest that more than 280 000 Jovian Trojans are expected to be discovered (LSST Science Collaboration 2009). Of those objects, it is likely that more than 150 observations will be made of at least 50 000, which will be sufficient for those objects to be characterized in five broad-band colours (LSST Science Collaboration 2009). This will provide a much larger context for taxonomy in the Jovian Trojan population, and small Solar system bodies in general. Astrocladistics is a tool that could be used to further analyse these data, and that is ideally suited to the analysis of such vast and sprawling data sets. Assuming that the currently observed L₄/L₅ numerical asymmetry holds (Jewitt et al. 2000; Nakamura & Yoshida 2008; Yoshida & Nakamura 2008; Vinogradova & Chernetenko 2015), it is expected that those observations would yield results for approximately 33 000 objects in the vicinity of L₄, and 17 000 around L₅. Given that the computational requirements for cladistical analysis increases approximately with a trend of $n^{3/2}$ (Goloboff et al. 2008; Goloboff & Catalano 2016), we estimate that, using current computational architecture, the analysis of such large data sets would require approximately 2700 CPU-hours for the L₅ analysis and 7500 CPU-hours for the population around L₄. In order for this to be feasible, further testing into the TNT 1.5 parallelization (Goloboff & Catalano 2016) will be required.

The James Web Space Telescope (JWST) is currently scheduled for launch in 2021. The telescope will provide detailed analysis of many Solar system objects (Rivkin et al. 2020). In contrast to the work of *Gaia* and the Vera Rubin observatory, which are undertaking wide ranging surveys, the *JWST* is instead a targeted mission, providing detailed IR spectra on specific objects, rather than broad-band colours on many objects. Whilst the time required for such observations will doubtless be incredibly highly sought after, two members of the Jovian Trojan population, 617 Patroclus (1906 VY) and 624 Hektor (1907 XM), have already been approved for study under the Guaranteed Time Observations program (Rivkin et al. 2020). Once those observations are complete, the results can be placed in a wider context due to this work. As *JWST* is a limited time mission, we recommend the prioritization of those targets identified in Section 4 to provide the most benefit.

Twinkle is a low-cost, community funded, space telescope, scheduled for launch in 2023 or 2024 (Savini et al. 2018). The mission will provide spectral analysis in three bands in the visible and near-IR (0.4–1, 1.3–2.42, and 2.42–4.5 μ m). In terms of the Jovian Trojans, the mission will be able to provide detailed observations down to approximately 15th magnitude. Over the seven year initial lifetime, *Twinkle* is expected to observe 50 or so of the largest Trojans (Edwards et al. 2019a, b), all of which are included in this work. This will provide further characterization of these bodies, particularly in the IR range. Astrocladistics can offer added value to analysis of *Twinkle* observations, through associations within clans.

The Nancy Grace Roman Space Telescope (RST, formally *WFIRST*) is currently in development, with an expected launch date in 2025. Once launched, there will be a number of opportunities for small body Solar system science using *RST*, including the ability to obtain a wealth of data for the Jovian Trojans (Holler et al. 2018). Using the wide-field imaging system, in the near-IR (0.6–2.0 μ m), *RST* will be able to observe the majority of the currently known Jovian Trojans. In conjunction with the broad-band Rubin Observatory LSST colours, those observations will yield a large data base of Jovian Trojan characteristics. As computational capabilities and algorithm optimizations increases prior to launch, astrocladistics will provide a tool capable of analysing such large data sets.

7 CONCLUSION

In this work, we apply the new astrocladistical technique to the Jovian Trojans. We combine dynamical characteristics with colour information from the SDSS, *WISE*, *Gaia* DR2, and *MOVIS*, into a holistic taxonomic analysis. We create two matrices, one for the L_4 and one for the L_5 Trojans, comprised of 398 and 407 objects, respectively. As part of this analysis, we find clustering beyond the previously identified collisional families (Nesvorný et al. 2015). These clusters we term ‘clans’, which provide the beginnings of a taxonomic framework, the results of which are presented visually using a consensus dendritic tree. Our results yield a hierarchical structure, with individual clans often congregating within a larger ‘superclan’, and with other clans being further broken down into one or more ‘subclans’. These subclans, clans, and superclans form clusters of objects with a possible common origin. With the next-generation wide-field surveys and the *Lucy* mission, these clusters will be able to be placed in a wider context under the new paradigm.

In our analysis of the members of the L_4 swarm, we identify a total of ten unaffiliated clans and eight superclans that, in turn, contain an additional seventeen clans. Within our analysis, we include 13 members of the Eurybates collisional family (Nesvorný et al. 2015), the largest in the Trojan population. Seven of these, including 3548 Eurybates (1973 SO), a *Lucy* target, cluster into the Eurybates clan, a part of the Greater Ajax superclan. Other canonical family members cluster together, though are separated, possibly indicating that they are not true collisional family members, but suffer from one of the inherent issues with the methodology used to identify families.

The L_5 swarm shows more hierarchical structure: seven unaffiliated clans, with six subclans within them. The L_5 swarm is found to contain at least three large superclans, with each superclan containing a larger number of clans and subclans. In total, there are 14 clans containing 14 subclans in the L_5 swarm. The only *Lucy* target in the L_5 swarm, 617 Patroclus (1906 VY), is the type object of the Greater Patroclus superclan, though it is not specifically part of any clan, it is close to the Memnon clan, which includes 2001 UV₂₀₉ collisional family member, 37519 Amphios (3040 T-3). The other members of the larger Ennomios collisional family (Nesvorný et al. 2015) are distributed throughout the dendritic tree, indicating that perhaps the original HCM (Zappala et al. 1990) is inappropriate for describing the history of the swarm.

A key outcome of our astrocladistical analysis is that we identify 15 high priority targets for follow-up observations. These are all comparatively large and bright objects that should be observed to provide further context for the Jovian Trojan swarms as a whole. Several are closely related to *Lucy* targets that could provide additional information in preparation for *in-situ* observations.

All of the future *Lucy* targets (Levison et al. 2017) are included in our analysis. Our results therefore provide a taxonomic context for the mission, and extend the value of discoveries made. By associating the *Lucy* targets with other clan members, inferences can be made about their nearest relatives, and the swarms as a whole.

Whilst the focus of this work is on the current generation of wide-field surveys, several new observatories will be coming on line in the next few decades. The Vera Rubin Observatory, with the Legacy Survey of Space and Time (Rubin Obs. LSST), the *James Web Space Telescope (JWST)*, *Twinkle*, and the *Nancy Grace Roman Space Telescope (RST)*, formerly *WFIRST* will all be able to observe the Jovian Trojan population and further characterize these objects. Astrocladistics offers a method of analysis that will allow a timely and detailed analysis of the relationships between the Jovian Trojans, based on the observations made by these next-

generation telescopes, and helps us to identify high priority targets for competitive observational time. The Jovian Trojans are the remnants of the early Solar system, held dynamically stable for the past 4.5×10^9 yr. They are vital clues to this early period in the story of the Solar system. Astrocladistical analysis of these objects provides us with insights into their history and how they are related to one another.

ACKNOWLEDGEMENTS

This research was in part supported by the University of Southern Queensland’s Strategic Research Initiative program. TRH was supported by the Australian Government Research Training Program Scholarship. Dr. Pablo Goloboff provided assistance with TNT, which is subsidized by the Willi Hennig Society, as well as additional comments on the methodology. We thank Dr. Didier Fraix-Burnet and an anonymous reviewer for their comments in improving the manuscript. Some analysis was conducted in Python 3.7 under the Anaconda software environment (Continuum Analytics 2016).

DATA AVAILABILITY

A GitHub repository has been created for this study <https://github.com/TimHoltastro/holt-et-al-2021-Jovian-Trojan-astrocladistics.git>, and is publicly available. Matrices, trees, and clan dispersal velocity data sets are stored in this repository. The Python 3 binning and dispersal velocity programs, as well as the tree-search parameters and nexis (.nex) files containing the tree-banks are also available.

REFERENCES

- Beauge C., Roig F., 2001, *Icarus*, 153, 391
 Bendjoya P., Cellino A., Di Martino M., Saba L., 2004, *Icarus*, 168, 374
 Bolin B. T., Delbó M., Morbidelli A., Walsh K. J., 2017, *Icarus*, 282, 290
 Bolin B. T., Walsh K. J., Morbidelli A., Delbó M., 2018, *MNRAS*, 473, 3949
 Bolin B. T. et al., 2021, *AJ*, 161, 116
 Bottke W. F., Vokrouhlický D., Rubincam D., Nesvorný D., 2006, *Annu. Rev. Earth Planet. Sci.*, 34, 157
 Brandley M. C., Warren D. L., Leaché A. D., McGuires J. A., 2009, *Syst. Biol.*, 58, 184
 Brooks D. R., O’Grady R. T., Wiley E. O., 1986, *Syst. Zool.*, 35, 571
 Brož M., Rozehnal J., 2011, *MNRAS*, 414, 565
 Buie M. W. et al., 2015, *AJ*, 149, 113
 Buie M. W., Zangari A. M., Marchi S., Levison H. F., Mottola S., 2018, *AJ*, 155, 245
 Bus S. J., 2002, *Icarus*, 158, 146
 Cardone V. F., Fraix-Burnet D., 2013, *MNRAS*, 434, 1930
 Carruba V., Michtchenko T. A., 2007, *A&A*, 475, 1145
 Carruba V., Domingos R. C., Nesvorný D., Roig F., Huaman M. E., Souami D., 2013, *MNRAS*, 433, 2075
 Carvano J. M., Hasselmann P. H., Lazzaro D., Mothé-Diniz T., 2010, *A&A*, 510, A43
 Chamberlain A., Wood B., 1987, *J. Hum. Evol.*, 16, 119
 Continuum Analytics, 2016, Anaconda Software Distribution. Version 2.4.0. Available at: <https://continuum.io>
 Darwin C., 1859, *On the Origin of the Species by Natural Selection*. Murray, London, UK
 Deienno R., Morbidelli A., Gomes R., Nesvorný D., 2017, *AJ*, 153, 153
 Deienno R., Walsh K. J., Delbo M., 2020, *Icarus*, 357, 114218
 DeMEO F. E., Carry B., 2013, *Icarus*, 226, 723
 DeMEO F. E., Carry B., 2014, *Nature*, 505, 629
 DeMEO F. E., Binzel R. P., Slivan S. M., Bus S. J., 2009, *Icarus*, 202, 160
 DeMEO F. E., Binzel R. P., Carry B., Polishook D., Moskovitz N. A., 2014, *Icarus*, 229, 392

- DeMeo F. E., Alexander C. M. O., Walsh K. J., Chapman C. R., Binzel R. P., 2015, in Michel P., DeMeo F. E., Bottke W. F., eds, *Asteroids IV*. Univ. Arizona Press, Tucson, AZ, p. 13
- Di Sisto R. P., Ramos X. S., Beaugé C., 2014, *Icarus*, 243, 287
- Di Sisto R. P., Ramos X. S., Gallardo T., 2019, *Icarus*, 319, 828
- Dotto E. et al., 2006, *Icarus*, 183, 420
- Durech J., Carry B., Delbo M., Kaasalainen M., Viikinkoski M., 2015, in Michel P., DeMeo F. E., Bottke W. F., eds, *Asteroids IV*. Univ. Arizona Press, Tucson, AZ, p. 183
- Ebell M., 1909, *Astron. Nachr.*, 180, 213
- Edwards B., Savini G., Tinetti G., Tessenyi M., Arena C., Lindsay S., Bowles N., 2019a, *J. Astron. Telesc. Instrum. Syst.*, 5, 1
- Edwards B., Lindsay S., Savini G., Tinetti G., Arena C., Bowles N., Tessenyi M., 2019b, *J. Astron. Telesc. Instrum. Syst.*, 5, 1
- Emery J. P., Brown R. H., 2003, *Icarus*, 164, 104
- Emery J. P., Cruikshank D. P., Van Cleve J., 2006, *Icarus*, 182, 496
- Emery J. P., Burr D. M., Cruikshank D. P., 2011, *AJ*, 141, 25
- Emery J. P., Marzari F., Morbidelli A., French L. M., Grav T., 2015, in Michel P., DeMeo F., Bottke W., eds, *Asteroids IV*. Univ. Arizona Press, Tucson, AZ, p. 203
- Evans D. W. et al., 2018, *A&A*, 616, A4
- Farris J. S., 1970, *Syst. Biol.*, 19, 83
- Farris J. S., 1982, *Syst. Biol.*, 31, 328
- Farris J. S., 1989, *Cladistics*, 5, 417
- Fornasier S., Dotto E., Marzari F., Barucci M., Boehnhardt H., Hainaut O., Debergh C., 2004, *Icarus*, 172, 221
- Fornasier S., Dotto E., Hainaut O., Marzari F., Boehnhardt H., Deluise F., Barucci M., 2007, *Icarus*, 190, 622
- Fowler J., Chillemi J. R., 1992, in Tedesco E. F., ed., *IRAS Minor planet Surv.*, tech. repo edn. Philips Laboratory, Hanscom Air Force Base, MA, USA
- Fraix-Burnet D., Choler P., Douzery E. J. P., 2006, *A&A*, 455, 845
- Fraix-Burnet D., Dugué M., Chattopadhyay T., Chattopadhyay A. K., Davoust E., 2010, *MNRAS*, 407, 2207
- Fukugita M., Ichikawa T., Gunn J. E., Doi M., Shimasaku K., Schneider D. P., 1996, *AJ*, 111, 1748
- Gascuel O., 2005, *Mathematics of Evolution and Phylogeny*. OUP Oxford, Oxford, UK
- Giorgini J. D. et al., 1996, *AAS/Division Planet. Sci. Meet. Abstr. #28*. p. 1158
- Givnish T., Sytsma K., 1997, *Mol. Phylogenet. Evol.*, 7, 320
- Goloboff P. A., 1996, *Cladistics*, 12, 199
- Goloboff P. A., 2015, *Cladistics*, 31, 210
- Goloboff P. A., Catalano S. A., 2016, *Cladistics*, 32, 221
- Goloboff P. A., Farris J. S., Nixon K. C., 2008, *Cladistics*, 24, 774
- Grav T. et al., 2011, *ApJ*, 742, 40
- Grav T., Mainzer A. K., Bauer J. M., Masiero J. R., Nugent C. R., 2012, *ApJ*, 759, 49
- Hasselmann P. H., Carvano J. M., Lazzaro D., 2012, *NASA Planet. Data Syst.*, Available at: <https://sbn.psi.edu/pds/resource/sdsstax.html>
- Heinrich V., 1907, *Astron. Nachr.*, 176, 193
- Hellmich S., Mottola S., Hahn G., Kührt E., de Niem D., 2019, *A&A*, 630, A148
- Hennig W., 1965, *Annu. Rev. Entomol.*, 10, 97
- Holler B. J., Milam S. N., Bauer J. M., Alcock C., Bannister M. T., Bjoraker G. L., 2018, *J. Astron. Telesc. Instrum. Syst.*, 4, 1
- Holt T. R., Brown A. J., Nesvorný D., Horner J., Carter B. D., 2018, *ApJ*, 859, 97
- Holt T. R. et al., 2020a, *MNRAS*, 495, 4085
- Holt T. R., Vokrouhlický D., Nesvorný D., Brož M., Horner J., 2020b, *MNRAS*, 499, 3630
- Horner J., Wyn Evans N., 2006, *MNRAS*, 367, L20
- Horner J., Müller T. G., Lykawka P. S., 2012, *MNRAS*, 423, 2587
- Horner J. et al., 2020, *PASP*, 132, 102001
- Hsieh H. H., Fitzsimmons A., Novaković B., Denneau L., Heinze A. N., 2021, *Icarus*, 354, 114019
- Hug L. A. et al., 2016, *Nat. Microbiol.*, 1, 16048
- Ivezić Ž. et al., 2002, *AJ*, 124, 2943
- Jewitt D. C., Trujillo C. A., Luu J. X., 2000, *AJ*, 120, 1140
- Jofré P., Das P., Bertranpetit J., Foley R., 2017, *MNRAS*, 467, 1140
- Johanson D., White T., 1979, *Science*, 203, 321
- Karlsson O., Lagerkvist C., Davidsson B., 2009, *Icarus*, 199, 106
- Knežević Z., Milani A., 2003, *A&A*, 403, 1165
- Knežević Z., Milani A., 2017, *AstDys: Synthetic proper elements 5553 numbered and multiopposition Trojans*. Available at: <https://newton.spa.cedys.com/astdys2/propsynth/tro.syn>
- Lazzaro D., Angeli C. A., Carvano J. M., Mothé-Diniz T., Duffard R., Florczak M., 2004, *Icarus*, 172, 179
- Levison H. F., Shoemaker E. M., Shoemaker C. S., 1997, *Nature*, 385, 42
- Levison H. F., Bottke W. F., Gounelle M., Morbidelli A., Nesvorný D., Tsiganis K., 2009, *Nature*, 460, 364
- Levison H. F., Morbidelli A., Tsiganis K., Nesvorný D., Gomes R., 2011, *AJ*, 142, 152
- Levison H. F., Olkin C. B., Noll K., Marchi S., Lucy Team, 2017, in *Lunar Planet. Sci. Conf.*, p. 2025
- Linnaeus C., 1758, *Systema Naturae per regna tria naturae, secundum classes, ordines, genera, species, cum characteribus, differentiis, synonymis, locis* LSST Science Collaboration, 2009, preprint ([arXiv:0912.0201](https://arxiv.org/abs/0912.0201))
- Lykawka P. S., Horner J., 2010, *MNRAS*, 405, 1375
- Maddison W. P., Maddison D. R., 2015, *Zephyr: a Mesquite package for interacting with external phylogeny inference programs*. Version 1.1. Available at: <https://mesquitezephyr.wikispaces.com>
- Maddison W. P., Maddison D. R., 2017, *Mesquite: a modular system for evolutionary analysis*. Version 3.20. Available at: <http://mesquiteproject.org>
- Maddison W. P., Donoghue M. J., Maddison D. R., 1984, *Syst. Biol.*, 33, 83
- Marchis F. et al., 2006, *Nature*, 439, 565
- Marchis F. et al., 2014, *ApJ*, 783, L37
- Margush T., McMorris F. R., 1981, *Bull. Math. Biol.*, 43, 239
- Masiero J. R. et al., 2011, *ApJ*, 741, 68
- Merline W. J. et al., 2001, *Int. Astron. Union Circ.*, 7741, 2
- Milam S. N., Stansberry J. A., Sonneborn G., Thomas C., 2016, *PASP*, 128, 018001
- Milani A., 1993, *Celest. Mech. Dyn. Astron.*, 57, 59
- Milani A., Cellino A., Knežević Z., Novaković B., Spoto F., Paolicchi P., 2014, *Icarus*, 239, 46
- Morate D., Licandro J., Popescu M., de León J., 2018, *A&A*, 617, A72
- Morbidelli A., 2010, *C. R. Phys.*, 11, 651
- Morbidelli A., Levison H. F., Tsiganis K., Gomes R., 2005, *Nature*, 435, 462
- Mottola S., Hellmich S., Buie M. W., Zangari A. M., Marchi S., Brown M. E., Levison H. F., 2020, *Planet. Sci. J.*, 1, 73
- Nakamura T., Yoshida F., 2008, *PASJ*, 60, 293
- Naylor G., Kraus F., 1995, *Syst. Biol.*, 44, 559
- Nesvorný D., 2002, *Icarus*, 160, 271
- Nesvorný D., 2018, *ARA&A*, 56, 137
- Nesvorný D., Morbidelli A., 2012, *AJ*, 144, 117
- Nesvorný D., Vokrouhlický D., 2019, *Icarus*, 331, 49
- Nesvorný D., Beaugé C., Dones L., 2004, *AJ*, 127, 1768
- Nesvorný D., Vokrouhlický D., Morbidelli A., 2013, *ApJ*, 768, 45
- Nesvorný D., Brož M., Carruba V., 2015, in Michel P., DeMeo F. E., Bottke W. F., eds, *Asteroids IV*. University of Arizona Press, Tucson, AZ, p. 297
- Nicholson S. B., 1961, *Astron. Soc. Pacific Leaflet*, 8, 239
- Parins-Fukuchi C., Greiner E., MacLachy L. M., Fisher D. C., 2019, *Paleobiology*, 45, 378
- Parker A. H., Ivezić Ž., Jurić M., Lupton R. H., Sekora M., Kowalski A., 2008, *Icarus*, 198, 138
- Perna D., Bott N., Hromakina T., Mazzotta Epifani E., Dotto E., Doressoundiram A., 2018, *MNRAS*, 475, 974
- Pirani S., Johansen A., Bitsch B., Mustill A. J., Turrini D., 2019a, *A&A*, 623, A169
- Pirani S., Johansen A., Mustill A. J., 2019b, *A&A*, 631, A89
- Popescu M. et al., 2016, *A&A*, 591, A115
- Popescu M. et al., 2018, *A&A*, 617, A12
- Pravec P. et al., 2019, *Icarus*, 333, 429
- Radović V., Novaković B., Carruba V., Marčeta D., 2017, *MNRAS*, 470, 576

- Reddy V., Dunn T. L., Thomas C. A., Moskovitz N. A., Burbine T. H., 2015, in Michel P., DeMeo F. E., Bottke W. F., eds, *Asteroids IV*. Univ. Arizona Press, Tucson, AZ
- Rein H., Liu S.-F., 2012, *A&A*, 537, A128
- Rein H., Tamayo D., 2015, *MNRAS*, 452, 376
- Rivkin A. S., Marchis F., Stansberry J. A., Takir D., Thomas C., Group t. J. A. F., 2016, *PASP*, 128, 018003
- Rivkin A. S., Milam, Stefanie N., Thomas C. A., 2020, STScI: Web Observing Program: GTO 1244. Available at: <https://www.stsci.edu/jwst/observing-programs/program-information?id=1244>
- Robutel P., Gabern F., 2006, *MNRAS*, 372, 1463
- Roig F., Nesvorný D., 2015, *AJ*, 150, 186
- Roig F., Ribeiro A. O., Gil-Hutton R., 2008, *A&A*, 483, 911
- Romanishin W., Tegler S. C., 2018, *AJ*, 156, 19
- Rozehnal J., Brož M., Nesvorný D., Durda D. D., Walsh K., Richardson D. C., Asphaug E., 2016, *MNRAS*, 462, 2319
- Savini G. et al., 2018, *Sp. Telesc. Instrum. 2016 Opt. Infrared, Millim. Wave*, 9904, 175
- Slyusarev I. G., Belskaya I. N., 2014, *Sol. Syst. Res.*, 48, 139
- Souza-Feliciano A. C. et al., 2020, *Icarus*, 338, 113463
- Spoto F. et al., 2018, *A&A*, 616, A13
- Steckloff J. K., Sarid G., Volk K., Karetka T., Womack M., Harris W., Woodney L., Schambeau C., 2020, *ApJ*, 904, L20
- Strömgren E., 1908, *Astron. Nachr.*, 177, 123
- Sutherland W. et al., 2015, *A&A*, 575, A25
- Szabo G. M., Ivezić Ž., Jurić M., Lupton R. H., 2007, *MNRAS*, 377, 1393
- Tholen D. J., 1984, PhD thesis, University of Arizona, Tucson
- Tholen D. J., 1989, in Binzel R.P., Gehrels T., Shapley Matthews M., eds, *Asteroids II*. Univ. Arizona Press, Tucson, p. 1139
- Tsiganis K., Varvoglis H., Dvorak R., 2005a, *Celest. Mech. Dyn. Astron.*, 92, 71
- Tsiganis K., Gomes R., Morbidelli A., Levison H. F., 2005b, *Nature*, 435, 459
- Turrini D., Marzari F., Beust H., 2008, *MNRAS*, 391, 1029
- Vinogradova T. A., 2015, *MNRAS*, 454, 2436
- Vinogradova T. A., Chernetenko Y. A., 2015, *Sol. Syst. Res.*, 49, 391
- Vokrouhlický D., Nesvorný D., 2008, *AJ*, 136, 280
- Walsh K. J., Delbó M., Bottke W. F., Vokrouhlický D., Lauretta D. S., 2013, *Icarus*, 225, 283
- Wang X., Hou X., 2017, *MNRAS*, 471, 243
- Warner B. D., Harris A. W., Pravec P., 2009, *Icarus*, 202, 134
- Wolf M., 1907, *Astron. Nachr.*, 174, 47
- Wong I., Brown M. E., 2017, *AJ*, 153, 69
- Wyse A., 1938, *Astron. Soc. Pacific Leaflet*, 3, 113
- Yoshida F., Nakamura T., 2008, *PASJ*, 60, 297
- Zappala V., Cellino A., Farinella P., Knežević Z., 1990, *AJ*, 100, 2030
- Zappala V., Cellino A., Dell'Oro A., Migliorini F., Paolicchi P., 1996, *Icarus*, 124, 156

SUPPORTING INFORMATION

Supplementary data are available at [MNRAS](https://www.mnras.org/) online.

Figure 5. Consensus tree of cladistical analysis of 398 L₄ Jovian Trojans.

Figure 6. Consensus tree of cladistical analysis of 407 L₅ Jovian Trojans.

Please note: Oxford University Press is not responsible for the content or functionality of any supporting materials supplied by the authors. Any queries (other than missing material) should be directed to the corresponding author for the article.

APPENDIX A: CHARACTERISTICS USED IN THE MATRIX

This appendix details the characteristics used in the analysis. In total there are 17 values that are binned using the Python 3 (Continuum Analytics 2016) program, available at the associated Github (<https://github.com/TimHoltastro/holt-et-al-2021-Jovian-Trojan-astrocladistics.git>). This binning program is based on one developed in Holt et al. (2018). R^2 values are the correlation between the binned values and the original data. The binning program sets the number of bins once an R^2 value greater than 0.99 is reached, or the maximum number of bins, 15 is reached. Each characteristic is binned independently for the L₄ and L₅ Trojan matrices.

A1 Δa_p

Proper Δ semimajor axis of the object. From AsyDys data base <https://newton.spacedys.com/astdys/>

Reference: Knežević & Milani (2017)

Units: au

L4 Bin Number: 13

L4 R^2 value: 0.9902

L4 Bin delimiters: [0.0004417 0.01277692 0.02495385 0.03713077 0.04930769 0.06148462 0.07366154 0.08583846 0.09801538 0.11019231 0.12236923 0.13454615 0.14672308 0.1589]

L5 Bin Number: 13

L5 R^2 value: 0.9902

L5 Bin delimiters: [0.0041526 0.01563846 0.02697692 0.03831538 0.04965385 0.06099231 0.07233077 0.08366923 0.09500769 0.10634615 0.11768462 0.12902308 0.14036154 0.1517]

A2 e_p

Proper eccentricity of the object. From AsyDys data base <https://newton.spacedys.com/astdys/>

Units: n/a

Reference: Knežević & Milani (2017)

L4 Bin Number: 15

L4 R^2 value: 0.9900

L4 Bin delimiters: [0.0035364 0.01460667 0.02551333 0.03642 0.04732667 0.05823333 0.06914 0.08004667 0.09095333 0.10186 0.11276667 0.12367333 0.13458 0.14548667 0.15639333 0.1673]

L5 Bin Number: 15

L5 R^2 value: 0.9876

L5 Bin delimiters: [0.0041151 0.01662667 0.02895333 0.04128 0.05360667 0.06593333 0.07826 0.09058667 0.10291333 0.11524 0.12756667 0.13989333 0.15222 0.16454667 0.17687333 0.1892]

A3 $\sin i_p$

Sine of the proper inclination of the object. From AsyDys data base <https://newton.spacedys.com/astdys/>

Units: n/a

Reference: Knežević & Milani (2017)

L4 Bin Number: 15

L4 R^2 value: 0.9870

L4 Bin delimiters: [0.0101936 0.06476 0.11852 0.17228 0.22604 0.2798 0.33356 0.38732 0.44108 0.49484 0.5486 0.60236 0.65612 0.70988 0.76364 0.8174]

L5 Bin Number: 13

L5 R^2 value: 0.9901

L5 Bin delimiters: [0.012521 0.06543077 0.11766154 0.16989231 0.22212308 0.27435385 0.32658462 0.37881538 0.43104615 0.48327692 0.53550769 0.58773846 0.63996923 0.6922]

A4 MeanLib

Mean libration value, relative to Jupiter. Calculated using REBOUND (Rein & Liu 2012; Rein & Tamayo 2015) as outlined in Section 2.1 of the text.

Units: degree

Reference: n/a

L4 Bin Number: 15

L4 R^2 value: 0.9838

L4 Bin delimiters: [56.4248396 57.77509172 59.10538938 60.43568704 61.7659847 63.09628236 64.42658001 65.75687767 67.08717533 68.41747299 69.74777065 71.07806831 72.40836597 73.73866362 75.06896128 76.39925894]

L5 Bin Number: 14

L5 R^2 value: 0.9908 L5 Bin delimiters: [285.72582824 286.91482596 288.0862523 289.25767863 290.42910496 291.60053129 292.77195762 293.94338395 295.11481029 296.28623662 297.45766295 298.62908928 299.80051561 300.97194195 302.14336828 303.31479461]

A5 LibRange

Range of the objects libration, relative to Jupiter. Calculated using REBOUND (Rein & Liu 2012; Rein & Tamayo 2015) as outlined in Section 2.1 of the text.

Units: degree

Reference: n/a

L4 Bin Number: 14

L4 R^2 value: 0.9904

L4 Bin delimiters: [4.04450175 9.22096281 14.325954 19.43094519 24.53593638 29.64092757 34.74591876 39.85090995 44.95590114 50.06089233 55.16588352 60.27087471 65.3758659 70.48085709 75.58584828]

L5 Bin Number: 14

L5 R^2 value: 0.9908

L5 Bin delimiters: [2.7354308 7.67859255 12.55350552 17.42841848 22.30333145 27.17824441 32.05315738 36.92807035 41.80298331 46.67789628 51.55280924 56.42772221 61.30263518 66.17754814 71.05246111]

A6 albedo

Geometric albedo of the object. From NASA-JPL HORIZONS Solar System Dynamics Data base <https://ssd.jpl.nasa.gov/> Giorgini et al. (1996).

Units: n/a

Reference: Giorgini et al. (1996)

L4 Bin Number: 15

L4 R^2 value: 0.9830

L4 Bin delimiters: [0.024827 0.03653333 0.04806667 0.0596 0.07113333 0.08266667 0.0942 0.10573333 0.11726667 0.1288 0.14033333 0.15186667 0.1634 0.17493333 0.18646667 0.198]

L5 Bin Number: 15

L5 R^2 value: 0.9817

L5 Bin delimiters: [0.030831 0.04226667 0.05353333 0.0648 0.07606667 0.08733333 0.0986 0.10986667 0.12113333 0.1324 0.14366667 0.15493333 0.1662 0.17746667 0.18873333 0.2]

A7 W1Alb

Near infrared values from the *WISE* survey using the W1 filter (3.4).

Units: magnitude

Reference: Grav et al. (2011, 2012)

L4 Bin Number: 15

L4 R^2 value: 0.9824

L4 Bin delimiters: [0.055661 0.0786 0.1012 0.1238 0.1464 0.169 0.1916 0.2142 0.2368 0.2594 0.282 0.3046 0.3272 0.3498 0.3724 0.395]

L5 Bin Number: 15

L5 R^2 value: 0.9794

L5 Bin delimiters: [0.065666 0.08826667 0.11053333 0.1328 0.15506667 0.17733333 0.1996 0.22186667 0.24413333 0.2664 0.28866667 0.31093333 0.3332 0.35546667 0.37773333 0.4]

A8 W2Alb

Near infrared values from the *WISE* survey using the W2 filter (4.6 μ m).

Units: magnitude

Reference: Grav et al. (2011, 2012)

L4 Bin Number: 15

L4 R^2 value: 0.9838

L4 Bin delimiters: [0.035641 0.05993333 0.08386667 0.1078 0.13173333 0.15566667 0.1796 0.20353333 0.22746667 0.2514 0.27533333 0.29926667 0.3232 0.34713333 0.37106667 0.395]

L5 Bin Number: 15

L5 R^2 value: 0.9773

L5 Bin delimiters: [0.027628 0.0528 0.0776 0.1024 0.1272 0.152 0.1768 0.2016 0.2264 0.2512 0.276 0.3008 0.3256 0.3504 0.3752 0.4]

A9 $g_{\text{mag-mean}}$

Mean *G*-band magnitude from the *GAIA* survey. Filter passband from 330 to 1050 nm (Evans et al. 2018).

Units: magnitude

Reference: Spoto et al. (2018) L4 Bin Number: 15

L4 R^2 value: 0.9894

L4 Bin delimiters: [15.10926146 15.38560874 15.65787207 15.9301354 16.20239873 16.47466206 16.74692539 17.01918872 17.29145205 17.56371538 17.83597871 18.10824204 18.38050537 18.65276871 18.92503204 19.19729537]

L5 Bin Number: 12

L5 R^2 value: 0.9904

L5 Bin delimiters: [15.85627031 16.11791172 16.37645066 16.6349896 16.89352854 17.15206747 17.41060641 17.66914535 17.92768429 18.18622323 18.44476217 18.7033011 18.96184004]

A10 ($b - v$)

Index of Johnson *B* (442 nm) and Johnson *V* (540 nm) band magnitudes, calculated from SDSS photometry (Fukugita et al. 1996).

Units: magnitude

Reference: Szabo et al. (2007)

L4 Bin Number: 15

L4 R^2 value: 0.9591

L4 Bin delimiters: [0.50896 0.57933333 0.64866667 0.718 0.78733333 0.85666667 0.926 0.99533333 1.06466667 1.134 1.20333333 1.27266667 1.342 1.41133333 1.48066667 1.55]

L5 Bin Number: 15

L5 R^2 value: 0.9878

L5 Bin delimiters: [0.60968 0.63133333 0.65266667 0.674 0.69533333 0.71666667 0.738 0.75933333 0.78066667 0.802 0.82333333 0.84466667 0.866 0.88733333 0.90866667 0.93]

A11 ($u - g$)

Index of U (354.3 nm) and G (477 nm) band magnitudes taken from the SDSS (Fukugita et al. 1996).

Units: magnitude

Reference: Szabo et al. (2007)

L4 Bin Number: 15

L4 R^2 value: 0.9656

L4 Bin delimiters: [0.873585 0.96933333 1.06366667 1.158 1.25233333 1.34666667 1.441 1.53533333 1.62966667 1.724 1.81833333 1.91266667 2.007 2.10133333 2.19566667 2.29]

L5 Bin Number: 15

L5 R^2 value: 0.9724

L5 Bin delimiters: [0.62835 0.74 0.85 0.96 1.07 1.18 1.29 1.4 1.51 1.62 1.73 1.84 1.95 2.06 2.17 2.28]

A12 ($g - r$)

Index of G (477 nm) and R (623.1 nm) band magnitudes taken from the SDSS (Fukugita et al. 1996).

Units: magnitude

Reference: Szabo et al. (2007)

L4 Bin Number: 15

L4 R^2 value: 0.9560

L4 Bin delimiters: [0.299 0.36666667 0.43333333 0.5 0.56666667 0.63333333 0.7 0.76666667 0.83333333 0.9 0.96666667 1.03333333 1.1 1.16666667 1.23333333 1.3]

L5 Bin Number: 15

L5 R^2 value: 0.9851

L5 Bin delimiters: [0.4197 0.44 0.46 0.48 0.5 0.52 0.54 0.56 0.58 0.6 0.62 0.64 0.66 0.68 0.7 0.72]

A13 ($r - i$)

Index of R (623.1 nm) and I (762.5 nm) band magnitudes taken from the SDSS (Fukugita et al. 1996).

Units: magnitude

Reference: Szabo et al. (2007)

L4 Bin Number: 15

L4 R^2 value: 0.9890

L4 Bin delimiters: [0.09976 0.116 0.132 0.148 0.164 0.18 0.196 0.212 0.228 0.244 0.26 0.276 0.292 0.308 0.324 0.34]

L5 Bin Number: 15

L5 R^2 value: 0.9841

L5 Bin delimiters: [0.06824 0.09066667 0.1127619 0.13485714 0.15695238 0.17904762 0.20114286 0.2232381 0.24533333 0.26742857 0.28952381 0.31161905 0.33371429 0.35580952 0.37790476 0.4]

A14 ($i - z$)

Index of I (762.5 nm) and Z (913.4 nm) band magnitudes taken from the SDSS (Fukugita et al. 1996).

Units: magnitude

Reference: Szabo et al. (2007)

L4 Bin Number: 15

L4 R^2 value: 0.9614

L4 Bin delimiters: [-0.55087 -0.492 -0.434 -0.376 -0.318 -0.26 -0.202 -0.144 -0.086 -0.028 0.03 0.088 0.146 0.204 0.262 0.32]

L5 Bin Number: 15

L5 R^2 value: 0.9656

L5 Bin delimiters: [-0.37082 -0.31533333 -0.26066667 -0.206 -0.15133333 -0.09666667 -0.042 0.01266667 0.06733333 0.122 0.17666667 0.23133333 0.286 0.34066667 0.39533333 0.45]

A15 ($Y - J$)

Index of Y (1.02 μm) and J (1.25 μm) band magnitudes from the VISTA survey (Sutherland et al. 2015), in the MOVIS data base (Popescu et al. 2016).

Units: magnitude

Reference: Popescu et al. (2018)

L4 Bin Number: 15

L4 R^2 value: 0.9875

L4 Bin delimiters: [0.02060934 0.0655506 0.1098277 0.1541048 0.1983819 0.242659 0.2869361 0.3312132 0.3754903 0.4197674 0.4640445 0.5083216 0.5525987 0.5968758 0.6411529 0.68543]

L5 Bin Number: 15

L5 R^2 value: 0.9886

L5 Bin delimiters: [0.05425359 0.09975333 0.14458067 0.189408 0.23423533 0.27906267 0.32389 0.36871733 0.41354467 0.458372 0.50319933 0.54802667 0.592854 0.63768133 0.68250867 0.727336]

A16 ($J - K_s$)

Index of J (1.25 μm) and K (2.15 μm) band magnitudes from the VISTA survey (Sutherland et al. 2015), in the MOVIS data base (Popescu et al. 2016).

Units: magnitude

Reference: Popescu et al. (2018)

L4 Bin Number: 15

L4 R^2 value: 0.9846

L4 Bin delimiters: [0.14045928 0.25723273 0.37228047 0.4873282 0.60237593 0.71742367 0.8324714 0.94751913 1.06256687 1.1776146 1.29266233 1.40771007 1.5227578 1.63780553 1.75285327 1.867901]

L5 Bin Number: 15

L5 R^2 value: 0.9890

L5 Bin delimiters: [0.06778045 0.16160333 0.25403967 0.346476 0.43891233 0.53134867 0.623785 0.71622133 0.80865767 0.901094 0.99353033 1.08596667 1.178403 1.27083933 1.36327567 1.455712]

A17 ($H - K_s$)

Index of H (1.65 μm) and K (2.15 μm) band magnitudes from the VISTA survey (Sutherland et al. 2015), in the MOVIS data base (Popescu et al. 2016).

Units: magnitude

Reference: Popescu et al. (2018)

L4 Bin Number: 8

L4 R^2 value: 0.9991

L4 Bin delimiters: [−0.33295512 −0.2505985 −0.1688955
−0.0871925 −0.0054895 0.0762135 0.1579165 0.2396195
0.3213225]

L5 Bin Number: 14

L5 R^2 value: 0.9906

L5 Bin delimiters: [−0.1558507 −0.05802146 0.03845707
0.13493561 0.23141414 0.32789268 0.42437121 0.52084975
0.61732829 0.71380682 0.81028536 0.90676389 1.00324243
1.09972096 1.1961995]

A18 tax_c

Canonical taxonomic designation, based on the (DeMeo et al. 2009). Note: any ‘P-type’ have been modernized into the X-types. Reference used is in tax_{ref} .

A19 tax_{ref}

Source of canonical taxonomic classification (tax_c) Tholen1989: Tholen (1989); Bendjoya2004: Bendjoya et al. (2004); Fornasier2004 (Fornasier et al. 2004); Lazzaro2004: Lazzaro et al. (2004); Fornasier2007: Fornasier et al. (2007); H2012: Hasselmann et al. (2012).

APPENDIX B: INDIVIDUAL SUPERCLANS, CLANS, AND SUBCLANS

The figures here (Figs B1–B12) show each of the separate superclans, along with the L4 unassociated clans (Fig. B1) and unassociated L5 clans (Fig. B9). These are additionally available individually from the PDS. We include Table B1 as an example of those included in the

data archive, available from the PDS. In this data set, the dispersal velocity calculated from inverse Gauss equations, see Section 2.3, to the reference object (ΔV_{ref}) and to a fictitious cluster centre (ΔV_{cent}) are given for each superclan, clan, and subclan independently, for the subset of Jovian Trojans used in this analysis.

Table B1. Ulysses clan-D: Diameter of the object. From NASA-JPL HORIZONS Solar System Dynamics Data base <https://ssd.jpl.nasa.gov/> (Giorgini et al. 1996). Where not available, generated from H magnitude and mean geometric albedo (0.075); ΔV_{ref} : dispersal velocity calculated from inverse Gauss equations, see Section 2.3, to the reference object; ΔV_{cent} : as ΔV_{ref} , with calculations to the fictitious cluster centre; F_{esc} : Fraction of clones that escape the Jovian Trojan population in Holt et al. (2020a).

full_name	D (km)	ΔV_{ref} (m s^{-1})	ΔV_{cent} (m s^{-1})	F_{esc}
4834 Thoas (1989 AM2)	72.33	9.83	23.99	2.20E-01
5254 Ulysses (1986 VG1)	76.15	0.00	17.81	–
5264 Telephus (1991 KC)	68.47	34.09	16.83	–
11396 (1998 XZ77)	37.11	33.67	14.19	–
13782 (1998 UM18)	24.97	13.89	28.86	8.90E-01
16099 (1999 VQ24)	36.77	28.36	11.69	–
20424 (1998 VF30)	45.80	17.92	3.48	–
20716 (1999 XG91)	26.37	11.34	9.36	–
21595 (1998 WJ5)	35.18	12.63	6.26	–
21599 (1998 WA15)	28.31	48.31	28.04	–
23958 (1998 VD30)	46.00	18.02	5.02	–
24501 (2001 AN37)	24.54	17.78	1.21	–
63195 (2000 YN120)	24.69	35.93	18.19	–
111819 (2002 DD1)	19.34	17.35	9.23	3.30E-01
252173 (2001 DL10)	15.45	40.86	20.81	–
310027 (2010 AH95)	11.10	36.22	16.84	–
355768 (2008 RY57)	11.72	10.25	10.38	–

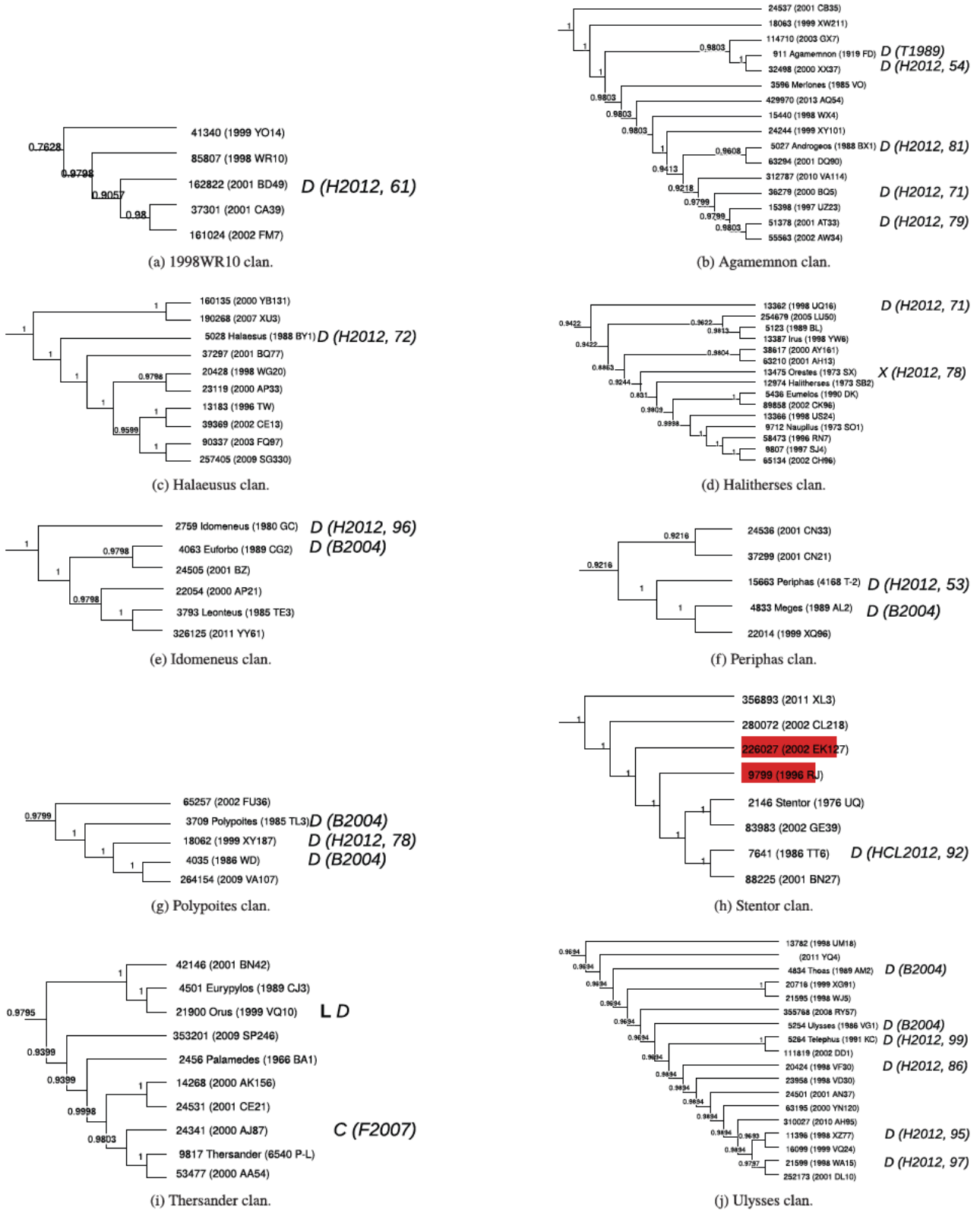


Figure B1. Consensus trees of L4 Trojans that are not associated with any superclan. Numbers indicate fraction of 10 000 trees where branch is present. *Letters* associate objects with Bus–Demeo taxonomy (Bus 2002; DeMeo et al. 2009), classified by associated reference T1989: Tholen (1989); B2004: Bendjoya et al. (2004); F2007: Fornasier et al. (2007); H2012, with associated confidence rating: Hasselmann et al. (2012). *L* indicates objects to be visited by the *Lucy* spacecraft (Levison et al. 2017). The red highlights are members of the 1996 RJ collisional family.

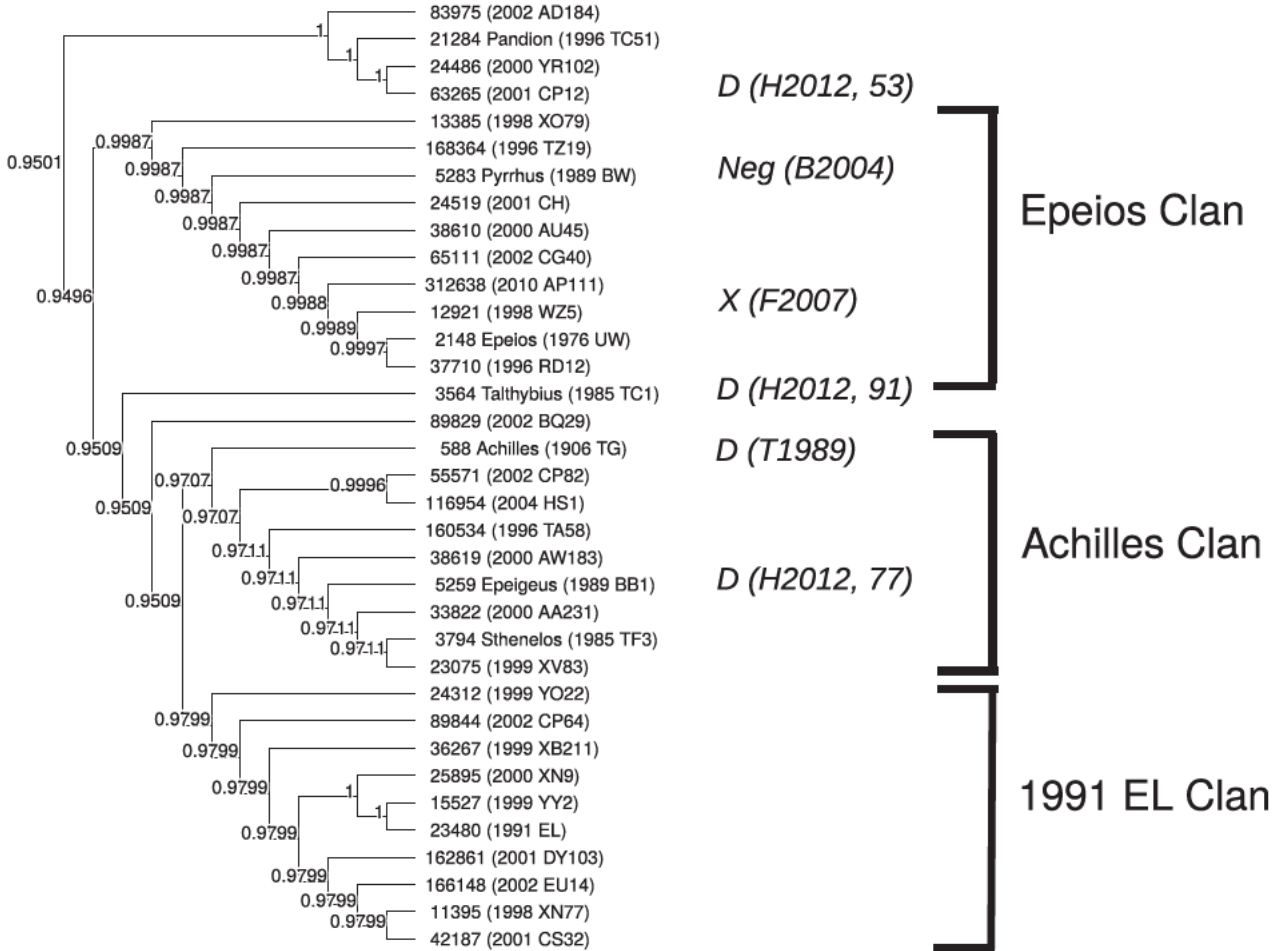


Figure B2. Consensus tree of the L4 Greater Achilles superclan, including Epeios, achilles and 1991 EL clans. Numbers indicate fraction of 10 000 trees where branch is present. *Letters* associate objects with Bus–Demeo taxonomy (Bus 2002; DeMeo et al. 2009), classified by associated reference T1989: Tholen (1989); B2004: Bendjoya et al. (2004); F2007: Fornasier et al. (2007); H2012, with associated confidence rating: Hasselmann et al. (2012).

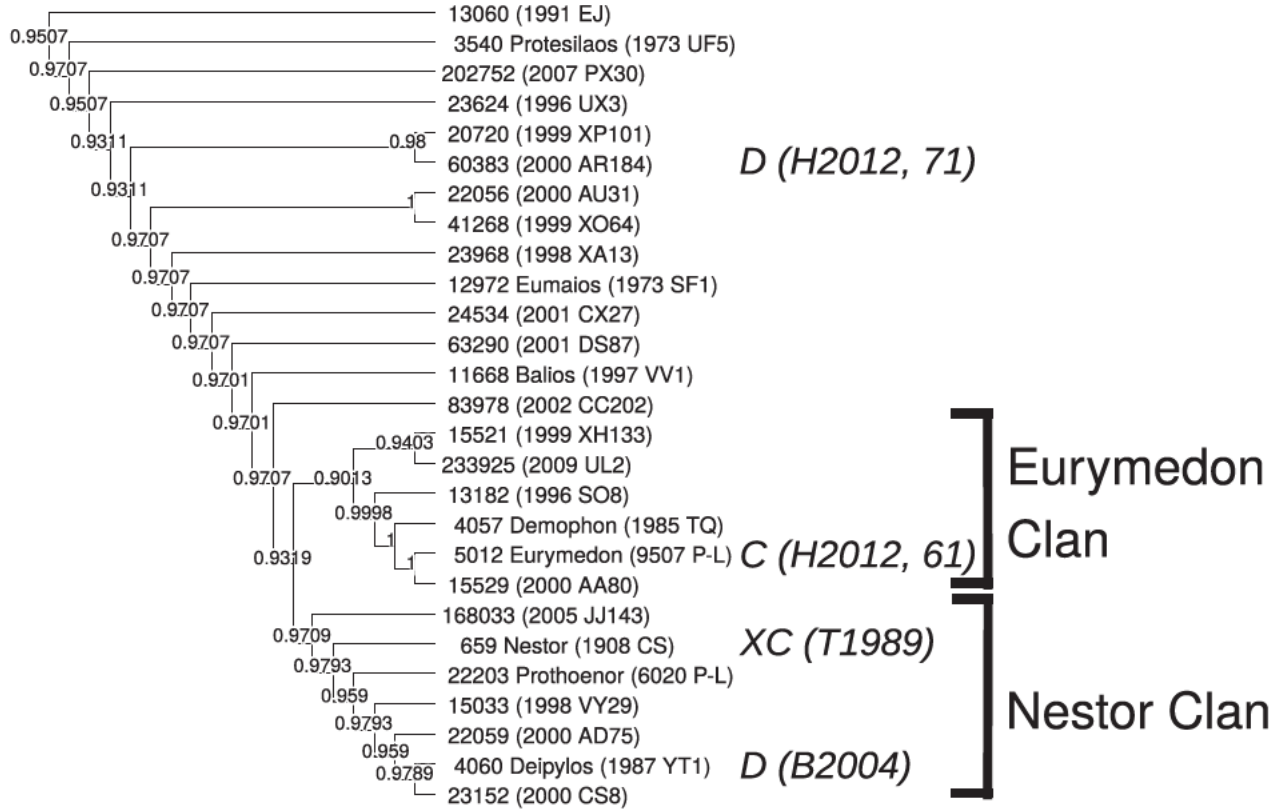


Figure B3. Consensus tree of the L4 Greater Nestor superclan, including Eurymedon and Nestor clans. Numbers indicate fraction of 10 000 trees where branch is present. *Letters* associate objects with Bus–Demeo taxonomy (Bus 2002; DeMeo et al. 2009), classified by associated reference T1989: Tholen (1989); B2004: Bendjoya et al. (2004); F2007: Fornasier et al. (2007); H2012, with associated confidence rating: Hasselmann et al. (2012).

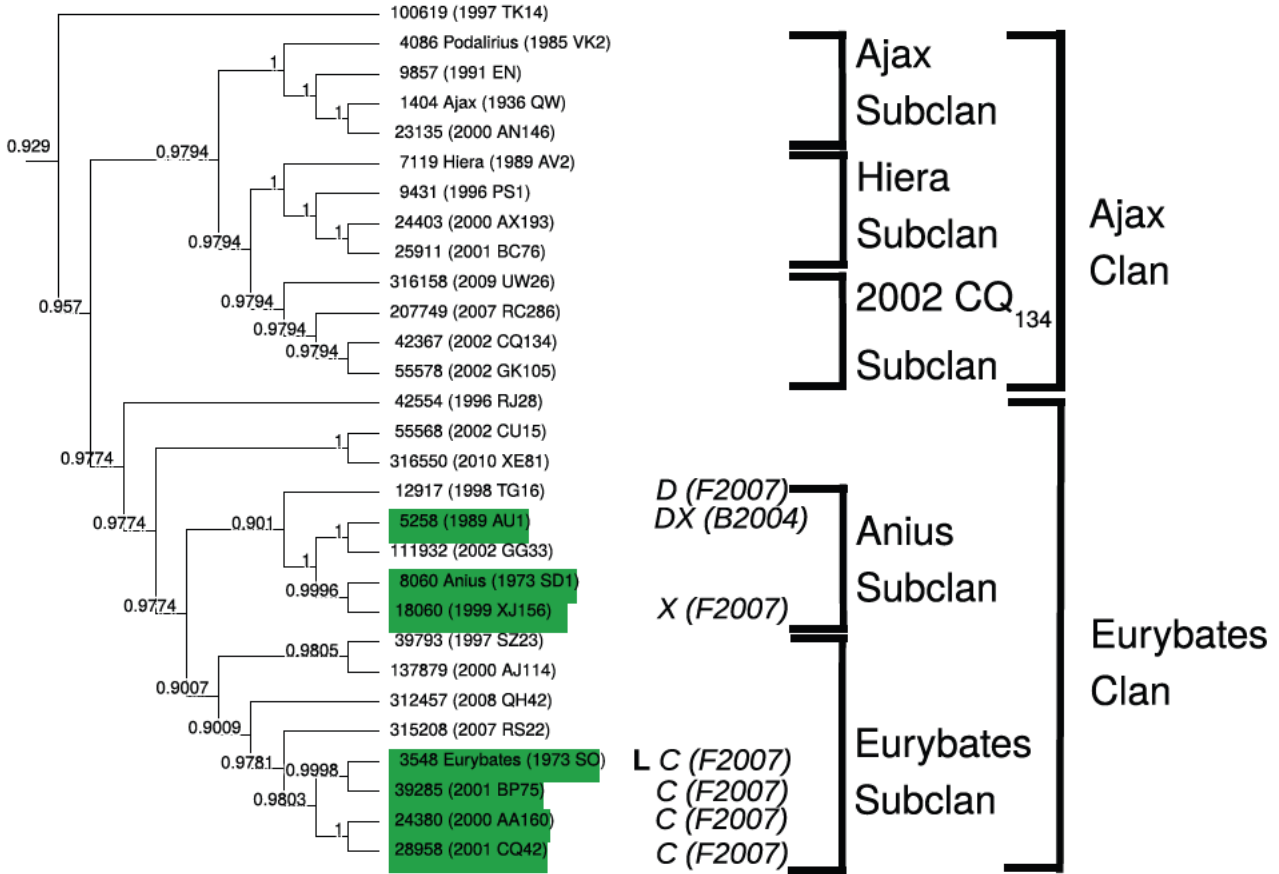


Figure B4. Consensus tree of the L4 Greater Ajax superclan, including Ajax and Eurybates clans. This is a duplicate of Fig. 4, and is included here for completeness. Numbers indicate fraction of 10 000 trees where branch is present. *Letters* associate objects with Bus–Demeo taxonomy (Bus 2002; DeMeo et al. 2009), classified by associated reference T1989: Tholen (1989); B2004: Bendjoya et al. (2004); F2007: Fornasier et al. (2007); H2012, with associated confidence rating: Hasselmann et al. (2012). *L* indicates objects to be visited by the *Lucy* spacecraft (Levison et al. 2017). The green highlights are members of the Eurybates collisional family.

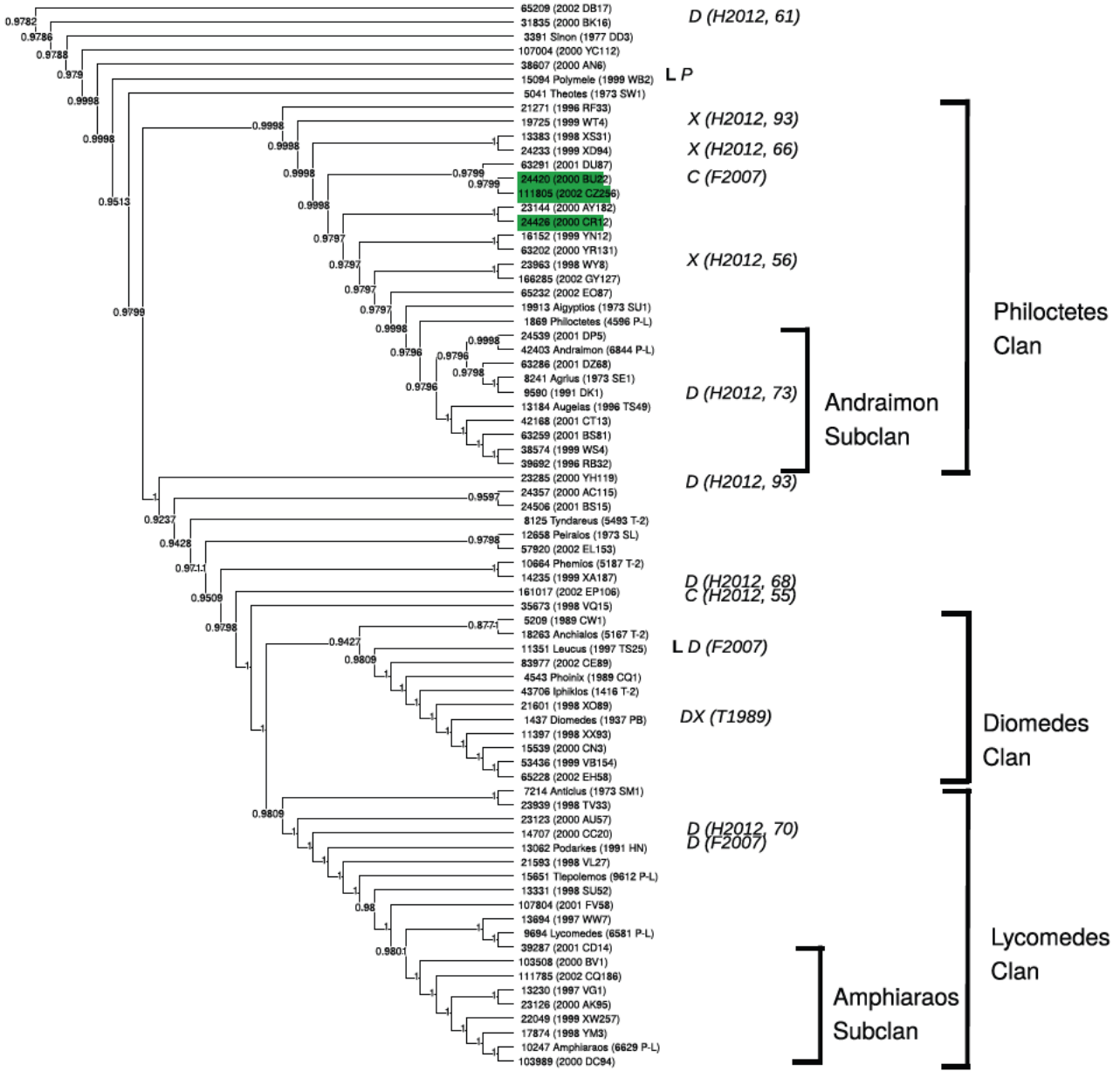


Figure B6. Consensus tree of the L4 Greater Diomedes superclan, including Philoctetes, Diomedes, and Lycomedes clans. Numbers indicate fraction of 10 000 trees where branch is present. Letters associate objects with Bus–Demeo taxonomy (Bus 2002; DeMeo et al. 2009), classified by associated reference T1989: Tholen (1989); B2004: Bendjoya et al. (2004); F2007: Fornasier et al. (2007); H2012, with associated confidence rating: Hasselmann et al. (2012). L indicates objects to be visited by the *Lucy* spacecraft (Levison et al. 2017). The green highlights are members of the Eurybates collisional family.

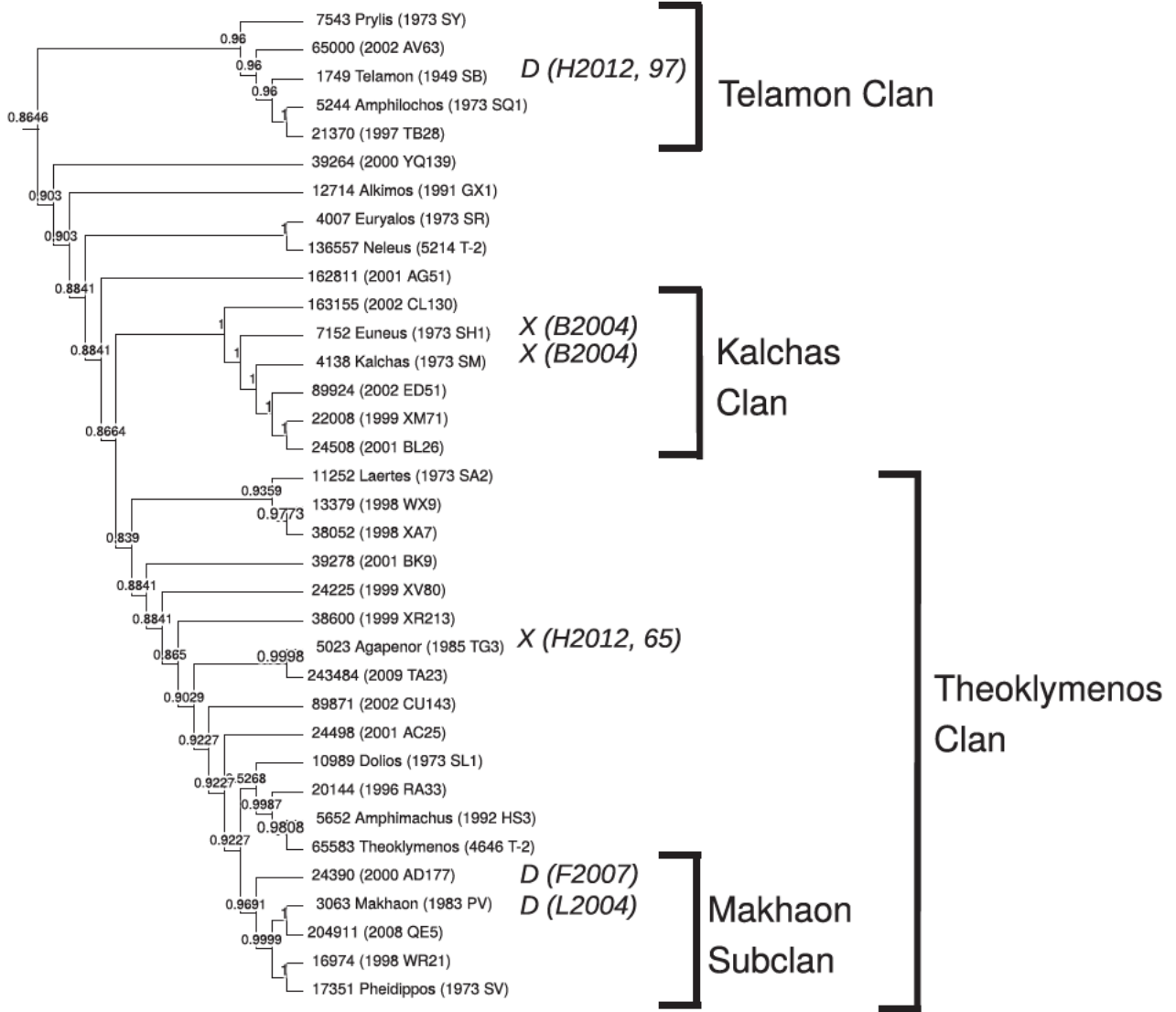


Figure B7. Consensus tree of the L4 Greater Telamon superclan, including Telamon, Kalchas, and Theoklymenos clans. Numbers indicate fraction of 10 000 trees where branch is present. *Letters* associate objects with Bus–Demeo taxonomy (Bus 2002; DeMeo et al. 2009), classified by associated reference T1989: Tholen (1989); B2004: Bendjoya et al. (2004); L2004: Lazzaro et al. (2004); F2007: Fornasier et al. (2007); H2012, with associated confidence rating: Hasselmann et al. (2012).

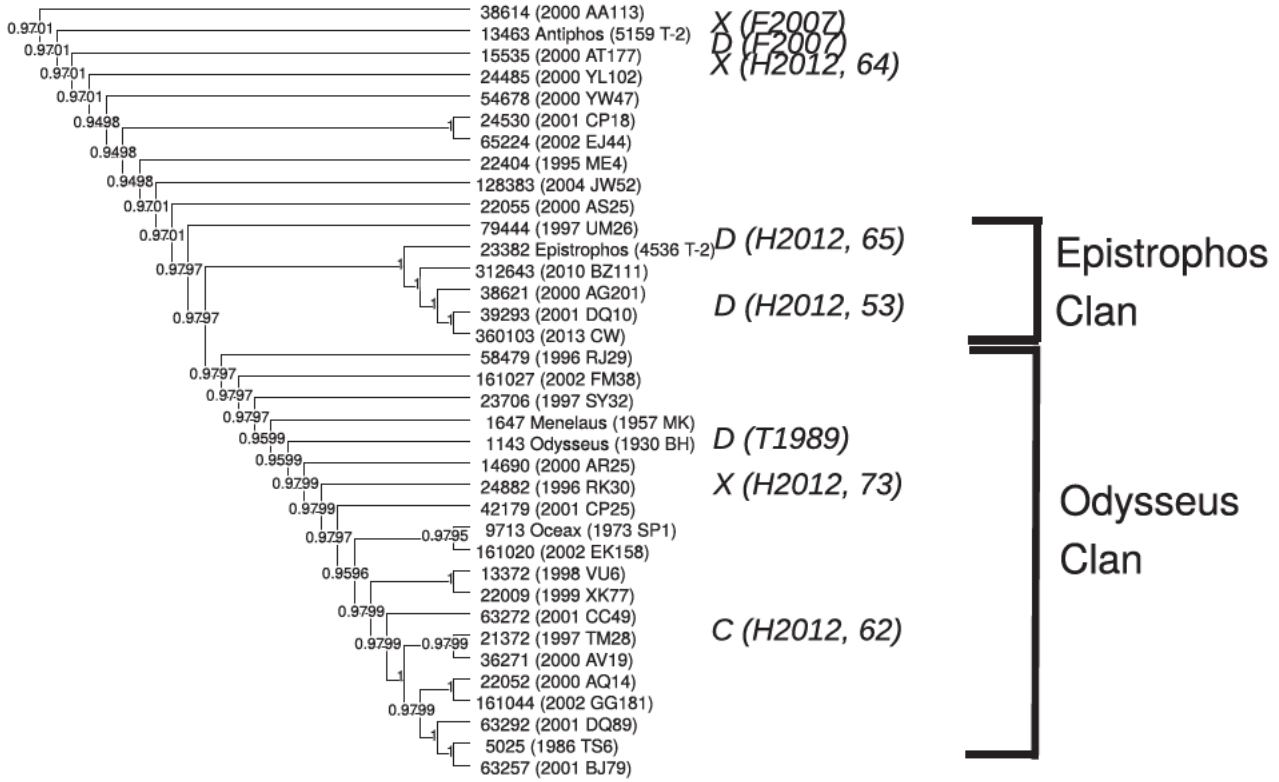


Figure B8. Consensus tree of the L4 Greater Odysseus superclan, including Epistrophos and Odysseus clans. Numbers indicate fraction of 10 000 trees where branch is present. *Letters* associate objects with Bus–Demeo taxonomy (Bus 2002; DeMeo et al. 2009), classified by associated reference T1989: Tholen (1989); B2004: Bendjoya et al. (2004); F2007: Fornasier et al. (2007); H2012, with associated confidence rating: Hasselmann et al. (2012).

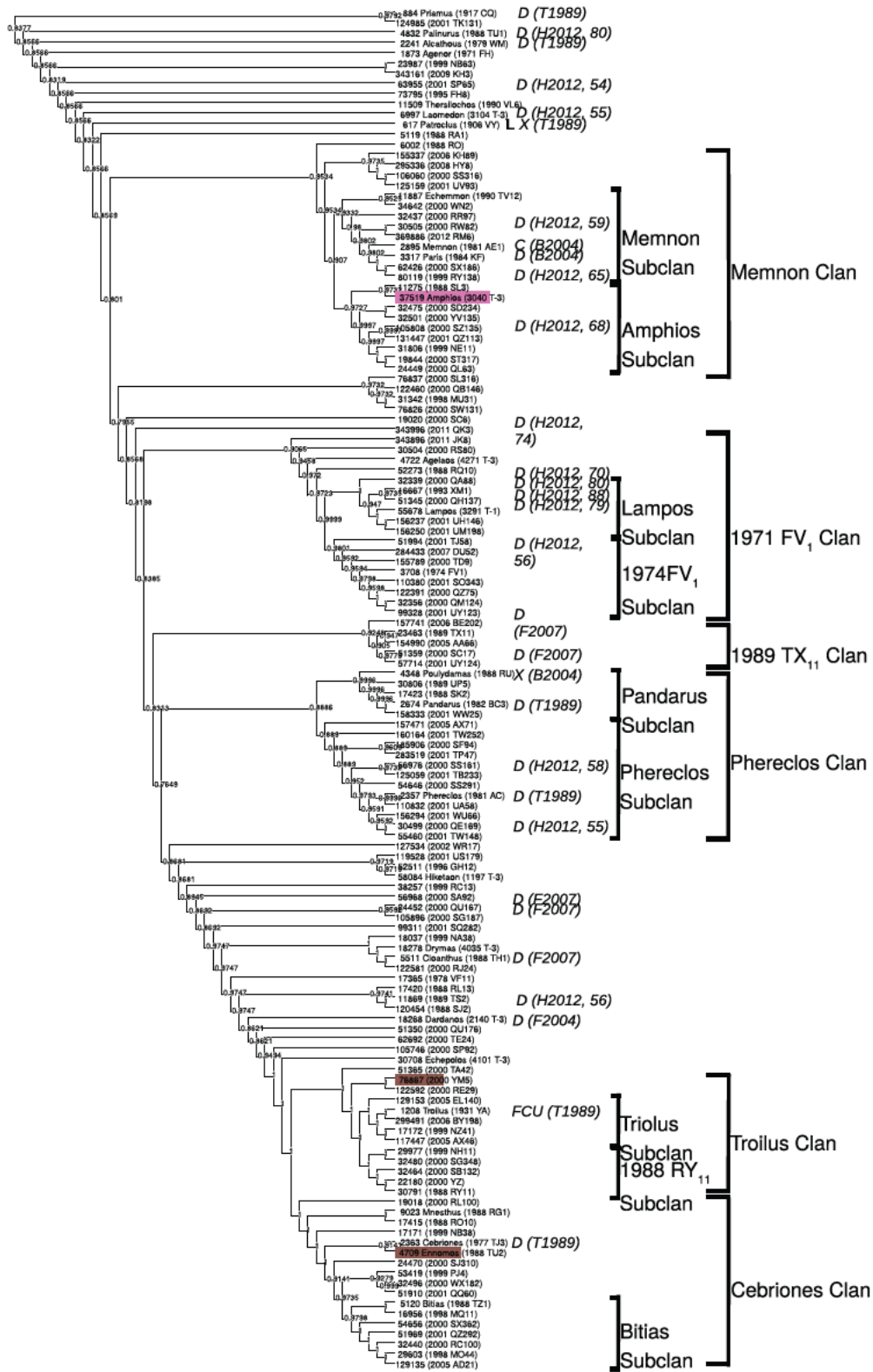


Figure B10. Consensus trees of the L5 Greater Patroclus superclan, including Memnon, 1971 FV₁, 1989 TX₁₁, Phereclos, Troilus and Cebriones clans. Numbers indicate fraction of 10 000 trees where branch is present. *Letters* associate objects with Bus–Demeo taxonomy (Bus 2002; DeMeo et al. 2009), classified by associated reference T1989: Tholen (1989); B2004: Bendjoya et al. (2004); F2007: Fornasier et al. (2007); H2012, with associated confidence rating: Hasselmann et al. (2012). L indicates objects to be visited by the *Lucy* spacecraft (Levison et al. 2017). The brown and purple highlights are members of the Ennomos and 2001 UV₂₀₉ collisional families, respectively.

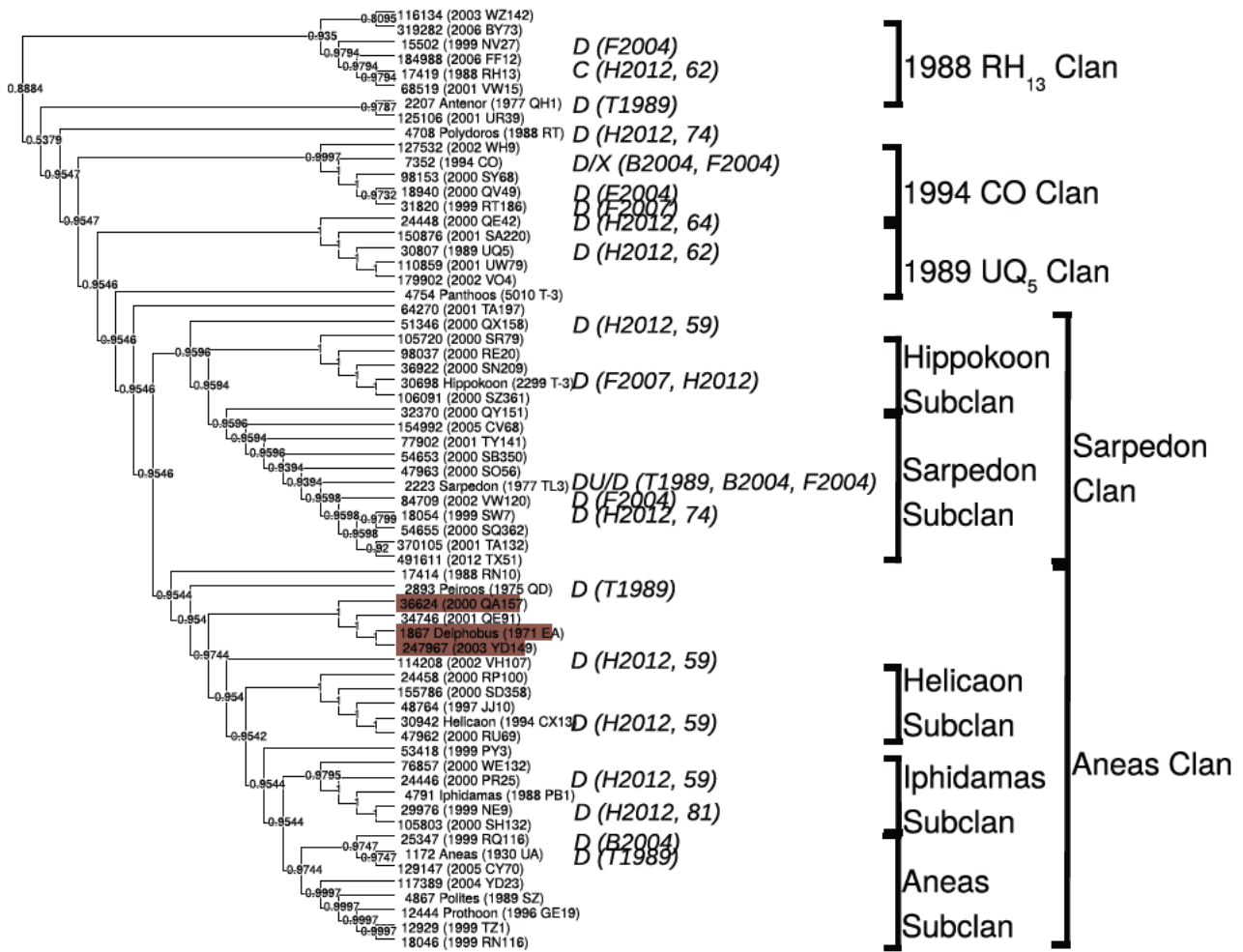


Figure B11. Consensus trees of the L5 Greater Aeneas superclan, including 1988 RH₁₃, 1994 CO, 1989 UQ₅, Sarpedon and Aeneas clans. Numbers indicate fraction of 10 000 trees where branch is present. Letters associate objects with Bus–Demeo taxonomy (Bus 2002; DeMeo et al. 2009), classified by associated reference T1989: Tholen (1989); B2004: Bendjoya et al. (2004); F2007: Fornasier et al. (2007); H2012, with associated confidence rating: Hasselmann et al. (2012). The brown highlights are members of the Ennomos collisional family.

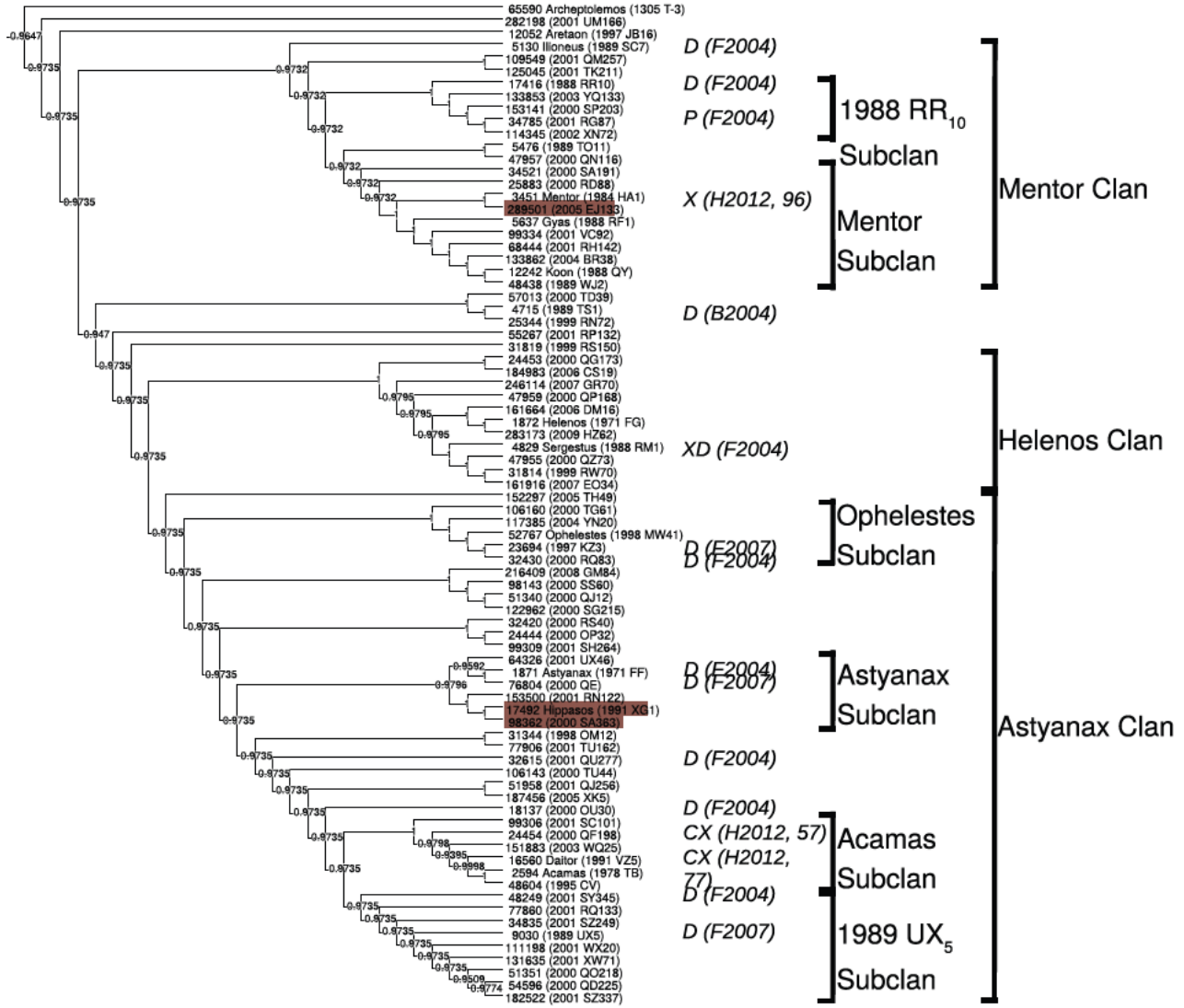


Figure B12. Consensus trees of the L5 Greater Astyanax superclan, including Mentor, Helenos, and Astyanax clans. Numbers indicate fraction of 10 000 trees where branch is present. *Letters* associate objects with Bus–Demeo taxonomy (Bus 2002; DeMeo et al. 2009), classified by associated reference T1989: Tholen (1989); B2004: Bendjoya et al. (2004); F2007: Fornasier et al. (2007); H2012, with associated confidence rating: Hasselmann et al. (2012). The brown highlights are members of the Ennomos collisional family.

This paper has been typeset from a $\text{\TeX}/\text{\LaTeX}$ file prepared by the author.

6

Additional works and Coauthor projects

In this chapter, I outline additional first author works that are peripherally related to the four first-author papers. In section 6.2, I outline several coauthor projects with which I have been involved.

6.1 ADDITIONAL WORKS

6.1.1 SIMULATIONS OF A SYNTHETIC EURYBATES COLLISIONAL FAMILY

Holt, T. R., Nesvorný, D., Horner, J., King, R., Carter, B. D., & Brookshaw, L. (2019). Simulations of a Synthetic Eurybates Collisional Family. AAS Division on Dynamical Astronomy Meeting 50, id. 100.01.

Of the six recognized collisional families in the Jovian Trojan swarms, the Eurybates family is the largest, with over 200 recognized members. Located around the Jovian L_4 Lagrange point, librations of the members make this family an interesting study in orbital dynamics. The Jovian Trojans are thought to have been captured during an early period of instability in the Solar system. The parent body of the family, 3548 Eurybates is one of the targets for the *Lucy* spacecraft, and our work will provide a dynamical context for the mission. Recent modeling has suggested that some members of the family have escaped the swarm on a time

scale comparable to the age of the Solar system. The aim of the present work is to provide a dynamical simulation of the early history of the Eurybates family to explain its origins. Our modeling involved the creation of a 1000 member synthetic fragment cloud, centered on 3548 Eurybates as the parent body. The synthetic family was created using the Gauss equations, with a 1000 m/s escape velocity and random ejection angles. The dynamical evolution of the synthetic cloud was modeled using high precision n-body simulations with the REBOUND code on a variety of time scales. From these simulations, we find that the synthetic family stabilizes into the modern observed libration pattern within a relatively short time span. By using statistical comparisons with the observed family members, our results provide the first estimate of the minimum age of the Eurybates family. The Eurybates collisional family also provides a unique opportunity to examine the dynamical evolution of the fragments of break-up event around a Lagrange point.

This was to form a basis for an investigation into the Eurybates collisional family (Brož and Rozehnal, 2011; Nesvorný et al., 2015). In the presented work, I found a minimal age for the Eurybates family of approximately 114,000 years after the collisional family creation event. Using the escape rate in Holt et al. (2020a), I also found an age estimation for the family of around 1 billion years. The synthetic simulations would form the basis for a more robust statistical analysis using a method described in Parker (2015). The method uses Approximate Bayesian Computational methods (see Marin et al., 2011, for review), to estimate the age of the family statistically. Unfortunately the results were inconclusive and the project was put on hiatus.

6.1.2 CAPTURED SMALL SOLAR SYSTEM BODIES IN THE ICE GIANT REGION:

Community Science White Paper for the Planetary and Astrobiology Decadal Survey, 2023-2032

This white paper advocates for the inclusion of small, captured Outer Solar system objects, found in the Ice Giant region in the next US Decadal Survey. These objects include the Trojans and Irregular satellite populations of Uranus and Neptune. The captured small bodies provide vital clues as to the formation of our Solar system. They have unique dynamical situations, which any model of Solar system formation needs to explain. The major issue is that so few of these objects have been discovered, with very little information known about them. The purpose of this document is to prioritize further discovery and characterization of these objects. This will require the use of NASA and NSF facilities over the 2023-2032 decade, including additional support for analysis. This is in preparation for potential future

insitu missions in the following decades.

In the USA, NASA funding for projects is dependent upon a proposal system. The success of proposals is dependent upon the community input, which begins during a decadal survey. These surveys drive NASA funding, and are constructed based by the community under a NASA and NSF mandate. The basis for these are community contributed white papers. I chose to lead one of these white papers, to ensure that the subject, Trojans and Irregular satellites of Uranus and Neptune, are part of the conversation in the next decade.

6.2 COAUTHOR

In this section, I overview several refereed papers that I have been involved with over the course of my PhD program.

6.2.1 HORNER ET AL. 2020 - SOLAR SYSTEM PHYSICS FOR EXOPLANET RESEARCH

Horner, J., Kane, S. R., Marshall, J. P., Dalba, P. A., Holt, T. R., Wood, J., ... Tylor, C. C. E. (2020). Solar System Physics for Exoplanet Research. Publications of the Astronomical Society of the Pacific, 132(1016), 102001.

Over the past three decades, we have witnessed one of the great revolutions in our understanding of the cosmos - the dawn of the Exoplanet Era. Where once we knew of just one planetary system (the Solar system), we now know of thousands, with new systems being announced on a weekly basis. Of the thousands of planetary systems we have found to date, however, there is only one that we can study up-close and personal - the Solar system. In this review, we describe our current understanding of the Solar system for the exoplanetary science community - with a focus on the processes thought to have shaped the system we see today. In section one, we introduce the Solar system as a single well studied example of the many planetary systems now observed. In section two, we describe the Solar system's small body populations as we know them today - from the two hundred and five known planetary satellites to the various populations of small bodies that serve as a reminder of the system's formation and early evolution. In section three, we consider our current knowledge of the Solar system's planets, as physical bodies. In section four, we discuss the research that has been carried out into the Solar system's formation and evolution, with a focus on the information gleaned as a result of detailed studies of the system's small body populations. In section five, we discuss our current knowledge of planetary systems beyond our own - both in terms of the planets they host, and in terms of the debris that we observe orbiting their host stars. As

we learn ever more about the diversity and ubiquity of other planetary systems, our Solar system will remain the key touchstone that facilitates our understanding and modelling of those newly found systems, and we finish section five with a discussion of the future surveys that will further expand that knowledge.

MY CONTRIBUTION: Horner et al. (2020) is a recent major overview of Solar system physics, presented in the context of exoplanet science. In this work, I helped to create many of the plots of Solar system populations. Some examples are shown in the figures 1.2 and 1.4, plots in Semi-major axis, eccentricity and inclination for the inner and outer Solar system. I also created figures for individual populations, such as Figure 1.8. Another example, of the NEO populations, shown here in Figure 6.1. Each figure was created using data from HORIZONS Solar system Dynamics Database <https://ssd.jpl.nasa.gov/> (Giorgini et al., 1996). I also made plots of the Solar system as it stood on Jan 1st, 2000.

6.2.2 BOLIN ET AL. 2020 - CHARACTERIZATION OF TEMPORARILY CAPTURED MINIMOON 2020 CD₃ BY KECK TIME-RESOLVED SPECTROPHOTOMETRY

Bolin, B. T., Fremling, C., Holt, T. R., Hankins, M. J., Ahumada, T., Anand, S., ... Zolkower, J. (2020). Characterization of Temporarily Captured Minimoon 2020 CD₃ by Keck Time-resolved Spectrophotometry. *The Astrophysical Journal*, 900(2), L45.

We present time-resolved visible spectrophotometry of 2020 CD₃, the second known minimoon. The spectrophotometry was taken with the Keck I/Low Resolution Imaging Spectrometer between wavelengths 434 and 912 nm in the B, g, V, R, I, and RG850 filters as it was leaving the Earth–Moon system on 2020 March 23 UTC. The spectrum of 2020 CD₃ resembles V-type asteroids and some lunar rock samples with a 434–761 nm reddish slope of $\sim 18\%/100$ nm ($g-r = 0.62 \pm 0.08$ and $r-i = 0.21 \pm 0.06$) with an absorption band at ~ 900 nm corresponding to $i-z = -0.54 \pm 0.10$. Combining our measured H of 31.9 ± 0.1 with an albedo of 0.35 typical for V-type asteroids, we determine 2020 CD₃'s diameter to be $\sim 0.9 \pm 0.1$ m, making it the first minimoon and one of the smallest asteroids to be spectrally studied. We use our time-series photometry to detect significant periodic light-curve variations with a period of ~ 573 s and amplitude of ~ 1 . In addition, we extend the observational arc of 2020 CD₃ to 37 days, to 2020 March 23 UTC. From the improved orbital solution for 2020 CD₃, we estimate the likely duration of its capture to be ~ 2 yr and the nongravitational perturbation on its orbit due to radiation pressure with an area-to-mass ratio of $(6.9 \pm 2.4) \times 10^{-4}$ m² kg⁻¹

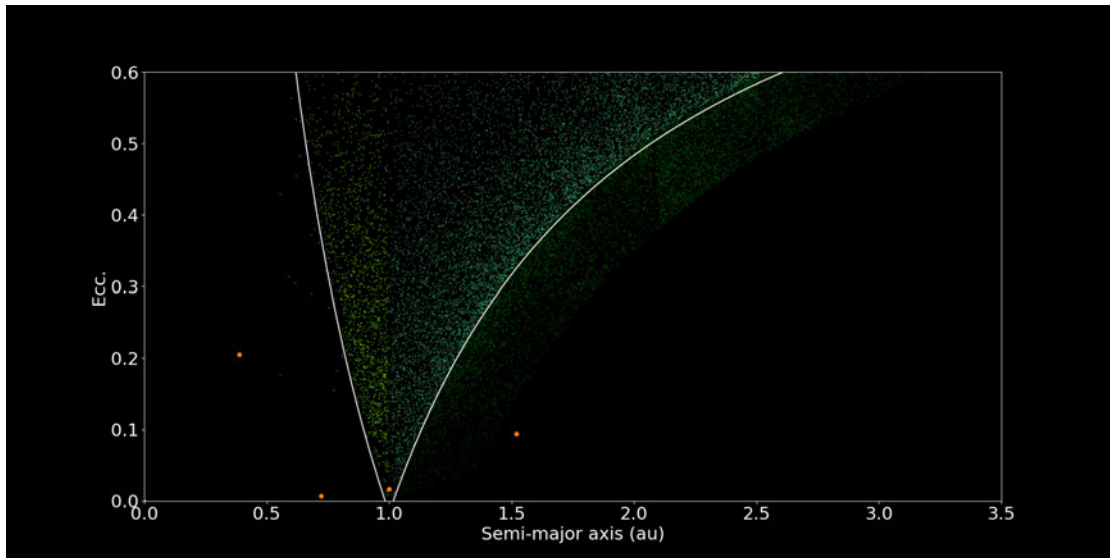


Figure 6.1: The orbital element distribution of the known near-Earth asteroids, in semi-major axis eccentricity space (top) after Horner et al. (2020). The four sub-groups within the near-Earth asteroid population are shown in different shades of green. The Atira asteroids are shown in aquamarine, the Atens in chartreuse, Apolos in sea green and Amors in dark green. The impact of observational bias is clearly seen here, particularly in the upper panel. Objects are easier to detect closer to Earth than farther away - and the smallest (but most numerous) objects can only be discovered during close approaches to our planet. For that reason, the greatest population in a-e space is bounded by lines of constant perihelion = 0.9833 au (curving outward to the right) and aphelion = 1.0167 au (moving inwards toward higher eccentricities), which we show in white in the top panel. The wedge bounded by these two lines contains those objects that can reach a heliocentric distance at a distance within the bounds set by Earth's perihelion and aphelion distances and can therefore experience very close encounters with our planet.

implying a density of $2.3 \pm 0.8 \text{ g cm}^{-3}$, broadly compatible with other meter-scale asteroids and lunar rock. We searched for predisccovery detections of 2020 CD₃ in the Zwicky Transient Facility archive as far back as 2018 October but were unable to locate any positive detections.

MY CONTRIBUTION: In Bolin et al. (2020), I undertook the dynamical simulations. The following is reproduced from that paper, showing my major contributions.

The second-known minimoons 2020 CD₃ was discovered while it was captured by the Earth-Moon system. To determine its orbital evolution before, during and after its captured state, we implemented the REBOUND n -body orbit integration package (Rein and Liu, 2012) with our fitted orbit. In addition to its nominal orbit, we cloned ~ 10 additional massless test particles defined from the vertices of a cuboid represented by the heliocentric orbital elements and σ orbital parameter semi-major axis a , eccentricity e and inclination i uncertainties and an initial ephemeris time of 2020 March 23 UTC. The simulations are run using the IAS15 integrator (Rein and Liu, 2012) and the Sun, eight major masses of the Solar system, along with the Moon, Vesta, Ceres and Pluto ¹. The simulations were run using a timestep of 0.00249 y (21.825 hours, 0.03 times the Lunar orbital period), with an output of 0.01 y for 5-y and 100-y time-frames.

We adopt the definition of geocentric capture from Fedorets et al. (2017) and Jedicke et al. (2018) to describe the geocentric orbital evolution of 2020 CD₃, namely that while captured, 2020 CD₃ remains within 3 Hill radii ($\sim 0.03 \text{ au}$) of the Earth, has a $e_g < 1$, and approaches the Earth to within 1 Hill radius ($\sim 0.01 \text{ au}$) at some point during its captures. As seen in Fig. 6.2, 2020 CD₃ approaches the Earth-Moon system opposite from the Sun's direction in the direction of the L₂ Lagrange point with its capture beginning in mid 2018 with a low $\sim 1 \text{ km/s}$ encounter velocity. Almost half of minimoons pass through the L₂ Lagrange point while becoming temporarily geocentrically bound (Granvik et al., 2012), therefore, it seems 2020 CD₃'s capture is non-exceptional in the case of temporarily captured asteroids. In addition, we see from the top panels of Fig. 6.2 that 2020 CD₃ is captured on a retrograde orbit $\sim 100^\circ$ and completes ~ 5 revolutions around the Earth-Moon system while remaining within three Hill radii of geocenter. Integrating its orbit forward and backward, the majority of 2020 CD₃ orbital clones remained captured within the Earth-Moon for $\sim 2 \text{ y}$ as seen in the bottom right panel of Fig.6.2 leaving the Earth-Moon system in mid 2020. Integrating the orbit with and without a Solar radiation pressure component does not significantly affect the capture dura-

¹Taken from the JPL HORIZONS Solar System Dynamics Database <https://ssd.jpl.nasa.gov/> (Giorgini et al., 1996), on 10th April, 2020.

tion of 2020 CD₃. The geocentric orbit of 2020 CD₃ is retrograde for nearly the entirety of its capture and its final orbit will result in it having a slightly larger heliocentric semi-major axis of a of 1.027 au compared to its pre-capture a of 0.973 au as seen in the bottom left panel of Fig. 6.2. Overall it seems the capture of 2020 CD₃ is a typical, however, having a longer duration than the ~ 1 y capture duration of 2006 RH₁₂₀, the only other known minimoon, and the ~ 9 month capture duration averaged over the minimoon population (Granvik et al., 2012).

In addition, we take a look at the longer term, 100 y heliocentric orbital evolution of 2020 CD₃ as presented in Figs. 6.3 and 6.4. Integrating the orbit of 2020 CD₃ 100 years into the past and into the future show similar behavior in that 2020 CD₃ has close encounters with the Earth placing 2020 CD₃ inside the Hill radius of the Earth every ~ 20 -30 years as seen in the bottom right panels of Figs. 6.3 and 6.4. The long-term orbit of 2020 CD₃ resembles a horseshoe orbit as seen in the upper left panels of Figs. 6.3 and 6.4 where its status as temporarily capture asteroids has resulted from its similar orbital plane and low encounter velocity relative to Earth’s (Granvik et al., 2013; Jedicke et al., 2018). Interestingly, some of the 2020 CD₃ orbit clones when integrated into the future switch from a max inclination of 0.012° to 0.031° during the next encounter with the Earth. In addition, we have undertaken preliminary, long-term simulations using the hybrid MERCURIUS REBOUND integrator, (Rein et al., 2019) using the same initial conditions as above, including the eight clones. These initial simulations indicate that the horse-shoe dynamical situation is stable for at least $\sim 10^6$ years.

6.2.3 HORNER ET AL. 2021 - DYNAMICAL PROSPECTING IN THE π MENSÆ SYSTEM

Horner, J., Marshall, J. P., Witenmyer, R. A., Kane, S. R., Okumura, J., Holt, T. R., Errico, A. and Carter, B. D. (2021). Dynamical prospecting in the π Mensæ system. *The Astronomical Journal*. Under review.

We present the results of a “dynamical prospecting” study of the π Mensæ system, in an attempt to constrain the possibilities for additional undiscovered planets and debris disc structures therein. π Mensæ is a Sun-like star known to host a hot super-Earth, a cold, massive, and eccentric giant planet, and a cold debris disc (analogous to the Edgeworth-Kuiper belt). We find that the system could indeed host further, as yet undiscovered planets, but that those planets must orbit closer than ~ 0.4 au from the central star. We can explicitly rule out the presence of planets in the optimistic habitable zone around π Mensæ – such planets would be ejected from the system by π Mensæ b on timescales of a thousand years, or less. By com-

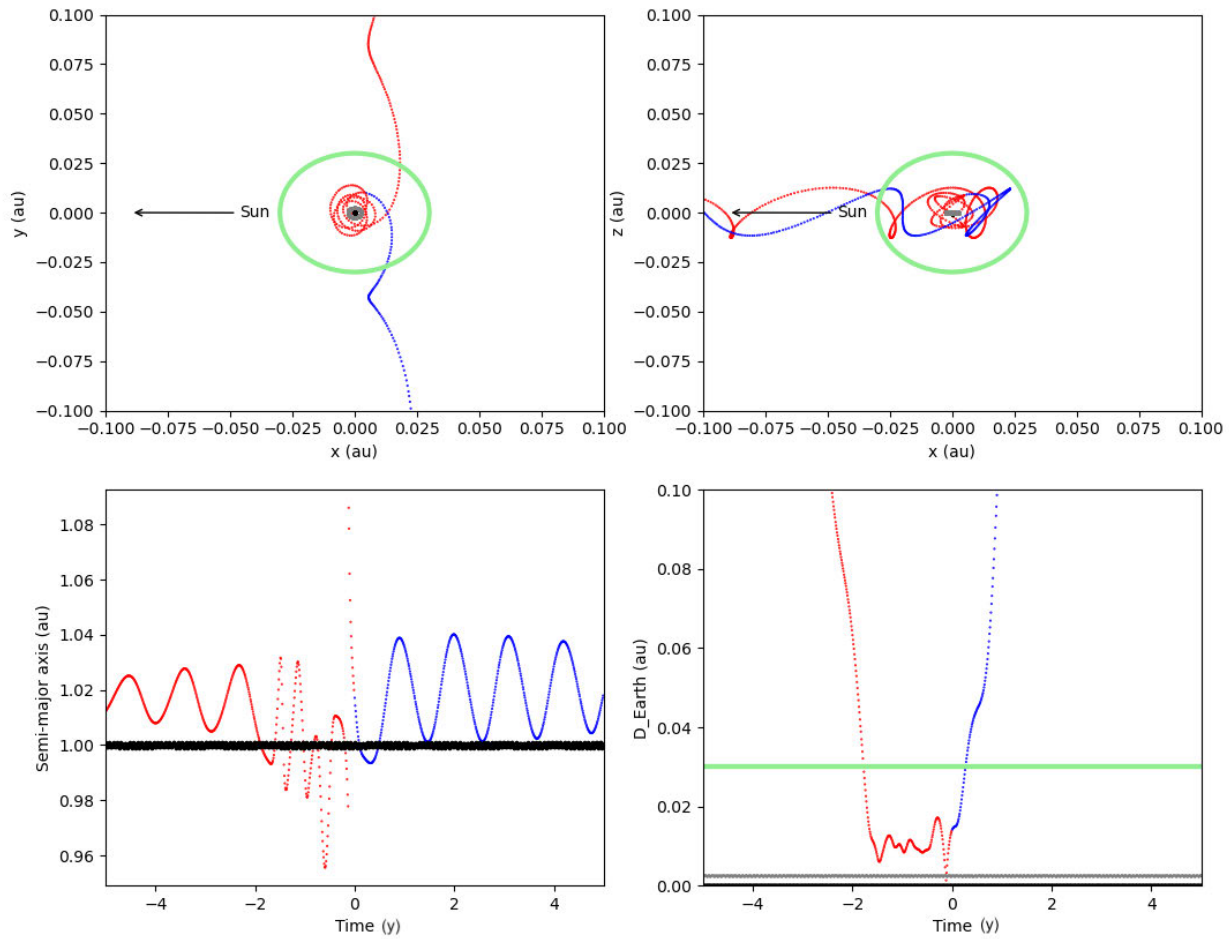


Figure 6.2: Top left pane mean geocentric, co-rotating Cartesian y and x coordinates of 2020 CD₃ orbita c ones ± 5 y centered on 2020 March 23 UTC encompassing its ~ 700 day capture competing ~ 5 revolutions around the Earth-Moon system. The red dotted line indicates the trajectory of 2020 CD₃ before 2020 March 23 UTC and the blue dotted line indicates the trajectory of 2020 CD₃ after 2020 March 23 UTC. A green circle with a radius of three times the Earth's Hill radii of ~ 0.03 au is overlotted. The direction towards the Sun in the co-rotating frame is indicated. Top right pane same as the top left pane except for mean geocentric, co-rotating Cartesian x and z coordinates. Bottom left pane the evolution of 2020 CD₃'s orbita c ones mean semi-major axes ± 5 y centered on 2020 March 23 UTC. The color code of the dotted lines is the same as in the top panes. Bottom right pane the mean geocentric distance of 2020 CD₃ orbita c ones ± 5 y centered on 2020 March 23 UTC. A horizontal green line indicates three times the Hill radii in distance. The color code of the dotted lines is the same as in the previous three panes.

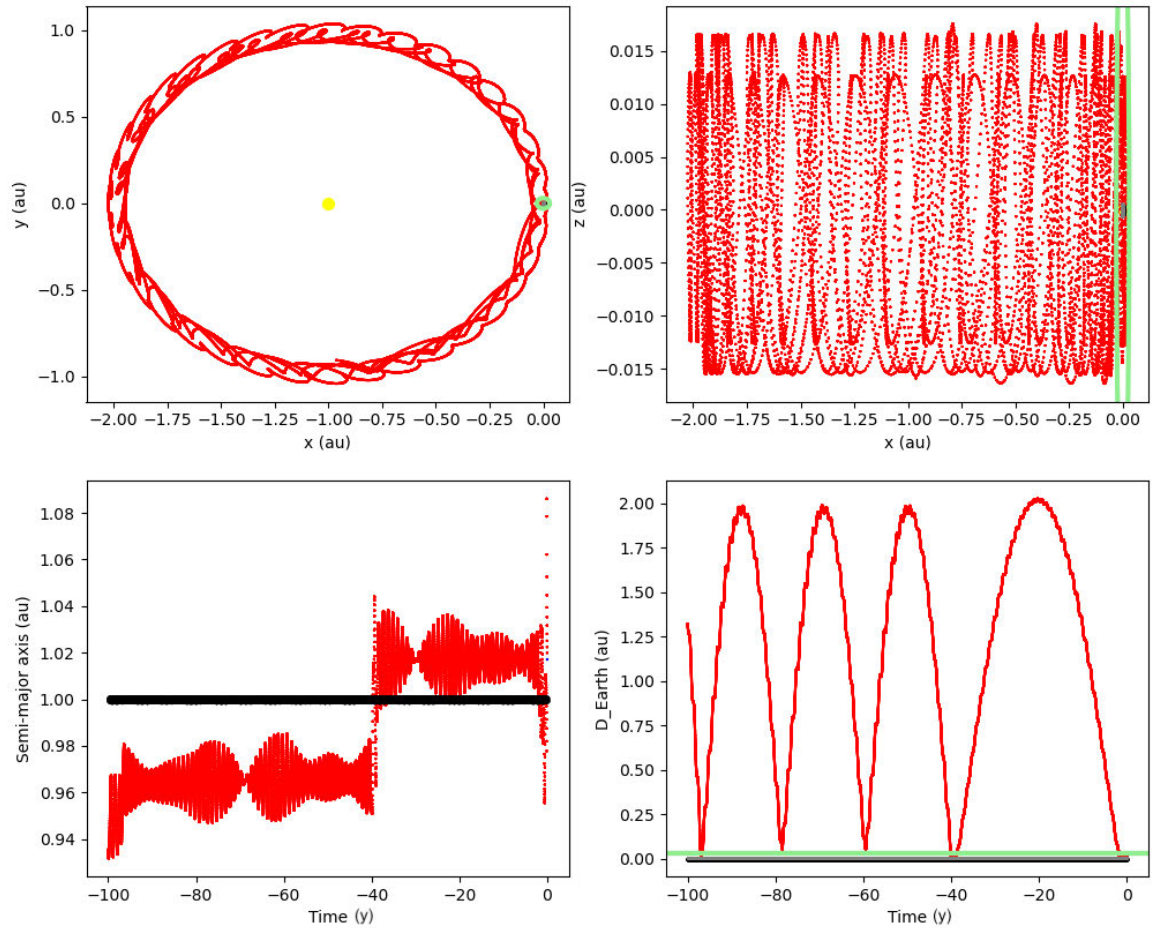


Figure 6.3: Top left pane mean geocentric Cartesian y and x coordinates of 2020 CD₃ orbita c ones integrated backwards 100 y from 2020 March 23 UTC (blue line) with the Earth's three Hill radii marked in green. Top right pane same as the top left pane except for the mean geocentric Cartesian x and z coordinates of 2020 CD₃ orbita c ones integrated backwards 100 y from 2020 March 23 UTC. Bottom left pane the evolution in 2020 CD₃'s orbita c ones mean semi-major axis integrated backwards 100 y from 2020 March 23 UTC with the Earth's orbit in black. Bottom right pane the geocentric distance of 2020 CD₃ orbita c ones integrated backwards 100 y from 2020 March 23 UTC.

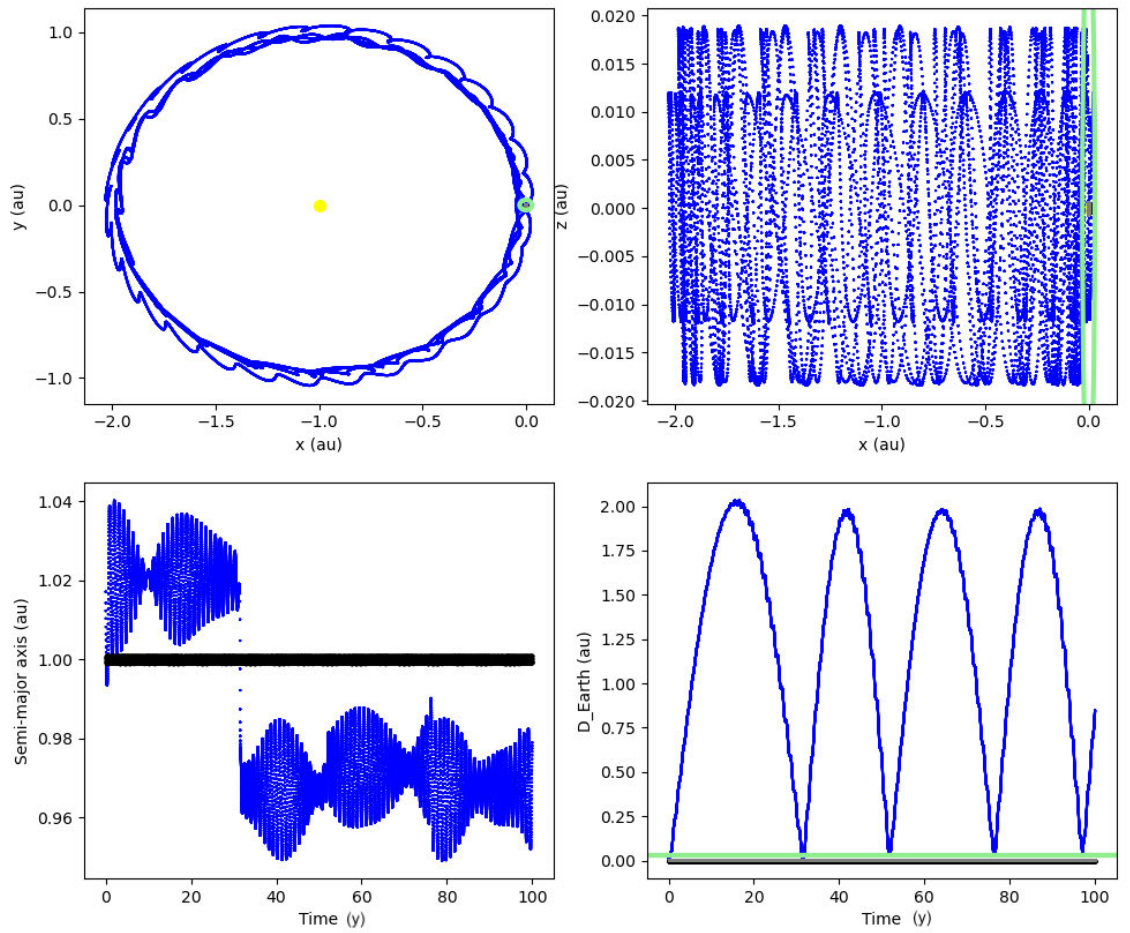


Figure 6.4: Top left pane same as in Fig. 6.3 except for orbitals of 2020 CD₃ integrated forwards 100 y from 2020 March 23 UTC (red line) with the Earth's three Hill radii marked in green. Top right pane same as the top left pane except for the mean geocentric Cartesian x and z coordinates of 2020 CD₃ orbitals integrated forwards 100 y from 2020 March 23 UTC. Bottom left pane the evolution in 2020 CD₃'s orbitals mean semi-major axis integrated forwards 100 y from 2020 March 23 UTC with the Earth's orbit in black. Bottom right pane the geocentric distance of 2020 CD₃ orbitals integrated forwards 100 y from 2020 March 23 UTC.

binning our dynamical constraints with a reanalysis of available radial velocity data, we can rule out the presence of planets more massive than $\sim 4M_{\oplus}$ interior to π Mensæ c, and exclude the presence of planets above $10M_{\oplus}$ anywhere between the orbits of the two known planets. Our simulations also reveal the possibility that the π Mensæ system could host a warm debris belt, analogous to the Asteroid belt, between ~ 0.2 and 0.65 au. Such a belt would yield an infrared excess around the star at wavelengths of $\sim 5\mu\text{m}$. However, the available observational data is only sufficient to exclude the presence of an extremely bright disc at such wavelengths – leaving the presence (or absence) of such a debris belt to be determined by future observations.

MY CONTRIBUTION: This work looks into the dynamical parameter space of the exoplanetary system, π Mensæ. My contribution to this work was calculating the Habitable zone (Kopparapu et al., 2013, 2014) for the system. The optimistic habitable zone in the π Mensæ system, the inner boundary of which falls at $a \sim 0.902$ au, with the outer boundary at $a \sim 2.121$ au. For the π Mensæ system, there have been two planets discovered, π Mensæ b (3.10 ± 0.02 au) and π Mensæ b (0.06839 ± 0.00050 au, $0.0152^{+0.0026}_{-0.0027} M_{jup}$) (Huang et al., 2018). Using the simulation setup shown in the top images of Figure 6.5 the results mean that we can definitively rule out the existence of planets within the optimistic habitable zone of π Mensæ solely on dynamical grounds – the influence of π Mensæ b renders the entire region dynamically unstable. In addition to the habitable zone calculations, I also helped to update the figures 6 and 7, shown in Figure 6.5 and 6.6.

6.2.4 BOLIN ET AL. 2021 - INITIAL VISIBLE AND MID-IR CHARACTERIZATION OF P/2019 LD₂ (ATLAS), AN ACTIVE TRANSITIONING CENTAUR AMONG THE TROJANS, WITH HUBBLE, SPITZER, ZTF, KECK, APO AND GROWTH IMAGING AND SPECTROSCOPY

Bolin, B. T., Fernandez, Y. R., Lisse, M.C., Holt, T. R., Lin, Z., Purdum, J.N., ... Zolkower, J. (2020). Initial Visible and Mid-IR Characterization of P/2019 LD₂ (ATLAS), an Active Transitioning Centaur Among the Trojans, with Hubble, Spitzer, ZTF, Keck, APO and GROWTH Imaging and Spectroscopy. *The Astronomical Journal*, Volume 161, Issue 3, id.116, 15 pp.

We present visible and mid-infrared imagery and photometry of Jovian co-orbital comet P/2019 LD₂ (ATLAS) taken with Hubble Space Telescope/WFC3 on 2020 April 1, Spitzer Space Telescope/IRAC on 2020 January 25, Zwicky Transient Facility between 2019 April 9 and

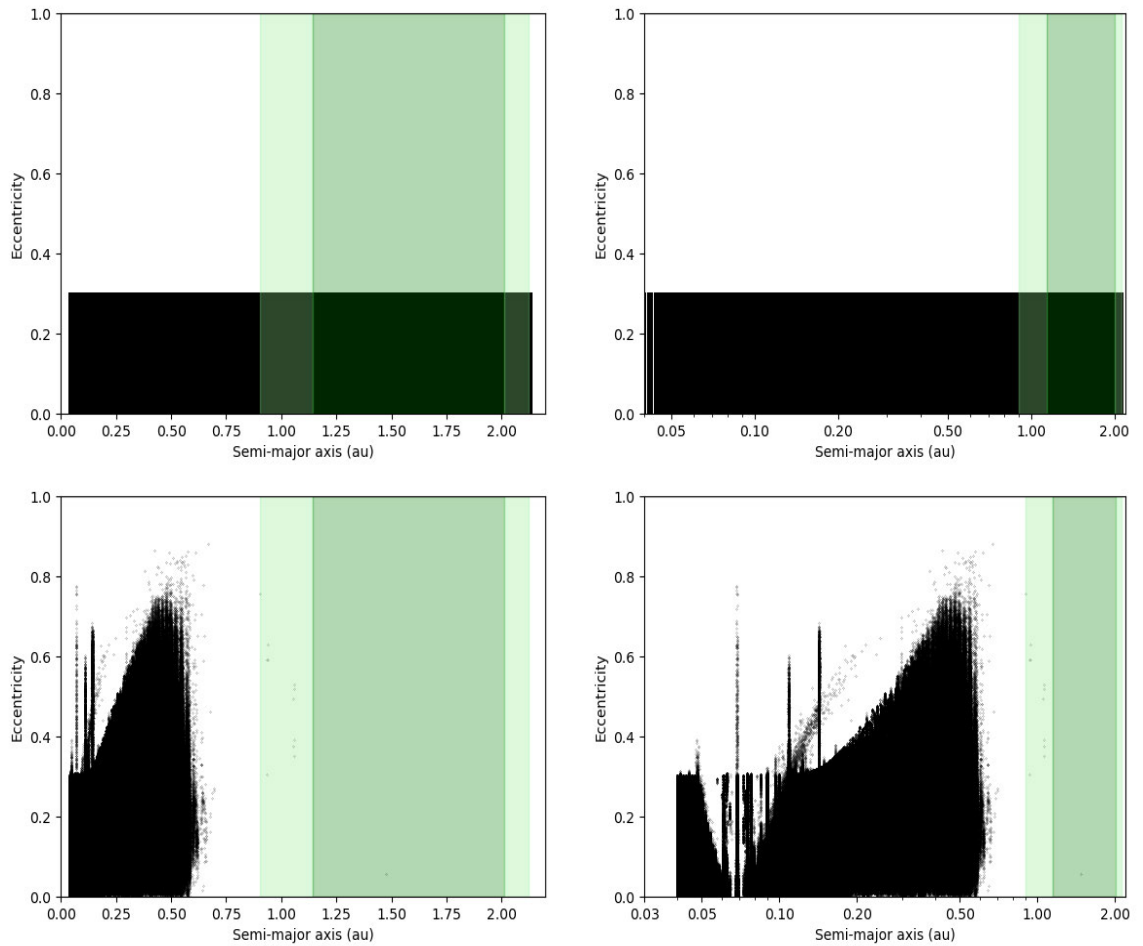


Figure 6.5: The distribution of test particles at the start (top) and end (bottom) of our simulations, in semi-major axis (a) vs eccentricity (e) space. We highlight the extent of the conservative and optimistic habitable zones for the system, following Kopparapu et al. (2013, 2014), in green - with the conservative habitable zone shown in dark green, and the optimistic zone marked in pale green. The influence of π Mensæ b is readily apparent - clearing the entirety of the optimistic habitable zone, and beyond (inwards to ~ 0.6 au), and exciting the eccentricities of particles inwards to within 0.2 au. Similarly, the influence π Mensæ c can be seen in the form of the 'wedge' of cleared space in the inner area of the system.

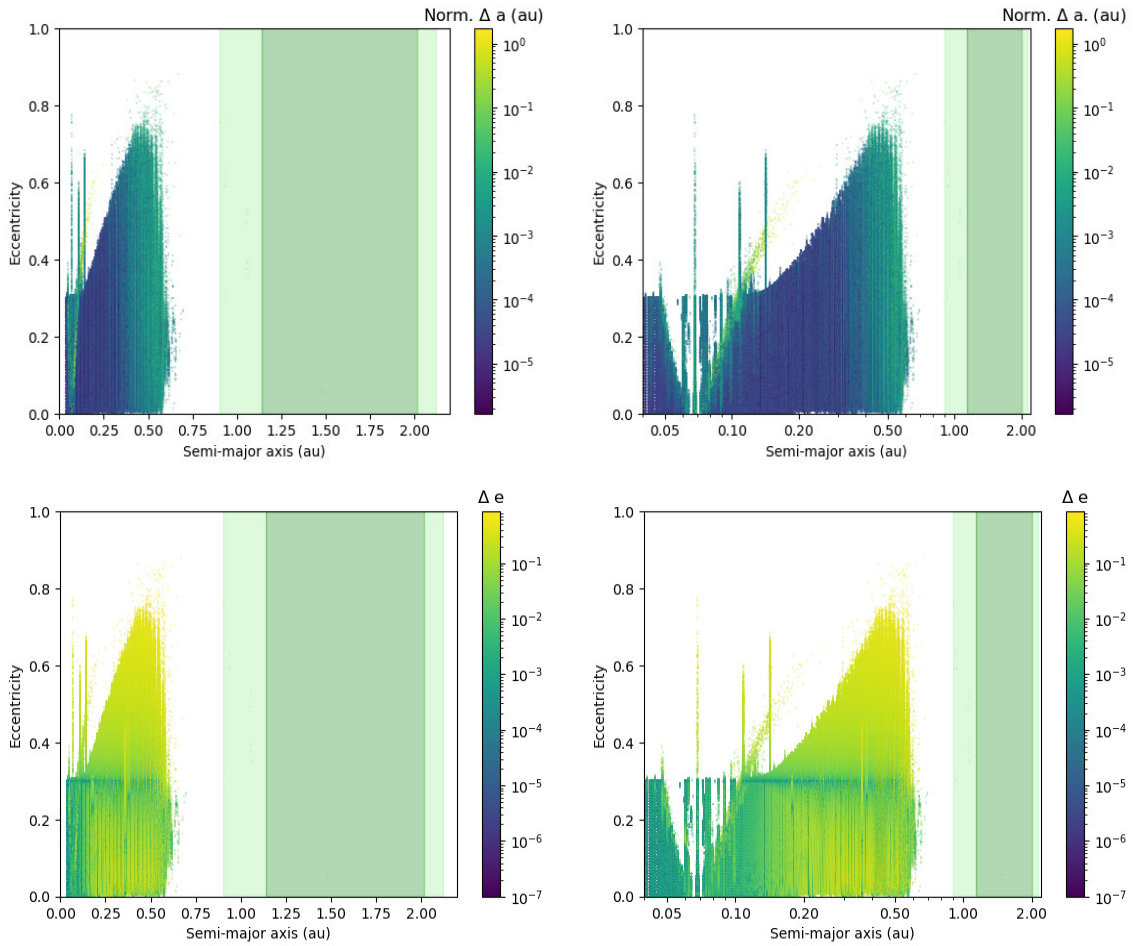


Figure 6.6: The distribution of test particles at the end of our simulations, in semi-major axis (a) vs eccentricity (e) space. The colour bar shows, in each plot, the normalised fractional change in the test particles semi-major axis (top) and the distance that it has moved in eccentricity space (bottom). The regions shown in green mark the conservative (dark green) and optimistic (light green) habitable zones, following Kopparapu et al. (2013, 2014). It is immediately apparent that, through the great majority of the region studied, the surviving test particles exhibit excitation in orbital eccentricity without moving much in semi-major axis space. The exception to this comes in the form of those particles scattered by π Mensæ c along lines of constant periapse and apoapse.

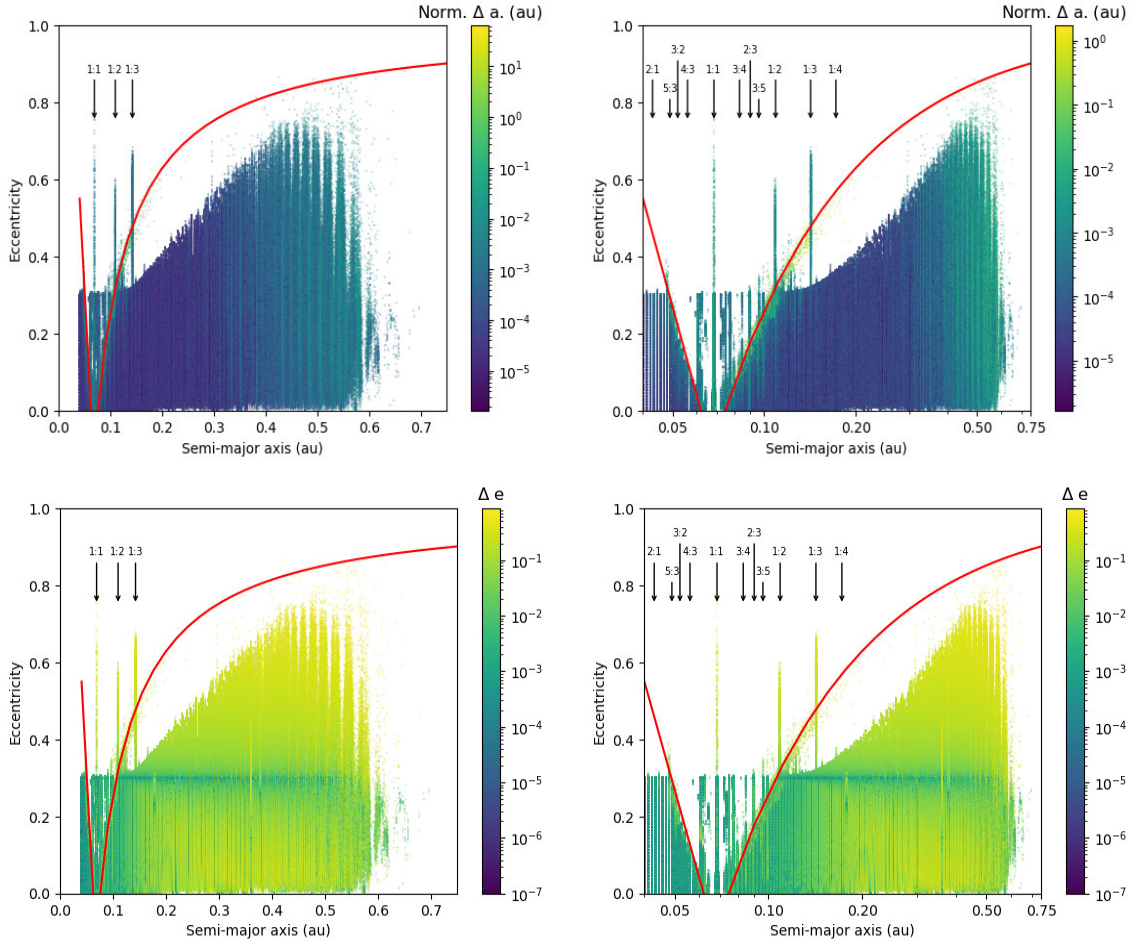


Figure 6.7: The distribution of the surviving test particles at the conclusion of our simulations, after 1 Myr of evolution, zoomed to the region where particles survived. The panels show the particle distribution in semi-major axis (a) vs. eccentricity (e) space, with the left panel showing a linear presentation of a , and the right plotting a logarithmically. The red lines denote paths of constant apoapse at 0.062 au and periapse at 0.074 au, and the locations of key mean-motion resonances with π Mensæ c are marked at the top. As in Figure 6.6, the colour scale shows the degree to which test particles are excited in semi-major axis (upper panels) and eccentricity (lower panels). The striped structure visible in the logarithmic plot is the result of the initial spacing process, showing the spacing of the innermost suite of test particles in a -space, which is preserved as those test particles are not strongly stirred in semi-major axis. The sculpting of the test particle disk exterior to ~ 0.2 au as a result of the influence of π Mensæ b is clearly visible.

2019 Nov 8 and the GROWTH telescope network from 2020 May to July, as well as visible spectroscopy from Keck/LRIS on 2020 August 19. Our observations indicate that LD₂ has a nucleus with radius 0.2-1.8 km assuming a 0.08 albedo and that the coma is dominated by $\sim 100 \mu\text{m}$ -scale dust ejected at $\sim 1 \text{ m/s}$ speeds with a $\sim 1^\circ$ jet pointing in the SW direction. LD₂ experienced a total dust mass loss of $\sim 10^8 \text{ kg}$ and dust mass loss rate of $\sim 6 \text{ kg/s}$ with $Af\rho$ /cross-section varying between $\sim 85 \text{ cm}/125 \text{ km}^2$ and $\sim 200 \text{ cm}/310 \text{ km}^2$ between 2019 April 9 and 2019 Nov 8. If the $Af\rho$ /cross-section increase remained constant, it implies that LD₂ has remained active since ~ 2018 November when it came within 4.8 au of the Sun, a typical distance for comets to begin sublimation of H₂O. From our $4.5 \mu\text{m}$ Spitzer observations, we set a limit on CO/CO₂ gas production of $\sim 10^{27}/\sim 10^{26} \text{ mol/s}$. Multiple bandpass photometry of LD₂ taken by the GROWTH network measured in a 10,000 km aperture provide color measurements of $g-r = 0.59 \pm 0.03$, $r-i = 0.18 \pm 0.05$, and $i-z = 0.01 \pm 0.07$, colors typical of comets. We set a spectroscopic upper limit to the production of H₂O gas of $\sim 80 \text{ kg/s}$. Improving the orbital solution for LD₂ with our observations, we determine that the long-term orbit of LD₂ is that of a typical Jupiter Family Comet having close encounters with Jupiter coming within ~ 0.5 Hill radius in the last $\sim 3 \text{ y}$ to within 0.8 Hill radius in $\sim 9 \text{ y}$ and has a 95% chance of being ejected from the Solar System in $< 10 \text{ Myr}$.

MY CONTRIBUTION: As in Bolin et al. (2020), I assisted with the dynamical simulations. In the case of this object, 2019 LD₂ has been investigated using short term simulations by Hsieh et al. (2021) and Steckloff et al. (2020). In Bolin et al. (2021), I validate their short-term simulations (± 100 years) using REBOUND MERCURIUS (Rein et al., 2019) hybrid integrator, and run long-term 10 million year simulations, with 27,000 clones. This confirmed 2019 LD₂ as a Centaur transitioning into a Jupiter Family Comet through the Jovian Lagrange region, before being ejected from the Solar system on million year time scales. Using this larger number of clones, I can look statistically at the fraction of the clones that escape the Solar system. The half-life of these clones, as per Centaurs in (Horner et al., 2004), is 3.4×10^5 years. This is an order of magnitude smaller than the mean half-life of Centaurs (2.7×10^6 years, Horner et al., 2004) and more comparable to lifetimes of Jupiter Family group comets of $\sim 5 \times 10^5$ (Levison and Duncan, 1994). 78.8% of the clones escape the Solar system within the first 1×10^6 years as seen in fig 6.8. After $\sim 3.8 \times 10^6$ years, 95% of the P/2019 LD₂ clones have escaped.

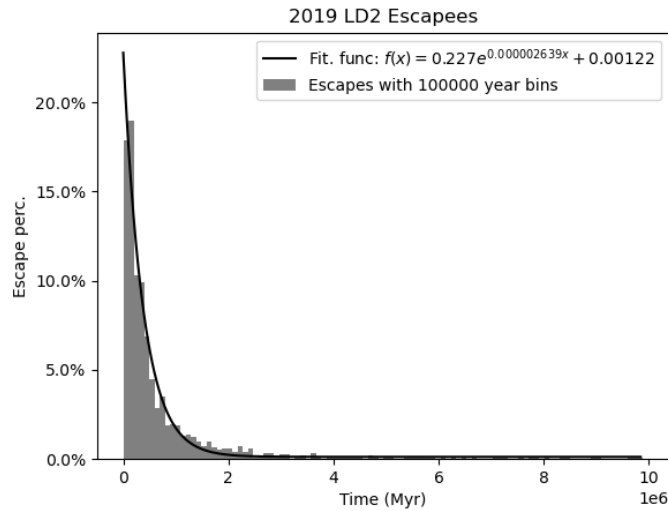


Figure 6.8: The percentage of orbita P/2019 LD 2 c ones that have escaped the So ar System (reached >1000 au from the Sun) per bin in duration of time. Each bin is $\sim 100,000$ years wide. Within the first million years of the simulation, 78.8% have escaped the So ar System. By 10 million years, $\sim 95\%$ have escaped the So ar System.

6.2.5 BUIE ET AL. 2021 -SIZE AND SHAPE OF (11351) LEUCUS FROM FIVE STELLAR OCCULTATIONS

Buie, M.W., Keeney, B.A. et al. (2021). Size and shape of (11351) Leucus from five stellar occultations. Planetary Science Journal. Under review.

We present observations of five stellar occultations for (11351) Leucus and reports from two efforts on (21900) Orus. Both objects are prime mission candidate targets for the *Lucy* Discovery mission. The combined results for Leucus indicate a very dark surface with $p_V = 0.037 \pm 0.001$. The albedo is from the average of the multi-chord occultations with each being corrected to the appropriate lightcurve phase. Our estimate of the triaxial ellipsoidal shape is for axial diameters of 63.8 x 36.6 x 29.6 km assuming that the spin pole is normal to the line of sight. The actual shape of the object is only roughly elliptical in profile at each epoch. A considerable amount of correlated topography is see with horizontal scales up to 30 km and vertical scales up to 5 km. The largest feature seen is on the southern end of the object as seen from a terrestrial view point. The predictions for these occultations required the use of differential refraction corrections to account for the difference in color between the target object and the reference stars used from ground-based observing stations.

MY CONTRIBUTION: In this work, I attended the occultation events and helped to take data. This involved making observations of a star as the asteroid, in this case 11351 Leucus and 21900 Orus, passes in front. This is similar to a Solar eclipse, and is very location dependent. I was part of the team for the November 2018 Leucus event in Arizona USA, the November 2019 Orus event in Northern Australia and the October 2020 Leucus event in Texas, USA. I also improved the initial parts of the introduction to read: The NASA Discovery mission, *Lucy*, is scheduled to visit at least six targets in the Jovian Trojan population (Levison et al., 2017). These two captured swarms, located near Jupiters' L_4 and L_5 Lagrange points, are vital to our understanding of the early Solar system (Nesvorný, 2018; Holt et al., 2020a). The population also contains a diversity of taxonomic types (DeMeo et al., 2009; Grav et al., 2012), with possible links to the outer Solar system populations (Emery et al., 2015; Wong and Brown, 2016). The work discussed here is in regard to (11351) Leucus, a D-type object (Fornasier et al., 2007), and to a lesser extent (21900) Orus, both of which are among the selected targets for *Lucy*.

7

Outcomes, Future works and conclusions

This thesis is comprised of four papers, each in relation to the hypothesis: Astrocladistics can be used to classify small Solar system objects into groups, including the Jovian Trojans and gas giant Irregular satellites, using incomplete datasets. The dynamical evolution of these populations can be simulated, giving insight into their long term stability and origins. Papers one (Holt et al., 2018) and four (Holt et al., 2021), use the astrocladistical technique to demonstrate that the technique is valid in the Solar system context. Papers two (Holt et al., 2020b) and three (Holt et al., 2020a) are related to the dynamics of the Jovian Trojans, and help to understand the history of these objects.

7.1 OUTCOMES

HOW CAN ASTROCLADISTICS BE USED TO GIVE INSIGHTS INTO THE THE HISTORY OF SOLAR SYSTEM OBJECTS? A major outcome from his project has been to successfully introduce astrocladistics into a planetary science context. The first paper to do this investigated the Jovian and Saturnian Satellites (Holt et al., 2018). This paper looked specifically at using the dynamical and compositional components to place each of the objects in context. The study mostly confirmed the previously identified collisional families, and separated out the

regular and irregular satellites. This work indicated that astrocladistics would be applicable in a planetary science context.

To follow up on this work, and expand astrocladistics, I investigated the Jovian Trojan swarms (Holt et al., 2021). This work looked at an order of magnitude more objects than Holt et al. (2018) and expanded the technique to include colour observations from wide field surveys. In our analysis of the members of the L₄ swarm, we identify a total of ten unaffiliated clans and eight superclans that, in turn, contain an additional seventeen clans. The L₅ swarm shows more hierarchical structure: seven unaffiliated clans, with six subclans within them. The L₅ swarm is found to contain at least three large superclans, with each superclan containing a larger number of clans and subclans. In total, there are 14 clans containing 14 subclans in the L₅ swarm. The paper forms the basis for the use of astrocladistics in small Solar system body science.

WHAT ARE THE LONG TERM DYNAMICS OF THE JUPITER TROJAN COLLISIONAL FAMILIES? In the second paper (Holt et al., 2020a), I looked at the long-term dynamics of 5553 initially stable Jovian Trojans. This study considered nearly double the number of objects than the next largest study (Di Sisto et al., 2014, 2019). I found that the escape rates were consistent with other studies (e.g. Hellmich et al., 2019; Di Sisto et al., 2014, 2019), showing that the rate of population escape is consistent on the scale of 4.5×10^9 years.

The other focus of the second paper was on the six collisional families previously identified in the Trojan population (Nesvorný et al., 2015). In order to further investigate these, I created a set of 125 clones per family member. Three of the six families (the Hektor, 1996 RJ and 2001 UV₂₀₉ families) have too few members for us to say anything beyond calculating an estimation of their escape rate. One of the L₄ families, Arkesilaos, has 37 members, but is located in the stable parameter space, and so only has a single member for which any clones escape. The Enomminos clan in the L₅ swam, with 30 members possibly could show some trends, though these were inconclusive. The major outcome from this work was a tentative age for the Eurybates family. Being the largest family in the population, with 218 members, this created the opportunity to undertake statistically significant analysis. This study found that the escape rate of the family members is increasing. By extending the linear trend into the past, I was able to calculate a minimum age for the family at approximately $1.045 \pm 0.364 \times 10^9$ years.

ARE THERE ANY ASTEROID PAIRS IN THE JOVIAN TROJANS, AND WHAT ARE THE IMPLICATIONS FOR THE HISTORY OF THE POPULATION? Asteroid pairs, two dynamically linked

objects, help inform us about the dynamical history of various small body populations, including the Main belt and Hungaria populations (Vokrouhlický and Nesvorný, 2008; Pravec and Vokrouhlický, 2009; Rozek et al., 2011; Pravec et al., 2019). Prior to work that I conducted with David Vokrouhlický, David Nesvorný and Miroslav Brož (Holt et al., 2020b), no asteroid pairs had been found in the Jovian Trojans. In this work, instead of using the standard proper elements, we used the derived, delta-semi major axis. From this we discovered the first pair in the Trojan population, (258656) 2002 ES₇₆ and 2013 CC₄₁ in the L₄ swarm. We use *n*-body integrations to discover a convergence in Eulerian parameters, indicating an age of around 360 Myr, though it could be as high as several Gyrs.

7.1.1 ADDITIONAL OUTCOMES

IDENTIFICATION OF HIGH PRIORITY TARGETS One of the outcomes from the astrocladistical investigation of the Jovian Trojans was the identification of fourteen priority targets for follow-up observations. These comparatively large objects could provide insights on the nature of the population as a whole. This also improves the usefulness of astrocladistics as a tool to characterise a population. Details on these priority targets, along with their light curve information, are given in Table 7.1.

HIGH PRECISION DATABASE OF JOVIAN TROJAN PROPER ELEMENTS An additional outcome from Holt et al. (2020b) was the creation of a high precision dataset of Trojan proper elements. In the astrocladistics work, I use the AstDyS dataset (Knežević and Milani, 2017). This dataset of proper elements is well regarded as a reference set. The reason we created an alternative dataset was two fold. The first reason is the number of significant digits. The AstDyS dataset has the proper elements of the Jovian Trojans to four significant digits. While this was sufficient for the binning program used in astrocladistic analysis, the search for pairs requires higher precision proper elements. In this new dataset we include the proper elements to sixteen significant figures. The second reason for the update is the new number of discovered Trojans. The AstDyS dataset includes 5553 Trojans as of June, 2017. Our new dataset, as of April 2020, includes 7328 identified objects. The database of Jovian Trojan proper elements is accessible at https://sirrah.troja.mff.cuni.cz/~mira/mp/trojans_hildas/.

Table 7.1: Physical and observational parameters for the priority targets identified in HOLT REF., taken from the Asteroid Lightcurve Database, (<http://www.minorplanet.info/lightcurvedatabase.html>, retrieved 2020 October 22 Warner et al., 2009). Here, P denotes the rotation period of the asteroid, and A_{\min} and A_{\max} are the minimum and maximum amplitudes of the asteroid's lightcurve. H is the absolute magnitude of the asteroid, and p_V the geometric albedo.

$Ast_{no.}$	P [hrs]	A_{\min} [mag]	A_{\max} [mag]	H [mag]	p_V
659	15.98	0.22	0.31	8.71	0.040 ± 0.004
1173	11.60	0.16	0.73	8.91	0.035 ± 0.002
1208	56.17	-	0.20	9.00	0.037 ± 0.002
1404	29.38	-	0.30	9.41	0.050 ± 0.003
1437	24.49	0.34	0.70	8.21	0.028 ± 0.001
2456	7.24	0.05	0.27	9.37	0.026 ± 0.002
2895	7.52	0.08	0.48	10.14	-
4086	10.43	0.08	0.16	9.29	0.056 ± 0.004
4138	29.20	0.10	0.40	10.12	0.057 ± 0.007
4709	12.28	0.31	0.47	8.77	0.078 ± 0.005
5283	7.32	-	0.11	9.76	0.072 ± 0.007
7119	400.00	-	0.10	9.85	0.036 ± 0.005
7152	9.73	-	0.09	10.34	-
37519	50.93	-	0.30	11.10	-

7.2 FUTURE WORKS

7.2.1 OTHER SMALL BODY POPULATIONS

Several other small body populations could be further analysed using astrocladistics. In the coming years, these small body populations will be characterised by the The Vera Rubin Observatory, with the Legacy Survey of Space and Time (Rubin Obs. LSST), in multiple colours, see 7.2.2 for more details.

THE NEAR EARTH OBJECTS (NEO) are a population of objects that move on orbits that approach or cross that of the Earth. This population is dynamically chaotic (e.g. Binzel et al., 2015), and are of particular interest from a planetary protection perspective. Consequently, identifying the compositional aspects of the population is a priority. In this astrocladistics can help to decipher relationships between objects. By using a similar method to Paper 4 (Holt et al., 2020b), it should be possible to examine the relationships between NEOs, and identify targets for follow up. This methodology would also be able to place NEOs that have been visited by spacecraft, such as the *OSIRIS-REX* mission to 101955 Benu. There is additional value in placing 101955 Benu and 162173 Ryugu (target of the *Hyabusa 2* mission) in context. The *Hyabusa 2* returned a sample from 162173 Ryugu to Earth in December 2020, and we are awaiting publication of the analysis. *OSIRIS-REX* left 101955 Benu very recently (May 2021), with the samples due to Earth in September 2023.

THE INNER MAIN BELT (IMB) contains 18 collisional families (Nesvorný et al., 2015) and many different taxonomic types (DeMeo and Carry, 2014). These families are thought to be the source of many Near Earth Objects (Bottke et al., 2002), including 101955 Benu (Campins et al., 2010; Bottke et al., 2015) and 162173 Ryugu (Campins et al., 2013), both the targets for two separate sample return missions. Through astrocladistics, we could further place these samples in context, and identify related objects. In such a diverse region, astrocladistics could also provide further insights into the history of the population.

THE EDGEWORTH-KUIPER BELT AND SCATTERED DISK OBJECTS are located in the outer Solar system, beyond the orbit of Neptune. The ‘Cold’ and ‘Warm’ classical Edgeworth-Kuiper belts are in dynamical stable orbits, set during an early instability in Solar system history (Levison et al., 2008). The ‘cold’ classical, which includes 486958 Arrokoth (2014 MU₆₉), target of the *New Horizons* mission, are thought to be have been stable since the early Solar

system. The Scattered disk contains objects that have been moved by Neptune during its migration (Duncan, 1997). Astrocladistics could help to further understand the small objects in the outer Solar system, and help place the *New Horizons* discoveries in context.

7.2.2 FUTURE SURVEYS

In this work, we use astrocladistics to investigate the Jovian Trojan population, drawing upon observational data obtained by the latest generation of wide-field surveys. In the coming decade, several new surveys will come online, providing a wealth of new data that could be incorporated in future studies. Here, we comment on the potential for the use of the astrocladistical methodology in the analysis of that data, and discuss how those surveys will improve our understanding of the Jovian Trojan population.

Gaia DR3: In this work we use single G-band (330 to 1050 nm) data taken from *Gaia* DR2 (Spoto et al., 2018). Whilst this single band data can provide some information about the objects, The *Gaia* G-band magnitudes are clearly linked to size, to first approximation, but also to some extent albedo and distance. Albedos within the Jovian Trojans are low, and relatively consistent (Romanishin and Tegler, 2018). Distance is also normalised somewhat, due to the librations of the population around the Lagrange points. In the *Gaia* DR2 dataset, there are two additional two bands, G_{BP} -band (330 – 680 nm) and G_{RP} -band (630 – 1050 nm) (Evans et al., 2018) for stellar objects, but data in these bands is not available for Solar system objects. These data are expected to be included in the full *Gaia* DR3 release, which is currently scheduled for release in early 2022, and once available, could be incorporated into future astrocladistical surveys in a similar way to the SDSS and MOVIS colours.

THE VERA RUBIN OBSERVATORY, with the Legacy Survey of Space and Time (Rubin Obs. LSST), is expected to receive first light in 2023. During the first few years that Vera Rubin is active, estimates suggest that more than 280,000 Jovian Trojans are expected to be discovered (LSST Science Collaboration et al., 2009). Of those objects, it is likely that more than 150 observations will be made of at least 50,000, which will be sufficient for those objects to be characterised in five broadband colours (LSST Science Collaboration et al., 2009). This will provide a much larger context for taxonomy in the Jovian Trojan population, and small Solar system bodies in general. Astrocladistics is a tool that could be used to further analyse these data, and that is ideally suited to the analysis of such vast and sprawling datasets. Assuming that the currently observed L_4/L_5 numerical asymmetry holds (Jewitt et al., 2000; Nakamura

and Yoshida, 2008; Yoshida and Nakamura, 2008; Vinogradova and Chernetenko, 2015), it is expected that those observations would yield results for approximately 33,000 objects in the vicinity of L₄, and 17,000 around L₅. Given that the computational requirements for cladistical analysis increases approximately with a trend of $n^{3/2}$ (Goloboff et al., 2008; Goloboff and Catalano, 2016), we estimate that, using current computational architecture, the analysis of such large datasets would require approximately 2700 CPU-hours for the L₅ analysis and 7500 CPU-hours for the population around L₄. In order for this to be feasible, further testing into the TNT 1.5 parallelisation (Goloboff and Catalano, 2016) will be required.

In addition to examining these new objects with astrocladistics, the discovery of more objects will require dynamical characterisation as well. In each population, there is an opportunity to discover new collisional families (e.g. Nesvorný et al., 2015) and asteroidal pairs (e.g. Pravec et al., 2019) in each of the small Solar system body populations. This may also be an opportunity to consolidate the spectral taxonomy (e.g. DeMeo et al., 2015) and dynamical taxonomy (see Horner et al., 2020, for review) into a revised system.

THE *JAMES WEB SPACE TELESCOPE (JWST)* is currently scheduled for launch in 2021. The telescope will provide detailed analysis of many Solar system objects (Rivkin et al., 2020). In contrast to the work of *Gaia* and the Vera Rubin observatory, which are undertaking wide ranging surveys, the *JWST* is instead a targeted mission, providing detailed IR spectra on specific objects, rather than broadband colours on many objects. Whilst the time required for such observations will doubtless be incredibly highly sought after, two members of the Jovian Trojan population (617 Patroclus and 624 Hektor) have already been approved for study under the Guaranteed Time Observations program (Rivkin et al., 2020). Once those observations are complete, the results can be placed in a wider context due to the work in Paper 4 (Holt et al., 2020b). As *JWST* is a limited time mission, we recommend the prioritisation of those targets identified in Paper 4 (Holt et al., 2020b) to provide the most benefit.

TWINKLE is a low-cost, community funded, space telescope, scheduled for launch in 2023 or 2024 (Savini et al., 2018). The mission will provide spectral analysis in three bands in the visible and near-IR (0.4 μm to 1 μm , 1.3 μm to 2.42 μm , and 2.42 μm to 4.5 μm). In terms of the Jovian Trojans, the mission will be able to provide detailed observations down to approximately 15th magnitude. Over the seven year initial lifetime, *Twinkle* is expected to observe 50 or so of the largest Trojans (Edwards et al., 2019a,b), all of which are included in this work. This will provide further characterisation of these bodies, particularly in the IR range. Astrocladistics can offer added value to analysis of *Twinkle* observations, through associations

within clans.

THE *NANCY GRACE ROMAN SPACE TELESCOPE* (*RST*, FORMALLY *WFIRST*) is currently in development, with an expected launch date in 2025. Once launched, there will be a number of opportunities for small body Solar system science using *RST*, including the ability to obtain a wealth of data for the Jovian Trojans (Holler et al., 2018). Using the wide-field imaging system, in the near-IR ($0.6\ \mu\text{m}$ - $2.0\ \mu\text{m}$), *RST* will be able to observe the majority of the currently known Jovian Trojans. In conjunction with the broadband Rubin Observatory LSST colours, those observations will yield a large database of Jovian Trojan characteristics. As computational capabilities and algorithm optimisations increase prior to launch, astrocladistics will provide a tool capable of analysing such large data-sets.

7.3 CONCLUDING REMARKS

In this section I present some of the conclusions of the four papers that form the core of this thesis. They can be divided into two main sections. Section 7.3.1 discusses the two dynamical works (Holt et al., 2020a,b). The second broad theme of this thesis considers the novel astrocladistical approach in planetary science, discussed in section 7.3.2.

7.3.1 DYNAMICS OF THE JOVIAN TROJANS

Dynamics form a core part of this thesis. Here I present some of the conclusions reached by the two dynamics focused papers that have been published.

7.3.1.1 JOVIAN TROJAN ESCAPES

Paper 2 (Holt et al., 2020a) presents the results of detailed n -body simulations of the known Jovian Trojan population, using nearly double the number of objects of the previous largest study (Di Sisto et al., 2014, 2019). We simulate the orbital evolution of a population of 49,977 massless test particles, nine particles for each of the 5553 known Jovian Trojans, for a period of 4.5×10^9 years into the future, under the gravitational influence of the Sun and the four giant planets. Our simulations reveal that the populations of both the L_4 and L_5 swarms are predominately stable, however a significant number of objects from both swarms can escape over the lifetime of the Solar system. In the case of the leading L_4 swarm, we find that 23.35% of objects escape, by volume. Similarly, only 24.89% escape the trailing L_5 swarm. Overall, 23.95% by volume of all test particles simulated in this work escape the Jovian population. As

discussed by other authors (Nesvorný, 2002; Tsiganis et al., 2005b; Nesvorný et al., 2013; Di Sisto et al., 2014, 2019), we find that the escape rates can not explain the current observed asymmetry between the two swarms. This supports the conclusion that the observed asymmetry between the L_4 and L_5 swarms are the result of their initial capture implantation (Nesvorný et al., 2013; Pirani et al., 2019a).

The escape rates of objects from the two Trojan swarms are in accordance with the idea that the Jovian Trojans act as a source of material to the other small Solar system body populations, as noted in Levison et al. (1997); Di Sisto et al. (2014, 2019), particularly with regards to the Centaurs (Horner et al., 2004, 2012). The majority of escaped Trojans, 58.63%, are ejected from the population and the Solar system within a single 1×10^5 year timestep. For those that remain in the Solar system, 99.25% are ejected by 1×10^7 years, after joining the Centaur population.

In the Jovian Trojan swarms, a total of six collisional families have been identified to date (Nesvorný et al., 2015), with four in the L_4 swarm and two located around L_5 . We find that three of the families are highly dynamically stable, with no particles escaping the Trojan population through the course of our integrations (the 1996 RJ, Arkesilaos and 2001 UV₂₀₉ families). Two other collisional groups, the L_4 Hektor and L_5 Ennomos families did have members that escape. These unstable families all have a small number of known members, which limits our ability to study their stability further in this work. The largest known Trojan family, the Eurybates L_4 family, has a smaller escape rate than the overall population. Contrary to the escape trends in the population, however, the escape rate of the Eurybates family is found to increase with time in our simulations. This might point to the diffusion of its members into unstable parameter space as they evolve away from the location of the family's creation. From this escape rate, we can obtain an estimate of the age of the Eurybates family on the order of $1.045 \pm 0.364 \times 10^9$ years.

7.3.1.2 JOVIAN TROJAN PAIR

The first potential dynamical pair in the Jovian Trojan population is identified in Paper 3 (Holt et al., 2020b), by myself and coauthors. In particular, we analysed the distribution of Trojans in their proper orbital element space. Using information about the local density of objects, we also assessed the statistical significance of the proximity of potential couples. This procedure lead us to select a pair of bodies, (258656) 2002 ES₇₆ and 2013 CC₄₁, in the L_4 swarm as a potential candidate pair. Interestingly, this suggested pair is located very close to the L_4 Lagrange point, with low proper elements, semimajor axis (da_P), eccentricity e_P and

sine of inclination ($\sin I_p$) values. Finally, as part of our effort, we developed an up-to-date, highly accurate set of proper elements for the all Jovian Trojans, which we have made publicly available.

In order to further investigate the selected pair, we ran a series of n -body simulations, which were used to look for past convergences in the osculating nodal ($\delta\varpi$) and perihelion longitude ($\delta\Omega$) value for the two objects, whilst ensuring that, at the time of such convergences the differences in the osculating eccentricity and inclination were also sufficiently small. Our simulations included both geometric clones, created from the uncertainties in the orbital elements of the bodies, and Yarkovsky clones, based on the estimated thermal accelerations that the two objects could experience, for a variety of realistic rotation rates. As a result, we obtained a statistical set of convergences, finding a larger pool of possibilities once the Yarkovsky clones were included. Our results reveal that the pair is at least $\simeq 360$ Myr old, but are compatible with the age being significantly older, potentially in the Gyr time scale. By finding such possible convergences, we increase the confidence that the (258656) 2002 ES₇₆–2013 CC₄₁ couple is a legitimate pair.

We then considered the mechanisms by which the (258656) 2002 ES₇₆–2013 CC₄₁ pair could have formed (compared with Vokrouhlický and Nesvorný, 2008). The pair is not associated with any known collisional family, and as such we do not favour the possibility of the pair having been formed as a result of a catastrophic impact on a putative parent body. The pair might have been formed through the rotational fission of their parent Trojan, since, for certain initial conditions, the timescale for such an object to be spun-up by the YORP effect to the point that it undergoes fission could be somewhat shorter than the age of the Solar system. However, this pair consists of two nearly equal-sized components, whilst the vast majority of observed pairs formed by rotational fission have a size ratio of at least 1.5 (see Pravec et al., 2010, 2019). For that reason, we consider that the pair most likely formed as a result of the dissociation of an equal-size binary. We can confirm that such a scenario is indeed feasible using an estimation of the binary survival rate in the size range of the (258656) 2002 ES₇₆–2013 CC₄₁ pair, $D \simeq 7$ km, over 4.5 Gyr, after implantation to the Trojan population early in Solar system’s history. Statistically, this indicates that there should be many such pairs within the Trojan population in this 5 – 10 km size range. As the Rubin Observatory’s Legacy Survey of Space and Time (LSST) comes online, it is expected to discover many Jovian Trojans in this size range (e.g., Schwamb et al., 2018). As new Trojans are discovered, our results suggest that further pairs should be revealed.

The (258656) 2002 ES₇₆–2013 CC₄₁ pair provides an interesting clue to the past history of the Jovian Trojans, and the Solar system as a whole. So far, we know little beyond their

dynamical properties and size estimations. In particular, lightcurve analysis could assist in constraining the formation mechanism, as this would provide an estimate of the rotational periods of the two objects. Due to their small size, and dark albedo, the objects have relatively low apparent magnitudes, at best ≈ 20.5 magnitude in visible band. In order to further characterise these objects, observations using large Earth-based facilities, such as the SUBARU (Kashikawa et al., 2002) or Keck (Oke et al., 1995) telescopes, will be required. These objects would also benefit from future observations using the *James Webb* (*JWST*, Rivkin et al., 2016) and *Nancy Grace Roman Space Telescopes* (RST, formerly known as WFIRST, Holler et al., 2018). Time on these telescopes is competitive, but we recommend proposals for observations of (258656) 2002 ES₇₆ and 2013 CC₄₁ be selected to further extend our understanding of this interesting pair of Trojans.

7.3.2 ASTROCLADISTICS IN PLANETARY SCIENCE

In Paper 1 (Holt et al., 2018), I and my coauthors have shown that the new application of cladistics on the Jovian and Saturnian satellite systems is valid for investigating the relationships between orbital bodies. In the Jovian system, the traditional classification categories (Nesvorný et al., 2003; Sheppard and Jewitt, 2003; Jewitt and Haghighipour, 2007) are preserved. We support the hypothesis put forward by Nesvorný et al. (2007) that each Jovian irregular satellite family can be represented by the largest member, and that each family is the remnants of a dynamical capture event, and subsequent breakup. We can also assign recently discovered, as yet unnamed, satellites to each of their respective Jovian families. Cladistical analysis of the Saturnian system broadly preserves the traditional classifications (Nesvorný et al., 2003; Sheppard and Jewitt, 2003; Jewitt and Haghighipour, 2007; Turrini et al., 2008), strengthening the validity of the cladistical method. In the Phoebe family of retrograde, irregular satellites, we assign two subfamilies similar to those found by (Turrini et al., 2008). We rename the classical mythological designations for the Saturnian irregular satellites, to represent the largest member of the subfamily, in order to be consistent with the Jovian naming convention. Newly discovered unnamed Saturnian satellites are easily assigned to various subfamilies. Through the application of the technique to the Jovian and Saturnian systems, we show that cladistics can be used as a valuable tool in a planetary science context, providing a systematic method for future classification.

Following on from (Holt et al., 2018), Paper 4 (Holt et al., 2021) applies the new astrocladistical technique to the Jovian Trojans. Myself and coauthors combine dynamical characteristics with colour information from the Sloan Digital Sky Survey (SDSS), *WISE*, *Gaia* DR2

and MOVIS, into a holistic taxonomic analysis. We create two matrices, one for the L₄ and one for the L₅ Trojans, comprised of 398 and 407 objects respectively. As part of this analysis, we find clustering beyond the previously identified collisional families (Nesvorný et al., 2015). These clusters we term ‘clans’, which provide the beginnings of a taxonomic framework, the results of which are presented visually using a consensus dendritic tree. Our results yield a hierarchical structure, with individual clans often congregating within a larger ‘superclan’, and with other clans being further broken down into one or more ‘subclans’. In our analysis of the members of the L₄ swarm, we identify a total of ten unaffiliated clans and eight superclans that, in turn, contain an additional seventeen clans. Within our analysis, we include 13 members of the Eurybates collisional family (Nesvorný et al., 2015), the largest in the Trojan population. Seven of these, including 3548 Eurybates (1973 SO), a *Lucy* target, cluster into the Eurybates clan, a part of the Greater Ajax superclan. The L₅ swarm shows more hierarchical structure: seven unaffiliated clans, with six subclans within them. The L₅ swarm is found to contain at least three large superclans, with each superclan containing a larger number of clans and subclans. In total, there are 14 clans containing 14 subclans in the L₅ swarm. The only *Lucy* target in the L₅ swarm, 617 Patroclus (1906 VY), is the type object of the Greater Patroclus superclan, though it is not specifically part of any clan, it is close to the Memnon clan, which includes 2001 UV₂₀₉ collisional family member, 37519 Amphios (3040 T-3). A key outcome of our astrocladistical analysis is that we identify 14 high priority targets for follow-up observations. These are all comparatively large and bright objects that should be observed to provide further context for the Jovian Trojan swarms as a whole. Several are closely related to *Lucy* targets that could provide additional information in preparation for *in-situ* observations. All of the future *Lucy* targets (Levison et al., 2017) are included in our analysis. Our results therefore provide a taxonomic context for the mission, and extend the value of discoveries made. By associating the *Lucy* targets with other clan members, inferences can be made about their nearest relatives, and the swarms as a whole.

Whilst the focus of this thesis is on the current generation of wide-field surveys, several new observatories will be coming on line in the next few decades. The Vera Rubin Observatory, with the Legacy Survey of Space and Time (Rubin Obs. LSST), the *James Web Space Telescope* (*JWST*), *Twinkle* and the *Nancy Grace Roman Space Telescope* (*RST*, formerly *WFIRST*) will all be able to observe the Jovian Trojan population and further characterise these objects. Astrocladistics offers a method of analysis that will allow a timely and detailed analysis of the relationships between the Jovian Trojans, based on the observations made by these next generation telescopes, and helps to identify high priority targets for competitive observational time. The Jovian Trojans are the remnants of the early Solar system, held dynamically stable

for the past 4.5×10^9 years. They are vital clues to this early period in the story of the Solar system. Astrocladistical analysis of these objects provides us with insights into their history and how they are related to one another.

The Jovian Trojans and the irregular Satellites are fascinating populations, remnants of the early stages of the Solar system's formation. In the future, as more members of the populations and their taxonomic groupings are identified, it will be interesting to see whether these dynamical methods can be used to help constrain the ages of the smaller clusters. If this is possible, such results would shed light on the variability of the collision rates within the Jovian Trojan swarms and the irregular satellites. The results I present in this thesis, and these potential future works, highlight the importance of these populations, their taxonomic groups and collisional families, to understanding the history of the Solar system.

References

- Agnor, C. B. and Hamilton, D. P. (2006). Neptune's capture of its moon Triton in a binary-planet gravitational encounter. *Nature*, 441(7090):192–194.
- Archie, J. W. (1989). Homoplasy Excess Ratios: New Indices for Measuring Levels of Homoplasy in Phylogenetic Systematics and a Critique of the Consistency Index. *Syst. Zool.*, 38(3):253.
- Aria, C. and Caron, J.-B. (2017). Burgess Shale fossils illustrate the origin of the mandibulate body plan. *Nature*, 545(7652):89–92.
- Asphaug, E. and Reufer, A. (2013). Late origin of the Saturn system. *Icarus*, 223(1):544–565.
- Bakker, R. T. and Galton, P. M. (1974). Dinosaur monophyly and a new class of vertebrates. *Nature*, 248(5444):168–172.
- Barnard, E. E. (1892). Discovery and observations of a fifth satellite to Jupiter. *Astron. J.*, 12:81.
- Barnes, R. and Quinn, T. R. (2004). The (In)stability of Planetary Systems. *Astron. J.*, 611:494–516.
- Barucci, M. M. A., Cruikshank, D. P., Mottola, S., and Lazzarin, M. (2002). Physical Properties of Trojan and Centaur Asteroids. In Bottke Jr., W., Cellino, A., Paolicchi, P., and Binzel, R., editors, *Asteroids III*, pages 273–287.
- Baum, W., Kreidl, T., Westphal, J., Danielson, G. E., Seidelmann, P., Pascu, D., and Currie, D. (1981). Saturn's E ring. *Icarus*, 47(1):84–96.
- Beaugé, C. and Nesvorný, D. (2007). Proper Elements and Secular Resonances for Irregular Satellites. *Astron. J.*, 133(6):2537–2558.

- Beauge, C. and Roig, F. (2001). A Semianalytical Model for the Motion of the Trojan Asteroids: Proper Elements and Families. *Icarus*, 153(2):391–415.
- Bendjoya, P., Cellino, A., Di Martino, M., and Saba, L. (2004). Spectroscopic observations of Jupiter Trojans. *Icarus*, 168(2):374–384.
- Binzel, R. P., Reddy, V., and Dunn, T. (2015). The Near-Earth Object Population: Connections to Comets, Main-Belt Asteroids, and Meteorites. In Michel, P., DeMeo, F. E., and Bottke, W. F., editors, *Asteroids IV*. University of Arizona Press, Tucson, AZ.
- Bolin, B. T., Delbó, M., Morbidelli, A., and Walsh, K. J. (2017). Yarkovsky V-shape identification of asteroid families. *Icarus*, 282:290–312.
- Bolin, B. T., Fernandez, Y. R., Lisse, C. M., Holt, T. R., Lin, Z.-Y., Purdum, J. N., Deshmukh, K. P., Bauer, J. M., Bellm, E. C., Bodewits, D., Burdge, K. B., Carey, S. J., Copperwheat, C. M., Helou, G., Ho, A. Y. Q., Horner, J., van Roestel, J., Bhalerao, V., Chang, C.-K., Chen, C., Hsu, C.-Y., Ip, W.-H., Kasliwal, M. M., Masci, F. J., Ngeow, C.-C., Quimby, R., Burruss, R., Coughlin, M., Dekany, R., Delacroix, A., Drake, A., Duev, D. A., Graham, M., Hale, D., Kupfer, T., Laher, R. R., Mahabal, A., Mróz, P. J., Neill, J. D., Riddle, R., Rodriguez, H., Smith, R. M., Soumagnac, M. T., Walters, R., Yan, L., and Zolkower, J. (2021). Initial Characterization of Active Transitioning Centaur, P/2019 LD 2 (ATLAS), Using Hubble, Spitzer, ZTF, Keck, Apache Point Observatory, and GROWTH Visible and Infrared Imaging and Spectroscopy. *Astron. J.*, 161(3):116.
- Bolin, B. T., Fremling, C., Holt, T. R., Hankins, M. J., Ahumada, T., Anand, S., Bhalerao, V., Burdge, K. B., Copperwheat, C. M., Coughlin, M., Deshmukh, K. P., De, K., Kasliwal, M. M., Morbidelli, A., Purdum, J. N., Quimby, R., Bodewits, D., Chang, C.-K., Ip, W.-H., Hsu, C.-Y., Laher, R. R., Lin, Z.-Y., Lisse, C. M., Masci, F. J., Ngeow, C.-C., Tan, H., Zhai, C., Burruss, R., Dekany, R., Delacroix, A., Duev, D. A., Graham, M., Hale, D., Kulkarni, S. R., Kupfer, T., Mahabal, A., Mróz, P. J., Neill, J. D., Riddle, R., Rodriguez, H., Smith, R. M., Soumagnac, M. T., Walters, R., Yan, L., and Zolkower, J. (2020). Characterization of Temporarily Captured Minimoons 2020 CD 3 by Keck Time-resolved Spectrophotometry. *Astrophys. J.*, 900(2):L45.
- Bolin, B. T., Walsh, K. J., Morbidelli, A., and Delbó, M. (2018). Initial velocity V-shapes of young asteroid families. *Mon. Not. R. Astron. Soc.*, 473(3):3949–3968.

- Bottke, W. F., Morbidelli, A., Jedicke, R., Petit, J. M., Levison, H. F., Michel, P., and Metcalfe, T. S. (2002). Debaised orbital and absolute magnitude distribution of the near-Earth objects. *Icarus*, 156(2):399–433.
- Bottke, W. F., Vokrouhlický, D., Brož, M., Nesvorný, D., and Morbidelli, A. (2001). Dynamical Spreading of Asteroid Families by the Yarkovsky Effect. *Science (80-.)*, 294:1693–1696.
- Bottke, W. F., Vokrouhlický, D., Rubincam, D., and Nesvorný, D. (2006). The Yarkovsky and Yorp Effects: Implications for Asteroid Dynamics. *Annu. Rev. Earth Planet. Sci.*, 34:157–191.
- Bottke, W. F., Vokrouhlický, D., Walsh, K. J., Delbo, M., Michel, P., Lauretta, D. S., Campins, H., Connolly, H. C., Scheeres, D. J., and Chelsey, S. R. (2015). In search of the source of asteroid (101955) Bennu: Applications of the stochastic YORP model. *Icarus*, 247:191–217.
- Brandley, M. C., Warren, D. L., Leaché, A. D., and McGuire, J. A. (2009). Homoplasy and Clade Support. *Syst. Biol.*, 58(2):184–198.
- Brož, M. and Rozehnal, J. (2011). Eurybates - the only asteroid family among Trojans? *Mon. Not. R. Astron. Soc.*, 414(1):565–574.
- Brož, M., Vokrouhlický, D., Roig, F., Nesvorný, D., Bottke, W. F., and Morbidelli, A. (2005). Yarkovsky origin of the unstable asteroids in the 2/1 mean motion resonance with Jupiter. *Mon. Not. R. Astron. Soc.*, 359:1437–1455.
- Brozović, M. and Jacobson, R. A. (2017). The Orbits of Jupiter’s Irregular Satellites. *Astron. J.*, 153(4):147.
- Buie, M. W., Olkin, C. B., Merline, W. J., Walsh, K. J., Levison, H. F., Timerson, B., Herald, D., William, M. O., Abramson, H. B., Abramson, K. J., Breit, D. C., Caton, D. B., Conard, S. J., Croom, M. A., Dunford, R. W., Dunford, J. A., Dunham, D. W., Ellington, C. K., Liu, Y., Maley, P. D., Olsen, A. M., Preston, S., Royer, R., Scheck, A. E., Sherrod, C., Sherrod, L., Swift, T. J., Taylor, L. W., and Venable, R. (2015). Size and shape from stellar occultation observations of the double jupiter trojan patroclus and menoetius. *Astron. J.*, 149(3):113.
- Bus, S. J. (2002). Phase II of the Small Main-Belt Asteroid Spectroscopic Survey A Feature-Based Taxonomy. *Icarus*, 158(1):146–177.

- Camin, J. H. and Sokal, R. R. (1965). A Method for Deducing Branching Sequences in Phylogeny. *Evolution (N. Y.)*, 19(3):311.
- Campins, H., León, J. D., Morbidelli, A., Licandro, J., Gayon-Markt, J., Delbo, M., and Michel, P. (2013). The origin of asteroid 162173 (1999 JU₃). *Astron. J.*, 146(2):26.
- Campins, H., Morbidelli, A., Tsiganis, K., De León, J., Licandro, J., and Lauretta, D. (2010). The origin of asteroid 101955 (1999 RQ₃₆). *Astrophys. J. Lett.*, 721(1 PART 2):53–57.
- Canup, R. M. (2010). Origin of Saturn’s rings and inner moons by mass removal from a lost Titan-sized satellite. *Nature*, 468(7326):943–946.
- Canup, R. M. and Ward, W. R. (2002). Formation of the Galilean Satellites: Conditions of Accretion. *Astron. J.*, 124(6):3404–3423.
- Cardone, V. F. and Fraix-Burnet, D. (2013). Hints for families of gamma-ray bursts improving the Hubble diagram. *Mon. Not. R. Astron. Soc.*, 434(3):1930–1938.
- Carruba, V., Domingos, R. C., Nesvorný, D., Roig, F., Huaman, M. E., and Souami, D. (2013). A multidomain approach to asteroid families’ identification. *Mon. Not. R. Astron. Soc.*, 433(3):2075–2096.
- Carruba, V. and Nesvorný, D. (2016). Constraints on the original ejection velocity fields of asteroid families. *Mon. Not. R. Astron. Soc.*, 457(2):1332–1338.
- Carry, B. (2012). Density of asteroids. *Planet. Space Sci.*, 73(1):98–118.
- Carvano, J. M., Hasselmann, P. H., Lazzaro, D., and Mothé-Diniz, T. (2010). SDSS-based taxonomic classification and orbital distribution of main belt asteroids. *Astron. Astrophys.*, 510:A43.
- Chamberlain, A. and Wood, B. (1987). Early hominid phylogeny. *J. Hum. Evol.*, 16(1):119–133.
- Chambers, J. E. (1999). A hybrid symplectic integrator that permits close encounters between massive bodies. *Mon. Not. R. Astron. Soc.*, 304(4):793–799.
- Charnoz, S., Salmon, J., and Crida, A. (2010). The recent formation of Saturn’s moonlets from viscous spreading of the main rings. *Nature*, 465(7299):752–754.

- Chesley, S. R. (2003). Direct Detection of the Yarkovsky Effect by Radar Ranging to Asteroid 6489 Golevka. *Science (80-.)*, 302(5651):1739–1742.
- Christou, A. A. and Asher, D. J. (2011). A long-lived horseshoe companion to the Earth. *Mon. Not. R. Astron. Soc.*, 414(4):2965–2969.
- Clark, R. N., Brown, R. H., Jaumann, R., Cruikshank, D. P., Nelson, R. M., Buratti, B. J., McCord, T. B., Lunine, J. I., Baines, K. H., Bellucci, G., Bibring, J. P., Capaccioni, F., Ceroni, P., Coradini, A., Formisano, V., Langevin, Y., Matson, D. L., Mennella, V., Nicholson, P. D., Sicardy, B., Sotin, C., Hoefen, T. M., Curchin, J. M., Hansen, G. B., Hibbits, K., and Matz, K.-D. (2005). Compositional maps of Saturn’s moon Phoebe from imaging spectroscopy. *Nature*, 435(7038):66–69.
- Colombo, G. and Franklin, F. (1971). On the formation of the outer satellite groups of Jupiter. *Icarus*, 15(2):186–189.
- Ćuk, M. and Burns, J. A. (2004). Gas-drag-assisted capture of Himalia’s family. *Icarus*, 167(2):369–381.
- Ćuk, M., Christou, A. A., and Hamilton, D. P. (2015). Yarkovsky-driven spreading of the Eureka family of Mars Trojans. *Icarus*, 252:339–346.
- Cuzzi, J. N., Whizin, A., Hogan, R., Dobrovolskis, A., Dones, L., Showalter, M. R., Colwell, J., and Scargle, J. (2014). Saturn’s F Ring core: Calm in the midst of chaos. *Icarus*, 232:157–175.
- Darwin, C. (1859). *On the Origin of the Species by Natural Selection*. Murray, London, UK.
- Davis, A. B. and Scheeres, D. J. (2020). Doubly synchronous binary asteroid mass parameter observability. *Icarus*, 341:113439.
- de la Fuente Marcos, C. and de la Fuente Marcos, R. (2016). A trio of horseshoes: past, present and future dynamical evolution of Earth co-orbital asteroids 2015 XX 169, 2015 YA and 2015 YQ 1. *Astrophys. Space Sci.*, 361(4):121.
- Deienno, R., Morbidelli, A., Gomes, R., and Nesvorný, D. (2017). Constraining the Giant Planets’ Initial Configuration from Their Evolution: Implications for the Timing of the Planetary Instability. *Astron. J.*, 153(4):153.

- Deienno, R., Nesvorný, D., Vokrouhlický, D., and Yokoyama, T. (2014). ORBITAL PERTURBATIONS OF THE GALILEAN SATELLITES DURING PLANETARY ENCOUNTERS. *Astron. J.*, 148(2):25.
- Deienno, R., Walsh, K. J., and Delbo, M. (2020). Efficiency characterization of the V-shape asteroid family detection method. *Icarus*, 357:114218.
- Delbó, M., Mueller, M., Emery, J., Rozitis, B., and Capria, M. (2015). Asteroid Thermo-physical Modeling. In Michel, P., DeMeo, F., and Bottke, W., editors, *Asteroids IV*, pages 107–128. University of Arizona Press.
- DeMeo, F. E., Alexander, C. M. O., Walsh, K. J., Chapman, C. R., and Binzel, R. P. (2015). The Compositional Structure of the Asteroid Belt. In Michel, P., DeMeo, F. E., and Bottke, W. F., editors, *Asteroids IV*, pages 13–41. University of Arizona Press.
- DeMeo, F. E., Binzel, R. P., Carry, B., Polishook, D., and Moskovitz, N. A. (2014). Unexpected D-type interlopers in the inner main belt. *Icarus*, 229:392–399.
- DeMeo, F. E., Binzel, R. P., Slivan, S. M., and Bus, S. J. (2009). An extension of the Bus asteroid taxonomy into the near-infrared. *Icarus*, 202(1):160–180.
- DeMeo, F. E. and Carry, B. (2013). The Taxonomic Distribution of Asteroids from Multi-filter All-sky Photometric Surveys. *Icarus*, 226(1):723–741.
- DeMeo, F. E. and Carry, B. (2014). Solar System evolution from compositional mapping of the asteroid belt. *Nature*, 505(7485):629–634.
- Denk, T. and Mottola, S. (2019). Studies of irregular satellites: I. Lightcurves and rotation periods of 25 Saturnian moons from Cassini observations. *Icarus*, 322:80–102.
- Deo, S. N. and Kushvah, B. S. (2017). Yarkovsky effect and solar radiation pressure on the orbital dynamics of the asteroid (101955) Bennu. *Astron. Comput.*, 20:97–104.
- DePater, I. and Lissauer, J. J. (2010). *Planetary Sciences, Second Edition*. Cambridge University Press, Cambridge, UK.
- Di Sisto, R. P., Ramos, X. S., and Beaugé, C. (2014). Giga-year evolution of Jupiter Trojans and the asymmetry problem. *Icarus*, 243:287–295.

- Di Sisto, R. P., Ramos, X. S., and Gallardo, T. (2019). The dynamical evolution of escaped Jupiter Trojan asteroids, link to other minor body populations. *Icarus*, 319:828–839.
- Dotto, E., Fornasier, S., Barucci, M. M. A., Licandro, J., Boehnhardt, H., Hainaut, O., Marzari, F., de Bergh, C., and De Luise, F. (2006). The surface composition of Jupiter Trojans: Visible and near-infrared survey of dynamical families. *Icarus*, 183(2):420–434.
- Duncan, M. J. (1997). A Disk of Scattered Icy Objects and the Origin of Jupiter-Family Comets. *Science (80-.)*, 276(5319):1670–1672.
- Duncan, M. J., Levison, H. F., and Lee, M. H. (1998). A Multiple Time Step Symplectic Algorithm for Integrating Close Encounters. *Astron. J.*, 116(4):2067–2077.
- Ebell, M. (1909). Ephemeride des Planeten (659) [1908 CS]. *Astron. Nachrichten*, 180(13):213–214.
- Edwards, B., Lindsay, S., Savini, G., Tinetti, G., Arena, C., Bowles, N., and Tessenyi, M. (2019a). Small bodies science with the Twinkle space telescope. *J. Astron. Telesc. Instruments, Syst.*, 5(03):1.
- Edwards, B., Savini, G., Tinetti, G., Tessenyi, M., Arena, C., Lindsay, S., and Bowles, N. (2019b). Remote-sensing characterization of major Solar System bodies with the Twinkle space telescope. *J. Astron. Telesc. Instruments, Syst.*, 5(01):1.
- El Moutamid, M., Nicholson, P. D., French, R. G., Tiscareno, M. S., Murray, C. D., Evans, M. W., French, C. M., Hedman, M. M., and Burns, J. A. (2016). How Janus’ orbital swap affects the edge of Saturn’s A ring? *Icarus*, 279:125–140.
- Emery, J. P. and Brown, R. H. (2003). Constraints on the surface composition of Trojan asteroids from near-infrared (0.8–4.0 μm) spectroscopy. *Icarus*, 164(1):104–121.
- Emery, J. P., Burr, D. M., and Cruikshank, D. P. (2011). Near-Infrared Spectroscopy of Trojan Asteroids: Evidence for two Compositional Groups. *Astron. J.*, 141(1):25.
- Emery, J. P., Cruikshank, D. P., and Van Cleve, J. (2006). Thermal emission spectroscopy (5.2–38 μm) of three Trojan asteroids with the Spitzer Space Telescope: Detection of fine-grained silicates. *Icarus*, 182(2):496–512.

- Emery, J. P., Marzari, F., Morbidelli, A., French, L. M., and Grav, T. (2015). The Complex History of Trojan Asteroids. In Michel, P., DeMeo, F., and Bottke, W., editors, *Asteroids IV*, pages 203–220. University of Arizona Press, Tucson, AZ.
- Euler, L. (1767). De motu rectilineo trium corporum se mutuo attrahentium. *Novi Comment. Acad. Sci. Petropolitanae*, 11:144–151.
- Evans, D. W., Riello, M., De Angeli, F., Carrasco, J. M., Montegriffo, P., Fabricius, C., Jordi, C., Palaversa, L., Diener, C., Busso, G., Cacciari, C., van Leeuwen, F., Burgess, P. W., Davidson, M., Harrison, D. L., Hodgkin, S. T., Pancino, E., Richards, P. J., Altavilla, G., Balaguer-Núñez, L., Barstow, M. A., Bellazzini, M., Brown, A. G. A., Castellani, M., Cocozza, G., De Luise, F., Delgado, A., Ducourant, C., Galleti, S., Gilmore, G., Giuffrida, G., Holl, B., Kewley, A., Koposov, S. E., Marinoni, S., Marrese, P. M., Osborne, P. J., Piersimoni, A., Portell, J., Pulone, L., Ragaini, S., Sanna, N., Terrett, D., Walton, N. A., Wevers, T., and Wyrzykowski, Ł. (2018). Gaia Data Release 2. *Astron. Astrophys.*, 616:A4.
- Everhart, E. (1985). An Efficient Integrator that Uses Gauss-Radau Spacings. In Carusi, A. and Valsecchi, G. B., editors, *Dyn. Comets Their Orig. Evol. Proc. IAU Colloq. 83, held Rome, Italy, June 11-15, 1984.*, pages 185–202. Astrophysics and Space Science Library.
- Farnocchia, D., Chesley, S. R., Vokrouhlický, D., Milani, A., Spoto, F., and Bottke, W. F. (2013). Near Earth Asteroids with measurable Yarkovsky effect. *Icarus*, 224(1):1–13.
- Farris, J. S. (1970). Methods for Computing Wagner Trees. *Syst. Biol.*, 19(1):83–92.
- Farris, J. S. (1982). Outgroups and Parsimony. *Syst. Biol.*, 31(3):328–334.
- Farris, J. S. (1989). THE RETENTION INDEX AND THE RESCALED CONSISTENCY INDEX. *Cladistics*, 5(4):417–419.
- Fedorets, G., Granvik, M., and Jedicke, R. (2017). Orbit and size distributions for asteroids temporarily captured by the Earth-Moon system. *Icarus*, 285:83–94.
- Feibelman, W. A. (1967). Concerning the “D” Ring of Saturn. *Nature*, 214(5090):793–794.
- Filacchione, G., Capaccioni, F., Ciarniello, M., Clark, R. N., Cuzzi, J. N., Nicholson, P. D., Cruikshank, D. P., Hedman, M. M., Buratti, B. J., Lunine, J. I., Soderblom, L. A., Tosi, F., Cerroni, P., Brown, R. H., McCord, T. B., Jaumann, R., Stephan, K., Baines, K. H., and Flamini, E. (2012). Saturn’s icy satellites and rings investigated by Cassini–VIMS: III – Radial compositional variability. *Icarus*, 220(2):1064–1096.

- Fornasier, S., Dotto, E., Hainaut, O., Marzari, F., Boehnhardt, H., Deluise, F., and Barucci, M. (2007). Visible spectroscopic and photometric survey of Jupiter Trojans: Final results on dynamical families. *Icarus*, 190(2):622–642.
- Fornasier, S., Dotto, E., Marzari, F., Barucci, M., Boehnhardt, H., Hainaut, O., and Debergh, C. (2004). Visible spectroscopic and photometric survey of L₅ Trojans: investigation of dynamical families. *Icarus*, 172(1):221–232.
- Fraix-Burnet, D., Chattopadhyay, T., Chattopadhyay, A. K., Davoust, E., and Thuillard, M. (2012). A six-parameter space to describe galaxy diversification. *Astron. Astrophys.*, 545:A80.
- Fraix-Burnet, D., Choler, P., and Douzery, E. J. P. (2006). Towards a phylogenetic analysis of galaxy evolution: a case study with the dwarf galaxies of the Local Group. *Astron. Astrophys.*, 455(3):845–851.
- Fraix-Burnet, D. and Davoust, E. (2015). Stellar populations in ω Centauri: a multivariate analysis. *Mon. Not. R. Astron. Soc.*, 450(4):3431–3441.
- Fraix-Burnet, D., Davoust, E., and Charbonnel, C. (2009). The environment of formation as a second parameter for globular cluster classification. *Mon. Not. R. Astron. Soc.*, 398(4):1706–1714.
- Fraix-Burnet, D., Dugué, M., Chattopadhyay, T., Chattopadhyay, A. K., and Davoust, E. (2010). Structures in the fundamental plane of early-type galaxies. *Mon. Not. R. Astron. Soc.*, 407(4):2207–2222.
- Fraix-Burnet, D., Thuillard, M., and Chattopadhyay, A. K. (2015). Multivariate approaches to classification in extragalactic astronomy. *Front. Astron. Sp. Sci.*, 2:3.
- Galilei, G. (1610). *Sidereus Nuncius*.
- Gascuel, O. (2005). *Mathematics of Evolution and Phylogeny*. OUP Oxford, Oxford, UK.
- Giese, B., Neukum, G., Roatsch, T., Denk, T., and Porco, C. C. (2006). Topographic modeling of Phoebe using Cassini images. *Planet. Space Sci.*, 54(12):1156–1166.
- Gillon, M., Jehin, E., Lederer, S. M., Delrez, L., de Wit, J., Burdanov, A., Van Grootel, V., Burgasser, A. J., Triaud, A. H. M. J., Opitom, C., Demory, B.-O., Sahu, D. K., Bardalez Gagliuffi, D., Magain, P., and Queloz, D. (2016). Temperate Earth-sized planets transiting a nearby ultracool dwarf star. *Nature*, 533(7602):221–224.

- Giorgini, J. D., Yeomans, D., Chamberlin, A., Chodas, P., Jacobson, R. A., Keesey, M., Lieske, J., Ostro, S., Standish, E., and Wimberly, R. (1996). JPL's On-Line Solar System Data Service. In *AAS/Division Planet. Sci. Meet. Abstr. #28*, volume 28 of *Bulletin of the American Astronomical Society*, page 1158.
- Givnish, T. and Sytsma, K. (1997). Consistency, Characters, and the Likelihood of Correct Phylogenetic Inference. *Mol. Phylogenet. Evol.*, 7(3):320–330.
- Gladman, B. J., Kavelaars, J. J., Holman, M. J., Nicholson, P. D., Burns, J. A., Hergenrother, C. W., Petit, J.-M., Marsden, B. G., Jacobson, R. A., Gray, W., and Grav, T. (2001). Discovery of 12 satellites of Saturn exhibiting orbital clustering. *Nature*, 412(6843):163–166.
- Gladman, B. J., Sheppard, S. S., and Marsden, B. G. (2003a). S/2003 J 19 and S/2003 J 20. *IAU Circ.*, 8125.
- Gladman, B. J., Sheppard, S. S., and Marsden, B. G. (2003b). S/2003 J 21. *IAU Circ.*, 8138.
- Goloboff, P. A. (1993). CHARACTER OPTIMIZATION AND CALCULATION OF TREE LENGTHS. *Cladistics*, 9(4):433–436.
- Goloboff, P. A. (1996). METHODS FOR FASTER PARSIMONY ANALYSIS. *Cladistics*, 12(3):199–220.
- Goloboff, P. A. (2015). Computer science and parsimony: a reappraisal, with discussion of methods for poorly structured datasets. *Cladistics*, 31(2):210–225.
- Goloboff, P. A. and Catalano, S. A. (2016). TNT version 1.5, including a full implementation of phylogenetic morphometrics. *Cladistics*, 32(3):221–238.
- Goloboff, P. A., Farris, J. S., and Nixon, K. C. (2008). TNT, a free program for phylogenetic analysis. *Cladistics*, 24(5):774–786.
- Golubov, O. and Scheeres, D. J. (2019). Systematic Structure and Sinks in the YORP Effect. *Astron. J.*, 157(3):105.
- Granvik, M., Jedicke, R., Bolin, B., Chyba, M., Patterson, G., and Picot, G. (2013). Earth's Temporarily-Captured Natural Satellites – The First Step towards Utilization of Asteroid Resources. In Badescu, V., editor, *Asteroids Prospect. Energy Mater. Resour.*, pages 151–167. Springer Berlin Heidelberg, Berlin, Heidelberg.

- Granvik, M., Vaubaillon, J., and Jedicke, R. (2012). The population of natural Earth satellites. *Icarus*, 218(1):262–277.
- Grav, T. and Bauer, J. M. (2007). A deeper look at the colors of the saturnian irregular satellites. *Icarus*, 191(1):267–285.
- Grav, T., Holman, M. J., Gladman, B. J., and Aksnes, K. (2003). Photometric survey of the irregular satellites. *Icarus*, 166(1):33–45.
- Grav, T., Mainzer, A. K., Bauer, J. M., Masiero, J. R., and Nugent, C. R. (2012). WISE/NEOWISE observations of the Jovian Trojan Population: Taxonomy. *Astrophys. J.*, 759(1):49.
- Grav, T., Mainzer, A. K., Bauer, J. M., Masiero, J. R., Spahr, T. B., McMillan, R. S., Walker, R. G., Cutri, R. M., Wright, E. L., Eisenhardt, P. R. M., Blauvelt, E., DeBaun, E., Elsbury, D., Gautier, T., Gomillion, S., Hand, E., and Wilkins, A. (2011). WISE /NEOWISE OBSERVATIONS OF THE JOVIAN TROJANS: PRELIMINARY RESULTS. *Astrophys. J.*, 742(1):40.
- Greenberg, R. (2010). The icy Jovian satellites after the Galileo mission. *Reports Prog. Phys.*, 73(3):036801.
- Grundy, W. M., Buratti, B. J., Cheng, A. F., Emery, J. P., Lunsford, A. W., McKinnon, W. B., Moore, J. M., Newman, S. F., Olkin, C. B., Reuter, D. C., Schenk, P. M., Spencer, J. R., Stern, A., Throop, H. B., and Weaver, H. A. (2007). New Horizons Mapping of Europa and Ganymede. *Science (80-.)*, 318(5848):234–237.
- Hamilton, A. (2014). *The Evolution of Phylogenetic Systematics*. Number volume 5 in Species and Systematics. University of California Press.
- Hasselmann, P. H., Carvano, J. M., and Lazzaro, D. (2012). SDSS-based Asteroid Taxonomy V1.1. EAR-A-10035-5-SDSSTAX-V1.1. *NASA Planet. Data Syst.*
- Hedman, M. M., Burns, J. A., Hamilton, D. P., and Showalter, M. R. (2012). The three-dimensional structure of Saturn’s E ring. *Icarus*, 217(1):322–338.
- Hedman, M. M., Burns, J. A., Tiscareno, M. S., Porco, C. C., Jones, G., Roussos, E., Krupp, N., Paranicas, C., and Kempf, S. (2007). The Source of Saturn’s G Ring. *Science (80-.)*, 317:653.

- Hedman, M. M., Murray, C. D., Cooper, N., Tiscareno, M. S., Beurle, K., Evans, M. W., and Burns, J. A. (2009). Three tenuous rings/arcs for three tiny moons. *Icarus*, 199(2):378–386.
- Heinrich, V. (1907). Elemente und Ephemeride des Planeten (617) Patroklus. *Astron. Nachrichten*, 176(12):193–194.
- Hellmich, S., Mottola, S., Hahn, G., Kührt, E., and de Niem, D. (2019). Influence of the Yarkovsky force on Jupiter Trojan asteroids. *Astron. Astrophys.*, 630:A148.
- Hemingway, D., Nimmo, F., Zebker, H. A., and Iess, L. (2013). A rigid and weathered ice shell on Titan. *Nature*, 500(7464):550–552.
- Hennig, W. (1965). Phylogenetic systematics. *Annu. Rev. Entomol.*, 10(1):97–116.
- Heppenheimer, T. A. and Porco, C. C. (1977). New contributions to the problem of capture. *Icarus*, 30(2):385–401.
- Hergenrother, C. W., Maleszewski, C. K., Nolan, M. C., Li, J.-Y., Drouet d’Aubigny, C. Y., Shelly, F. C., Howell, E. S., Kareta, T. R., Izawa, M. R. M., Barucci, M. M. A., Bierhaus, E. B., Campins, H., Chesley, S. R., Clark, B. E., Christensen, E. J., DellaGiustina, D. N., Fornasier, S., Golish, D. R., Hartzell, C. M., Rizk, B., Scheeres, D. J., Smith, P. H., Zou, X.-D., and Loretta, D. S. (2019). The operational environment and rotational acceleration of asteroid (101955) Bennu from OSIRIS-REx observations. *Nat. Commun.*, 10(1):1291.
- Hillier, J. K., Green, S. F., McBride, N., Schwanethal, J. P., Postberg, F., Srama, R., Kempf, S., Moragas-Klostermeyer, G., McDonnell, J. A. M., and Grün, E. (2007). The composition of Saturn’s E ring. *Mon. Not. R. Astron. Soc.*, 377(4):1588–1596.
- Holler, B. J., Milam, S. N., Bauer, J. M., Alcock, C., Bannister, M. T., and Bjoraker, G. L. (2018). Solar system science with the Wide-Field Infrared Survey Telescope. *J. Astron. Telesc. Instruments, Syst.*, 4(03):1.
- Holt, T. R., Brown, A. J., and Nesvorný, D. (2016). Cladistical Analysis of the Jovian Satellites. In *Lunar Planet. Sci. Conf.*, volume 47 of *Lunar and Planetary Science Conference*, page 2676.
- Holt, T. R., Brown, A. J., Nesvorný, D., Horner, J., and Carter, B. D. (2018). Cladistical Analysis of the Jovian and Saturnian Satellite Systems. *Astrophys. J.*, 859(2):97.

- Holt, T. R., Horner, J., Nesvorný, D., King, R., Popescu, M., Carter, B. D., and Tylor, C. C. E. (2021). Astrocladistics of the Jovian Trojan Swarms. *Mon. Not. R. Astron. Soc.*, 504(2):1571–1608.
- Holt, T. R., Nesvorný, D., Horner, J., King, R., Marschall, R., Kamrowski, M., Carter, B. D., Brookshaw, L., and Tylor, C. (2020a). Stability of Jovian Trojans and their collisional families. *Mon. Not. R. Astron. Soc.*, 495(4):4085–4097.
- Holt, T. R., Vokrouhlický, D., Nesvorný, D., Brož, M., and Horner, J. (2020b). A pair of Jovian Trojans at the L₄ Lagrange point. *Mon. Not. R. Astron. Soc.*, 499(3):3630–3649.
- Homer. *The Iliad & The Odyssey*. Barnes & Noble, New York, NY, 2013 colle edition.
- Horner, J., Evans, N. W., and Bailey, M. E. (2004). Simulations of the population of Centaurs - I. The bulk statistics. *Mon. Not. R. Astron. Soc.*, 354(3):798–810.
- Horner, J., Kane, S. R., Marshall, J. P., Dalba, P. A., Holt, T. R., Wood, J., Maynard-Casely, H. E., Wittenmyer, R., Lykawka, P. S., Hill, M., Salmeron, R., Bailey, J., Löhne, T., Agnew, M., Carter, B. D., and Tylor, C. C. E. (2020). Solar System Physics for Exoplanet Research. *Publ. Astron. Soc. Pacific*, 132(1016):102001.
- Horner, J. and Lykawka, P. S. (2011). The Neptune Trojans: a window on the birth of the solar system. *Astron. Geophys.*, 52(4):4.24–4.30.
- Horner, J., Müller, T. G., and Lykawka, P. S. (2012). (1173) Anchises - thermophysical and dynamical studies of a dynamically unstable Jovian Trojan. *Mon. Not. R. Astron. Soc.*, 423(3):2587–2596.
- Hsieh, H. H., Fitzsimmons, A., Novaković, B., Denneau, L., and Heinze, A. N. (2021). The transient Jupiter Trojan-like orbit of P/2019 LD₂ (ATLAS). *Icarus*, 354:114019.
- Huang, C. X., Burt, J., Vanderburg, A., Günther, M. N., Shporer, A., Dittmann, J. A., Winn, J. N., Wittenmyer, R., Sha, L., Kane, S. R., Ricker, G. R., Vanderspek, R. K., Latham, D. W., Seager, S., Jenkins, J. M., Caldwell, D. A., Collins, K. A., Guerrero, N., Smith, J. C., Quinn, S. N., Udry, S., Pepe, F., Bouchy, F., Ségransan, D., Lovis, C., Ehrenreich, D., Marmier, M., Mayor, M., Wöhler, B., Haworth, K., Morgan, E. H., Fausnaugh, M., Ciardi, D. R., Christiansen, J., Charbonneau, D., Dragomir, D., Deming, D., Glidden, A., Levine, A. M., McCullough, P. R., Yu, L., Narita, N., Nguyen, T., Morton, T., Pepper, J., Pál, A.,

and Rodriguez, J. E. (2018). TESS discovery of a transiting Super-Earth in the π Mensae system.

Hug, L. A., Baker, B. J., Anantharaman, K., Brown, C. T., Probst, A. J., Castelle, C. J., Butterfield, C. N., Hemsdorf, A. W., Amano, Y., Ise, K., Suzuki, Y., Dudek, N., Relman, D. A., Finstad, K. M., Amundson, R., Thomas, B. C., and Banfield, J. F. (2016). A new view of the tree of life. *Nat. Microbiol.*, 1(5):16048.

Hunter, R. B. (1967a). Motions of Satellites and Asteroids Under the Influence of Jupiter and the Sun: I. Stable and Unstable Satellite Orbits. *Mon. Not. R. Astron. Soc.*, 136(3):245–265.

Hunter, R. B. (1967b). Motions of Satellites and Asteroids Under the Influence of Jupiter and the Sun: II. Asteroid Orbits Close to Jupiter. *Mon. Not. R. Astron. Soc.*, 136(3):267–277.

Huygens, C. (1659). *Systema saturnium*.

Ivezić, Ž., Lupton, R. H., Jurić, M., Tabachnik, S., Quinn, T. R., Gunn, J. E., Knapp, G. R., Rockosi, C. M., and Brinkmann, J. (2002). Color Confirmation of Asteroid Families. *Astron. J.*, 124(5):2943–2948.

Jacobson, R. A., Brozović, M., Gladman, B. J., Alexandersen, M., Veillet, C., and Williams, G. (2011). New Satellites of Jupiter: S/2010 J 1 and S/2010 J 2. *IAU Circ.*, 9222.

Jedicke, R., Bolin, B. T., Bottke, W. F., Chyba, M., Fedorets, G., Granvik, M., Jones, L., and Urrutxua, H. (2018). Earth's Minimoons: Opportunities for Science and Technology. *Front. Astron. Sp. Sci.*, 5(13):13.

Jewitt, D. C. (2018). The Trojan Color Conundrum. *Astron. J.*, 155(2):56.

JEWITT, D. C., DANIELSON, G. E., and SYNNOTT, S. P. (1979). Discovery of a New Jupiter Satellite. *Science (80-.)*, 206(4421):951–951.

Jewitt, D. C. and Haghighipour, N. (2007). Irregular Satellites of the Planets: Products of Capture in the Early Solar System. *Annu. Rev. Astron. Astrophys.*, 45(1):261–295.

Jewitt, D. C., Sheppard, S. S., Kleyna, J., and Marsden, B. G. (2005). Satellites of Saturn. *IAU Circ.*, 8727.

- Jewitt, D. C., Trujillo, C. A., and Luu, J. X. (2000). Population and Size Distribution of Small Jovian Trojan Asteroids. *Astron. J.*, 120(2):1140–1147.
- Jofré, P., Das, P., Bertranpetit, J., and Foley, R. (2017). Cosmic phylogeny: reconstructing the chemical history of the solar neighbourhood with an evolutionary tree. *Mon. Not. R. Astron. Soc.*, 467(1):1140–1153.
- Johnson, T. V. and Lunine, J. I. (2005). Saturn’s moon Phoebe as a captured body from the outer Solar System. *Nature*, 435(7038):69–71.
- Jones, E., Oliphant, T., Peterson, P., and Others (2015). SciPy: Open Source Scientific Tools for Python, 2001 (<http://www.scipy.org/>).
- Kaplan, M. and Cengiz, S. (2020). Horseshoe co-orbitals of Earth: current population and new candidates. *Mon. Not. R. Astron. Soc.*, 496(4):4420–4432.
- Karkoschka, E. (1994). Spectrophotometry of the Jovian Planets and Titan at 300- to 1000-nm Wavelength: The Methane Spectrum. *Icarus*, 111(1):174–192.
- Karlsson, O., Lagerkvist, C., and Davidsson, B. (2009). (U)BVRI photometry of Trojan L₅ asteroids. *Icarus*, 199(1):106–118.
- Kary, D. M. and Lissauer, J. J. (1995). Nebular gas drag and planetary accretion. ii. planet on an eccentric orbit. *Icarus*, 117(1):1–24.
- Kashikawa, N., Aoki, K., Asai, R., Ebizuka, N., Inata, M., Iye, M., Kawabata, K. S., Kosugi, G., Ohyama, Y., Okita, K., Ozawa, T., Saito, Y., Sasaki, T., Sekiguchi, K., Shimizu, Y., Taguchi, H., Takata, T., Yadoumaru, Y., and Yoshida, M. (2002). FOCAS: The Faint Object Camera and Spectrograph for the Subaru Telescope. Technical Report 6.
- Kepler, J. (1609). *Astronomia nova*. Pragae.
- Kluge, A. G. and Farris, J. S. (1969). Quantitative Phyletics and the Evolution of Anurans. *Syst. Biol.*, 18(1):1–32.
- Knežević, Z. and Milani, A. (2017). AstDys: Synthetic proper elements 5553 numbered and multiopposition Trojans.
- Kopff, A. (1909). Beobachtungen der Planeten (624) Hektor und (659) [1908 CS]. *Astron. Nachrichten*, 182(2):25–26.

- Kopparapu, R. K., Ramirez, R., Kasting, J. F., Eymet, V., Robinson, T. D., Mahadevan, S., Terrien, R. C., Domagal-Goldman, S., Meadows, V., and Deshpande, R. (2013). HABITABLE ZONES AROUND MAIN-SEQUENCE STARS: NEW ESTIMATES. *Astrophys. J.*, 765(2):131.
- Kopparapu, R. K., Ramirez, R. M., SchottelKotte, J., Kasting, J. F., Domagal-Goldman, S., and Eymet, V. (2014). HABITABLE ZONES AROUND MAIN-SEQUENCE STARS: DEPENDENCE ON PLANETARY MASS. *Astrophys. J.*, 787(2):L29.
- Kowal, C. T., Aksnes, K., Marsden, B. G., and Roemer, E. (1975a). Thirteenth satellite of Jupiter. *Astron. J.*, 80:460.
- Kowal, C. T., Roemer, E., Daniel, M., McCarthy, C., Aksnes, K., and Marsden, B. G. (1975b). Probable New Satellite of Jupiter. *IAU Circ.*, 2855.
- Kuiper, G. P. (1944). Titan: a Satellite with an Atmosphere. *Astrophys. J.*, 100:378.
- Kvist, S., Laumer, C. E., Junoy, J., and Giribet, G. (2014). New insights into the phylogeny, systematics and DNA barcoding of Nemertea. *Invertebr. Syst.*, 28(3):287.
- Lagrange, J.-L. (1772). Essai sur le probleme des trois corps. *Essai sur le Probl\`eme des Trois Corps, Prix l'Acad\`emie R. des Sci. Paris (printed 1868, {\OE}uvres Lagrange, Tome VI, Gauthier-Villars, p. 229)*, 9:292.
- Lassell (1849). Lassell's Satellite of Neptune. *Mon. Not. R. Astron. Soc.*, 10(1):8–8.
- Lauretta, D. S., Drake, M., and Team, O. (2011). OSIRIS-REx - Exploration of Asteroid (101955) 1999 RQ36. *AGU Fall Meet. Abstr.*, pages P21E–01.
- Lazzaro, D., Angeli, C. A., Carvano, J. M., Mothé-Diniz, T., Duffard, R., and Florczak, M. (2004). S₃OS₂: The visible spectroscopic survey of 820 asteroids. *Icarus*, 172(1 SPEC.ISS.):179–220.
- Lebreton, J.-P., Witasse, O., Sollazzo, C., Blancquaert, T., Couzin, P., Schipper, A.-M., Jones, J. B., Matson, D. L., Gurvits, L. I., Atkinson, D. H., Kazeminejad, B., and Pérez-Ayúcar, M. (2005). An overview of the descent and landing of the Huygens probe on Titan. *Nature*, 438(7069):758–764.

- Levison, H. F., Bottke, W. F., Gounelle, M., Morbidelli, A., Nesvorný, D., and Tsiganis, K. (2009). Contamination of the asteroid belt by primordial trans-Neptunian objects. *Nature*, 460(7253):364–366.
- Levison, H. F. and Duncan, M. J. (1994). The Long-Term Dynamical Behavior of Short-Period Comets. *Icarus*, 108(1):18–36.
- Levison, H. F., Morbidelli, A., Tsiganis, K., Nesvorný, D., and Gomes, R. (2011). LATE ORBITAL INSTABILITIES IN THE OUTER PLANETS INDUCED BY INTERACTION WITH A SELF-GRAVITATING PLANETESIMAL DISK. *Astron. J.*, 142(5):152.
- Levison, H. F., Morbidelli, A., VanLaerhoven, C., Gomes, R., and Tsiganis, K. (2008). Origin of the structure of the Kuiper belt during a dynamical instability in the orbits of Uranus and Neptune. *Icarus*, 196(1):258–273.
- Levison, H. F., Olkin, C. B., Noll, K., Marchi, S., and Lucy Team (2017). Lucy: Surveying the Diversity of the Trojan Asteroids: The Fossils of Planet Formation. In *Lunar Planet. Sci. Conf.*, volume 48 of *Lunar and Planetary Science Conference*, page 2025.
- Levison, H. F., Shoemaker, E. M., and Shoemaker, C. S. (1997). Dynamical evolution of Jupiter’s Trojan asteroids. *Nature*, 385(6611):42–44.
- Liberato, L. and Winter, O. C. (2020). The structure of the co-orbital stable regions as a function of the mass ratio. *Mon. Not. R. Astron. Soc.*, 496(3):3700–3707.
- Lissauer, J. J. (1987). Timescales for planetary accretion and the structure of the protoplanetary disk. *Icarus*, 69(2):249–265.
- LSST Science Collaboration, Abell, P. A., Allison, J., Anderson, S. F., Andrew, J. R., Angel, J. R. P., Armus, L., Arnett, D., Asztalos, S. J., Axelrod, T. S., Bailey, S., Ballantyne, D. R., Bankert, J. R., Barkhouse, W. A., Barr, J. D., Barrientos, L. F., Barth, A. J., Bartlett, J. G., Becker, A. C., Becla, J., Beers, T. C., Bernstein, J. P., Biswas, R., Blanton, M. R., Bloom, J. S., Bochanski, J. J., Boeshaar, P., Borne, K. D., Bradac, M., Brandt, W. N., Bridge, C. R., Brown, M. E., Brunner, R. J., Bullock, J. S., Burgasser, A. J., Burge, J. H., Burke, D. L., Cargile, P. A., Chandrasekharan, S., Chartas, G., Chesley, S. R., Chu, Y.-H., Cinabro, D., Claire, M. W., Claver, C. F., Clowe, D., Connolly, A. J., Cook, K. H., Cooke, J., Cooray, A., Covey, K. R., Culliton, C. S., de Jong, R., de Vries, W. H., Debattista, V. P., Delgado, F., Dell’Antonio, I. P., Dhital, S., Di Stefano, R., Dickinson, M., Dilday, B., Djorgovski, S. G., Dobler, G.,

Donalek, C., Dubois-Felsmann, G., Durech, J., Eliasdottir, A., Eracleous, M., Eyer, L., Falco, E. E., Fan, X., Fassnacht, C. D., Ferguson, H. C., Fernandez, Y. R., Fields, B. D., Finkbeiner, D., Figuerao, E. E., Fox, D. B., Francke, H., Frank, J. S., Frieman, J., Fromenteau, S., Furqan, M., Galaz, G., Gal-Yam, A., Garnavich, P., Gawiser, E., Geary, J., Gee, P., Gibson, R. R., Gilmore, K., Grace, E. A., Green, R. F., Gressler, W. J., Grillmair, C. J., Habib, S., Haggerty, J. S., Hamuy, M., Harris, A. W., Hawley, S. L., Heavens, A. F., Hebb, L., Henry, T. J., Hileman, E., Hilton, E. J., Hoadley, K., Holberg, J. B., Holman, M. J., Howell, S. B., Infante, L., Ivezić, Z., Jacoby, S. H., Jain, B., R., Jedicke, Jee, M. J., Jernigan, J. G., Jha, S. W., Johnston, K. V., Jones, R. L., Juric, M., Kaasalainen, M., Styliani, Kafka, Kahn, S. M., Kaib, N. A., Kalirai, J., Kantor, J., Kasliwal, M. M., Keeton, C. R., Kessler, R., Knezevic, Z., Kowalski, A., Krabbendam, V. L., Krughoff, K. S., Kulkarni, S., Kuhlman, S., Lacy, M., Lepine, S., Liang, M., Lien, A., Lira, P., Long, K. S., Lorenz, S., Lotz, J. M., Lupton, R. H., Lutz, J., Macri, L. M., Mahabal, A. A., Mandelbaum, R., Marshall, P., May, M., McGehee, P. M., Meadows, B. T., Meert, A., Milani, A., Miller, C. J., Miller, M., Mills, D., Minniti, D., Monet, D., Mukadam, A. S., Nakar, E., Neill, D. R., Newman, J. A., Nikolaev, S., Nordby, M., O'Connor, P., Oguri, M., Oliver, J., Olivier, S. S., Olsen, J. K., Olsen, K., Olszewski, E. W., Oluseyi, H., Padilla, N. D., Parker, A. H., Pepper, J., Peterson, J. R., Petry, C., Pinto, P. A., Pizagno, J. L., Popescu, B., Prsa, A., Radcka, V., Raddick, M. J., Rasmussen, A., Rau, A., Rho, J., Rhoads, J. E., Richards, G. T., Ridgway, S. T., Robertson, B. E., Roskar, R., Saha, A., Sarajedini, A., Scannapieco, E., Schalk, T., Schindler, R., Schmidt, S., Schmidt, S., Schneider, D. P., Schumacher, G., Scranton, R., Sebag, J., Seppala, L. G., Shemmer, O., Simon, J. D., Sivertz, M., Smith, H. A., Smith, J. A., Smith, N., Spitz, A. H., Stanford, A., Stassun, K. G., Strader, J., Strauss, M. A., Stubbs, C. W., Sweeney, D. W., Szalay, A., Szkody, P., Takada, M., Thorman, P., Trilling, D. E., Trimble, V., Tyson, A., Van Berg, R., Berk, D. V., VanderPlas, J., Verde, L., Vrsnak, B., Walkowicz, L. M., Wandelt, B. D., Wang, S., Wang, Y., Warner, M., Wechsler, R. H., West, A. A., Wiecha, O., Williams, B. F., Willman, B., Wittman, D., Wolff, S. C., Wood-Vasey, W. M., Wozniak, P., Young, P., Zentner, A., and Zhan, H. (2009). LSST Science Book, Version 2.0. *ArXiv e-prints*.

Lykawka, P. S. and Horner, J. (2010). The capture of Trojan asteroids by the giant planets during planetary migration. *Mon. Not. R. Astron. Soc.*, 405:1375–1383.

Maddison, W. P., Donoghue, M. J., and Maddison, D. R. (1984). Outgroup analysis and parsimony. *SystBio*, 33(1):83–103.

- Maddison, W. P. and Maddison, D. R. (2015). Zephyr: a Mesquite package for interacting with external phylogeny inference programs. Version 1.1. <http://mesquitezephyr.wikispaces.com>.
- Maddison, W. P. and Maddison, D. R. (2017). Mesquite: a modular system for evolutionary analysis. Version 3.20. <http://mesquiteproject.org>.
- Marchis, F., Durech, J., Castillo-Rogez, J. C., Vachier, F., Cuk, M., Berthier, J., Wong, M. H., Kalas, P., Duchene, G., van Dam, M. A., Hamanowa, H., and Viikinkoski, M. (2014). THE PUZZLING MUTUAL ORBIT OF THE BINARY TROJAN ASTEROID (624) HEKTOR. *Astrophys. J.*, 783(2):L37.
- Marchis, F., Hestroffer, D., Descamps, P., Berthier, J., Bouchez, A. H., Campbell, R. D., Chin, J. C. Y., van Dam, M. A., Hartman, S. K., Johansson, E. M., Lafon, R. E., Mignant, D. L., de Pater, I., Stomski, P. J., Summers, D. M., Vachier, F., Wizinovich, P. L., and Wong, M. H. (2006). A low density of 0.8 g cm⁻³ for the Trojan binary asteroid 617 Patroclus. *Nature*, 439(7076):565–567.
- Margot, J.-L., Pravec, P., Taylor, P., Carry, B., and Jacobson, S. (2015). Asteroid Systems: Binaries, Triples, and Pairs. *Asteroids IV*, pages 355–373.
- Margush, T. and McMorris, F. R. (1981). Consensus-trees. *Bull. Math. Biol.*, 43(2):239–244.
- Marin, J.-M., Pudlo, P., Robert, C. P., and Ryder, R. (2011). Approximate Bayesian Computational methods. *Stat. Comput.*, 22(6):1167–1180.
- Marzari, F., Scholl, H., Murray, C., and Lagerkvist, C. (2002). Origin and Evolution of Trojan Asteroids. In Bottke Jr., W., Cellino, A., Paolicchi, P., and Binzel, R. P., editors, *Asteroids III*, pages 725–738. University of Arizona Press, Tucson, AZ.
- Masiero, J. R., Mainzer, A. K., Grav, T., Bauer, J. M., Cutri, R. M., Dailey, J., Eisenhardt, P. R. M., McMillan, R. S., Spahr, T. B., Skrutskie, M. F., Tholen, D. J., Walker, R. G., Wright, E. L., DeBaun, E., Elsbury, D., Gautier, T., Gomillion, S., and Wilkins, A. (2011). MAIN BELT ASTEROIDS WITH WISE /NEOWISE. I. PRELIMINARY ALBEDOS AND DIAMETERS. *Astrophys. J.*, 741(2):68.

- Matson, D. L., Castillo-Rogez, J. C., Schubert, G., Sotin, C., and McKinnon, W. B. (2009). *The Thermal Evolution and Internal Structure of Saturn's Mid-Sized Icy Satellites*, pages 577–612. Springer Netherlands, Dordrecht.
- Melotte, J. and Perrine, C. D. (1908). Recent Observations of the Moving Object Near Jupiter, Discovered at Greenwich. *Publ. Astron. Soc. Pacific*, 20:184.
- Michel, P., Jutzi, M., Richardson, D. C., and Benz, W. (2011). The Asteroid Veritas: An intruder in a family named after it? *Icarus*, 211(1):535–545.
- Mikkola, S. and Innanen, K. (1992). A numerical exploration of the evolution of Trojan-type asteroidal orbits. *Astron. J.*, 104(4):1641.
- Milani, A. (1993). The Trojan asteroid belt: Proper elements, stability, chaos and families. *Celest. Mech. Dyn. Astron.*, 57(1-2):59–94.
- Milani, A., Cellino, A., Knežević, Z., Novaković, B., Spoto, F., and Paolicchi, P. (2014). Asteroid families classification: Exploiting very large datasets. *Icarus*, 239:46–73.
- Mitchell, P. C. (1901). VII. On the Intestinal Tract of Birds; with Remarks on the Valuation and Nomenclature of Zoological Characters. *Trans. Linn. Soc. London. 2nd Ser. Zool.*, 8(7):173–275.
- Morbidelli, A. (2010). A coherent and comprehensive model of the evolution of the outer Solar System. *Comptes Rendus Phys.*, 11(9-10):651–659.
- Morbidelli, A., Levison, H. F., Tsiganis, K., and Gomes, R. (2005). Chaotic capture of Jupiter's Trojan asteroids in the early Solar System. *Nature*, 435(7041):462–465.
- Morbidelli, A., Zappala, V., Moons, M., Cellino, A., and Gonczi, R. (1995). Asteroid Families Close to Mean Motion Resonances: Dynamical Effects and Physical Implications. *Icarus*, 118(1):132–154.
- Moskovitz, N. A., Fatka, P., Farnocchia, D., Devogèle, M., Polishook, D., Thomas, C. A., Mommert, M., Avner, L. D., Binzel, R. P., Burt, B., Christensen, E., DeMeo, F. E., Hinkle, M., Hora, J. L., Magnusson, M., Matson, R., Person, M., Skiff, B., Thirouin, A., Trilling, D., Wasserman, L. H., and Willman, M. (2019). A common origin for dynamically associated near-Earth asteroid pairs. *Icarus*, 333:165–176.

- Nakamura, T. and Yoshida, F. (2008). A New Surface Density Model of Jovian Trojans around Triangular Libration Points. *Publ. Astron. Soc. Japan*, 60(2):293–296.
- Naylor, G. and Kraus, F. (1995). The Relationship Between s and m and the Retention Index. *Syst. Biol.*, 44(4):559.
- Nesvorný, D. (2002). How Long-Lived Are the Hypothetical Trojan Populations of Saturn, Uranus, and Neptune? *Icarus*, 160(2):271–288.
- Nesvorný, D. (2006). The Breakup of a Main-Belt Asteroid 450 Thousand Years Ago. *Science (80-.)*, 312(5779):1490–1490.
- Nesvorný, D. (2018). Dynamical Evolution of the Early Solar System. *Annu. Rev. Astron. Astrophys.*, 56(1):137–174.
- Nesvorný, D., Alvarillos, J. L. A., Dones, L., and Levison, H. F. (2003). Orbital and Collisional Evolution of the Irregular Satellites. *Astron. J.*, 126(1):398–429.
- Nesvorný, D., Beaug, C., and Dones, L. (2004). Collisional Origin of Families of Irregular Satellites. *Astron. J.*, 127(3):1768–1783.
- Nesvorný, D. and Bottke, W. F. (2004). Detection of the Yarkovsky effect for main-belt asteroids. *Icarus*, 170(2):324–342.
- Nesvorný, D., Bottke, W. F., Dones, L., and Levison, H. F. (2002a). The recent breakup of an asteroid in the main-belt region. *Nature*, 417(6890):720–721.
- Nesvorný, D., Brož, M., and Carruba, V. (2015). Identification and Dynamical Properties of Asteroid Families. In Michel, P., DeMeo, F. E., and Bottke, W. F., editors, *Asteroids IV*, pages 297–321. University of Arizona Press, Tucson, AZ.
- Nesvorný, D. and Morbidelli, A. (2012). STATISTICAL STUDY OF THE EARLY SOLAR SYSTEM'S INSTABILITY WITH FOUR, FIVE, AND SIX GIANT PLANETS. *Astron. J.*, 144(4):117.
- Nesvorný, D., Morbidelli, A., Vokrouhlický, D., Bottke, W. F., and Brož, M. (2002b). The Flora family: A case of the dynamically dispersed collisional swarm? *Icarus*, 157(1):155–172.
- Nesvorný, D. and Vokrouhlický, D. (2006). New Candidates for Recent Asteroid Breakups. *Astron. J.*, 132(5):1950–1958.

- Nesvorný, D. and Vokrouhlický, D. (2019). Binary survival in the outer solar system. *Icarus*, 331:49–61.
- Nesvorný, D., Vokrouhlický, D., Bottke, W. F., and Levison, H. F. (2018). Evidence for very early migration of the Solar System planets from the Patroclus–Menoetius binary Jupiter Trojan. *Nat. Astron.*, 2(11):878–882.
- Nesvorný, D., Vokrouhlický, D., and Deienno, R. (2014). CAPTURE OF IRREGULAR SATELLITES AT JUPITER. *Astrophys. J.*, 784(1):22.
- Nesvorný, D., Vokrouhlický, D., and Morbidelli, A. (2007). Capture of Irregular Satellites during Planetary Encounters. *Astron. J.*, 133(5):1962–1976.
- Nesvorný, D., Vokrouhlický, D., and Morbidelli, A. (2013). Capture of Trojans by Jumping Jupiter. *Astrophys. J.*, 768(1):45.
- Newton, I. (1687). *Philosophiæ naturalis principia mathematica (Mathematical principles of natural philosophy)*. Jussu Societatis Regiæ ac Typis Joseph Streater, London.
- Nicholson, P. D., Hamilton, D. P., Matthews, K., and Yoder, C. F. (1992). New observations of Saturn’s coorbital satellites. *Icarus*, 100(2):464–484.
- Nicholson, S. B. (1914). Discovery of the Ninth Satellite of Jupiter. *Publ. Astron. Soc. Pacific*, 26:197.
- Nicholson, S. B. (1938). Two New Satellites of Jupiter. *Publ. Astron. Soc. Pacific*, 50:292.
- Nicholson, S. B. (1951). An Unidentified Object Near Jupiter, Probably a New Satellite. *Publ. Astron. Soc. Pacific*, 63:297.
- Nicholson, S. B. (1961). The Trojan Asteroids. *Astron. Soc. Pacific Leaflet*, 8:239.
- Niemann, H. B., Atreya, S. K., Bauer, S. J., Carignan, G. R., Demick, J. E., Frost, R. L., Gautier, D., Haberman, J. A., Harpold, D. N., Hunten, D. M., Israel, G., Lunine, J. I., Kasprzak, W. T., Owen, T. C., Paulkovich, M., Raulin, F., Raaen, E., and Way, S. H. (2005). The abundances of constituents of Titan’s atmosphere from the GCMS instrument on the Huygens probe. *Nature*, 438(7069):779–784.
- Noll, K. S., Brown, M. E., Weaver, H. A., Grundy, W. M., Porter, S. B., Buie, M. W., Levison, H. F., Olkin, C., Spencer, J. R., Marchi, S., and Statler, T. (2020a). Detection of a Satellite

- of the Trojan Asteroid (3548) Eurybates - A Lucy Mission Target. In *51st Lunar Planet. Sci. Conf. held 16-20 March, 2020 Woodlands, Texas.*, number 2326, page 2981.
- Noll, K. S., Grundy, W. M., Nesvorný, D., and Thirouin, A. (2020b). Trans-Neptunian binaries. In Pralnik, D., Barucci, M. A., and Young, L., editors, *Trans-Neptunian Sol. Syst.*, pages 205–224. Elsevier, Cambridge, MA, USA.
- North, J. (2008). *Cosmos: An Illustrated History of Astronomy and Cosmology (revised)*. University of Chicago Press, Chicago, USA.
- Ockert-Bell, M. E., Burns, J. A., Daubar, I. J., Thomas, P. C., Veverka, J., Belton, M., and Klaasen, K. P. (1999). The Structure of Jupiter's Ring System as Revealed by the Galileo Imaging Experiment. *Icarus*, 138(2):188–213.
- Oke, J. B., Cohen, J. G., Carr, M., Cromer, J., Dingizian, A., Harris, F. H., Labrecque, S., Lucinio, R., Schaal, W., Epps, H., and Miller, J. (1995). The Keck Low-Resolution Imaging Spectrometer. *Publ. Astron. Soc. Pacific*, 107(710):375.
- Olsen, G. J., Woese, C. R., and Overbeek, R. (1994). The winds of (evolutionary) change: breathing new life into microbiology. *J. Bacteriol.*, 176(1):1–6.
- Parker, A. H. (2015). The intrinsic Neptune Trojan orbit distribution: Implications for the primordial disk and planet migration. *Icarus*, 247:112–125.
- Parker, A. H., Ivezić, Ž., Jurić, M., Lupton, R. H., Sekora, M., and Kowalski, A. (2008). The size distributions of asteroid families in the SDSS Moving Object Catalog 4. *Icarus*, 198(1):138–155.
- Peale, S. J. (1993). The Effect of the Nebula on the Trojan Precursors. *Icarus*, 106(1):308–322.
- Perna, D., Bott, N., Hromakina, T., Mazzotta Epifani, E., Dotto, E., and Doressoundiram, A. (2018). Rotationally resolved spectroscopy of Jupiter Trojans (624) Hektor and (911) Agamemnon. *Mon. Not. R. Astron. Soc.*, 475(1):974–980.
- Perrine, C. D. (1905). The Sixth Satellite of Jupiter. *Publ. Astron. Soc. Pacific*, 17(101):62.
- Perrine, C. D. and Aitken, R. G. (1905). The Seventh Satellite of Jupiter. *Publ. Astron. Soc. Pacific*, 17(101):62–63.
- Pickering, E. C. (1899). A New Satellite of Saturn. *Astrophys. J.*, 9:274.

- Pickering, W. (1905). Phoebe, the ninth satellite of Saturn. *AnHvaCOB*, 53:85–100.
- Pirani, S., Johansen, A., Bitsch, B., Mustill, A. J., and Turrini, D. (2019a). Consequences of planetary migration on the minor bodies of the early solar system. *Astron. Astrophys.*, 623:A169.
- Pirani, S., Johansen, A., and Mustill, A. J. (2019b). On the inclinations of the Jupiter Trojans. *Astron. Astrophys.*, 631:A89.
- Pollack, J. B., Burns, J. A., and Tauber, M. E. (1979). Gas drag in primordial circumplanetary envelopes: A mechanism for satellite capture. *Icarus*, 37(3):587–611.
- Pollack, J. B., Hubickyj, O., Bodenheimer, P., Lissauer, J. J., Podolak, M., and Greenzweig, Y. (1996). Formation of the Giant Planets by Concurrent Accretion of Solids and Gas. *Icarus*, 124(1):62–85.
- Popescu, M., Licandro, J., Morate, D., de León, J., Nedelcu, D. A., Rebolo, R., McMahon, R. G., Gonzalez-Solares, E., and Irwin, M. (2016). Near-infrared colors of minor planets recovered from VISTA-VHS survey (MOVIS). *Astron. Astrophys.*, 591:A115.
- Porco, C. C., Baker, E., Barbara, J., Beurle, K., Brahic, A., Burns, J. A., Charnoz, S., Cooper, N., Dawson, D. D., Del Genio, A. D., Denk, T., Dones, L., Dyudina, U., Evans, M. W., Giese, B., Grazier, K., Helfenstein, P., Ingersoll, A. P., Jacobson, R. A., Johnson, T. V., McEwen, A., Murray, C. D., Neukum, G., Owen, W. M., Perry, J., Roatsch, T., Spitale, J. N., Squyres, S., Thomas, P. C., Tiscareno, M. S., Turtle, E., Vasavada, A. R., Veverka, J., Wagner, R., and West, R. (2005). Cassini Imaging Science: initial results on Saturn’s rings and small satellites. *Science*, 307(5713):1226–36.
- Porco, C. C., Thomas, P. C., Weiss, J. W., and Richardson, D. C. (2007). Saturn’s Small Inner Satellites: Clues to Their Origins. *Science (80-.)*, 318(5856):1602–1607.
- Pravec, P., Fatka, P., Vokrouhlický, D., Scheirich, P., Ďurech, J., Scheeres, D. J., Kušnirák, P., Hornoch, K., Galád, A., Pray, D. P., Krugly, Y. N., Burkhonov, O., Ehgamberdiev, S. A., Pollock, J., Moskovitz, N. A., Thirouin, A., Ortiz, J. L., Morales, N., Husárik, M., Inasaridze, R. Y., Oey, J., Polishook, D., Hanuš, J., Kučáková, H., Vraštil, J., Világi, J., Gajdoš, Kornoš, L., Vereš, P., Gaftonyuk, N. M., Hromakina, T., Sergeyev, A. V., Slyusarev, I. G., Ayvazian, V. R., Cooney, W. R., Gross, J., Terrell, D., Colas, F., Vachier, F., Slivan, S., Skiff, B., Marchis, F., Ergashev, K. E., Kim, D. H., Aznar, A., Serra-Ricart, M., Behrend, R.,

- Roy, R., Manzini, F., and Molotov, I. E. (2019). Asteroid pairs: A complex picture. *Icarus*, 333:429–463.
- Pravec, P. and Harris, A. (2007). Binary asteroid population. *Icarus*, 190(1):250–259.
- Pravec, P. and Vokrouhlický, D. (2009). Significance analysis of asteroid pairs. *Icarus*, 204(2):580–588.
- Pravec, P., Vokrouhlický, D., Polishook, D., Scheeres, D. J., Harris, A. W., Galád, A., Vaduvescu, O., Pozo, F., Barr, A., Longa, P., Vachier, F., Colas, F., Pray, D. P., Pollock, J., Reichart, D., Ivarsen, K., Haislip, J., Lacluyze, A., Kušnirák, P., Henych, T., Marchis, F., Macomber, B., Jacobson, S. A., Krugly, Y. N., Sergeev, A. V., and Leroy, A. (2010). Formation of asteroid pairs by rotational fission. *Nature*, 466(7310):1085–1088.
- Rabe, E. (1968). Stability Characteristics of the Short-Period Trojan Librations. *Astron. J.*, 73:732.
- Radović, V., Novaković, B., Carruba, V., and Marčeta, D. (2017). An automatic approach to exclude interlopers from asteroid families. *Mon. Not. R. Astron. Soc.*, 470(1):576–591.
- Ragozzine, D. and Brown, M. E. (2007). Candidate Members and Age Estimate of the Family of Kuiper Belt Object 2003 EL61. *Astron. J.*, 134(6):2160–2167.
- Rein, H., Hernandez, D. M., Tamayo, D., Brown, G., Eckels, E., Holmes, E., Lau, M., Leblanc, R., and Silburt, A. (2019). Hybrid symplectic integrators for planetary dynamics. *Mon. Not. R. Astron. Soc.*, 485(4):5490–5497.
- Rein, H. and Liu, S.-F. (2012). REBOUND: an open-source multi-purpose N -body code for collisional dynamics. *Astron. Astrophys.*, 537:A128.
- Rein, H. and Spiegel, D. S. (2015). ias15: a fast, adaptive, high-order integrator for gravitational dynamics, accurate to machine precision over a billion orbits. *Mon. Not. R. Astron. Soc.*, 446(2):1424–1437.
- Rein, H. and Tamayo, D. (2015). whfast: a fast and unbiased implementation of a symplectic Wisdom–Holman integrator for long-term gravitational simulations. *Mon. Not. R. Astron. Soc.*, 452(1):376–388.

- Ričan, O., Pialek, L., Almiron, A., and Casciotta, J. (2011). Two new species of Australoheros (Teleostei: Cichlidae), with notes on diversity of the genus and biogeography of the Rio de la Plata basin. *Zootaxa*, 2982(1):1–26.
- Rivkin, A. S., Marchis, F., Stansberry, J. A., Takir, D., Thomas, C., and Group, t. J. A. F. (2016). Asteroids and the James Webb Space Telescope. *Publ. Astron. Soc. Pacific*, 128(959):018003.
- Rivkin, A. S., Milam, Stefanie, N., and Thomas, C. A. (2020). STScI: Web Observing Program: GTO 1244.
- Robutel, P., Gabern, F., and Jorba, A. (2005). The Observed Trojans and the Global Dynamics Around The Lagrangian Points of the Sun–Jupiter System. *Celest. Mech. Dyn. Astron.*, 92(1-3):53–69.
- Roig, F., Nesvorný, D., and Ferraz-Mello, S. (2002). Asteroids in the 2 : 1 resonance with Jupiter: Dynamics and size distribution. *Mon. Not. R. Astron. Soc.*, 335(2):417–431.
- Roig, F., Ribeiro, A. O., and Gil-Hutton, R. (2008). Taxonomy of asteroid families among the Jupiter Trojans: comparison between spectroscopic data and the Sloan Digital Sky Survey colors. *Astron. Astrophys.*, 483(3):911–931.
- Romanishin, W. and Tegler, S. C. (2018). Albedos of Centaurs, Jovian Trojans, and Hildas. *Astron. J.*, 156(1):19.
- Ross, F. (1905). Investigations on the orbit of Phoebe. *AnHvaCOB*, 53:101–142.
- Rozehnal, J., Brož, M., Nesvorný, D., Durda, D. D., Walsh, K. J., Richardson, D. C., and Asphaug, E. (2016). Hektor – an exceptional D-type family among Jovian Trojans. *Mon. Not. R. Astron. Soc.*, 462(3):2319–2332.
- Rozek, A., Breiter, S., and Jopek, T. J. (2011). Orbital similarity functions - application to asteroid pairs. *Mon. Not. R. Astron. Soc.*, 412(2):987–994.
- Rubincam, D. (2000). Radiative Spin-up and Spin-down of Small Asteroids. *Icarus*, 148(1):2–11.
- Ryan, E. L., Sharkey, B. N. L., and Woodward, C. E. (2017). Trojan Asteroids in the Kepler Campaign 6 Field. *Astron. J.*, 153(3):116.

- Salisbury, S. W., Molnar, R. E., Frey, E., and Willis, P. M. A. (2006). The origin of modern crocodyliforms: new evidence from the Cretaceous of Australia. *Proc. R. Soc. B Biol. Sci.*, 273(1600):2439–2448.
- Salmon, J. and Canup, R. M. (2017). Accretion of Saturn’s Inner Mid-sized Moons from a Massive Primordial Ice Ring. *Astrophys. J.*, 836(1):109.
- Sanderson, M. J. and Donoghue, M. J. (1989). Patterns of Variation in Levels of Homoplasy. *Evolution (N. Y.)*, 43(8):1781.
- Savini, G., Tinetti, G., Arena, C., Tennyson, J., Pascale, E., Ade, P. A. R., Griffin, M. J., Knowles, P., Crook, M., Saad, A., Eccleston, P., Shaughnessy, B., Brooke, T., Macleod, A., Wright, G. S., Jason, S., Williams, J., Winter, B., Smith, A., Tessenyi, M., Zingales, T., Sudiwala, R., Papageorgiou, A., Sarkar, S., Barnes, K., Hipwood, L., Patel, M., Leese, M., Mason, J. P., Tosh, I., Wells, M., Bryson, I., Taylor, W., Bezawada, N., Friend, J., Johnston, G., Prasad, S., Vora, A., Saunders, C., and Curry, P. (2018). TWINKLE: a low earth orbit visible and infrared exoplanet spectroscopy observatory. *Sp. Telesc. Instrum. 2016 Opt. Infrared, Millim. Wave*, 9904:175.
- Schwamb, M. E., Jones, R. L., Chesley, S. R., Fitzsimmons, A., Fraser, W. C., Holman, M. J., Hsieh, H., Ragozzine, D., Thomas, C. A., Trilling, D. E., Brown, M. E., Bannister, M. T., Bodewits, D., de Val-Borro, M., Gerdes, D., Granvik, M., Kelley, M. S. P., Knight, M. M., Seaman, R. L., Ye, Q.-Z., and Young, L. A. (2018). Large Synoptic Survey Telescope Solar System Science Roadmap. *ArXiv e-prints*, 1802.01783.
- Scotti, J., Spahr, T. B., McMillan, R. S., Larsen, J., Montani, J., Gleason, A., Gehrels, T., Marsden, B. G., and Williams, G. (2000). S/1999 J 1. *IAU Circ.*, 7460.
- Sheppard, S. S., Gladman, B. J., and Marsden, B. G. (2003a). Satellites of Jupiter and Saturn. *IAU Circ.*, 8116.
- Sheppard, S. S., Gladman, B. J., and Marsden, B. G. (2004). S/2003 J 22. *IAU Circ.*, 8276.
- Sheppard, S. S., Jewitt, D., Kleyna, J., and Marsden, B. (2006). Satellites of Saturn. *iaucirc*, 8727.
- Sheppard, S. S. and Jewitt, D. C. (2003). An abundant population of small irregular satellites around Jupiter. *Nature*, 423(6937):261–263.

- Sheppard, S. S., Jewitt, D. C., Fernández, Y. R., Magnier, G., Marsden, B. G., Dahm, S., and Evans, A. (2001). Satellites of Jupiter. *IAU Circ.*, 7555.
- Sheppard, S. S., Jewitt, D. C., Fernández, Y. R., Magnier, G., Marsden, B. G., Holman, M. J., Kowal, C. T., Roemer, E., and Williams, G. (2000). S/1975 J 1 = S/2000 J 1. *IAU Circ.*, 7525.
- Sheppard, S. S., Jewitt, D. C., Kleyana, J., and Marsden, B. G. (2007). S/2007 S 1, S/2007 S 2, and S/2007 S 3. *IAU Circ.*, 8836.
- Sheppard, S. S., Jewitt, D. C., Kleyana, J., Marsden, B. G., and Jacobson, R. (2002). Satellites of Jupiter. *IAU Circ.*, 7900.
- Sheppard, S. S., Jewitt, D. C., Kleyana, J., Marsden, B. G. B., Jacobson, R. A., Fernández, Y. R., Hsieh, H., and Fernandez, Y. (2003b). Satellites of Jupiter. *IAU Circ.*, 8087.
- Sheppard, S. S. and Marsden, B. G. (2003). S/2003 J 8. *IAU Circ.*, 8088.
- Sheppard, S. S. and Marsden, B. G. (2004). S/2003 J 23. *IAU Circ.*, 8281.
- Sheppard, S. S. and Williams, G. (2012). S/2011 J 1 and S/2011 J 2. *IAU Circ.*, 9252.
- Sheppard, S. S., Williams, G. V., Tholen, D. J., Trujillo, C. A., Brozović, M., Thirouin, A., Devoegele, M., Fohring, D., Jacobson, R. A., and Moskovitz, N. A. (2018). New Jupiter Satellites and Moon-Moon Collisions. *Res. Notes AAS*, 2(3):155.
- Shoemaker, E. M., Shoemaker, C. S., and Wolfe, R. F. (1989). Trojan asteroids: populations, dynamical structure and origin of the L₄ and L₅ swarms. In Binzel, R. P., Gehrels, T., and Matthews, M. S., editors, *Asteroids II*, page 523. University of Arizona Press, Tucson, AZ.
- Showalter, M. R. (1991). Visual detection of 1981S₁₃, Saturn's eighteenth satellite and its role in the Encke gap. *Nature*, 351(6329):709–713.
- Šidlichovský, M. and Nesvorný, D. (1996). Frequency modified fourier transform and its application to asteroids. *Celest. Mech. Dyn. Astron.*, 65(1-2):137–148.
- Slyusarev, I. G. and Belskaya, I. N. (2014). Jupiter's Trojans: Physical properties and origin. *Sol. Syst. Res.*, 48(2):139–157.
- Smith, B. A., Soderblom, L. A., Johnson, T. V., Ingersoll, A. P., Collins, S. A., Shoemaker, E. M., Hunt, G. E., Masursky, H., Carr, M. H., Davies, M. E., Cook, A. F., Boyce, J., Danielson, G. E., Owen, T. C., Sagan, C., Beebe, R. F., Veverka, J., Strom, R. G., McCauley, J. F.,

Morrison, D., Briggs, G. A., Suomi, V. E., Tiscareno, M. S., and Vasavada, A. R. (1979). The jupiter system through the eyes of voyager 1. *Science*, 204(4396):951–72.

Smith, S. Y., Stockey, R. A., Rothwell, G. W., and Little, S. A. (2017). A new species of *Pityostrobus* (Pinaceae) from the Cretaceous of California: moving towards understanding the Cretaceous radiation of Pinaceae. *JSysPalaeo*, 15(1):69–81.

Spahn, F., Schmidt, J., Albers, N., Hörning, M., Makuch, M., Seiß, M., Kempf, S., Srama, R., Dikarev, V., Helfert, S., Moragas-Klostermeyer, G., Krivov, A., Sremčević, M., Tuzzolino, A., Economou, T., and Grün, E. (2006). Cassini Dust Measurements at Enceladus and Implications for the Origin of the E Ring. *Science (80-.)*, 311:1416–1418.

Spoto, F., Tanga, P., Mignard, F., Berthier, J., Carry, B., Cellino, A., Dell’Oro, A., Hestroffer, D., Muinonen, K., Pauwels, T., Petit, J.-M., David, P., De Angeli, F., Delbo, M., Frézouls, B., Galluccio, L., Granvik, M., Guiraud, J., Hernández, J., Ordénovic, C., Portell, J., Poujoulet, E., Thuillot, W., Walmsley, G., Brown, A. G. A., Vallenari, A., Prusti, T., de Bruijne, J. H. J., Babusiaux, C., Bailer-Jones, C. A. L., Biermann, M., Evans, D. W., Eyer, L., Jansen, F., Jordi, C., Klioner, S. A., Lammers, U., Lindegren, L., Luri, X., Panem, C., Pourbaix, D., Randich, S., Sartoretti, P., Siddiqui, H. I., Soubiran, C., van Leeuwen, F., Walton, N. A., Arenou, F., Bastian, U., Cropper, M., Drimmel, R., Katz, D., Lattanzi, M. G., Bakker, J., Cacciari, C., Castañeda, J., Chaoul, L., Cheek, N., Fabricius, C., Guerra, R., Holl, B., Masana, E., Messineo, R., Mowlavi, N., Nienartowicz, K., Panuzzo, P., Riello, M., Seabroke, G. M., Thévenin, F., Gracia-Abril, G., Comoretto, G., Garcia-Reinaldos, M., Teysier, D., Altmann, M., Andrae, R., Audard, M., Bellas-Velidis, I., Benson, K., Blomme, R., Burgess, P., Busso, G., Clementini, G., Clotet, M., Creevey, O., Davidson, M., De Ridder, J., Delchambre, L., Ducourant, C., Fernández-Hernández, J., Fouesneau, M., Frémat, Y., García-Torres, M., González-Núñez, J., González-Vidal, J. J., Gosset, E., Guy, L. P., Halbwachs, J.-L., Hambly, N. C., Harrison, D. L., Hodgkin, S. T., Hutton, A., Jasiewicz, G., Jean-Antoine-Piccolo, A., Jordan, S., Korn, A. J., Krone-Martins, A., Lanzafame, A. C., Lebzelter, T., Löffler, W., Manteiga, M., Marrese, P. M., Martín-Fleitas, J. M., Moitinho, A., Mora, A., Osinde, J., Pancino, E., Recio-Blanco, A., Richards, P. J., Rimoldini, L., Robin, A. C., Sarro, L. M., Siopis, C., Smith, M., Sozzetti, A., Süveges, M., Torra, J., van Reeven, W., Abbas, U., Abreu Aramburu, A., Accart, S., Aerts, C., Altavilla, G., Álvarez, M. A., Alvarez, R., Alves, J., Anderson, R. I., Andrei, A. H., Anglada Varela, E., Antiche, E., Antoja, T., Arcay, B., Astraatmadja, T. L., Bach, N., Baker, S. G., Balaguer-Núñez, L., Balm, P., Barache, C., Barata, C., Barbato, D., Barblan, F., Barklem, P. S., Barrado, D., Barros, M.,

Barstow, M. A., Bartholomé Muñoz, L., Bassilana, J.-L., Becciani, U., Bellazzini, M., Berihuete, A., Bertone, S., Bianchi, L., Bienaymé, O., Blanco-Cuaresma, S., Boch, T., Boeche, C., Bombrun, A., Borrachero, R., Bossini, D., Bouquillon, S., Bourda, G., Bragaglia, A., Bramante, L., Breddels, M. A., Bressan, A., Brouillet, N., Brüsemeister, T., Brugaletta, E., Bucciarelli, B., Burlacu, A., Busonero, D., Butkevich, A. G., Buzzì, R., Caffau, E., Cancelliere, R., Cannizzaro, G., Cantat-Gaudin, T., Carballo, R., Carlucci, T., Carrasco, J. M., Casamiquela, L., Castellani, M., Castro-Ginard, A., Charlot, P., Chemin, L., Chiavassa, A., Cocozza, G., Costigan, G., Cowell, S., Crifo, F., Crosta, M., Crowley, C., Cuypers, J., Daffont, C., Damerdj, Y., Dapergolas, A., David, M., de Laverny, P., De Luise, F., De March, R., de Souza, R., de Torres, A., Debosscher, J., del Pozo, E., Delgado, A., Delgado, H. E., Diakite, S., Diener, C., Distefano, E., Dolding, C., Drazinos, P., Durán, J., Edvardsson, B., Enke, H., Eriksson, K., Esquej, P., Eynard Bontemps, G., Fabre, C., Fabrizio, M., Faigler, S., Falcão, A. J., Farràs Casas, M., Federici, L., Fedorets, G., Fernique, P., Figueras, F., Filippi, F., Findeisen, K., Fonti, A., Fraile, E., Fraser, M., Gai, M., Galletti, S., Garabato, D., García-Sedano, F., Garofalo, A., Garralda, N., Gavel, A., Gavras, P., Gerssen, J., Geyer, R., Giacobbe, P., Gilmore, G., Girona, S., Giuffrida, G., Glass, F., Gomes, M., Gueguen, A., Guerrier, A., Gutiérrez, R., Haignon, R., Hatzidimitriou, D., Hauser, M., Haywood, M., Heiter, U., Helmi, A., Heu, J., Hilger, T., Hobbs, D., Hofmann, W., Holland, G., Huckle, H. E., Hypki, A., Icardi, V., Janßen, K., Jevardat de Fombelle, G., Jonker, P., Juhász, Á. L., Julbe, F., Karamelas, A., Kewley, A., Klar, J., Kochoska, A., Kohley, R., Kolenberg, K., Kontizas, M., Kontizas, E., Koposov, S. E., Kordopatis, G., Kostrzewa-Rutkowska, Z., Koubsky, P., Lambert, S., Lanza, A. F., Lasne, Y., Lavigne, J.-B., Le Fustec, Y., Le Poncin-Lafitte, C., Lebreton, Y., Leccia, S., Leclerc, N., Lecoœur-Taïbi, I., Lenhardt, H., Leroux, F., Liao, S., Licata, E., Lindstrøm, H. E. P., Lister, T., Livanou, E., Lobel, A., López, M., Managau, S., Mann, R. G., Mantelet, G., Marchal, O., Marchant, J. M., Marconi, M., Marinoni, S., Marschalkó, G., Marshall, D. J., Martino, M., Marton, G., Mary, N., Massari, D., Matijević, G., Mazeh, T., McMillan, P. J., Messina, S., Michalik, D., Millar, N. R., Molina, D., Molinaro, R., Molnár, L., Montegriffo, P., Mor, R., Morbidelli, R., Morel, T., Morris, D., Mulone, A. F., Murave (2018). Gaia Data Release 2. *Astron. Astrophys.*, 616:A13.

Steckloff, J. K., Sarid, G., Volk, K., Kareta, T., Womack, M., Harris, W., Woodney, L., and Schambeau, C. (2020). P/2019 LD₂ (ATLAS): An Active Centaur in Imminent Transition to the Jupiter Family. *Astrophys. J.*, 904(2):L20.

Strömgren, E. (1908). Oppositions-Ephemeride des Planeten (624) Hektor. *Astron. Nachrichten*, 177(8):123–126.

- Suárez-Díaz, E. and Anaya-Muñoz, V. H. (2008). History, objectivity, and the construction of molecular phylogenies. *SHPBioSci*, 39(4):451–468.
- Sun, K.-L. K.-L., Seiß, M., Hedman, M. M., and Spahn, F. (2017). Dust in the arcs of Methone and Anthe. *Icarus*, 284:206–215.
- Synnott, S. P. (1980). 1979J2 - Discovery of a previously unknown Jovian satellite. *Science (80-.)*, 210:786–788.
- Synnott, S. P. (1981). 1979J3 - Discovery of a previously unknown satellite of Jupiter. *Science (80-.)*, 212:1392.
- Szabo, G. M., Ivezić, Ž., Jurić, M., and Lupton, R. H. (2007). The properties of Jovian Trojan asteroids listed in SDSS Moving Object Catalogue 3. *Mon. Not. R. Astron. Soc.*, 377(4):1393–1406.
- Tholen, D. J. (1984). *Asteroid taxonomy from cluster analysis of photometry*. PhD thesis, University of Arizona, Tucson.
- Tholen, D. J. (1989). Asteroid taxonomic classifications. In *Asteroids II*, page 1139. University of Arizona Press.
- Thomas, P. C. (2010). Sizes, shapes, and derived properties of the saturnian satellites after the Cassini nominal mission. *Icarus*, 208(1):395–401.
- Thomas, P. C., Burns, J. A., Hedman, M. M., Helfenstein, P., Morrison, S., Tiscareno, M. S., and Veverka, J. (2013). The inner small satellites of Saturn: A variety of worlds. *Icarus*, 226(1):999–1019.
- Thomas, P. C., Burns, J. A., Rossier, L., Simonelli, D., Veverka, J., Chapman, C., Klaasen, K. P., Johnson, T. V., and Belton, M. (1998). The Small Inner Satellites of Jupiter. *Icarus*, 135(1):360–371.
- Throop, H. B. (2004). The jovian rings: new results derived from Cassini, Galileo, Voyager, and Earth-based observations. *Icarus*, 172(1):59–77.
- Tillyard, R. J. (1926). *The Insects of Australia and New Zealand*. Sydney, Angus & Robertson, Ltd.

- Tiscareno, M. S., Burns, J. A., Hedman, M. M., Porco, C. C., Weiss, J. W., Dones, L., Richardson, D. C., and Murray, C. D. (2006). 100-metre-diameter moonlets in Saturn's A ring from observations of 'propeller' structures. *Nature*, 440(7084):648–650.
- Treffenstädt, L. L., Mourão, D. C., and Winter, O. C. (2015). Formation of the Janus-Epimetheus system through collisions. *Astron. Astrophys.*, 583:A80.
- Tsiganis, K., Gomes, R., Morbidelli, A., and Levison, H. F. (2005a). Origin of the orbital architecture of the giant planets of the Solar System. *Nature*, 435(7041):459–461.
- Tsiganis, K., Varvoglis, H., and Dvorak, R. (2005b). Chaotic Diffusion And Effective Stability of Jupiter Trojans. *Celest. Mech. Dyn. Astron.*, 92(1-3):71–87.
- Turrini, D., Marzari, F., and Beust, H. (2008). A new perspective on the irregular satellites of Saturn - I. Dynamical and collisional history. *Mon. Not. R. Astron. Soc.*, 391(3):1029–1051.
- Turrini, D., Marzari, F., and Tosi, F. (2009). A new perspective on the irregular satellites of Saturn - II. Dynamical and physical origin. *Mon. Not. R. Astron. Soc.*, 392(1):455–474.
- Van Dung, V., Giao, P. M., Chinh, N. N., Tuoc, D., Arctander, P., and MacKinnon, J. (1993). A new species of living bovid from Vietnam. *Nature*, 363(6428):443–445.
- Vasundhara, R., Selvakumar, G., and Anbazhagan, P. (2017). Analysis of mutual events of Galilean satellites observed from VBO during 2014–2015. *Mon. Not. R. Astron. Soc.*, 468(1):501–508.
- Verbiscer, A. J., Skrutskie, M. F., and Hamilton, D. P. (2009). Saturn's largest ring. *Nature*, 461(7267):1098–1100.
- Vinogradova, T. A. (2015). Identification of asteroid families in Trojans and Hildas. *Mon. Not. R. Astron. Soc.*, 454(3):2436–2440.
- Vinogradova, T. A. and Chernetenko, Y. A. (2015). Total mass of the Jupiter Trojans. *Sol. Syst. Res.*, 49(6):391–397.
- Vokrouhlický, D. (1998). Diurnal Yarkovsky effect as a source of mobility of meter-sized asteroidal fragments. I. Linear theory. *Astron. Astrophys.*, 335:353–363.
- Vokrouhlický, D., Brož, M., Bottke, W. F., Nesvorný, D., and Morbidelli, A. (2006). Yarkovsky/YORP chronology of asteroid families. *Icarus*, 182(1):118–142.

- Vokrouhlický, D. and Čapek, D. (2002). YORP-Induced Long-Term Evolution of the Spin State of Small Asteroids and Meteoroids: Rubincam's Approximation. *Icarus*, 159(2):449–467.
- Vokrouhlický, D. and Nesvorný, D. (2008). Pairs of Asteroids probably of a common origin. *Astron. J.*, 136(1):280–290.
- Vokrouhlický, D., Pravec, P., Ďurech, J., Hornoch, K., Kušnirák, P., Galád, A., Vraštil, J., Kučáková, H., Pollock, J. T., Ortiz, J. L., Morales, N., Gaftonyuk, N. M., Pray, D. P., Krugly, Y. N., Inasaridze, R. Y., Ayvazian, V. R., Molotov, I. E., and Colazo, C. A. (2017). Detailed Analysis of the Asteroid Pair (6070) Rheinland and (54827) 2001 NQ8. *Astron. J.*, 153(6):270.
- Walsh, K. J., Delbó, M., Bottke, W. F., Vokrouhlický, D., and Lauretta, D. S. (2013). Introducing the Eulalia and new Polana asteroid families: Re-assessing primitive asteroid families in the inner Main Belt. *Icarus*, 225(1):283–297.
- Walsh, K. J., Morbidelli, A., Raymond, S. N., O'Brien, D. P., and Mandell, A. M. (2011). A low mass for Mars from Jupiter's early gas-driven migration. *Nature*, 475(7355):206–209.
- Wang, X. and Hou, X. (2017). Dynamical spreading of small bodies in 1:1 resonance with planets by the diurnal Yarkovsky effect. *Mon. Not. R. Astron. Soc.*, 471(1):243–254.
- Warner, B. D., Harris, A. W., and Pravec, P. (2009). The asteroid lightcurve database. *Icarus*, 202(1):134–146.
- Wilkens, A. (1918). Die absolute Bewegung des Trojaners 884 Priamus. *Astron. Nachrichten*, 208(16):233–240.
- Winter, O., Souza, A., Sfait, R., Giuliatti-Winter, S., Mourão, D. C., and Foryta, D. (2016). On the Janus-Epimetheus Ring. In *AAS/Division Planet. Sci. Meet. Abstr.*, volume 48 of *AAS/Division for Planetary Sciences Meeting Abstracts*, page 203.03.
- Wisdom, J. and Holman, M. J. (1991). Symplectic maps for the n-body problem. *Astron. J.*, 102:1528.
- Wolf, M. (1907). Wiederauffindung des Planeten (588) [1906 TG]. *Astron. Nachrichten*, 174(3):47–48.

- Wong, I. and Brown, M. E. (2015). THE COLOR–MAGNITUDE DISTRIBUTION OF SMALL JUPITER TROJANS. *Astron. J.*, 150(6):174.
- Wong, I. and Brown, M. E. (2016). A Hypothesis fo the color Bimodality of Jupiter Trojans. *Astron. J.*, 152(4):90.
- Wong, I. and Brown, M. E. (2017). THE COLOR–MAGNITUDE DISTRIBUTION OF HILDA ASTEROIDS: COMPARISON WITH JUPITER TROJANS. *Astron. J.*, 153(2):69.
- Wong, I., Brown, M. E., and Emery, J. P. (2014). THE DIFFERING MAGNITUDE DISTRIBUTIONS OF THE TWO JUPITER TROJAN COLOR POPULATIONS. *Astron. J.*, 148(6):112.
- Wyse, A. (1938). The Trojan Group. *Astron. Soc. Pacific Leaflet.*, 3:113.
- Yoder, C. F. (1979). Notes on the origin of the Trojan asteroids. *Icarus*, 40(3):341–344.
- Yoder, C. F., Colombo, G., Synnott, S. P., and Yoder, K. (1983). Theory of motion of saturn’s coorbiting satellites. *Icarus*, 53(3):431–443.
- Yoder, C. F., Synnott, S. P., and Salo, H. (1989). Orbits and masses of Saturn’s co-orbiting satellites, Janus and Epimetheus. *Astron. J.*, 98:1875.
- Yoshida, F. and Nakamura, T. (2008). A Comparative Study of Size Distributions for Small L4 and L5 Jovian Trojans. *Publ. Astron. Soc. Japan*, 60(2):297–301.
- Zappala, V., Cellino, A., Dell’Oro, A., Migliorini, F., and Paolicchi, P. (1996). Reconstructing the Original Ejection Velocity Fields of Asteroid Families. *Icarus*, 124(1):156–180.
- Zappala, V., Cellino, A., Farinella, P., and Knežević, Z. (1990). Asteroid families. I - Identification by hierarchical clustering and reliability assessment. *Astron. J.*, 100:2030.
- Zebker, H. A., Marouf, E. A., and Leonard Tyler, G. (1985). Saturn’s rings: Particle size distributions for thin layer models. *Icarus*, 64(3):531–548.
- Zhou, L., Xu, Y.-B., Zhou, L.-Y., Dvorak, R., and Li, J. (2019). Orbital stability of Earth Trojans. *Astron. Astrophys.*, 622:A97.
- Zimmermann, W. and Schultz, W. (1931). *Arbeitsweise der botanischen Phylogenetik und anderer Gruppierungswissenschaften*. Urban & Schwarzenberg.

A

Appendix

Appendix

A.1 CALCULATIONS

A.1.1 CALCULATION OF $\left(\frac{da}{dt}\right)_{JT}$

As an approximation of the Yarkovsky effect on a 10km $\left(\frac{da}{dt}\right)_{MB}$ main belt asteroid from (Bottke et al., 2006).

$$\left(\frac{da}{dt}\right)_{MB} = 10^{-5} au/my \left(\frac{10km}{D}\right) \left(\frac{2.5au}{a}\right)^2 \left(\frac{2.5gcm^{-3}}{g}\right) \left(\frac{A}{0.2}\right)^{1/2} \cos\gamma \quad (A.1)$$

Added in values as an approximation for a Jovian Trojan (5.2au) with a density of $0.8gcm^{-3}$ (Marchis et al., 2006) and 0.07 albedo (ref) and solved per year and per km.

$$\left(\frac{da}{dt}\right)_{JT} = 10^{-11} au/y \left(\frac{10km}{D}\right) \left(\frac{2.5au}{5.2au}\right)^2 \left(\frac{2.5gcm^{-3}}{0.8gcm^{-3}}\right) \left(\frac{0.07}{0.2}\right)^{1/2} \cos\gamma \quad (A.2)$$

$$\left(\frac{da}{dt}\right)_{JT} = 3.798 \times 10^{-11} au/y \left(\frac{1km}{D}\right) \cos\gamma \quad (A.3)$$

A.1.2 MEAN OBLIQUITY OF YARKOVSKY

Obliquity range of angles is a $\sin\gamma$ function. If it were a linear function m , the mean is found using the inverse of integral $\int_0^{90 \text{ deg}} \sin\gamma = \cos\gamma$ at 0.5 , $\gamma = \cos^{-1}0.5$ which is 60° .

As the Yarkovsky effect is dependent on $\cos\gamma$ (Bottke et al., 2006), from equation $\left(\frac{da}{dt}\right)_{JT}$, ignoring the constant and dependence on diameter, I get the integral of:

$$\frac{1}{\pi/2} \int_0^{\pi/2} \cos\gamma \sin\gamma d\gamma \quad (A.4)$$

$$\frac{1}{\pi} \int_0^{\pi/2} d\gamma \sin 2\gamma \quad (A.5)$$

with: $X = 2\gamma$ and therefore $\frac{dX}{d\gamma} = 2$ and $d\gamma = \frac{dX}{2}$

$$\frac{1}{2\pi} \int_0^{\pi/2} [-\cos 2\gamma] \quad (A.6)$$

$$\frac{1}{2\pi} [-\cos\pi + \cos 0] \quad (A.7)$$

$$= \frac{1}{\pi} \quad (A.8)$$

$$\gamma = \cos^{-1}1/\pi \quad (A.9)$$

The resolution is that the mean Yarkovsky effect occurs at an obliquity of 71.44° .